PhD Thesis

DESIGN, SYNTHESIS AND APPLICATION OF SUPRAMOLECULAR LIGANDS IN ASYMMETRIC HYDROGENATION AND HYDROFORMYLATION

Ignacio Mon Quílez

Supervised by Prof. Dr. Anton Vidal i Ferran

(ICIQ - Universitat Rovira i Virgili)

Tarragona 2014

UNIVERSITAT ROVIRA I VIRGILI
DEPARTAMENT DE QUIMICA ANALITICA I QUIMICA ORGANICA

Prof. Dr. ANTON VIDAL I FERRAN, Group Leader in the Institute of Chemical Research of Catalonia (ICIQ) and Research Professor of the Catalan Institution for Research and Advanced Studies (ICREA),

CERTIFIED:

That the present research work entitled “Design, Synthesis and Application of Supramolecular Ligands in Asymmetric Hydrogenation and Hydroformylation” that Ignacio Mon Quílez presents to obtain the PhD degree in Chemistry, has been carried out under his supervision in the corresponding research group of the ICIQ.

Tarragona, February 2014

Prof. Dr. Anton Vidal i Ferran

ICIQ
Institut Català d'Investigació Química

UNIVERSITAT ROVIRA I VIRGILI
DEPARTAMENT DE QUIMICA ANALITICA I QUIMICA ORGANICA

AGRADECIMIENTOS

En primer lugar, quiero expresar mi agradecimiento a mi director de Tesis, Dr. Anton Vidal i Ferran, por la oportunidad que me brindó para realizar este trabajo de investigación en un instituto de tan alto nivel como es el ICIQ. Agradezco especialmente toda su dedicación prestada para que esta tesis llegara a buen puerto.

También quiero expresar mi aprecio a todos los compañeros de laboratorio que siguen en las vitrinas o que ya se fueron. Ha sido una experiencia muy positiva poder compartir unos cuantos años con gente de tan diversas procedencias y de las que tanto he llegado a aprender.

No debo olvidarme tampoco de todas las personas del Área de Soporte que me han ayudado durante la realización de esta Tesis. Mi más profundo agradecimiento a la gente de CRTU, masas, rayos-X, RMN, etc…

Por último, pero no menos importante, quiero agradecer al Prof. Toni Frontera su esfuerzo dedicado a la determinación de las geometrías y los parámetros estructurales, a nivel teórico, de algunos de los complejos supramoleculares detallados en el capítulo 2 de esta Tesis. Estos estudios han sido de gran utilidad durante mi estancia en el laboratorio y necesarios en la elaboración de esta Tesis doctoral.

El trabajo desarrollado en esta tesis doctoral ha sido posible gracias a la financiación de l'Institut Català d'Investigació Química (ICIQ) y a su programa de becas pre-doctorales (ICIQ PhD Fellowship ref. 11/09). Esta investigación se ha desarrollado en el marco de los proyectos: CTQ-2008-00950/BQU, CTQ2011-28512 del MICINN (actualmente MINECO), Consolider Ingenio 2010 (CSD2006-0003) y del proyecto 2009SGR623 del DURSI, Generalitat de Catalunya.

At the submission of this Thesis, the results contained herein have so far resulted in the following publications:

Allosteric P=O Receptors for Dicarboxylic Acids. Jose, D. A.; Mon, I.; Fernández-Pérez, H.; Escudero-Adán, E. C.; Benet-Buchholz, J.; Vidal-Ferran A. *Org. Lett.* **2011**, *13*, 3632.

Bis(phosphite) Ligands with Distal Regulation: Application in Rhodium-mediated Asymmetric Hydroformylations. Mon, I.; Jose, D. A.; Vidal-Ferran, A. *Chem. Eur. J.* **2013**, *19*, 2720.

TABLE OF CONTENTS

TABLE OF CONTENTS

INTRODUCTION AND AIMS OF RESEARCH

INTRODUCTION AND AIMS OF RESEARCH

Chirality (or the property of an object not being superimposable on its mirror image) is a common occurrence in living systems. Thus, chirality is omnipresent in nature and, not surprisingly, chiral compounds have a vast importance in many sectors of industrial chemistry (*e.g.* biologically active compounds, pharmaceutical ingredients, agrochemicals, flavors, fragrances, and materials as polymers or crystals).

The demand for chiral compounds, as single enantiomers, has exponentially increased in the last decades mainly driven by the demands of pharmaceutical companies that were forced to fulfill strong regulations[1] issued by the U.S. Food and Drug Administration (FDA) in 1993 after the Thalidomide tragedy.[2] This policy ensured that most of future marketable chiral drugs be pharmacologically tested as single enantiomers. Due to the high demand of structurally diverse enantiomerically pure compounds, synthetic chemists have become more interested in developing new and more efficient methods to gain access to enantiopure compounds.[3]

A detailed description of all strategies to prepare enantiopure compounds is beyond the scope of this Thesis introduction. However, they can be categorized into three main strategies, depending on the kind of starting material used (Figure 1). Resolution of racemates (racemate or racemic mixture is one that has equal amounts of left- and right-handed enantiomers of a chiral molecule) was one of the first methods to be used and is still the widest used for the industrial preparation of pure enantiomers.[3a] Theoretical yields of 100% of pure enantiomers are achievable for both crystallization types under certain

[1] For example see a) FDA Policy Statement for the Development of New Stereoisomeric Drugs, Washington DC, 1992: http://www.fda.gov/drugs/GuidanceComplianceRegulatoryInformation/Guidances/ucm122883.htm. b) Investigation of Chiral Active Substance: http://www.ema.europa.eu/docs/en_GB/document_library/Scientific_guideline/2009/09/WC500002816.pdf.
[2] Kim, J. H.; Scialli, A. R. *Toxicol. Sci.* **2011**, *122*, 1.
[3] For example, see the following comprehensive books on the field: a) *Comprehensive Chirality*; Carreira, E. M.; Yamamoto, H., Eds.; Elsevier Science: Oxford, 2012. b) *Comprehensive Asymmetric Catalysis: Supplement I*; Jacobsen, E. N.; Pfaltz, A.; Yamamoto, H., Eds; Springer-Verlag: Heidelberg, 2004. c) *Comprehensive Asymmetric Catalysis: Supplement II*; Jacobsen, E. N.; Pfaltz, A.; Yamamoto, H., Eds; Springer-Verlag: Heidelberg, 2004. d) *Comprehensive Asymmetric Catalysis*; Jacobsen, E. N.; Pfaltz, A.; Yamamoto, H., Eds; Springer-Verlag: Heidelberg, 1999.

conditions.[4] However, the more common cases result in theoretical yields of only 50%, which represents a drawback unless the undesired enantiomer can be racemized and recycled, or there is a demand for both enantiomers.

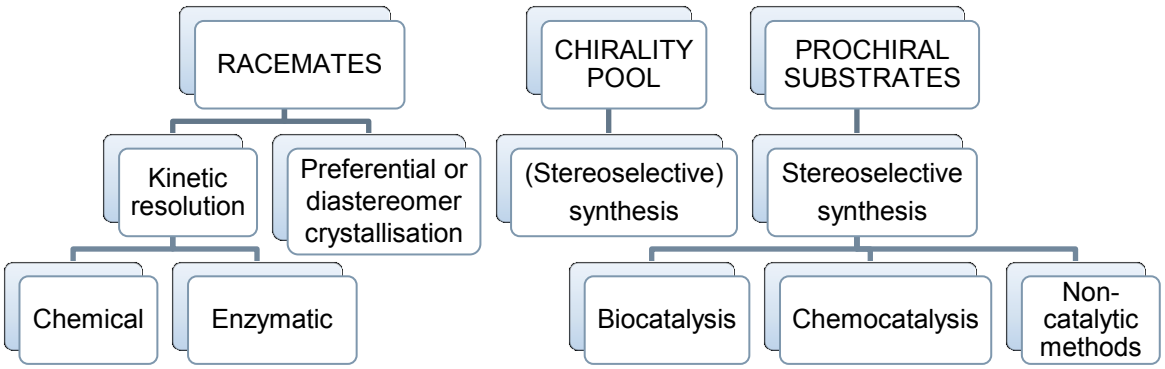

Figure 1. Methodologies for preparing enantiopure compounds from different sources[5]

Large-scale chromatographic separation techniques (*e.g. simulated moving bed (SMB) chromatography*)[6] are becoming important preparation methods for APIs, especially at the early phases of product development.[7]

Kinetic resolution is a suitable method to prepare enantiopure compounds when one of two enantiomers of a given starting material reacts at a different rate with a chiral reagent or interacts differently with a chiral catalyst. Ideally, one of the enantiomers is transformed whereas the other remains unreacted.[8]

[4] Spontaneous *in situ* racemization for preferential crystallization and spontaneous diastereomer interconversion for diastereomer crystallization render racemate separation in a 100% theoretical yield.
[5] Extracted from Sheldon, R.A. *Chirotechnology: Industrial Synthesis of Optically Active Compounds*; Marcel Dekker: New York, 1993.
[6] For instance, see: a) Rajendran, A.; Paredes, G.; Mazzotti, M. *J. Chromatogr. A* **2009**, *1216*, 709. and b) Subramanian, G. *Chiral Separation Techniques: A Practical Approach*; Wiley-VCH: Weinheim, 2001.
[7] Lorenz, H.; Seidel-Morgenstern, A. *Angew. Chem., Int. Ed.* **2014**, *53*, 1218.
[8] Koskinen, A. *Asymmetric synthesis of natural products*; Wiley-VCH: Chichester, 1993.

Some of these preparation methods (*e.g.* diastereomer crystallization and non-catalytic kinetic resolution) require stoichiometric amounts of a chiral reagent or resolving agent, which in industrial processes calls for recycling of the enantiomerically pure derivative.

The transformation of inexpensive and readily available enantiomerically pure natural products or their derivatives into the desired product using well-established chemical transformations is known as the "chiral pool" approach. One inherent weakness of this method results from the limited structural diversity of the starting materials of the chiral pool that cannot hope to cover all of the desired target molecules. Furthermore, both enantiomers of natural products might not occur naturally, which constitutes the second major disadvantage of this strategy.

Stereoselective synthesis involves a chemical reaction (or reaction sequence) that introduces in a controlled manner one or more new and desired stereogenic elements in a molecule. Enantioselective synthesis generates stereogenic units (*i.e.* stereogenic centers, planes or axes) from substrates that contain the corresponding pro-stereogenic element.

Among the different possibilities in stereoselective synthesis (use of chiral reagents or chiral auxiliaries),[9] asymmetric catalysis is the more advantageous method, as each molecule of a chiral catalyst can produce many molecules of the target enantiomer by virtue of being continually regenerated and not becoming itself permanently involved. Asymmetric catalysis allows for a diverse scope of enantiomerically pure compounds in good yields using small amounts of a chiral catalyst, which offers greater economy than using chiral reagents or chiral auxiliaries in stoichiometric amounts. Moreover, the isolation of the product is often easier, since there are fewer by-products generated. Although asymmetric catalysis is limited by the range and scope of available synthetic methodology, the explosive development of new chemical transformations in the last decades has made asymmetric catalysis a very general and practical approach to enantiomerically pure (or enriched) compounds. Indeed, enantiomerically pure compounds are also ubiquitous in nature and are produced in living systems by asymmetric catalysis mediated by highly efficient biocatalysts called enzymes.

[9] a) Rouf, A.; Taneja, S. C. *Chirality* **2014**, *26*, 63. b) Blaser, H. U. *Chem. Rev.* **1992**, *92*, 935.

Despite what is commonly believed, the seminal work of Horner[10] and Knowles[11] in the field of asymmetric hydrogenation of olefins mediated by optically pure rhodium complexes containing organophosphorus ligands[12] is not the first known example of enantioselective catalysis not involving bio-catalysts. A non-enzymatic enantioselective catalytic transformation can be traced back to the infancy of organic synthesis (1904). In that year, Marckwald reported the catalytic enantioselective decarboxylation of a malonic acid derivative mediated by brucine in 10% ee.[13] Some years later (1913), Bredig *et al.* also developed an enantioselective catalytic method for the preparation of mandelonitrile from benzaldehyde and hydrogen cyanide using an alkaloid as catalyst.[14] These pieces of work did not receive much attention by contemporary chemists, mainly because of the low enantioselectivities obtained (*ca.* 10% ee), but they are now considered as conceptually important pieces of work. It was not until 1960, when Natta *et al.* reported the first example of homogeneous asymmetric catalysis mediated by a metal complex. Natta's enantioselective polymerization of benzofurane was carried out by generating catalysts derived from aluminium trichloride and optically pure D- or L-phenylalanine.[15] This process resulted in optically active polymers, but the level of enantioinduction was difficult to estimate. A successful level of enantioselectivity (80% ee) was achieved in the 1960s by Izumi *et al*., who developed a catalytic enantioselective hydrogenation of a ketoester into an enantioenriched secondary alcohol in the presence of a catalyst derived from Raney nickel and tartaric acid.[16] In 1966, Wilkinson's catalyst $[RhCl(PPh_3)_3]$[17] demonstrated that it was possible to activate and to

[10] Horner, L.; Siegel, H.; Büthe, H. *Angew. Chem., Int. Ed.* **1968**, *7*, 942.
[11] Knowles, W. S.; Sabacky, M. J. *J. Chem. Soc., Chem. Commun.* **1968**, 1445.
[12] In coordination chemistry, a ligand is a molecule that binds to a central metal atom to form a coordination complex. The key step in most catalytic organometallic enantioselective processes involves the assembly of a supramolecular system around a metal center, with participation of the substrate molecule, the reagent, and of an enantiopure chiral molecule (a *chiral ligand*), generally bonded to the metal through one or more functional groups. In this complex system, the metal provides a low energy reaction pathway (*is responsible for catalysis*), while the chiral ligand, besides activating the metal, creates asymmetry around the metal center and ultimately allows the preferential recognition of one of the pro-stereogenic elements of the substrate.
[13] a) Marckwald, W. *Ber. Dtsch. Chem. Ges.* **1904**, *37*, 1368. b) Marckwald, W. *Ber. Dtsch. Chem. Ges.* **1904**, *37*, 349.
[14] Bredig, G.; Fiske, P. S. *Biochem. Z.* **1913**, *46*, 7.
[15] a) Natta, G.; Farina, M.; Peraldo, M.; Bressan, G. *Makromol. Chem.* **1961**, *43*, 68. b) Natta, G.; Farina, M.; Donati, M.; Peraldo, M. *Chim. Ind.* **1960**, *42*, 1363.
[16] Review: Izumi, Y. *Adv. Catal.* **1983**, *32*, 215.
[17] Osborn, J. A.; Jardine, F. H.; Young, J. F.; Wilkinson, G. *J. Chem. Soc. A* **1966**, 1711.

transfer molecular hydrogen to an olefin without the need for a metallic surface. This discovery culminated in the discovery of rhodium chelating chiral bisphosphine ligands for the asymmetric hydrogenation of substituted olefins resulting in high levels of enantioselection, such as for example Kagan's DIOP ligand **1**[18] (ee's up to 88%) and Knowles' DIPAMP ligand **2**[19] developed at Monsanto in 1975 (ee's up to 96%). Rhodium(I) complexes derived from DIPAMP **2** proved to be highly efficient catalysts (both in terms of conversion and enantioselectivity) for the asymmetric hydrogenation of dehydroamino acids and allowed for the preparation of L-DOPA at the industrial scale (Scheme 1). The associated production process utilizing this enantioselective catalyst is considered to be the first industrial process involving asymmetric catalysis and is known as the Monsanto L-DOPA process.[20]

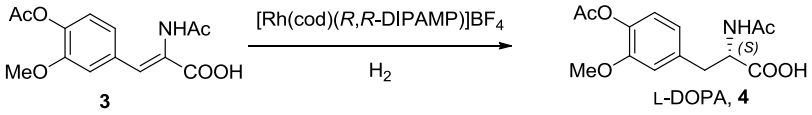

Scheme 1. Asymmetric hydrogenation step in Monsanto's L-DOPA process

As might be expected from the possibilities that the L-DOPA process offered, many chemists in academia and industry focused their work on the asymmetric hydrogenation reaction. From that time until now, many other highly efficient enantioselective catalysts were developed and tested.[21] Optically pure atropisomeric bisphosphine BINAP ligand **5** (atropisomers are stereoisomers resulting from hindered rotation about single bonds where the steric strain energy barrier to rotation is high enough to allow for the isolation of the conformers) is a clear example. Metal complexes derived from BINAP **5** are powerful catalysts in asymmetric hydrogenation as reported by Noyori *et al.* in 1980.[22] Whilst this ligand did not give exceptional results in the Rh-mediated asymmetric

[18] a) Kagan, H. B.; Dang Tuan, P. *J. Am. Chem. Soc.* **1972**, *94*, 6429. b) Kagan, H. B.; Dang, T. P. *J. Chem. Soc., Chem. Commun.* **1971**, 481.
[19] Knowles, W. S.; Sabacky, M. J.; Vineyard, B. D.; Weinkauff, D. J. *J. Am. Chem. Soc.* **1975**, *97*, 2567.
[20] Blaser, H. U.; Schmidt, E. *Asymmetric Catalysis on Industrial Scale: Challenges, Approaches and Solutions*; Wiley-VCH: Weinheim, 2004.
[21] a) Ager, D. J.; de Vries, A. H. M.; de Vries, J. G. *Chem. Soc. Rev.* **2012**, *41*, 3340. b) Luehr, S.; Holz, J.; Boerner, A. *ChemCatChem* **2011**, *3*, 1708. c) Klosin, J.; Landis, C. R. *Acc. Chem. Res.* **2007**, *40*, 1251.
[22] Noyori, R.; Takaya, H. *Acc. Chem. Res.* **1990**, *23*, 345.

hydrogenation of functionalized olefins, it exhibited an excellent performance as a ligand for ruthenium(II) precursors in the asymmetric hydrogenation of C=C and C=O bonds. Nowadays, BINAP **5** is still finding many applications as a metal ligand[23] and its chiral binaphthyl backbone is considered a privileged structure for asymmetric catalysis.[24]

Asymmetric hydroformylation is also an important reaction in academia and industry, whose study was closely related to the development of asymmetric hydrogenation.[25] Hydroformylation, also known as oxo synthesis or as the oxo process, involves the formal addition of a formyl group (CHO) and a hydrogen atom (H) to a carbon-carbon double bond, in which two different regioisomers can be obtained (Scheme 2).

The first excellent results on asymmetric hydroformylation of styrene **6a** were achieved with Pt-Sn systems (ee up to 85% with ligand **10**, see Scheme 2 for the hydroformylation reaction and Figure 2 for the structure of ligand **10**).[26] However, the low reaction rates, the low regioselectivity towards branched products and the presence of by-products derived from the parallel hydrogenation of the substrates turned the attention of investigators to rhodium-based catalysts for this transformation.[27]

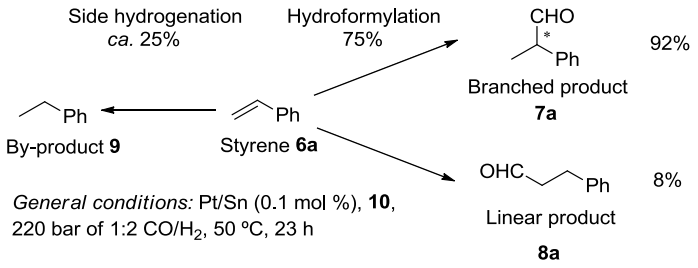

Scheme 2. Hydroformylation of **6a** with Pt/Sn/**10** catalytic system

[23] Ohkuma T., Kurono N. in *Privileged Chiral Ligands and Catalysts*; Zhou, Q.-L., Ed.; Wiley-VCH: Weinheim, 2011.
[24] a) Pereira, M. M.; Calvete, M. J. F.; Carrilho, R. M. B.; Abreu, A. R. *Chem. Soc. Rev.* **2013**, *42*, 6990. b) Aikawa, K.; Mikami, K. *Chem. Commun.* **2012**, *48*, 11050. c) Li, Y.-M.; Kwong, F.-Y.; Yu, W.-Y.; Chan, A. S. C. *Coord. Chem. Rev.* **2007**, *251*, 2119. d) Yoon, T. P.; Jacobsen, E. N. *Science* **2003**, *299*, 1691.
[25] van Leeuwen, P. W. N. M. *Homogeneous Catalysis: Understanding the Art*; Kluwer Academic Publishers: Dordrecht, 2004.
[26] Consiglio, G.; Nefkens, S. C. A. *Tetrahedron: Asymmetry* **1990**, *1*, 417.
[27] Claver, C.; van Leeuwen, P. W. N. M. in *Rhodium Catalyzed Hydroformylation*; Claver, C.; van Leeuwen, P. W. N. M., Eds.; Kluwer Academic Publishers: Dordrecht, 2000.

The first attempts to catalyze the rhodium-mediated asymmetric hydroformylation were carried out using the same bisphosphine ligands prepared for asymmetric hydrogenation. However, bisphosphine ligands turned out to be unsuitable for this transformation. Indeed, enantioselectivities were only moderate until the development of a new kind of organophosphorus ligands by Wink *et al.*: the bisphosphites.[28] The use of bisphosphites is one of the most important breakthroughs in asymmetric hydroformylation. The original underlying idea was to improve the reactivity and/or the selectivity of the catalyst by making the metal center more electrophilic. Bisphosphite ligand **11** (Figure 2) could, indeed, help to dramatically change the electronic properties of the metal, but in first instance it did not show any enantioselectivity in the asymmetric hydroformylation of styrene.[28] Fortunately, only one year later, promising results were obtained by Takaya *et al.* in the asymmetric hydroformylation of vinyl acetate (50% ee) with bisphosphite ligand **12**.[29] They claimed that hydroformylation catalysts derived from bisphosphite ligands were more stable than those derived from bisphosphines under hydroformylation conditions since less P-ligand decomplexation was probably occurring. Styrene was successfully hydroformylated by Babin and Whiteker at Union Carbide with an excellent enantioselectivitiy (90% ee) by using chiral bisphosphite **13**.[30] van Leeuwen *et al.* thoroughly studied the influence of the different parameters present in ligand **13** including the phosphite substituents, the length of the alkyl chain between the two phosphite groups in the ligand skeleton and the matched/mismatched effects of the different stereogenic elements on the catalyst performance.[31] In 1993, Takaya and Nozaki synthesized a new ligand named BINAPHOS **14**, which was structurally related to BINAP **5** and combined phosphine and phosphite with axial stereogenic elements moieties.[32] From this combination it was expected that BINAPHOS **14** could take advantage of the excellent-performance of axial stereogenic elements in asymmetric hydrogenation catalysts and the recently discovered advantages of phosphite groups for asymmetric hydroformylation. The result constituted the highest performing and one of the most general ligands

[28] Wink, D. J.; Kwok, T. J.; Yee, A. *Inorg. Chem.* **1990**, *29*, 5006.
[29] Sakai, N.; Nozaki, K.; Mashima, K.; Takaya, H. *Tetrahedron: Asymmetry* **1992**, *3*, 583.
[30] Babin, J. E.; Whiteker, G. T. PCT Int. Appl. 1993, WO 9303839.
[31] Buisman, G. J. H.; Vos, E. J.; Kamer, P. C. J.; van Leeuwen, P. W. N. M. *J. Chem. Soc., Dalton Trans.* **1995**, 409.
[32] Sakai, N.; Mano, S.; Nozaki, K.; Takaya, H. *J. Am. Chem. Soc.* **1993**, *115*, 7033.

for asymmetric hydroformylation. (R_a,S_a)-BINAPHOS **14** was capable of catalyzing in a highly enantioselective way (up to 95% ee) the hydroformylation of diverse families of alkenes. Noteworthy, other outstanding bidentate ligands such as the bisphosphite ligand KELLIPHITE developed by Dowpharma **15**,[33] Landis' bisphospholane ligand **16**[34] or Zhang and Yan's phosphine-phosphoramidite YANPHOS **17**[35] have been presented until the date; a wide selection of them and their results on asymmetric hydroformylation have been published on a recent review.[36]

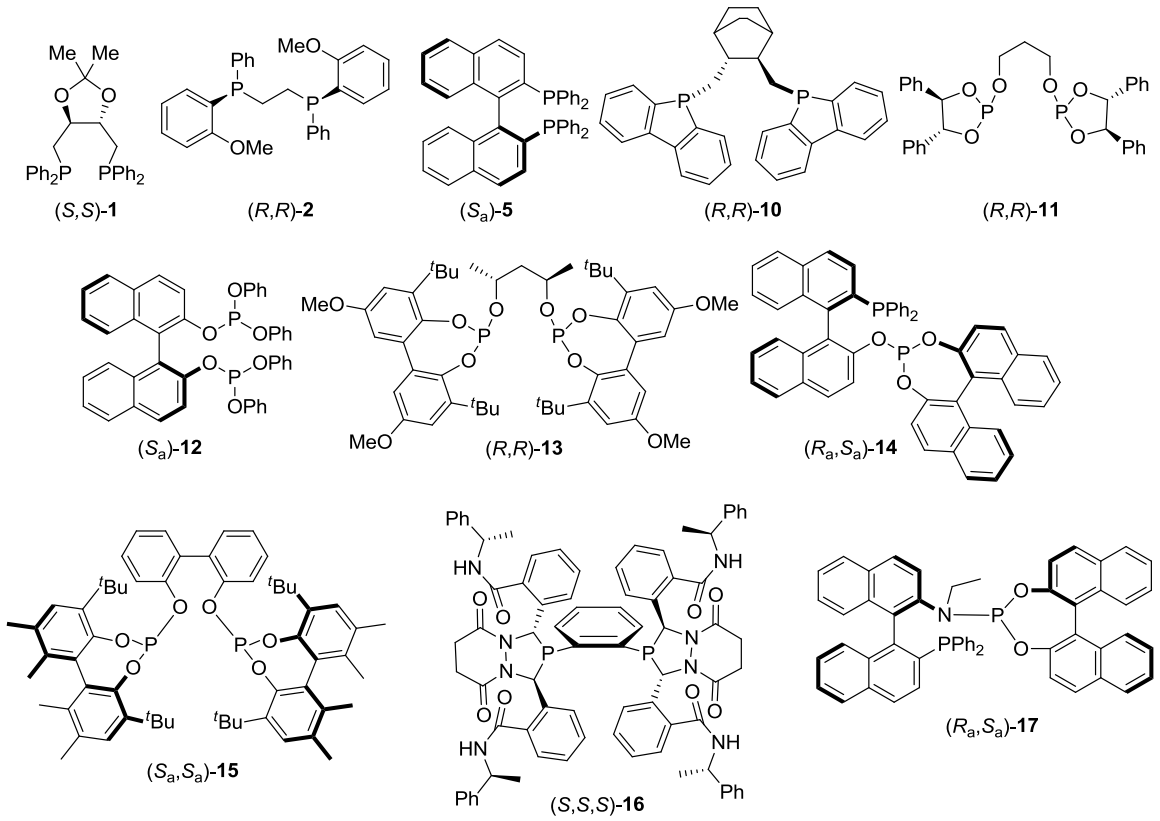

Figure 2. Examples of phosphorus-based chiral ligands used for asymmetric hydroformylation and hydrogenation

One can conclude that many of the catalyst's properties depend on the ligand, and therefore, advances in asymmetric catalysts have led to the

[33] Cobley, C. J.; Gardner, K.; Klosin, J.; Praquin, C.; Hill, C.; Whiteker, G. T.; Zanotti-Gerosa, A.; Petersen, J. L.; Abboud, K. A. *J. Org. Chem.* **2004**, *69*, 4031.
[34] a) McDonald, R. I.; Wong, G. W.; Neupane, R. P.; Stahl, S. S.; Landis, C. R. *J. Am. Chem. Soc.* **2010**, *132*, 14027. b) Watkins, A. L.; Hashiguchi, B. G.; Landis, C. R. *Org. Lett.* **2008**, *10*, 4553. c) Thomas, P. J.; Axtell, A. T.; Klosin, J.; Peng, W.; Rand, C. L.; Clark, T. P.; Landis, C. R.; Abboud, K. A. *Org. Lett.* **2007**, *9*, 2665. d) Clark, T. P.; Landis, C. R.; Freed, S. L.; Klosin, J.; Abboud, K. A. *J. Am. Chem. Soc.* **2005**, *127*, 5040.
[35] Yan, Y.; Zhang, X. *J. Am. Chem. Soc.* **2006**, *128*, 7198.
[36] Chikkali, S. H.; van der Vlugt, J. I.; Reek, J. N. H. *Coord. Chem. Rev.* **2014**, *262*, 1.

development of a myriad of structurally diverse enantiomerically pure ligands for almost every synthetic transformation susceptible to be asymmetrically catalyzed. For this reason, an ideal chiral ligand should not only be easily accessible but also be structurally modifiable in a systematic way. The feasibility of rational ligand design in asymmetric catalysis is limited in many cases by a lack of deep understanding of the catalytic process. Thus, much of the development of an efficient asymmetric catalyst for a given transformation and a particular substrate relies on empirical strategies. The standard strategy involves developing and synthesizing a number of structurally related ligands that incorporate subtle structural differences with the hope that one of them in the series performs the desired catalytic asymmetric transformation for the required substrate in good stereoselectivity and acceptable catalytic activity. The preparation of ligands through conventional covalent chemistry is normally tedious and highly time-consuming, as well as expensive. Combinatorial and high-throughput synthetic strategies have enabled the generation of ligand libraries with unprecedented ease for different asymmetric reactions and substrates.[37] Furthermore, synthetic chemists have shown great interest in developing innovative methodologies that allow for easy modification of the structure (and thus the properties) of a chiral catalyst in an easier way than standard covalent chemistry allows.

A promising approach was established in the field of supramolecular chemistry which has attracted the attention of chemists in recent years because of the high level of development achieved. The term supramolecular[38] reflects the fact that this chemistry deals with complex chemical entities formed by more than one species that are associated by means of intermolecular reversible binding forces. Furthermore, the properties of this association are expected to overcome the sum of the individual components and permit to hold together the diverse entities that form the supramolecular complex (see Table 1).

[37] a) Schmink, J. R.; Bellomo, A.; Berritt, S. *Aldrichim. Acta* **2013**, *46*, 71. b) Leung, D.; Kang, S. O.; Anslyn, E. V. *Chem. Soc. Rev.* **2012**, *41*, 448. c) Busacca, C. A.; Fandrick, D. R.; Song, J. J.; Senanayake, C. H. *Adv. Synth. Catal.* **2011**, *353*, 1825. d) Jäkel, C.; Paciello, R. *Chem. Rev.* **2006**, *106*, 2912.
[38] Lehn, J. M. *Pure Appl. Chem.* **1978**, *50*, 871.

Table 1. Strength of supramolecular interactions[39]

Interaction	Strength (kJ mol^{-1})	Example
Ion-ion	200 – 300	Tetrabutylammonium chloride
Ion-dipole	50 – 200	Sodium [15]crown-5
Dipole-dipole	5 – 50	Acetone
Hydrogen bonding	4 – 120	DNA/RNA
Cation-π	5 – 80	K^+ in benzene
π-π	0 – 50	Benzene in graphite
Anion-π[40]	20 – 70	$C_6F_6 \bullet F^-$ interactions
Van der Waals	< 5	Argon, packing in molecular crystals
Hydrophobic	Related to solvent-solvent interaction energy	Cyclodextrin inclusion compounds

After gaining a deep understanding of the principles that govern these forces, supramolecular chemists have used them as a toolbox to build a highly diverse array of supramolecular structures. A brief summary of the main tools available for supramolecular chemists is presented below.[41]

- Metal-ligand interactions: The use of metal-ligand interactions is a common tool for the construction of supramolecular assemblies. Indeed, metal-ligand interactions present an array of properties that are particularly interesting for the construction of complex supramolecular entities. The variation of the ligand denticity, polarizability, and steric hindrance and structure of metal used allows for the generation of a wide range of different supramolecular complexes. These type of interactions are present, for example, between Zn(II) or Ru(II) metal centers with the pyridine units indicated in Figure 8 and between the Rh(I) metal center with carbon monoxide (CO) and chloride anion (Cl^-) (shown in Scheme 4).

[39] Extracted from: Steed, J. W.; Turner, D. R.; Wallace, K. J. *Core Concepts in Supramolecular Chemistry and Nanochemistry;* Jhon Wiley & Sons: Chichester, 2007. Metal-ligand interactions have been commonly used in supramolecular chemistry. However, scales of bond energies for metal ligand interactions are hardly ever tabulated in the literature. For this reason, metal-ligand interactions have not been included in Table 1.
[40] Chifotides, H. T.; Dunbar, K. R. *Acc. Chem. Res.* **2013**, *46*, 894.
[41] Steed, J. W.; Atwood, J. L. *Supramolecular Chemistry*; John Wiley & Sons: Chichester, 2009.

- Ionic and dipolar interactions:[41] Up to three subdivisions can be made within this category of interactions: ion-ion interactions, ion-dipole and dipole-dipole. Whereas all of them are electrostatic interactions based in the Coulombic attraction between two opposite charges, the main difference between them is the nature of the charge and the directionality of the interaction. Ion-ion interactions between net charges are non-directional, which means that the attractive forces are acting in every direction. These forces are responsible, for example, for keeping sodium and chloride ions close together in sodium chloride salt. On the other hand, ion-dipole and dipole-dipole interactions involve a pair of electric charges of equal magnitude but opposite sign separated by a distance (*i.e.* a dipole) and these are directional. Although these interactions are weaker than ion-ion interactions, they are very useful since the directional interaction forces the molecules to aggregate in a predictable and particular way, if they complement each other (Figure 3).

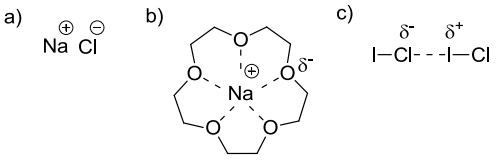

Figure 3. Examples of: a) Ion-ion interaction in sodium chloride; b) Ion-dipole interactions in a sodium complex of [15]crown-5; c) Dipole-dipole interactions in iodine monochloride

- Hydrogen bonding:[41] This interaction combines two interesting properties: a high degree of directionality and a notable binding strength. Hydrogen bonding can be considered as a special kind of dipole-dipole interaction between a proton acceptor (A) and a proton donor (D). The hydrogen bond donor is formed by an electronegative functional group with a bound proton. This electronegative functional group creates a dipole by withdrawing electron density and leaving the proton partially positively charged (δ^+). The proton acceptor (A) is also a dipole with electron-withdrawing groups that has a high level of electron density (δ^-) allowing the directional electrostatic attraction between A and D. As an example of strong hydrogen bonding, the complementary hydrogen bonding binding motifs based in the quadruple array in **18** (Figure 4a) display *ca.* 20% of the

thermodynamic stability of a C-C covalent bond.[42] Not surprisingly, hydrogen bonding was nature's choice for many interesting biological processes like substrate recognition by enzymes as well as protein and nucleic acid folding (see **19** in Figure 4b).

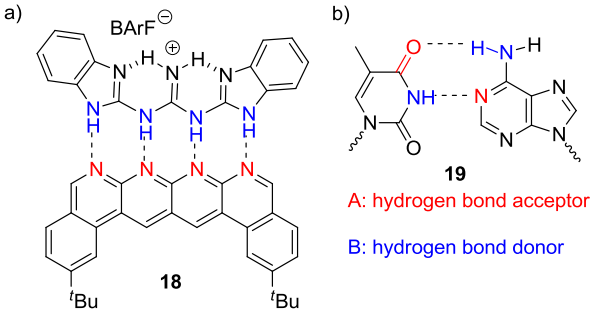

Figure 4. Example of molecular recognition using hydrogen bond: a) Strong artificial quadrupole hydrogen bond array **18**; b) Thymine and adenine primary hydrogen bond interactions (**19**)

- Cation-π interactions: This attractive interaction is now recognized as a major force in molecular recognition and an important factor in chemical and biocatalysis.[43] For example, it is present in biological processes such as the binding of neurotransmitters to their receptors and many drug-receptor interactions, such as those in nicotine-acetylcholine receptors in the brain.[44] However, it is also a key interaction in non-natural catalytic reactions, such as the organocatalytic bio-inspired processes developed by Jacobsen *et al.*, which involve organocatalyzed cationic polycyclizations and Claisen rearrangements.[45] The driving force of the binding event comes from a partial negative charge of a π-electron cloud that interacts with positively charged species. The binding strength was early proved when it was demonstrated that the potassium cation binds benzene more tightly than water in the gas phase (see Figure 5a).[46] This interaction has been recently applied in the development of the first artificial receptor **20** that selectively binds the asymmetric dimethyl arginine (aRMe$_2$)

[42] Blight, B. A.; Hunter, C. A.; Leigh, D. A.; McNab, H.; Thomson, P. I. T. *Nat. Chem.* **2011**, *3*, 244.
[43] a) Dougherty, D. A. *Acc. Chem. Res.* **2013**, *46*, 885. b) Hunter, C. A.; Low, C. M. R.; Rotger, C.; Vinter, J. G.; Zonta, C. *Proc. Natl. Acad. Sci. U. S. A.* **2002**, *99*, 4873. c) Zacharias, N.; Dougherty, D. A. *Trends Pharmacol. Sci.* **2002**, *23*, 281.
[44] Xiu, X.; Puskar, N. L.; Shanata, J. A. P.; Lester, H. A.; Dougherty, D. A. *Nature* **2009**, *458*, 534.
[45] a) Uyeda, C.; Jacobsen, E. N. *J. Am. Chem. Soc.* **2011**, *133*, 5062. b) Knowles, R. R.; Lin, S.; Jacobsen, E. N. *J. Am. Chem. Soc.* **2010**, *132*, 5030.
[46] Sunner, J.; Nishizawa, K.; Kebarle, P. *J. Phys. Chem.* **1981**, *85*, 1814.

amino acid derivative **21a** over the symmetric dimethyl arginine (sRMe$_2$) **21b** (see Figure 5b).[47]

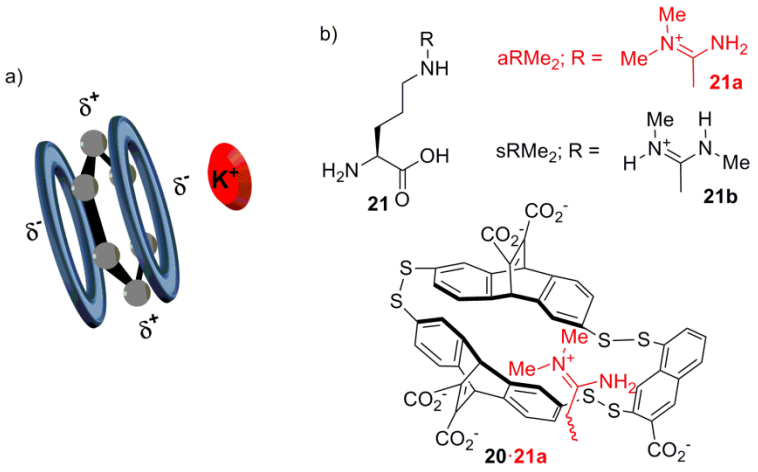

Figure 5. Examples of supramolecular systems bound through cation–π interactions: a) Schematic drawing of the benzene-potassium cation system; b) Artificial receptor **20** for dimethyl arginine guests **21**

- π-π interactions:[48] The nature of aromatic π-π interactions is still under debate. Early investigations by Sanders[49] and Hunter[49,50] proposed an electrostatic model whereas Cozzi and Siegel[51] suggested a "polar/π" model. In both cases, the substitution effects in π-stacking interactions are explained as changes induced to the π-aryl system. For example, in the electrostatic model, electron-withdrawing elements remove electron density from the π-cloud diminishing the repulsion between aromatic cores resulting in a favored π-π stacking interaction. Nevertheless, π-π interactions have been intensively studied both experimentally and computationally by other researchers.[52] π-

[47] James, L. I.; Beaver, J. E.; Rice, N. W.; Waters, M. L. *J. Am. Chem. Soc.* **2013**, *135*, 6450.
[48] a) Wheeler, S. E. *Acc. Chem. Res.* **2013**, *46*, 1029. b) Sherrill, C. D. *Acc. Chem. Res.* **2013**, *46*, 1020. c) Wheeler, S. E. *J. Am. Chem. Soc.* **2011**, *133*, 10262. d) Salonen, L. M.; Ellermann, M.; Diederich, F. *Angew. Chem., Int. Ed.* **2011**, *50*, 4808.
[49] Hunter, C. A.; Sanders, J. K. M. *J. Am. Chem. Soc.* **1990**, *112*, 5525.
[50] a) Cockroft, S. L.; Perkins, J.; Zonta, C.; Adams, H.; Spey, S. E.; Low, C. M. R.; Vinter, J. G.; Lawson, K. R.; Urch, C. J.; Hunter, C. A. *Org. Biomol. Chem.* **2007**, *5*, 1062. b) Cockroft, S. L.; Hunter, C. A.; Lawson, K. R.; Perkins, J.; Urch, C. J. *J. Am. Chem. Soc.* **2005**, *127*, 8594.
c) Hunter, C. A.; Lawson, K. R.; Perkins, J.; Urch, C. J. *J. Chem. Soc., Perkin Trans. 2* **2001**, 651.
[51] a) Cozzi, F.; Annunziata, R.; Benaglia, M.; Baldridge, K. K.; Aguirre, G.; Estrada, J.; Sritana-Anant, Y.; Siegel, J. S. *Phys. Chem. Chem. Phys.* **2008**, *10*, 2686. b) Cozzi, F.; Cinquini, M.; Annuziata, R.; Siegel, J. S. *J. Am. Chem. Soc.* **1993**, *115*, 5330. c) Cozzi, F.; Cinquini, M.; Annunziata, R.; Dwyer, T.; Siegel, J. S. *J. Am. Chem. Soc.* **1992**, *114*, 5729.
[52] a) Watt, M.; Hardebeck, L. K. E.; Kirkpatrick, C. C.; Lewis, M. *J. Am. Chem. Soc.* **2011**, *133*, 3854. b) Wheeler, S. E.; McNeil, A. J.; Müller, P.; Swager, T. M.; Houk, K. N. *J. Am. Chem. Soc.* **2010**, *132*, 3304. c) Wheeler, S. E.; Houk, K. N. *J. Am. Chem. Soc.* **2008**, *130*, 10854.

π interactions are normally present between aromatic groups; most commonly, two different aromatic π-π interactions can be found: i) *face to face* (called also π-stacking), in which the centers of two aromatic rings interact with each other (sandwich type) or with the corner of another one (parallel-displaced). This kind of interaction is known to be present in the molecular structure of graphite; ii) *Edge to face* (also referred to as T-shaped or CH-π interaction); in this case one of the aromatic rings is perpendicularly aligned to the center of another aromatic ring (Figure 6).

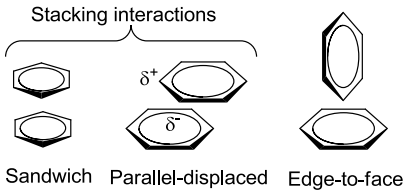

Figure 6. Prototypical π-stacking interactions between two phenyl groups

- Anion-π interactions:[40,53] Although the origins of attractive anion-interactions have been known for some time,[54] interest in anion-π interactions is relatively recent. One of the possible explanations for this is because, in contrast to cation-π interactions, anion-π interactions could be considered to be as counterintuitive. Actually, it was not until 2002 when Deyà, Frontera, Ballester *et al.*[55] first proposed the term anion-π interactions for the attractive forces between π-acidic aromatic rings and anions. In that work, a combination of crystallographic and computational studies revealed an energetically favorable interaction between the π-electron cloud from hexafluorobenzene and several different anions **22** (Figure 7). Nowadays, the scientific community is aware of the important role of anion-π interactions in many key biological systems, such as enzymes and proteins.[53] Not surprisingly, the knowledge gained on this topic is

d) Sinnokrot, M. O.; Sherrill, C. D. *J. Phys. Chem. A* **2006**, *110*, 10656. e) Ringer, A. L.; Sinnokrot, M. O.; Lively, R. P.; Sherrill, C. D. *Chem. Eur. J.* **2006**, *12*, 3821. f) Sinnokrot, M. O.; Sherrill, C. D. *J. Phys. Chem. A* **2003**, *107*, 8377. g) Rashkin, M. J.; Waters, M. L. *J. Am. Chem. Soc.* **2002**, *124*, 1860. h) Kim, E.-i.; Paliwal, S.; Wilcox, C. S. *J. Am. Chem. Soc.* **1998**, *120*, 11192.

[53] a) Ballester, P. *Acc. Chem. Res.* **2012**, *46*, 874. b) Frontera, A.; Gamez, P.; Mascal, M.; Mooibroek, T. J.; Reedijk, J. *Angew. Chem., Int. Ed.* **2011**, *50*, 9564. c) Berryman, O. B.; Johnson, D. W. *Chem. Commun.* **2009**, 3143. d) Schottel, B. L.; Chifotides, H. T.; Dunbar, K. R. *Chem. Soc. Rev.* **2008**, *37*, 68.

[54] Hiraoka, K.; Mizuse, S.; Yamabe, S. *J. Phys. Chem.* **1987**, *91*, 5294.

[55] Quiñonero, D.; Garau, C.; Rotger, C.; Frontera, A.; Ballester, P.; Costa, A.; Deyà, P. M. *Angew. Chem., Int. Ed.* **2002**, *41*, 3389.

being applied in the design of new anionic receptors, hosts, catalysts and other materials.[56]

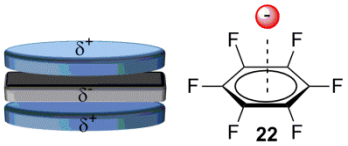

Figure 7. Schematic representation of the quadrupole moment of hexafluorobenzene (left) and the anion-π interaction (right)

In order to have a more complete vision of the supramolecular interactions that can be present in a supramolecular complex or aggregate other non-directional or less specific forces should be also considered including van der Waals forces (London and exchange-repulsion forces), closed shell interactions[57] such as aurophilic interactions[58] or halogen bonding,[59] solvation[60] and hydrophobic effects.[61]

In any catalytic process, supramolecular forces are always present since the catalyst recognizes and organizes substrates and reagents in a certain way and contributes to the assembly of a new molecule. In general, the term supramolecular catalysis is used for supramolecular interactions that are not present in the basic catalytic reaction. However, and despite this definition, it is also true that there is not always a clear cut-division between supramolecular and non-supramolecular catalysis.

In the 1970s,[62] supramolecular catalysis was equivalent to mimicking enzymes *via* host-guest catalysis. Early studies dealt only with reactions that also take place in enzymes. Other non-enzymatic reactions (*e.g.* Diels-Alder cycloadditions) were also studied successfully with this approach. Progress in supramolecular organometallic host-guest chemistry was not straightforward at that time, since the synthesis of host-guest systems equipped with a metallic

[56] See, for example, this recent review on ligand design: Watt, M. M.; Collins, M. S.; Johnson, D. W. *Acc. Chem. Res.* **2013**, *46*, 955.
[57] Pyykkoe, P. *Chem. Rev.* **1997**, *97*, 597.
[58] Schmidbaur, H.; Schier, A. *Chem. Soc. Rev.* **2008**, *37*, 1931.
[59] Priimagi, A.; Cavallo, G.; Metrangolo, P.; Resnati, G. *Acc. Chem. Res.* **2013**, *46*, 2686.
[60] Smithrud, D. B.; Sanford, E. M.; Chao, I.; Ferguson, S. B.; Carcanague, D. R.; Evanseck, J. D.; Houk, K. N.; Diederich, F. *Pure Appl. Chem.* **1990**, *62*, 2227.
[61] Southall, N. T.; Dill, K. A.; Haymet, A. D. J. *J. Phys. Chem. B* **2002**, *106*, 521.
[62] van Leeuwen, P. W. N. M. *Supramolecular Catalysis*; Wiley-VCH: Weinheim, 2008.

catalytic site is not trivial. In recent years, supramolecular, homogeneous catalysis has experienced an exponential growth, and many supramolecular catalysts, not only operating under the host-guest principle, have been designed and constructed with exquisite detail using supramolecular forces.[63] With regard to the construction of supramolecular catalysts for asymmetric reactions, four general strategies can be found in the literature:

i) the preparation of ditopic ligands by assembling two chiral monotopic building blocks *via* supramolecular interactions around a template or between them[64]

ii) allosteric control of the active site's geometry[63a]

iii) substrate-ligand interactions[65]

iv) construction of chiral cavities[66]

Enantioselective catalysis is mainly based on favoring/disfavoring the formation of one of the possible enantiomers in a given transformation. Certainly, steric interactions and supramolecular forces (cation-π, C-H-π, π-π interactions, etc.) play a central role in the stereodiscriminating processes in enantioselective catalysis (*e.g.* control of the metal coordination spheres in organometallic enantioselective catalysis). The idea of using the tool box of supramolecular forces to design new and more efficient enantioselective catalysts by controlling the different reaction paths may not seem too naïve. However, supramolecular forces are not always completely predictable and the field of supramolecular enantioselective catalysis engineering is still nowadays underdeveloped.

The progress of supramolecular enantioselective catalysis in all the fields already mentioned has been comprehensively reviewed recently. A detailed summary of all aspects falls beyond the scope of this introduction.[63]

---

[63] a) Raynal, M.; Ballester, P.; Vidal-Ferran, A.; van Leeuwen, P. W. N. M. *Chem. Soc. Rev.* **2014**, *43*, 1734. b) Raynal, M.; Ballester, P.; Vidal-Ferran, A.; van Leeuwen, P. W. N. M. *Chem. Soc. Rev.* **2014**, *43*, 1660. c) Meeuwissen, J.; Reek, J. N. H. *Nat. Chem.* **2010**, *2*, 615.
[64] Bellini, R.; van, d. V. J. I.; Reek, J. N. H. *Isr. J. Chem.* **2012**, *52*, 613.
[65] Carboni, S.; Gennari, C.; Pignataro, L.; Piarulli, U. *Dalton Trans.* **2011**, *40*, 4355.
[66] a) Brown, C. J.; Bergman, R. G.; Raymond, K. N. *J. Am. Chem. Soc.* **2009**, *131*, 17530. b) Fiedler, D.; van Halbeek, H.; Bergman, R. G.; Raymond, K. N. *J. Am. Chem. Soc.* **2006**, *128*, 10240. c) Fiedler, D.; Leung, D. H.; Bergman, R. G.; Raymond, K. N. *Acc. Chem. Res.* **2005**, *38*, 351. d) Fiedler, D.; Bergman, R. G.; Raymond, K. N. *Angew. Chem., Int. Ed.* **2004**, *43*, 6748. e) Fiedler, D.; Pagliero, D.; Brumaghim, J. L.; Bergman, R. G.; Raymond, K. N. *Inorg. Chem.* **2004**, *43*, 846.

Whilst the preparation of catalysts by the supramolecular assisted assembly of two chiral constituent monotopic blocks, either around a template (an ion or a platform bearing a coordinative center) or themselves is a well-studied strategy to easily synthesize enantioselective catalysts,[64] the control of the size and/or shape of the catalytic site (sometimes also referred to as "chiral pocket") by means of supramolecular interactions is an underdeveloped field of research.

Again, Nature has served as a model, since some enzymes have developed a very efficient way for adjusting the catalytic performance to optimal conditions by participation of another molecule which can enhance or decrease the enzyme's activity. This phenomenon is generally referred to as allosteric control and the regulation event does not necessarily have to take place in the immediacy of the active catalytic site (generally it does not). Allosteric regulation[67] generally arises from a conformational change induced by the binding of a molecule (allosteric effector) at a site that may be remote from the catalytic center.

The first efforts towards the development of artificial allosteric catalysts for asymmetric catalysis were reported in 2003 by Mirkin *et al*.[68] Reversible interactions (metal-ligand interactions) were used by these authors for allosteric modulation (Weak-Link Approach, WLA) in the multimetallic macrocyclic complexes depicted in Scheme 3. These macrocycles can be chemically interconverted *in situ* using small molecules (A) between their *condensed* **23** and *open* states **24**. First investigations showed a two-fold enhancement of the rate of the asymmetric ring opening of cyclohexene oxide **25** with $TMSN_3$ upon addition of the chloride anion and carbon monoxide to the *condensed* state complex **23a** to generate the *open* state complex **24a** *in situ*. However, no conclusions on the regulation effects on enantioselectivity were drawn by the authors.[68c] With this Weak-Link approach, the authors designed other types of allosteric catalysts that differ in the shape of their structural center, and consequently, in their catalytic activity. For example, they developed the metallo-macrocycles **26** and **27**, which

[67] a) Edelstein, S. J. *J. Mol. Biol.* **2013**, *425*, 1391. b) Goodey, N. M.; Benkovic, S. J. *Nat. Chem. Biol.* **2008**, *4*, 474.
[68] a) Gianneschi, N. C.; Masar, M. S., III; Mirkin, C. A. *Acc. Chem. Res.* **2005**, *38*, 825. b) Gianneschi, N. C.; Cho, S.-H.; Nguyen, S. B. T.; Mirkin, C. A. *Angew. Chem., Int. Ed.* **2004**, *43*, 5503. c) Gianneschi, N. C.; Bertin, P. A.; Nguyen, S. T.; Mirkin, C. A.; Zakharov, L. N.; Rheingold, A. L. *J. Am. Chem. Soc.* **2003**, *125*, 10508.

can be interconverted between them by the addition or removal of CO gas (Scheme 4). These compounds that contain two units of the salen[69] ligand were used in the enantioselective ring-opening of cyclohexene oxide by trimethylsilylazide ($TMSN_3$). The ability to reversibly convert the far less active and selective catalyst **27** to the more reactive **26** by *in situ* CO saturation or CO desaturation in the presence of chloride ions allowed to conveniently cycle the catalyst through two modes (*open* **27** and *condensed* **26**). With the introduction and removal of CO (1 atm) as a switch between the *open* **27** and *condensed* forms **26** of the catalyst, they demonstrated the allosteric effect with respect to the rate and enantioselectivity in the formation of 1-azido-2-(trimethylsiloxy)cyclohexane **28** (Scheme 4).

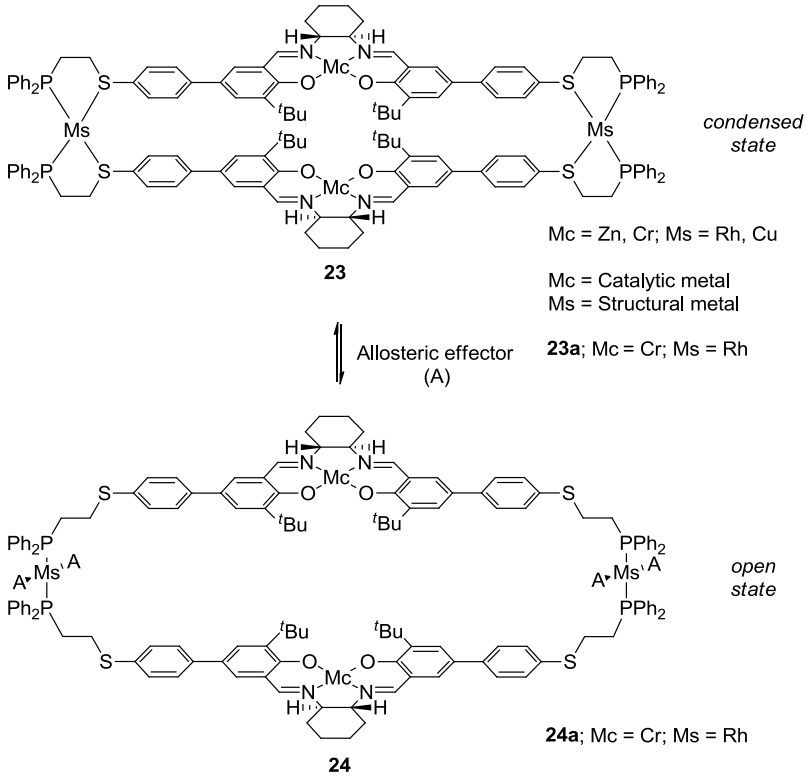

Scheme 3. General structure of the supramolecular allosteric catalysts designed by Mirkin *et al.*, shown in the *condensed* **23** and *open* states **24**

[69] Salen-type compounds **29** are Schiff bases that can act as *N*,*N*',*O*,*O*'-tetradentate ligands and derive from ethylenediamine and 2-hydroxybenzaldehyde. The name salen is a contraction for Bis(**sa**licylaldehyde)ethy**len**ediamine.

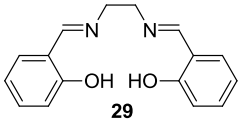

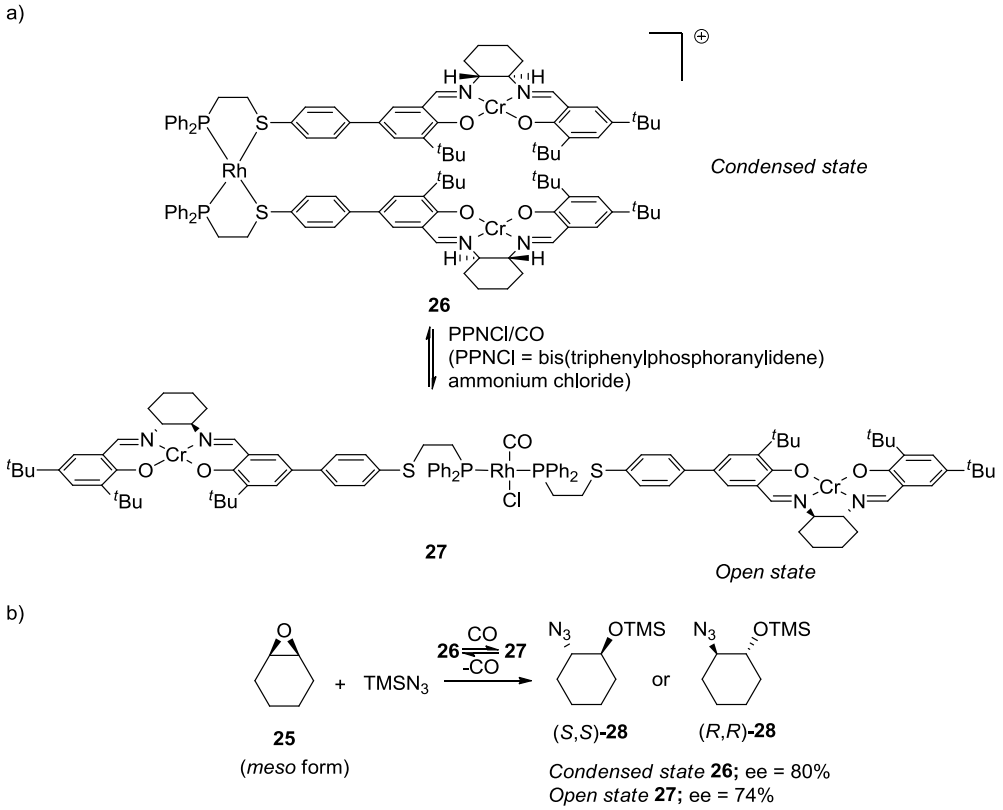

Scheme 4. a) Mirkin's supramolecular allosteric catalysts **26**/**27**, shown in *condensed* **26** and *open* states **27**; b) Asymmetric epoxide-opening mediated by *condensed* **26** and *open* states **27**

In a second approach, an organic ligand binds to a structural metal center (Ms) within the same chiral complex and induces a conformational change that affects the ability of a catalytic metal center (Mc) to function. Basically, the change in the coordination sphere of the structural metal generates a new molecular shape in the supramolecular complex, which in combination with a catalytic metal center is suitable for catalysis and may result in improved activity and/or selectivity in a given transformation. From a biological point of view, this strategy is more reminiscent of the way various enzymes use structural metals to define their tertiary structure in a static fashion rather than behaving dynamically and reversibly (Scheme 5).[70]

[70] Some early examples: a) Horiuchi, Y.; Gnanadesikan, V.; Ohshima, T.; Masu, H.; Katagiri, K.; Sei, Y.; Yamaguchi, K.; Shibasaki, M. *Chem. Eur. J.* **2005**, *11*, 5195. b) Hua, J.; Lin, W. *Org. Lett.* **2004**, *6*, 861. c) Lee, S. J.; Hu, A.; Lin, W. *J. Am. Chem. Soc.* **2002**, *124*, 12948. d) Morris, G. A.; Nguyen, S. T.; Hupp, J. T. *J. Mol. Catal. A: Chem.* **2001**, *174*, 15.

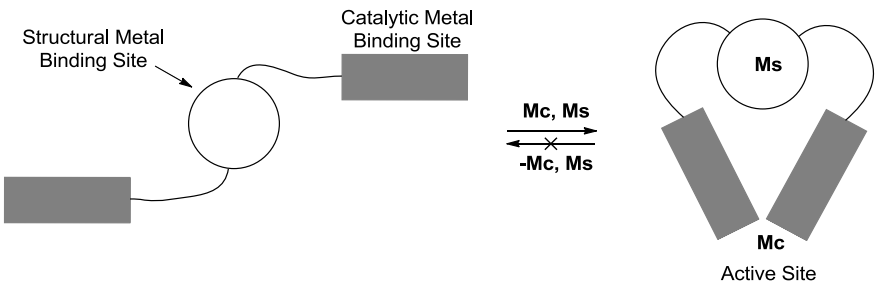

Scheme 5. A ligand binds to one or more structural metal ions (Ms), and the resulting intermediate, having adopted the appropriate configuration, then binds to one or more catalytic metal ions (Mc) to form a catalytically active complex.

Researchers have also sought to extrapolate this principle of allosteric regulation to much smaller and synthetically accessible organic ligands. Reek *et al.* recently described monodentate phosphoramidite **30** or bidentate phosphine-phosphoramidite **31** ligands with two appended pyridyl units at the *ortho* position of the axially chiral octahydro-[1,1'-binaphthalene]-2,2'-diol-derived group. The nitrogen atoms of the pyridyl units exclusively bind Ru(II) or Zn(II) structural metals from porphyrin **32** or salphen[71] moieties **33**, whereas phosphorus atoms preferably bind to Rh(I) centers (Figure 8) and which will only be utilized for catalysis. For example, the coordination behavior of monodentate phosphoramidite ligand **30** is affected by the presence or absence of Zn(II) porphyrin **32a**. High pressure (HP-NMR) complexation studies of ligand and rhodium precursor under CO/H_2 pressure and in the absence or presence of Zn(II) porphyrin **32a** show that one major rhodium complex is formed in which the hydrido ligand occupies an axial position and the phosphorus binding group is located *cis* to it (Scheme 6). Addition of two equivalents of Zn(II) porphyrin **32a** induces a change of the coordination geometry, in which the hydrido ligand still occupies an apical position, but with the phosphorus group now coordinated *trans* to it. As a consequence of the supramolecularly induced change in the coordination mode of the different ligands at the rhodium center and the

[71] Salphen-type compounds **34** are Schiff bases that can act as *N*,*N*',*O*,*O*'-tetradentate ligands and derive from *o*-phenylenediamine and 2-hydroxybenzaldehyde. The name salphen **34** is a contraction for bis(**sal**icylaldehyde)-*o*-**phen**ylenediamine.

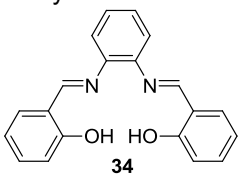

34

increased steric bulk in the active metal surroundings, the catalytic properties of **30** in the asymmetric hydroformylation of *trans*-2-octene (*trans*-**35**) are improved (see Scheme 6).[72]

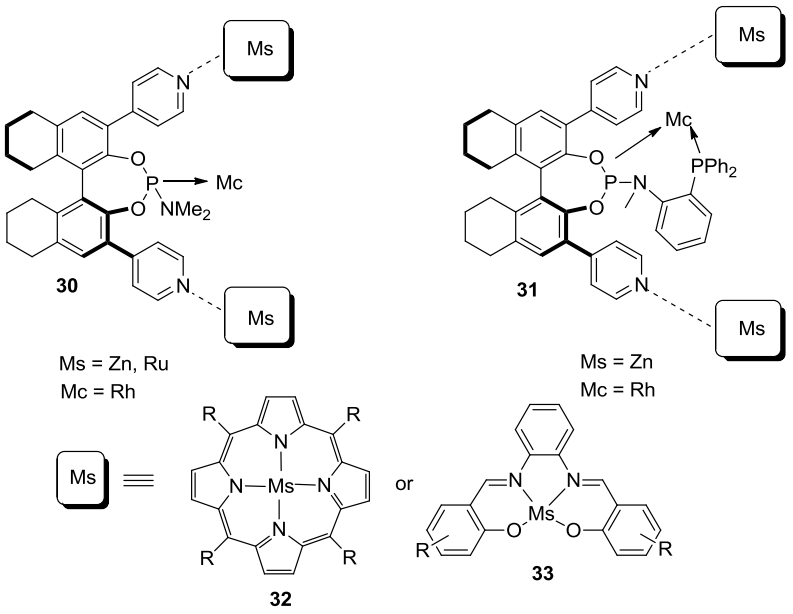

Figure 8. Schematic representation of Reek's monophosphoramidite ligand **30** and phosphine-phosphoramidite **31** with supramolecular regulation

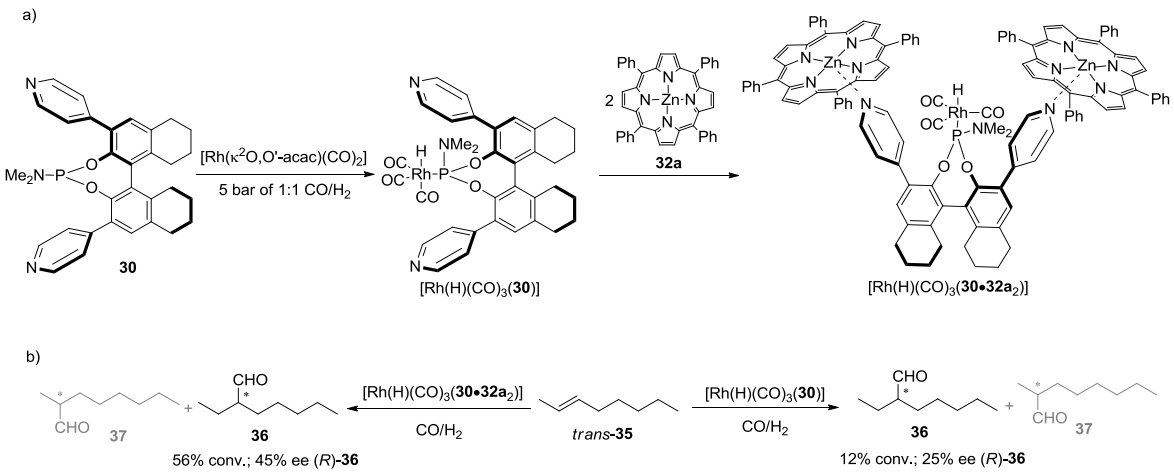

Scheme 6. a) Supramolecular control of monodentate ligand **30** coordination to Rh and b) Implications in asymmetric hydroformylation of *trans*-**35**

Encouraged by the previous results with monodentate ligand **30**, Reek *et al.* applied the same supramolecular strategy with bidentate ligand **31** (Figure 8).

[72] Bellini, R.; Chikkali, S. H.; Berthon-Gelloz, G.; Reek, J. N. H. *Angew. Chem., Int. Ed.* **2011**, *50*, 7342.

Key catalytic properties such as activity and selectivity in the Rh-mediated asymmetric hydroformylation[73] of styrene **6a** and *para*-substituted styrene derivatives **38** (Scheme 7) and asymmetric hydrogenation[74] of dimethyl itaconate **39a**, α-dehydroamino acid ester derivatives **39b–d** and Roche ester derivative **40** were tailored by binding different Zn(II) or Ru(II)-containing regulators differing in their steric and electronic properties to the chiral ligand **31** (Scheme 8). Some representative results are summarized in Table 2 and Table 3.

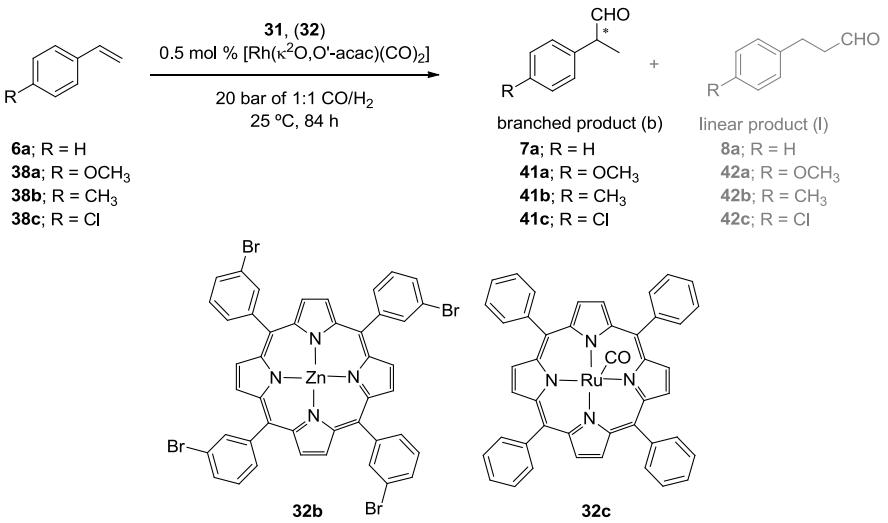

Scheme 7. Asymmetric hydroformylation of styrene **6a** and *para*-substituted styrene derivatives **38** with ligand **31** and binders **32**

[73] Bellini, R.; Reek, J. N. H. *Chem. Eur. J.* **2012**, *18*, 13510.
[74] Bellini, R.; Reek, J. N. H. *Eur. J. Inorg. Chem.* **2012**, *2012*, 4684.

Table 2. Representative results for the asymmetric hydroformylation of styrene **6a** and derivatives **38** with Rh(I) catalysts derived from ligand **31** and different binders **32**

Substrate	Binder	Conv.	b/l[75]	ee
6a	**-**	5%	95:5	51% (*S*)
6a	**32a**	52%	91:9	59% (*S*)
6a	**32b**	10%	97:3	64% (*S*)
6a	**32c**	9%	99:1	**72% (*S*)**
38a	**-**	21%	91:9	18% (*S*)
38a	**32c**	10%	90:10	**82% (*S*)**
38b	**-**	22%	92:8	15% (*S*)
38b	**32c**	16%	95:5	**80% (*S*)**
38c	**-**	18%	99:1	13% (*S*)
38c	**32c**	12%	99:1	**66% (*S*)**

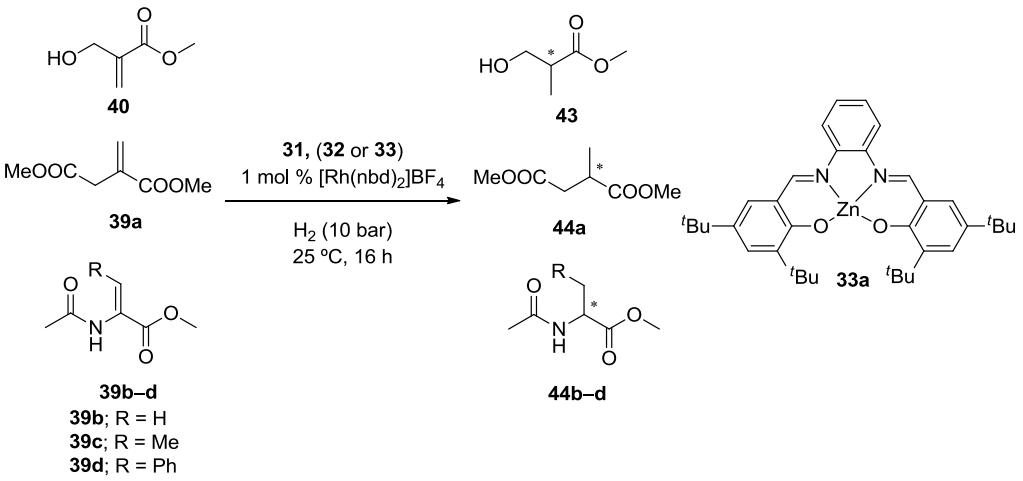

Scheme 8. Rh-mediated asymmetric hydrogenation of diverse alkenes with ligand **31** and different binders (**32** and **33**)

[75] Branched-to-linear product ratio in the hydroformylation reaction.

Table 3. Representative results for the asymmetric hydrogenation of diverse alkenes with Rh(I) catalysts derived from ligand **31** and different binders (**32** and **33a**)

Substrate	Binder	Conv.	ee
39a	**-**	2%	0
39a	**32a**	5%	57% (*R*)
39a	**33a**	> 99%	> 99% (*R*)
39a	**32c**	> 99%	> 99% (*R*)
40	**-**	0	-
40	**32a**	59%	39% (*S*)
40	**33a**	> 99%	55% (*S*)
40	**32c**	> 99%	57% (*S*)
39b	**-**	4%	0
39b	**33a**	> 99%	98% (*R*)
39c	**-**	0	-
39c	**33a**	> 99%	> 99% (*R*)
39d	**-**	3%	0
39d	**33a**	70%	91% (*R*)

All of these examples show that the objective of regulating the activity of an enantioselective catalyst by interaction of an effector, which interacts *via* supramolecular forces with a regulation site already present in the original catalyst, is indeed achievable. The presented examples represent pioneering work and show the potential of the supramolecular approach to generate efficient catalysts for different asymmetric reactions and substrate families. Therefore, the potential of this approach is still both promising and innovative.

In his PhD Thesis,[76] Dr. Héctor Fernández-Pérez envisaged using predictable, structurally well-defined binding interactions to generate supramolecular catalysts with a distal regulation mechanism. Dr. Fernández-Pérez designed a distal regulable ligand **45b**, which incorporates a conformationally stable biaryl bisphosphine as the active catalytic site and a crown ether unit as the remote regulation site. Changes in the biaryl dihedral angle were considered to be the linking mechanism capable of communicating

[76] H. Fernández-Pérez, PhD Thesis, Universitat Rovira i Virgili, September 2009.

the regulation and catalytic sites. Thus, modulation of the catalytic activity of our proposed ligands *via* regulation effects (alkali metal or ammonium-type cations) that bind *via* ion-dipole interactions to the crown ether moiety rigidifying the structure, modifying the dihedral angle (θ) and ultimately causing a change in the bite angle (β) of the phosphorus groups to the metal center seemed to us feasible (Figure 9).

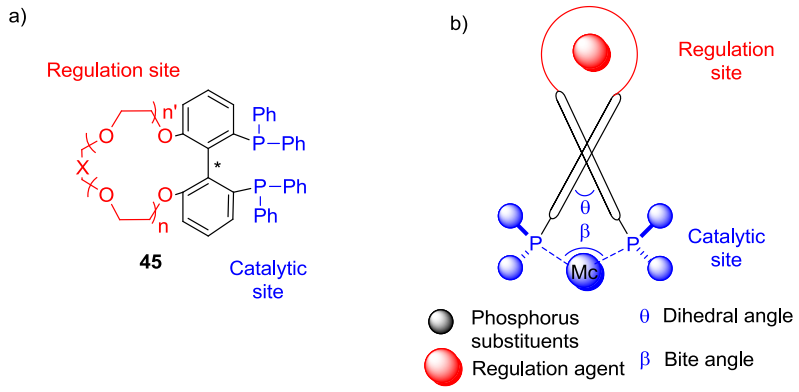

Figure 9. a) Designed system with potential distal modulation for enantioselective catalysis b) Schematic drawing of the regulation strategy

In the aforementioned PhD Thesis, only the synthesis of compounds **45b** with a potential regulation mechanism for catalysis was described.[76] These compounds were prepared in both enantiomeric forms, although low amounts of material were obtained (Figure 10).

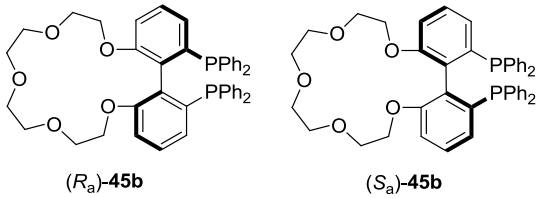

Figure 10. Designed systems with potential distal modulation for enantioselective catalysis

In the present PhD Thesis, we also aim to develop another strategy to generate a set of supramolecular ligands which resemble a privileged structure, yet at the same time offer a range of closely geometrically related active sites. The main advantage of this approach rests on the ability to modify the geometry of the catalytic site through reversible interactions. This strategy should allow for rapid generation of ligand libraries, in which the ligands preserve most of the

structural generalities of their predecessors, but they incorporate "subtle" changes in their three-dimensional structure that might improve the catalytic properties of the resulting supramolecular structures. We aim to develop conformationally transformable bisphosphites **46** as ligands for asymmetric catalysis. Together with the bisphosphite binding groups for organometallic asymmetric catalysis, our design incorporates a polyether unit as the distal regulation site. It is envisaged that the binding of cationic species (regulation agents) within the polyether moieties by ion-dipole interactions would not only serve to bring the two terminal phosphorus ligating groups close together (*template effect*), but also to confer a particular geometry to the catalytic site associated to the shape and size of the regulation agent (*adaptive effect of the catalyst*). Geometric changes around the metal center should result in modified catalytic properties and constitute the basis of our regulation mechanism. The concept is shown in Scheme 9.

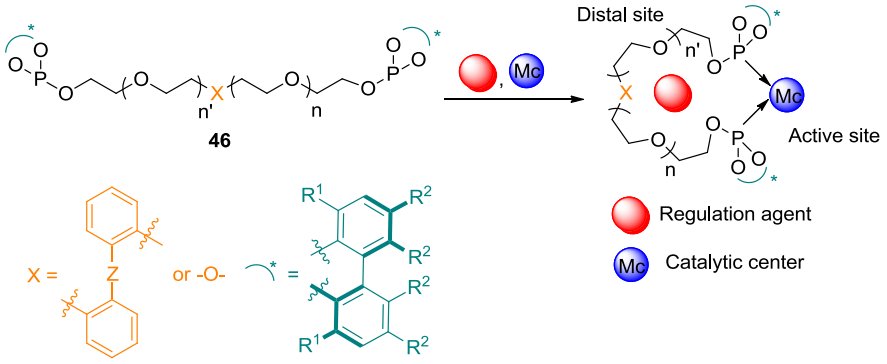

Scheme 9. Strategy for distal modulation of open crown ether bisphosphite ligands **46**

Consequently, the aims of this work are as follows:

1. A preparation method for an array of enantiomerically pure biaryl bisphosphine ligands **45** with a distal regulation site (in the form of crown ether groups of different size and topology) will be devised and developed. The binding properties of these biaryl derivatives with structurally diverse cationic species using different spectroscopic techniques will be studied. The catalytic properties of these ligands in transformations of interest (*i.e.* enantioselective hydrogenation) and the efficiency of the regulation mechanism (binding inside the

polyether moiety) between the distal regulation and catalytic sites will also be assessed.

2. Enantiomerically pure bisphosphite ligands **46** with structurally diverse polyether chains will be synthesized. Binding studies with structurally diverse cationic species and catalytic studies in asymmetric transformations of interest (*i.e.* enantioselective hydrogenation and hydroformylation) will be carried out. Our aim is also to study the potential of different binding agents as regulators of the catalyst structure and, therefore, activity and (stereo)selectivity.

CHAPTER 1: DEVELOPMENT OF BISPHOSPHINE LIGANDS WITH A DISTAL REGULATION SITE IN THE FORM OF CROWN ETHER GROUPS OF DIFFERENT SIZE AND TOPOLOGY

LITERATURE REVIEW

CHAPTER 1: DEVELOPMENT OF BISPHOSPHINE LIGANDS WITH A DISTAL REGULATION SITE IN THE FORM OF CROWN ETHER GROUPS OF DIFFERENT SIZE AND TOPOLOGY

1.1 LITERATURE REVIEW

1.1.1 Artificial receptors with distal modulation

Allosteric modulation is a quite common feature in nature and has allowed for the regulation of the structure and activity of enzymes in many biological systems. As relevant and well-studied processes, the regulation of oxygen binding by haemoglobin,[77] the hexamerization of an arginine repressor,[78] and the change in the binding cooperativity as a function of the concentration of arachidonate-containing phospholipids in cytosolic phospholipase A2[79] deserve mention. Allosteric regulation is also present in the exquisite control observed in many enzymatic processes.[80] The term allosterism entails the change of the binding or catalytic properties of the biologically active site by the interaction of an external unit (effector) within a specific regulatory site in the biological system (allosteric site, Scheme 10). This effector can enhance (positive allostery) or decrease the functional properties of the biological system (negative allostery).

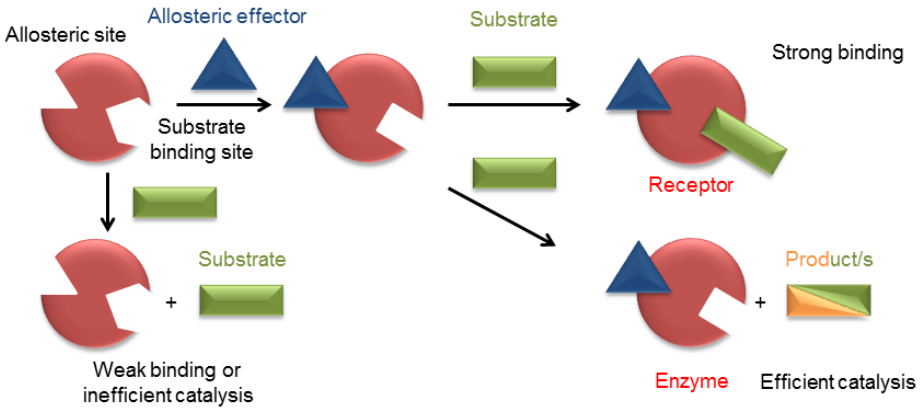

Scheme 10. Activation of substrate binding or catalyst activity by an allosteric effector in the case of receptors or biocatalysts, respectively

[77] a) Perutz, M. F.; Fermi, G.; Luisi, B.; Shaanan, B.; Liddington, R. C. *Acc. Chem. Res.* **1987**, *20*, 309. b) Perutz, M. F. *Annu. Rev. Biochem.* **1979**, *48*, 327. c) Monod, J.; Changeux, J.-P.; Jacob, F. *J. Mol. Biol.* **1963**, *6*, 306.
[78] Grandori, R.; Lavoie, T. A.; Pflumm, M.; Tian, G. L.; Niersbach, H.; Maas, W. K.; Fairman, R.; Carey, J. *J. Mol. Biol.* **1995**, *254*, 150.
[79] Burke, J. R.; Witmer, M. R.; Tredup, J.; Micanovic, R.; Gregor, K. R.; Lahiri, J.; Tramposch, K. M.; Villafranca, J. J. *Biochemistry* **1995**, *34*, 15165.
[80] Stryer, L. *Biochemistry*; Freeman: New York, 1995.

The design of artificial allosteric receptors is of great significance for controlling molecular function by external stimuli. Pioneering contributions by Rebek based on the binding ability and predictable flexibility of bipyridine system **47** can be considered as a first step towards allosteric receptors or catalysts.[81] Initial studies focused on the binding of a transition metal cation to the bipyridine group in **47** and the influence of binding on the racemization barrier of the biarylic molecule **47** depicted in Scheme 11.[82]

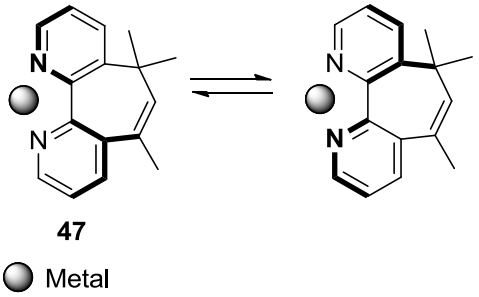

Scheme 11. Enhanced bipyridine racemization by metal chelation developed by Rebek *et al.*

Table 4. Activation energies for the racemization of **47**

Metal	$\Delta G_c^{\neq}$ (Kcal/mol)[a]
None	14.5
$HgCl_2$	10.5
$ZnCl_2$	10.5

[a] Calculated from NMR spectra at coalescence temperatures.

The results in Table 4 show that chelation to metals reduces the barrier of racemization by about 4 Kcal/mol. The enhancement in the racemization rate is probably due to the fact that both aromatic rings are brought close to planarity upon metal binding, which stabilizes the transition state to racemization.

Rebek exploited a similar molecular design in the catalysis of chemical reactions. For example, the cyclization of the bipyridine derivative **48** depicted in Scheme 12 needs the addition of $NiCl_2$ to proceed at low temperatures (45 ºC).

[81] See: Rebek, J., Jr. *Acc. Chem. Res.* **1984**, *17*, 258.
[82] Rebek, J.; Trend, J. E. *J. Am. Chem. Soc.* **1978**, *100*, 4315.

The metal coordination to the N atoms brings the two reactive sites in close proximity by forcing, again, a planar conformation with an overall enhancement of the rate of the intramolecular reaction.[83]

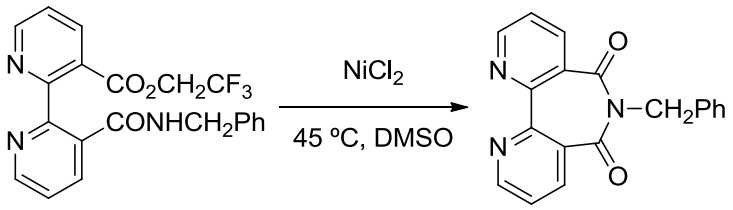

48 **49**

Scheme 12. Cyclization reaction enhanced by the addition of a coordinating Ni(II) precursor

These pioneering contributions by Rebek and co-workers were accompanied by the description of the first allosteric receptor based on the same 2,2'-bipyridine chelation motif.[84] The crown ether containing a 3,3'-disubstituted 2,2'-bipyridine unit (**50** in Figure 11) showed negative cooperative binding of alkali metal ions, which have a strong affinity for the N atoms, in the presence of crown ether binders such as Hg^{2+}, Zn^{2+} or Pd^{2+} cations or $W(CO)_4$.[84b,c] On the contrary, Hg^{2+}-binding to the crown ether unit induced a positive cooperative effect on the binding of Pd^{2+} to the bipyridine group.[84a]

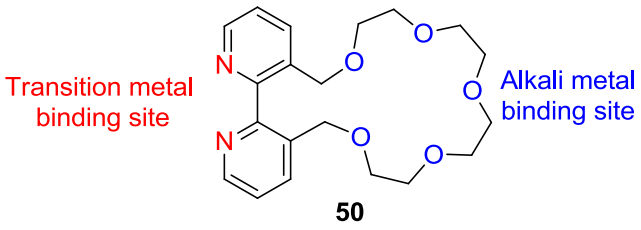

50

Figure 11. Rebek's allosteric supramolecular receptor

In parallel with the development of supramolecular host-guest chemistry, other systems have been designed and studied to control catalysis and binding by combining allosteric sites and effectors of a diverse nature.[85] Since the

[83] Rebek, J., Jr.; Costello, T.; Wattley, R. *J. Am. Chem. Soc.* **1985**, *107*, 7487.
[84] a) Rebek, J.; Marshall, L. *J. Am. Chem. Soc.* **1983**, *105*, 6668. b) Rebek, J.; Wattley, R. V. *J. Am. Chem. Soc.* **1980**, *102*, 4853. c) Rebek, J., Jr.; Trend, J. E.; Wattley, R. V.; Chakravorti, S. *J. Am. Chem. Soc.* **1979**, *101*, 4333.
[85] Reviews on allosteric receptors: a) Kremer, C.; Luetzen, A. *Chem. Eur. J.* **2013**, *19*, 6162. b) Kubo, Y.; Ishii, Y. *J. Nanosci. Nanotechnol.* **2006**, *6*, 1489. c) Takeuchi, M.; Ikeda, M.; Sugasaki, A.; Shinkai, S. *Acc. Chem. Res.* **2001**, *34*, 865. d) Nabeshima, T. *Coord. Chem. Rev.*

quantity and diversity of allosteric systems described in the literature is vast, they have been classified into four main groups: Heterotropic or homotropic[86] and subsequently divided into positive or negative allosteric systems. In artificial systems, homotropic allosterism is more difficult to reproduce, and examples are accordingly rare. Nevertheless, the first example can be traced to the early 1980s, when Rebek and co-workers studied a bis(crown ether) system that exhibited negative cooperative binding of alkali metal ions.[87] In homotropic systems, the initial binding of guest species to the allosteric receptor must produce a conformational change that makes the other binding site(s) more or less suitable for the same guest (positive and negative homotropic allosterism, respectively). On the other hand, in the case of a heterotropic allosteric system, the binding of the effector at the allosteric site produces a conformational change that affects the binding event of the binding guest at a remote site. Positive heterotropic allosterism indicates that a conformational change induced by the effector makes the second binding event tighter. Conversely, negative heterotropic allosterism indicates that the second binding event is made less favorable.

1.1.1.1 Crown ether-based receptors with distal modulation for neutral molecules

A wide variety of receptors for neutral molecules (aromatic derivatives, nucleic bases, sugars, ureas, etc.) incorporating an appended crown ether unit as the allosteric site have been reported. With the possibility to easily vary the crown ether size, shape, and topology together with well-established synthetic strategies for their preparation, they have become popular artificial allosteric sites. In addition, the relatively large amount of energy that is gained in the cation binding process easily overcomes energetic differences between different conformations of the allosteric receptors.[85a]

1996, *148*, 151. Review on allosteric receptors and catalysts: e) Kovbasyuk, L.; Kraemer, R. *Chem. Rev.* **2004**, *104*, 3161. Reviews on allosteric catalysts: f) Kumagai, N.; Shibasaki, M. *Catal. Sci. Technol.* **2013**, *3*, 41. g) Zhu, L.; Anslyn, E. V. *Angew. Chem., Int. Ed.* **2006**, *45*, 1190.

[86] Heterotropic or homotropic allosterism indicates that the binding of a molecule to the receptor influences the interaction of this receptor with a different or the same molecule, respectively.

[87] Rebek, J.; Costello, T.; Marshall, L.; Wattley, R.; Gadwood, R. C.; Onan, K. *J. Am. Chem. Soc.* **1985**, *107*, 7481.

The first example of a receptor for the recognition of neutral molecules with allosteric modulation was presented by Dervan *et al.* in 1987. They designed an allosterically regulable DNA-binder **51** that contained two netropsin[88] units separated by a tetraethylene glycol tether, which acts as a multidentate acyclic neutral ligand for cations (Figure 12). The binding of alkaline earth metal cations to the polyether unit caused a conformational change that favored the binding in water of both netropsin units to the double-stranded DNA molecule.[89]

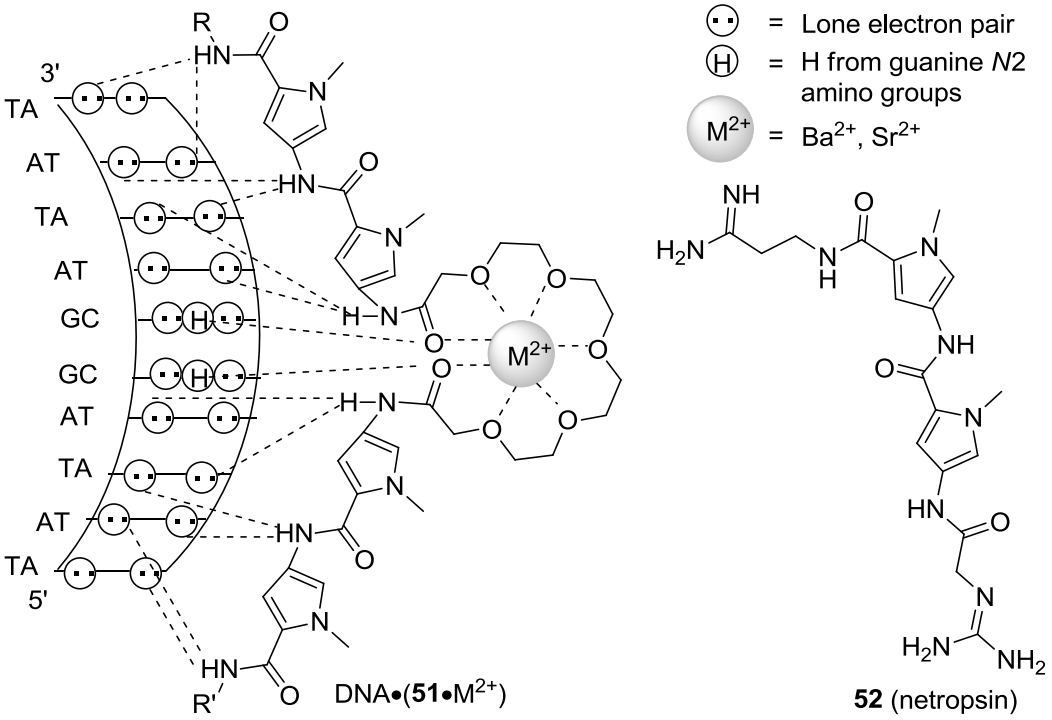

Figure 12. Heterotropic allosterically regulated binding of bis(netropsin) **51** to DNA by alkaline earth metal cations. Anti-infective drug netropsin **52**

Another receptor with a polyether chain as allosteric site for the recognition of nucleotide bases was reported in 1993 by Inouye and co-workers.[90] In this case, binding of 1-^{n}Bu-thymine to receptor **53** by hydrogen bonding was enhanced by a factor of 4 – 6 after sodium cation binding to the oxygen atoms of **53** (Figure 13). This increase of the binding constant was governed by π-stacking interactions of the closer anthracene unit to the substrate and coulombic interactions of the complexed cations.

[88] Netropsin **52** is an oligopeptide with antibiotic and antiviral activity. See: Barrett, M. P.; Gemmell, C. G.; Suckling, C. J. *Pharmacol. Ther.* **2013**, *139*, 12.
[89] Griffin, J. H.; Dervan, P. B. *J. Am. Chem. Soc.* **1987**, *109*, 6840.
[90] Inouye, M.; Konishi, T.; Isagawa, K. *J. Am. Chem. Soc.* **1993**, *115*, 8091.

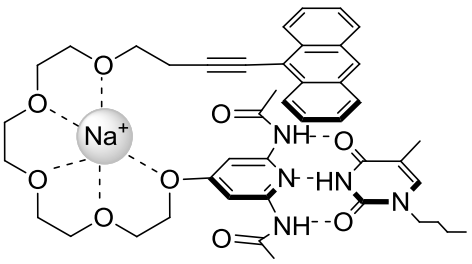

53•Na^+•1-^{n}Bu-thymine

Figure 13. Positive heterotropic allosteric receptor **53** for 1-^{n}Bu-thymine

Remarkable contributions were made by Shinkai et *al.* in the 1990s, when they presented a number of allosteric receptors for the recognition of carbohydrates that bind mono- or dissacharides by formation of boronic acid esters. Some examples of Shinkai's receptors using crown ethers as allosteric sites are briefly summarized in Figure 14. The affinity of receptor **54**[91] with D-glucose, D-talose and D-allose before and after addition of allosteric effectors was monitored by Circular Dichroism (CD) spectroscopy analysis. Binding constants diminished from 3.1 x 10^4 to 2.5 x 10^4, 1.4 x 10^4 to 8.4 x 10^3 and 1.2 x 10^3 to 3 x 10^2 M^{-1} respectively after addition of Ca^{2+} as allosteric effector. Presumably, the conformational changes induced by binding of the calcium ion to the crown ether chain forces the boronic acids into an orientation which is less favorable for 1:1 binding with monosaccharides.

Receptors **55**[92] and **56**[93] were found as relatively complicated mixtures of conformers in the absence of a cation (effector) and a substrate (monosaccharides). In both cases, the binding of alkali metal ions induced conformational changes to the receptors that favored or disfavored the binding ability towards monosaccharides depending on the cation employed. Potassium ions, for example, were found to act as negative effectors for both receptors, whereas sodium and lithium cations enhanced the binding ability of the receptors **55** and **56** towards monosaccharides, respectively.

[91] Deng, G.; James, T. D.; Shinkai, S. *J. Am. Chem. Soc.* **1994**, *116*, 4567.
[92] Ohseto, F.; Yamamoto, H.; Matsumoto, H.; Shinkai, S. *Tetrahedron Lett.* **1995**, *36*, 6911.
[93] James, T. D.; Shinkai, S. *J. Chem. Soc., Chem. Commun.* **1995**, 1483.

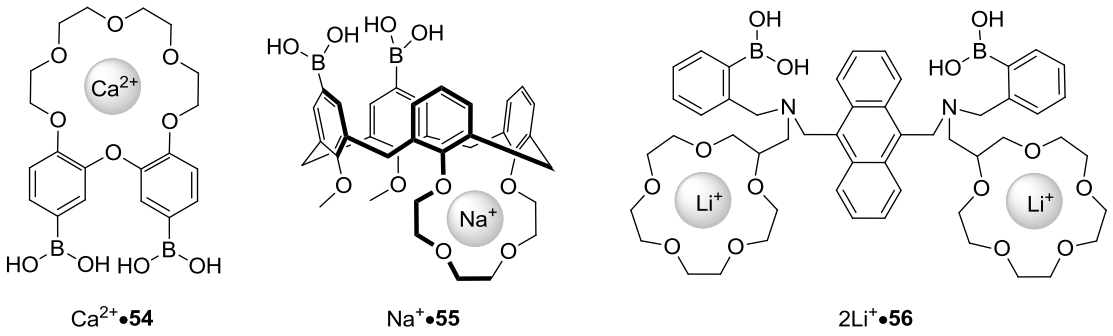

Ca^{2+}•**54** Na^{+}•**55** $2Li^{+}$•**56**

Figure 14. Shinkai's allosteric boronic acid-based receptors for monosaccharides

An example from the work of Fukazawa *et al.* is depicted in Figure 15. Their monodeoxycalix[4]arene crown ether **57** exhibited affinity towards urea-type molecules *via* hydrogen bonding involving the carboxylic acid units. Sodium and potassium cations increased the binding constants of **57** towards the urea substrates. These positive allosteric effects were explained by molecular mechanics calculations. In the presence of an appropriate cation, the crown ether moiety changes its conformation to fit the cation into the cavity. As a result of this conformational change, the intramolecular hydrogen bonding between the two dicarboxylic acids is disrupted and the two arms of the receptor equipped with a carboxylic acid group are then available for a four-point hydrogen bonding interaction with the urea guest molecule.[94]

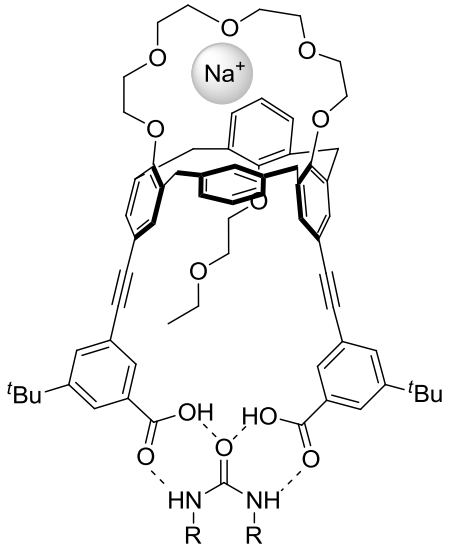

Na^{+}•**57**•urea

Figure 15. Complex between receptor **57**, Na^{+} ion and ureas

[94] Haino, T.; Katsutani, Y.; Akii, H.; Fukazawa, Y. *Tetrahedron Lett.* **1998**, *39*, 8133.

Notably, Kubo and co-workers described one of the first heterotropic allosteric receptors for neutral molecules with negative cooperative binding. Receptor **58** binds diamine substrate **59** with a binding constant of 7.9 x 10^5 M^{-1}. Binding of a Ba^{2+} ion into the crown ether increases the distance of the Zn(II) ions through the rotation of the biphenyl units and, hence, the receptor binding affinity towards substrate **59** decreases (Figure 16).[95]

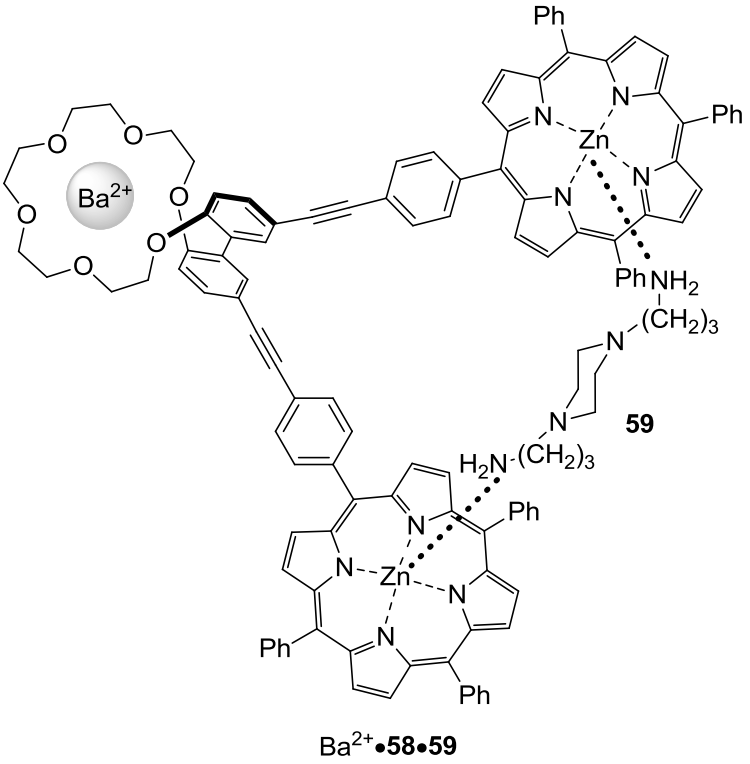

Ba^{2+}•**58**•**59**

Figure 16. Complex of Kubo's heterotropic allosteric receptor **58**, Ba^{2+} ion, and diamine substrate **59**

More recently, Liu and co-workers reported on a positively cooperative bis(β-cyclodextrin) crown ether receptor **60** for dye molecules such as **61**. Allosteric regulation is produced by sodium ion binding to the crown ether unit that induces a change in the conformation of the receptor that improves the cooperative binding of both cyclodextrin arms towards the guest dye molecule.[96]

[95] Kubo, Y.; Murai, Y.; Yamanaka, J.-i.; Tokita, S.; Ishimaru, Y. *Tetrahedron Lett.* **1999**, *40*, 6019.
[96] Liu, Y.; Yang, Y.-W.; Li, L.; Chen, Y. *Org. Biomol. Chem.* **2004**, *2*, 1542.

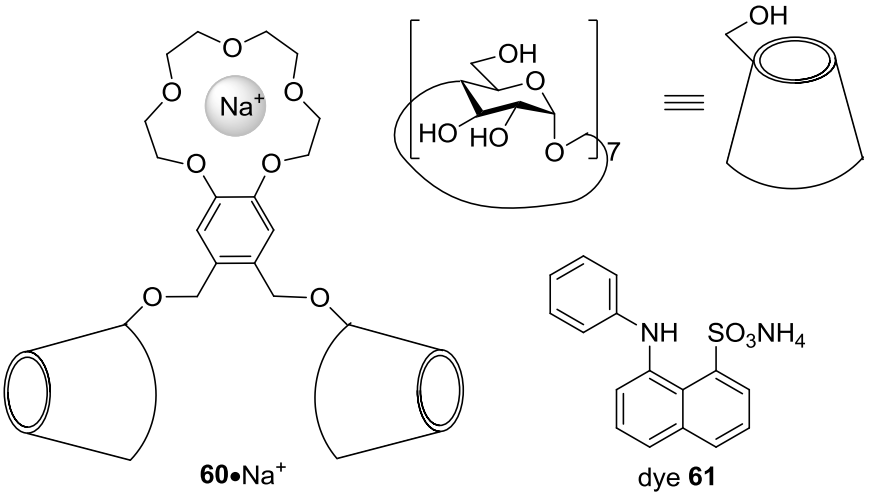

Figure 17. Liu's crown ether bridged bis(β-cyclodextrin) receptor **60** bound to Na^+ ion and substrate dye **61**

1.1.2 Mimicking biological regulation of catalysis *via* distal modulation

In catalysis, three different parts are required for a successful system involving a regulation mechanism: an active or catalytic site, a remote or regulation site, and finally, a mechanical mechanism linking these sites that provokes conformation changes in the catalytic site. Therefore, we envisaged using predictable, structurally well-defined binding interactions to assemble supramolecular catalysts with a plausible regulation mechanism. Our distal modulated systems **45** are enantiomerically pure biaryl derivatives containing crown ether groups of different size and topology as the regulation site. Far from the remote site, a bisphosphine moiety is located that acts as the active site after coordination to transition metals. The biaryl unit also belongs to the crown ether moiety which is expected to behave as the regulation site. Finally, binding of cationic species to the crown ethers *via* ion-dipole or hydrogen bonding interactions would not only rigidify the catalyst structure but also induce conformational changes that modify the biaryl dihedral angle.

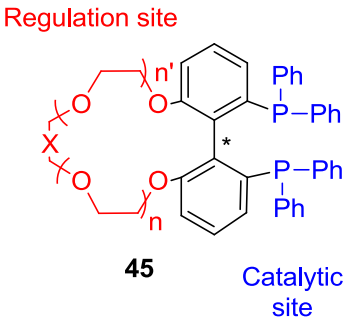

45

Figure 18. General structure of bisphosphine ligands **45** with a regulation mechanism

Extensive studies have demonstrated that changing the bite angle of chelating bisphosphines leads to dramatic changes in the activity and/or enantioselectivity of the derived catalysts.[97] A complete summary of all known biaryl derivatives, and the effect of the dihedral angle change in asymmetric catalysis would be beyond the scope of this section. However, representative examples can be extracted from the literature. For instance, Saito *et al.* studied the relationship between the dihedral angle of known bisphosphine ligands (*i.e.*

[97] Shimizu, H.; Nagasaki, I.; Saito, T. *Tetrahedron* **2005**, *61*, 5405.

(R_a)-BINAP (R_a)-**5**, (R_a)-BIPHEMP (R_a)-**62**, (R_a)-MeO-BIPHEP (R_a)-**63a** and its narrower dihedral angle analogue named (R_a)-SEGPHOS (R_a)-**64**) and the catalytic activity of the derived ruthenium catalysts in the asymmetric hydrogenation of 1-hydroxypropan-2-one **65** to yield chiral propane-1,2-diol **66** (Scheme 13).

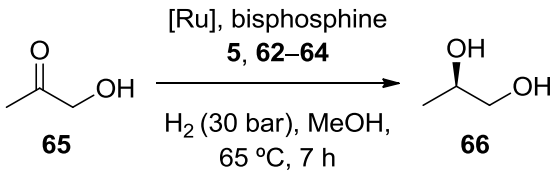

Scheme 13. Ru(II)-mediated asymmetric hydrogenation of substrate **65**

Highest enantioselectivities were obtained with (R_a)-SEGPHOS (R_a)-**64** ligand demonstrating the importance of the dihedral angle in asymmetric catalysis (see Table 5).[98]

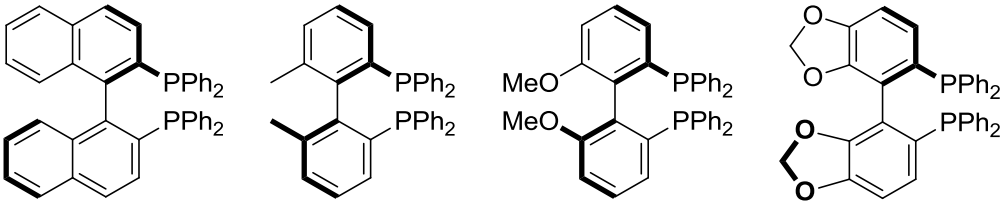

(R_a)-**5** (R_a)-**62** (R_a)-**63a** (R_a)-**64**

Table 5. Correlation between dihedral angles in the Ru-complexes and enantioselectivity in Ru-mediated asymmetric hydrogenation of **65**

Ligand	BINAP **5**	BIPHEMP **62**	MeO-BIPHEP **63a**	SEGPHOS **64**
Dihedral angle θ (deg)[a]	73.5	72.1	68.6	65.0
ee (%)	89	93	96	99

[a] As estimated by CAChe[99] MM2 calculations.

[98] Saito, T.; Yokozawa, T.; Ishizaki, T.; Moroi, T.; Sayo, N.; Miura, T.; Kumobayashi, H. *Adv. Synth. Catal.* **2001**, *343*, 264.
[99] **C**omputer-**A**ided **Che**mistry; molecular modeling software package by Fujitsu Limited.

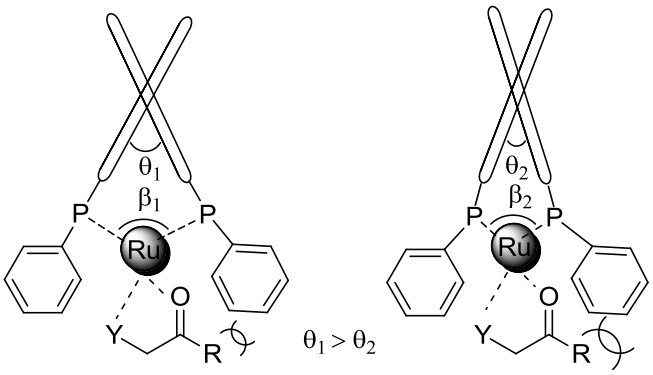

Figure 19. Altering the sterics of the phosphine groups by modifying the dihedral θ and the bite angle β

Nevertheless, strategies to modify the dihedral angle in biaryl derivatives without altering the nature of the biaryl group, such as those developed by Saito *et al.* that have been already summarized,[98] would be more attractive and are similar to the intended regulation mechanism in this Thesis.

Relevant examples can be found in the literature where very subtle changes in the skeleton of the biaryl ligand have a deep impact in the dihedral angle without affecting the nature of the ligand. For example, Zhang *et al.* suggested that although ligands **5**, **62** or **63a** had proved to be effective in asymmetric catalysis, they were not rigid enough for some substrates such as γ-aryl-β-ketoesters.[100] Thus, they prepared a series of bridged ligands with different alkylic linkers named C_n-TunaPHOS **67a–f** (Table 6). These ligands are more rigid than the analogous ligand **63a** and exhibit different dihedral angles. The authors demonstrated the importance of this structural parameter in the enantioselective hydrogenation of different substrates. The best ligand, in terms of enantioselectivity, for β-ketoesters was C_4-TunaPHOS,[100] C_1- and C_2-TunaPHOS for enol acetates,[101] C_3-TunaPHOS for α-phthalimide ketones,[102] and C_2–C_5-TunaPHOS for β-acylaminoacrylates.[103]

[100] Zhang, Z. G.; Qian, H.; Longmire, J.; Zhang, X. M. *J. Org. Chem.* **2000**, *65*, 6223.
[101] Wu, S.; Wang, W.; Tang, W.; Lin, M.; Zhang, X. *Org. Lett.* **2002**, *4*, 4495.
[102] Lei, A.; Wu, S.; He, M.; Zhang, X. *J. Am. Chem. Soc.* **2004**, *126*, 1626.
[103] Tang, W.; Wu, S.; Zhang, X. *J. Am. Chem. Soc.* **2003**, *125*, 9570.

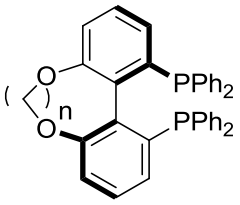

67a–f

67a n = 1, C_1-TunaPHOS
67b n = 2, C_2-TunaPHOS
67c n = 3, C_3-TunaPHOS
67d n = 4, C_4-TunaPHOS
67e n = 5, C_5-TunaPHOS
67f n = 6, C_6-TunaPHOS

Table 6. Calculated dihedral angles of ligands C_n-TunaPHOS **67a–f**

Ligand	**67a**	**67b**	**67c**	**67d**	**67e**	**67f**
Dihedral angle θ (deg)[a]	60	74	77	88	94	106

[a] As estimated by CAChe MM2 calculations.

Chan *et al.* designed a series of chiral bisphosphine ligands named PQ-Phos **68** that were prepared by atropdiastereoselective Ullmann coupling and ring-closure reactions.[104] The Ullmann coupling reaction of the biarylbisphosphine dioxides was selected for a highly efficient central-to-axial chirality transfer method resulting in enantiomerically pure bisphosphines of different dihedral angles **68a–c** without having to perform the traditional optical resolution of the racemic bisphosphine dioxides. Chan's strategy is depicted in Scheme 14.

[104] a) Qiu, L.; Kwong, F. Y.; Wu, J.; Lam, W. H.; Chan, S.; Yu, W.-Y.; Li, Y.-M.; Guo, R.; Zhou, Z.; Chan, A. S. C. *J. Am. Chem. Soc.* **2006**, *128*, 5955. b) Qiu, L.; Wu, J.; Chan, S.; Au-Yeung, T. T. L.; Ji, J.-X.; Guo, R.; Pai, C.-C.; Zhou, Z.; Li, X.; Fan, Q.-H.; Chan, A. S. C. *Proc. Natl. Acad. Sci. U. S. A.* **2004**, *101*, 5815.

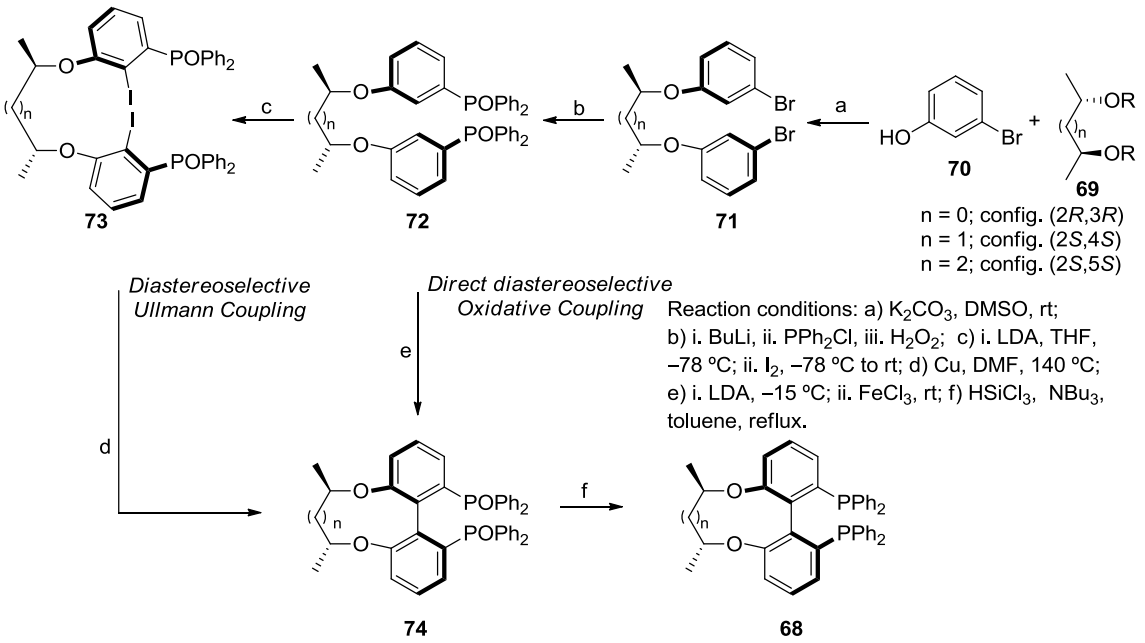

Scheme 14. Synthetic protocols for synthesizing PQ-Phos ligands **68** involving intramolecular diastereoselective biaryl couplings

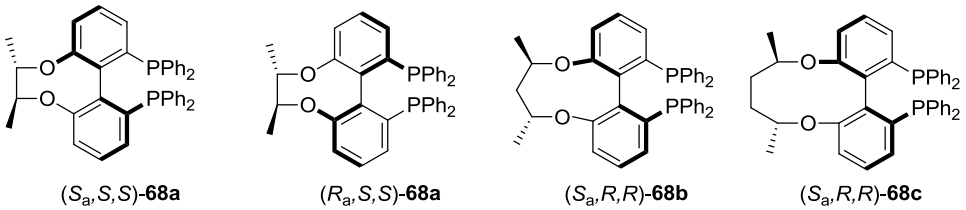

Table 7. Calculated dihedral angles for PQ-PHOS ligands **68a–c**

	(*S*a,*S*,*S*)-**68a**	(*R*a,*S*,*S*)-**68a**	(*S*a,*R*,*R*)-**68b**	(*S*a,*R*,*R*)-**68c**
Dihedral angle θ (deg)[a]	64.8	–66.5	80.0	88.8

[a] Calculated using Chem 3D MM2 modelling.

Thus, optically pure derivatives **71** were prepared by treatment of enantiopure butanediol derivatives **69** with bromophenol **70** (Scheme 14, step a). The bisphosphine oxides **72** were synthesized from **71**, which contains two stereogenic centers in their backbone, by halogen/lithium exchange followed by capture of the dilithium derivative with chlorodiphenylphosphine and, finally, oxidation of the phosphino groups with H_2O_2 (Scheme 14, step b). The diiodo derivatives **73** were easily prepared by direct *ortho*-lithiation of **72** and

subsequent quenching with iodine (Scheme 14, step c). Finally, diastereomerically pure biaryl derivatives **74** were obtained by intramolecular Ullmann coupling of **73** (Scheme 14, step d). Alternatively, bisphosphine oxides **74** were also directly prepared by an asymmetric ring-closure reaction, *via* oxidative intramolecular coupling of **72** (Scheme 14, step e). It should be noted that the stereogenic centers in the bridging chain of **72** provided very high diastereoselectivity in both routes (d.e. > 99% both for the diastereoselective Ullmann and the oxidative couplings), as reflected in the fact that the other possible diastereomers were not detected in either case. Finally, the target bisphosphines **68** were readily obtained by reduction of the P=O bonds with trichlorosilane (Scheme 14, step f).

These ligands were successfully applied to a myriad of asymmetric reactions. The effect of the dihedral angle of the ligands on the efficiency of the catalyst was shown to be very important in the Ir-catalyzed asymmetric hydrogenation of *N*-heteroaromatic compounds. For example, the substrate 2-methyl-quinoxaline **75** was hydrogenated in only 39% ee with ligands (S_a,*S*,*S*)-**68a** and (R_a,*S*,*S*)-**68a** and below 30% ee with MeO-BIPHEP or (S_a,*R*,*R*)-**68c**, whereas (S_a,*R*,*R*)-**68b** raised the enantioselectivity of the process up to a moderate 61% ee.[104]

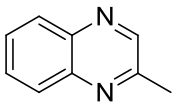

75

Figure 20. *N*-heteroaromatic compound 2-methyl-quinoxaline **75**

The aforementioned strategies to tune the dihedral angle of biaryl bisphosphine ligands rely on structural changes *via* covalent chemistry.

Very relevant studies from Benniston *et al.* have focused on the possibility to control the torsion angle in the biphenyl derivative **76** by the binding of cationic species to an embedded crown ether moiety.[105] In one of the first studies, they described a set of detailed molecular-dynamics simulations on the related crown

[105] a) Benniston, A. C.; Harriman, A.; Li, P. Y.; Patel, P. V.; Sams, C. A. *J. Org. Chem.* **2006**, *71*, 3481. b) Benniston, A. C.; Harriman, A.; Patel, P. V.; Sams, C. A. *Eur. J. Org. Chem.* **2005**, 4680. c) Benniston, A. C.; Li, P.; Sams, C. *Tetrahedron Lett.* **2003**, *44*, 3947.

ether system **76** alone, as well as in the presence of added cations (H^+, Li^+, Na^+, K^+, Rb^+ or NH_4^+). A good correlation between the calculated torsion angles of the biphenyl moiety and the Pauling cation radii was found (Table 8).[105c]

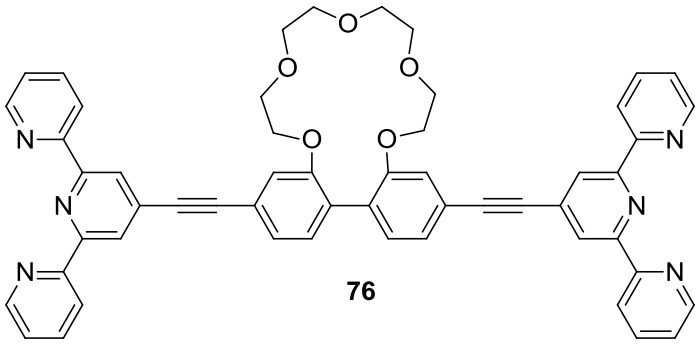

76

Table 8. Dihedral angles in the biphenyl unit of crown ether-containing receptor **76**

Cation	Dihedral angle[a] (deg)	Variation in dihedral angle[b] (deg)	Pauling cation radius (Å)[c]
None	142.6	76.7 – 159	-
H^+	59.9	22.9 – 98.0	-
Li^+	50.9	25.5 – 95.1	0.60
Na^+	61.9	30.8 – 104	0.95
K^+	79.8	34.3 – 156	1.33
Rb^+	83.3	49.5 – 146	1.48
NH_4^+	81.3	39.7 – 142	1.48

[a] Dihedral angle taken from the energy-minimized structure. [b] Taken from molecular dynamics simulations. Molecular dynamics and geometry optimization calculations were carried out using the Discover 3 module available in Insight II running on a Silicon Graphics O2 workstation (see ref. 105c for details). [c] Tabulated Pauling radii are those indicated in ref. 105c.

These studies not only demonstrated that supramolecular interactions are capable of changing the torsion angle of the biphenyl unit in **76**, but also that this structural parameter (torsion angle of the biphenyl unit) can be modulated depending on the size of the cation introduced in the crown ether moiety.

A related system (**77a–c**) was studied by the same research group. In this case, the strength of the binding of cationic species (*i.e.* Li^+, Na^+ and K^+) to crown

ether receptors **77a–c** was determined by fluorescence spectroscopic studies. The geometry for the corresponding 1:1 complexes was theoretically calculated (Table 9).[105b] Again, it was computationally demonstrated that the torsion angle of the 2,2'-biphenyl units with embedded crown ethers **77a–c** can be modulated *via* cation binding at the crown ether moiety. The fluorescence behavior of receptors **77** is consistent with the molecular dynamics simulations performed. The bound cation imposes restrictions on the geometry and forces the rings further from planarity, which results in fluorescence quenching.

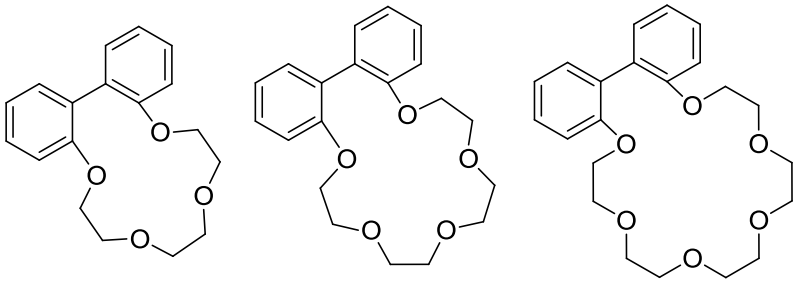

77a **77b** **77c**

Table 9. Cation binding effect on the dihedral angle of the biphenyl unit

	Torsion angle: mean value and range (deg)[a]			
Receptor	None	Li^+	Na^+	K^+
77b	130 (70 – 165)	55 (23 – 99)	65 (30 – 105)	91
77c	120	-	65	70

[a] Taken from molecular dynamics simulations. Computational studies were performed with several different packages. Minimum energy conformations were obtained using the Gaussian03 and Insight II programs. See ref. 105b for details.

It should also be mentioned that similar control of the molecular structure upon cation binding to crown ether or related systems has been reported by other groups.[106] Moreover, this rotation angle mechanism found applicability as allosteric modulator on the binding affinity of a Zn(II) porphyrin dimer receptor towards diamine substrates in the previously mentioned Kubo's system **58** (Figure 16 in Section *1.1.1.1*).[95]

[106] a) Interaction between tetrathiafulvalene units was modulated by binding of Pb^{2+} to a crown ether moiety due to rotation of a biphenyl unit: Delogu, G.; Fabbri, D.; Dettori, M. A.; Sallé, M.; Le Derf, F.; Blesa, M.-J.; Allain, M. *J. Org. Chem.* **2006**, *71*, 9096. b) Fluorescence studies on a Ru(bipyridyl) complex with different cation binding: McFarland, S. A.; Finney, N. S. *Chem. Commun.* **2003**, 388. c) Fluorescence studies on crown ether biphenyl systems after metal binding: McFarland, S. A.; Finney, N. S. *J. Am. Chem. Soc.* **2001**, *123*, 1260. d) Crown ether containing polythiophenes: Marsella, M. J.; Swager, T. M. *J. Am. Chem. Soc.* **1993**, *115*, 12214. e) Chiral biphenyl bis(crown ethers): Lindsten, G.; Wennerstroem, O.; Isaksson, R. *J. Org. Chem.* **1987**, *52*, 547.

RESULTS AND DISCUSSION

1.2 RESULTS AND DISCUSSION

1.2.1 Synthesis of crown ether-containing bisphosphine ligands 45

The synthetic strategy chosen for the preparation of bisphosphines **45** is indicated in Scheme 15. In the first place, the synthetic strategy involves the preparation of the key biaryl derivative (*rac*)-**78**, from 1-bromo-3-methoxybenzene **79** employing well-established and already published synthetic transformations.[107] Secondly, our synthetic strategy involves resolution of the racemic biaryl derivative (*rac*)-**78**[107] and cleavage of the methoxy group into its fenolic analogue.[108]. Finally, cyclization of enantiopure [1,1'-biphenyl]-2,2'-diol **80** with the corresponding polyether derivative and reduction of the P=O bonds in compounds **81** into the corresponding bisphosphines should render the target compounds in enantiomerically pure form.

It should be mentioned that, whilst Dr. Fernández Pérez prepared in his PhD Thesis compound (S_a)- and (R_a)-**45b** in enantiomerically pure form and in milligram amounts following a different synthetic strategy,[109] the preparation of the remaining compounds was tackled for the first time within this present PhD Thesis.

The synthetic strategy for the preparation of (*rac*)-**78** is based on an *ortho*-lithiation/iodination followed by a Ullmann homocoupling process. The route comprises the following key steps: reaction of 1-bromo-3-methoxybenzene **79** to form (2-iodo-3-methoxyphenyl)diphenylphosphine oxide **82** and Ullmann homocoupling to form the desired compound **78** in its racemic form (Scheme 16).

[107] Schmid, R.; Foricher, J.; Cereghetti, M.; Schoenholzer, P. *Helv. Chim. Acta* **1991**, *74*, 370.
[108] Qiu, L. Q.; Qi, J. Y.; Ji, J. X.; Zhou, Z. Y.; Yeung, C. H.; Choi, M. C. K.; Chan, A. S. C. *Acta Crystallogr., Sect. C: Cryst. Struct. Commun.* **2003**, *C59*, o33.
[109] Dr. Fernández Pérez prepared (S_a)- and (R_a)-**45b** using another synthetic strategy which involved an upgrading of the optical purity by semipreparative HPLC chromatography on chiral stationary phases. See: H. Fernández-Pérez, PhD Thesis, Universitat Rovira i Virgili, September 2009.

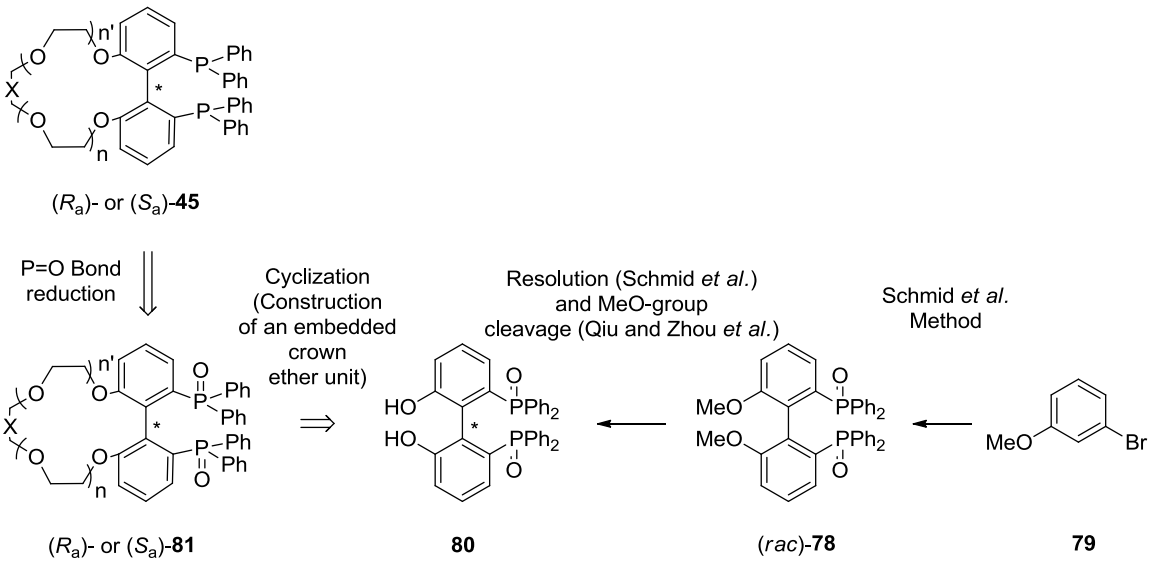

Scheme 15. Retrosynthetic strategy for the synthesis of enantiomerically pure bisphosphines **45**

In general terms, the conditions of the reported method[107] could be reproduced. The first transformations comprised lithiation of **79** followed by the capture of the corresponding organolithium derivative with chlorodiphenylphosphine followed by oxidation of the phosphorus atoms with 30% H_2O_2 in MeOH as solvent to provide the corresponding diarylphosphine oxide **83** in good overall yield (83%). Directed *ortho*-lithiation of **83** with LDA at –78 ºC followed by quenching with iodine provided the iodo derivative **82** in 72% yield. Finally, the racemate of **78** was prepared *via* Ullmann homocoupling of **82** using activated - by I_2 treatment - copper powder in DMF. Compound (*rac*)-**78** was easily purified by precipitation and was obtained in 80% yield.

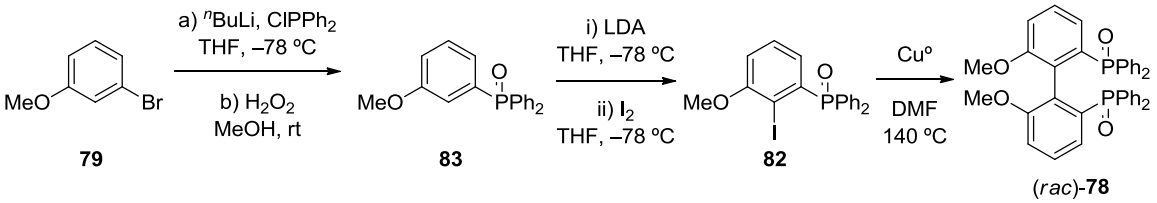

Scheme 16. Synthesis of (*rac*)-**78**

With regard to the next steps in the synthetic sequence indicated in Scheme 15, enantiomerically pure compound was obtained by optical resolution of the racemic intermediate (*rac*)-**78** with (–)- and (+)-DBTA (2,3-O,O'-dibenzoyl tartaric acid) following a reported procedure.[107]

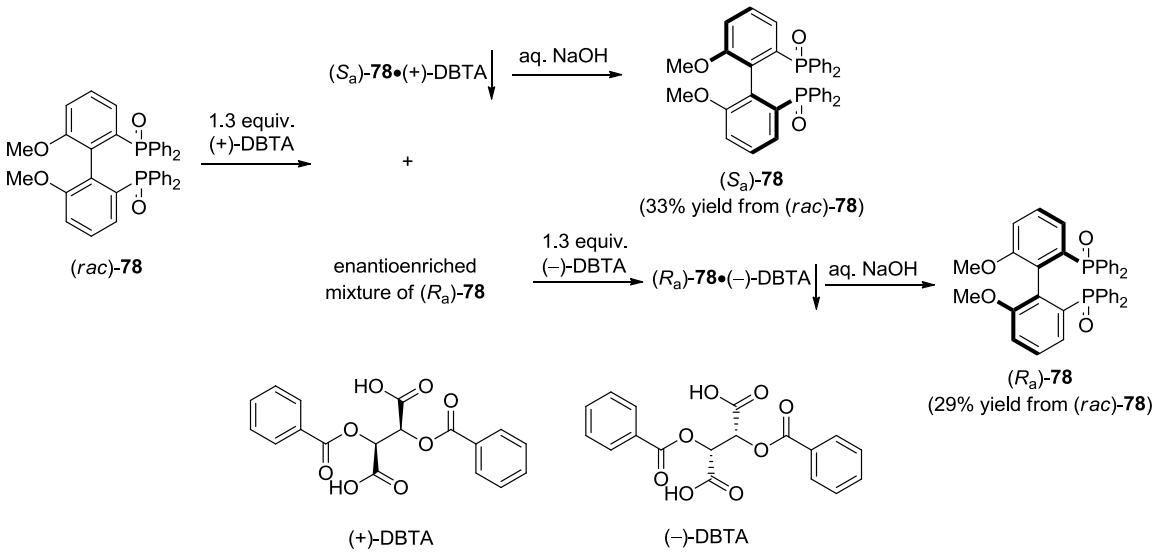

Figure 21. Optical resolution of (*rac*)-**78** using (–)- and (+)-DBTA as resolving agents

Thus, (*rac*)-**78** was first resolved with (+)-DBTA, by fractional crystallization. Compound (*rac*)-**78** was allowed to interact with an excess of resolving agent in the right solvent (a mixture of CH_2Cl_2/EtOAc in a 1/1.2 v/v final ratio). A precipitate was formed corresponding to a 1:1 complex between the substrate and resolving agent (complex (S_a)-**78**•(+)-DBTA). After filtering and washing, the (S_a)-**78**•(+)-DBTA complex was cleaved under aqueous basic conditions and enantiomerically pure (S_a)-**78** could be isolated (66% yield, ≥ 99% ee according to HPLC analysis[110], see Figure 22). The mother liquors and the washing phases from the previous crystallization were gathered and treated with (–)-DBTA under the same conditions. The other enantiomer of the biaryl derivative (R_a)-**78** was thus obtained (59% yield, ≥ 99% ee).

[110] DAICEL Chiralcel IA column (isopropanol/water 75/25, 0.2 mL/min, λ = 216 nm, t_R (S_a) = 31.0, t_R (R_a) = 48.9 min)

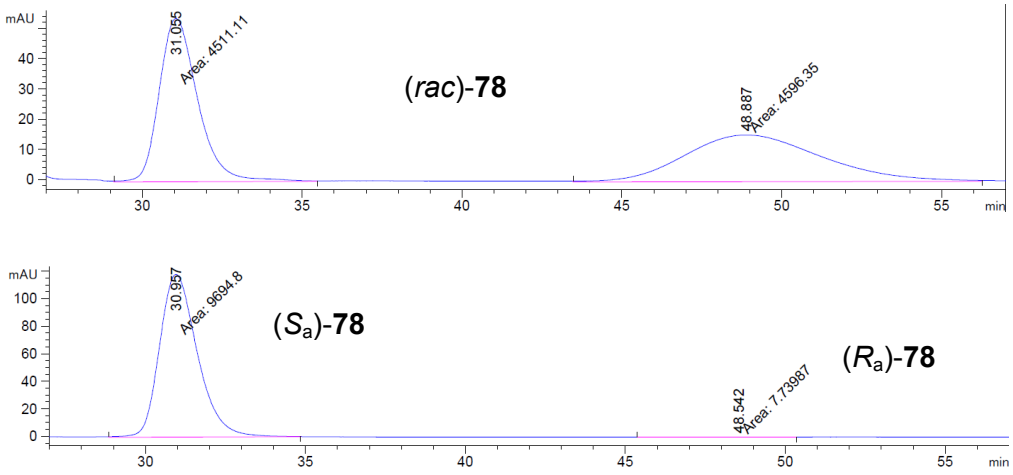

Figure 22. HPLC chromatograms of (*rac*)-**78** (top) and enantiomerically pure (S_a)-**78** (bottom)

With regard to the preparation of enantiomerically pure (R_a)- and (S_a)-**80**, the deprotection of **78** was carried out with BBr_3 as Lewis acid according to the previously reported procedure (treatment of the methoxy-containing biaryl derivative with an excess of BBr_3 at low temperature, followed by aqueous work-up) and afforded diol **80** in 71% yield (average yield of the reaction for the methoxy cleavage in (*rac*)-**78**, (R_a)-**78** and (S_a)-**78**). This reaction suffered in the past from a lack of reproducibility when BBr_3 was used as the commercially available solution.[111] However, the use of neat BBr_3 led to the desired product in good yield without any problems. $^{31}P\{^1H\}$ NMR and ^1H spectra are presented in Figure 23 and Figure 24, respectively.

[111] Dr. P. Molas, unpublished results.

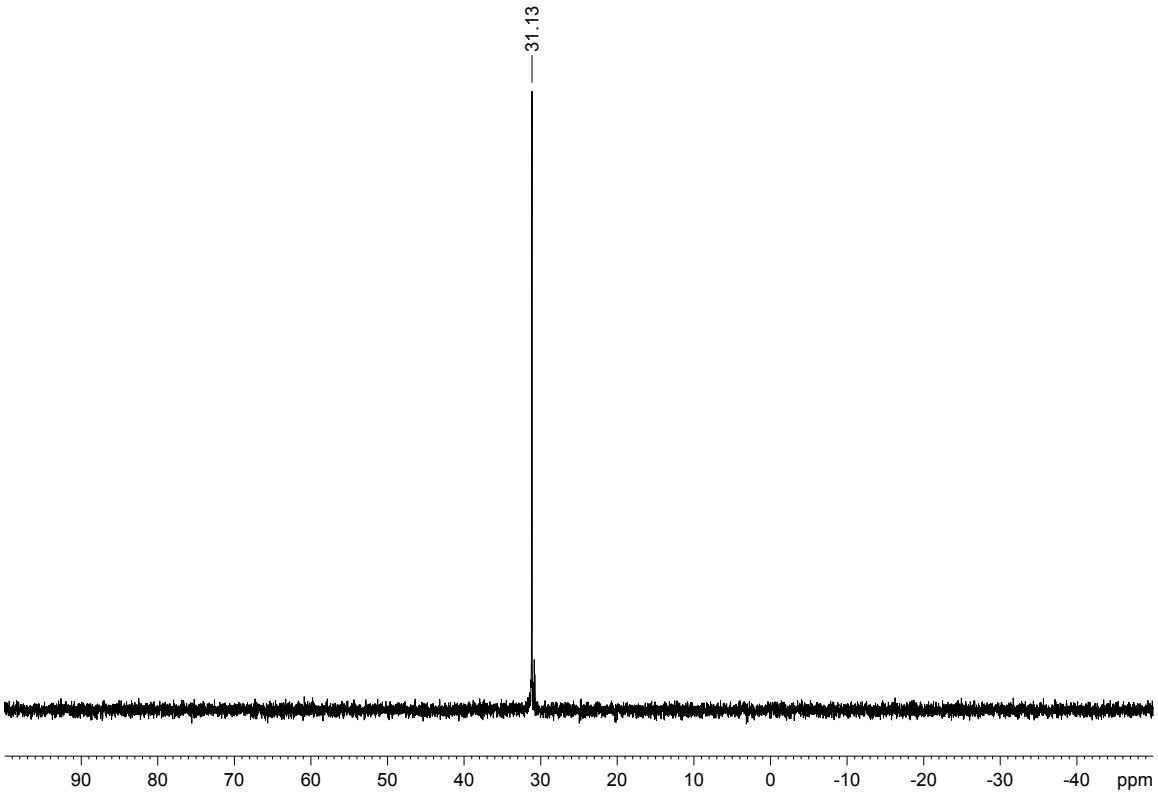

Figure 23. $^{31}P\{^{1}H\}$ NMR spectrum of compound **80** in DMSO-d_6

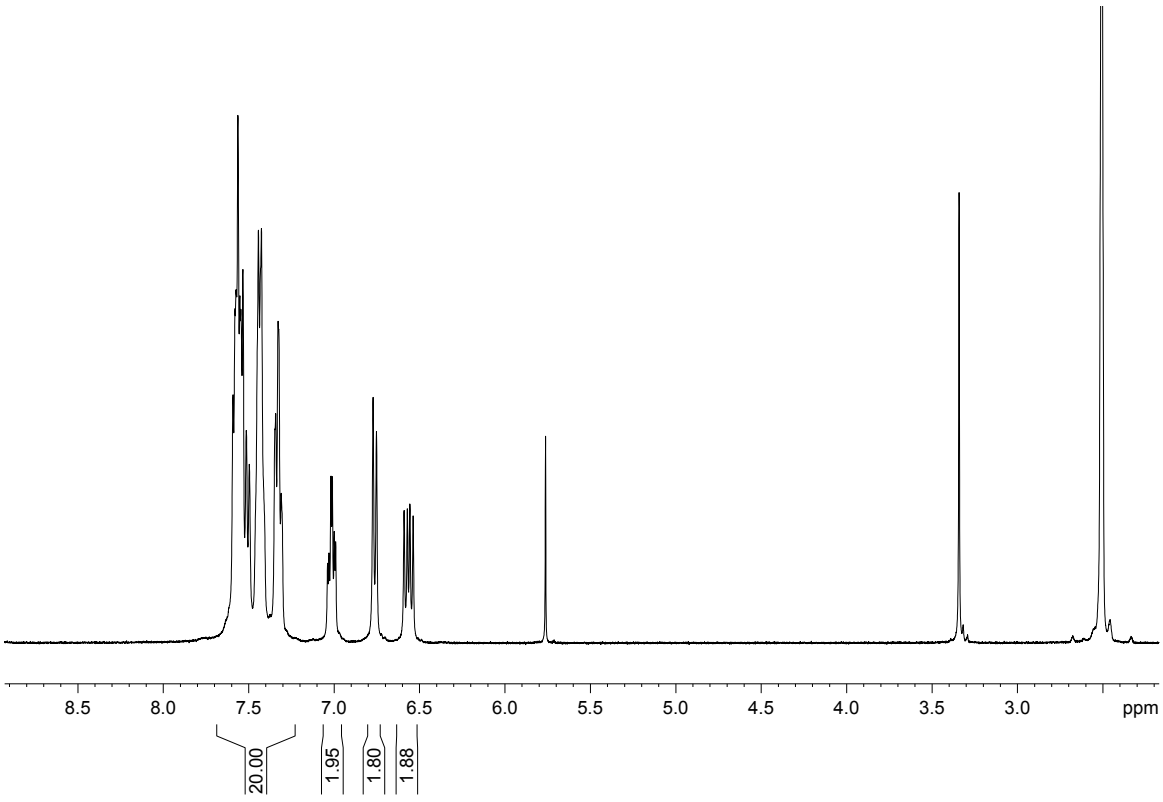

Figure 24. ^{1}H NMR spectrum of compound **80** in DMSO-d_6

As has already been mentioned in the introduction, Dr. Héctor Fernández Pérez described an efficient synthetic method for the preparation of a crown ether containing (1,1'-biphenyl-2,2'-diyl)bis(diphenylphosphine oxide) derivative (S_a)-**81b** (Scheme 17).

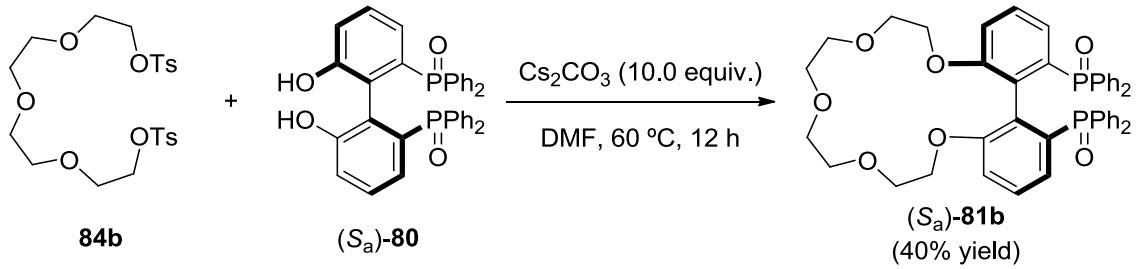

84b (S_a)-**80** (S_a)-**81b** (40% yield)

Scheme 17. Synthetic method of crown ether containing (1,1'-biphenyl-2,2'-diyl)bis(diphenylphosphine oxide) derivative (S_a)-**81b** developed by Dr. H. Fernández-Pérez

(S_a)-**80** was reacted with the corresponding bistosylated polyethylene oxide derivative **84b** and an excess of Cs_2CO_3 in DMF at 60 ºC for 12 h. The target compound (S_a)-**81b** was purified by column chromatography and isolated as a white solid in 40% yield. The reaction was carried out under high-dilution conditions by slow addition of a solution of **84b** to the deprotonated biaryl derivative of (S_a)-**80** to prevent the formation of oligomers and to favor the intramolecular cyclization reaction. One of Dr. Fernández-Pérez's concerns was the possibility of racemization of the enantiomerically pure deprotected diol during the cyclization reaction. This possibility was already discarded by H. Fernández-Pérez in his Thesis by directly checking the enantiomeric purity of compound (S_a)-**81b** just after the cyclization reaction: no loss of enantiomeric purity was observed.

At this point, we became interested in developing and optimizing synthetic strategies for expanding the structural diversity of the polyether chain in the target compounds. For the sake of convenience, we decided to carry out these studies with the racemic series by using (*rac*)-**80** as starting material instead of the more valuable enantiomerically pure analogues (R_a)-**80** or (S_a)-**80**. An array of structurally diverse crown ether-containing bisphosphine dioxide derivatives (*rac*)-**81a–e** was efficiently synthesized by reaction of (*rac*)-**80** and several polyether bistosylate derivatives **84a–e** (Scheme 18). The starting material (*rac*)-**80** was

reacted with the corresponding bistosylated polyether derivatives **84a–e** and an excess of Cs_2CO_3 in DMF at 60 ºC for 12 h. The target compounds (*rac*)-**81** were purified by column chromatography and isolated as white solids in 42 – 65% yield. The reaction was carried out under high-dilution conditions by slow addition of a solution of **84** to the deprotonated biaryl derivative (*rac*)-**80** to prevent the formation of oligomers and to favor the intramolecular cyclization reaction.

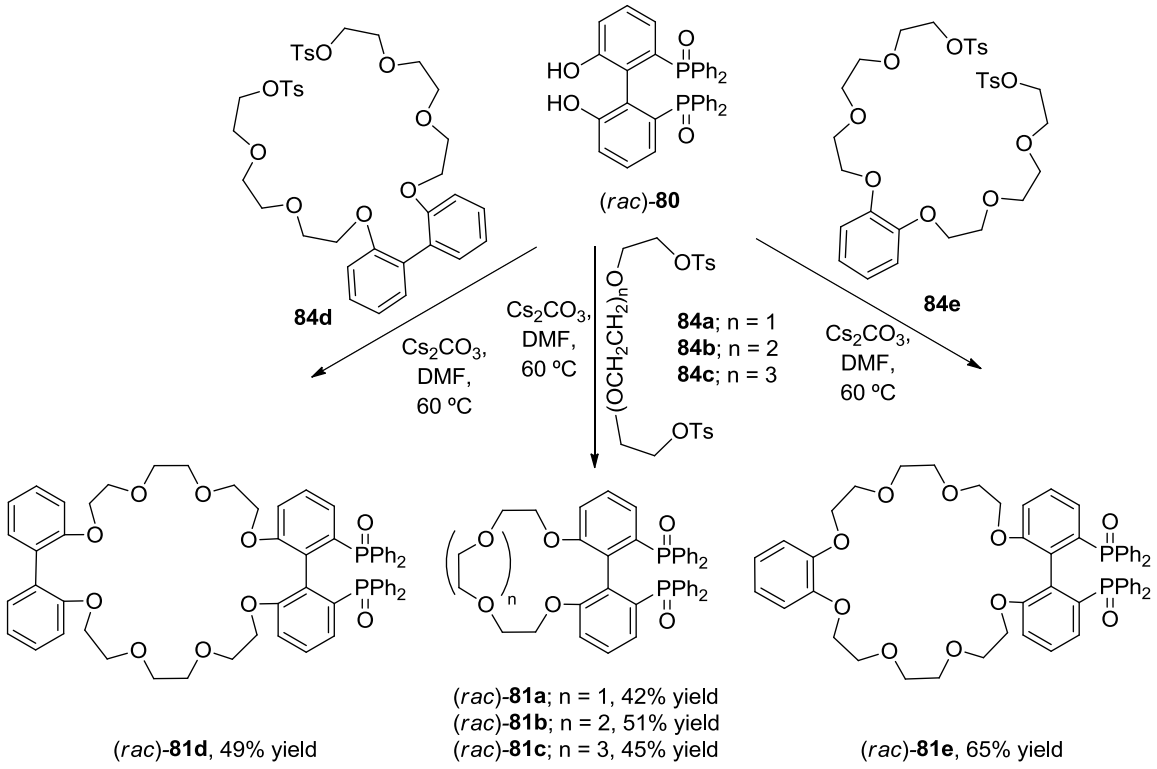

Scheme 18. Synthesis of bisphosphine dioxide derivatives with an appended crown ether moiety, (*rac*)-**81**

With regard to the preparation of the required bistosylated polyethylene oxide derivatives **84a–c**, these compounds were obtained from commercial sources, whereas the large bistosylated chain **84e** was synthesized as previously reported in the literature[112] and **84d** was synthesized for the first time in the present Thesis following the same synthetic strategy as for **84e** (Scheme 19).

[112] Zhu, X.-Z.; Chen, C.-F. *J. Am. Chem. Soc.* **2005**, *127*, 13158.

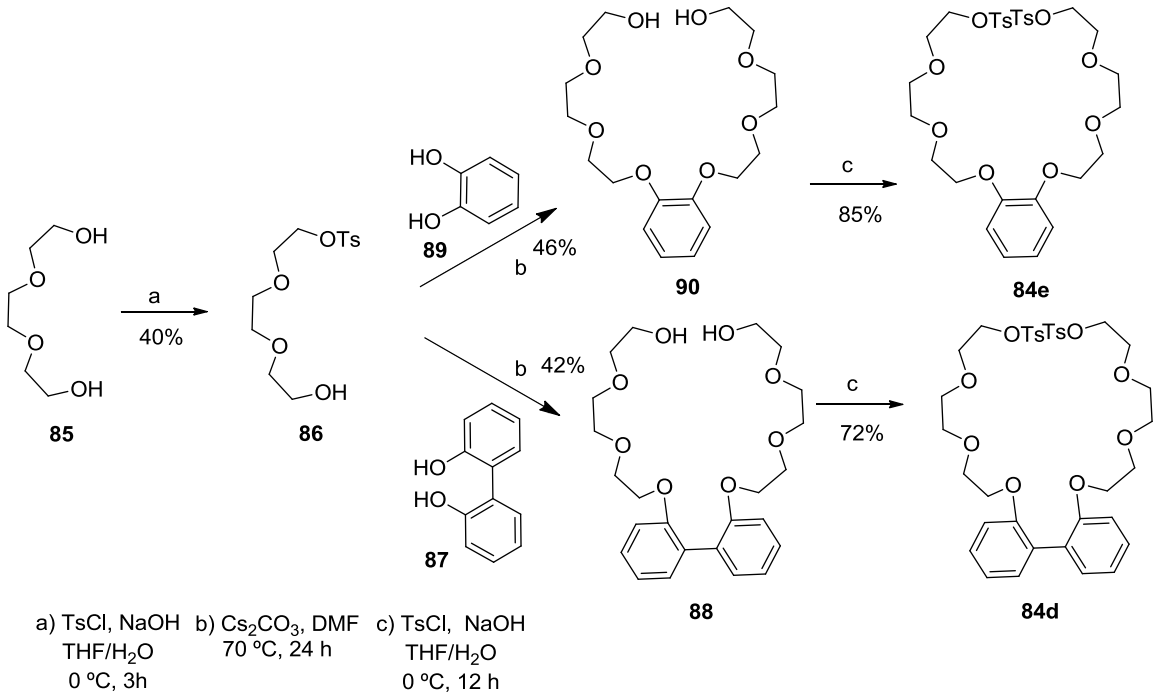

Scheme 19. Synthetic strategy for compounds **84e** and **84d**

Thus, the first step in the preparation of **84d** was the treatment of triethylene glycol **85** with NaOH in a mixture of H_2O and THF under slow addition of tosyl chloride in THF at 0 ºC for 3 h to afford monotosylated derivative **86** in moderate yield (40%). In the next step, a mixture of diol **87** and monotosylated alcohol derivative **86** with Cs_2CO_3 as a base in DMF was heated at 70 ºC and left to react for 24 h, affording diol **88** in moderate yield (42%). In the last step, **84d** was obtained in good yield (72%) by treatment of a solution of diol **88** with NaOH in a mixture of H_2O and THF with a dropwise addition of a THF solution of tosyl chloride at 0 ºC for 12 h. The preparation of **84e** is analogous to that previously described for **84d** where catechol **89** is used instead of diol **87** in the second step of the synthetic strategy to afford diol **90**.

Most interestingly, the structure of all cyclized compounds could be confirmed by X-ray analysis, as all of them proved to be highly crystalline. Crystals of compounds (*rac*)-**81a–e** were grown by slow evaporation of their solutions in organic solvents, such as dichloromethane or deuterated chloroform (See Appendix II for the X-Ray structure data).

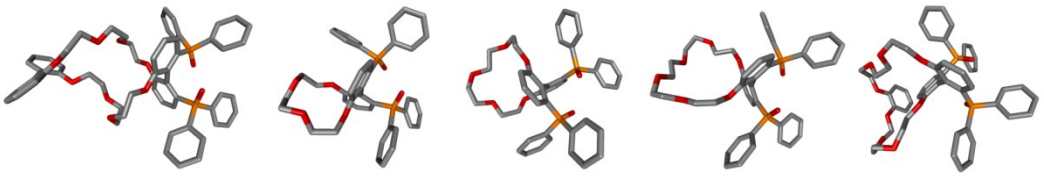

(*rac*)-**81d** (*rac*)-**81a** (*rac*)-**81b** (*rac*)-**81c** (*rac*)-**81e**

Figure 25. X-Ray structures of compounds (*rac*)-**81**

X-Ray structures of compounds (*rac*)-**81** revealed that, in the solid state, the dihedral angle involving the carbon atoms between the two phosphorus groups (θ) increases from (*rac*)-**81a** to (*rac*)-**81c** as the size of the crown ether unit does. Large dihedral angles bring the two P atoms a part making P-P distances larger ($d_{P=O\text{-}P=O}$). In the case of (*rac*)-**81e** and (*rac*)-**81d**, smaller dihedral angles than expected are found. The addition of a phenyl or a biphenyl group on the crown ether moiety breaks the aforementioned trend for (*rac*)-**81a–c** and the dihedral angle becomes smaller though the size of the crown ether moiety grows. Thus, the size and topology of the appended crown ethers appear to have an important effect on the geometry of the compounds and particularly on the relative spatial orientation of the P=O groups (Table 10). These results demonstrate that important structural parameters in bisphosphine dioxides (*rac*)-**81** (*i.e.* the dihedral angle or the distance between P atoms) are affected by the geometry of the distal appended crown ether moiety. Overall, these observations demonstrate that the geometry of the crown ether moiety and the relative spatial orientation of the P=O groups are intercommunicated, which validates the main premise of the proposed regulation mechanism for the first type of supramolecular ligands with a distal regulation site within the present Thesis.

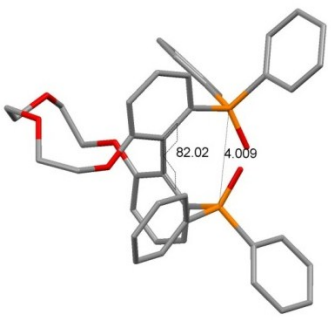

Figure 26. X-Ray structure of compound (*rac*)-**81a** showing torsion angle (θ) and distance between phosphorus atoms ($d_{P=O\text{-}P=O}$) in Å

Table 10. X-Ray structural parameters for (*rac*)-**81a–e**: distance between phosphorus atoms ($d_{P=O\text{-}P=O}$) and between oxygen atoms ($d_{P=O\text{-}P=O}$) in Å and dihedral angles in degrees (θ)

	X-Ray structural parameters		
Compound	$d_{P=O\text{-}P=O}$ (Å)	$d_{P=O\text{-}P=O}$ (Å)	Dihedral angle (θ)
(*rac*)-**81a**	4.009	3.046	82.0
(*rac*)-**81b**	4.158	3.27	88.4
(*rac*)-**81c**	4.55	3.892	102.5
(*rac*)-**81d**	4.355	3.694	95.1
(*rac*)-**81e**	4.233	3.623	87.5

With regard to the final steps towards the preparation of enantiomerically pure bisphosphine ligands **45**, the cyclization conditions and results obtained were the same as those for the racemic compounds (Scheme 18). The final reductive step consisted of adding an excess of $HSiCl_3$ to enantiomerically pure compounds **81** in the presence of an excess of tri-*n*butylamine in refluxing xylene (Scheme 20). The reductions were complete after 3 hours of reaction. Compounds (R_a)-**45a**, (S_a)-**45b** and (R_a)-**45e** were precipitated and isolated as white solids in *ca.* 45% yield. Spectroscopic and spectrometric data were in agreement with the proposed structure. ^{1}H, $^{13}C\{^{1}H, ^{31}P\}$ and $^{31}P\{^{1}H\}$ NMR spectra for (R_a)-**45e** are presented in Figure 27, Figure 28 and Figure 29, respectively.

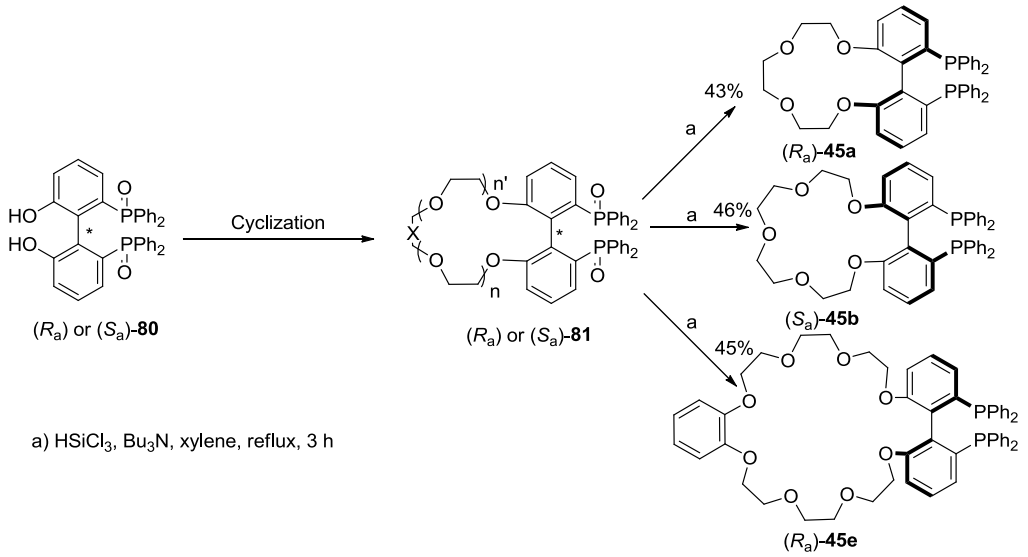

Scheme 20. Synthesis of enantiomerically pure bisphosphine ligands **45** from enantiomerically pure compound **80**

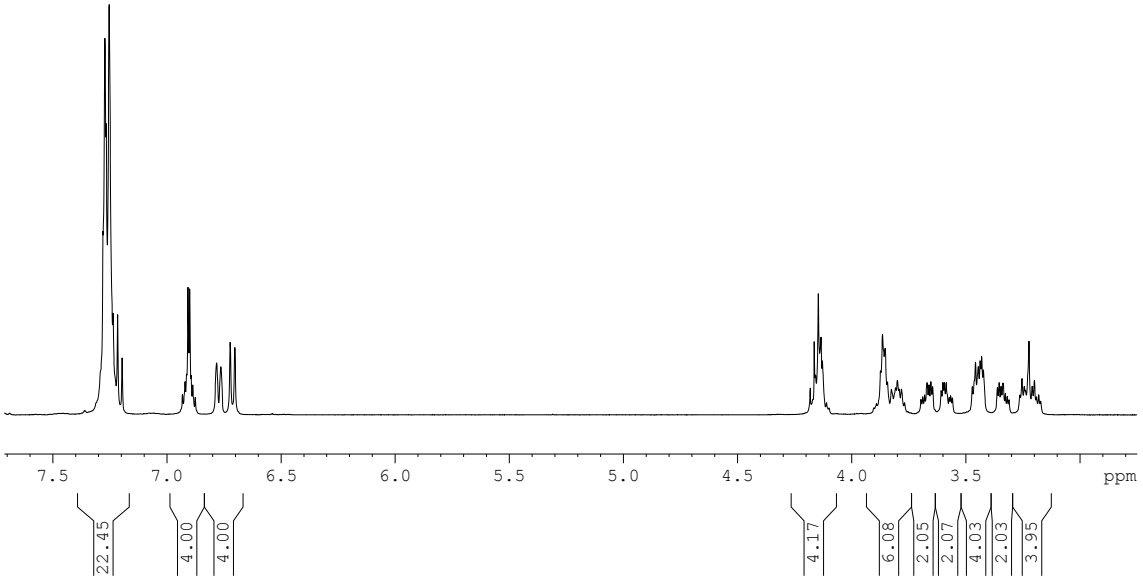

Figure 27. ^{1}H NMR spectrum of compound (R_a)-**45e** in $CDCl_3$

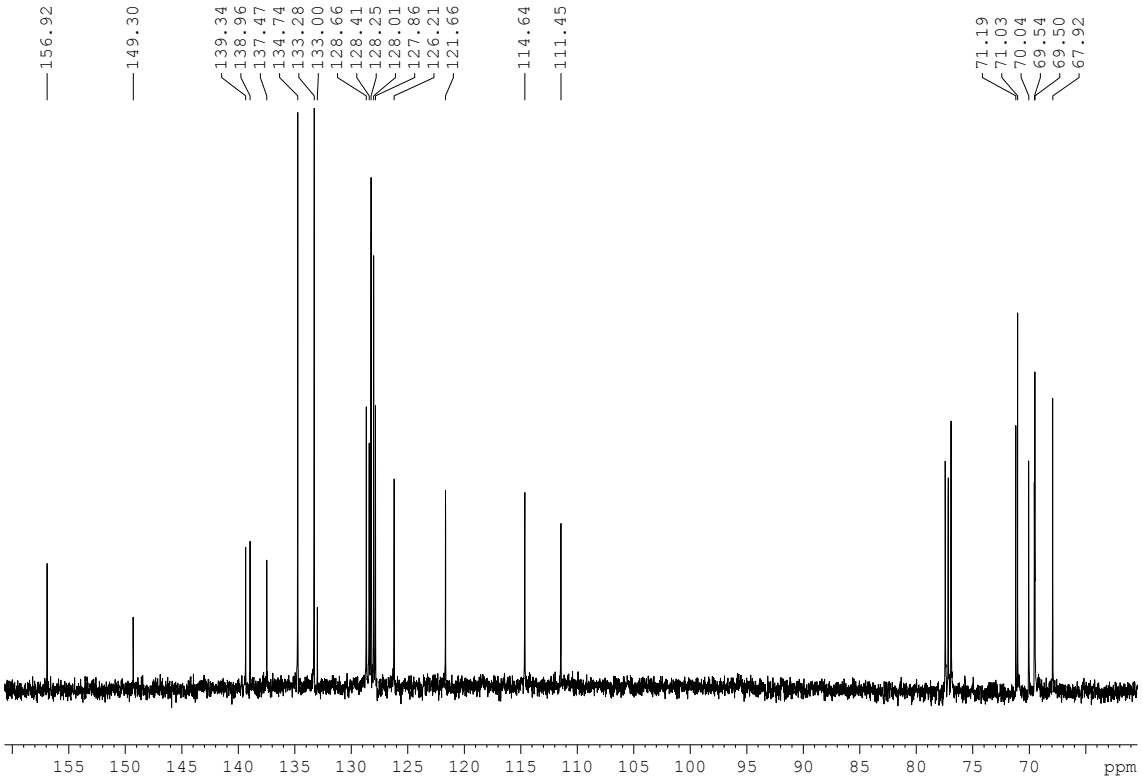

Figure 28. $^{13}C\{^{1}H,^{31}P\}$ NMR spectrum of compound (R_a)-**45e** in $CDCl_3$

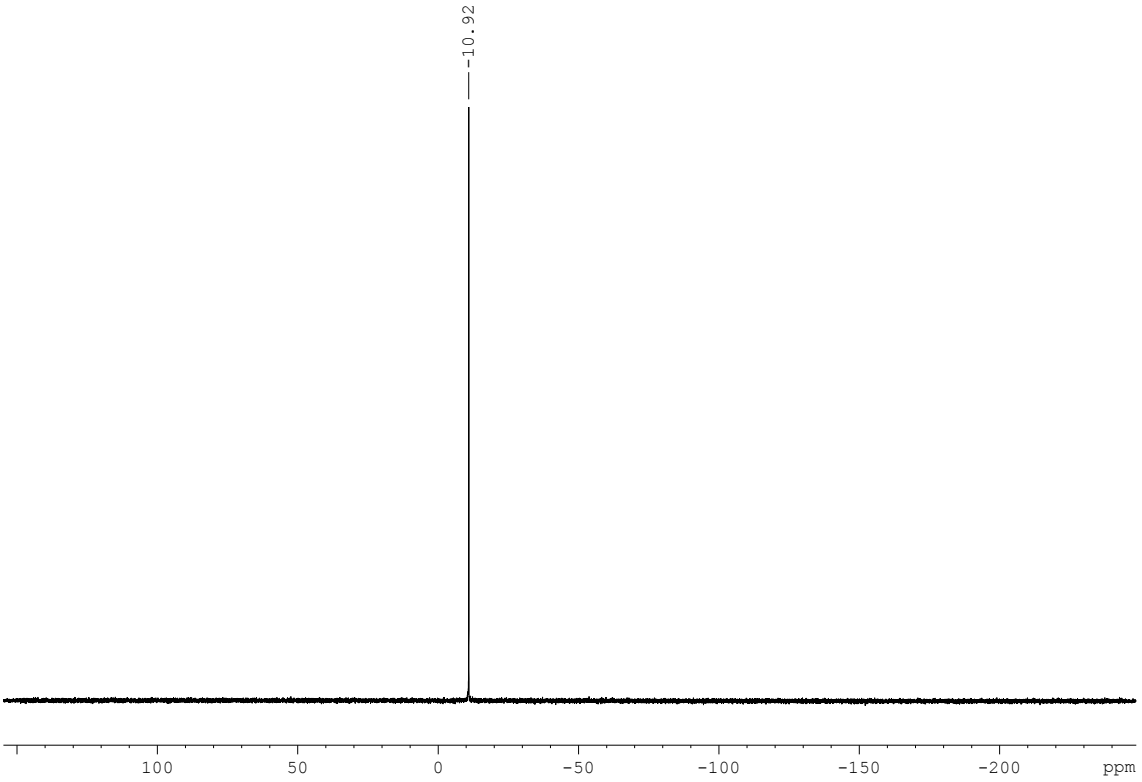

Figure 29. $^{31}P\{^{1}H\}$ NMR spectrum of compound (R_a)-**45e** in $CDCl_3$

1.2.2 Binding studies between cationic species and crown ether-containing bisphosphine dioxides (*rac*)-81

It should be recalled at this point that the underlying principle of this project relies on the binding of a suitable cationic guest into the crown ether moiety-containing phosphorus ligands with a distal regulation site. We envisaged that the binding of such species might lead to a change in the conformation of the receptor, and this conformational change may be transmitted to the catalytic site by changing its geometry (Figure 30).

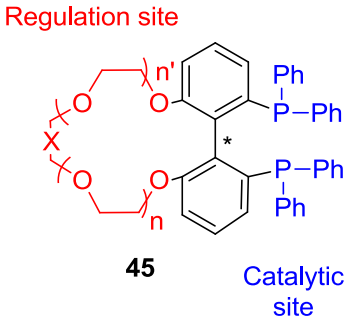

Figure 30. Designed system with potential distal modulation for enantioselective catalysis

Metal cations *via* ion-dipole interactions and ammonium salts *via* hydrogen bonding are known to bind crown ethers.[113] It is generally accepted that when the size of the crown ether and the ionic radius of the guest match, high binding constants are usually observed as pointed out by Pedersen in his pioneering work on crown ethers.[114] Nowadays, although the early reported conclusions by Pedersen are still generally accepted and are taken into account in the design of new crown ether based molecules, other factors such as preorganization and complementarity,[115] solvation and chelate ring size[116] are considered as important factors in the selectivity of crown ethers. These parameters are, however, difficult to predict *a priori.* Thus, preliminary studies were required both for future applications in catalysis and for recognition purposes involving experiments on the inclusion of different cations in the synthesized phosphorus

[113] a) A review in recognition of organic ammonium ions with synthetic receptors: Spaeth, A.; Koenig, B. *Beilstein J. Org. Chem.* **2010**, *6*, No. 32. b) A review about the coordination chemistry of alkali metals and crown ethers: Steed, J. W. *Coord. Chem. Rev.* **2001**, *215*, 171.
[114] Pedersen, C. J. *J. Am. Chem. Soc.* **1967**, *89*, 7017.
[115] Cram, D. J. *Angew. Chem., Int. Ed.* **1986**, *25*, 1039.
[116] Hancock, R. D. *J. Chem. Educ.* **1992**, *69*, 615.

ligands (*rac*)-**81** to find out the most suitable guest in each case (binding selectivity).[117]

For the sake of convenience, binding studies to our synthesized crown ether-containing phosphorus derivatives were carried out on the racemic series. In order to get first estimates of the value of the binding constants, we decided to use emission spectrophotometry. Fluorescence spectroscopy has been demonstrated to be a useful tool for monitoring host-guest interactions in solution.[118] Benniston *et al.*[119] previously reported an in-depth study for similar systems. They prepared three different crown ether ligands, **77a**–**c**, based upon the 2,2'-biphenyl unit with different chain length (Figure 31). By means of fluorescence spectrophotometry they were able to measure the binding constants of their hosts **77a**–**c** with different cations: Li^+, Na^+ and K^+. It was also determined by molecular modeling that the complexation event affects the fluorescence properties by controlling the average conformation around the emitting biphenyl group. The bound cation rigidifies the structure imposing restrictions on the geometry and forcing the rings further from the optimum conformation for emission: planarity. We assumed that the behavior of the emission spectrum of **77** upon addition of different cationic species (Figure 32) would be similar to our receptors (*rac*)-**81** and suitable for binding constant determination. Furthermore, emission spectroscopy is a quick and very sensitive technique that requires very small amounts of material making this technique ideal for our studies.

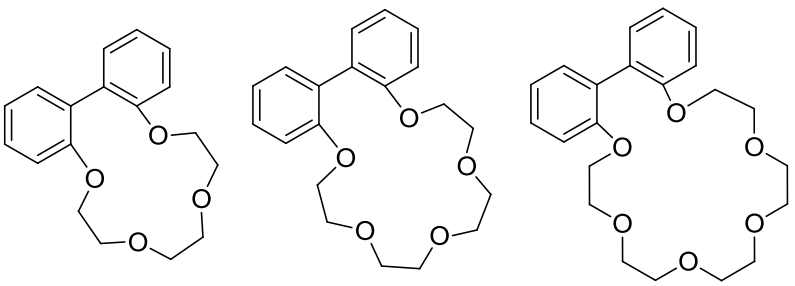

Figure 31. Receptors **77** used by Benniston *et al.* in their study

[117] These binding studies were carried out in collaboration with Dr. Amilan D. Jose.
[118] Some examples: a) Cody, J.; Fahrni, C. J. *Tetrahedron* **2004**, *60*, 11099. b) Charbonnière, L. J.; Ziessel, R. F.; Sams, C. A.; Harriman, A. *Inorg. Chem.* **2003**, *42*, 3466.
[119] Benniston, A. C.; Harriman, A.; Patel, P. V.; Sams, C. A. *Eur. J. Org. Chem.* **2005**, 4680.

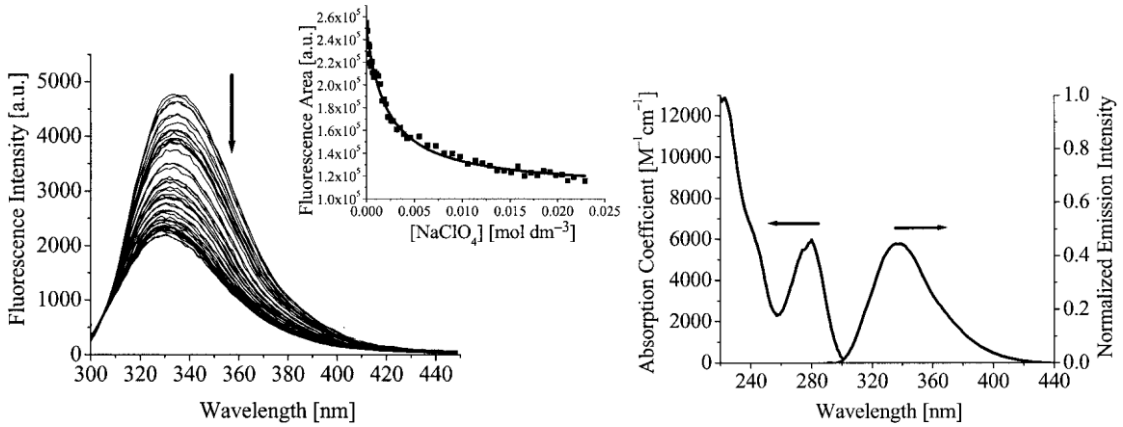

Figure 32. Fluorescence quenching of **77b** upon addition of $NaClO_4$ (left) and absorption and emission profiles of **77b** (right). Figures taken from ref.119

The UV-vis spectra of the compounds (*rac*)-**81a**–**e** showed an absorption band peak at *ca.* 290 nm. Although the general shape of the fluorescence spectrum was preserved, the emission band was partially quenched and red-shifted (*ca.* 5 – 7 nm) during the titration with different cations. Figure 33 shows, as a generic example, the behavior of the emission band of receptor **81a** upon addition of a large excess (5 equivalents) of different salts: $LiClO_4$, $NaClO_4$, KCF_3SO_3, $Mg(ClO_4)_2$, $Ca(ClO_4)_2$, $Ba(ClO_4)_2$ and NH_4PF_6. Dichloromethane, with a minimum amount of methanol (0.5%) for solubilizing the salts, was the solvent of choice for these studies. We thought that such an aprotic solvent would result in high binding constants since dichloromethane is not prone to compete for cation coordination with our hosts. Moreover, the binding constants determined in this media would be relevant and applicable because it is also a suitable solvent for further binding or catalytic studies.

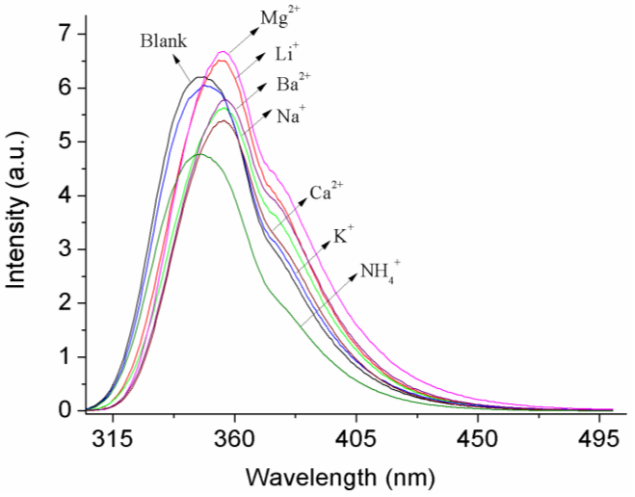

Figure 33. Emission spectra of (*rac*)-**81a** (1.7 x 10^{-4} M) with an excess of different cationic species (5 equivalents) in DCM/MeOH (99.5/0.5 v/v) at 298 K

Cationic crown ether binding solutions were prepared from the corresponding perchlorates, except for K^+ solutions, which were prepared from potassium triflate and for NH_4^+ solutions, which were prepared from ammonium hexafluorophosphate for solubility issues.

Thus, stock solutions of the receptors **81a–e** (*ca.* 10^{-4} M) were prepared in DCM/MeOH (99.5/0.5 v/v). Solutions of the corresponding salts (*ca.* 10^{-3} M) were also prepared in the same solvent mixture. The titration was carried out at 298 K by adding incremental amounts of cationic species to the host solution (compounds **81a**–**e**) leading to changes in the emission spectra. Excitation of the bisphosphine dioxides with an appended crown ether at 290 nm produced a fluorescence emission band at 350 nm. This emission, in most cases, decreased upon addition of guest; however, quenching of the intensity was almost stopped after complete formation of the complex (Figure 34). The binding constants were extracted by non-linear curve fitting of the emission data at 350 nm considering a 1:1 binding model.[117]

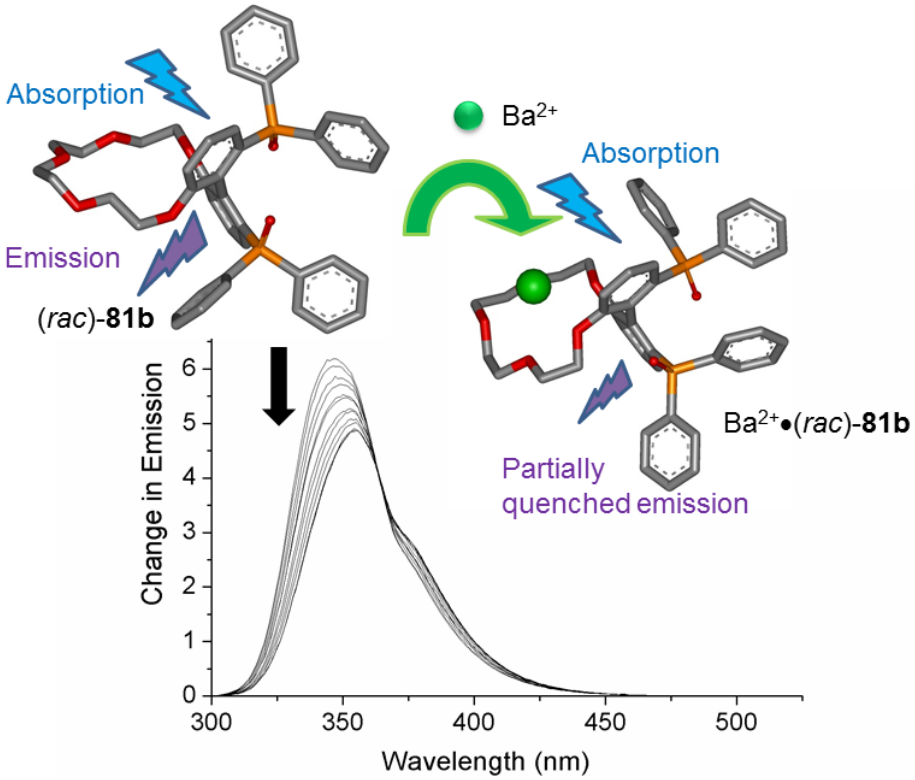

Figure 34. Example of emission titration,[120] compound (*rac*)-**81b** acts as a host for Ba^{2+}

At a very low receptor concentration, and with the assumption that no excited state association occurs, the observed emission intensity can be represented by equation:[121]

$$\frac{I_{max} \cdot [G]^n + K_d \cdot I_{min}}{K_d + [G]^n} = I([G])$$

Where:

$I([G])$ = Emission intensity for a given guest concentration

n = Number of bound guest molecules

[G] = Concentration of cation

K_d = Dissociation constant

K = Binding constant = 1 / K_d

[120] Geometry of (*rac*)-**81b** and Ba^{2+}•(*rac*)-**81b** system were optimized with Scigress Explorer Ultra, Version 7.7.0.47.
[121] Novikov, E.; Stobiecka, A.; Boens, N. *J. Phys. Chem. A* **2000**, *104*, 5388.

I_{min} = Emission intensity without any cation

I_{max} = Emission intensity with maximum amount of cation

As an example, the plot of added concentration of cation [G] ($LiClO_4$) *versus* the change in emission intensity (I–Io) for receptor (*rac*)-**81b** is represented in Figure 35. Non-linear curve fitting of the experimental data to the previous equation results in a *K*-value = 1.4 x 10^4 M^{-1}.

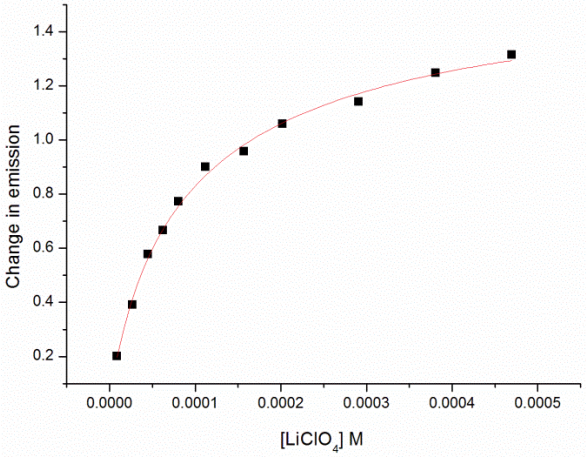

Figure 35. Change in emission intensity of (*rac*)-**81b** (I–Io) plotted against concentration of $LiClO_4$ guest

The table below (Table 11) shows the binding constant values obtained from the emission titrations of our receptors (*rac*)-**81** with $LiClO_4$, $NaClO_4$, KCF_3SO_3, $Mg(ClO_4)_2$, $Ca(ClO_4)_2$, $Ba(ClO_4)_2$ and NH_4PF_6. The same results are presented in Figure 36.[117]

Table 11. Association constants of receptors (*rac*)-**81** with crown ether binding species

Binding constants: K (M^{-1})[a]						
Entry	Guests	Hosts				
		81a	**81b**	**81c**	**81d**	**81e**
1	Li^+	5.0×10^4	1.4×10^4	5.0×10^3	3.3×10^4	5.0×10^4
2	Na^+	2.5×10^4	3.0×10^4	2.5×10^4	1.1×10^4	6.0×10^3
3	K^+	1.2×10^4	5.0×10^4	2.0×10^3	5.0×10^4	1.5×10^3
4	Mg^{2+}	<100	2.0×10^3	1.6×10^4	5.0×10^4	5.0×10^4
5	Ca^{2+}	2.6×10^4	3.0×10^4	1.4×10^4	1.3×10^5	2.0×10^5
6	Ba^{2+}	3.0×10^4	3.3×10^4	6.6×10^4	2.0×10^4	5.0×10^4
7	NH_4^+	5.0×10^4	3.3×10^4	2.0×10^4	5.0×10^4	5.0×10^4

[a] Measured in DCM/MeOH (99.5/0.5 v/v) at 25 ºC by emission titration, the values reported are the mean value of at least two independent measurements.

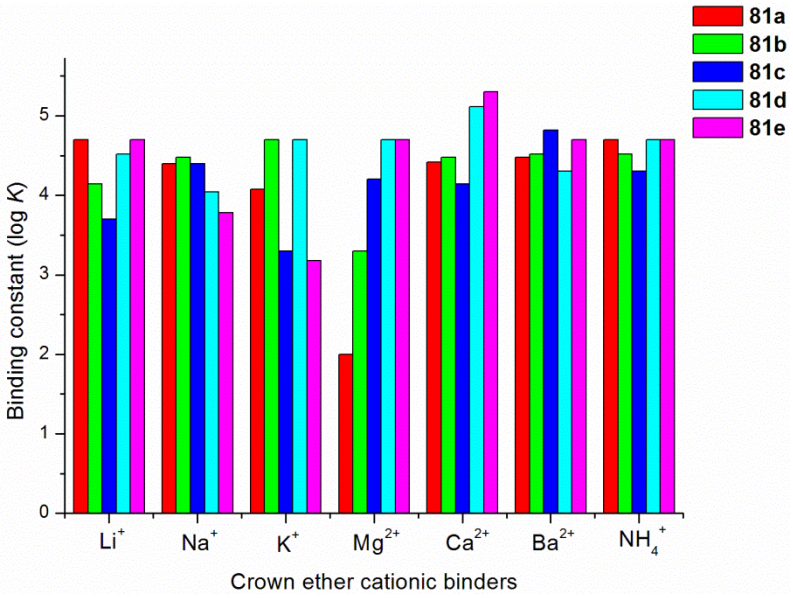

Figure 36. Binding constants calculated from emission titrations for different receptors **81** and guests

Our binding studies revealed that the receptors studied did not show a pronounced selectivity for any of the different cationic species that were analyzed; *K*-values were around 10^4 M^{-1} for almost every case. However, and as expected from the ring size, the receptor incorporating the smallest ring (*rac*)-**81a** showed a small preference for Li^+ over Na^+ and K^+. Receptor (*rac*)-**81b** presented

a slightly higher binding affinity for Na^+ and K^+ over Li^+; (*rac*)-**81c** had a small preference for divalent Ba^{2+} cation whereas (*rac*)-**81d** and (*rac*)-**81e** for Ca^{2+}. All receptors bound NH_4^+ with similar affinities.

As a background experiment we tested the affinity of [1,1'-biphenyl]-2,2'-diylbis(diphenylphosphine oxide) or BIPHEPO **91**,[122] an analogous molecule of our receptors (*rac*)-**81** but without the crown ether moiety, to different monovalent cations: Li^+ and NH_4^+ but also to divalent Ba^{2+}. The binding constants determined were found to be 2 to 3 orders of magnitude lower than those obtained with receptors (*rac*)-**81** (6.7 x 10^1, 1.0 x 10^2, and 2.6 x 10^2 M^{-1}, respectively), proving that the cations had a strong preference to bind the crown ether rather than the P=O groups.

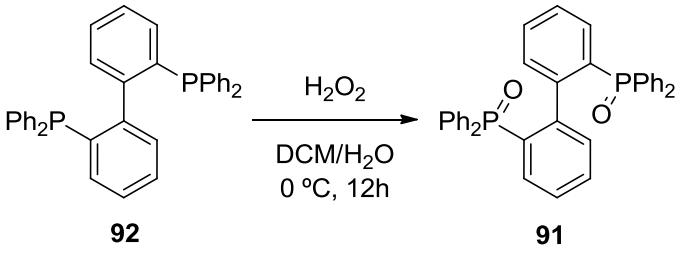

92 **91**

Scheme 21. Synthetic strategy for BIPHEPO **91**

Binding site-selectivity on receptor (*rac*)-**81a** was also established in a qualitative sense by NMR spectroscopy. For example, methylene signals in the spectrum of (*rac*)-**81a** suffered considerable changes upon addition of increasing Li^+ and Na^+ amounts, indicating that the crown ether moiety was the binding site (Figure 37).

[122] Compound **91** was synthesized following a previously reported procedure from biaryl derivative **92**: Harada, T.; Nakano, Y.; Fujiki, M.; Naito, M.; Kawai, T.; Hasegawa, Y. *Inorg. Chem.* **2009**, *48*, 11242.

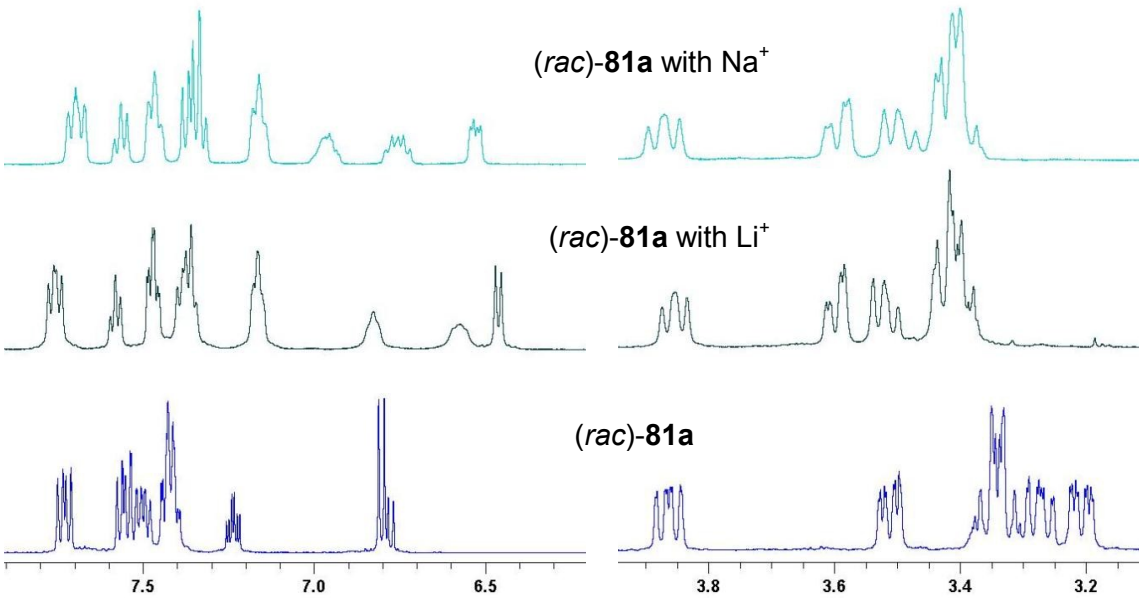

Figure 37. Spectral ^{1}H NMR changes on receptor (*rac*)-**81a** after the addition of Li^{+} and Na^{+} salts

We also investigated the binding behavior between (*rac*)-**81b** and Ba^{2+} by isothermal titration calorimetry (ITC).[123] A solution of (*rac*)-**81b** (7.3×10^{-4} M) in DCM/MeOH (98/2 v/v) was added in the cell of an isothermal calorimeter. Known volumes of a solution of barium perchlorate in the same solvent mixture (6.1×10^{-3} M) were syringed into the host solution and the evolved heat measured. The binding constant determined by ITC had the same order of magnitude than that measured by fluorescence ($K = 2 \times 10^{4}$ M^{-1} by ITC in DCM/MeOH (98/2 v/v) and $K = 3 \times 10^{4}$ M^{-1} by fluorescence in DCM/MeOH (99.5/0.5 v/v) at 25 ºC). A 1:1 ratio between Ba^{2+} and (*rac*)-**81b** was deduced from the ITC data. ΔH and ΔS values (7.5 kcal/mol, 44.4 cal/mol/K, 298 K in DCM/MeOH (98/2 v/v)) were also extracted from the titration data and revealed that complexation towards the 1:1 complex is an entropically driven process (Figure 38).

[123] Binding studies of other positively charged species were not possible by ITC, since heat evolved due to dilution was much higher than the heat involved in the binding process.

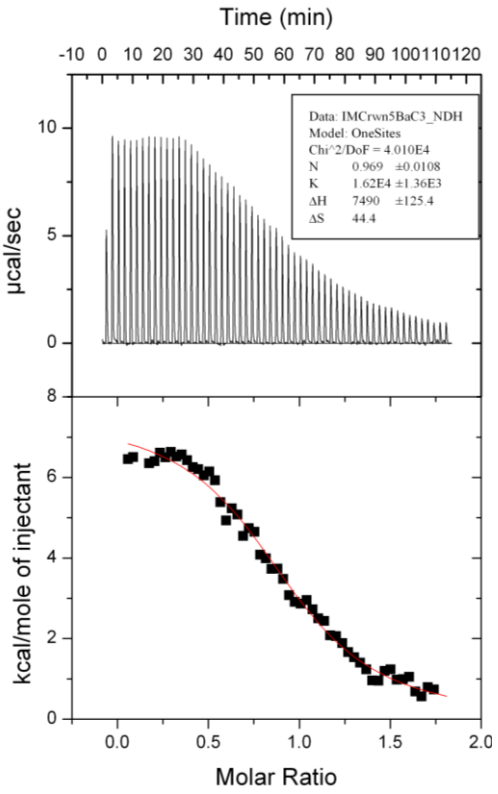

Figure 38. ITC titration experiment for (*rac*)-**81b** and barium perchlorate. Top: raw data. Bottom: normalized integration data of the evolved heat per injection in terms of kcal mol^{-1} of injectant $Ba(ClO_4)_2$ plotted against the molar ratio. To determine the values of the thermodynamic variables (ΔH and ΔS) the ITC data was fitted to a 1:1 binding model (red line).

1.2.3 Crown ether-containing bisphosphine ligands 45 for rhodium-mediated asymmetric hydrogenation

Having obtained enantiomerically pure bisphosphines with appended crown ether moieties (R_a)-**45a**, (S_a)-**45b** and (R_a)-**45e**, we decided to assess their catalytic activity as ligands for Rh-mediated asymmetric hydrogenation of functionalized alkenes. The possibility to modulate the catalytic efficiency of the Rh(I) complexes of the enantiomerically pure bisphosphines prepared *via* complexation with cationic species, namely Li^+, Ba^{2+} and NH_4^+, was first tested with ligand (R_a)-**45a**. We chose these cationic species as representative examples of monovalent and divalent cations of chemically diverse species (one alkali metal, one alkaline earth and one ammonium cation). The substrates of choice were three benchmark substrates for rhodium mediated asymmetric hydrogenation of functionalized alkenes: dimethyl itaconate **39a**, methyl 2-acetamidoacrylate **39b** and (*Z*)-methyl 2-acetamido-3-phenylacrylate **39d** (also abbreviated as ZMac). Dichloromethane with small amounts of methanol was chosen as a proper solvent to carry out the hydrogenation reactions, as this solvent mixture both solubilizes the ligand and cationic species and facilitates strong binding between them according to the previous binding studies (section 1.2.2). To aid comparison, commercially available ligand (S_a)-MeO-BIPHEP (S_a)-**63a** was also assessed in the catalytic studies as a reference ligand due to its similar structure but lack of regulation mechanism.[124]

[124] Ligand (S_a)-**63a** ((S_a)-MeO-BIPHEP) was purchased from Aldrich and used as received:

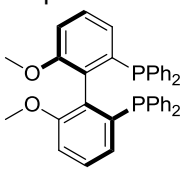

(S_a)-**63a**

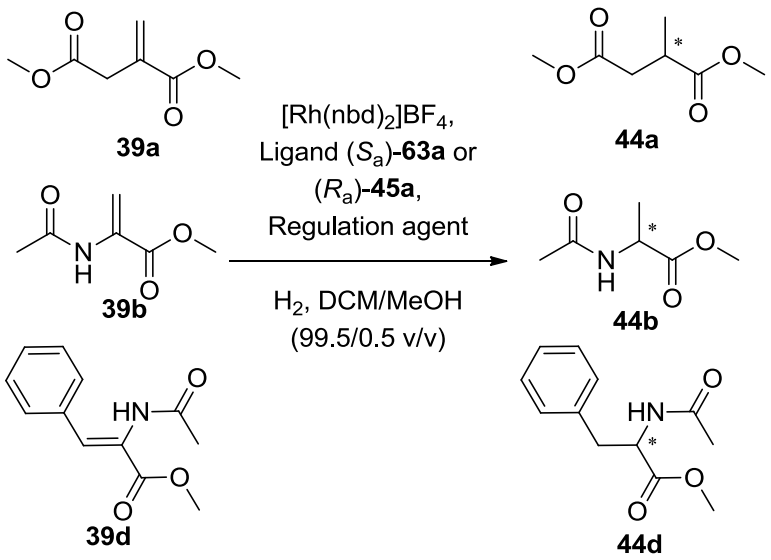

Scheme 22. Rh-mediated asymmetric hydrogenation of substrates **39a**,**b**,**d** with different cationic species (regulation agents)

Table 12. Results of the asymmetric hydrogenation of substrates **39a**,**b**,**d** with ligands (R_a)-**45a** and (S_a)-**63a** and different cationic species as potential regulation agents of the catalytic activity[a]

Entry	Ligand	Substrate	Regulation agent	ee
1	(R_a)-**45a**	**39a**	-	66% (*R*)
2	(R_a)-**45a**	**39a**	$LiClO_4$	68% (*R*)
3	(R_a)-**45a**	**39a**	$Ba(ClO_4)_2$	67% (*R*)
4	(R_a)-**45a**	**39a**	NH_4PF_6	67% (*R*)
5	(R_a)-**45a**	**39b**	-	15% (*R*)
6	(R_a)-**45a**	**39b**	$LiClO_4$	16% (*R*)
7	(R_a)-**45a**	**39b**	$Ba(ClO_4)_2$	18% (*R*)
8	(R_a)-**45a**	**39b**	NH_4PF_6	19% (*R*)
9	(R_a)-**45a**	**39d**	-	2% (*S*)
10	(R_a)-**45a**	**39d**	$LiClO_4$	2% (*S*)
11	(R_a)-**45a**	**39d**	$Ba(ClO_4)_2$	6% (*R*)
12	(R_a)-**45a**	**39d**	NH_4PF_6	9% (*R*)
13	(S_a)-**63a**	**39a**	-	61% (*S*)
14	(S_a)-**63a**	**39b**	-	28% (*S*)
15	(S_a)-**63a**	**39d**	-	15% (*S*)

[a] Hydrogenation reactions were carried out at 5 bar of H_2 pressure at room temperature. Rh/ligand/regulator/substrate ratio = 1/1.1/5.5/100. Substrate concentration [S] = 0.025 M. Reaction time = 60 hours. Results obtained at full conversion in all cases.

The results summarized in Table 12 clearly indicated that only **39a** was hydrogenated in relatively good enantiomeric excesses. Compound **44a** was obtained in 66% enantiomeric excess in favor of the (*R*) enantiomer without any additive salt present when ligand (R_a)-**45a** was used. This result was slightly better in terms of enantioselectivity than that obtained with ligand (S_a)-**63a** for the same substrate (61% ee, entry 13). Enantiomeric excesses for substrates **39b** and **39d** were very poor: 15% and 2%, respectively.

Unfortunately, the addition of the potential regulators of the catalytic activity (*i.e.* Li^+, Ba^{2+} and NH_4^+ salts) to the reaction media did not provoke any noticeable change in the enantioselectivity of the hydrogenation product mediated by the catalytic system. The highest increase in ee was found by combining ligand (R_a)-**45a** and NH_4^+ in the hydrogenation of **39b** (compare entries 5 and 8 in Table 12). However, the enantioselectivity observed was only four percentage points higher than that obtained with ligand (R_a)-**45a** alone, and the optical purity of the product was still very low (19% ee). Product **44d** was obtained practically as a racemic mixture when using ligand (R_a)-**45a** alone or in combination with Li^+ (entries 9 and 10). When NH_4^+ was present in the reaction media, the enantiomeric excess determined was found to increase up to 9% ee towards product (*R*)-**44d** (entry 12). In general terms, the observed improvements in the enantiomeric excesses obtained were considered too low to draw any conclusions.

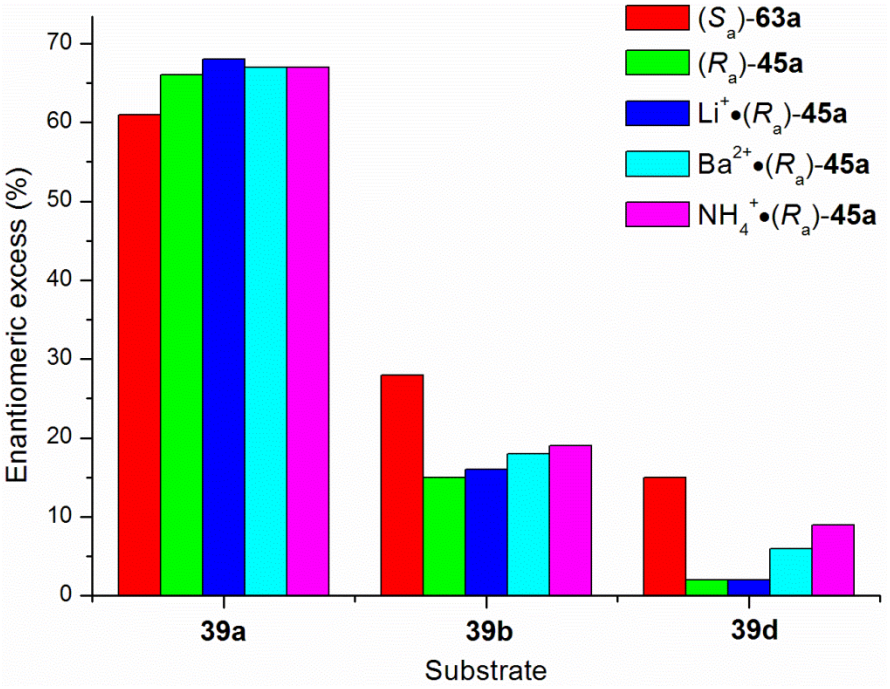

Figure 39. Summary on the results of asymmetric hydrogenation of substrates **39a**,**b**,**d** with Rh(I) catalysts derived from ligands (S_a)-**63a** and (R_a)-**45a** with different cationic species

The cation sources that we used in the aforementioned catalytic studies were the lithium, barium or ammonium perchlorates or hexafluorophosphates. These compounds are not soluble in pure dichloromethane and a small amount of methanol was required for full solubilization in the reaction media. The binding strength of cationic species within crown ethers in methanol is expected to be lower than those in dichloromethane, as methanol competes with the cationic species in binding with the crown ether moieties. In a first approximation, we considered that this effect could be detrimental for our strategy and be the reason for the low efficiency of our regulation mechanism.

With the aim of facilitating higher binding strength between the regulation agents (mainly salts of alkali metal and ammonium cations) and the crown ether moiety, we decided to use salts, not only with a better solubility in non-polar solvents such as dichloromethane but also with an even less coordinating anion. Thus, the bulky and weakly coordinating [B(3,5-$(CF_3)_2C_6H_3)_4$] anion (hereafter

abbreviated as BArF[125]) seemed to us an attractive option for our catalytic studies (Figure 40).

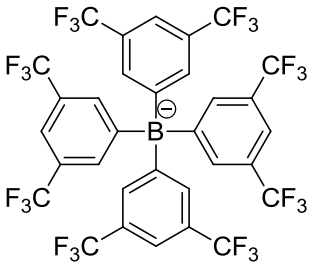

BArF anion

Figure 40. $[B(3,5\text{-}(CF_3)_2C_6H_3)_4]$ (BArF) anion

Besides, NaBArF is commercially available and can be used as a source of BArF anion for the preparation of the required BArF salts.[126] Indeed, we prepared not only a series of alkaline metal BArF salts, such as KBArF, RbBArF and CsBArF, in a straightforward way but also ammonium-type BArF salts such as the optically pure ammonium BArF salts (*R*)-**93**, (*S*)-**93**, (*R*,*R*)-**94** and (*S*,*S*)-**94** and the achiral: dibenzylammonium BArF **95**,[127] whose synthesis was already described.

Most of the required BArF salts were synthesized by anion-exchange processes over another salt of a given cation by the commercially available NaBArF salt.

The high insolubility of CsBArF and RbBArF in water was exploited for the preparation of these compounds from their sodium analogue. NaBArF was dissolved in water (90 ºC). Subsequent portion wise addition of $CsNO_3$ or $RbNO_3$ led to the formation of a new solid, which was precipitated corresponding to CsBArF or RbBArF, respectively. CsBArF and RbBArF were isolated by filtration, washed with water, and recrystallized in THF (*ca.* 70% yield). The salts obtained in this way were dried at 120 ºC under vacuum overnight. The BArF ammonium salts **93**, **94** and **95** (see Scheme 23) were prepared using a similar strategy. Mixing the highly soluble NaBArF and the sparingly soluble hydrochloride

[125] Krossing, I.; Raabe, I. *Angew. Chem., Int. Ed.* **2004**, *43*, 2066.
[126] Buschmann, W. E.; Miller, J. S.; Bowman-James, K.; Miller, C. N. *Inorg. Synth.* **2002**, *33*, 83.
[127] South, C. R.; Higley, M. N.; Leung, K. C. F.; Lanari, D.; Nelson, A.; Grubbs, R. H.; Stoddart, J. F.; Weck, M. *Chem. Eur. J.* **2006**, *12*, 3789.

precursors **96**,[128] **97** and **98** in diethyl ether for 12 hours resulted in the precipitation of NaCl. Filtration of the crude mixture to remove the precipitated NaCl and evaporation of the crude mixture afforded analytically pure products **93**, **94**, and **95**, respectively, as white solids in quantitative yields.

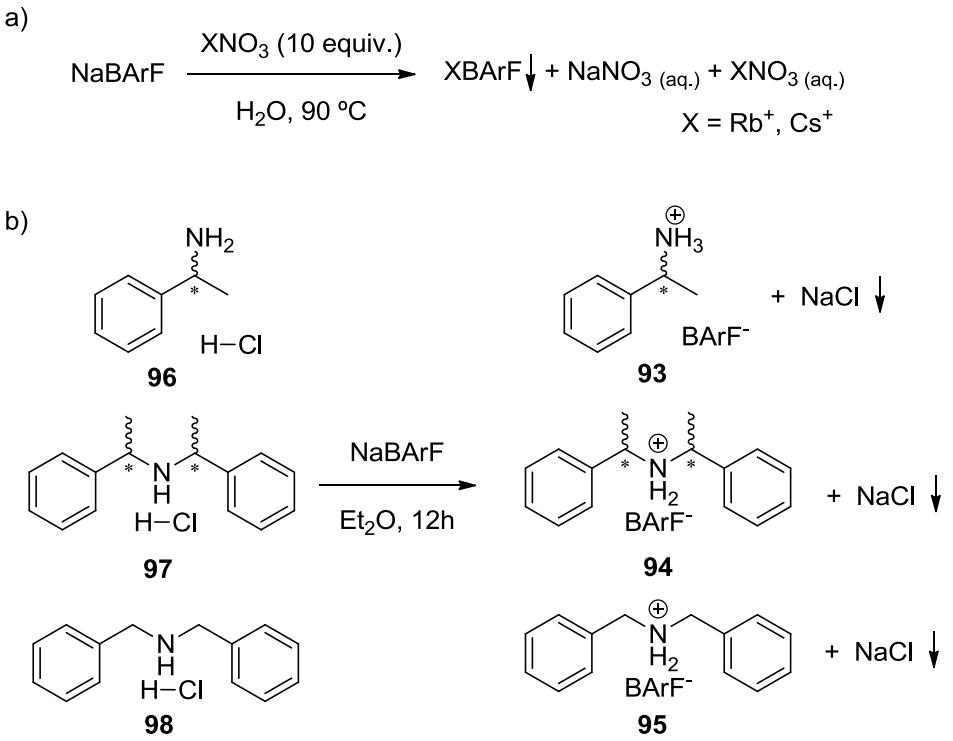

Scheme 23. a) Preparation rubidium and cesium BArF salts and b) synthesis of primary and secondary amine derived BArF salts

Lastly, KBArF was synthesized following a well-established methodology (Scheme 24).[126] Thus, compound **99** was added dropwise to a stirred solution of magnesium turnings in diethyl ether to form the aryl-magnesium halide MgI[$C_6H_3(CF_3)_2$]. After stirring for 1 hour, boron trifluoride diethyl etherate was added drop wise and the reaction mixture was refluxed overnight. Finally, the crude reaction mixture was poured into a solution of K_2CO_3 in water to generate the potassium salt. The $MgCO_3$ precipitate was filtered off. The organic solvent was concentrated under reduced pressure, leaving a brown residue. The residue was dissolved in a DCM/THF mixture (1/1) and the resulting solution was layered with hexane to induce precipitation of the desired product at room temperature. This process was repeated three consecutive times to obtain colorless crystals of

[128] Compounds **96** were synthesized following the reported procedure: Halloran, K.J.; Comely, A.; Chen, Z.; Krishnan, S. Stereoselective Synthesis of Metyrosine. WO 2011/053835 A1, 2011.

pure KBArF salt. The solid became white after drying at 120 ºC *in vacuo* overnight (60% yield).

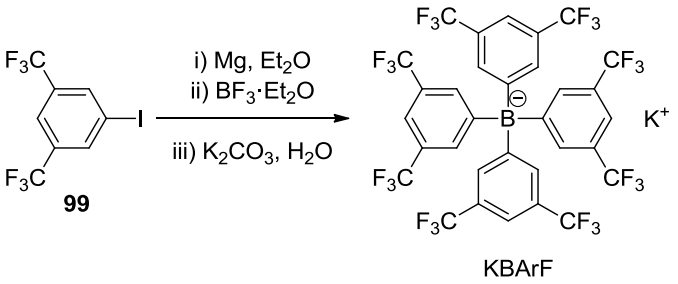

Scheme 24. Synthesis of KBArF salt from compound **99**

To summarize, we prepared 8 potential cationic regulators for the catalytic activity in our approach, which are represented in Figure 41. In total, we had at our disposal four alkaline metal cation BArF salts with increasing cationic radius: Na^+, K^+, Rb^+, Cs^+ and five ammonium analogues, of which four were enantiomerically pure (Figure 41).

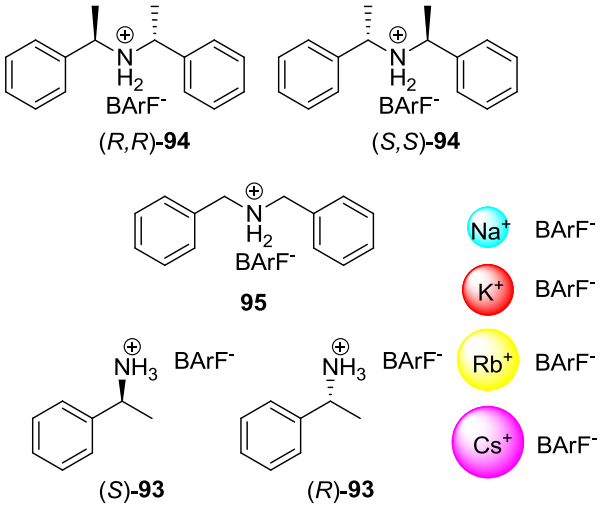

Figure 41. BArF salts as cationic sources for distal regulation

With this array of BArF derivatives of cationic species in hand, we then performed new catalytic studies on the rhodium mediated asymmetric hydrogenation of alkenes using ligand (S_a)-**45b**. Dimethyl itaconate **39a** and (*Z*)-methyl 2-acetamido-3-phenylacrylate **39d** were chosen as model substrates for asymmetric hydrogenation with bisphosphine (S_a)-**45b** as ligand and the BArF salts depicted in Figure 41 as regulation agents. The catalytic experiments were conducted in pure dichloromethane at room temperature under 20 bar of H_2

pressure for 24 hours, as the BArF salts were soluble in this solvent. The commercially available rhodium precursor $[Rh(cod)_2]BArF$ was chosen for these studies instead of $[Rh(nbd)_2]BF_4$ to avoid possible cross effects on the enantioselectivity of the process due to the presence of two different counterions in the vicinity of the catalytic site.

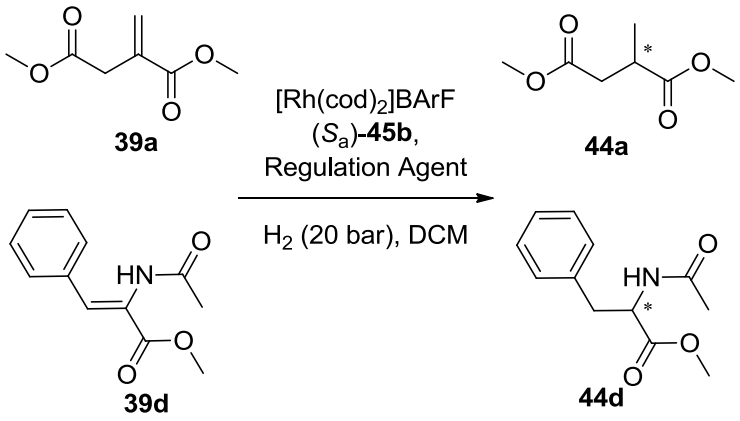

Scheme 25. Rh-mediated asymmetric hydrogenation of substrates **39a**,**d** with different BArF salts

Table 13. Results on the asymmetric hydrogenation of substrates **39a**,**d** with ligand (S_a)-**45b** and different BArF salts[a]

Entry	Substrate	Regulation Agent (as BArF salt)	ee
1	**39a**	-	64% (*S*)
2	**39a**	Na^+	50% (*S*)
3	**39a**	K^+	64% (*S*)
4	**39a**	Rb^+	64% (*S*)
5	**39a**	Cs^+	64% (*S*)
6	**39a**	(*S*)-**93**	64% (*S*)
7	**39a**	(*R*)-**93**	64% (*S*)
8	**39a**	(*S*,*S*)-**94**	64% (*S*)
9	**39a**	(*R*,*R*)-**94**	64% (*S*)
10	**39a**	**95**	64% (*S*)
11	**39d**	-	17% (*S*)
12	**39d**	Na^+	21% (*S*)
13	**39d**	K^+	21% (*S*)
14	**39d**	Rb^+	21% (*S*)
15	**39d**	Cs^+	18% (*S*)
16	**39d**	(*S*)-**93**	19% (*S*)
17	**39d**	(*R*)-**93**	18% (*S*)
18	**39d**	(*S*,*S*)-**94**	18% (*S*)
19	**39d**	(*R*,*R*)-**94**	18% (*S*)
20	**39d**	**95**	19% (*S*)

[a] Hydrogenations were carried out at 20 bar of H_2 pressure at room temperature. Rh/ligand/regulation agent/substrate ratio = 1/1.1/1.4/200. Substrate concentration [S] = 0.1 M. Reaction time = 24 hours. Results obtained at full conversion in all cases.

No clear improvements in the enantioselectivity were achieved with the regulation agents employed according to the results in Table 13. Actually, in the case of substrate **39a** the reaction afforded product **44a** in a moderate 64% ee without any added additive (entry 1) and in the presence of most of the salts employed (entries 3 – 10). Surprisingly, only the Na^+ cation modified the enantioselectivity of the process and the corresponding hydrogenation product **44a** was obtained in lower ee (50% of ee, entry 2). In the case of substrate **39d**

the enantioselectivities obtained were very low, ranging from 17 (entry 11) to 21% (entries 12 – 14). Again, it can be concluded that no significant changes in the enantioinduction of the catalyst were observed when the cationic crown ether binders were added to the reaction mixture.

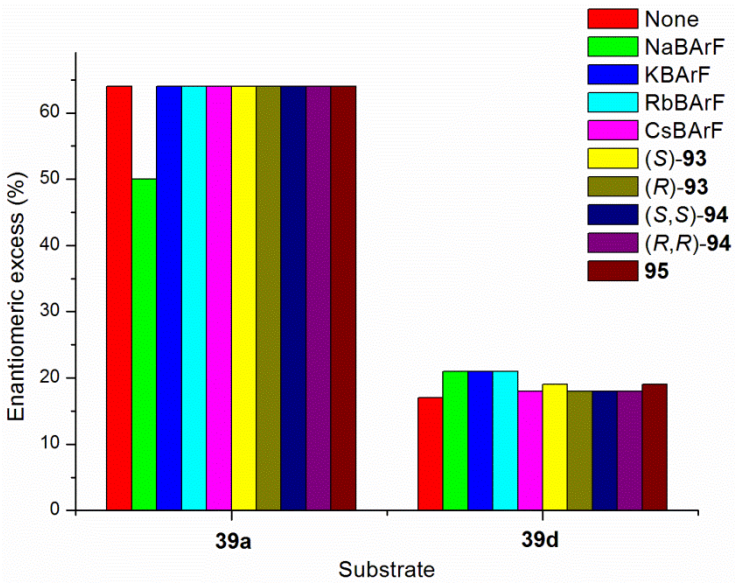

Figure 42. Summary on the results of asymmetric hydrogenation of substrates **39a**,**d** with Rh(I) catalysts derived from ligands (S_a)-**45b** with different cationic species

The low enantiomeric excesses of the asymmetric hydrogenation of substrates **39** with ligands **45** are in good agreement with literature reports. This lack of enantioinduction has been rationalized on the basis of the orientation of the four phenyl groups attached to the phosphorus atoms, which originate the asymmetric environment around the metal center. Then, the two equatorial P-phenyl rings exert a greater steric influence on the two diagonal quadrants while the two axial ones stay relatively open in the other two quadrants. The rotation and flexible orientation of the two equatorial P-phenyl groups can decrease the effectiveness of the chiral induction (See b in Figure 43). Indeed, this problem has been solved by some authors introducing covalently attached substituents at the 3,3'-positions on the chiral ligand backbone.[129] With this structural change, rotation of the equatorial phenyl groups could be restricted and an improvement of the enantioinduction level of the derived catalyst was observed (See c in

[129] a) Rankic, D. A.; Parvez, M.; Keay, B. A. *Tetrahedron: Asymmetry* **2012**, *23*, 754. b) Hopkins, J. M.; Dalrymple, S. A.; Parvez, M.; Keay, B. A. *Org. Lett.* **2005**, *7*, 3765. c) Wu, S.; He, M.; Zhang, X. *Tetrahedron: Asymmetry* **2004**, *15*, 2177.

Figure 43).[129c] For example, substrates **39b** and **39d** are hydrogenated in only 25 and 21% ee with Rh catalyst derived from ligand (S_a)-**63a**, whereas almost perfect enantioselectivity is achieved when ligand (S_a)-**63b** is employed for both substrates: > 99 and 98% ee, respectively.

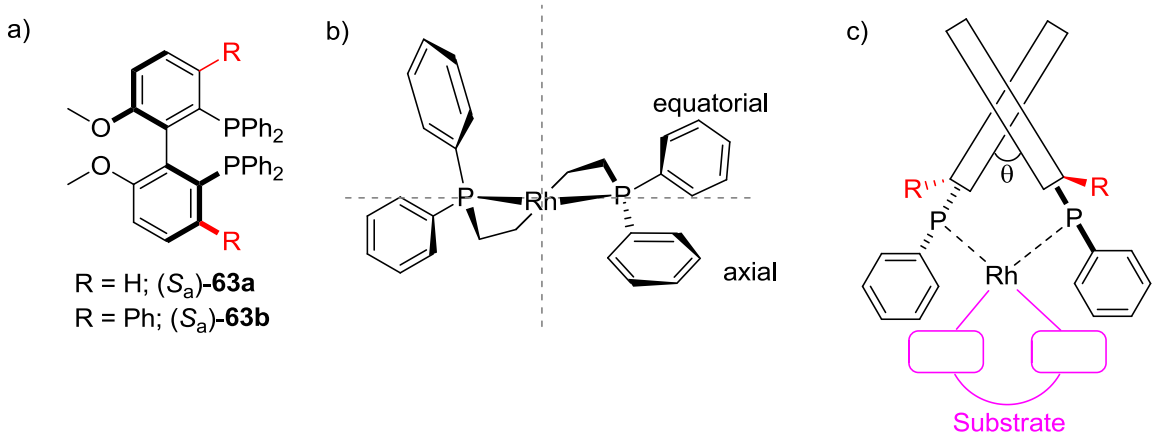

Figure 43. a) Unsubstituted (S_a)-**63a** and *ortho*-phenyl substituted analogue ligand (S_a)-**63b**. b) Quadrant diagram of (S_a)-**63a**. c) Design of (S_a)-**63b**

We assumed that the introduction of *ortho*-substituents to the P-groups in the bisphosphine ligands with appended crown ethers **45** would not be necessary. Since the binding of cationic species in the distal crown ether moiety could be sufficient to rigidify the catalyst structure and to restrict the flexibility of the P-phenyl groups. This idea would have permitted not only to obtain high levels of enantioselectivity but also to easily modulate the catalyst efficiency depending on the demands of the different substrates by addition of different cationic species.

Unfortunately, our predictions were not accomplished and the binding event inside the crown ether appears not to affect the free rotation and flexibility of the P-phenyl groups, whose spatial orientation generates the chiral pocket of the derived rhodium catalysts. As a future aim, it is proposed to prepare enantiomerically pure 3,3'-substituted biaryl ligands with appended crown ethers (Figure 44) and to study their regulation potential in the aforementioned transformation and in other interesting ones. These ligands would combine the improved active site of an *ortho*-substituted biaryl ligand with the possibility to fine-tune the geometry and flexibility of the ligand through non-covalent interactions.

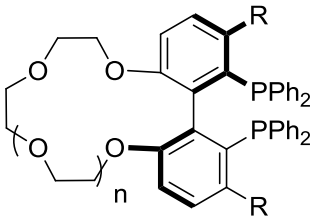

100

Figure 44. Target ligands with a distal regulation mechanism with a 3,3'-substituted biaryl backbone

EXPERIMENTAL PART

1.3 EXPERIMENTAL PART

1.3.1 General remarks

All syntheses were carried out using chemicals as purchased from commercial sources unless otherwise cited. All manipulations and reactions were performed under inert atmosphere. Glassware was dried *in vacuo* before use with a hot air gun. All solvents were dried and deoxygenated by using a Solvent Purification System (SPS). Silica gel 60 (230 – 400 mesh) or spherical Silica-C18 (200 – 400 mesh) was used for column chromatography. NMR spectra were recorded in $CDCl_3$ unless otherwise cited using a Bruker Avance 400 and 500 MHz Ultrashield spectrometers. ^{1}H NMR and ^{13}C NMR chemical shifts were quoted in ppm relative to residual solvent peaks, whereas $^{31}P\{^{1}H\}$ NMR chemical shifts were quoted in ppm relative to 85% phosphoric acid in water. IR spectra were recorded using Attenuated Total Reflection (ATR) technique unless otherwise cited. High-resolution mass spectra (HRMS) were recorded by using an electrospray ionization (ESI) method in positive mode on a Waters LCT Premier mass spectrometer. Melting points were determined in open capillaries and are uncorrected. UV spectra were recorded on a UV-vis spectrometer using 10 mm quartz cells. Emission spectra were recorded on an Aminco·Bowman Series 2 spectrofluorimeter using 10 mm quartz cells. Optical rotations were measured on a Jasco P-1030 polarimeter. ITC data were obtained on a VP-ITC Microcalorimeter, MicroCal, LLC (Northampton, MA). Enantiomeric excesses were determined by GC or HPLC on using chiral stationary phases. GC analyses were performed on an Agilent 6890N chromatograph equipped with a FID detector. HPLC analyses were performed on an Agilent 1200 Series chromatograph equipped with a diode array UV detector. Elemental analyses were performed on a LECO CHNS-932 elemental analyzer.

1.3.2 Synthetic procedure of crown ether-containing P=O receptors 81

*1.3.2.1 Synthetic procedure of the bistosylated polyethylene oxide derivatives **84a–e***

Bistosylated polyethylene oxide derivatives **84a–c** are commercially available. Compound **84e** was synthesized from catechol **89** and 8-Tosyloxy-3,6-dioxaoctanol **86** following a previously reported procedure.[130] Compound **84d** was synthesized following the same strategy than for **84e**.

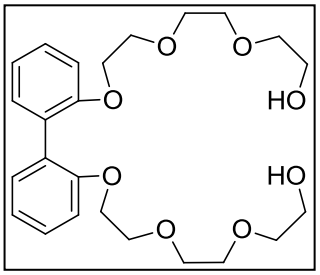

Compound 88: 8-Tosyloxy-3,6-dioxaoctanol **86**[130] (3.23 g, 10.61 mmol) and Cs_2CO_3 (4.89 g, 15 mmol) were added to [1,1'-biphenyl]-2,2'-diol **87** (1.00 g, 5.4 mmol) in dry DMF (140.0 mL) and the resulting mixture was heated at 70 °C for 24 h. The brown mixture was quenched with ice and then concentrated under reduced pressure. The crude product was purified by column chromatography over silica gel (EtOAc/MeOH 90/10 as the eluent) to afford the desired product **88** as yellow oil (1.02 g, 42% yield). ^{1}H NMR (400 MHz, $CDCl_3$) δ 7.26–7.20 (m, 4H), 6.97–6.91 (m, 4H), 4.07–4.04 (m, 4H), 3.65–3.49 (m, 16H), 2.92–2.84 (m, 4H); $^{13}C\{^1H\}$ NMR (100 MHz, $CDCl_3$) δ 156.6, 131.6, 128.42, 128.38, 120.6, 112.4, 72.5, 70.8, 70.4, 69.6, 68.5, 61.6. Spectroscopic data for this compound were in agreement with the reported ones.[131]

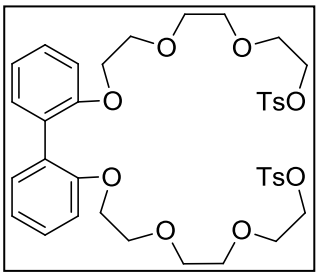

Compound 84d: Compound **88** (0.25 g, 0.55 mmol) was dissolved in 30.0 mL of THF and a solution of sodium hydroxide (80 mg, 2.00 mmol) in H_2O (20.0 mL) was added at 0 ºC (ice bath). A solution of tosyl chloride (1.05 g, 5.50 mmol) in THF (60.0 mL) was added dropwise (3 h) to the above solution. The mixture was further stirred overnight, THF was evaporated under reduced pressure and the residue was extracted with ethyl acetate (3 x 30 mL) and dried over anhydrous magnesium sulfate. The crude product was purified by column chromatography over silica gel (hexane/EtOAc 30/70 as the eluent) to afford **84d** (300 mg, 72% yield). IR (neat,

[130] Zhu, X.-Z.; Chen, C.-F. *J. Am. Chem. Soc.* **2005**, *127*, 13158.
[131] Czech, B.; Czech, A.; Bartsch, R. A. *J. Heterocycl. Chem.* **1984**, *21*, 341.

cm^{-1}) υ 3270, 3067, 2919, 2873, 1646, 1596, 1540, 1530, 1480, 1439, 1399, 1355, 1289, 1262, 1237, 1188, 1176, 1123, 1096, 1058, 921, 816, 755, 663, 554; ^{1}H NMR (400 MHz, $CDCl_3$) δ 7.78 (d, *J* = 8.2 Hz, 4H), 7.32 (d, *J* = 8.2 Hz, 4H), 7.29–7.24 (m, 4H), 6.99–6.92 (m, 4H), 4.12–4.03 (m, 8H), 3.66–3.58 (m, 8H), 3.45–3.40 (m, 8H), 2.43 (s, 6H); ^{13}C{^{1}H} NMR (100 MHz, $CDCl_3$) δ 156.3, 144.8, 133.0, 131.6, 129.8, 128.4, 128.3, 127.9, 120.5, 112.4, 70.8, 69.7, 69.2, 68.6, 68.5, 21.6; HRMS (ESI$^+$): m/z [M+Na]$^+$ calcd for $C_{38}H_{46}O_{12}S_2Na$ 781.2328, found 781.2294.

*1.3.2.2 General synthetic procedure for receptors (rac)-**81a–e***

In a 250 mL dry two-necked flask, a solution of (*rac*)-**80**[132] (0.85 mmol) and Cs_2CO_3 (8.50 mmol) in dry DMF (60.0 mL) was stirred for 1.5 h at 60 ºC under argon. To this solution, 0.85 mmol of the corresponding bistosylate derivative (**84a–e**) dissolved in 50.0 mL of DMF were added very slowly (6–8 h) under argon. The reaction mixture was stirred at 60 ºC for another 12–14 h. The mixture was then quenched with water (5.0 mL) and the solvents removed *in vacuo* at 50 ºC. The resulting aqueous solution was extracted with EtOAc (3 x 40.0 mL) and the combined organic layers were dried over $MgSO_4$, filtered and evaporated. The resulting residue was purified by flash chromatography on SiO_2 using EtOAc/MeOH as eluent to give the expected crown ether receptors (*rac*)-**81a–e**.

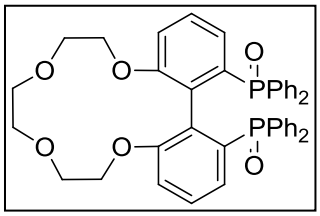

Compound (*rac*)-81a: Compound (*rac*)-**81a** was synthesized following the general procedure, from bistosylate **84a** (0.390 g, 0.85 mmol), Cs_2CO_3 (2.77 g, 8.50 mmol) and (*rac*)-**80** (0.500 g, 0.85 mmol). The product was obtained as a white solid (0.250 g, 42% yield) after chromatography with silica gel (EtOAc/MeOH 90/10 as the eluent). Mp: 298–305 °C; IR (neat, cm^{-1}) υ 3053, 2886, 1567, 1435, 1258, 1191, 1116, 742, 694, 533; ^{1}H NMR (400 MHz, $CDCl_3$) δ 7.74–7.58 (m, 8H), 7.44–7.33 (m, 12H), 7.21–7.17 (m, 2H), 6.82–6.75 (m, 4H), 3.90–3.84 (m, 2H), 3.55–3.52 (m, 2H), 3.40–3.21 (m, 8H).

[132] a) Schmid, R.; Foricher, J.; Cereghetti, M.; Schoenholzer, P. *Helv. Chim. Acta* **1991**, *74*, 370. b) Qiu, L. Q.; Qi, J. Y.; Ji, J. X.; Zhou, Z. Y.; Yeung, C. H.; Choi, M. C. K.; Chan, A. S. C. *Acta Crystallogr., Sect. C: Cryst. Struct. Commun.* **2003**, *C59*, o33.

$^{13}C\{^{1}H, ^{31}P\}$ NMR (100 MHz, $CDCl_3$) δ 156.0, 134.9, 133.9, 133.2, 132.6, 132.4, 130.9, 130.6, 130.5, 128.0, 127.6, 127.5, 124.7, 113.4, 70.2, 69.5, 66.1; $^{31}P\{^{1}H\}$ NMR (162 MHz, $CDCl_3$) δ 31.8 (s); HRMS (ESI^+): m/z $[M+H]^+$ calcd for $C_{42}H_{39}O_6P_2$ 701.2144, found 701.2199.

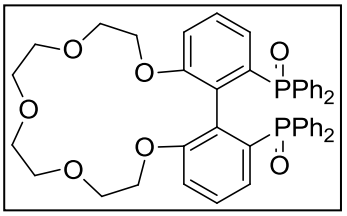

Compound (*rac*)-81b: Compound (*rac*)-**81b** was synthesized following the general procedure, from bistosylate **84b** (0.350 g, 0.68 mmol), Cs_2CO_3 (2.22 g, 6.80 mmol) and (*rac*)-**80** (0.400 g, 0.68 mmol). The product was obtained as a white solid (0.258 g, 51% yield) after chromatography with silica gel (EtOAc/MeOH 92/8 as the eluent). Mp: 268–275 °C; IR (neat, cm^{-1}) υ 3391, 3054, 2866, 1569, 1437, 1260, 1192, 1116, 749, 697, 534; ^{1}H NMR (400 MHz, $CDCl_3$) δ 7.71–7.64 (m, 8H), 7.48–7.28 (m, 12H), 7.21 (ddd, *J* = 7.8 Hz, *J* = 3.6 Hz, 2H), 6.91–6.81 (m, 4H), 3.87–3.83 (m, 2H), 3.47–3.28 (m, 10H), 3.17–3.02 (m, 4H); $^{13}C\{^{1}H,^{31}P\}$ NMR (125 MHz, $CDCl_3$) δ 156.7, 135.4, 134.0, 132.4, 132.3, 132.2, 131.0, 130.9, 130.8, 128.0, 127.8, 127.6, 125.3, 113.7, 71.4, 71.2, 69.7, 67.7; $^{31}P\{^{1}H\}$ NMR (162 MHz, $CDCl_3$) δ 31.8 (s); HRMS (ESI^+): m/z $[M+H]^+$ calcd for $C_{44}H_{43}O_7P_2$ 745.2406, found 745.2480.

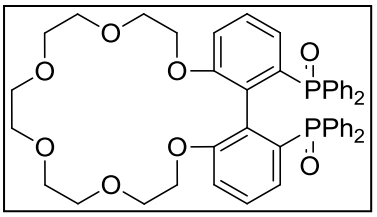

Compound (*rac*)-81c: Compound (*rac*)-**81c** was synthesized following the general procedure, from bistosylate **84c** (0.466 g, 0.85 mmol), Cs_2CO_3 (2.77 g, 8.50 mmol) and (*rac*)-**80** (0.500 g, 0.85 mmol). The product was obtained as a white solid (0.310 g, 45% yield) after chromatography with silica gel (EtOAc/MeOH 90/10 as the eluent). Mp: 274–278 °C; IR (neat, cm^{-1}) υ 3055, 2886, 1566, 1483, 1253, 1190, 1116, 1066, 742, 694, 533; ^{1}H NMR (400 MHz, $CDCl_3$) δ 7.69–7.63 (m, 8H), 7.50–7.21 (m, 12H), 7.26–7.21 (m, 2H), 6.88–6.83 (m, 4H), 3.87–3.81 (m, 2H), 3.62–3.21 (m, 16H), 3.07–3.01 (m, 2H); $^{13}C\{^{1}H,^{31}P\}$ NMR (125 MHz, $CDCl_3$) δ 156.6, 135.3, 134.0, 132.4, 132.3, 132.2, 130.9, 130.6, 128.0, 127.8, 127.7, 125.2, 113.6, 71.0, 70.8, 70.7, 69.0, 68.0; $^{31}P\{^{1}H\}$ NMR (162 MHz, $CDCl_3$) δ 31.5 (s); HRMS (ESI^+): m/z $[M+H]^+$ calcd for $C_{46}H_{47}O_8P_2$ 789.2668, found 789.2723.

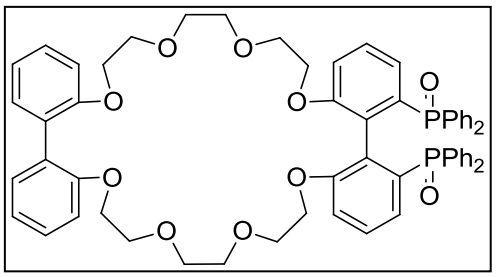

Compound (*rac*)-81d: Compound (*rac*)-**81d** was synthesized following the general procedure, from bistosylate **84d** (0.645 g, 0.85 mmol), Cs_2CO_3 (2.77 g, 8.50 mmol) and (*rac*)-**80** (0.500 g, 0.85 mmol). The product was obtained as a white solid (0.420 g, 49% yield) after chromatography with silica gel (EtOAc/MeOH 90/10 as the eluent). Mp: 125–130 ºC; IR (neat, cm^{-1}) υ 3407, 3192, 3088, 2917, 2870, 1627, 1568, 1436, 1393, 1283, 1258, 1202, 1153, 1112, 1050, 1035, 720, 709, 692, 531; ^1H NMR (400 MHz, $CDCl_3$) δ 7.74–7.61 (m, 8H), 7.52–7.35 (m, 8H), 7.34–7.14 (m, 10H), 7.03–6.79 (m, 8H), 4.07–3.99 (m, 4H), 3.85–3.73 (m, 2H), 3.68–3.52 (m, 4H), 3.39–3.17 (m, 10H), 3.15–3.06 (m, 2H), 2.98–2.88 (m, 2H); $^{13}C\{^1H,^{31}P\}$ NMR (100 MHz, $CDCl_3$) δ 156.5, 135.2, 133.9, 132.5, 132.4, 132.3, 131.2, 131.0, 130.9, 128.8, 128.5, 128.0, 127.9, 127.7, 125.2, 120.6, 113.4, 112.3, 70.8, 70.7, 69.7, 68.9, 68.0, 67.8; $^{31}P\{^1H\}$ NMR (162 MHz, $CDCl_3$) δ 31.5 (s); HRMS (ESI^+): m/z $[M+H]^+$ calcd for $C_{60}H_{59}O_{10}P_2$ 1001.3505, found 1001.3596.

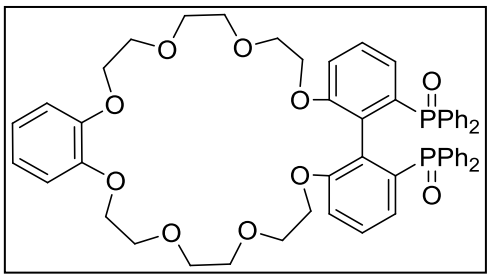

Compound (*rac*)-81e: Compound (*rac*)-**81e** was synthesized following the general procedure, from bistosylate **84e** (0.410 g, 0.60 mmol), Cs_2CO_3 (1.96 g, 6.01 mmol) and (*rac*)-**80** (0.352 g, 0.60 mmol). The product was obtained as a white solid (0.305 g, 65% yield) after chromatography with silica gel (EtOAc/MeOH 90/10 as the eluent). Mp: 148–150 ºC; IR (neat, cm^{-1}) υ 3055, 2864, 1567, 1504, 1434, 1254, 1195, 1114, 943, 745, 693, 523; ^1H NMR (400 MHz, $CDCl_3$) δ 7.71–7.63 (m, 8H), 7.49–7.30 (m, 12H), 7.23–7.19 (m, 2H), 6.91–6.83 (m, 8H), 4.14–4.08 (m, 4H), 3.82–3.79 (m, 6H), 3.61–3.48 (m, 4H), 3.36–3.17 (m, 8H), 2.97–2.92 (m, 2H); $^{13}C\{^1H,^{31}P\}$ NMR (100 MHz, $CDCl_3$) δ 156.5, 149.1, 135.2, 134.0, 132.5, 132.4, 132.2, 131.0, 130.9, 128.0, 127.8, 127.7, 125.2, 121.5, 114.4, 113.4, 71.0, 70.8, 69.9, 69.3, 69.0, 68.1; $^{31}P\{^1H\}$ NMR (162 MHz, $CDCl_3$) δ 31.5 (s); HRMS (ESI^+): m/z $[M+H]^+$ calcd for $C_{54}H_{55}O_{10}P_2$ 925.3192, found 925.3276.

1.3.3 Measurements of binding constants by UV-vis absorption spectroscopy

Solutions of the receptors (*rac*)-**81** (*ca.* 10^{-4} M) were prepared in DCM/MeOH (99.5/0.5 v/v). Solutions of the corresponding dicarboxylic acids (*ca.* 10^{-2} M) were also prepared in the same solvent mixture. The receptor solution was placed in a 1 cm quartz cell. The titration was carried out by adding at 298 K incremental amounts of guest (dicarboxylic acids) to the host solution (receptors (*rac*)-**81a**–**e** or Li^+ or Na^+•(*rac*)-**81a**–**e** [prepared *in situ* by adding 10 equivalents of the corresponding perchlorate to (*rac*)-**81a**–**e**]), which led to changes in the absorbance. UV-visible titration data was analyzed using multivariate factor analysis and considering a binding model with two colored stoichiometric states of the crown ethers: unbound, and 1:1 complex.[133] SPECFIT software (Version 3.0; Spectra Software Associates) was used.[134]

*1.3.3.1 Qualitative binding determination of (rac)-**81a** and different carboxylic acids*

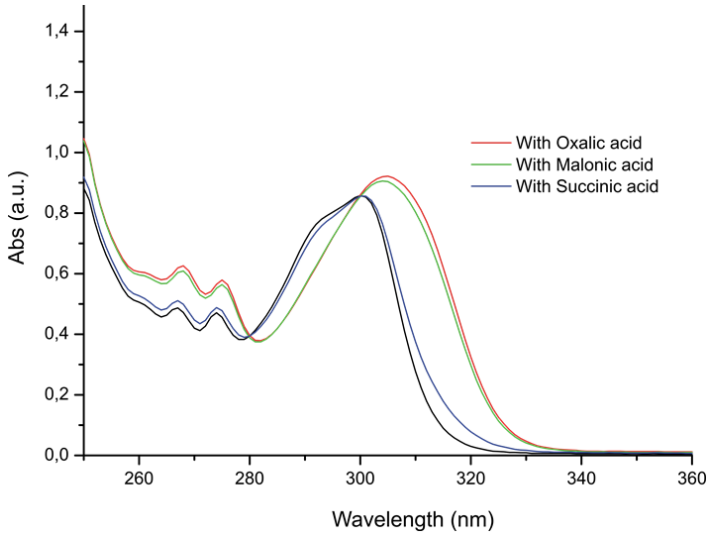

Figure 45. Change in UV-vis spectrum of (*rac*)-**81a** (1.17×10^{-4} M) upon addition of excess amount (10 equivalents) of different dicarboxylic acids in DCM/MeOH mixture (95.5/0.5 v/v) at 298 K (same type of spectral change was observed for other receptors)

[133] a) Connors, K. A. *Binding Constants: The measurement of Molecular Complex Stability*, John Wiley & Sons, New York, N. Y. 1987, 350 pp. b) Novikov, E.; Stobiecka, A.; Boens, N. *J. Phys. Chem. A* **2000**, *104*, 5388.
[134] a) Gampp, H.; Maeder, M.; Meyer, C. J.; Zuberbuehler, A. D. *Talanta* **1985**, *32*, 95. b) Gampp, H.; Maeder, M.; Meyer, C. J.; Zuberbuehler, A. D. *Talanta* **1986**, *33*, 943.

*1.3.3.2 Quantitative binding determination of **81** with different carboxylic acids*

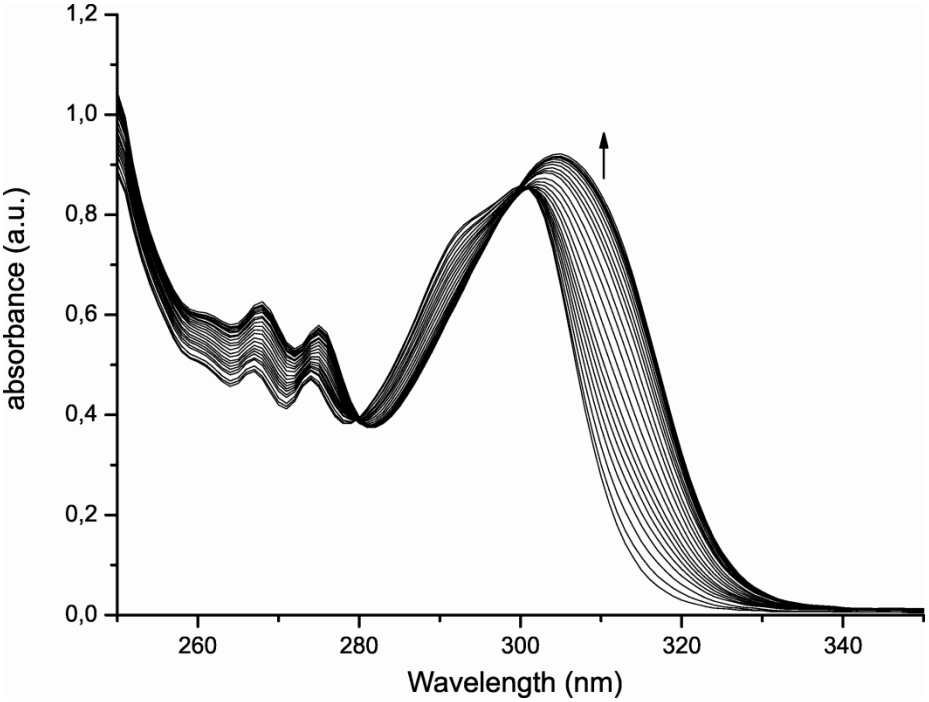

Figure 46. UV-vis titration: (*rac*)-**81a** (1.17 x 10^{-4} – 1.12 x 10^{-4} M) upon addition of different amounts of oxalic acid (0 M – 6.89 x 10^{-4} M) in DCM/MeOH (99.5/0.5 v/v) at 298 K

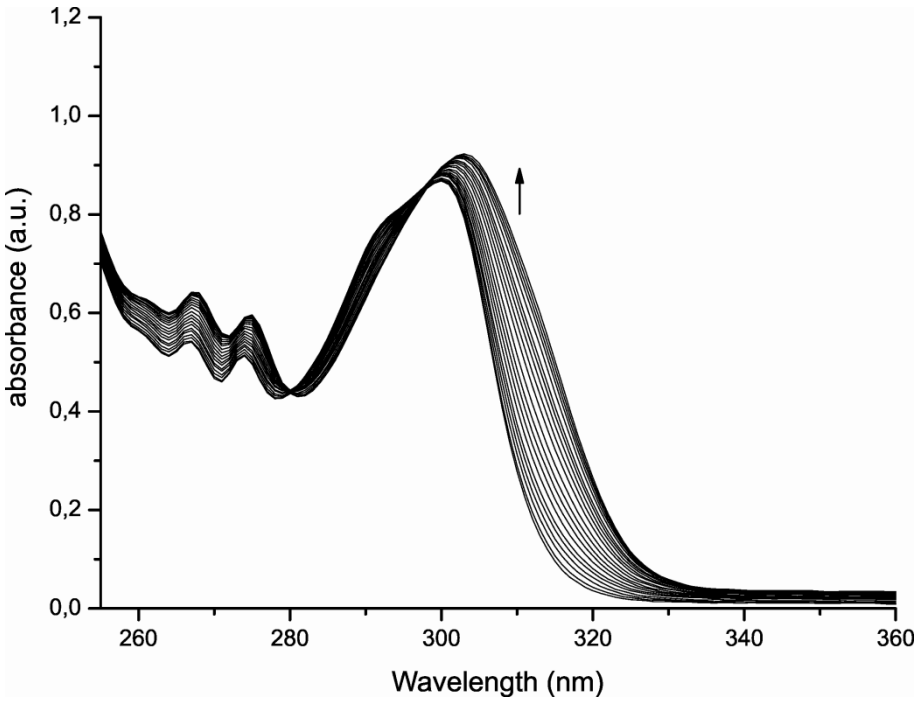

Figure 47. UV-vis titration: (*rac*)-**81a** (1.23 x 10^{-4} – 1.17 x 10^{-4} M) upon addition of different amounts of malonic acid (0 M – 6.80 x 10^{-4} M) in DCM/MeOH (99.5/0.5 v/v) at 298 K

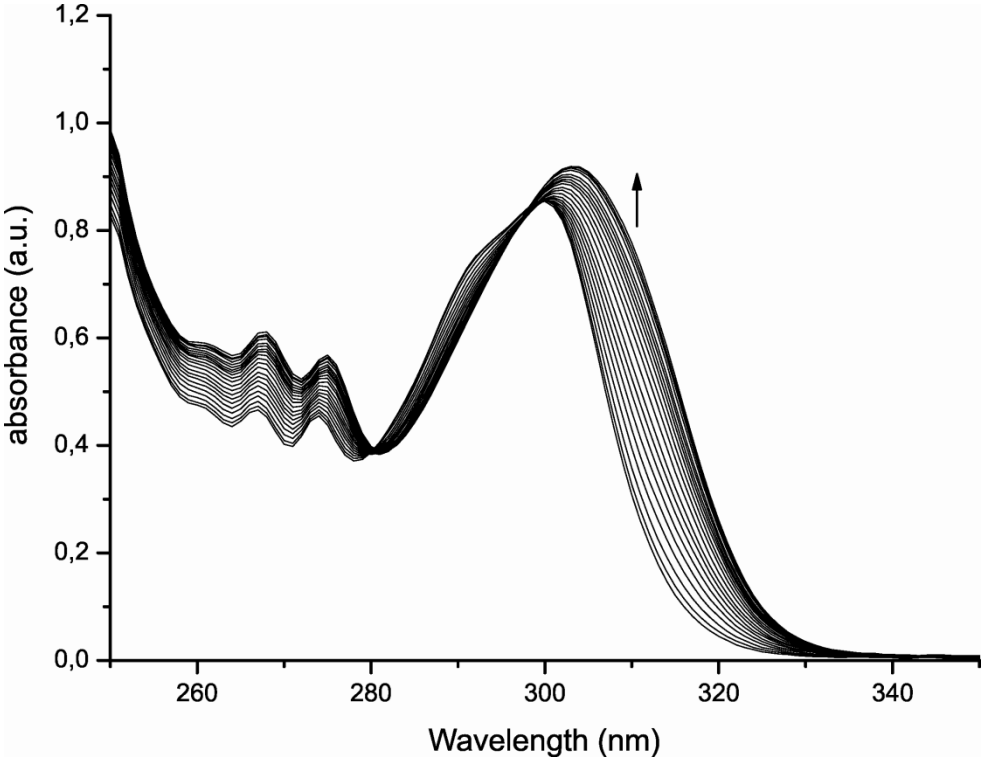

Figure 48. UV-vis titration: (*rac*)-**81b** (1.14×10^{-4} – 1.09×10^{-4} M) upon addition of different amounts of oxalic acid (0 M – 6.96×10^{-4} M) in DCM/MeOH (99.5/0.5 v/v) at 298 K

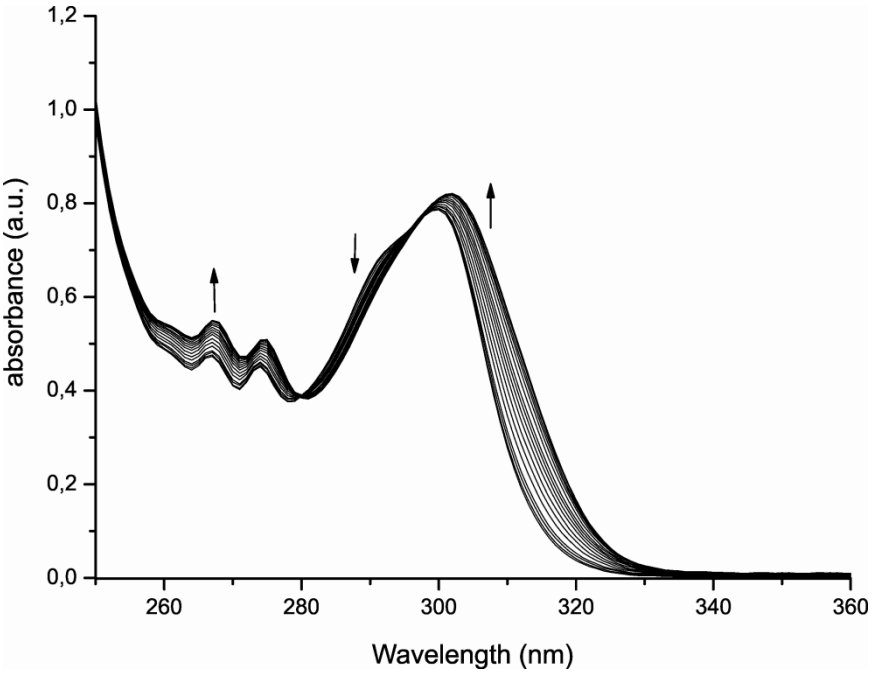

Figure 49. UV-vis titration: (*rac*)-**81b** (1.19×10^{-4} – 1.12×10^{-4} M) upon addition of different amounts of malonic acid (0 M – 8.72×10^{-4} M) in DCM/MeOH (99.5/0.5 v/v) at 298 K

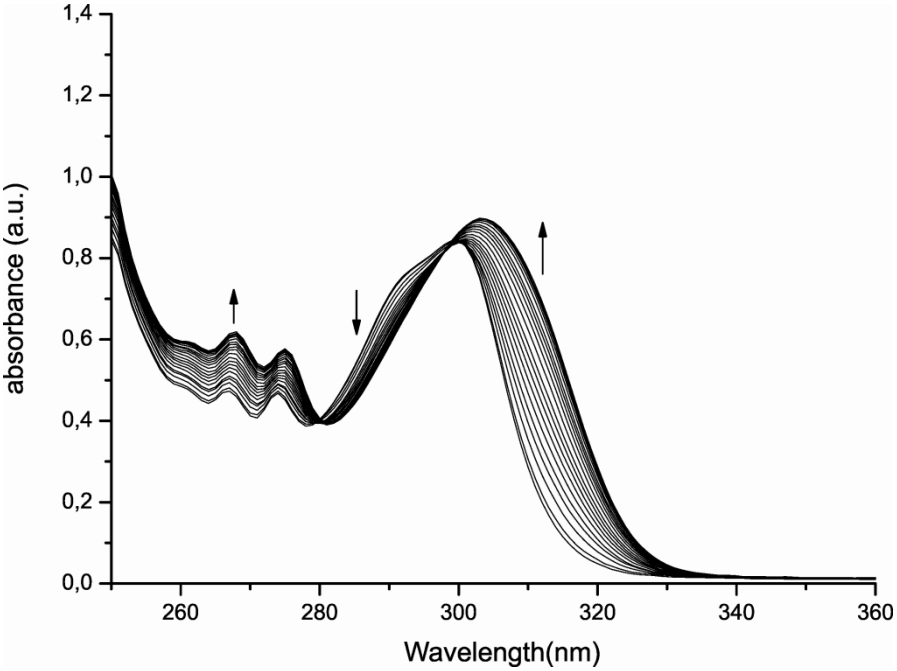

Figure 50. UV-vis titration: (*rac*)-**81c** (1.12×10^{-4} – 1.08×10^{-4} M) upon addition of different amounts of oxalic acid (0 M – 7.27×10^{-4} M) in DCM/MeOH (99.5/0.5 v/v) at 298 K

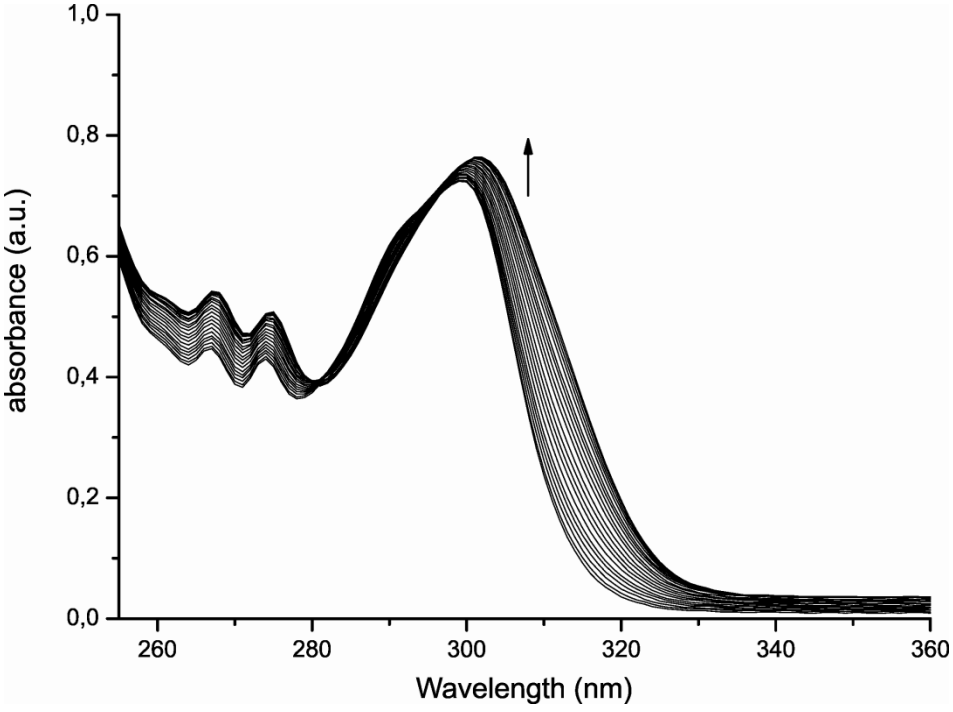

Figure 51. UV-vis titration: (*rac*)-**81c** (1.05×10^{-4} – 1.00×10^{-4} M) upon addition of different amounts of malonic acid (0 M – 6.80×10^{-4} M) in DCM/MeOH (99.5/0.5 v/v) at 298 K

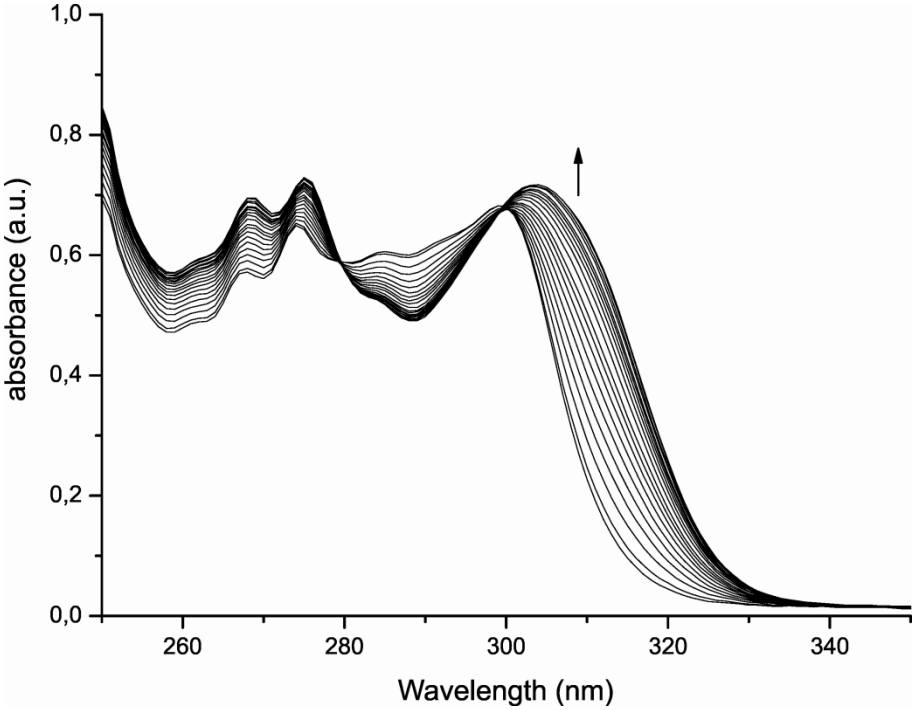

Figure 52. UV-vis titration: (*rac*)-**81e** (9.83 x 10^{-5} – 9.40 x 10^{-5} M) upon addition of different amounts of oxalic acid (0 M – 7.59 x 10^{-4} M) in DCM/MeOH (99.5/0.5 v/v) at 298 K

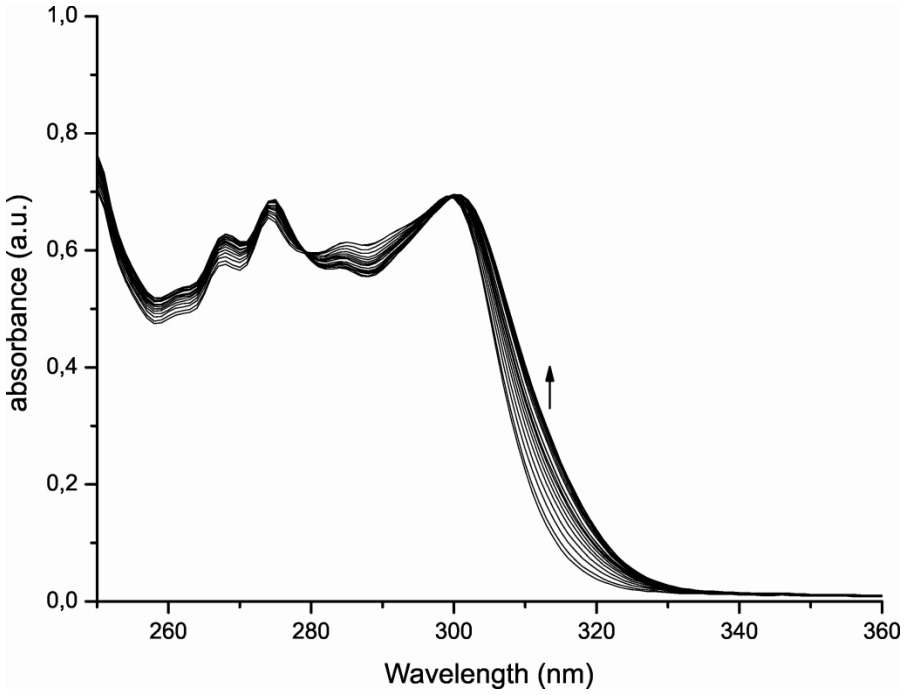

Figure 53. UV-vis titration: (*rac*)-**81e** (9.83 x 10^{-5} – 9.42 x 10^{-5} M) upon addition of different amounts of malonic acid (0 M – 1.32 x 10^{-3} M) in DCM/MeOH (99.5/0.5 v/v) at 298 K

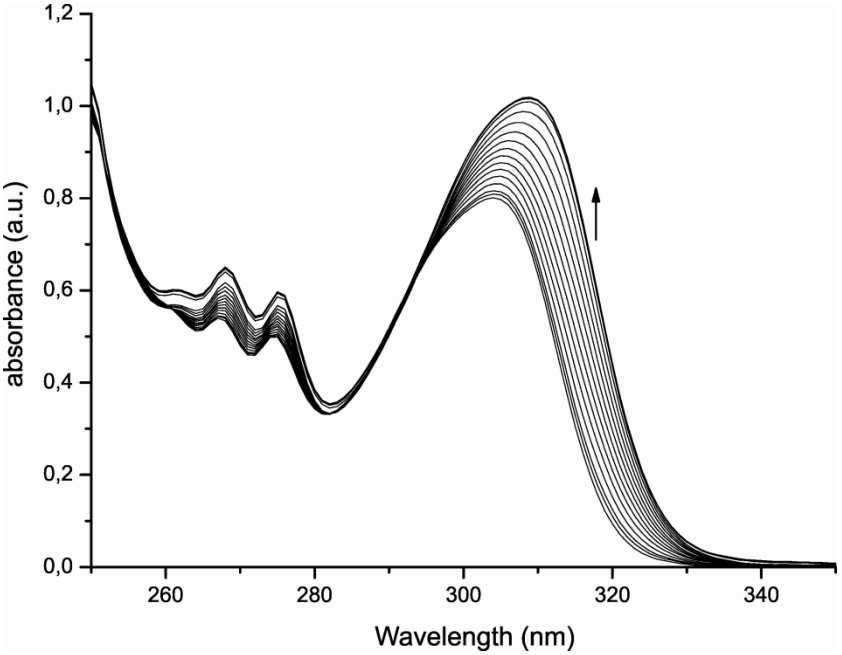

Figure 54. UV-vis titration: Li^+•(*rac*)-**81a** (1.20 x 10^{-4} M – 1.17x 10^{-4} M in (*rac*)-**81a** and 10 equivalents of $LiClO_4$) upon addition of different amounts of oxalic acid (0 M – 1.63 x 10^{-4} M) in DCM/MeOH (99.5/0.5 v/v) at 298 K

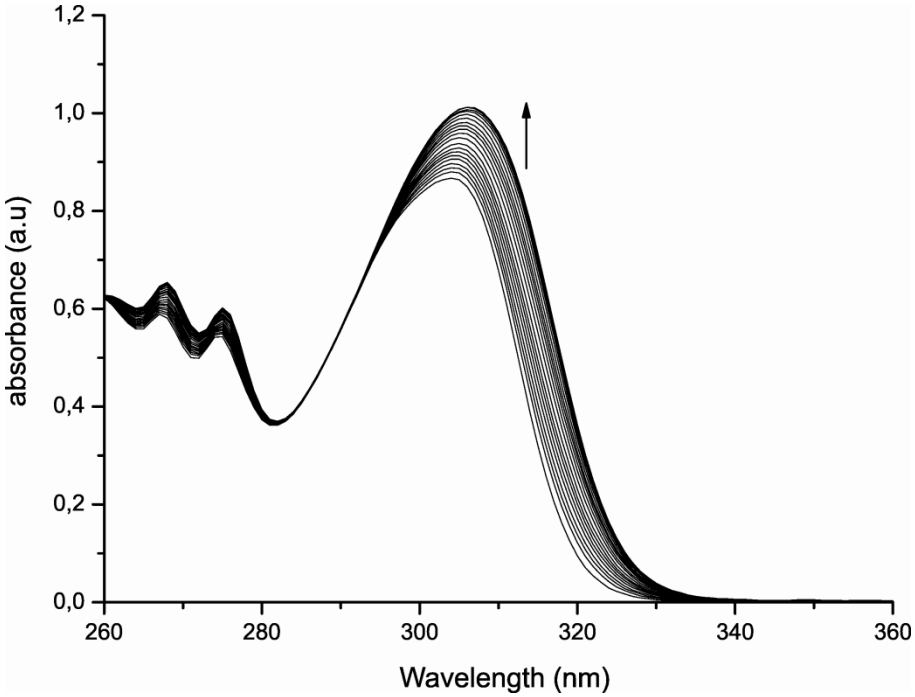

Figure 55. UV-vis titration: Li^+•(*rac*)-**81a** (1.17 x 10^{-4} M – 1.13 x 10^{-4} M in (*rac*)-**81a** and 10 equivalents of $LiClO_4$) upon addition of different amounts of malonic acid (0 M – 4.87 x 10^{-4} M) in DCM/MeOH (99.5/0.5 v/v) at 298 K

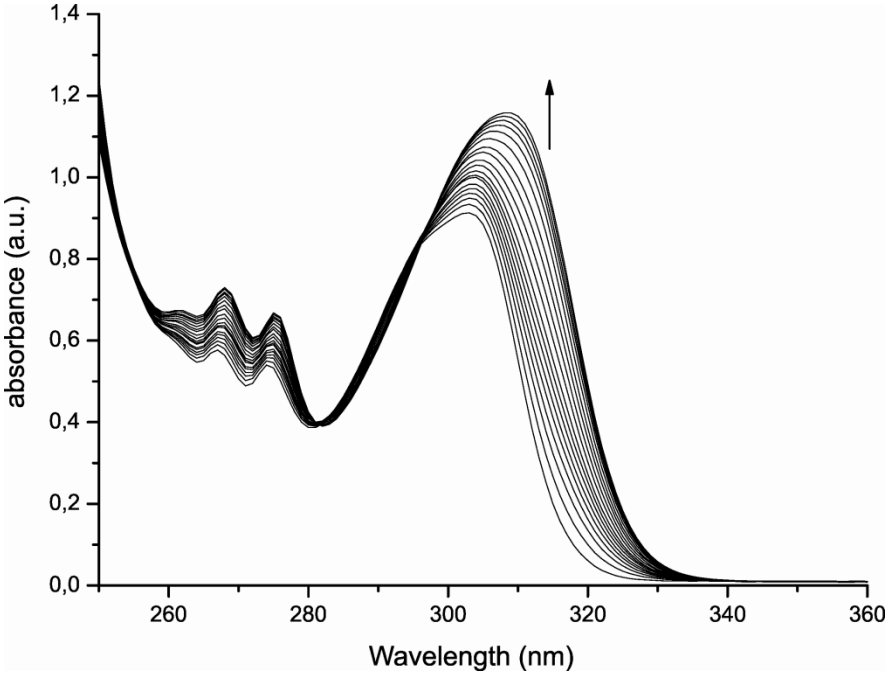

Figure 56. UV-vis titration: Na^+•(*rac*)-**81a** (1.23×10^{-4} M – 1.20×10^{-4} M in (*rac*)-**81a** and 10 equivalents of $NaClO_4$) upon addition of different amounts of oxalic acid (0 M – 2.88×10^{-4} M) in DCM/MeOH (99.5/0.5 v/v) at 298 K

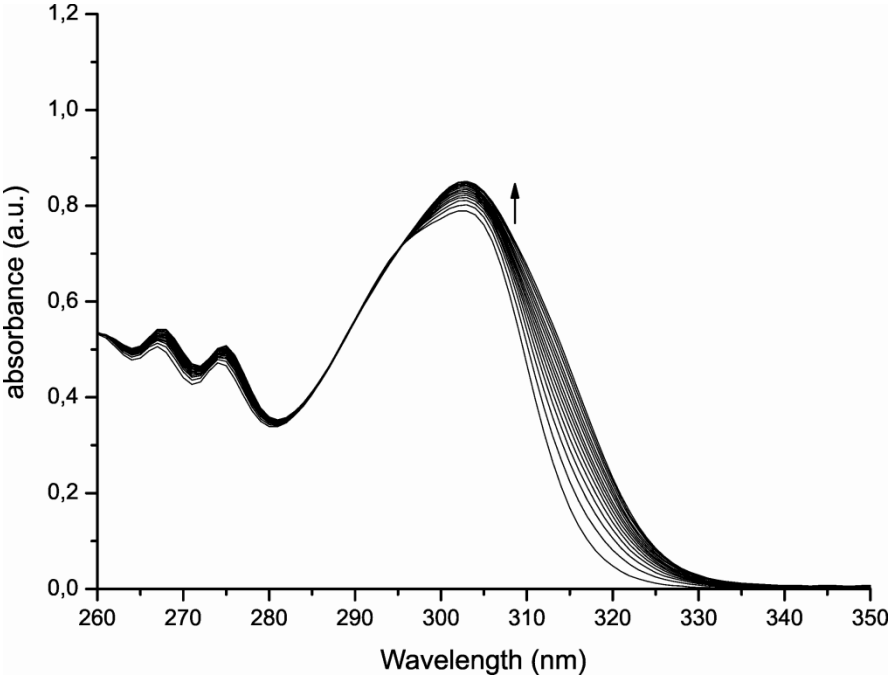

Figure 57. UV-vis titration: Na^+•(*rac*)-**81a** (1.20×10^{-4} M – 1.16×10^{-4} M in (*rac*)-**81a** and 10 equivalents of $NaClO_4$) upon addition of different amounts of malonic acid (0 M – 4.06×10^{-4} M) in DCM/MeOH (99.5/0.5 v/v) at 298 K

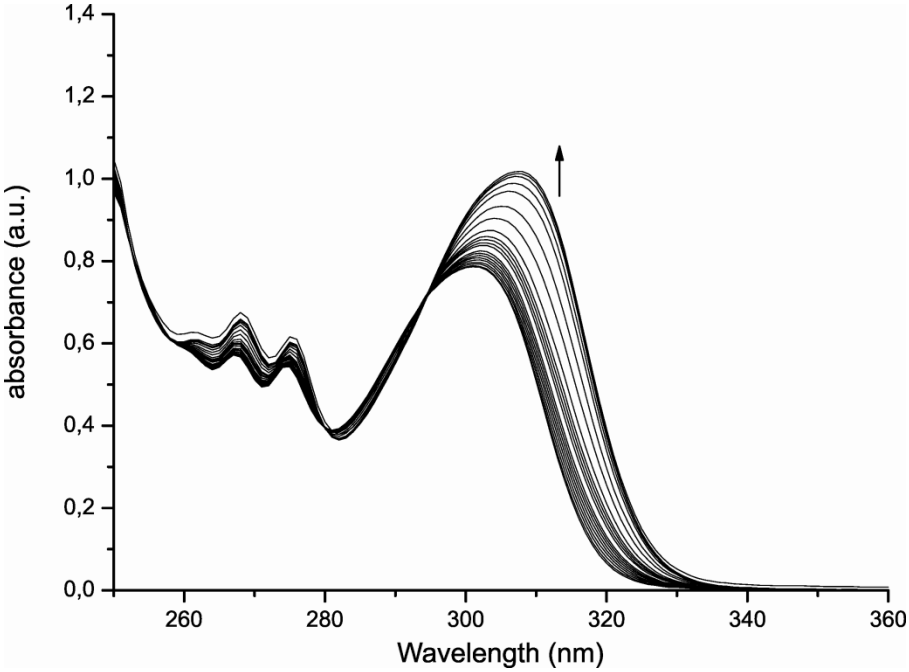

Figure 58. UV-vis titration: Li^+•(*rac*)-**81b** (1.14 x 10^{-4} M – 1.02 x 10^{-4} M in (*rac*)-**81b** and 10 equivalents of $LiClO_4$) upon addition of different amounts of oxalic acid (0 M – 2.75 x 10^{-4} M) in DCM/MeOH (99.5/0.5 v/v) at 298 K

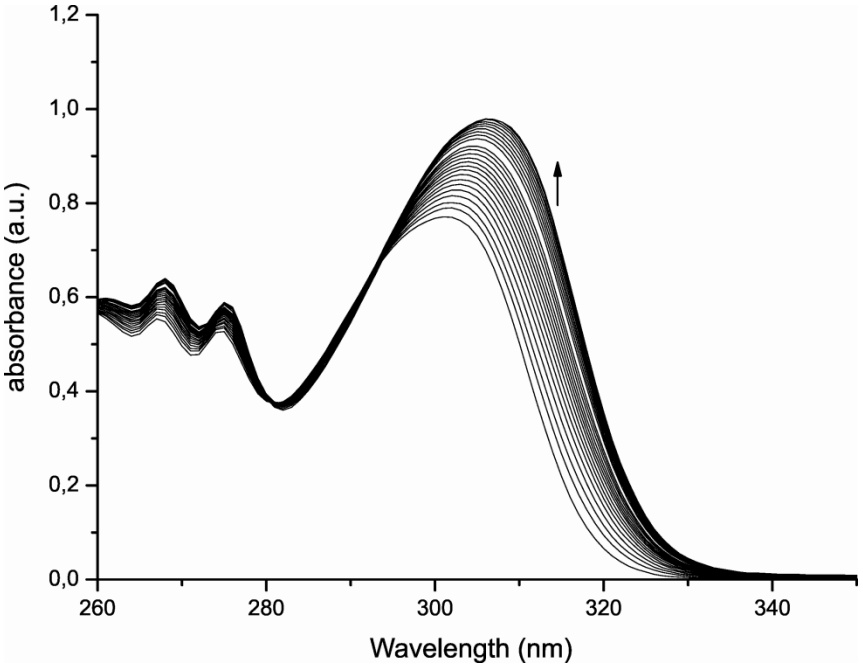

Figure 59. UV-vis titration: Li^+•(*rac*)-**81b** (1.14 x 10^{-4} M – 1.08 x 10^{-4} M in (*rac*)-**81b** and 10 equivalents of $LiClO_4$) upon addition of different amounts of malonic acid (0 M – 7.86 x 10^{-4} M) in DCM/MeOH (99.5/0.5 v/v) at 298 K

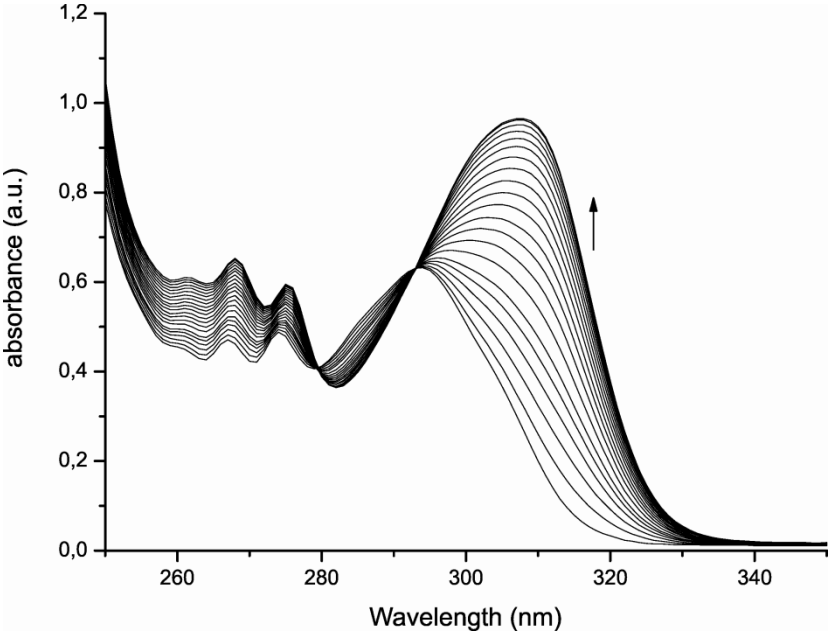

Figure 60. UV-vis titration: Na^+•(*rac*)-**81b** (1.20×10^{-4} M – 1.15×10^{-4} M in (*rac*)-**81b** and 10 equivalents of $NaClO_4$) upon addition of different amounts of oxalic acid (0 M – 4.12×10^{-4} M) in DCM/MeOH (99.5/0.5 v/v) at 298 K

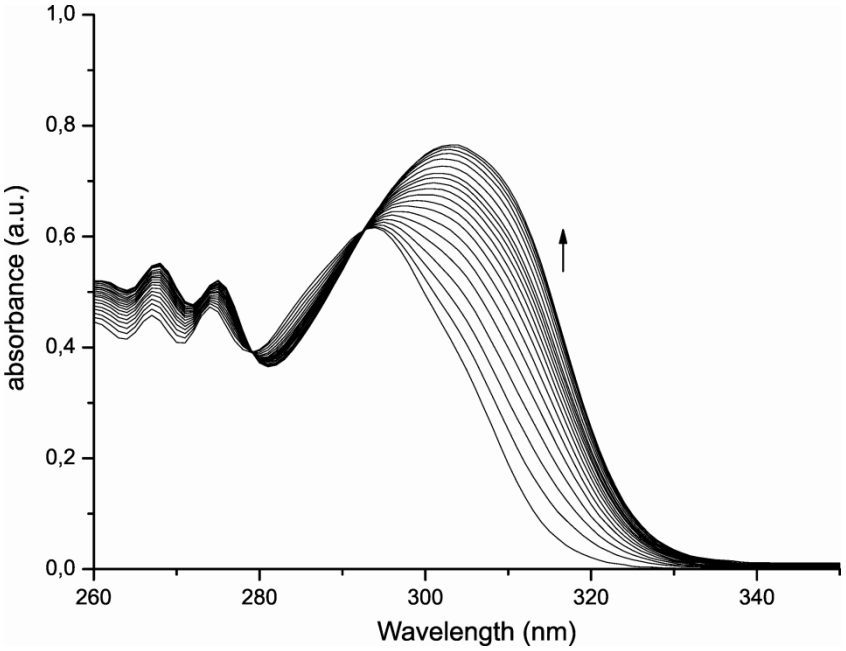

Figure 61. UV-vis titration: Na^+•(*rac*)-**81b** (1.10×10^{-4} M – 1.05×10^{-4} M in (*rac*)-**81b** and 10 equivalents of $NaClO_4$) upon addition of different amounts of malonic acid (0 M – 4.77×10^{-4} M) in DCM/MeOH (99.5/0.5 v/v) at 298 K

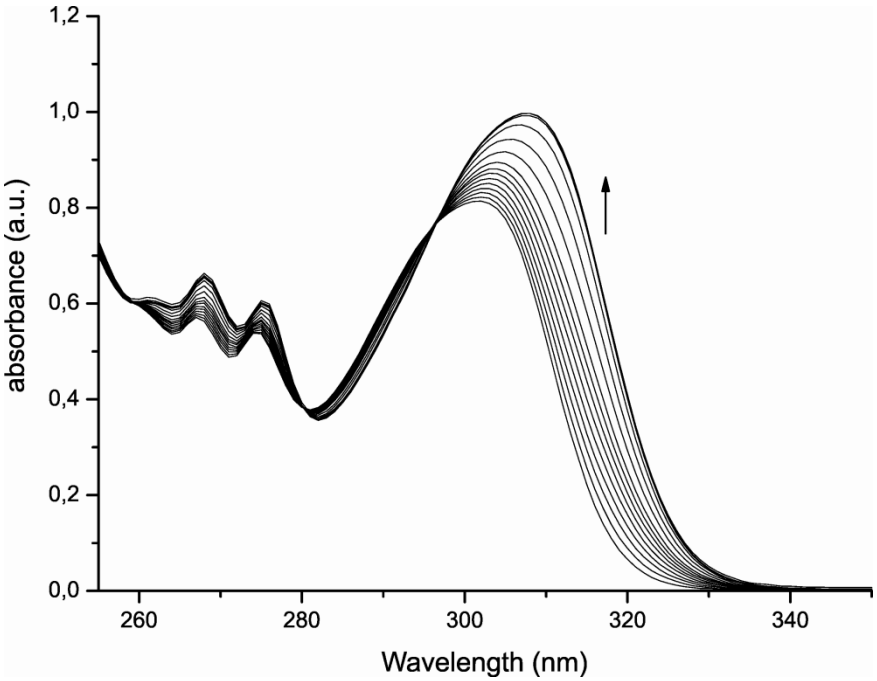

Figure 62. UV-vis titration: Li^+•(*rac*)-**81c** (1.12×10^{-4} M – 1.02×10^{-4} M in (*rac*)-**81c** and 10 equivalents of $LiClO_4$) upon addition of different amounts of oxalic acid (0 M – 2.48×10^{-4} M) in DCM/MeOH (99.5/0.5 v/v) at 298 K

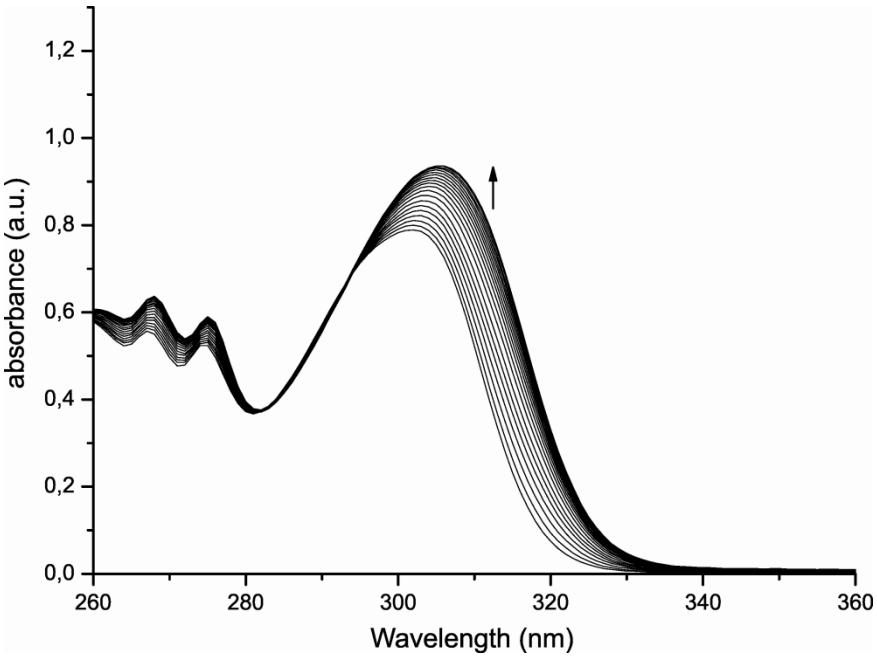

Figure 63. UV-vis titration: Li^+•(*rac*)-**81c** (1.12×10^{-4} M – 1.08×10^{-4} M in (*rac*)-**81c** and 10 equivalents of $LiClO_4$) upon addition of different amounts of malonic acid (0 M – 6.25×10^{-4} M) in DCM/MeOH (99.5/0.5 v/v) at 298 K

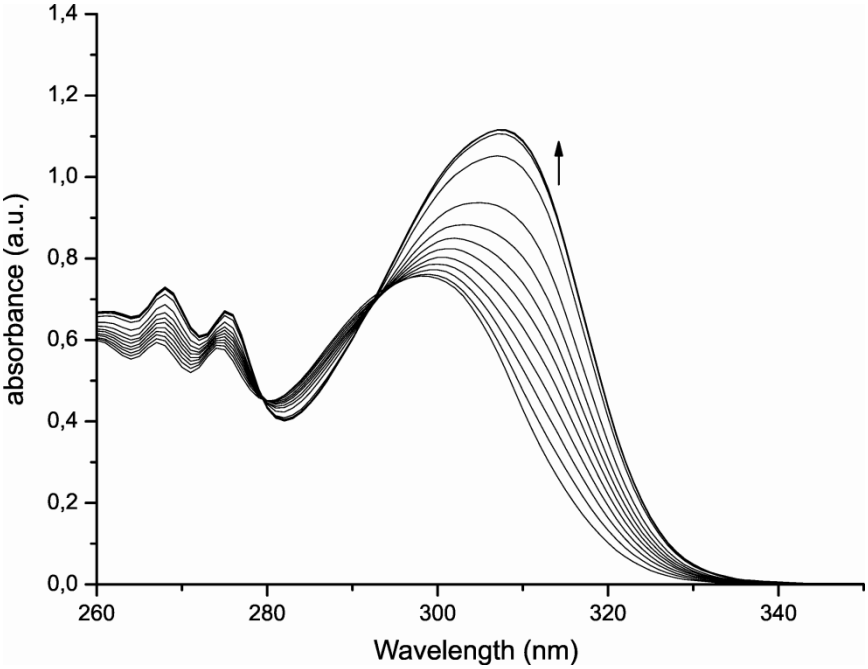

Figure 64. UV-vis titration: Na^+•(*rac*)-**81c** (1.12×10^{-4} M – 1.09×10^{-4} M in (*rac*)-**81c** and 10 equivalents of $NaClO_4$) upon addition of different amounts of oxalic acid (0 M – 2.12×10^{-4} M) in DCM/MeOH (99.5/0.5 v/v) at 298 K

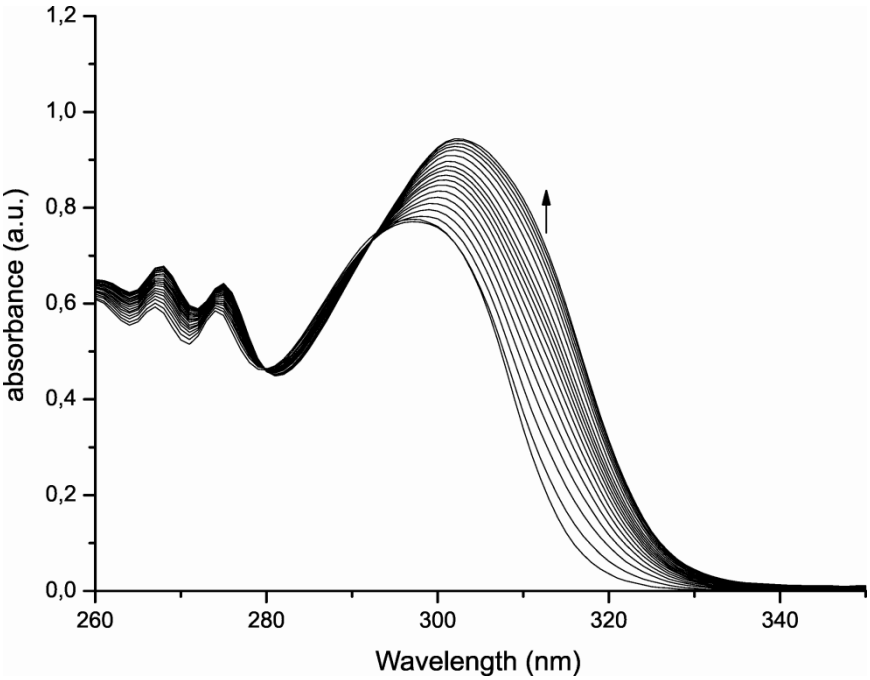

Figure 65. UV-vis titration: Na^+•(*rac*)-**81c** (1.12×10^{-4} M – 1.08×10^{-4} M in (*rac*)-**81c** and 10 equivalents of $NaClO_4$) upon addition of different amounts of malonic acid (0 M – 4.77×10^{-4} M) in DCM/MeOH (99.5/0.5 v/v) at 298 K

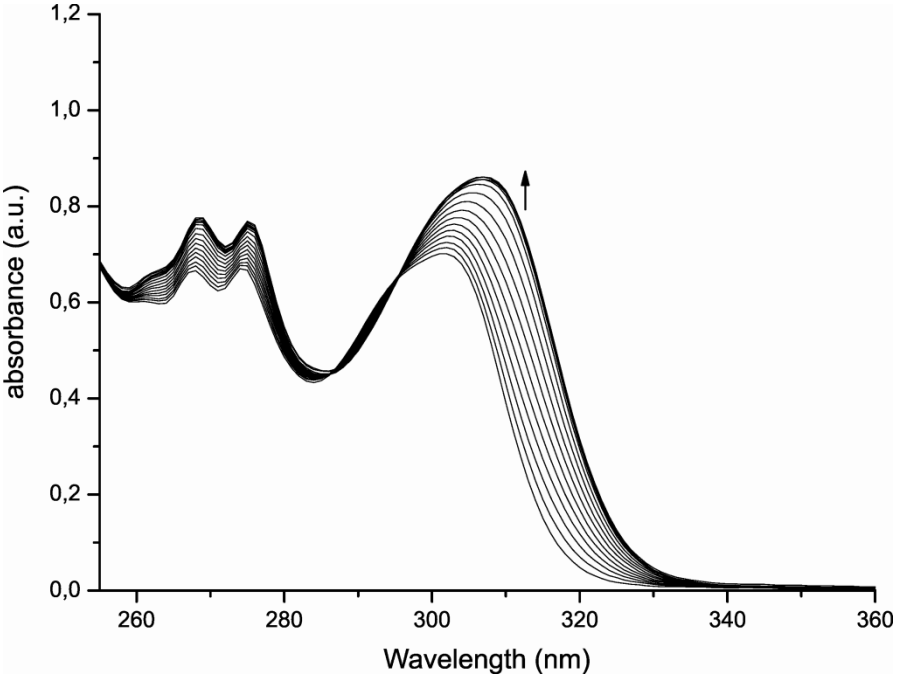

Figure 66. UV-vis titration: Li^+•(*rac*)-**81e** (9.83×10^{-5} M – 9.43×10^{-5} M in (*rac*)-**81e** and 10 equivalents of $LiClO_4$) upon addition of different amounts of oxalic acid (0 M – 3.62×10^{-4} M) in DCM/MeOH (99.5/0.5 v/v) at 298 K

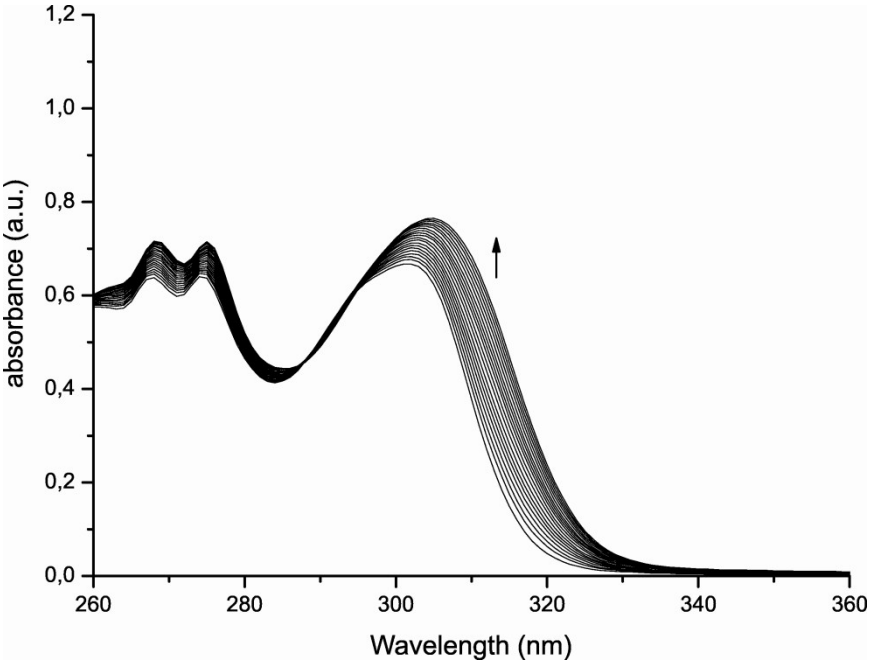

Figure 67. UV-vis titration: Li^+•(*rac*)-**81e** (9.83×10^{-5} M – 9.31×10^{-5} M in (*rac*)-**81e** and 10 equivalents of $LiClO_4$) upon addition of different amounts of malonic acid (0 M – 7.86×10^{-4} M) in DCM/MeOH (99.5/0.5 v/v) at 298 K

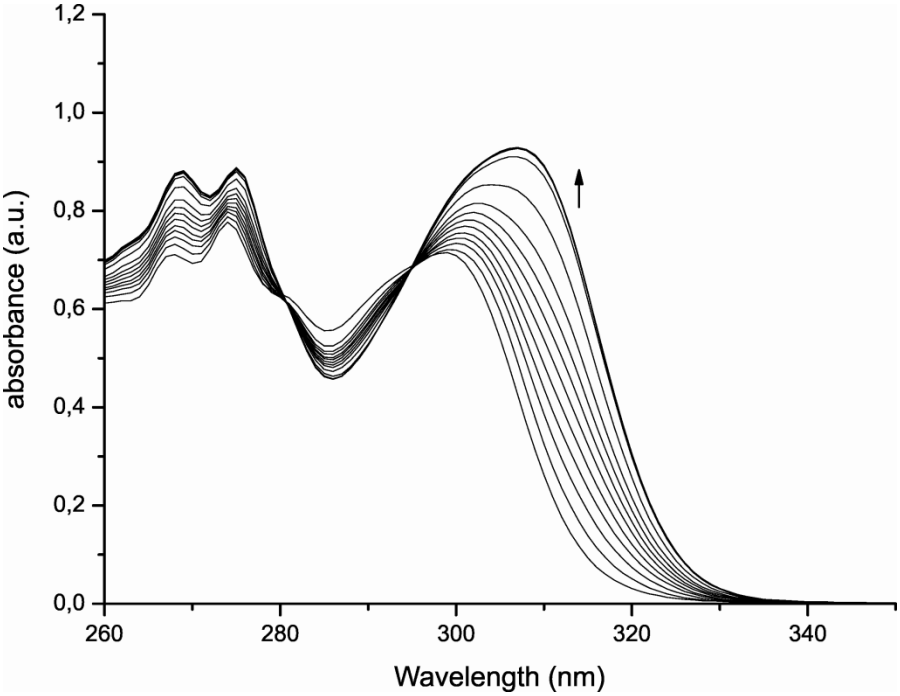

Figure 68. UV-vis titration: Na^+•(*rac*)-**81e** (9.83 x 10^{-5} M – 9.49 x 10^{-5} M in (*rac*)-**81e** and 10 equivalents of $NaClO_4$) upon addition of different amounts of oxalic acid (0 M – 2.27 x 10^{-4} M) in DCM/MeOH (99.5/0.5 v/v) at 298 K

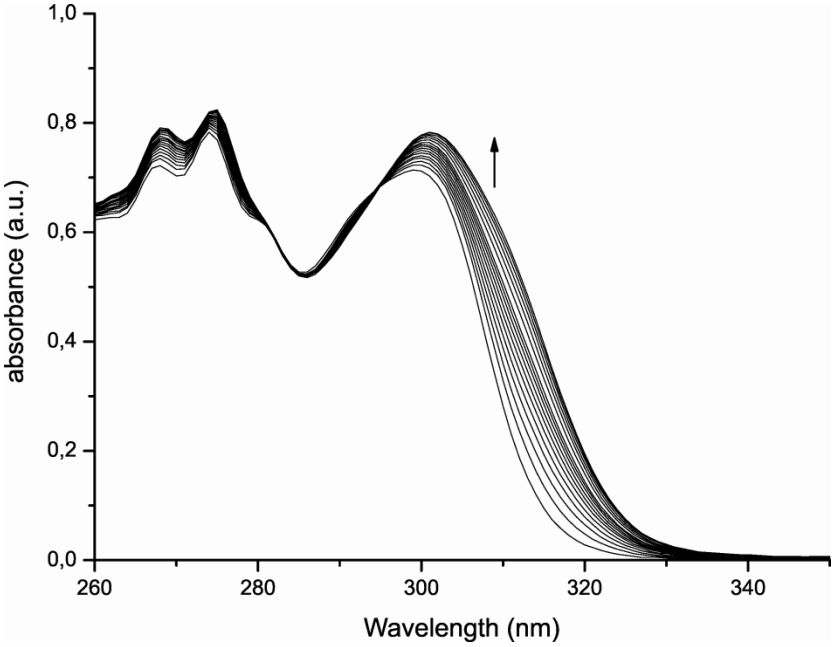

Figure 69. UV-vis titration: Na^+•(*rac*)-**81e** (9.83 x 10^{-5} M – 9.46 x 10^{-5} M in (*rac*)-**81e** and 10 equivalents of $NaClO_4$) upon addition of different amounts of malonic acid (0 M – 5.04 x 10^{-4} M) in DCM/MeOH (99.5/0.5 v/v) at 298 K

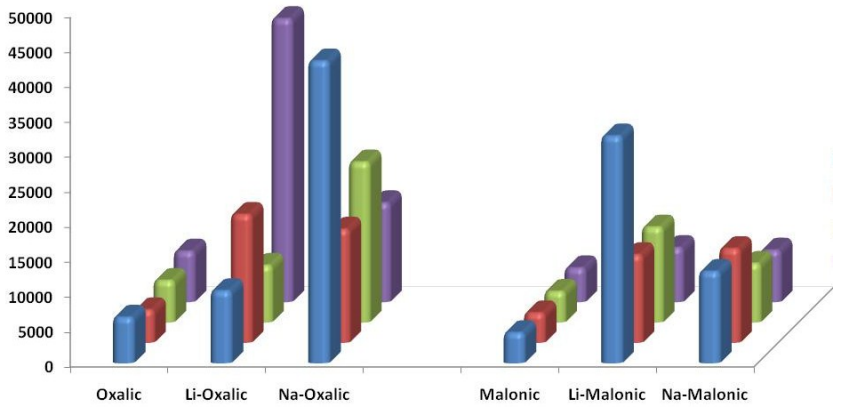

Figure 70. Comparative binding constant values (M^{-1}) of receptors (*rac*)-**81a**,**b**,**c**,**e** (blue, red, green and purple, respectively) with oxalic and malonic acids in presence of different cations such as Li^+ and Na^+ metal ions

1.3.4 Measurements of binding constants by emission spectroscopy

Stock solutions of the receptors (*rac*)-**81a–e** (*ca.* 10^{-4} M) were prepared in DCM/MeOH (99.5/0.5 v/v). Solutions of the corresponding cationic species (*ca.* 10^{-2} M) were also prepared in the same solvent mixture. The receptor solution was placed in a 1 cm quartz cell. The titration was carried out adding at 298 K incremental amounts of cationic species to the host solution (receptors (*rac*)-**81a–e**) leading to changes in the emission spectra. Binding constants were extracted by non-linear curve fitting of the emission data at 350 nm considering a 1:1 binding model.[133]

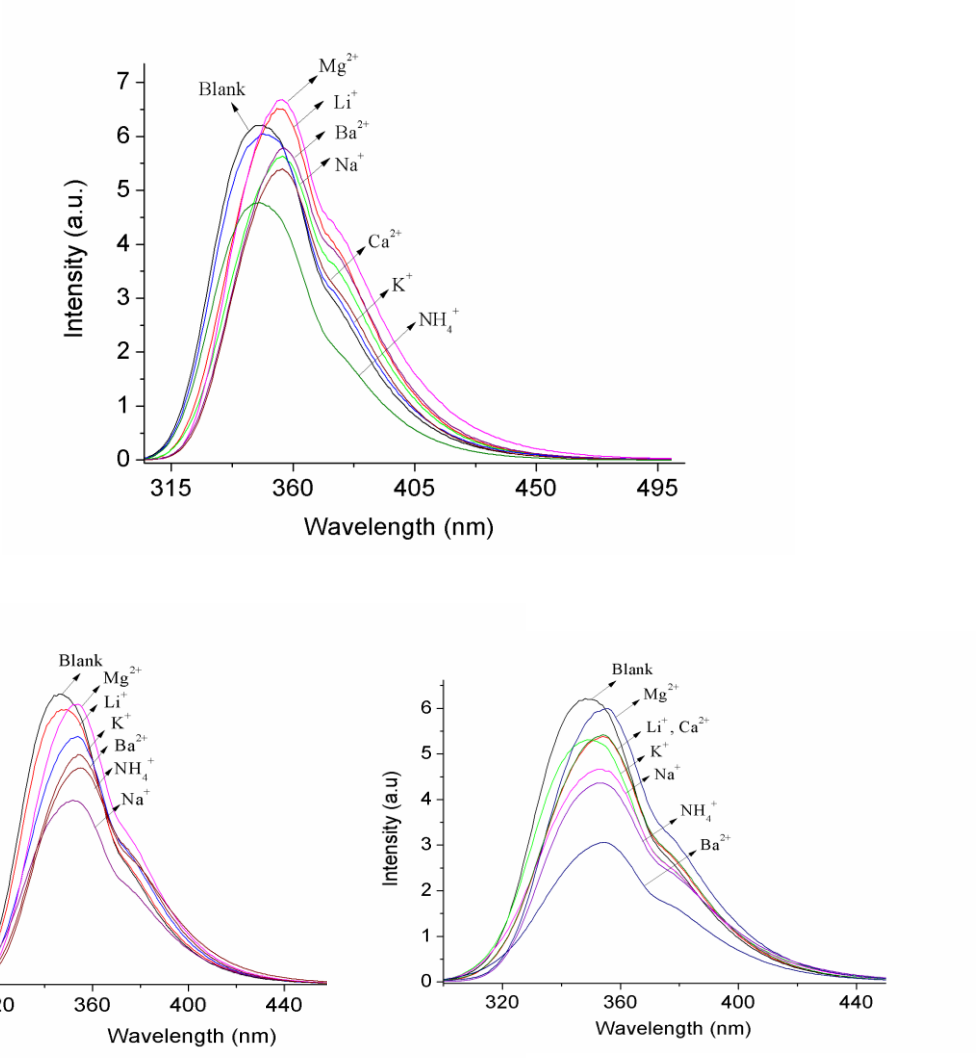

Figure 71. Emission spectrum of (top) (*rac*)-**81a** (1.7 x 10^{-4} M), (bottom left) (*rac*)-**81b** (1.5 x 10^{-4} M) and (bottom right) (*rac*)-**81c** (1.4 x 10^{-4} M) with an excess of different cationic species (5 equivalents) in DCM/MeOH (99.5/0.5 v/v) at 298 K

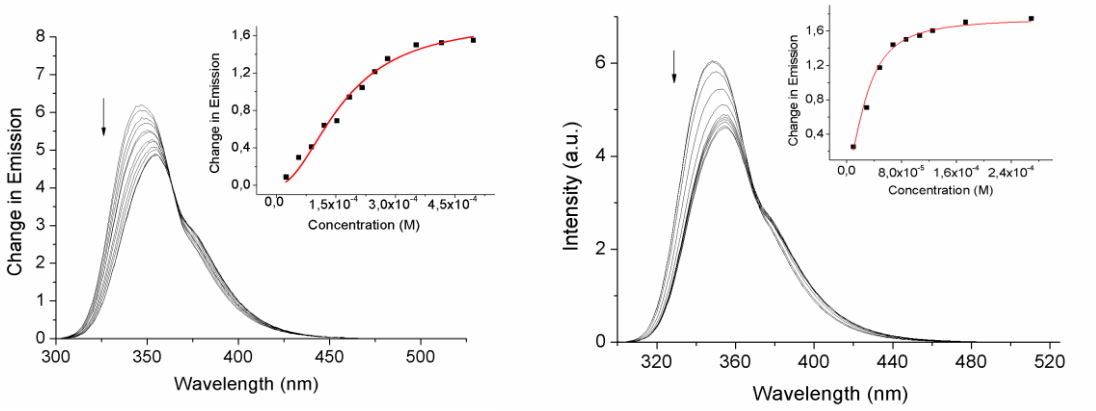

Figure 72. Emission titrations: as representative examples see (*rac*)-**81b** (1.5 x 10^{-4} M) upon addition of (left) Ba^{2+} (4.9 x 10^{-6} M – 4.70 x 10^{-4} M) and (right) NH_4^+ (9.6 x 10^{-6} M – 2.69 x 10^{-4} M) in DCM/MeOH (99.5/0.5 v/v) at 298 K

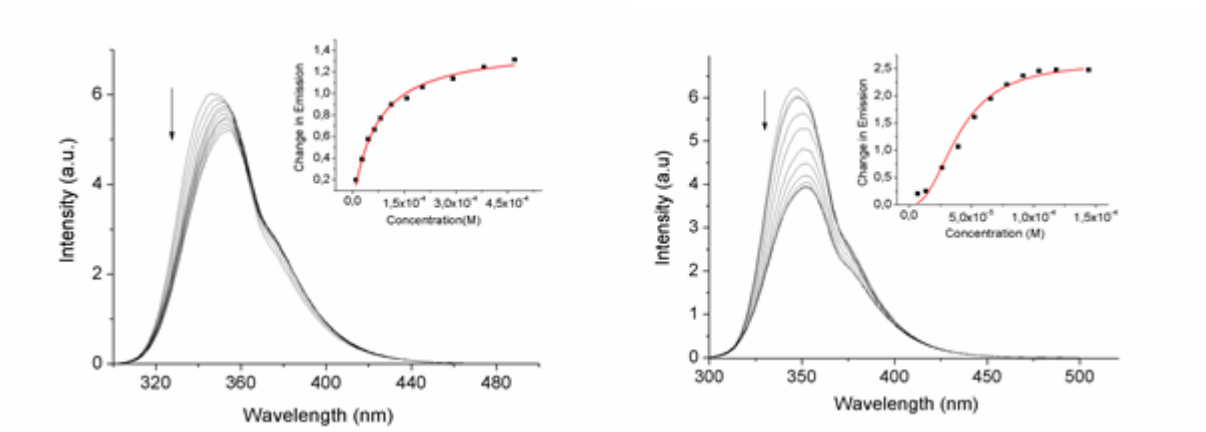

Figure 73.Emission titrations: as representative examples see (*rac*)-**81b** (1.5 x 10^{-4} M) upon addition of (left) Li^+ (9.0 x10^{-6} M – 4.7 x10^{-4} M) (right) and Na^+ (6.5 x10^{-6} M – 4.7 x10^{-4}) in DCM/MeOH (99.5/0.5 v/v) at 298 K

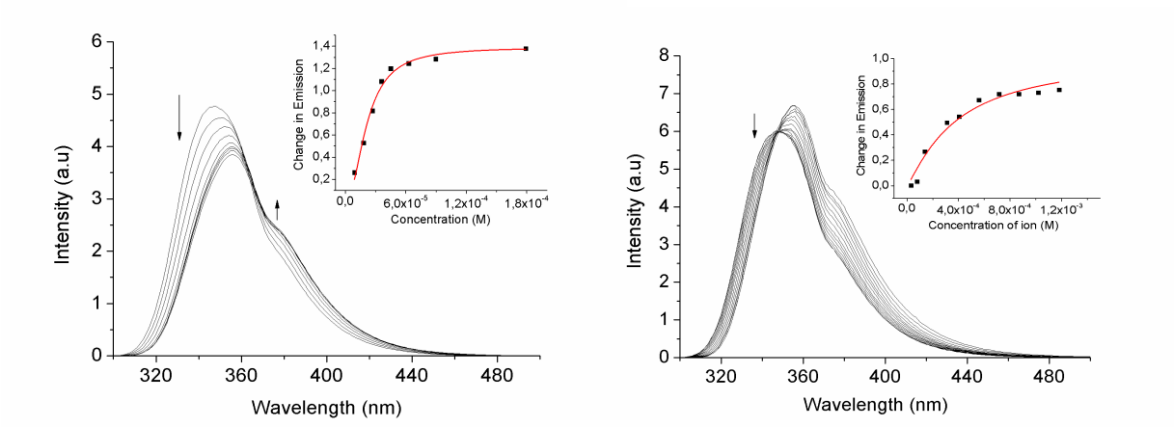

Figure 74. Emission titrations: as representative examples see (*rac*)-**81a** (1.7 x 10^{-4} M) upon addition of (left) NH_4^+ (9.0 x 10^{-5} M – 1.8 x 10^{-3} M) (right) and Mg^{2+} (3.2 x 10^{-6} M – 4.9 x 10^{-4} M) in DCM/MeOH (99.5/0.5 v/v) at 298 K

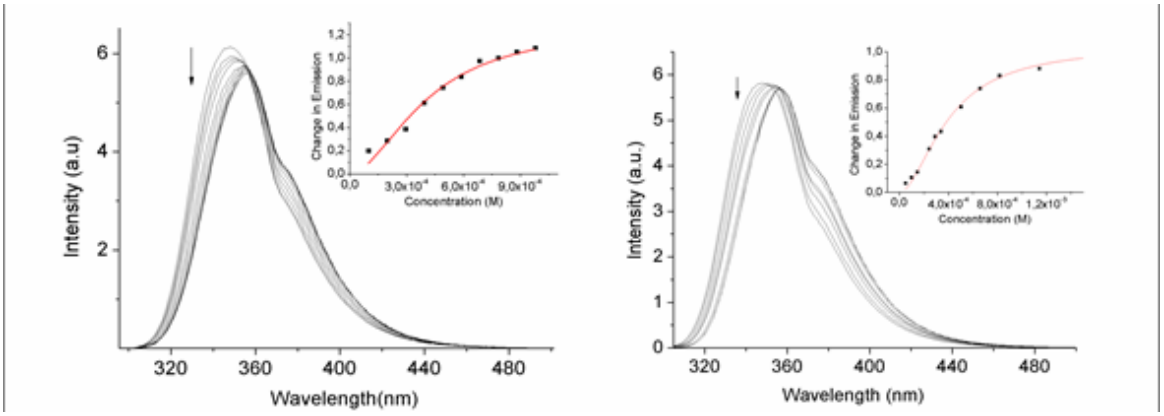

Figure 75. Emission titrations: as representative examples see (*rac*)-**81a** (1.7 x 10^{-4} M) upon addition of (left) Na^+ (9.79 x 10^{-5} M – 9.79 x 10^{-4} M) (right) and Ba^{2+} (4.8 x 10^{-5} M – 4.2 x 10^{-4} M) in DCM/MeOH (99.5/0.5 v/v) at 298 K

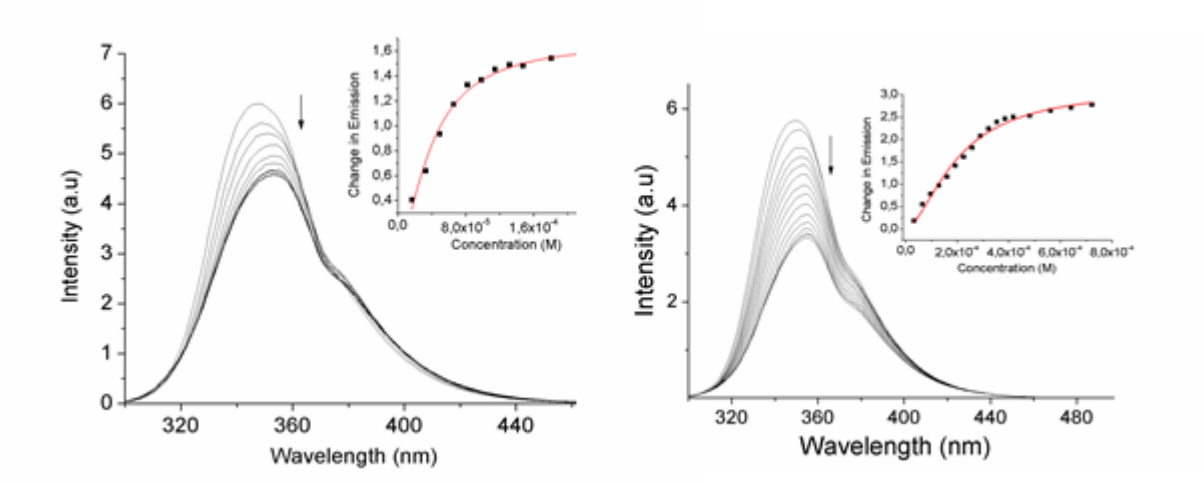

Figure 76. Emission titrations: as representative examples see (*rac*)-**81c** (1.4 x 10^{-4} M) upon addition of (left) Na^{+} (1.6 x 10^{-5} M – 4.9 x 10^{-4} M) (right) and Ba^{2+} (3.3 x 10^{-6} M – 7.2 x 10^{-4} M) in DCM/MeOH (99.5/0.5 v/v) at 298 K

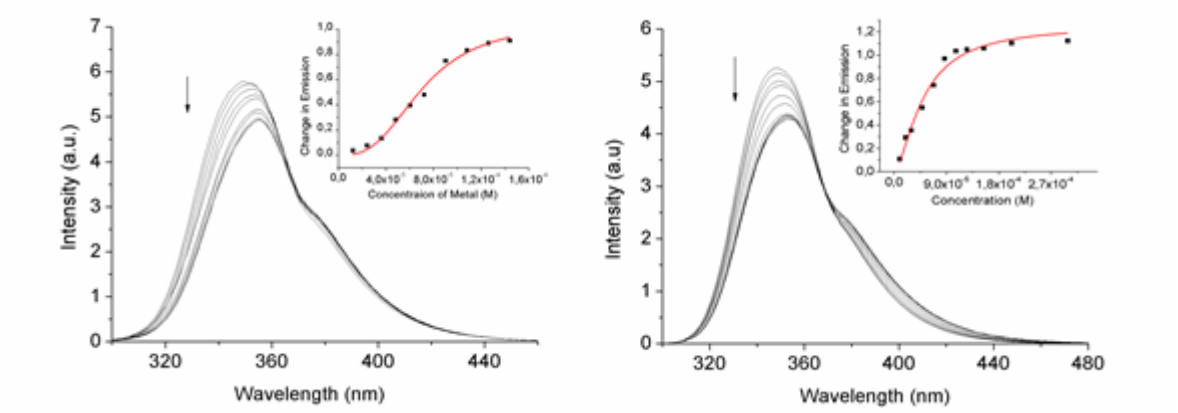

Figure 77. Emission titrations: as representative examples see (*rac*)-**81c** (1.4 x 10^{-4} M) upon addition of (left) Ca^{2+} (1.3 x 10^{-5} M – 4.9 x10^{-4} M) (right) and NH_4^{+} (9.6 x 10^{-6} M – 3.0 x 10^{-4} M) in DCM/MeOH (99.5/0.5 v/v) at 298 K

1.3.5 Stoichiometry determination: Job plots.

Stock solutions of the same concentration of receptor (*rac*)-**81b** (*ca.* 1 x 10^{-4} M) and the guests were prepared in DCM/MeOH (99.5/0.5 v/v). Emission spectra with different host-guest ratios at constant total concentration were recorded. Job plots were made by plotting changes in emission versus χ (host).

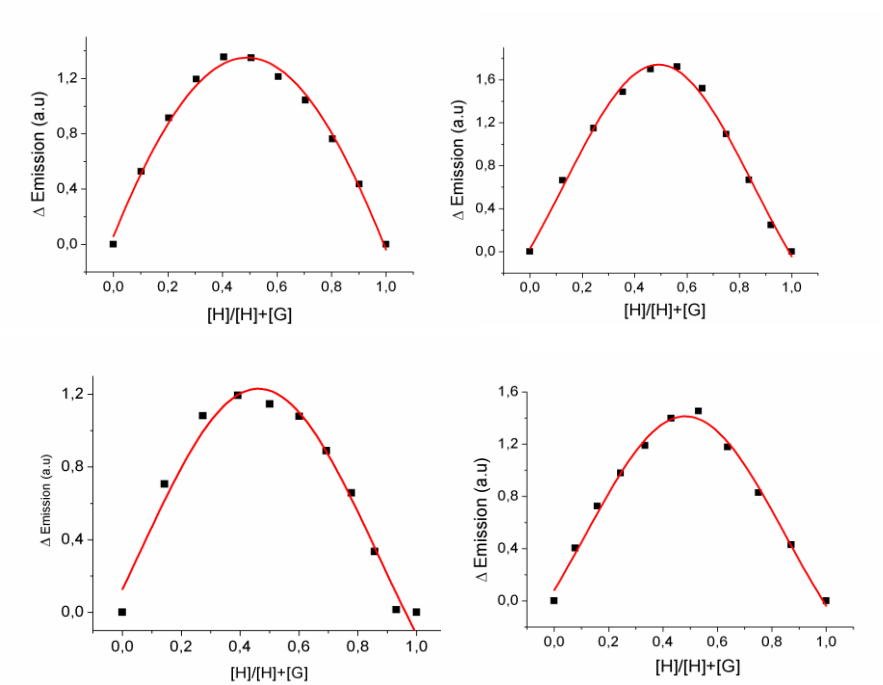

Figure 78. Job plots for (*rac*)-**81b** upon addition of (top left) Li^+, (top right) Na^+, (bottom left) K^+, and (bottom right) Ba^{2+} ions in DCM/MeOH (99.5/0.5 v/v) at 298 K

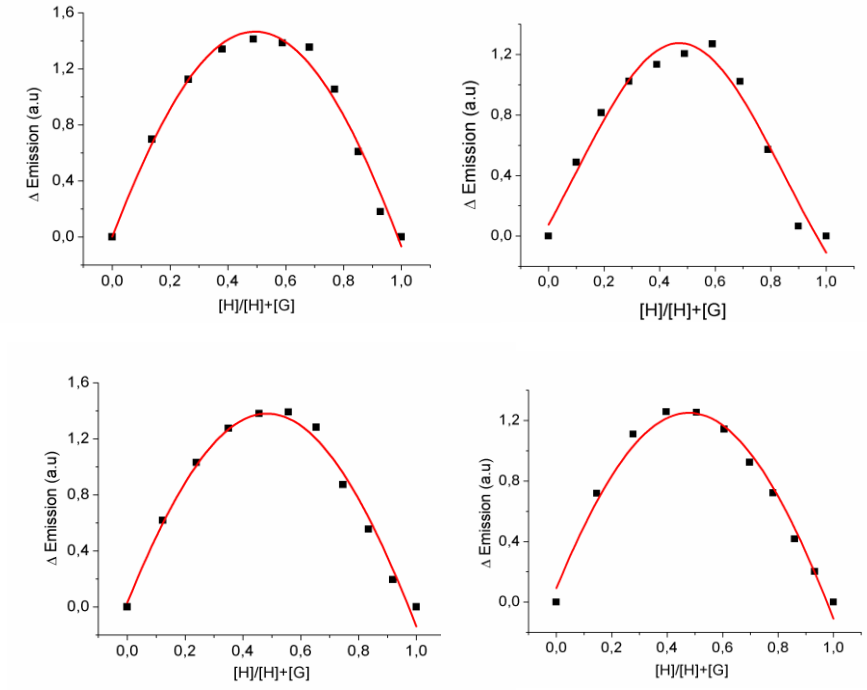

Figure 79. Job plots of (*rac*)-**81b** upon addition of (top left) Mg^{2+}, (top right) Ca^{2+}, (bottom left) NH_4^+, (bottom right) H-PheOMe•HCl (L-Phenylglycine methyl ester hydrochloride) in DCM/MeOH (99.5/0.5 v/v) at 298 K

Stock solutions of the same concentration of receptor (*rac*)-**81b** (*ca.* 1 x 10^{-4} M) and the guests were prepared in DCM/MeOH (99.5/0.5 v/v). UV-vis spectra with different host-guest ratios at constant total concentration were recorded. Job plots were made by plotting changes in absorbance versus χ (host).

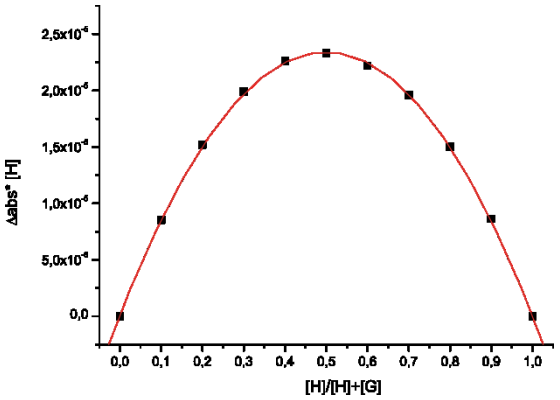

Figure 80. Job's plot of (*rac*)-**81b** upon addition of oxalic acid in DCM/MeOH (99.5/0.5 v/v) at 298 K. Plotted based on the spectral change of Uv-vis titrations

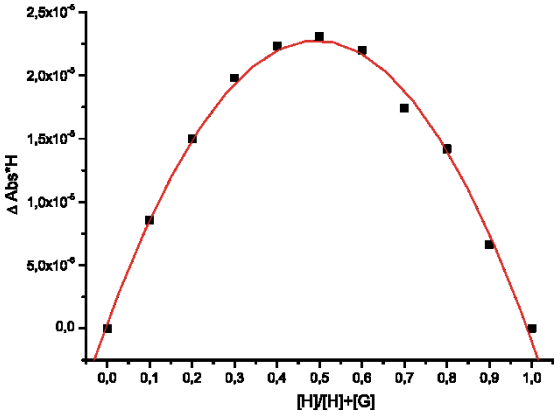

Figure 81. Job's plot of (*rac*)-**81b** upon addition of malonic acid in DCM/MeOH (99.5/0.5 v/v) at 298 K. Plotted based on the spectral change of Uv-vis titrations

1.3.6 Measurements of binding constants by ITC

A solution of (*rac*)-**81b** (7.3 x 10^{-4} M) in DCM/MeOH (98/2 v/v) was added in the cell of an isothermal calorimeter. Known volumes of a solution of barium perchlorate in the same solvent mixture (6.1 x 10^{-3} M) were syringed into the host solution and the evolved heat measured. After the reference titration was subtracted, the association constants and the thermodynamics parameters were obtained from the fit of the revised titration data to a theoretical titration curve using the one set of sites model of the MicroCal ITC Data Analysis module provided by MicroCal, LLC (Figure 82).

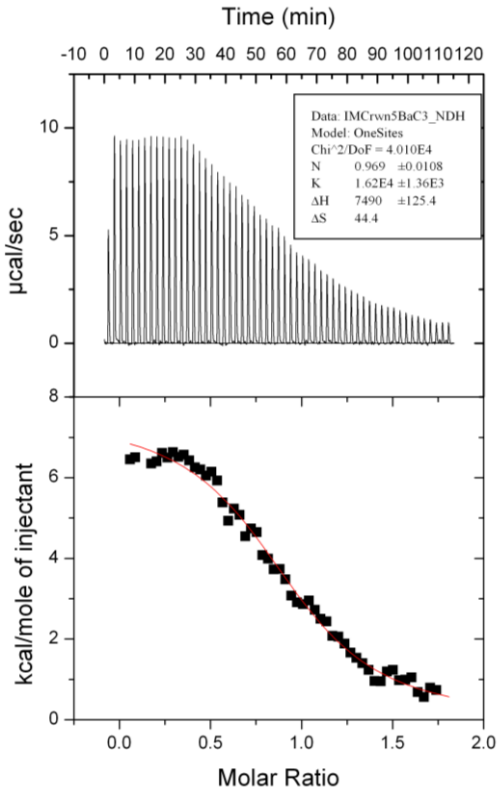

Figure 82. ITC titration data of (*rac*)-**81b** and $BaClO_4$ in DCM/MeOH (98/2 v/v)

A solution of (*rac*)-**81a** (7.7 x 10^{-4} M) in DCM/MeOH (98/2 v/v) was added in the cell of an isothermal calorimeter. Known volumes from a solution of barium perchlorate in the same solvent mixture (6.1 x 10^{-3} M) were syringed into the host solution and the evolved heat measured. Analysis of the titration data rendered the thermodynamic parameters in Figure 83.

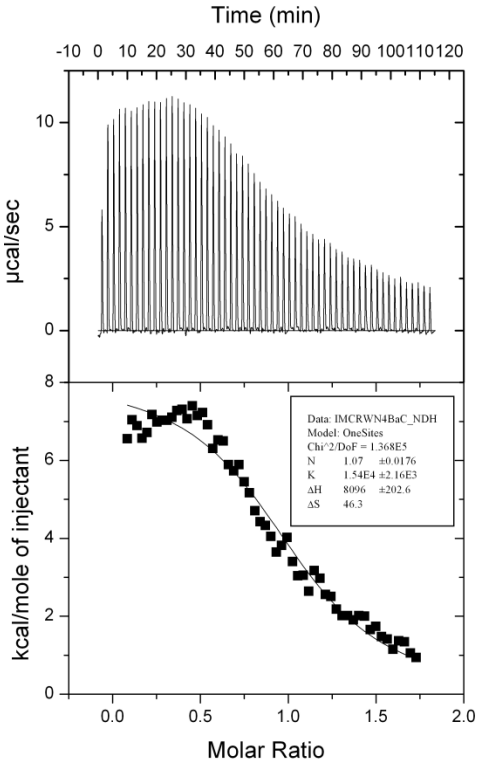

Figure 83. ITC titration data of (*rac*)-**81a** and $BaClO_4$ in DCM/MeOH (98/2 v/v)

1.3.7 NMR Titrations & Measurement of binding constants by NMR

1.3.7.1 Qualitative Titrations

Titrations were carried out on a 500 MHz spectrometer by using a solution of receptor (*rac*)-**81b** (*ca.* 1 x 10^{-2} M) in DCM-d_2/MeOH-d_4 (99.5/0.5 v/v) and adding aliquots of a solution of the corresponding dicarboxylic acid at 298 K.

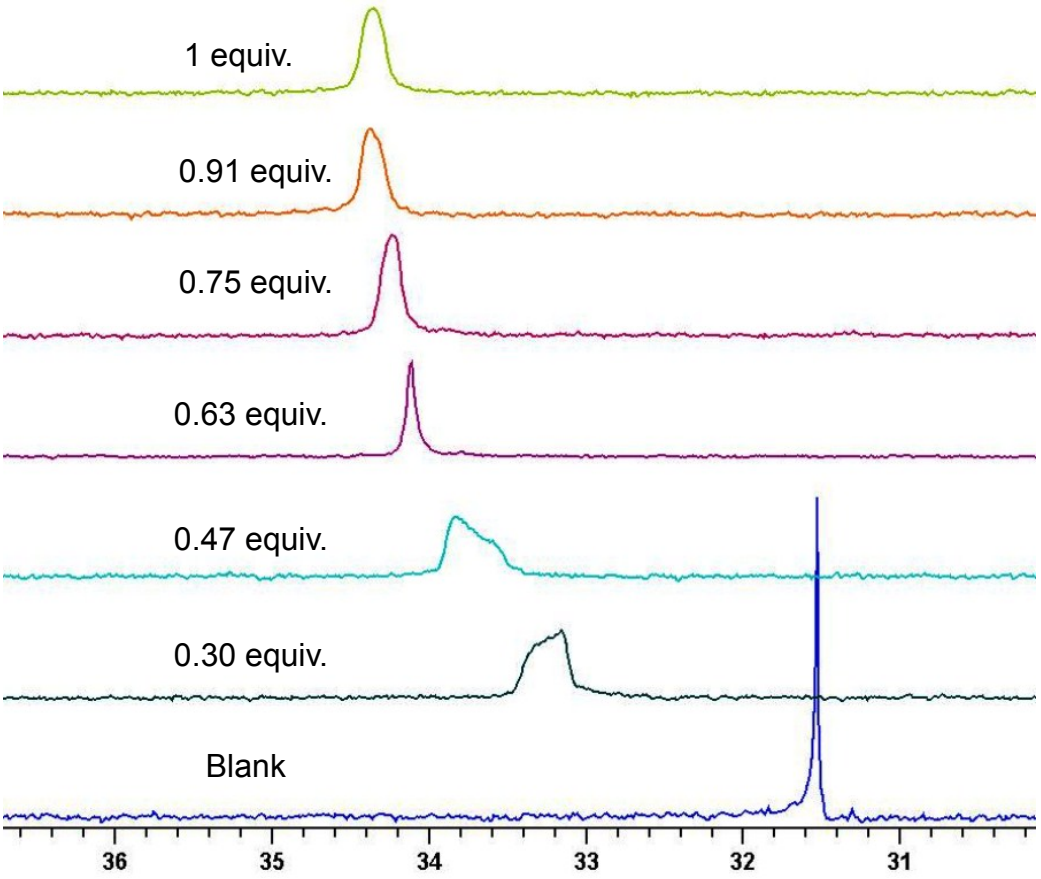

Figure 84. Changes in the ^{31}P NMR (202 MHz, DCM-d_2/MeOH-d_4 [99.5/0.5 v/v]) spectra acquired at 298 K during the titration of (*rac*)-**81b** with oxalic acid ([(*rac*)-**81b**] = 1.3 x 10^{-2} M)

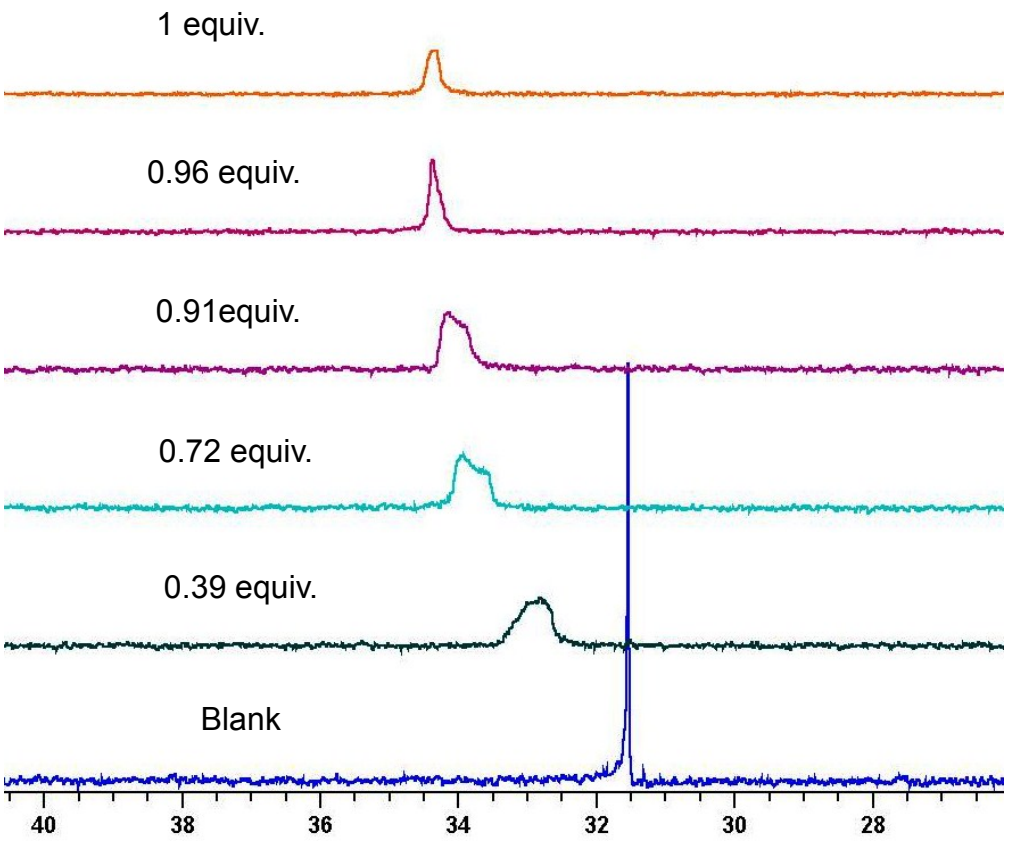

Figure 85. Changes in the ^{31}P NMR (202 MHz, DCM-d_2/MeOH-d_4 [99.5/0.5 v/v]) spectra acquired at 298 K during the titration of (*rac*)-**81b** with malonic acid ([(*rac*)-**81b**] = 1.3 x 10^{-2} M)

1.3.7.2 Measurement of binding constants by NMR spectroscopy

Solutions of the receptors (*rac*)-**81a** (*ca.* 10^{-4} M) and Li^+•(*rac*)-**81a** (*ca.* 10^{-4} M) were prepared in DCM-d_2/MeOH-d_4 (99.5/0.5 v/v). Solutions of malonic acid (*ca.* 10^{-2} M) were also prepared in the same solvent mixture. The host solution (0.6 mL) was placed in a NMR tube. The titration was carried out adding at 298 K incremental amounts of guest (malonic acid) to the host solution ((*rac*)-**81a** or Li^+•(*rac*)-**81a**), which led to changes in the chemical shift and signal width in the NMR spectra. Binding constants were extracted by multivariate factor analysis of the ^{31}P NMR chemical shift values, considering a 1:1 binding model in the fast exchange-limit. SPECFIT software (Version 3.0; Spectra Software Associates)[134] was used.

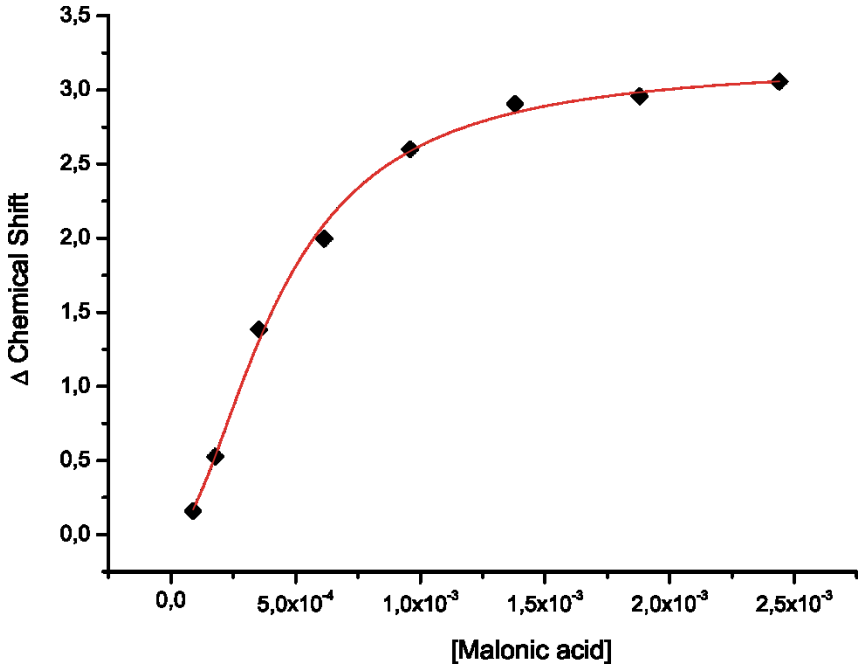

Figure 86. NMR Titration to measure the binding constant between (*rac*)-**81a** (8.91 x 10^{-4} M – 8.42 x 10^{-4} M) and malonic acid: Changes (ppm) in the ^{31}P NMR (202 MHz, DCM-d_2/MeOH-d_4 [99.5/0.5 v/v]) upon addition of malonic acid 8.90 x 10^{-5} – 2.44 x 10^{-3} M)

1.3.8 Synthetic procedure of crown ether-containing bisphosphine ligands 45

General synthetic procedure for crown ether-containing bisphosphine ligands **45**:

Under argon atmosphere enantiomerically pure compound **80**[132] (0.93 mmol) and Cs_2CO_3 were dissolved in dry DMF (100 mL). The obtained solution was stirred at 60 ºC for 2 hours. Then, a solution of the corresponding bistosylate derivative **84** (1.02 mmol) in dry DMF (25 mL) was slowly added through a dropping funnel. The reaction mixture was stirred at 60 ºC overnight. The reaction mixture was filtered and the solvent evaporated under reduced pressure. The remaining crude solid was purified by column chromatography on silica gel using dichloromethane/methanol (95/5 v/v) as elution solvent to provide the corresponding phosphine oxide derivative (58% yield), which was subsequently reduced by addition of xylene (5 mL), tri-^{n}butylamine (0.93 mL, 3.92 mmols) and trichlorosilane (0.27 mL, 2.69 mmols) under argon atmosphere. The reaction mixture was stirred at 140 ºC for 3 hours and then cooled to 0 ºC followed by slow addition of deoxygenated 30% NaOH solution (3 mL). Degassed dichloromethane (1.5 mL) was added and the reaction mixture was heated at 60 ºC until the two layers became clear. Aqueous layer was removed with a cannula. The organic layer was treated again with deoxygenated 30% NaOH solution (3 mL), washed with degassed water (3 mL) and brine (3 mL). Dried over $MgSO_4$, filtered and evaporated to dryness. The residue was heated on degassed EtOH (2.5 mL) at 80 ºC for 5 minutes, cooled to 0 ºC, and filtered. The solid was washed with degassed EtOH and dried *in vacuo* to obtain the final product as a white solid (34% yield).

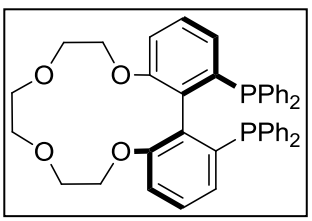

Compound (R_a)-45a: Compound (R_a)-**45a** was synthesized following the general procedure. From compound (R_a)-**80**[132] (200 mg, 0.34 mmol), Cs_2CO_3, bistosylate derivative **84a** (171 mg, 0.37 mmol), tri-^{n}butylamine (0.34 mL, 1.43 mmols) and trichlorosilane (0.10 mL, 0.98 mmols) the product (R_a)-**45a** was obtained as a white solid (41 mg, 18% overall yield). Mp: 209–211 ºC; $[\alpha]_D^{25}$ = –53.2 (*c* 0.97, chloroform); IR (neat, cm^{-1}) υ 1563, 740, 695;

^{1}H NMR (400 MHz, $CDCl_3$) δ 7.36–7.27 (m, 11H), 7.27–7.16 (m, 11H), 6.71–6.65 (m, 2H), 6.65–6.59 (m, 2H) 3.89–3.82 (m, 2H), 3.64–3.57 (m, 2H), 3.50–3.37 (m, 6H), 3.24–3.17 (m, 2H); ^{13}C{^{1}H,^{31}P} NMR (125 MHz, $CDCl_3$) δ 156.5, 139.7, 138.8, 137.5, 134.8, 133.5, 132.4, 128.5, 128.3, 128.2, 128.0, 127.7, 125.3, 110.8, 70.5, 69.7, 66.4; ^{31}P{^{1}H} NMR (202 MHz, $CDCl_3$) δ –9.4; HRMS (ESI^{+}): m/z [M+H]$^{+}$ calcd for $C_{42}H_{39}O_4P_2$ 669.2318, found 669.2329.

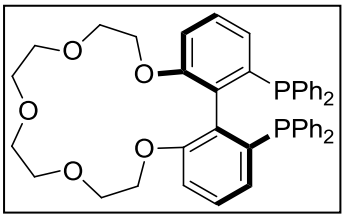

Compound (S_a)-45b: Compound (S_a)-**45b** was synthesized following the general procedure. From compound (S_a)-**80**[132] (545 mg, 0.93 mmol), Cs_2CO_3, bistosylate derivative **84b** (541 mg, 1.02 mmol), tri-^{n}butylamine (0.93 mL, 3.92 mmols) and trichlorosilane (0.27 mL, 2.69 mmols) the product (S_a)-**45b** was obtained as a white solid (140 mg, 23% overall yield). Mp: 163–167 ºC; $[\alpha]_D^{25}$ = –22.8 (*c* 1.02, chloroform); IR (neat, cm^{-1}) υ 1564, 740, 693; ^{1}H NMR (400 MHz, $CDCl_3$) δ 7.36–7.14 (m, 22H), 6.80–6.67 (m, 4H), 3.90–3.78 (m, 2H), 3.59–3.44 (m, 8H), 3.43–3.35 (m, 2H), 3.32–3.22 (m, 2H), 3.16–3.06 (m, 2H); ^{13}C{^{1}H,^{31}P} NMR (125 MHz, $CDCl_3$) δ 157.0, 139.2, 139.0, 137.5, 134.7, 133.3, 132.9, 128.5, 128.3, 128.2, 127.9, 127.8, 125.9, 111.4, 71.4, 71.3, 69.9, 67.5; ^{31}P{^{1}H} NMR (202 MHz, $CDCl_3$) δ –10.8; HRMS (ESI^{+}): m/z [M+H]$^{+}$ calcd for $C_{44}H_{43}O_5P_2$ 713.2560, found 713.2586.

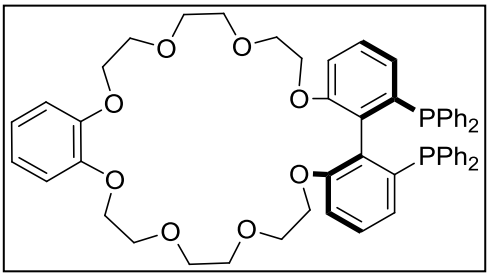

Compound (R_a)-45e: Compound (R_a)-**45e** was synthesized following the general procedure. From compound (R_a)-**80**[132] (220 mg, 0.37 mmol), Cs_2CO_3, bistosylate derivative **84e** (280 mg, 0.41 mmol), tri-^{n}butylamine (0.37 mL, 1.56 mmols) and trichlorosilane (0.11 mL, 1.07 mmols) the product (R_a)-**45e** was obtained as a white solid (96 mg, 29% overall yield). Mp: 63–67 ºC; $[\alpha]_D^{25}$ = 43.7 (*c* 1.15, chloroform); IR (neat, cm^{-1}) υ 1254, 740, 694; ^{1}H NMR (400 MHz, $CDCl_3$) δ 7.33–7.18(m, 22H), 6.96–6.85 (m, 4H), 6.81–6.67 (m, 4H), 4.22–4.06 (m, 4H), 3.93–3.73 (m, 6H), 3.72–3.62 (m, 2H), 3.62–3.52 (m, 2H), 3.49–3.39 (m, 4H), 3.38–3.29 (m, 2H) 3.28–3.14 (m, 4H); ^{13}C{^{1}H,^{31}P} NMR (125 MHz, $CDCl_3$) δ 156.9, 149.3, 139.3, 139.0, 137.5, 134.7, 133.3, 133.0, 128.7, 128.4, 128.2, 128.0, 127.9, 126.2, 121.7, 114.6, 111.4, 71.2,

71.0, 70.0, 69.5, 69.5, 67.9; $^{31}P\{^{1}H\}$ NMR (202 MHz, $CDCl_3$) δ –10.9; HRMS (ESI^+): m/z $[M+H]^+$ calcd for $C_{54}H_{54}NaO_8P_2$ 915.3186, found 915.3182.

1.3.9 Synthetic procedure of (tetra[3,5-bis(trifluoromethyl)phenyl]borate) BArF salts

NaBArF was purchased from a commercial supplier (Alfa Aesar®) and used as received.

CsBArF and RbBArF were obtained by ionic exchange following the next general procedure: $CsNO_3$ (1.81 mmol) or $RbNO_3$ were portionwise added to a hot solution (90 ºC) of NaBArF (0.36 mmol) in water (7 mL). The highly insoluble CsBArF or RbBArF precipitated and were isolated by filtration, washed with water, and recrystallized in THF (70% yield). The obtained salts were dried at 120 ºC under vacuum overnight.

KBArF was synthesized following a well-established methodology.[135]

Dibenzylammonium (tetra[3,5-bis(trifluoromethyl)phenyl]borate) (**95**) was synthesized following a previously reported procedure.[136]

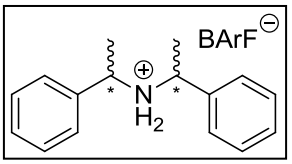

Compounds 94: Enantiomerically pure compounds (*S*,*S*)-**94** and (*R*,*R*)-**94** were prepared by mixing commercial NaBArF (266 mg, 0.3 mmol) with the corresponding enantiomerically pure amine hydrochloride salt **97** (80.1 mg, 0.3 mmol) in diethyl ether and allowing to react overnight. Filtration and evaporation of the solvent yielded compounds (*S*,*S*)-**94** and (*R*,*R*)-**94** (196 mg, 95% yield) as white solids. Mp: 117–119 ºC, IR (neat, cm^{-1}) υ 1611, 1578, 1353, 1273, 1094; ^{1}H NMR (400 MHz, $CDCl_3$) δ 7.82–7.66 (bs, 8H), 7.60–7.52 (bs, 4H), 7.52–7.43 (m, 6H), 7.26–7.14 (m, 4H), 4.13 (q, *J* = 6.8 Hz, 2H), 1.61 (d, *J* = 6.8 Hz, 6H); $^{13}C\{^{1}H\}$ NMR (125 MHz, $CDCl_3$) δ 161.8 (q, *J* = 50.0 Hz), 134.9, 133.5, 131.4, 130.6, 129.1 (q, *J* = 30.1 Hz), 126.6, 124.7 (q, *J* = 273.0 Hz), 117.7, 58.8, 20.4; Anal. Calcd for $C_{48}H_{32}BF_{24}N$: C, 52.91; H, 2.96; N, 1.29; Found: C, 53.03; H, 3.07, N, 1.48. $[\alpha]_D^{25}$ –18.5, (*c* 0.43, methanol) ((*S*,*S*)-**94**); $[\alpha]_D^{25}$ 19.7, (*c* 0.56, methanol) ((*R*,*R*)-**94**).

[135] Buschmann, W. E.; Miller, J. S.; Bowman-James, K.; Miller, C. N. *Inorg. Synth.* **2002**, *33*, 83.
[136] South, C. R.; Higley, M. N.; Leung, K. C. F.; Lanari, D.; Nelson, A.; Grubbs, R. H.; Stoddart, J. F.; Weck, M. *Chem. Eur. J.* **2006**, *12*, 3789.

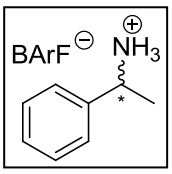

Compounds 93: (*R*) and (*S*)-**93** BArF salts were synthesized from (*R*) and (*S*)-phenylethylamine hydrochloride **96**,[137] respectively, as follows: NaBArF (281 mg, 0.32 mmol) in 5 mL of anhydrous diethyl ether was added to a solution of phenylethylamine hydrochloride **96** (50 mg, 0.32 mmol) in 5 mL of anhydrous diethyl ether. The mixture was stirred vigorously overnight and filtered. Subsequently, the filtrate was evaporated to dryness under reduced pressure at 60 ºC overnight to afford the product as a white solid: (292 mg, 94% yield). Mp: 149–154 ºC, IR (neat, cm^{-1}) υ 3686, 3606, 3323, 3281, 2857, 1612, 1492, 1353, 1275, 1098, 944, 930, 886, 837, 770, 709, 681, 670; ^{1}H NMR (500 MHz, $CDCl_3$) δ 7.72 (br s, 8H), 7.56 (br s, 4H), 7.53–7.41 (m, 3H), 7.24–7.15 (m, 2H), 4.40 (q, *J* = 6.8 Hz, 1H), 1.63 (d, *J* = 6.8 Hz, 3H); $^{13}C\{^{1}H\}$ NMR (125 MHz, $CDCl_3$) δ 161.8 (q, *J* = 50 Hz), 134.9, 134.7, 131.2, 130.3, 129.1, 126.0, 124.7 (q, *J* = 274.0 Hz), 117.8, 54.2, 19.6; Anal. Calcd for $C_{40}H_{24}BF_{24}N$: C, 48.75; H, 2.45; N, 1.42; Found: C, 48.12; H, 2.49, N, 1.49; $[\alpha]_D^{25}$ 1.0, (*c* 1.03, methanol) ((*R*)-**93**); $[\alpha]_D^{25}$ –1.0, (*c* 1.11, methanol) ((*S*)-**93**).

1.3.10 General procedure for the Rh-mediated asymmetric hydrogenation

In a glovebox filled with nitrogen, substrate (*ca.* 15 mg, 1 equiv.) and $[Rh(cod)_2]BArF$ (0.01 equiv. in dichloromethane) were placed into a 2 mL vial equipped with a magnetic bar. A stirred solution (10 minutes) of the corresponding ligand **45** (0.012 equiv.) and the corresponding additive (0.0156 equiv.) in dichloromethane were added that with substrate and rhodium precursor. Additional dichloromethane was charged to provide the desired final concentration of substrate (0.2 M). The vial was transferred into an autoclave and taken out of the glovebox. The autoclave was purged three times with H_2 at a pressure not higher than the desired pressure for the catalysis experiments and, finally, the autoclave was pressurized with H_2 to the desired pressure. The reaction mixture was stirred at room temperature for 18 h. The pressure was carefully released in a well-ventilated hood. The conversion was determined by ^{1}H NMR and enantiomeric excesses were determined by GC or HPLC analysis

[137] Halloran, K. J.; Comely, A.; Chen, Z.; Krishnan, S., 2011053835, 2011.

using chiral stationary phases (See section 2.3.11 from the experimental part of chapter 2 for further analytic details).

CHAPTER 2: DEVELOPMENT OF BISPHOSPHITE LIGANDS WITH A DISTAL REGULATION SITE IN THE FORM OF POLYETHER CHAINS OF DIFFERENT LENGTH AND TOPOLOGY

LITERATURE REVIEW

CHAPTER 2: DEVELOPMENT OF BISPHOSPHITE LIGANDS WITH A DISTAL REGULATION SITE IN THE FORM OF POLYETHER CHAINS OF DIFFERENT LENGTH AND TOPOLOGY

2.1 LITERATURE REVIEW

As early as 1984, McLain *et al*. pointed out the convenience of having bimetallic ligands capable of coordinating hard and soft metal cations for catalytic purposes.[138] In that patent, they described the design and synthesis of different phosphino-azacrown ethers like these depicted in Figure 87. The compounds described are formed by a polyether chain for hard metal cation binding such as alkali ions and a phosphorus group for binding the catalytically active transition metal, particularly rhodium(I).

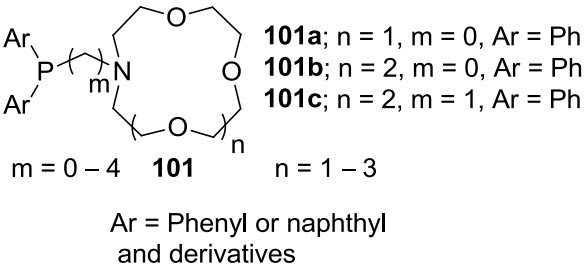

Figure 87. Phosphino-azacrown ether ligands

Interestingly, the interaction of alkali metal ions (E^+) with the formed catalysts resulted in favorable changes in the activity rate of the Rh(I)-mediated hydroformylation of propene. In order to determine the rate of the reaction, changes in the overall pressure as a function of time were monitored during the reaction. Thus, after GC analysis of the crude reaction mixture, the catalytic activity of each catalyst was calculated as the initial turnover frequency.[139] The results summarized in Table 14 showed that there was a clear rate enhancement for complexed phosphino-azacrown ether catalysts E^+•**101** when compared to the catalysts derived from free ligand **101**.

[138] McLain, S. J.; Waller, F. J. Phosphine Azacrown Ether Compounds. US Patent 4432904, 1984.
[139] Turnover frequency (TOF) can be defined as the number of molecular reactions or catalytic cycles occurring at the catalyst center per unit of time (mol product/(mol catalyst x time)).

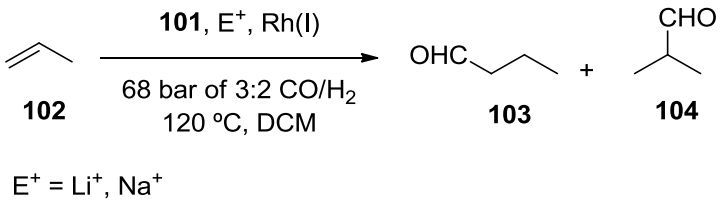

Scheme 26. Rh(I)-mediated hydroformylation of propene **102** with ligands **101** and additives E^+

Table 14. Enhancement of catalytic activity of ligands **101a–c** upon coordination to Na^+ or Li^+

Entry	E^+•Ligand/Ligand	Initial TOF[a] x 10^{-3} (E^+•L/L)	Initial TOF Enhancement (Ratio)
1	Na^+•**101a**/**101a**	7.62/2.99	2.55
2	Li^+•**101a**/**101a**	4.82/2.99	1.61
3	Na^+•**101b**/**101b**	7.49/5.99	1.25
4	Na^+•**101c**/**101c**	6.55/1.32	4.96

[a] In mol product x mol catalyst^{-1} x hour^{-1}

Previous studies by Powell *et al.* had also shown that binding of Li^+ and Na^+ to carbonyl ligands could result in the activation of carbonyl ligands toward nucleophilic attack, as shown in Scheme 27.[140]

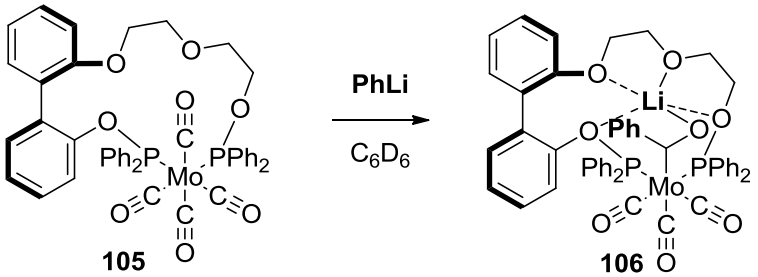

Scheme 27. Activation of carbonyl ligands by Li^+

Based in that work, Gray *et al.* pioneered studies aimed at varying the efficiency of rhodium bisphosphite catalyst in hydroformylation by means of coordinating alkali metal ions to the catalyst.[141] The authors claim that, if migratory-insertion reaction involving a carbonyl ligand is either the rate- or regio-

[140] See: a) Butler, J. M.; Jablonsky, M. J.; Gray, G. M. *Organometallics* **2003**, *22*, 1081. b) Powell, J.; Kuksis, A.; May, C. J.; Meindl, P. E.; Smith, S. J. *Organometallics* **1989**, *8*, 2933.
[141] Owens, S. B.; Gray, G. M. *Organometallics* **2008**, *27*, 4282.

determining step in the catalytic mechanism (step iv and iv' in Scheme 28), the presence of a hard metal cation bound to the catalyst, which interacts with carbonyl ligands, could significantly increase either the reaction rate or the regioselectivity of the hydroformylation reaction.

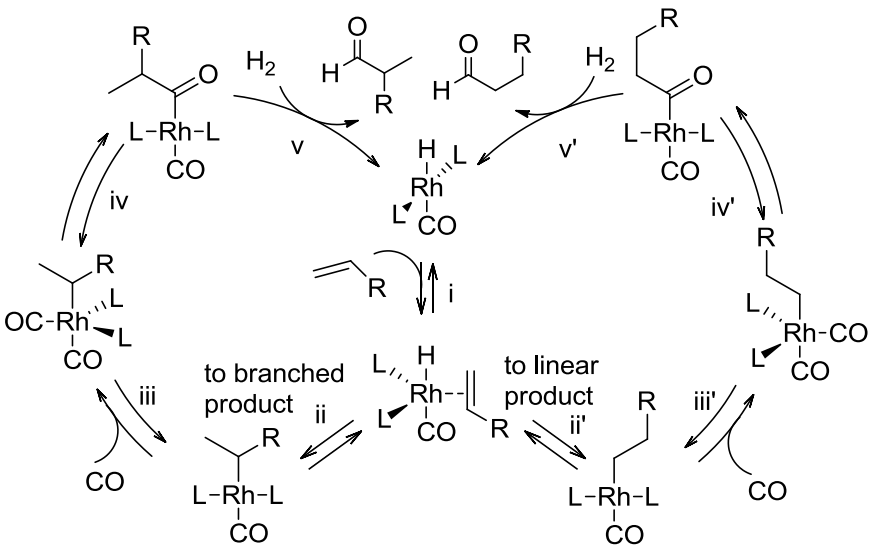

Scheme 28. General mechanism for the Rh-mediated hydroformylation showing two different paths for the branched and linear product isomers

The substrate of choice for these studies was styrene **6a** and, for this purpose, three different ligands were tested: i) (*R*,*R*)-CHIRAPHITE (*R*,*R*)-**13**, ii) 1,2-Bis(diphenylphosphino)ethane (dppe) **107** and iii) bisamido bisphosphite **108**. The first bisphosphite ligand of the series ((*R*,*R*)-**13**) is capable of binding hard metal cations through the oxygen atoms, as demonstrated by Powell and co-workers.[140b] Ligand dppe was used as an example of a bisphosphine ligand without the possibility for alkali metal cation coordination. On the contrary, bisphosphite ligand **108** possesses a flexible backbone with the potential advantage of an additional binding site for alkali metal cations (Figure 88). The results employing these three ligands and $NaBPh_4$ or $LiBPh_4$ salts are summarized in Table 15.

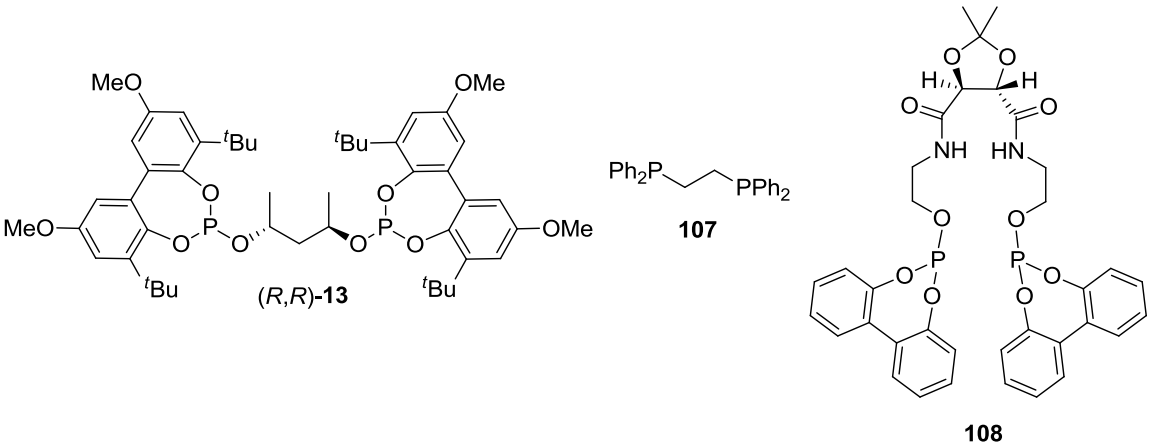

Figure 88. Ligands employed in Gray's hydroformylation studies

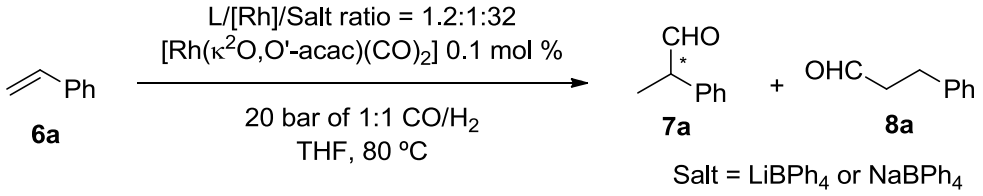

Table 15. Regioselectivity enhancement in the hydroformylation of styrene employing salts as additives[a]

Entry	Ligand	Added salt	Branched-to-linear product ratio	Enhancement[b]
1	**108**	-	3.9	-
2	**108**	$LiBPh_4$	6.2	1.6
3	**108**	$NaBPh_4$	6.6	1.7
4	(*R*,*R*)-**13**	-	10.1	-
5	(*R*,*R*)-**13**	$LiBPh_4$	33.6	3.3
6	(*R*,*R*)-**13**	$NaBPh_4$	16.6	1.6
7	**107**	-	1.8	-
8	**107**	$LiBPh_4$	2.2	1.2

[a] Regioselectivity data was obtained at total conversion in all cases, except for the results obtained with dppe ligand, in which conversion was 61%. [b] Expressed as the branched-to-linear product ratio with additive divided by that without additive.

The catalyst containing the ligand with a more rigid backbone ((*R*,*R*)-**13**) exhibited higher regioselectivities (entries 4 – 6) than catalysts with flexible backbones such as **108** or **107** did. More interestingly, the addition of alkali metal

salts to the catalysts derived from (*R*,*R*)-**13** or **108** significantly improved the regioselectivity of the process without altering the reaction rate. The amount and the nature of the alkali metal cation had a significant effect on the regioselectivity (see Figure 89). The increase in the regioselectivity was claimed not to be due to an increase of the ionic strength of the reaction medium for three main reasons: i) hydroformylation of styrene in the presence of the non-coordinating salt $TBABPh_4$[142] did not increase the regioselectivity observed, ii) the two studied alkali metal salts had different effects on the regioselectivity and iii) an ionic strength effect might be expected to be linear with concentration at the relatively low concentrations used.

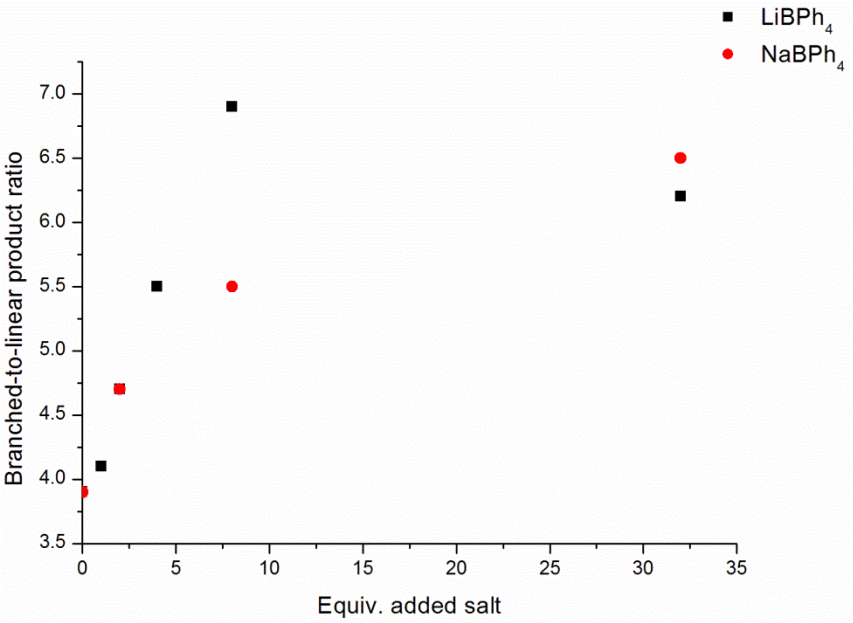

Figure 89. Dependence of the regioselectivity on the amount of salt used for the Rh(I) hydroformylation of styrene using ligand **108**

Thus, the original explanation for the effect of alkali metal added was that the coordination of the alkali metal cation to the oxygen of a carbonyl ligand activates the CO group towards migratory insertion. The different effects of the alkali metal cations could be either the different charge/size ratio of Li^+ and Na^+ ions or the differing abilities of the catalysts to bind these cations. Indeed, the nature of the ligand seemed to be of great importance. For example, regioselectivity enhancement with ligand (*R*,*R*)-**13** was very different with Na^+ or Li^+ whereas ligand **108** experimented almost the same level of enhancement

[142] $TBABPh_4$ stands for tetrabutylammonium tetraphenylborate.

(compare entries 5 and 6 with 2 and 3 in Table 15). Additionally, Rh(I) catalysts derived from ligand **107** showed almost no enhancement in regioselectivity after addition of Li^+ (entry 8). It is noteworthy to mention that although ligand **108** was used as an enantiomerically pure ligand, no studies were done on the enantioselectivity of the branched hydroformylation products derived from styrene. Therefore, the effect on the enantioselectivity of the addition of alkali metal cations was not explored in this example.

In further studies, Gray *et al.* designed two different achiral phosphite ligands that incorporated extra oxygen atoms on the backbone. Ligand **109**[143] is a monophosphite with an appended ether chain whereas ligand **110**[144] is a bisphosphite that forms a metallacrown ether after coordination to a transition metal (Figure 90). The effect of $LiBPh_4$ on the activity and regioselectivity of the Rh(I) catalysts derived from these ligands was studied on the hydroformylation of styrene.

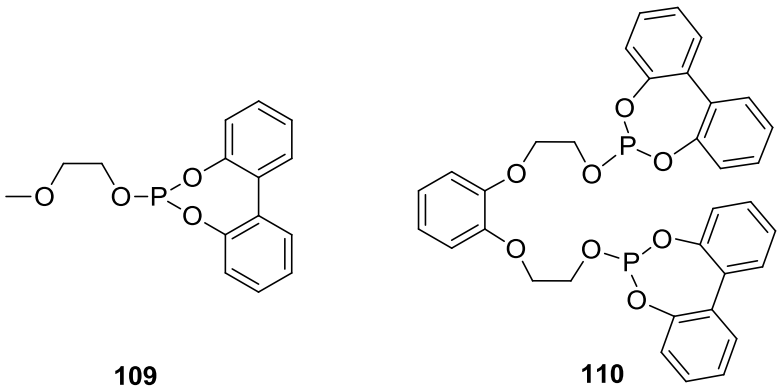

109 **110**

Figure 90. Ligands developed by Gray *et al.* and applied in styrene hydroformylation

[143] Kaisare, A. A.; Owens, S. B., Jr.; Valente, E. J.; Gray, G. M. *J. Organomet. Chem.* **2010**, *695*, 1472.
[144] Kaisare, A. A.; Owens Jr, S. B.; Valente, E. J.; Gray, G. M. *J. Organomet. Chem.* **2010**, *695*, 2658.

Table 16. Regioselectivity enhancement in the hydroformylation of styrene with ligands **109** and **110** employing $LiBPh_4$ as additive[a]

Entry	Ligand	Equiv. $LiBPh_4$[c]	Branched-to-linear product ratio	Rate constant k (s^{-1})[d]
1	**109**[b]	-	3.0	3.5×10^{-4}
2	**109**[b]	4	6.1	2.1×10^{-4}
3	**109**[b]	8	6.1	6.7×10^{-4}
4	**109**[b]	32	6.7	5.1×10^{-4}
5	**110**	-	3.2	1.9×10^{-4}
6	**110**	4	4.9	1.6×10^{-4}
7	**110**	8	6.1	1.5×10^{-4}
8	**110**	32	3.3	8.4×10^{-5}

[a] Same reaction conditions as described in Table 15. Regioselectivity data was obtained at total conversion. [b] L/[Rh] = 2.5:1. [c] Equivalents added with respect to rhodium. [d] Kinetic analysis indicated a pseudo first order rate law.

From these results, a direct observation can be made: regioselectivity could be increased by adding $LiBPh_4$ to the catalysts derived from ligands **109** and **110**. However, the use of high concentrations of $LiBPh_4$ with bisphosphite ligand **110** was detrimental to the catalytic activity (compare entries 5 and 8). On the other hand, ligand **109** showed an improved branched-to-linear product ratio and activity with 32 equivalents of $LiBPh_4$ (compare entries 1 and 4). Nevertheless, it should be emphasized that the addition of only 4 equivalents of Li^+ to catalysts derived from ligands **109** and **110** was enough to reach great regioselectivity enhancements, whereas ligand **108** needed 8 equivalents to show approximately the same level of improvement (see Figure 89). This might be an indication that the addition of extra oxygen atoms on the ligand backbone could improve the binding of alkali cations and, therefore, have those beneficial effects in hydroformylation reactions.

During the realization of this PhD Thesis, a very relevant paper regarding the studies we were carrying out was published by Fan *et al.*[145] In their article, they reported the preparation of conformationally tunable bisphosphites for

[145] Li, Y.; Ma, B.; He, Y.; Zhang, F.; Fan, Q.-H. *Chem. Asian J.* **2010**, *5*, 2454.

asymmetric hydrogenation (see Figure 91). The similarity of the supramolecular approach used by Fan *et al.* and the modulation design developed in our group was evident.

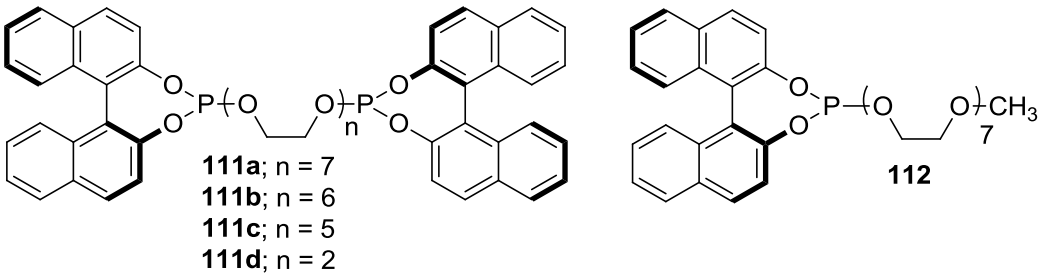

Figure 91. Conformationally tunable ligands employed by Fan *et al.*

Thus, complexation of these polyoxyethylene bisphosphite ligands **111a–d** with alkali-metal ions (E^+) and subsequent coordination to Rh(I) precursors gave the desired metallacrown ethers, which were used as catalysts for asymmetric hydrogenation. These catalysts were employed in the asymmetric hydrogenation of the dehydroamino acid derivative **39d**. First of all, they found the best combination of alkali metal ion and ligand for model substrate ZMac **39d**. Results without any cation and the best combination of ligand/cation are summarized in Table 17.

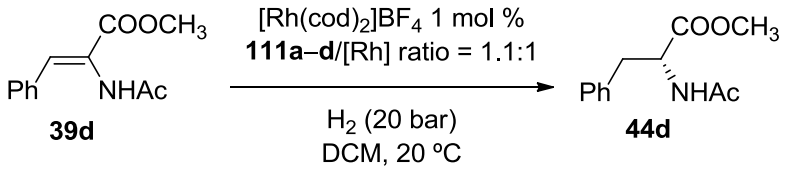

Table 17. Asymmetric hydrogenation of **39d** using Rh/bisphosphites **111a–d**[a]

Entry	Ligand	Additive (E^+/Ligand)	ee (%)
1	**111a**	-	87
2	**111a**	KBArF (3:1)	94
3	**111b**	-	84
4	**111b**	KBArF (3:1)	94[b]
5	**111b**	NaBArF (3:1)	**95**
6	**111c**	-	85
7	**111c**	NaBArF or LiBArF (3:1)	92
8	**111d**	-	74
9	**111d**	LiBArF (3:1)	79
10	**112**	-	88
11	**112**	KBArF (3:1)	32

[a] 100% conversion was observed in all cases. [b] Enantiomeric excess dropped to 84% when [18]crown-6 was added to the reaction mixture.

The best result was obtained with the combination of ligand **111b** and Na^+ as binder of the polyether chain to give the hydrogenation product **44d** in 95% ee, which represented an increase of 11% with respect to free ligand **111b** (compare entries 3 and 5). Ligand **111d** with a shorter polyether chain afforded the best result with the small Li^+ cation as additive. On the other hand, the best ligand/cation combination for the largest ligand **111a** involved using K^+ as the polyether chain binder, probably due to higher binding affinity between the ligand and cation. Monophosphite **112** was also employed in the hydrogenation of the substrate, with good enantioselectivity. In contrast to the bisphosphite ligands **111**, lower enantioselectivity was obtained when KBArF was present in the reaction media, suggesting a lower binding of the potassium cation to the 2,5,8,11,14,17,20-heptaoxadocosan-22-yl chain in the ligand **112**. Furthermore, to rule out the effect of the anion introduced with the cation of interest (BArF), an

extra experiment was carried out. [18]crown-6[146] was added to the catalyst system described in entry 4. Owing to the stronger binding ability of [18]crown-6 towards K^+ with respect to **111b**, K^+ was removed from the catalyst and the enantioselectivity of the process turned out to be the same as when no salt was added (see footnote b in Table 17).

Therefore, the Rh(I) catalyst derived from Na^+ coordinated to ligand **111b** (represented as [Rh(Na^+•**111b**)]), was employed for further asymmetric hydrogenation of similar substrates to check the tolerance of the reaction system to different functional groups present on the substrate of interest. A summary of the substrates studied and the results achieved with and without Na^+ as binder of the polyether chain are shown in Scheme 29.

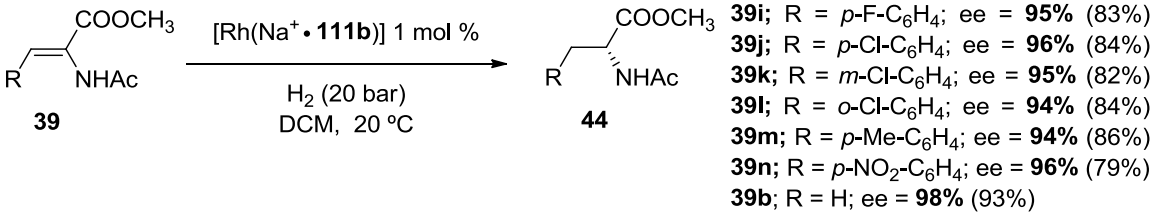

Scheme 29. Asymmetric hydrogenation of α-dehydroamino acid esters catalyzed by a) [Rh(Na^+•**111b**)] (results in bold letters) or b) [Rh(**111b**)] complexes (results in brackets)

To conclude, Fan *et al.* found that alkali metal ions were able to effectively modulate the enantioselectivity of the asymmetric hydrogenation of an array of substrates *via* coordination of alkali metal cations to the metallacrown ether formed by a bisphosphite ligand and a rhodium precursor. This study can be considered as the first publication on chiral metallacrown ethers as catalysts for asymmetric catalysis.

[146] [18]crown-6 corresponds to the compound 1,4,7,10,13,16-hexaoxacyclooctadecane (IUPAC name).

RESULTS AND DISCUSSION

2.2 RESULTS AND DISCUSSION

2.2.1 Design and synthesis of bisphosphite ligands 46

The preparation of enantiomerically pure bisphosphite ligands is a well-documented procedure.[147] Indeed, the key step in the synthesis of our target polyoxyethylene bisphosphite ligands is an *O*-phosphorylation reaction between two equivalents of a phosphochloridite with a diol in the presence of a base (Scheme 30).

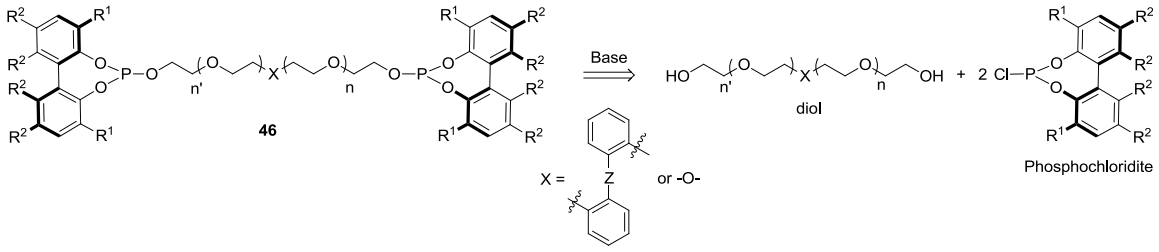

Scheme 30. Retrosynthetic strategy for polyoxyethylene bisphosphite ligands **46**

The design of our bisphosphite ligands permitted a modular approach, meaning that the achiral group deriving from the diol and the conformationally stable phosphite units could be easily changed without altering the general synthetic strategy. Indeed, five different achiral diols and four different enantiomerically pure, conformationally stable [1,1'-biaryl]-2,2'-diol derived phosphite units have been connected to generate an array of structurally diverse bisphosphite ligands. We considered, that such structural ligand diversity should allow us to prove our concept: regulation of the catalytic activity in several asymmetric transformations of interest as a function of the shape and size of an external regulation agent (a polyoxyethylene binder). The bisphosphite ligands that have been synthesized during the Thesis and the starting materials used are presented in Scheme 31. In summary, from the five different diols utilized, three of them contain a simple polyoxyethylene chain: **88**[148] incorporates an eight oxygen chain, **113** a ten oxygen one, and **114** contains three ethyleneoxy units and overall five oxygen atoms. Conversely, diol **116** is an analogue of compound **88** but where no oxygen atoms are present in the chain. The achiral diol **115**

[147] Pereira, M. M.; Calvete, M. J. F.; Carrilho, R. M. B.; Abreu, A. R. *Chem. Soc. Rev.* **2013**, *42*, 6990.
[148] Synthesis described in Section 1.2.1.

constitutes the largest achiral diol unit and contains eleven oxygen atoms and one configurationally labile 2,2'-oxydiphenol group. The phosphochloridites employed include enantiomerically pure, conformationally stable [1,1'-binaphthalene]-2,2'-diol groups with and without substituents at the 3 and 3' positions (phosphochloridites **117a** and **117b**, respectively). We also decided to include in the study the 3 and 3'-disubstituted phosphochloridite derived from partially hydrogenated [1,1'-binaphthalene]-2,2'-diol derivative **118** and, lastly, the 3 and 3'-disubstituted phosphochloridite derived from the enantiomerically pure, conformationally stable [1,1'-biphenyl]-2,2'-diol derivative **119**. All ligands **46a–i** were synthesized from the (R_a)-enantiomer of the phosphochloridites **117** – **119**.

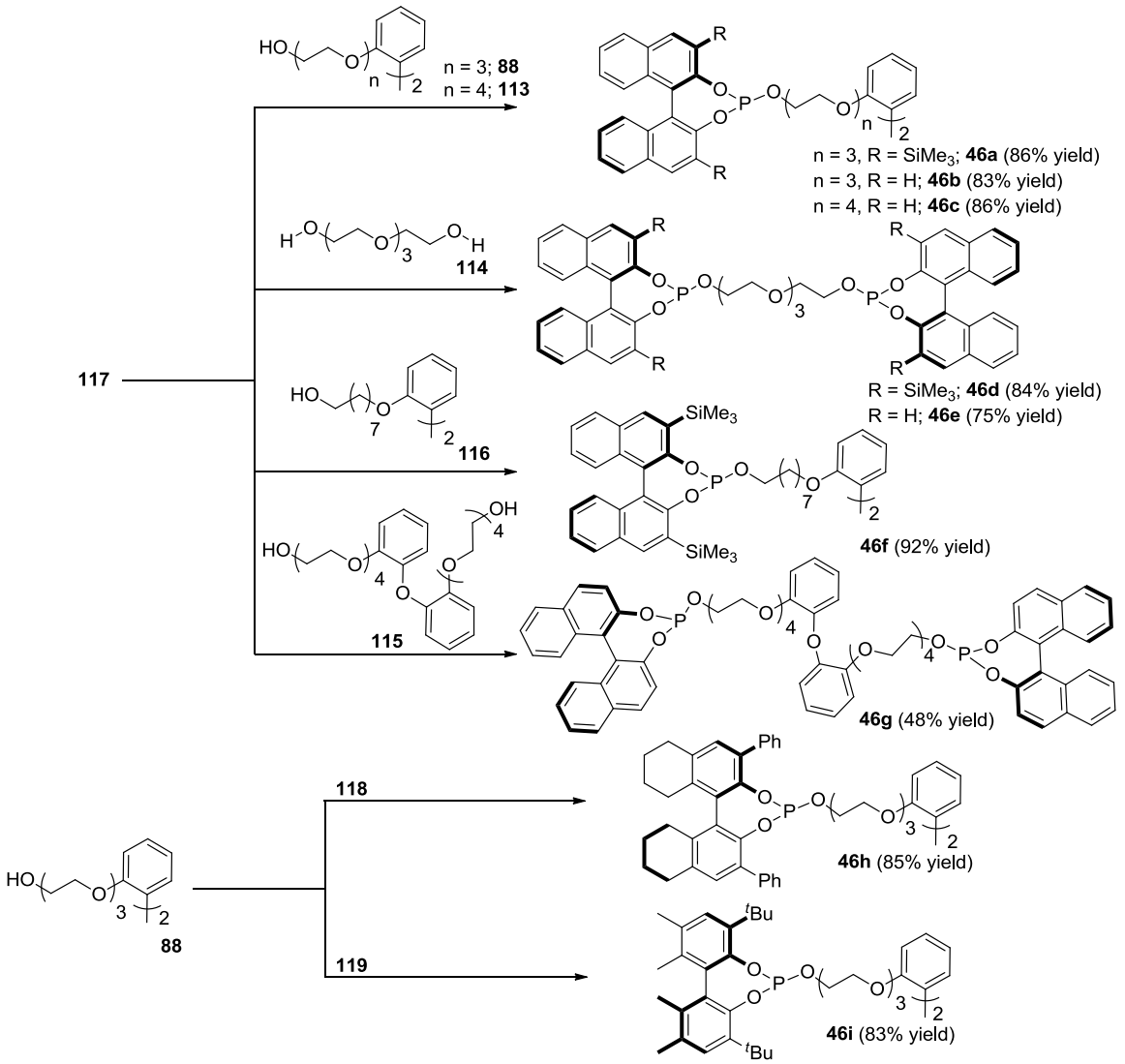

General conditions: Phosphochloridite **117** – **119** (1 equiv.), NEt_3 (2 equiv.), diol **88, 113** – **116** (0.46 equiv.), toluene, 0 ºC to rt, overnight.

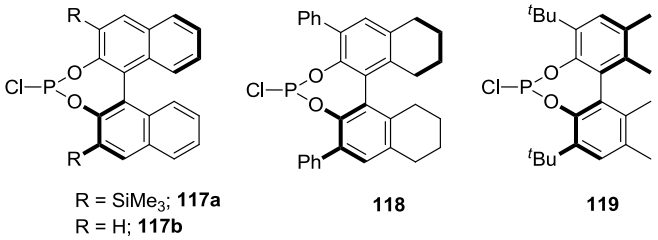

R = $SiMe_3$; **117a**
R = H; **117b**

118

119

Scheme 31. *O*-phosphorylation reactions towards ligands **46**

Thus, ligands **46a–i** were synthesized according to the general procedure indicated in Scheme 31. Reaction of diols **88** and **113** – **116** with the corresponding phosphochloridites **117** – **119** in the presence of an excess of NEt_3 led to the desired bisphosphite ligands. The final compounds were isolated after filtration of the precipitated triethylamine hydrochloride followed by filtration

through a short alumina pack eluting with dichloromethane. This was enough to obtain analytically pure ligands in most cases. However, when other impurities were present, standard preparative reversed-phase chromatography using a silica-based stationary phase was required. The desired bisphosphites were obtained in medium to high yields, which ranged from 48% to 92% (see Scheme 31). $^{31}P\{^{1}H\}$, ^{1}H and $^{13}C\{^{1}H,^{31}P\}$ NMR spectra of bisphosphite ligand **46g** are presented in Figure 92, Figure 93 and Figure 94, respectively.

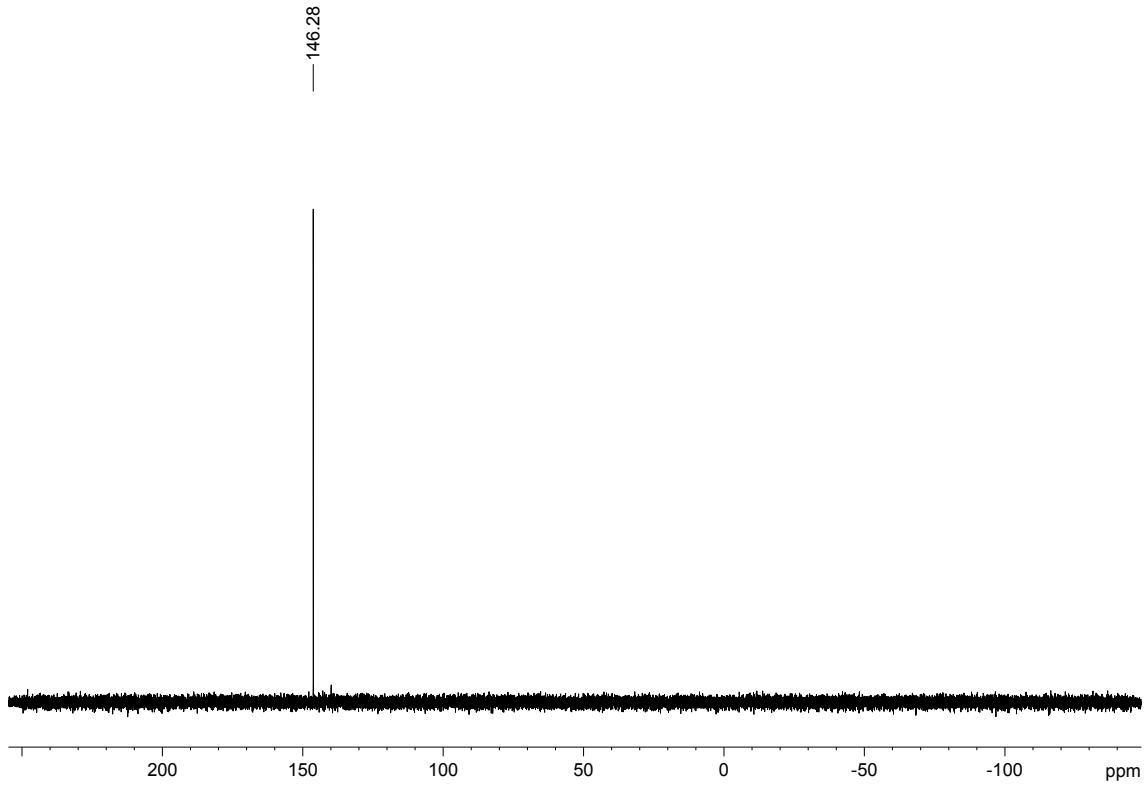

Figure 92. $^{31}P\{^{1}H\}$ NMR spectrum of compound **46g** in DCM-d_2

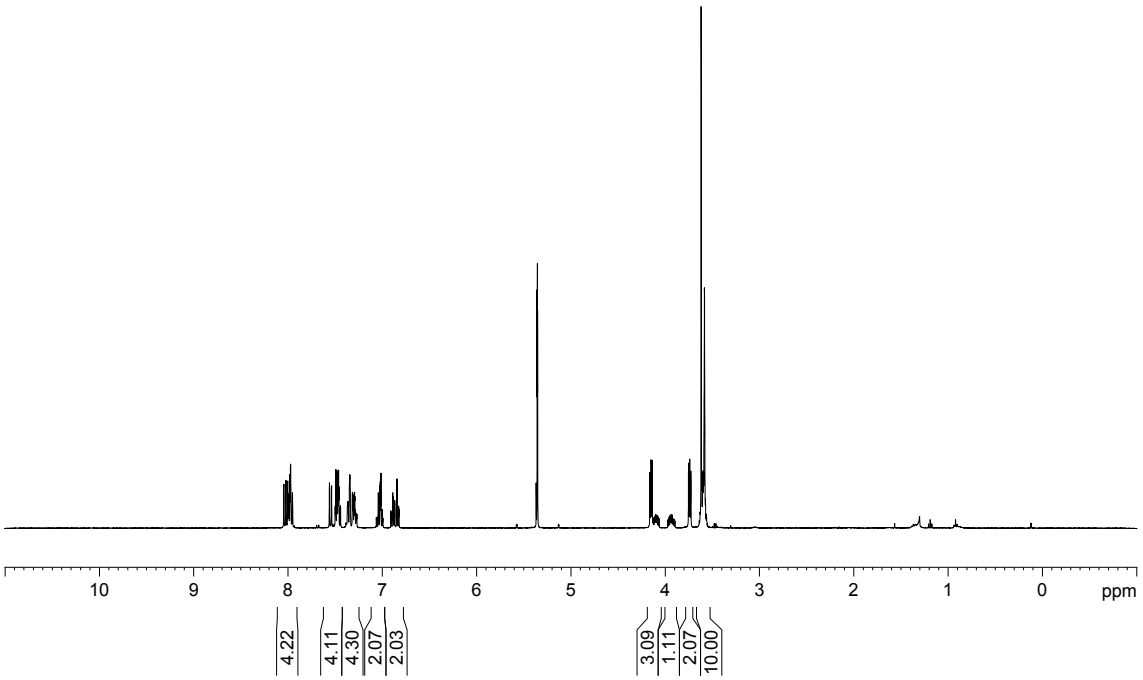

Figure 93. ^{1}H NMR spectrum of compound **46g** in DCM-d_2

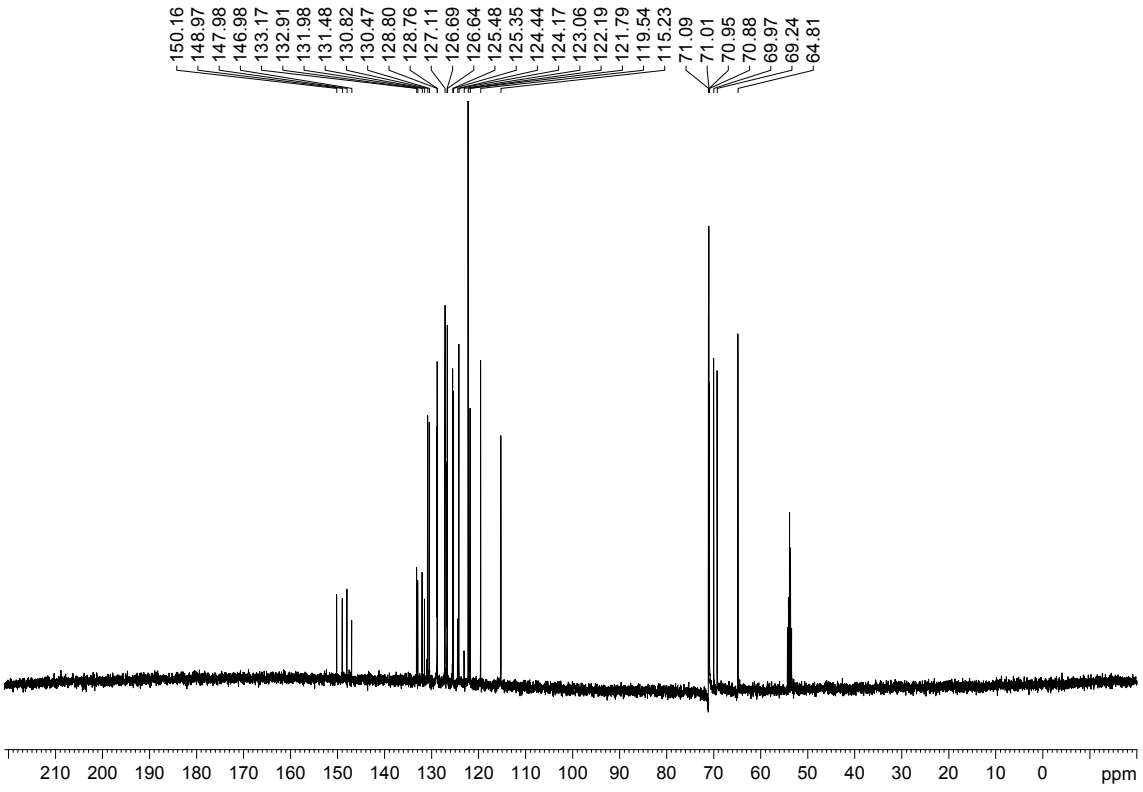

Figure 94. ^{13}C{^{1}H,^{31}P} NMR spectrum of compound **46g** in DCM-d_2

With regard to the required starting materials for preparing the target phosphochloridites, compound **117a** derives from diol **120**,[149] which was prepared according to a reported procedure (Scheme 32). Alternatively, phosphochloridite **117b** was used as received from commercial sources (Strem®) and phosphochloridite **118** was prepared from diol **124**, which was also synthesized following a reported procedure (Scheme 33).[150] Lastly, phosphochloridite **119** was prepared from commercially available diol **126** (Alfa Aesar®).

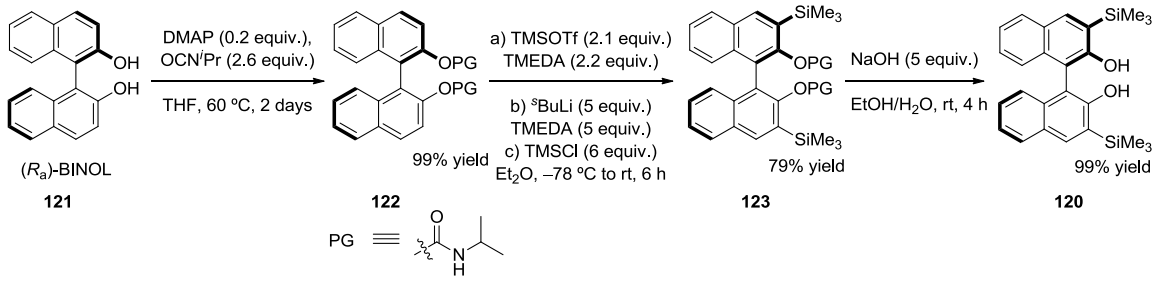

Scheme 32. Synthesis of diol **120**

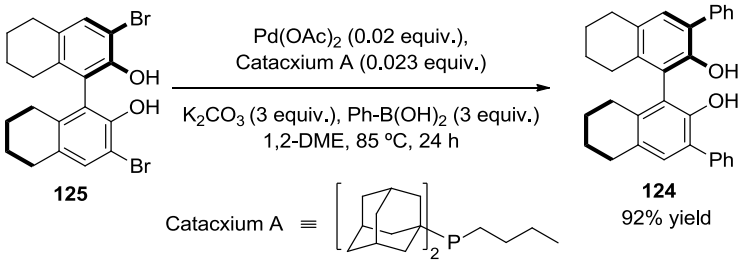

Scheme 33. Synthesis of diol **124**

The general procedure to prepare the non-commercially available phosphochloridites consisted in all cases in the reaction of the corresponding diol (compounds **120, 124** and **126**, respectively) with a mixture of PCl_3 and NEt_3 in toluene at 0 ºC (Scheme 34). The required phosphochloridites, which were obtained in quantitative yield, were directly used for the following *O*-phosphorylation reaction as obtained after filtration of the precipitated triethylamine hydrochloride and solvent removal *in vacuo* (the purity of the solid obtained was checked by ^{31}P NMR).

[149] Kauch, M.; Snieckus, V.; Hoppe, D. *J. Org. Chem.* **2005**, *70*, 7149.
[150] Erre, G.; Junge, K.; Enthaler, S.; Addis, D.; Michalik, D.; Spannenberg, A.; Beller, M. *Chem. - Asian J.* **2008**, *3*, 887.

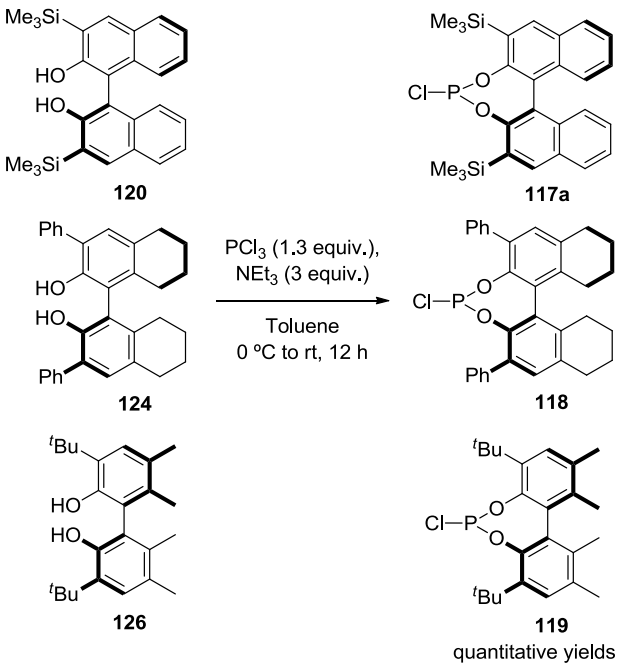

Scheme 34. Synthesis of phosphochloridites **117a**, **118** and **119**

With regard to the preparation of the required achiral diols, compound **116** was synthesized using the same strategy as that used for diol **88** (see Scheme 19 in section 1.2.1), which is indicated in Scheme 35. The first step entailed the preparation of monotosylated alcohol **127**, which was an already known compound and was synthesized as described in the literature.[151] In the final step, compound **127** was mixed with diol **87** and left to stir for 60 hours at reflux. After purification by column chromatography over silica gel, product **116** was isolated as a low melting point white solid (32 ºC) in moderate yield (56%).

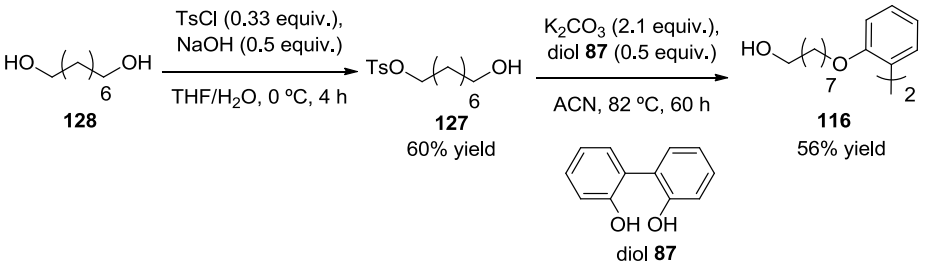

Scheme 35. Synthesis of diol **116**

[151] Junk, M. J. N.; Li, W.; Schlueter, A. D.; Wegner, G.; Spiess, H. W.; Zhang, A.; Hinderberger, D. *Angew. Chem., Int. Ed.* **2010**, *49*, 5683.

Diols **115** and **113** were prepared using the same synthetic strategy from the already described compound **129**[152] and diol **131** or **87**, respectively, under basic conditions (see Scheme 36 and Scheme 37). After purification of the crude mixtures by column chromatography over silica gel, diols **113** and **115** were isolated as pale yellow oils in moderate to low yield (45 and 46% yield, respectively).

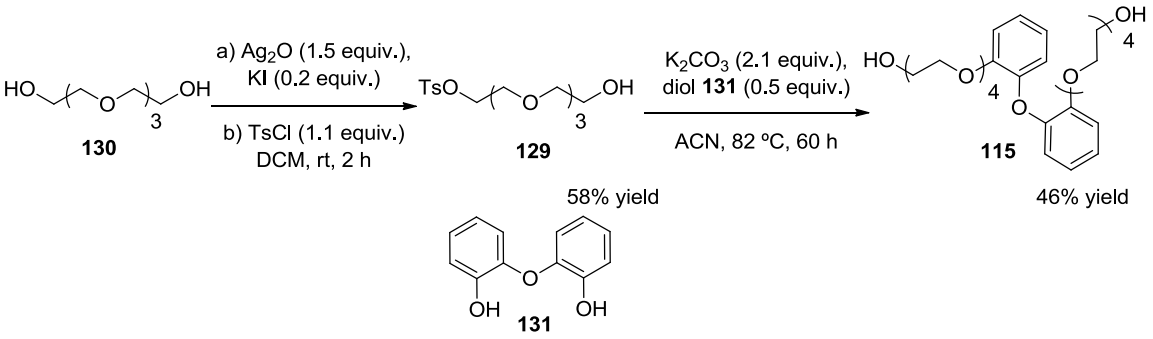

Scheme 36. Synthesis of diol **115**

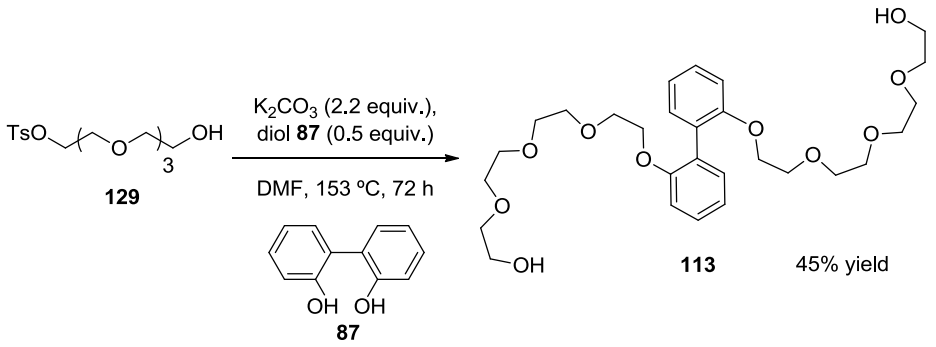

Scheme 37. Synthesis of diol **113**

Lastly, the preparation of diol **88** has already been described in the previous chapter (see Scheme 19 on section 1.2.1).

To summarize, an array of eight structurally diverse bisphosphite ligands with achiral polyether skeletons, bisphosphites **46**, were straightforwardly synthesized from simple starting materials. Isolation of the ligands as analytically pure solids was also easy, revealing this synthetic approach as economic and convenient towards the target bisphosphites with a binding motif for cationic

[152] Rubinshtein, M.; James, C. R.; Young, J. L.; Ma, Y. J.; Kobayashi, Y.; Gianneschi, N. C.; Yang, J. *Org. Lett.* **2010**, *12*, 3560.

species (the polyether chain), which constitutes the required distal regulation site in our approach.

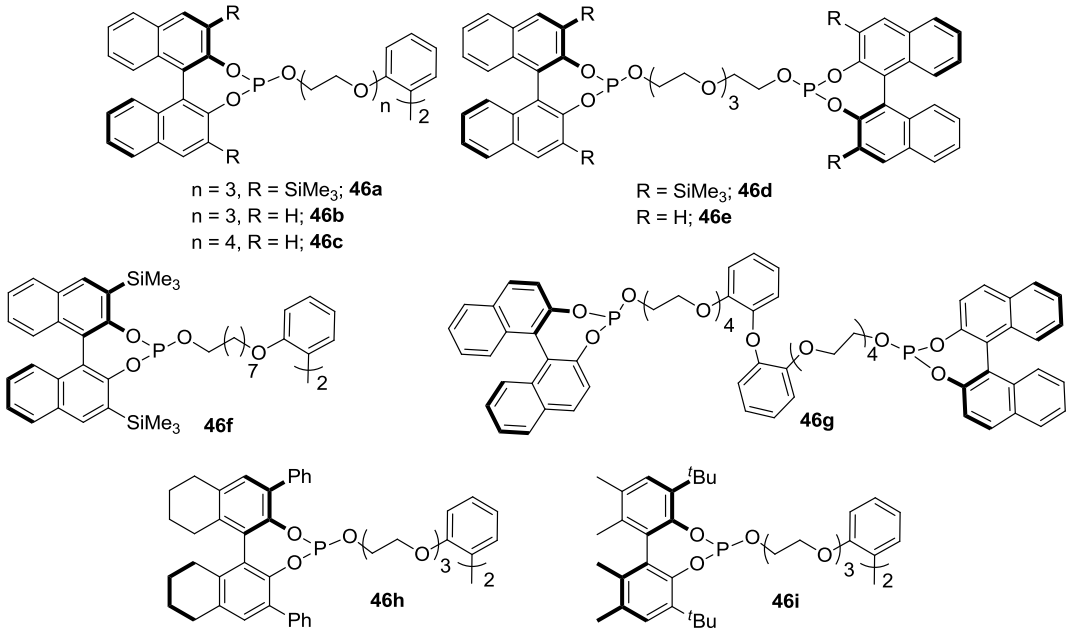

Figure 95. Array of structurally diverse enantiomerically pure bisphosphite ligands **46**

2.2.2 Binding constant determination for ligands 46a,b,d,e with cationic species

As a continuation in our studies towards supramolecular ligands with a distal regulation site for asymmetric catalysis, we examined the binding properties of ligands **46a**,**b** and **46d**,**e** toward different salts in suitable solvents for catalysis. We chose ligands **46a**,**b** and **46d**,**e** because they best represent the totality of the ligands synthesized within this PhD Thesis. Ligands **46a**,**b** have a large polyether chain for binding, whereas **46d**,**e** have a smaller binding site. On the other hand, **46a** and **46d** have a substituent at the 3 and 3' positions in the configurationally stable bisnaphthyl moieties, whereas **46b** and **46e** have no substituents at those positions on the phosphite unit.

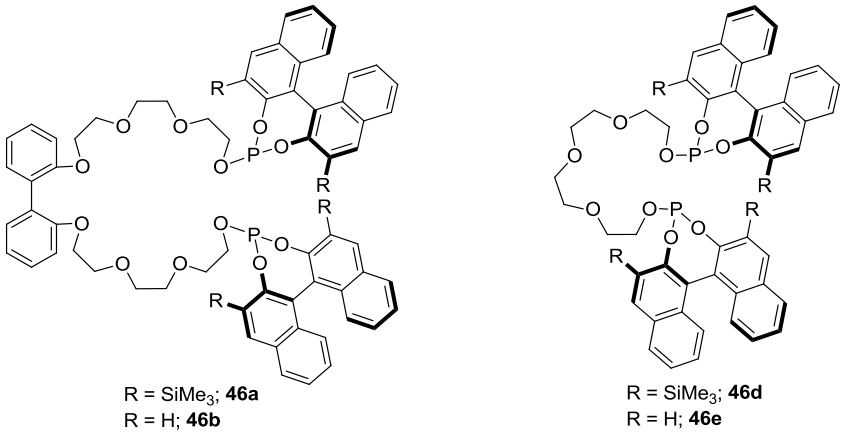

Figure 96. Enantiomerically pure bisphosphite ligands **46a**,**b**,**d**,**e**

Initial studies focused on the binding ability of the bisphosphite ligands towards alkali metal salts. Sodium, rubidium and cesium salts were chosen for these studies as representative examples of salts containing cations with small, medium and large ionic radius, respectively.[153] With regard to the most suitable anionic component of the salts, we turned our attention to the tetrakis[3,5-bis(trifluoromethyl)phenyl]borate $\{B[3,5\text{-}(CF_3)_2C_6H_3]_4\}^-$ anion and commonly referred to as BArF in chemical texts, as BArF salts are relatively soluble in the apolar solvents that we planned to use for our catalytic experiments (*i.e.* toluene, dichloromethane, tetrahydrofurane).

[153] The ionic radii for Na^+, Rb^+ and Cs^+ have been described to be 0.98, 1.48 and 1.67 Å (see: http://www.rsc.org/chemsoc/visualelements/PAGES/data/intro_groupi_data.html).

The methods that we have used for determining binding constants have been already detailed in the previous chapter (see section 1.2.2). Initial binding studies aimed at determining the association constants by NMR spectroscopy. In this case, the addition of increasing amounts of alkali metal BArF salts to ligands **46a** and **46d** in deuterated toluene with small amounts of deuterated THF (95/5 v/v) resulted in clear displacement of ^{1}H and/or ^{31}P NMR signals. Indeed, association constants between ligands **46a** and **46d** with different BArF salts could in this way be determined by nonlinear curve fitting, assuming a 1:1 binding mode (see, as a representative example, Figure 97).[154] The values of the binding constants determined by ^{1}H NMR spectroscopy between NaBArF, RbBArF and CsBArF salts and ligands **46a** and **46d** have been summarized in Table 18.

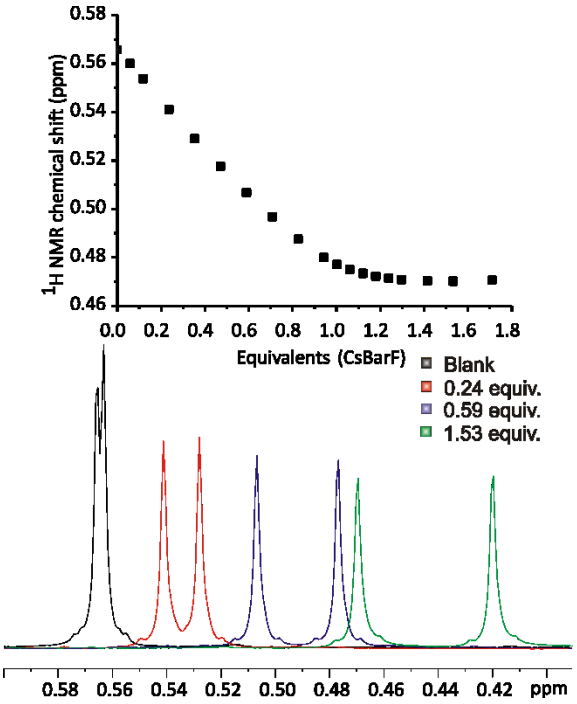

Figure 97. Top: Displacement of the Me_3Si signals in ^{1}H NMR as a function of the amounts of added salt. Bottom: Upfield Me_3Si- signal displacement upon addition of increasing amounts of CsBArF to a solution of **46d** (9 – 7 mM) in toluene-d_8/THF-d_8 (95/5 v/v) at 298K (The two Me_3Si groups in the bisphosphite moiety are observed at different chemical shifts)

[154] NMR titration data was analyzed using the HypNMR software (Version 2008: Protonic Software): a) Frassineti, C.; Alderighi, L.; Gans, P.; Sabatini, A.; Vacca, A.; Ghelli, S. *Anal. Bioanal. Chem.* **2003**, *376*, 1041. b) Frassineti, C.; Ghelli, S.; Gans, P.; Sabatini, A.; Moruzzi, M. S.; Vacca, A. *Anal. Biochem.* **1995**, *231*, 374.

Table 18. Results of binding constant determination of ligands **46a** and **46d** with different alkali metal salts by ^{31}P or ^{1}H NMR spectroscopy[a]

		Log *K*		
Entry	**Ligand**	**NaBArF**	**RbBArF**	**CsBArF**
1	**46a**	4.2	n.d.	3.8
2	**46d**	3.7	4.0	4.1[b]

[a] Average value of at least two independent measurements. Measured by NMR spectroscopy in toluene-d_8/THF-d_8 (95/5 v/v). [b] This binding constant was determined to be Log *K* = 4.1 by UV-vis titration in toluene /THF (95/5 v/v)

Conversely, the association constants between ligands **46b** and **46e** with the previously mentioned polyoxyethylene binders were found to be too high to be measured by NMR spectroscopy. Therefore, UV-vis spectrophotometry seemed to us a more convenient technique for the association processes involving these ligands. Changes in absorption bands ranging from 260 to 350 nm were observed during the titration (addition of increasing amounts of these BArF salts from different cations to ligands **46b** and **46e** in a dichloromethane/tetrahydrofuran 98/2 v/v mixture led to increased and decreased absorption intensities at around 260 and 290 nm, respectively; see Figure 98). Analysis of the UV-titration curve by nonlinear curve fitting assuming a 1:1 binding model allowed us to determine the *K*-values between **46b** and **46e** and the different BArF salts. Results are summarized in Table 19.

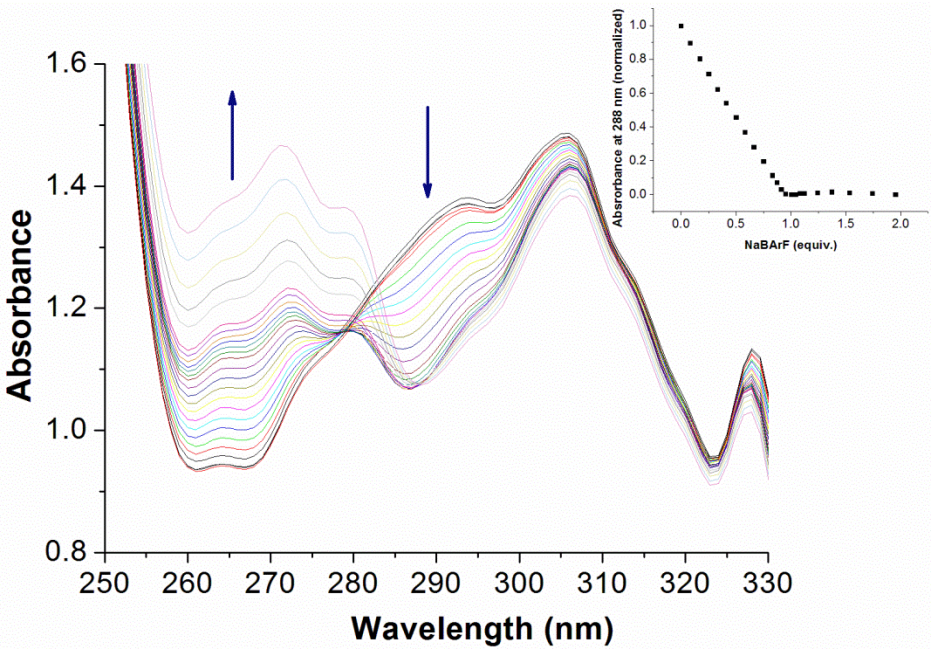

Figure 98. UV-vis titration: **46b** (0.06 mM) upon addition of increasing amounts of NaBArF (0 – 0.12 mM) in DCM/THF (98/2 v/v) at 298 K

Table 19. Results of binding constant determination of ligands **46b** and **46e** with different alkali metal salts by UV-vis spectrophotometry[a]

		Log *K*	
Entry	**Ligand**	**NaBArF**	**CsBArF**
1	**46b**	6.6	> 7.5[b]
2	**46e**	7.5	6.9

[a] Average value of at least two independent measurements. Measured by UV-vis spectrophotometry in dichloromethane/THF (98/2 v/v). [b] *K*-value was too high to be measured by UV-vis spectrophotometry.

Higher binding constants (log *K* > 6) were found between unsubstituted ligands **46b** and **46e** and metal alkali BArF salts than for the 3,3'-disubstituted analogous ligands **46a** and **46d** (log *K* = *ca.* 4). We rationalize that the presence of the Me_3Si- groups at the 3 and 3' positions of the phosphite moieties in ligands **46a** and **46d** decreased the binding constants due to the increase in steric bulk in the proximity of the polyether chain.

In order to study the effect of the solvent on the *K*-value, the binding affinity of ligand **46e** towards CsBArF[155] was also determined in toluene/THF (98/2 v/v) by emission and UV-vis spectrophotometry. The binding constant determined by emission (Log *K* = 7.1) and by UV-vis spectrophotometry (Log *K* = 7.0) for this ligand towards CsBArF were slightly higher than the value found in DCM/THF (98/2 v/v) by UV-vis spectrophotometry (Log *K* = 6.9, see entry 2 in Table 19). As already discussed in the previous chapter for the binding of 2,2'-diphosphino-1,1'-biphenyl derivatives with an appended crown ether, the strength of ion-dipole interactions increase as the relative permittivity or dielectric constant of the solvent (ε) decreases. Thus, the *K*-value for an association process for a given host and guest *via* ion-dipole interactions would be expected to be higher in toluene, followed by dichloromethane (ε for toluene and dichloromethane = 2.38 and 8.93[156] at 25 ºC, respectively).

In order to study whether the alkali metal BArF salts dissociate in the solvents that we planned to use in the catalytic studies (*i.e.* DCM or toluene, both with small amounts of THF) or tend to remain associated (*i.e.* ion pairs), we determined the molar conductivity of CsBArF in DCM/THF (99/1 v/v) and toluene/THF (95/5 v/v) at different CsBArF concentrations (Figure 99) with a conductivity meter.[157] Studies on the changes of the molar conductivity of a solution as a function of the concentration seemed to us a suitable technique to study the tendency of the BArF salts to dissociate.[158] Whilst the molar conductivitity of CsBArF increased upon decreasing its concentration in DCM/THF (99/1 v/v) in the whole range of studied concentrations (from 1 x 10^{-3} to 1 x 10^{-5} M), its conductivity in toluene only showed the same behavior in concentrations lower than 1 mM in toluene/THF (95/5 v/v), but increased for higher concentration. Typically, an increase in the molar conductivity as concentration decreases is associated with a dissociation process of the salt taking place in the range of studied concentrations (from 1 x 10^{-3} to 1 x 10^{-5} M in

[155] These studies were carried out only with CsBArF given its reasonably high solubility in toluene.
[156] Reichardt, C. *Solvents and Solvent Effects in Organic Chemistry*; Wiley-VCH: Weinheim, 2003.
[157] S30 SevenEasy apparatus equipped with Sensor INLAB718.
[158] a) Danil de Namor, A. F.; Khalife, R. *Phys. Chem. Chem. Phys.* **2010**, *12*, 753. b) Vrhovsek, A.; Cerar, J.; Bester-Rogac, M.; Skerjanc, J. *Phys. Chem. Chem. Phys.* **2001**, *3*, 2650. c) Duer, W. C.; Robinson, R. A.; Bates, R. G. *J. Chem. Soc., Faraday Trans. 1* **1972**, *68*, 716. d) Fuoss, R. M. *J. Am. Chem. Soc.* **1958**, *80*, 5059.

DCM/THF (99/1 v/v)). On the contrary, this tendency is not observed in toluene/THF (95/5 v/v), which indicates that a certain degree of association between the BArF and cesium ions remains in solution in this solvent mixture in the studied range of concentrations.

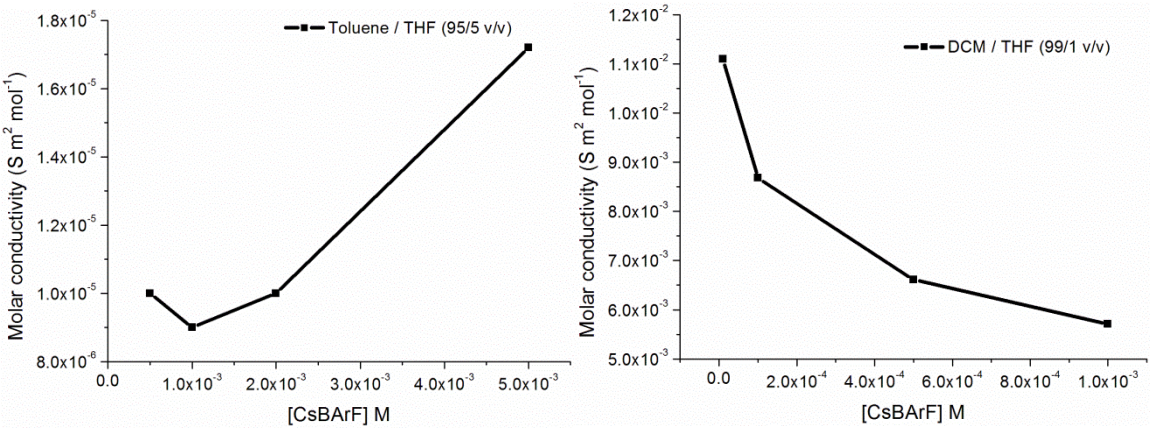

Figure 99. Molar conductivity versus CsBArF concentration in (left) toluene/THF (95/5 v/v) and (right) DCM/THF (99/1 v/v)

The stoichiometry of the formed complexes was determined by the method of continuous variations[159] (Job plot analysis), which is more commonly used for determining the relative stoichiometry of the components of a complex than other techniques, such as the slope ratio method or the mole ratio method, amongst others.[160] In order to determine the stoichiometry by the continuous variation method, the following process was followed:

1. The sum of $[Host]_o$ and $[Guest]_o$ concentrations must be kept constant (referred to as α in the following discussion).

2. Solutions of different host concentrations ranging from 0 to α have to be prepared.

3. A plot of a given analytical response (*e.g.* change of a band intensity in UV-vis absorption or emission spectrophotometry, or change in the chemical shift in NMR) from the formed complex as a function of the mole

[159] Renny, J. S.; Tomasevich, L. L.; Tallmadge, E. H.; Collum, D. B. *Angew. Chem., Int. Ed.* **2013**, *52*, 11998.
[160] Hirose, K. in *Analytical Methods in Supramolecular Chemistry*; Schalley, C. A., Ed.; Wiley-VCH: Weinheim, 2007.

fraction of host (χ)[161] is then made. This representation is known as a Job's Plot and the stoichiometry of the formed complex is obtained from the χ-coordinate at which the Job's plot presents a maximum.

For example, when 1:1 complexation is predominant at the equilibrium, the maximum appears at χ = 0.5. In the case of a 1:2 ($H{\bullet}G_2$) stoichiometric complexation, the maximum is located at χ = 0.333. On the other hand, when the predominant species is the 2:1 ($H_2{\bullet}G$) complex, the maximum of the Job's plot is located at χ = 0.666. Figure 100 represents three different Job's plot analysis for complexes of different stoichiometries: 1:1, 1:2 and 2:1 host to guest stoichiometries.

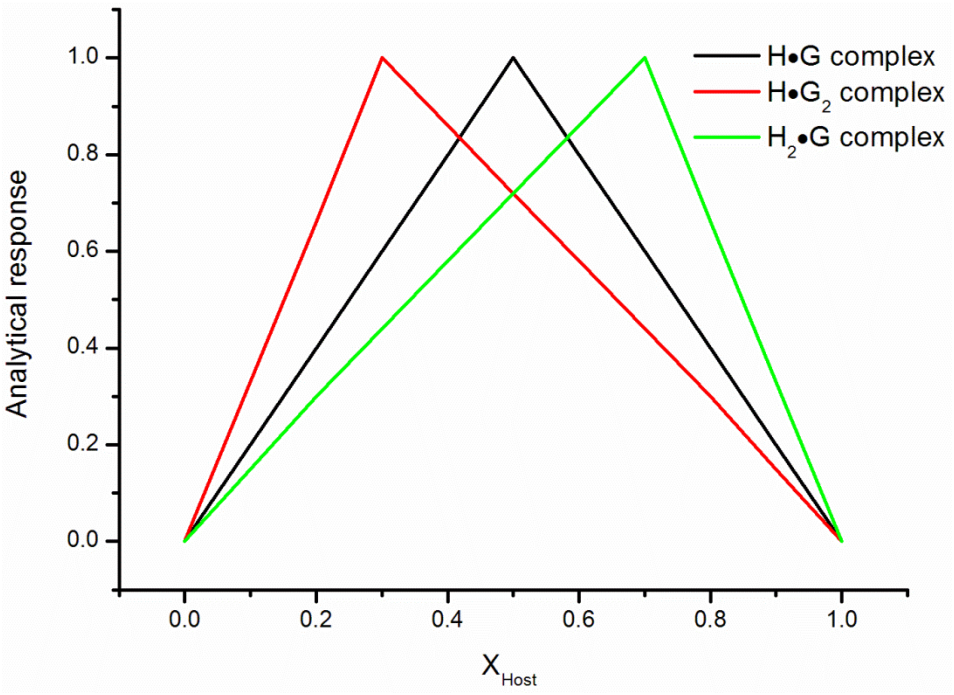

Figure 100. Determination of stoichiometry from the χ-coordinate at the maximum of the curve in Job's plots for complexes of different stoichiometries.

[161] The mole fraction of the host can be calculated with the following formula:

$$\frac{[\text{Host}]_o}{([\text{Host}]_o+[\text{Guest}]_o)} = \chi$$

Thus, the stoichiometry of the formed complexes from bisphosphite ligands **46a**,**b**,**d**,**e** was determined by the method of the continuous variations (Job plot analysis) using UV-vis or NMR techniques. UV-vis spectrophotometry measurements were carried out in DCM/THF (80/20 v/v) at 298 K with a ligand concentration ranging from 0 to *ca*. 5 x 10^{-5} M, whereas NMR spectroscopy measurements were made in toluene-d_8/THF-d_8 (80/20 v/v) at 298 K with a ligand concentration ranging from 0 to *ca*. 6 x 10^{-3} M (see Figure 101 and Figure 102). The results of these studies have been summarized in Table 20.

Table 20. Stoichiometry determination by Job Plot analysis of ligands **46a**,**b**,**d**,**e** with alkali metal BArF salts

		Stoichiometry determination by Job Plot analysis		
Entry	**Ligand**	**NaBArF**	**RbBArF**	**CsBArF**
1	**46a**	n.d.[a]	n.d.[a]	1:1
2	**46b**	1:1	n.d.[a]	n.d.[a]
3	**46d**	1:1	1:1	1:1
4	**46e**	n.d.[a]	n.d.[a]	1:1

[a] Not determined

These studies revealed that all ligands studied (**46a**,**b** and **46d**,**e**) were capable of adapting themselves to a 1:1 stoichiometry independently of the size of the host cavity and the size of the cation. For example, Job plots of ligand **46d** with salts containing the three different salts studied (*i.e.* CsBArF, RbBArF and NaBArF) present the maximum of the curve at a host mole fraction = *ca.* 0.5, which indicates the formation of a 1:1 complex, regardless of the size of the guest. Furthermore, CsBArF also forms 1:1 complexes with three ligands of different size (*i.e*. **46a**,**d**,**e**). This high adaptability might be attributed to the high flexibility of the hosts acting as podands[162] towards the alkali metal ions.

[162] For a recent review on podands and their applications see: Swinburne, A. N.; Steed, J. W. in *Supramolecular Chemistry: From Molecules to Nanomaterials;* Gale, P.; Steed, J. W., Eds.; John Wiley & Sons: New York, 2012.

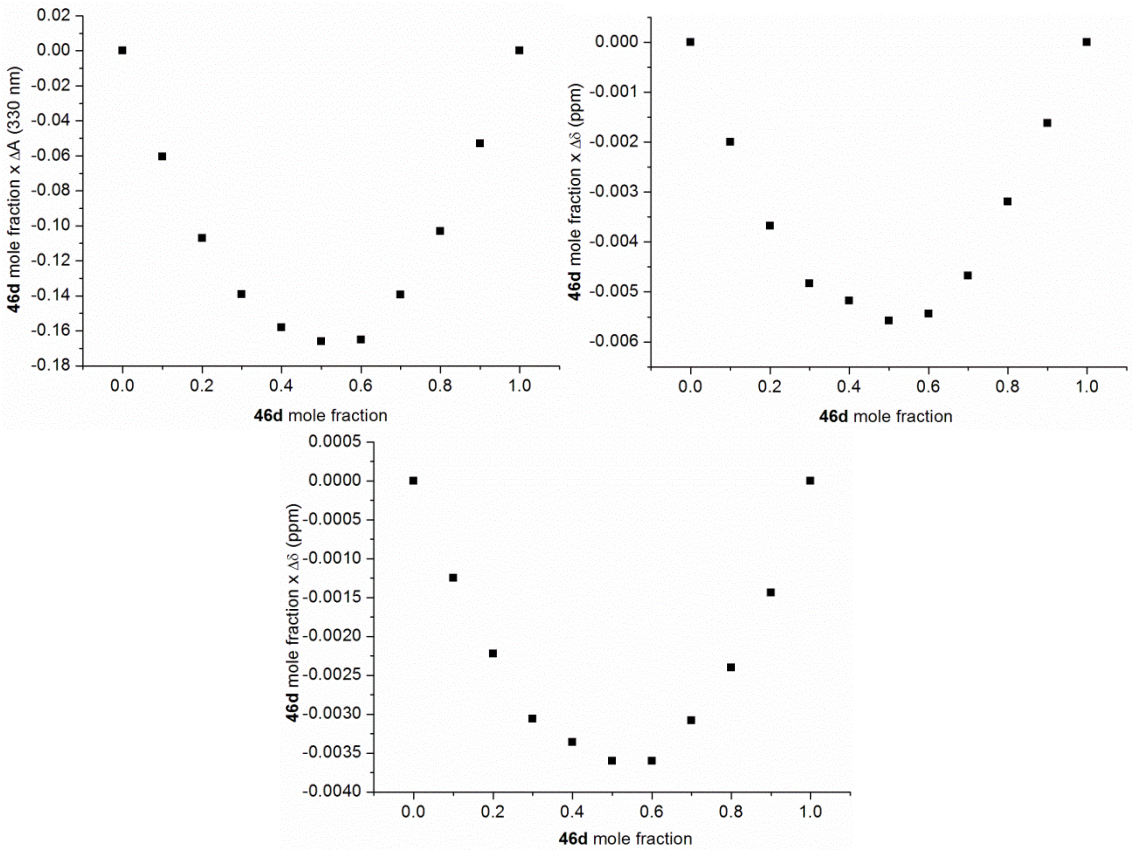

Figure 101. Job plots for **46d** upon addition of CsBArF (top left), RbBArF (top right) and NaBArF (bottom)

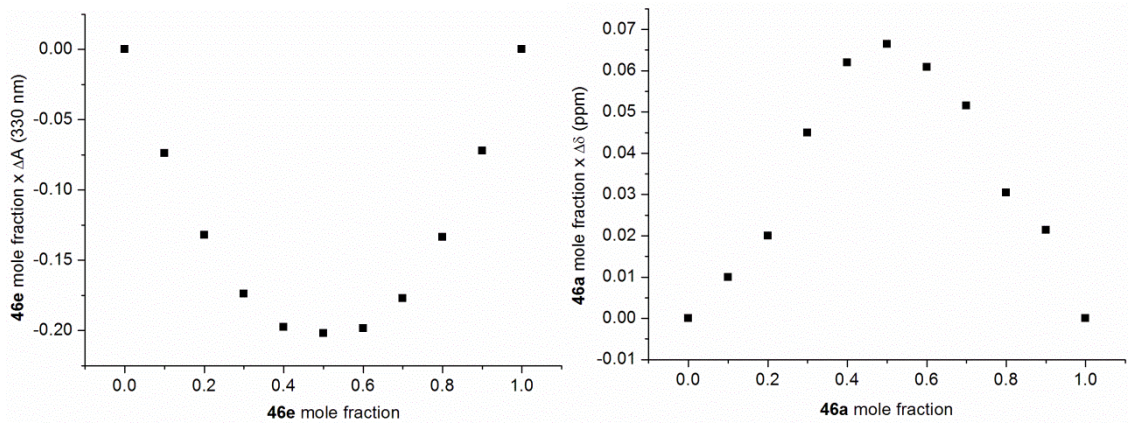

Figure 102. Job plots for **46e** (left) and **46a** (right) upon addition of CsBArF

According to the results obtained, **46e** and **46b** had a preference for NaBArF and CsBArF, respectively, as expected from the size of their cavities. The highest NaBArF affinity was found to be with ligand **46e**, while CsBArF was best fitted in ligand **46b**. This fact showed that the behavior of these ligands was very similar to standard crown ethers, where the size of the host receptor

determines the affinity to the guest. In the case of **46a**, the ^{31}P NMR signal remained almost invariable during the titration with NaBArF, indicating that the binding event was taking place far away from the phosphite moieties. On the other hand, a noteworthy chemical shift displacement in ^{31}P NMR was observed (*ca.* 0.8 ppm) in the case of CsBArF, showing that the binding event was taking place close to the phosphorus atoms and to the sterically demanding Me_3Si-groups. This justify a lower binding affinity of **46a** towards CsBArF than to NaBArF.

With regard to the binding affinities of enantiomerically pure ammonium salts **94** with ligands **46a**,**b** and **46d**,**e**; association constants were determined by fitting NMR titration data (see Figure 104 for the ^{31}P NMR titration curve) to a 1:1 binding model. In all cases, the *K*-values in dichloromethane at 25 ºC were found to be > 10^4 M^{-1}. Furthermore, the formation of a well-defined complex between ligands **46** and ammonium salts **94** was proved by NMR. In particular, 2D NMR NOESY experiments showed intense cross peaks arising from intermolecular through-space interactions between the methyl group of ammonium derivatives **94** and the O-C*H*$_2$C*H*$_2$-O units of the polyether moiety of ligands **46**. As an example, Figure 105 shows an expansion of the aliphatic region of the 2D NMR spectrum of the complex arising after mixing stoichiometric amounts of **46e** and (*R*,*R*)-**94**.

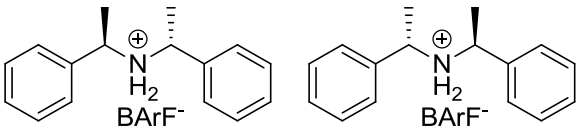

(*R*,*R*)-**94** (*S*,*S*)-**94**

Figure 103. Enantiomerically pure ammonium salts **94**

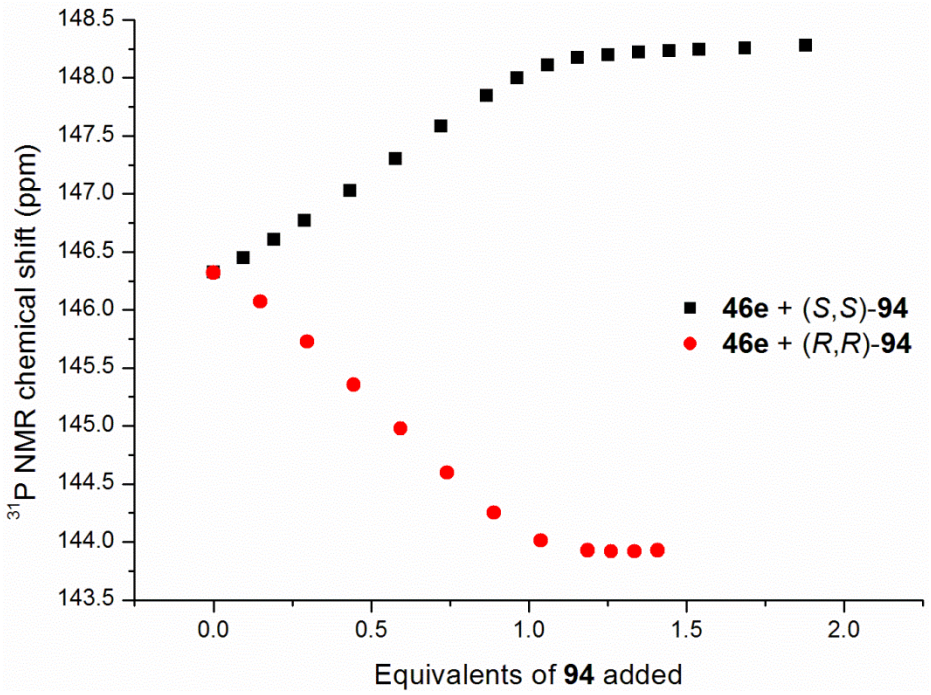

Figure 104. ^{31}P NMR titration curve in DCM-d_2 at 298 K of **46e** with (*R*,*R*)- and (*S*,*S*)-**94** ([**46e**]= 1 x 10^{-2} M)

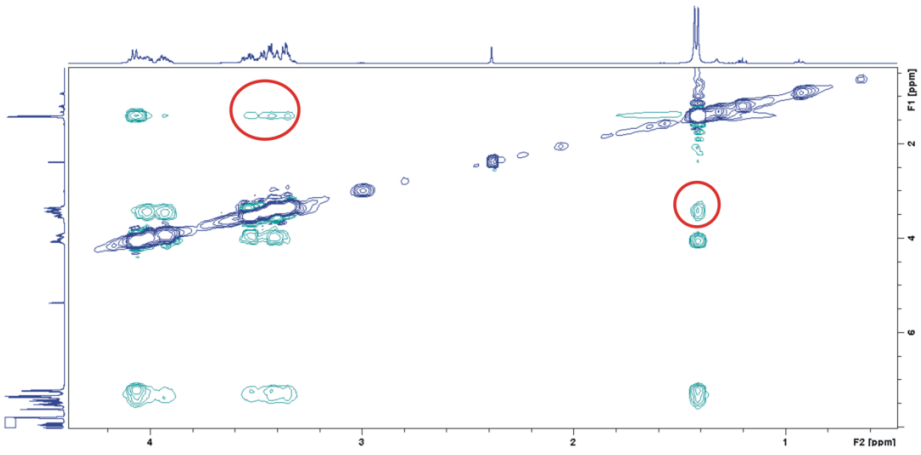

Figure 105. 2D NOESY NMR experiment for (*R*,*R*)-**94•46e** in DCM-d_2 at 298 K

In order to confirm the magnitude of the association constants, we also tried to use alternative techniques to NMR analysis for determining the magnitude of the binding constants. Unfortunately, no spectrophotometric changes were observed during the titration, neither by absorption nor emission spectrophotometry, of ligands **46a**,**b** and **46d**,**e** with ammonium derivatives **94**.

We then turned our attention to isothermal titration calorimetry (ITC),[163] which proved to be a convenient technique for the determination of these association constants. In this case, a solution of ligands **46b** or **46d**,**e** (*ca.* 1 x 10^{-4} M) in dichloromethane was added into the cell of an isothermal calorimeter. Known volumes of a solution of a given concentration of (*S*,*S*)- or (*R*,*R*)-**94** (*ca.* 7 x 10^{-4} M) in dichloromethane were syringed into the host solution. The evolved heat was measured and the analysis of the titration data rendered the thermodynamic parameters. The association constants, together with the thermodynamic parameters *(i.e.* ΔH and ΔS) that were determined by ITC are summarized in Table 21 and Table 22. Association constants were determined to be quite similar in all cases in dichloromethane at 298 K and were close to *ca.* 10^4 M^{-1}. A 1:1 ratio between ligands **46b** or **46d**,**e** and the ammonium salts **94** was deduced from the ITC data and the titration data revealed that all the complexation processes were exothermal ($\Delta H < 0$) but with an unfavorable entropic factor ($\Delta S < 0$). Figure 106 shows a representative example of the ITC raw data and plot of the titration data of the association process between ligand **46e** and (*S*,*S*)-**94**.

Table 21. Results of binding constant determination of ligands **46b** and **46d**,**e** with ammonium derivatives **94** by ITC

		Log *K*[a]	
Entry	**Ligand**	**(*S*,*S*)-94**	**(*R*,*R*)-94**
1	**46e**	4.0	4.1
2	**46d**	3.9	3.9
3	**46b**	4.1	4.2

[a] Average value of at least two independent measurements.

[163] Schmidtchen, F. P. in *Analytical Methods in Supramolecular Chemistry*; Schalley, C. A., Ed.; Wiley-VCH: Weinheim, 2007.

Table 22. Thermodynamic parameters of the binding event between ligands **46b** and **46d**,**e** with ammonium derivatives **94**

		Thermodynamic parameters[a]			
		(*S*,*S*)-**94**		(*R*,*R*)-**94**	
Entry	Ligand	ΔH^b	$T\Delta S^b$	ΔH^b	$T\Delta S^b$
1	**46e**	–7.3	–2.0	–7.2	–1.7
2	**46d**	–7.8	–2.6	–8.2	–2.9
3	**46b**	–7.9	–2.4	–7.0	–1.4

[a] Average value of at least two independent measurements. [b] Kcal mol^{-1}.

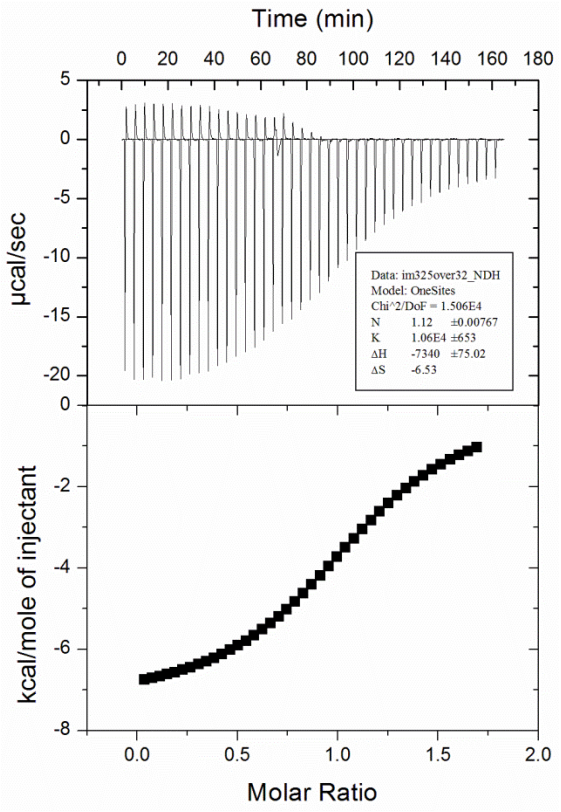

Figure 106. ITC titration data for **46e** and (*S*,*S*)-**94** in DCM at 298K. Top: raw ITC titration data. Bottom: normalized integration data of the evolved heat after each addition as a function of the molar ratio between **46e** and (*S*,*S*)-**94**

In summary, binding constants determined by different techniques (spectrophotometric, NMR or calorimetric titrations) for the ligands synthesized (**46a**,**b** and **46d**,**e**) and the different salts studied (NaBArF, RbBArF, CsBArF and ammonium derivatives **94**) in dichloromethane at 298 K ranged from *ca.* 1 x 10^4 to > 1 x 10^6 M^{-1}. In toluene, at the same temperature, binding constants were

found to be slightly higher. Therefore, the complexation between the two species is in general terms strong.

The importance of the strength of the binding (or the magnitude of the *K*-value) in the catalysis experiments that will be described in future sections, is related to the excess of regulation agent (salt derivative) with respect to ligand that has to be added to the reaction medium to ensure a high extent of complexation. For instance, in a catalysis experiment performed in toluene with a ligand concentration of *ca.* 3 x 10^{-3} M (as it will be described in the following sections, these are standard hydroformylation catalyst screening conditions), addition of 1.3 equivalents of regulation agent (*i.e.* NaBArF, KBArF, RbBArF, CsBArF and ammonium derivatives **94**) leads to the formation of the complex in a > 90% extent for an association constant of 10^4 M^{-1} (Figure 107). For the same complexation conditions as those described before, addition of 1.3 equivalents of regulation agent leads to the formation of complexes in a > 99% yield for an association constant of 10^6 M^{-1} (as will be described in the following sections, these are characteristic complexation conditions during hydrogenation).

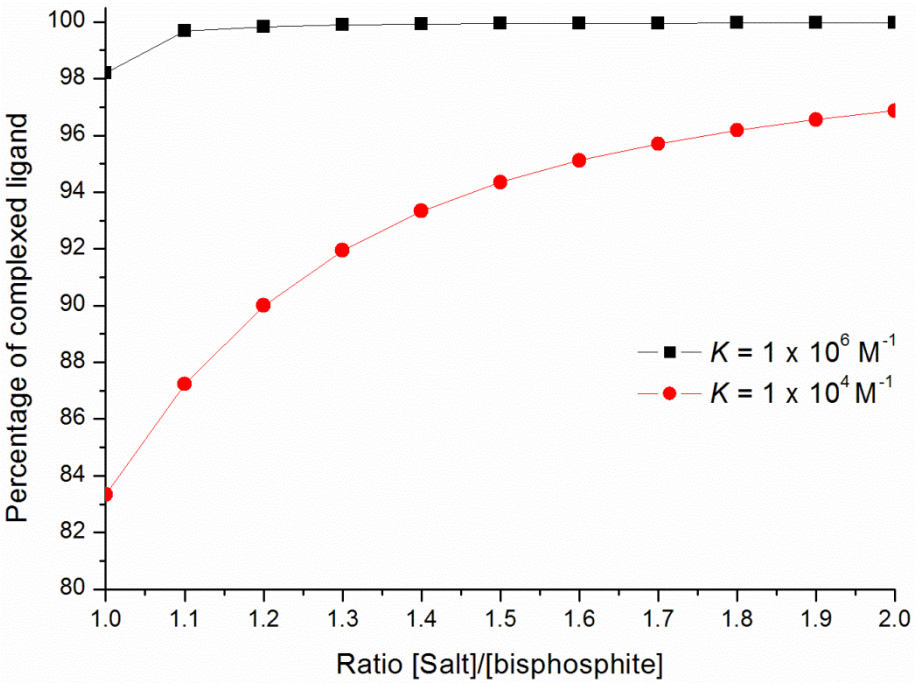

Figure 107. Percentage of complexed ligand depending on the ratio of [Salt]/[Ligand] assuming a *K*-value of 1 x 10^4 (red) or 1 x 10^6 M^{-1} (black)

2.2.3 Rh-mediated asymmetric hydroformylation of diverse alkenes

With the supramolecular ligands and relevant binding parameters of bisphosphite ligands **46a**,**b** and **46d**,**e** in hand, we then turned our attention to possible applications in asymmetric catalysis. We tested our bisphosphite ligands in asymmetric hydroformylation (AHF), which is a powerful synthetic methodology that converts olefins into enantiomerically enriched aldehydes in one synthetic step. Our ligands seemed to us most attractive for asymmetric hydroformylation, since bisphosphite ligands are well-known to efficiently catalyze this transformation upon coordination to a suitable rhodium precursor (*i.e.* [Rh(κ^2O,O'-acac)$(CO)_2$]). It is commonly accepted that bisphosphite ligands are good π-acceptors enhancing the CO dissociation from the rhodium catalysts improving the rate of the hydroformylation reaction.[164] Besides, the best results in hydroformylation have been achieved in low polar solvents, such as toluene or benzene. Therefore, our approach involving regulation using alkali metal or ammonium salts seemed also feasible due to the fact that high binding constants were achieved for CsBArF and **46e** in a toluene/THF mixture.

Branched chiral products obtained from AHF can be further transformed to different products, such as amines, imines, alcohols, and acids which can be used as versatile building blocks for the synthesis of polymer, macrocycle or pharmaceutical intermediates.[165] Styrene **6a** -together with vinyl acetate **6b**, allyl cyanide **6c** and allyl alcohol derivatives- is commonly used as a benchmark substrate to test new catalysts and/or catalytic parameters in asymmetric hydroformylation. For example, asymmetric hydroformylation of vinyl arenes gives access to enantiomerically pure 2-arylpropionic acids. Some of these compounds constitute an interesting class of nonsteroidal anti-inflamatory analgesics (NSAIAs) such as: (*S*)-Naproxen **132**, (*S*)-ibuprofen **133**, (*R*)-flurbiprofen **134** and (*S*)-ketoprofen **135** (Scheme 38). Asymmetric hydroformylation of vinyl acetate **6b** and derivatives have given access to optically active imidazoles[166] **136**, isoxazolines **137**, aminoalcohol **138** and the

[164] Claver, C.; van Leeuwen, P. W. N. M. in *Rhodium Catalyzed Hydroformylation*; Claver, C.; van Leeuwen, P. W. N. M., Eds.; Kluwer Academic Publishers: Dordrecht, 2000.
[165] Franke, R.; Selent, D.; Boerner, A. *Chem. Rev.* **2012**, *112*, 5675.
[166] Thomas, P. J.; Axtell, A. T.; Klosin, J.; Peng, W.; Rand, C. L.; Clark, T. P.; Landis, C. R.; Abboud, K. A. *Org. Lett.* **2007**, *9*, 2665.

antifungal and antibacterial compound (+)-Patulolide C[167] **139** (Scheme 39). Asymmetric hydroformylation of allyl cyanide **6c** leads to optically enriched amino alcohol derivative **142** after two reduction steps. Building block (*R*)-**142** was used for the synthesis of tachykinin NK_1 receptor antagonist **143** developed by Takeda. On the other hand, intermediate (*R*)-**144** was used by Merck in the synthesis of the gonadotropin-releasing hormone antagonist **145** depicted in Scheme 40.[168] Asymmetric hydroformylation of *O*-silyl protected allyl alcohols is also an interesting route to the "Roche aldehyde" **146**, which is usually prepared from the "Roche ester"[169] **43** in two steps: reduction to alcohol followed by selective oxidation to aldehyde.[170] The hydroformylation alternative route is faster and more economical compared to the usual one (Scheme 41).

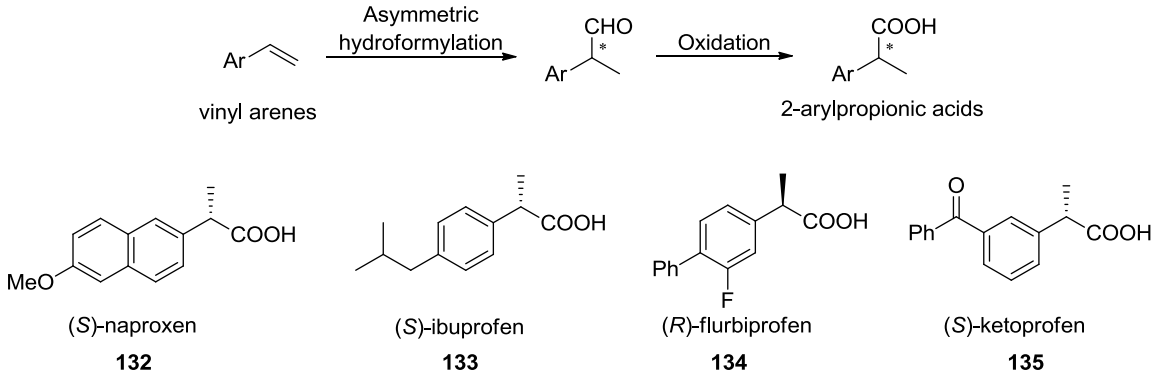

Scheme 38. Synthesis of enantiomerically pure 2-arylpropionic acids by hydroformylation from vinyl arenes

[167] Risi, R. M.; Burke, S. D. *Org. Lett.* **2012**, *14*, 1180.
[168] Cobley, C. J.; Gardner, K.; Klosin, J.; Praquin, C.; Hill, C.; Whiteker, G. T.; Zanotti-Gerosa, A.; Petersen, J. L.; Abboud, K. A. *J. Org. Chem.* **2004**, *69*, 4031.
[169] "Roche ester" **43** can be prepared by asymmetric hydrogenation of methyl-2-(hydroxymethyl)-prop-2-enoate.
[170] Wong, G.W.; Adint, T.T.; Landis, C.R. *Org. Synth.* **2012**, *89*, 243

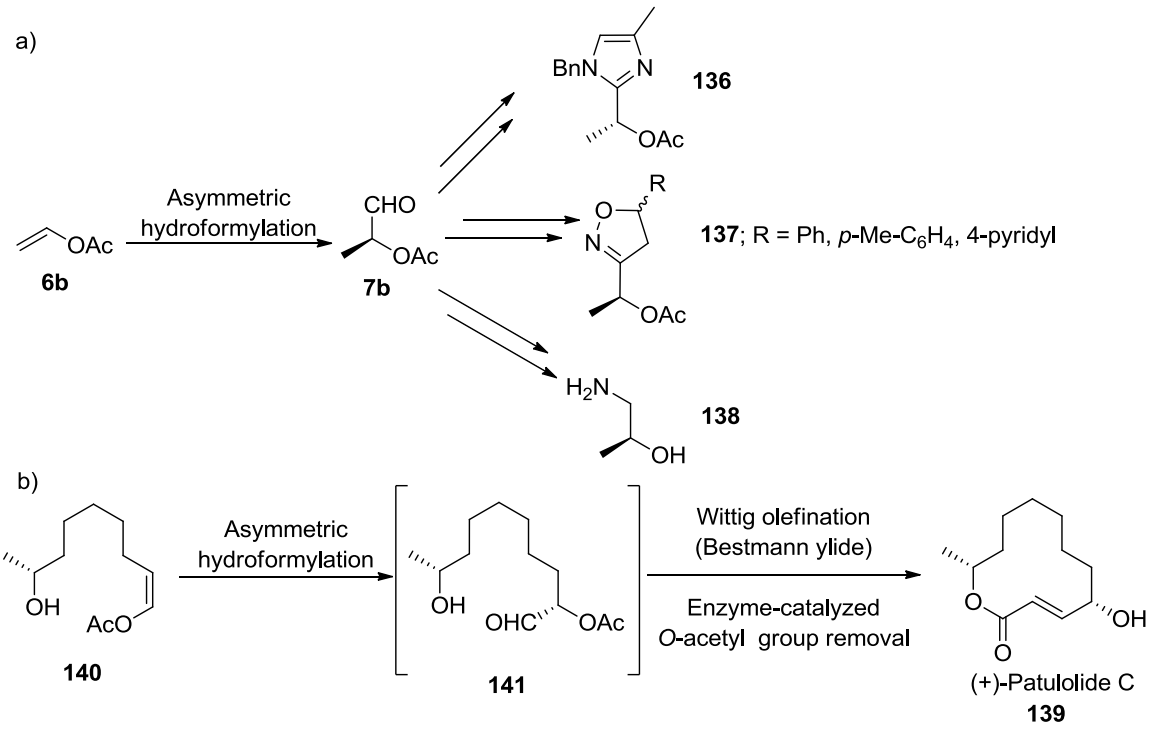

Scheme 39. Synthesis of enantiomerically pure biologically interesting compounds from a) vinyl acetate **6b** and b) an analogous substrate **140**

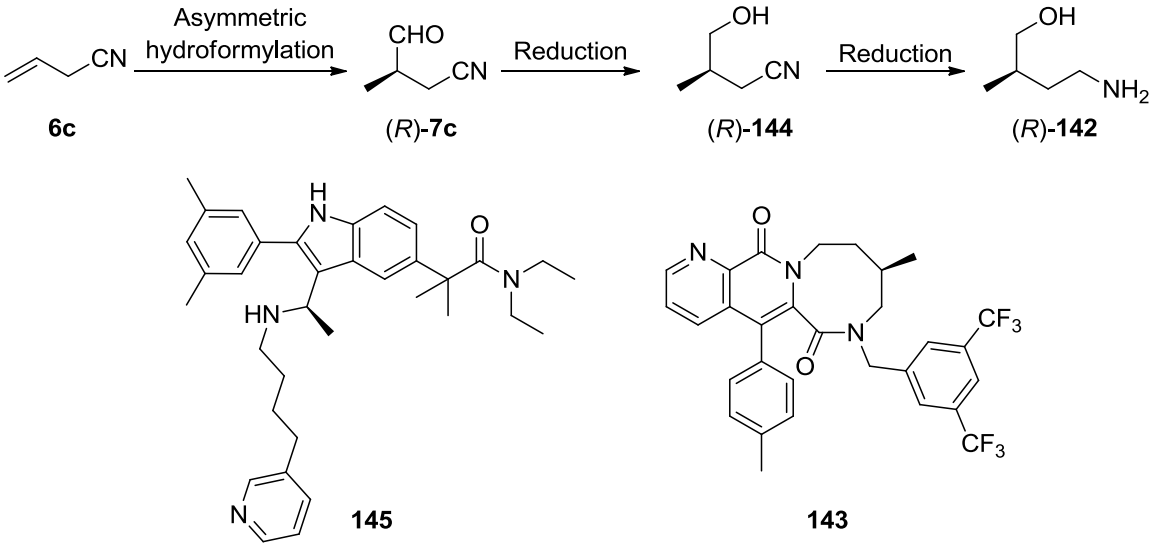

Scheme 40. Synthesis of chiral building blocks **142** and **144** by asymmetric hydroformylation of allyl cyanide **6c**

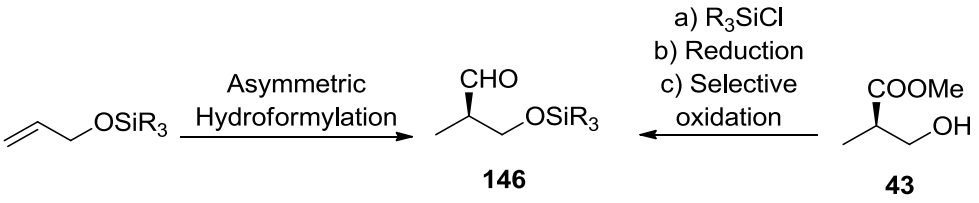

146 **43**

Scheme 41. Synthesis of Roche aldehyde **146** by asymmetric hydroformylation of *O*-silyl protected allyl alcohols or from **43** derivatization

Therefore, preliminary catalytic studies were conducted on the Rh-mediated asymmetric hydroformylation of vinyl acetate substrate **6b**. The Rh(I) catalyst derived from ligand **46b** and [Rh(κ^2O,O'-acac)$(CO)_2$] as metal precursor was tested in the presence of potential regulation agents, which were different salts, incorporating the Na^+, Mg^{2+}, Ba^{2+} and Zn^{2+} cations. To test the anion importance in the regulation of the catalyst activity, three different sodium salts were utilized: $NaBF_4$, $NaClO_4$ and NaBArF. The study was conducted as follows: the salt was solubilized in the minimum amount of THF and then added to a solution of the ligand in toluene, and to this solution [Rh(κ^2O,O'-acac)$(CO)_2$] in toluene, vinyl acetate **6b** and dodecane as internal standard were added. The reaction mixtures were placed into a computer-controlled autoclave (AMTEC reactors). After purging the system, the autoclave was pressurized with 10 bar of a 1:1 mixture of H_2/CO, and the reaction mixtures heated at 70 ºC for 5 hours. Some salts ($Mg(ClO_4)_2$, $Zn(OTf)_2$ and $CsClO_4$) required higher amounts of THF to be completely solubilized in the reaction media (up to toluene/THF 93/7 v/v). The results are summarized in Table 23.

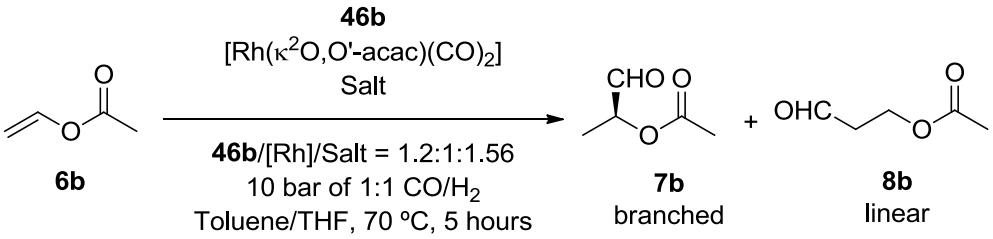

Table 23. AHF of vinyl acetate **6b** with Rh(I) catalysts derived from ligand **46b** in the presence of different salts as regulation agents[a]

Entry	Salt	Conversion (%)[b]	Branched-to-linear product ratio (b/l)[c]	ee (%)[d]
1	-	> 99	90.0:10.0	17
2	NaBArF	84	99.2:0.8	**26**
3	$NaBF_4$	> 99	90.1:9.9	17
4	$NaClO_4$	> 99	90.7:9.3	17
5	$Ba(ClO_4)_2$	37	98.2:1.8	16
6	$Mg(ClO_4)_2$	79	99.8:0.2	14
7	$Zn(OTf)_2$	96	98.8:1.2	16
8	$CsClO_4$	89	94.0:6.0	16

[a] Hydroformylations were done in an AMTEC reactor system. S/C = 200:1; [S] = 0.26 M. Solvent: toluene/THF (97/3 v/v) for entries 1 – 5 and toluene/THF (93:7 v/v) for entries 6 – 8. [b] Conversion, as determined by GC analysis (β-Dex™ 225) using *n*-dodecane as internal standard. [c] Branched-to-linear product ratio, as determined by GC analysis (β-Dex™ 225, ratio of areas). [d] Enantioselectivity towards the (*S*) product, as determined by GC using chiral stationary phases (β-Dex™ 225). Absolute configuration was assigned by comparison of the elution order in GC analysis with the reported data.[171]

The AHF of **6b** mediated by rhodium(I) catalysts derived from ligand **46b** took place in complete (or almost complete) conversion in all cases at 70 ºC for 5 hours, except when $Ba(ClO_4)_2$ was added. Regioselectivities ranged from branched-to-linear ratios = 90.0:10.0 when no cation source was added (entry 1), to > 99.0% of branched product when NaBArF was used (compare entries 1 and 2). It is noteworthy that the enantioselectivity of the process could be improved with NaBArF, from 17% ee for the (*S*) product without any regulation agent up to

[171] Enantiomeric excess determination method for **7a** and **7b** by GC analysis: a) Cobley, C. J.; Klosin, J.; Qin, C.; Whiteker, G. T. *Org. Lett.* **2005**, *7*, 1197. b) Cobley, C. J.; Klosin, J.; Qin, C.; Whiteker, G. T. *Org. Lett.* **2004**, *6*, 3277.

26% for the same configuration product (entries 1 and 2). Interestingly, not all the sodium salts showed this effect. Although all these salts contained low coordinating anions, only the large and least coordinating BArF anion proved to be a suitable counterion for our purposes (entries 2 – 4).

Our next catalytic studies on the AHF of vinyl acetate **6b** were performed with NaBArF and KBArF as cationic sources with rhodium(I) catalysts derived from four different ligands: **46a–c** and **46g**. Ligand **46a** incorporates $SiMe_3$ groups at the 3 and 3' positions of the enantiomerically pure naphthyl groups. **46c** was designed as a larger version of **46b** containing two more binding oxygen atoms in the polyoxyethylene chain. Ligand **46g** contains an oxygen atom between the two phenyl groups of the skeleton chain; this ligand variation was thought to improve the binding ability towards different cations. As in the previous experiments, the AHF reactions were conducted in the AMTEC system under the same conditions to the previously described reactions in Table 23, unless otherwise stated. The results are summarized in Table 24.

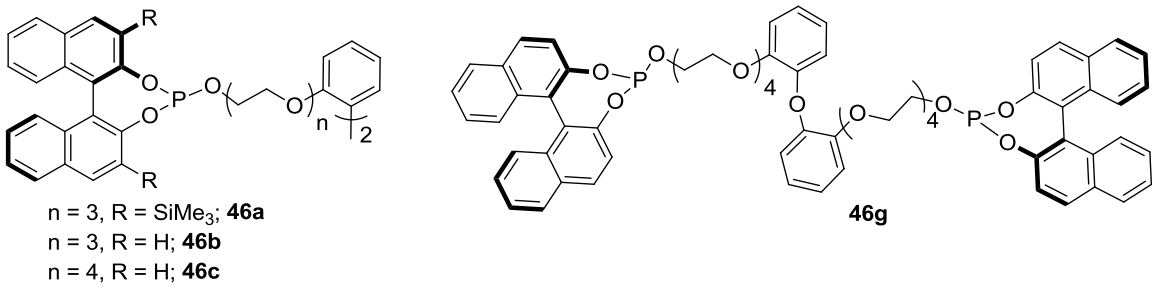

n = 3, R = $SiMe_3$; **46a**
n = 3, R = H; **46b**
n = 4, R = H; **46c**

46g

Figure 108. Bisphosphite ligands **46a–c** and **46g**

Table 24. AHF of vinyl acetate **6b** with Rh(I) catalysts derived from ligands **46a–c** and **46g** in the presence of different regulation agents[a]

Entry	Salt	**Ligand**	Conversion (%)[b]	Branched-to-linear product ratio (b/l)[c]	ee (%)[d]
1	KBArF	**46b**	88	94.9:5.1	27
2	-	**46a**	> 99	99.7:0.3	18
3	NaBArF	**46a**	71	99.9:0.1	19
4	KBArF	**46a**	> 99	99.5:0.5	**43**
5	NaBArF	**46c**	48	97.6:2.4	20
6	KBArF	**46c**	62	95.7:4.3	21
7	NaBArF	**46g**	38	96.2:3.8	26
8	KBArF	**46g**	41	92.8:7.2	24

[a] Hydroformylations were done in an AMTEC reactor system. S/C = 300:1; [S] = 0.42 M. Solvent: toluene/THF (97/3 v/v). For other experimental details (notes b, c and d), see Table 23.

The results in Table 24 clearly indicated that no improvement was achieved in the enantioselectivity of the process by increasing the number of oxygen atoms in the polyoxyethylene chain of the ligands employed (compare entries 5 – 8 in Table 24 for the results of ligands **46c** and **46g**). Most importantly, ligand **46a** showed an important increase in the enantioselectivity of the process when KBArF was added, in comparison to the results obtained when "free" ligand **46a** was used (see entries 2 and 4). The result obtained with KBArF•**46a** in the AHF of vinyl acetate (43% ee) overcomes the results obtained with NaBArF•**46b** or KBArF•**46b** (26 and 27% ee). In conclusion, substitution at the 3 and 3' positions of the biaryl phosphite group proved to be an essential key feature in the bisphosphites with a distal regulation site in AHF. On the other hand, the presence of additional oxygen binding groups in the skeleton chain resulted in poorer results (compare 24 and 21% ee for ligand KBArF•**46g** and KBArF•**46c**, respectively, with 27% ee for ligand KBArF•**46b**; entries 1, 6 and 8 in Table 24). The results obtained with ligand **46a** could be further improved by adding salts with larger cations as regulation agents. For this purpose RbBArF and CsBArF were used in the AHF of vinyl acetate. The results are presented in Table 25.

Table 25. AHF of vinyl acetate **6b** with Rh(I) catalysts derived from ligand **46a** and CsBArF and RbBArF as regulation agents[a]

Entry	Salt	**Ligand**	Conversion (%)[b]	Branched-to-linear product ratio (b/l)[c]	ee (%)[d]
1	CsBArF	**46a**	> 99	> 99.9:0.1	**79**
2	RbBArF	**46a**	91	99.9:0.1	75

[a] Hydroformylations were done in an AMTEC reactor. S/C = 200:1; [S] = 0.26 M. Solvent: toluene/THF (97/3 v/v). For other experimental details (notes b, c and d), see Table 23.

To our delight, enantioselectivity was improved up to 79% ee with the salt containing the large Cs^+ cation as regulation agent. Regioselectivity was also improved to almost complete conversion to the branched product under these conditions.

All the catalytic results previously reported were obtained from reactions carried out at 70 ºC. It is well-known that lowering the reaction temperature in AHF is normally beneficial in terms of enantioselectivity at the expense of diminishing the reaction rate.[164] Thus, we lowered the reaction temperature to 40 ºC, keeping the rest of the reaction conditions identical. The results are shown in Table 26.

Table 26. AHF of vinyl acetate with Rh(I) catalysts derived from ligand **46a** at different temperatures[a]

Entry	Salt	Temperature (ºC)	Conversion (%)[b]	Branched-to-linear product ratio (b/l)[c]	ee (%)[d]
1	-	60	> 99	99.5:0.5	21
2	CsBArF	60	> 99	> 99.9:0.1	83
3	-	50	90	99.2:0.8	21
4	CsBArF	50	> 99	> 99.9:0.1	87
5	-	40	48	99.5:0.5	46
6	CsBArF	40	70	> 99.9:0.1	**92**

[a] Hydroformylations were done in an AMTEC reactor system. S/C = 100:1; [S] = 0.26 M. Solvent: toluene/THF (97/3 v/v) For other experimental details (notes b, c and d), see Table 23.

As expected, the enantiomeric purity of the branched product increased from 79% ee to 92% ee in favor of the (*S*)-configured product just by lowering the temperature from 70 to 40 ºC. We decided not to lower further the temperature, as the conversion obtained in 5 hours with the catalytic system CsBArF•**46a** was not already complete (70%); showing a notable decrease in the rate of the hydroformylation reaction.

In order to expand the approach to other family substrates, the reactions were carried out in a HEL parallel autoclave that allows for a faster screening than the AMTEC reactor and permits lower amounts of substrate and catalyst to be used. To ensure the possibility of comparing results in both reactor systems (HEL and AMTEC), some results on the AHF of vinyl acetate were repeated in the HEL reactor. Conversion, enantioselectivity and regioselectivity were reproducible with these two different reactors as can be deduced from the results summarized in Table 27 (compare entry 2 in Table 27 and entry 6 in Table 26).

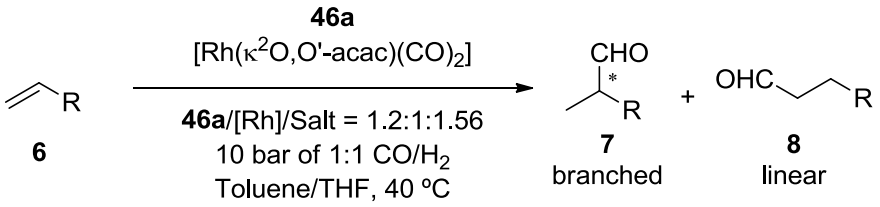
46a
[Rh(κ2O,O'-acac)(CO)2]
46a/[Rh]/Salt = 1.2:1:1.56
10 bar of 1:1 CO/H2
Toluene/THF, 40 ºC
R
6
CHO
R
7
branched
+
OHC
R
8
linear

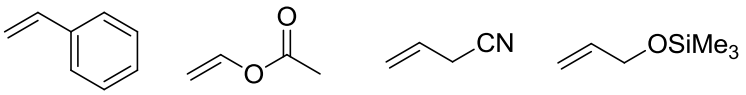
6a
O
O
6b
CN
6c
OSiMe3
6d

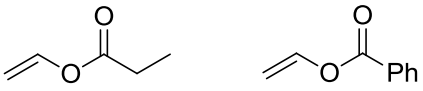
O
O
6e
O
O
Ph
6f

Table 27. AHF of different substrates with Rh(I) catalysts derived from ligand **46a** and regulation agents[a]

		Hydroformylation results			
Entry	**Alkene**	Conv. (%);[b] b/l;[c] ee (%)[d] -	Conv. (%);[b] b/l;[c] ee (%)[d] NaBArF	Conv. (%);[b] b/l;[c] ee (%)[d] KBArF	Conv. (%);[b] b/l;[c] ee (%)[d] CsBArF
1	**6a**	> 99, 94.4:5.6, 15 (*S*)	> 99, 92.3:7.7, 8 (*S*)	> 99, 94.7:5.3, *rac*	> 99, 94.1:5.9, **20** (*S*)
2	**6b**	76, 98.7:1.3, 28 (*S*)	57, > 99:1, 23 (*S*)	66, > 99:1, 64 (*S*)	95, > 99:1, **90** (*S*)
3	**6c**	> 99, 80.0:20.0, *rac*	> 99, 75.0:25.0, 1 (*S*)	> 99, 80.0:20.0, 8 (*S*)	> 99, 80.0:20.0, 3 (*R*)
4	**6d**	> 99,[e] 56.5:43.5,[e] 7 (*S*)	> 99,[e] 66.7:33.3,[e] 24 (*S*)	> 99,[e] 58.3:41.7,[e] 24 (*S*)	> 99,[e] 52.6:47.4,[e] 23 (*S*)
5	**6e**	> 99, 98.3:1.7, 27 (*S*)	> 99, > 99:1, 24 (*S*)	> 99, > 99:1, 58 (*S*)	> 99, > 99:1 **88** (*S*)
6	**6f**	> 99, > 99:1, 9 (*S*)	86, > 99:1, 9 (*S*)	88, > 99:1, 32 (*S*)	> 99, > 99:1 **71** (*S*)

[a] Hydroformylations were done in a HEL parallel autoclave. S/C = 100:1; [S] = 0.26 M. Solvent: toluene/THF (97/3 v/v). T = 40 ºC. Reaction time for **6b** and **6c** was 5 h, whilst for the rest was 18 h. [b] Conversion, as determined by GC analysis using *n*-dodecane as internal standard. [c] Branched-to-linear product ratio, as determined by GC analysis (ratio of areas). [d] Enantioselectivity, as determined by GC using chiral stationary phases. Absolute configurations were assigned by comparison of the elution order in GC analysis with the reported data.[171, 172, 173, 174] [e] Conversion and branched-to-linear product ratio determined by ^{1}H NMR analysis of the crude reaction mixture.

[172] Enantiomeric excess determination method for **7e** and **7f** by GC analysis: Zhang, X.; Cao, B.; Yan, Y.; Yu, S.; Ji, B.; Zhang, X. *Chem. Eur. J.* **2010**, *16*, 871.
[173] Enantiomeric excess determination method for **7d**, **7g**, **7j** and **7k** by GC analysis and **7h** by HPLC analysis: McDonald, R. I.; Wong, G. W.; Neupane, R. P.; Stahl, S. S.; Landis, C. R. *J. Am. Chem. Soc.* **2010**, *132*, 14027.
[174] Enantiomeric excess determination method for **7c** by GC analysis after derivatization of the product to its methyl ester: Zhao, B.; Peng, X.; Wang, Z.; Xia, C.; Ding, K. *Chem. Eur. J.* **2008**, *14*, 7847.

Together with vinyl acetate **6b**, vinyl propionate and vinyl benzoate (**6e** and **6f**, respectively) were also studied. Hydroformylation products from **6e** and **6f** were obtained in only 27% and 9% ee, respectively, when no regulation agent was present. However, the addition of salts with cations of increasing size in the hydroformylation of these three alkenes raised the level of optical purity of the obtained products: CsBArF was the regulation agent that induced the highest increase in enantioselectivity.

AHF products **7e** and **7f** were obtained in 88% and 71% ee in favor of the (*S*)-configured enantiomer and with excellent regioselectivity.

Hydroformylation product **7a** was obtained in only 15% ee in the blank experiment and addition of the diverse regulation agents barely improved the enantioselectivity.

Similarly, enantioselectivity in the hydroformylation of substrate **6d** was improved from 7% ee in the blank experiment to 23 – 24% towards the (*S*)-configured product by using any BArF salt of the considered alkali metals. On the contrary, a slightly higher ratio of the branched-to-linear products was observed with NaBArF (branched-to-linear ratio = 67:33, entry 4 in Table 27), whereas in the rest of the cases the ratio of branched-to-linear product remained constant at about a 56:44 ratio.

Unfortunately, hydroformylation product **7c** was obtained as nearly racemic mixtures in all cases and regioselectivity (branched-to-linear ratio = 80:20) could not be improved by any cationic regulation agent.

As a background experiment, ligand **46f** was employed as a non-supramolecular analogue of ligand **46a**. The peculiarity of this ligand is that it has no oxygen atoms capable of binding the cations of the salts that have been used as regulation agents. Therefore, the proposed regulation mechanism *via* supramolecular interactions on the ligand skeleton of **46f** is not possible. Indeed, no change in the enantioselectivity of the hydroformylation of vinyl acetate with ligand **46f** was observed when CsBArF was present in the reaction media, demonstrating that the interaction of the cation with the polyether chain of the ligand is crucial for improving the catalyst efficiency (Table 28).

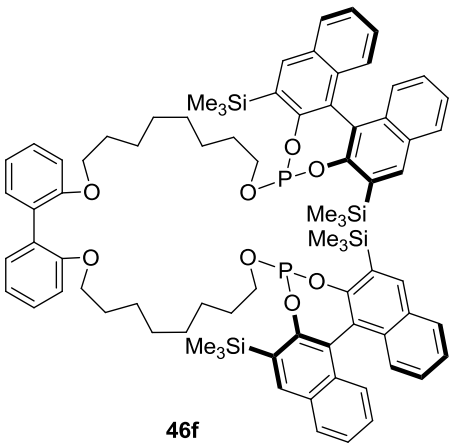

46f

Figure 109. Enantiomerically pure bisphosphite ligand **46f**

Table 28. AHF of vinyl acetate with Rh(I) complexes derived from ligand **46f** with and without CsBArF as the regulation agent[a]

	Hydroformylation results	
Alkene	Conv. (%);[b] b/l;[c] ee (%)[d] -	Conv. (%);[b] b/l;[c] ee (%)[d] CsBArF
6b	44, 94.3:5.7, 22 (*S*)	74, > 99:1 21 (*S*)
For the experimental details (notes a, b, c and d), see Table 27.		

Further AHF studies were conducted with ligand **46a** to expand the substrate scope of our distal regulation system. Different representative examples of substrates such as enamides: **6g**–**i** and the allylic substrates: **6j**–**m** were hydroformylated with and without CsBArF as regulation agent. Table 29 summarizes the results obtained.

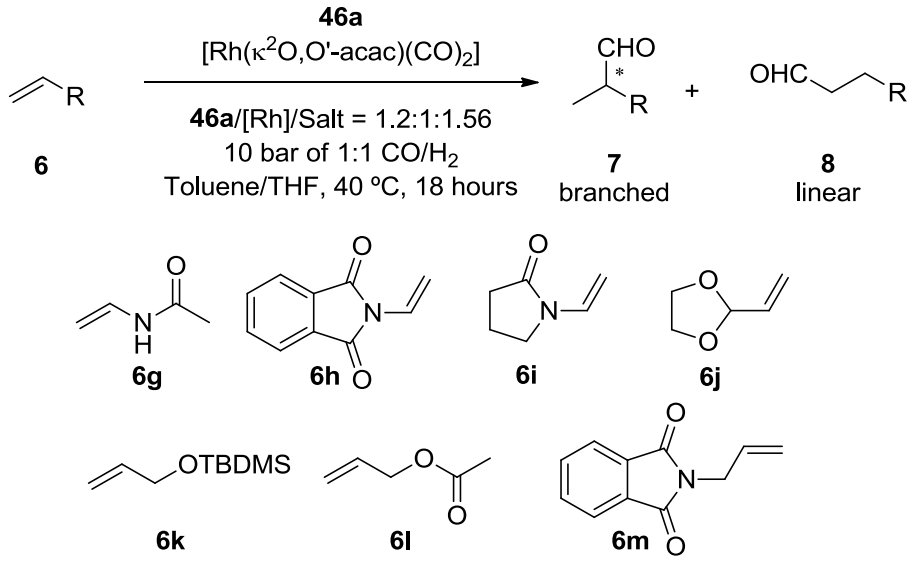

Table 29. AHF of substrates with Rh(I) complexes derived from ligand **46a** with and without CsBArF as regulation agent[a]

Entry	Salt	**Substrate**	Conversion (%)[b]	b/l[c]	ee (%)[d]
1	-	**6g**	> 99	74.4:25.6	18 (*S*)
2	CsBArF	**6g**	> 99	75.6:24.4	22 (*S*)
3	-	**6h**	83	97.0:3.0	61 (*R*)
4	CsBArF	**6h**	58	97.8:2.2	56 (*R*)
5	-	**6i**	45	56.5:43.5	*rac*
6	CsBArF	**6i**	60	61.5:38.5	*rac*
7	-	**6j**	> 99	68.8:31.2	3 (*S*)
8	CsBArF	**6j**	> 99	63.0:37.0	4 (*R*)
9	-	**6k**	> 99	56.5:43.5	12 (*S*)
10	CsBArF	**6k**	> 99	47.4:52.6	25 (*S*)
11	-	**6l**	> 99	77.3:22.7	5 (2)
12	CsBArF	**6l**	> 99	49.8:50.2	24 (1)
13	-	**6m**	> 99	74.4:25.6	9 (*S*)
14	CsBArF	**6m**	> 99	66.7:33.3	28 (*S*)

[a] Hydroformylations were done in a HEL parallel autoclave. S/C = 100:1; [S] = 0.26 M. Solvent: toluene/THF (97/3 v/v). [b,c] Conversion and branched-to-linear product ratio were determined by ^{1}H NMR analysis. [d] Enantioselectivity for products **7g**,[173] **7h**,[173] **7j**,[173] **7k**,[173] **7l**[175] and **7m**[175] was determined by GC or HPLC using chiral stationary phases according to reported methods (except in the case of product **7i**,[176] whose analytical method was developed in our laboratory). Absolute configurations were assigned by comparison of the elution order in GC or HPLC analysis with the reported data.

[175] Enantiomeric excess determination method for **7l** by GC analysis and **7m** by HPLC analysis after derivatization of the product to its methyl ester: Zhang, X.; Cao, B.; Yu, S.; Zhang, X. *Angew. Chem., Int. Ed.* **2010**, *49*, 4047.
[176] NMR data of hydroformylation product **7i**: Saidi, O.; Ruan, J.; Vinci, D.; Wu, X.; Xiao, J. *Tetrahedron Lett.* **2008**, *49*, 3516.

To summarize, the hydroformylation studies on substrates **6g–m** showed that no product was achieved with good enantioselectivity with or without CsBArF as the regulation agent. Moreover, only some allylic substrates presented noticeable improvements in the enantioselectivity of the process in the presence of CsBArF. For example, enantioselectivity for AHF of **6k** rose from 12 to 25% ee when CsBArF was added to the reaction medium, presenting a similar behavior to the analogous substrate **6d** (entry 4, Table 27). The hydroformylation of **6l** and **6m** also presented small improvements in terms of enantiomeric excess with a 28% ee for **6m** in favor of the (*S*)-configured hydroformylation product with CsBArF. Interestingly, product **7h** was obtained in a relatively high 61% enantiomeric excess in favor of the (*R*)-configured product in the absence of a regulation agent. Unfortunately, the enantiomeric excess could not be improved in this case with the addition of CsBArF (entries 3 and 4).

Changing the structure of the phosphite moiety was an interesting option that we decided to explore in order to try to improve the enantioinduction for types of substrates other than the vinyl esters. Bisphosphite ligands **46h** and **46i** incorporating an enantiomerically pure, conformationally stable partially hydrogenated binaphthyl unit (ligand **46h**) and a conformationally stable 3,3'-di-^{t}butyl-[1,1'-biphenyl]-2,2'-diol derived moiety (ligand **46i**), respectively, were utilized. We considered that both ligands could offer different asymmetric environments around the rhodium center capable of mediating the hydroformylation reactions of non-vinyl ester substrates with higher levels of enantioinduction. For these studies, we chose styrene **6a**, vinyl acetate **6b**, 2-vinyl-1,3-dioxolane **6j** and allyl alcohol derivative **6d** as substrates. Results of the AHF of these 4 substrates with and without CsBArF are presented in Table 30.

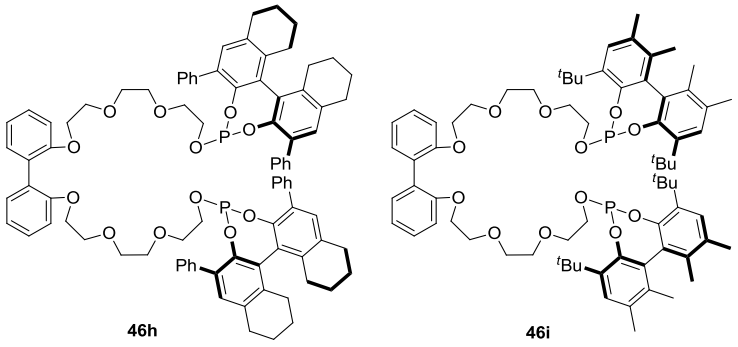

Figure 110. Bisphosphite ligands **46h** and **46i**

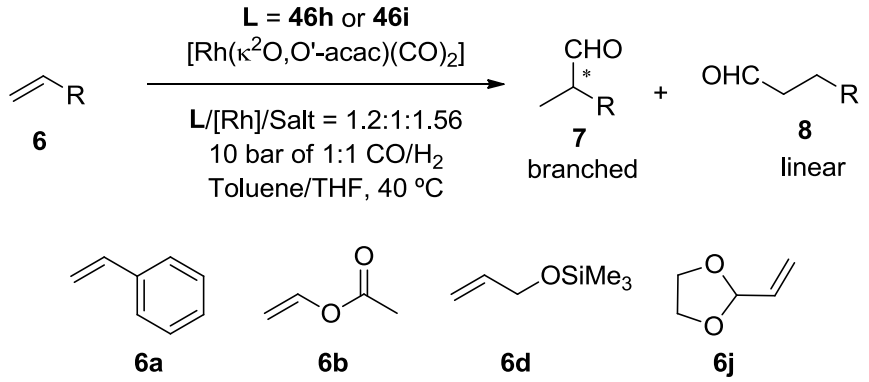

Table 30. AHF of substrates with Rh(I) complexes derived from ligands **46h** and **46i** with and without CsBArF as regulation agent[a]

Entry	Alkene	Hydroformylation results			
		Conv. (%); b/l; ee (%)[f] -		Conv. (%); b/l; ee (%)[f] CsBArF	
		46h	**46i**	**46h**	**46i**
1	**6a**	19[b] 95.6:4.4[c] 3 (*S*)	> 99[b] 95.5:4.5[c] 37 (*S*)	> 99[b] 95.2:4.8[c] 6 (*S*)	> 99[b] 93.8:6.2[c] 42 (*S*)
2	**6b**	55[b] 98.4:1.6[c] 65 (*S*)	92[b] 99.7:0.3[c] 18 (*S*)	> 99[b] 99.5:0.5[c], 80 (*S*)	> 99[b] 99.8.0.2[c] 86 (*S*)
3	**6d**	> 99[d] 70.6:29.4[e] 28 (*S*)	> 99[d] 61.3:38.7[e] 7 (*S*)	> 99[d] 76.2:23.8[e] 28 (*S*)	> 99[d] 43.2:56.8[e] 8 (*S*)
4	**6j**	> 99[d] 76.2:23.8[e] 23 (*R*)	> 99[d] 68.1:31.9[e] 9 (*S*)	> 99[d] 76.2:23.8[e] 23 (*R*)	> 99[d] 71.2:28.8[e] 15 (*R*)

[a] Hydroformylations were done in a HEL parallel autoclave. S/C = 100:1; [S] = 0.26 M. Solvent: toluene/THF (97/3 v/v). [b,c] Conversion and branched-to-linear product ratio was determined by GC analysis. [d,e] Conversion and branched-to-linear product ratio was determined by ^{1}H NMR. [f] Enantioselectivity was determined by GC analysis using chiral stationary phases according to established methods. Absolute configurations were assigned by comparison of the elution order in GC analysis with the reported data.

To summarize, the results obtained with ligands **46h** and **46i** did not show a clear improvement in the AHF of **6d** and **6j** (entries 3 and 4 in Table 30) with respect to other studied ligands.

After studying the effect of the addition of different cations in the AHF of different substrates mediated by Rh(I) complexes derived from the large bisphosphites **46a**, **46b**, **46h** and **46i**, we then focused our attention on the bisphosphite analogues of those previously studied with shorter polyether chain. These ligands **46d**,**e** were prepared as indicated in Section 2.2.1 and were studied in the asymmetric hydroformylation of styrene **6a**, vinyl esters **6b**, **6e** and **6f** and the allyl derivative **6d**.

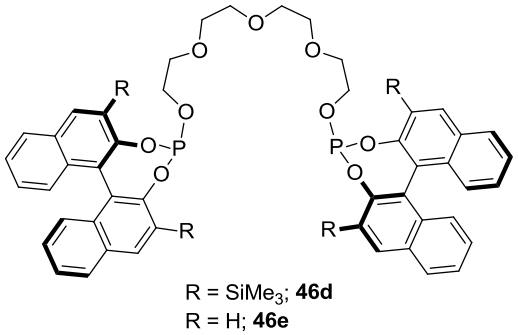

Figure 111. Bisphosphite ligands **46d** and **46e**

The first AHF studies were conducted on vinyl acetate **6b** with ligand **46d** and the whole set of alkali metal BArF salts in order to determine the optimal regulation agent for these ligands with a shorter polyether chain. Ligand **46e** was also included in these studies in order to get clear insight into the importance of the 3,3' substitution pattern in the catalytic efficiency. The results of these studies are summarized in Table 31.

Table 31. Catalytic studies on the hydroformylation of vinyl acetate **6b** using Rh(I) complexes derived from ligands **46d,e** and alkali metal BArF salts as regulation agents[a]

		Hydroformylation Results				
Entry	**Ligand**	Conv (%),[b] b/l ratio,[c] ee (%), (config.)[d]	Conv (%),[b] b/l ratio,[c] ee (%), (config.)[d]	Conv (%),[b] b/l ratio,[c] ee (%), (config.)[d]	Conv (%),[b] b/l ratio,[c] ee (%), (config.)[d]	Conv (%),[b] b/l ratio,[c] ee (%), (config.)[d]
		-	NaBArF	KBArF	RbBArF	CsBArF
1	**46d**	18, 90:10, 35, (*S*)	87, > 99:1, 74, (*S*)	> 99, > 99:1, 98, (*S*)	> 99, > 99:1, 99, (*S*)	> 99, > 99:1, 96, (*S*)
2	**46e**	33, 93:7, 15, (*S*)	-	10, 95:5, 16, (*S*)	-	-

For the experimental details (notes a, b, c and d), see Table 27

Ligands **46d** and **46e** showed similar behavior in the AHF of vinyl acetate **6b** to their analogue ligands **46** with a longer polyether chain. Again, the presence of substituents at the 3 and 3' positions of the [1,1'-binaphthalene]-2,2'-diol unit was key to obtain better enantioselectivities both in the absence or presence of regulation agents. The best result obtained, in terms of enantioselectivity, came from the combination of ligand **46d** and RbBArF. To our delight, the enantioselectvity obtained for the AHF product of **6b** using the combination of ligand **46d** and RbBArF (99% ee, entry 1 in Table 31) was higher than that obtained with ligand **46a** and CsBArF (90% ee, entry 2 in Table 27). Indeed, total conversion, perfect regioselectivity towards the branched product and 99% ee of the (*S*)-configured product product **7b** were obtained. These results equaled the best results obtained in the Rh-mediated AHF of **6b** by Landis *et al.*[177] In this example, highly versatile bisdiazaphospholane ligand **16** was applied in a one pot AHF-Wittig Olefination (AHF-WO) reaction. Olefins derived from α-chiral aldehydes **147** were isolated in up to 99% ee without racemization (Figure 112).

[177] Wong, G. W.; Landis, C. R. *Angew. Chem., Int. Ed.* **2013**, *52*, 1564.

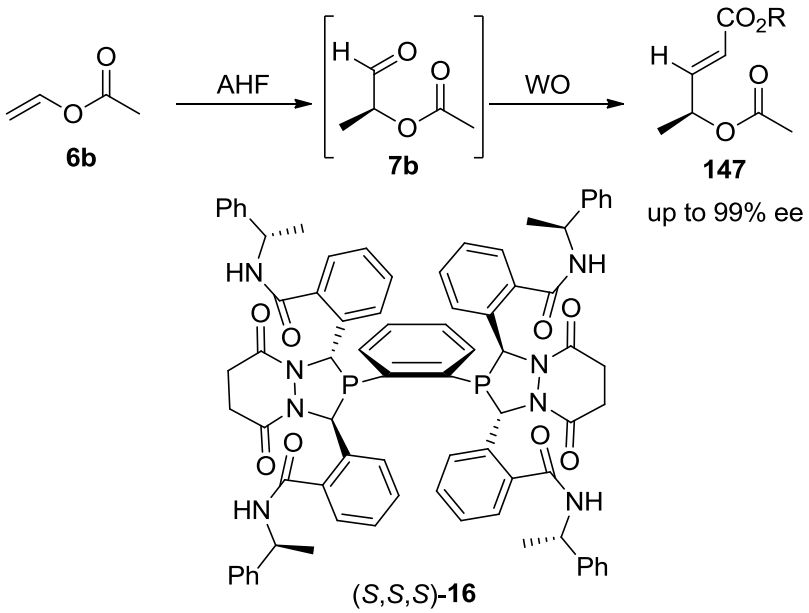

Figure 112. AHF-WO one-pot strategy developed by Landis *et al.* (AHF was mediated by Rh(I) complexes derived from ligand (*S*,*S*,*S*)-**16**)

Furthermore, non-supramolecular structurally related ligands **148**, **149** and **150** (Figure 113) gave poor results in the asymmetric hydroformylation of **6b** according to already published studies (ligand **148**: 2% conversion, 98:2 b/l ratio, 73% ee;[178] ligand **149**: 28% conversion, 92:8 b/l ratio, 10% ee; ligand **150**: 94% conversion, 99:1 b/l ratio, 9% ee);[179] demonstrating the superiority of our supramolecular approach.

[178] Cobley, C. J.; Froese, R. D. J.; Klosin, J.; Qin, C.; Whiteker, G. T.; Abboud, K. A. *Organometallics* **2007**, *26*, 2986.
[179] Whiteker, G. T.; Klosin, J.; Gardner, K. J. Asymmetric Catalysts Prepared from Optically Active Bisphosphites Bridged by Achiral Diols. US2004/0199023 A1, 2004.

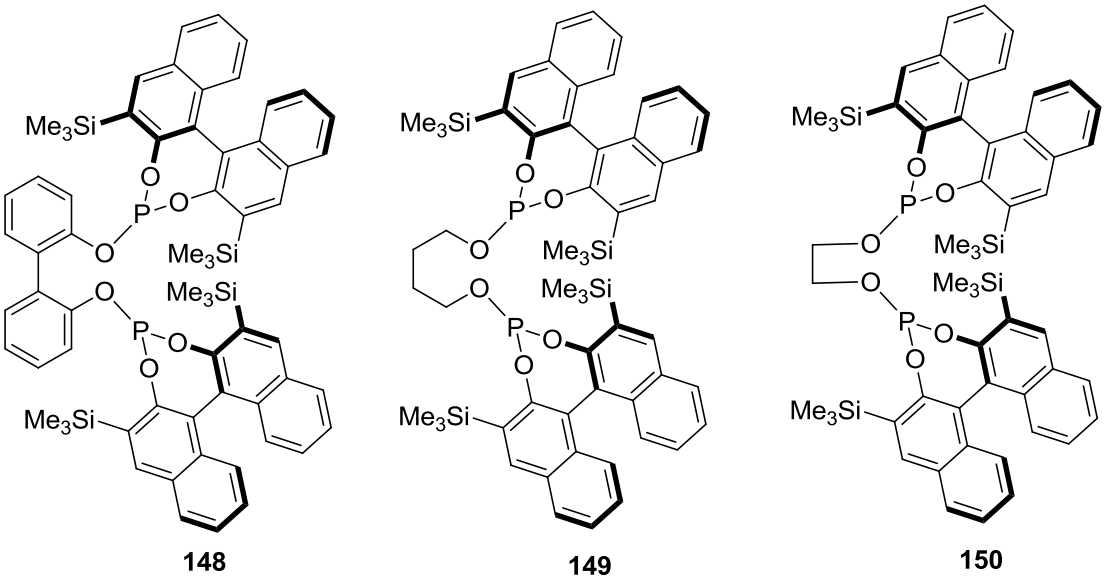

Figure 113. Other bisphosphite ligands employed in the Rh-mediated AHF of **6b**

Thus, the catalytic system RbBArF•**46d** was selected as the "lead" supramolecular ligand for subsequent hydroformylation studies.

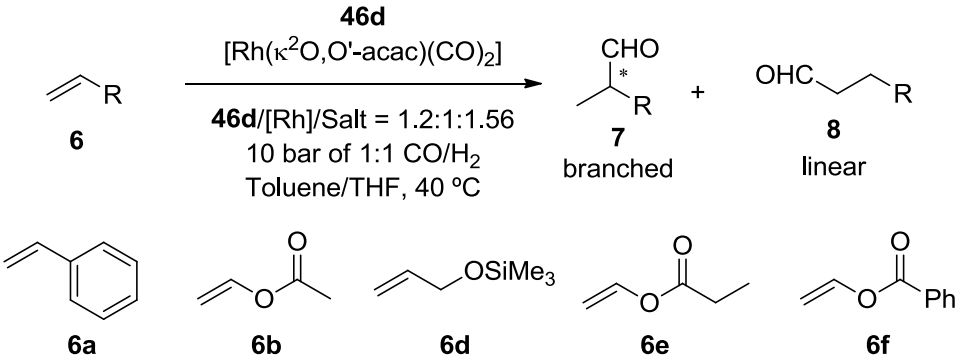

Table 32. Catalytic studies on the hydroformylation of **6a**,**b**,**d–f** using rhodium complexes derived from **46d** and RbBArF•**46d**[a]

Entry	Alkene	Hydroformylation Results	
		Conv (%),[b] b/l ratio,[c] ee (%), (config.)[d] -	Conv (%),[b] b/l ratio,[c] ee (%), (config.)[d] RbBArF
1	**6a**	> 99, 95:5, 12, (*S*)	57, 80:20, 5, (*S*)
2	**6b**	18,[f] 90:10,[f] 35, (*S*)[f]	> 99,[f] > 99:1,[f] 99, (*S*)[f]
3	**6d**	> 99,[e] 59:41,[e] 7, (*S*)	> 99,[e] 18:82,[e] 25, (*S*)
4	**6e**	93, 96:4, 36, (*S*)	> 99, > 99:1, 99, (*S*)
5	**6f**	97, 98:2, 14, (*S*)	99, > 99:1, 96, (*S*)

For the experimental details (notes a, b, c, d and e) see Table 27.
[f] Although these results were already presented in Table 31, they have been included again in this table to aid comparison.

Remarkably, substrate **6f** experienced an increase in the enantioselectivity from 14% ee to 96% ee when hydroformylated in the presence of RbBArF. Enantioselectivities obtained for **6e** (99% ee) and **6f** (96% ee) with RbBArF•**46d** are the best enantioselectivities obtained up to the present date when compared to highest reported ee values (results described by Zhang *et al.* using rhodium complexes derived from phosphine-phosphoramidites such as **17** as catalysts in the AHF of styrene **6a**, allyl cyanide **6c**, vinyl acetate **6b** and derivatives **6e**,**f** (Scheme 42)[172] and *N*-allylamides[175]).

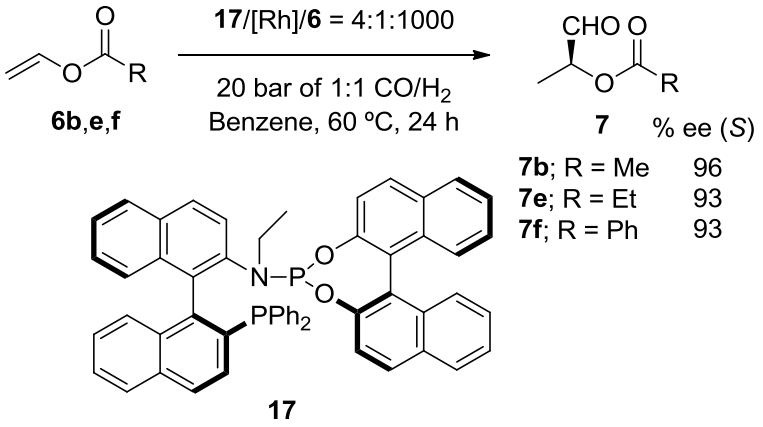

Scheme 42. Zhang's studies on the Rh(I) catalysed AHF of **6b** and derivatives **6e**,**f** with ligand **17**

As has also been observed for bisphosphite ligands incorporating longer polyether chains, **6a** and **6d** were hydroformylated in lower or close enantioselectivities with ligand **46d**, both in the presence or absence of RbBArF as regulation agent. It appears that changing the skeleton of the ligand determines the best cation to be added but it does not change the general behavior of the ligand towards the hydroformylation of the studied array of substrates.

With the aim of determining the minimum amount of catalyst required, we conducted the AHF of **6b** using different amounts of the supramolecular ligand RbBArF•**46d** and extending the reaction time to 24 hours, but keeping the rest of the experimental conditions constant. Results are summarized in Table 33.

Table 33. Catalyst loading studies on the AHF of **6b** with RbBArF•**46d**[a]

Entry	**46d**/[Rh]/RbBArF/**6b**	Conversion[b]	b/l[c]	ee[d]
1[e]	1.2:1:1.56:100	> 99%	> 99:1	99%
2	1.2:1:1.56:200	> 99%	> 99:1	98%
3	1.2:1:1.56:500	98%	> 99:1	98%
4	1.2:1:1.56:1000	83%	> 99:1	97%

For the experimental details (notes a, b, c, and d), see Table 27. [e] Although these results were already presented in Table 32, they have been included in this table to aid comparison.

Decreasing the catalyst loading to 1:1000 had a detrimental effect in the catalytic activity and conversion reached only 83%. On the other hand, enantioselectivity remained almost constant and ranged from 97% to 99% ee (compare entries 1 – 4 in Table 33).

We then studied the possibility of improving these results at 0.1 mol % of catalyst loading by increasing the amount of RbBArF and/or ligand **46d** added with respect to the rhodium precursor. In the current experiments, a reduction in the catalyst amount is evidently associated with a decrease in the concentration of the ligand in the reaction medium. Thus, we decided to double the amount of RbBArF (2.6 equiv. with respect to ligand **46d**, see entry 2 in Table 34) that is normally used (1.3 equiv. with respect to ligand **46d**, see entry 1 in Table 33).[180] Although using 2.6 equiv. of RbBArF instead of the usual 1.3 equiv. ensured a higher formation of the complex,[180] enantioselectivity was barely influenced by this parameter. The results are summarized in Table 34.

Table 34. Catalyst loading studies on the AHF of **6b** with RbBArF•**46d** using 0.1 mol % of rhodium precursor with respect to substrate[a]

Entry	**46d**/[Rh]/RbBArF	Conversion[b]	b/l[c]	ee[d]
1	1.8:1:2.34	82%	> 99:1	98%
2	1.2:1:3.12	82%	> 99:1	97%

For the experimental details (notes a, b, c, and d), see Table 27.

Changing the nature of the regulation agents employed from alkali metal cations to enantiomerically pure primary or secondary alkylammonium derivatives **94**, seemed to us a highly interesting approach to modulate the catalytic activity of the rhodium catalysts derived from our bisphosphite ligands. It should be noted at this point that using each of the two enantiomers from a chiral regulation agent, might lead to “matched” and “mismatched” effects in the regulation mechanism induced *via* ion-dipole/hydrogen bond interactions, as the bisphosphite ligands are used in enantiomerically pure form. Ligands **46a**,**b** and **46d**,**e** already demonstrated a strong binding with both enantiomers of chiral ammonium salt **94**

[180] Assuming a *K*-value = 10^4 M^{-1} for the association process between **46d** and RbBArF, and the ligand concentrations used in these experiments (0.3 – 0.5 mM), the use of 1.3 or 2.6 equiv. of RbBArF leads to the formation of the complex in a 73% or 85% extent, respectively.

(see Section 2.2.2). Therefore, AHF of vinyl acetate was conducted under the standard conditions with ligands **46a** and **46d** in the presence of different BArF alkylammonium salts (**93** – **95**), with the key point being that these salts were soluble in toluene. Therefore, the catalytic studies were carried out in pure toluene.

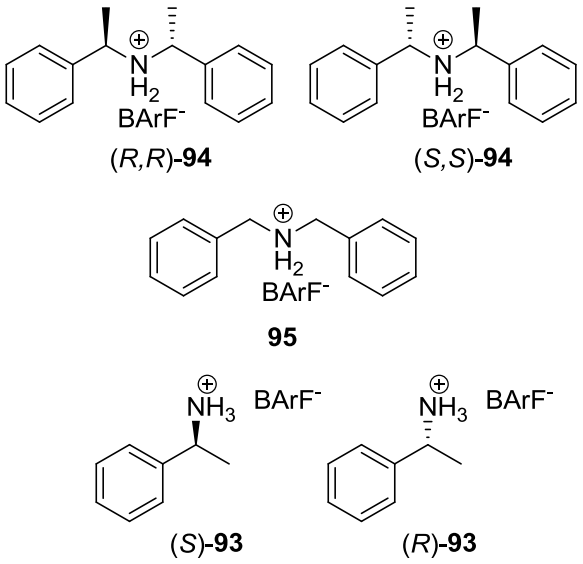

Figure 114. BArF alkylammonium salts (**93** – **95**)

Table 35. Catalytic studies on the hydroformylation of vinyl acetate **6b** using rhodium complexes derived from **46a** and **46d** with alkylammonium salts as regulation agents[a]

		Hydroformylation Results				
Entry	**Ligand**	Conv (%),[b] b/l ratio,[c] ee (%), (config.)[d] **95**	Conv (%),[b] b/l ratio,[c] ee (%), (config.)[d] (*S*)-**93**	Conv (%),[b] b/l ratio,[c] ee (%), (config.)[d] (*R*)-**93**	Conv (%),[b] b/l ratio,[c] ee (%), (config.)[d] (*S,S*)-**94**	Conv (%),[b] b/l ratio,[c] ee (%), (config.)[d] (*R,R*)-**94**
1	**46a**	33, > 99:1, 25, (*S*)	39, > 99:1, 25, (*S*)	37, > 99:1, 25, (*S*)	35, > 99:1, 26, (*S*)	< 1, n.d., 26, (*S*)
2	**46d**	n.d.	n.d.	n.d.	50, > 99:1, 40, (*S*)	46, > 99:1, 40, (*S*)

For the experimental details (notes a, b, c, and d), see Table 27. Results shown in this table were obtained in toluene, as salts **93** – **95** are completely soluble in pure toluene.

Results in Table 35 showed that ammonium-type cations had no effect on the enantioselectivity of the AHF of **6b** with ligands **46a** and **46d**. These results are in contrast with those in which the addition of alkali metal salts as regulation agents had a pronounced effect in the reaction outcome depending on the size of the cation introduced.

As a general conclusion, ligands **46a** and **46d** were shown to be highly efficient ligands for the rhodium-mediated asymmetric hydroformylation of vinyl acetate and related vinylic esters. The effective binding of cationic substances to the ligands employed were studied in section 2.2.2 of this Thesis and resulted in being crucial during catalysis. High enantiomeric excesses in the AHF of **6b**, **6e** or **6f** were found when different alkali metal BArF salts were used. Bisphosphite ligand **46a** with the longest polyether chain required CsBArF to obtain the highest enantioselectivities, whereas ligand **46d** gave better results when combined with a salt containing a smaller cation (RbBArF). Although some regulation effects were found in the AHF of other substrates such as protected allyl alcohols or vinyl arenes, these regulation effects were far from the optimal results obtained for vinyl esters.

*2.2.3.1 Comparative conversion curves in the enantioselective hydroformylation of vinyl acetate **6b** catalyzed by Rh(I) catalysts derived from bisphosphite ligands **46d** and **46a***

In order to have an insight into the catalytic activity profile of ligand **46d** and **46a** and the effect of the BArF salts on the catalyst activity, we decided to carry out a set of experiments monitoring the consumption of syngas (CO/H_2) during the AHF of vinyl acetate under standard reaction conditions.

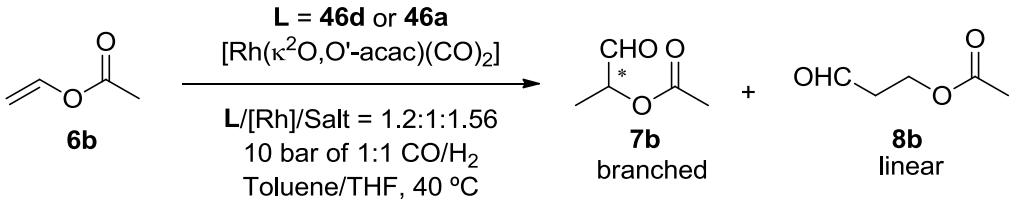

Scheme 43. Asymmetric hydroformylation of **6b** with Rh(I) catalysts derived from bisphosphite ligands **46d** or **46a**

For this purpose, a computer-controlled autoclave equipped with a gas flow-meter (AMTEC) was used. The existing instrumentation at our institute allows for accurate measurements of the consumed gas. For transforming the raw data on consumed gas volumes to conversion, three assumptions were made:

i) The dissolution of the syngas in the reaction medium is much faster than the studied reaction (the gas consumed in solution is immediately replaced by pressure effects).

ii) The catalyst loading is low enough to consider negligible the gas consumed for transforming the initial rhodium precursor into the hydroformylation reaction species.

iii) The concentration of syngas in solution is considered constant during the study.

These considerations allowed us to directly relate the gas up-take to conversion using the following equation:

$$\text{Conversion (\%)} = \frac{n_t - n_o}{n_f - n_o} \cdot 100$$

Where n_t is the gas up-take at a given time and n_o and n_f are the gas up-take data at the beginning of the reaction and at the end, respectively.

In this way, a plot of conversion as a function of time could be generated (Figure 115 and Figure 116). Turnover frequency at half conversion ($TOF_{1/2}$) was determined using the following equation:[181]

$$TOF_{1/2} = \frac{50}{I\ (\%) \cdot t_{1/2}}$$

Where I is the catalyst loading expressed in mol % respect to the substrate and $t_{1/2}$ is the time for half conversion expressed in time units (hours in our case).

In our case, conversion curves for **6b** using ligands **46d**, **46a**, RbBArF•**46d** and CsBArF•**46a** were independently recorded from the gas up-take profiles, and then used to calculate $TOF_{1/2}$ values at 50% conversion. Hydroformylations aimed at measuring the gas uptake were carried out at higher scale (*ca.* 25 times more amount of substrate **6b** was used with respect to catalyst screening experiments), decreasing the catalyst loading to 0.1 mol % and maintaining the rest of the reaction conditions when ligands **46d** or RbBArF•**46d** were used. The catalyst loading was kept at 1 mol % when ligands **46a** or CsBArF•**46a** were used and in this later case the experiments were carried out at lower scale (*ca.* 3 times more amount of substrate **6b** with respect to catalyst screening experiments). Gratifyingly, with the catalytic system RbBArF•**46d**, conversion was complete

[181] Kozuch, S.; Martin, J. M. L. *ACS Catal.* **2012**, *2*, 2787.

after 24 h and almost no loss of enantioselectivity was detected (97% ee in favor of the (*S*)-configured product). Conversely, ligand **46d** without any regulation agent led to *ca.* 55% conversion, which was in good agreement with the value determined by ^{1}H NMR of the final crude mixture at the end of the reaction (Figure 115).

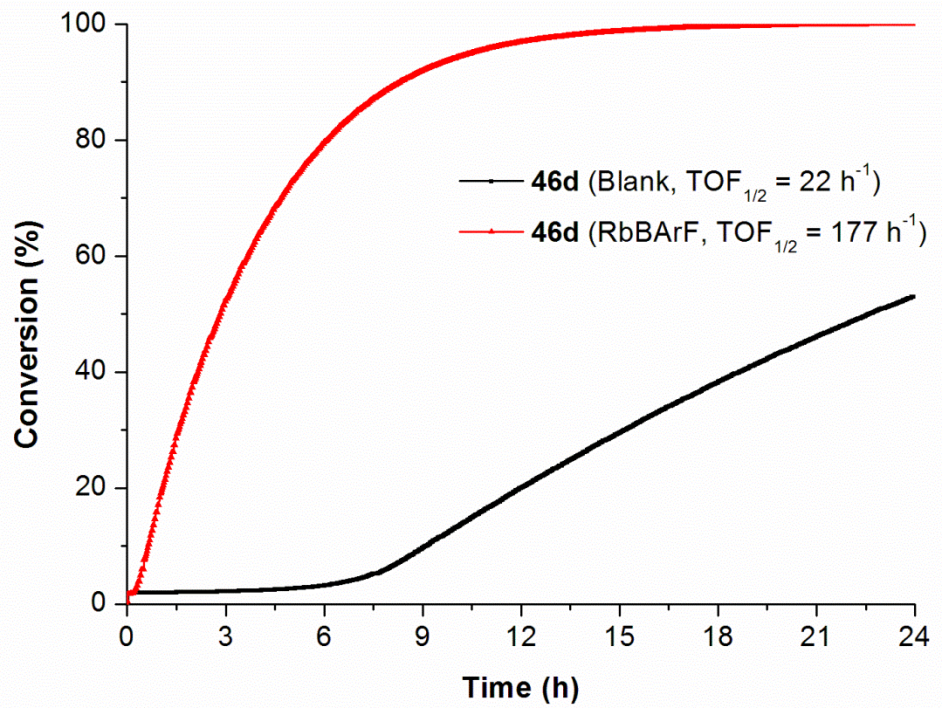

Figure 115. Plot of conversion against reaction time for the enantioselective hydroformylation of **6b** catalyzed by rhodium complexes derived from RbBArF•**46d** (red curve) and **46d** (black curve)

It is noteworthy to mention that the $TOF_{1/2}$ value of the hydroformylation mediated by the supramolecular ligand derived from bisphosphite **46d** and RbBArF was much higher than that obtained in the absence of RbBArF ($TOF_{1/2}$ = 177 h^{-1} for RbBArF•**46d** and $TOF_{1/2}$ = 22 h^{-1} for **46d**). This result clearly indicates that RbBArF not only increases the enantioselectivity of the AHF, but also accelerates the hydroformylation reaction of vinyl acetate **6b.** Interestingly, a template effect could be deduced from the activity rate of RbBArF•**46d**. A high consumption of syngas was detected from the beginning of the reaction with RbBArF•**46d** as the catalytic system, whereas **46d** needed almost 6 hours of incubation time to become active. This observation might point out to the importance of RbBArF as a catalyst template that facilitates preorganization.

Similar results were obtained with ligand **46a** and the catalytic system CsBArF•**46a**. In this case, the $TOF_{1/2}$ value of the hydroformylation mediated by the supramolecular ligand derived from bisphosphite **46a** and CsBArF was also higher than that obtained in the absence of CsBArF ($TOF_{1/2}$ = 27 h^{-1} for CsBArF•**46a** and $TOF_{1/2}$ = 12 h^{-1} for **46a**). Ligand **46a** needed also an incubation time (*ca.* 2 hours) before becoming active (Figure 116).

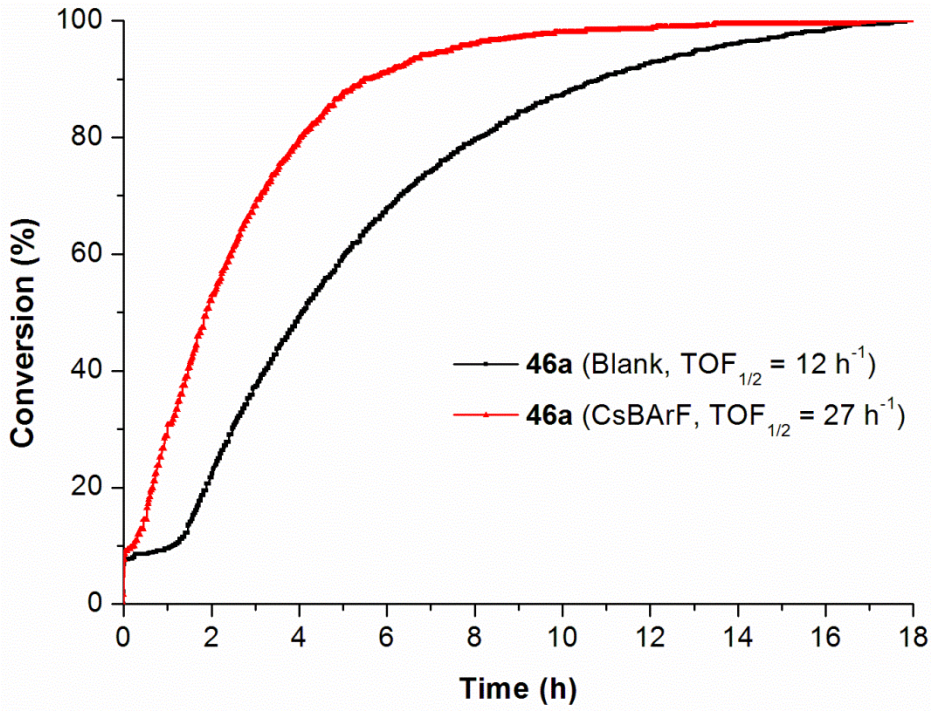

Figure 116. Plot of conversion against reaction time for the enantioselective hydroformylation of **6b** catalyzed by rhodium complexes derived from CsBArF•**46a** (red curve) and **46a** (black curve)

*2.2.3.2 In situ studies on the structure of Rh(I) catalysts derived from ligands CsBArF•**46a** and RbBArF•**46d***

In order to elucidate the structure of catalytic relevant species involved in the hydroformylation mediated by the rhodium complexes of RbBArF•**46d** and CsBArF•**46a**, we performed complexation experiments between the rhodium-precursor used [Rh(κ^2O,O'-acac)$(CO)_2$], ligands **46a** and **46d** and RbBArF and CsBArF as regulation agents under 10 bar of 1:1 CO/H_2 in a 5 mm high pressure HP-NMR sapphire tube. It is well known that phosphorus bidentate ligands normally react with [Rh(κ^2O,O'-acac)$(CO)_2$] under a CO/H_2 atmosphere yielding the neutral mono-hydrido, bis-carbonyl rhodium complex [Rh(H)$(CO)_2(P^1$-$P^2)$]

indicated in Scheme 44, which is considered to be the resting state in the "*type I kinetics*" hydroformylation catalytic cycle.[182]

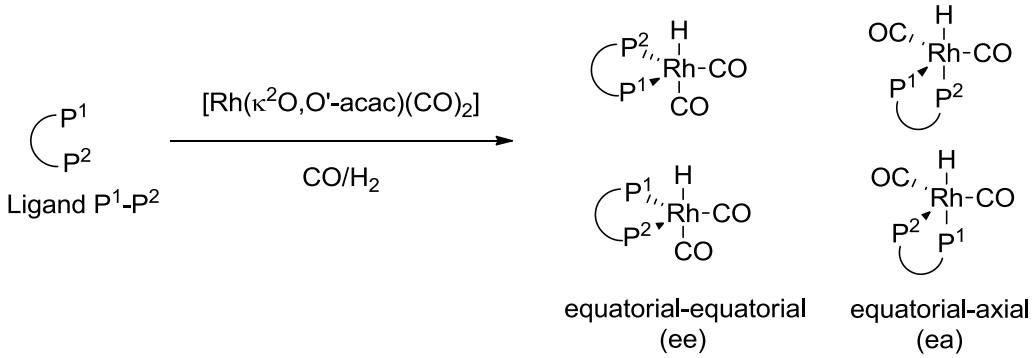

Scheme 44. Representative coordination modes of bidentate phosphorus ligands in a hydroformylation catalyst

In order to carry out these complexation experiments, a stoichiometric mixture of [Rh(κ^{2}O,O'-acac)(CO)$_2$] and RbBArF•**46d** or CsBArF•**46a** (*ca.* 10 mM) in toluene-d_8/THF-d_8 (97/3 v/v) was transferred into a 25 mL autoclave. The reactor was pressurized at 10 bar of 1:1 CO/H$_2$, heated to 40 ºC and stirred for 2 hours. The solution was subsequently transferred to a HP-NMR tube and pressurized at 10 bar of 1:1 CO/H$_2$. ^{31}P and ^{1}H NMR spectra were then acquired at variable temperatures. The rhodium species derived from RbBArF•**46d** or CsBArF•**46a** showed as expected a bidentate coordination mode, which was confirmed by ^{31}P NMR analysis on the basis of the presence of a doublet at δ = *ca.* 150 ppm ($^1J_{Rh-P}$ = *ca.* 250 Hz; see Table 36 for detailed spectral data of the rhodium complexes derived from RbBArF•**46d** or CsBArF•**46a**). According to symmetry considerations, the phosphorus atoms are equivalent in free ligands (C_2 symmetry). However, irrespective of the coordination mode to rhodium, the two possible complexes formed presenting a bis-equatorial or apical-equatorial coordination mode of the bisphosphite ligand (see Figure 117) have C_1 symmetry. Nevertheless, only one signal (*i.e.* a doublet) was observed in the ^{31}P NMR spectra, indicating that either both P-nuclei accidentally have the same

[182] "*Type I kinetics*" are considered to be operative in most of the Rh-mediated AHF reactions with phosphorus ligands and they are characterized by a first-order dependence on the catalyst and alkene concentration and a negative order dependence on the CO concentration, implying that alkene coordination and/or insertion into the Rh-H bond are the rate-determining step(s). On the other hand, *"type II kinetics"* are mainly operative with bulky monophosphite ligands. These hydroformylations are characterized by rate-limiting hydrogenolysis of the acyl species. See: Chikkali, S. H.; van der Vlugt, J. I.; Reek, J. N. H. *Coord. Chem. Rev.* **2014**, *262*, 1.

chemical shift or rapidly interconvert into each other on the NMR time scale. Variable temperature ^{31}P NMR experiments (from 40 ºC to –78 ºC) showed considerable line broadening at low temperatures but no splitting of the phosphorus signals was observed in the studied temperature range.

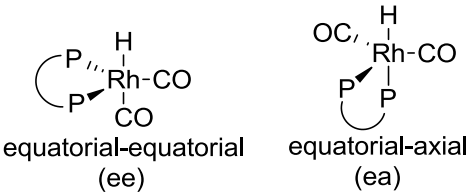

Figure 117. ee and ea coordination modes in [Rh(H)(CO)$_2$(P-P)] species with C_2 symmetric ligands

Only one hydride signal was observed in the ^{1}H NMR spectra of [Rh(H)(CO)$_2$(CsBArF•**46a**)] or [Rh(H)(CO)$_2$(RbBArF•**46d**)] as a broad singlet centered at δ *ca.* –10.5 ppm (width of the hydride signal at half height was *ca.* 9 Hz). The P-H coupling constant ($^2J_{H-P}$) was too small in both cases to be determined (see, as an example, the NMR spectra for [Rh(H)(CO)$_2$(RbBArF•**46d**)] in Figure 118.

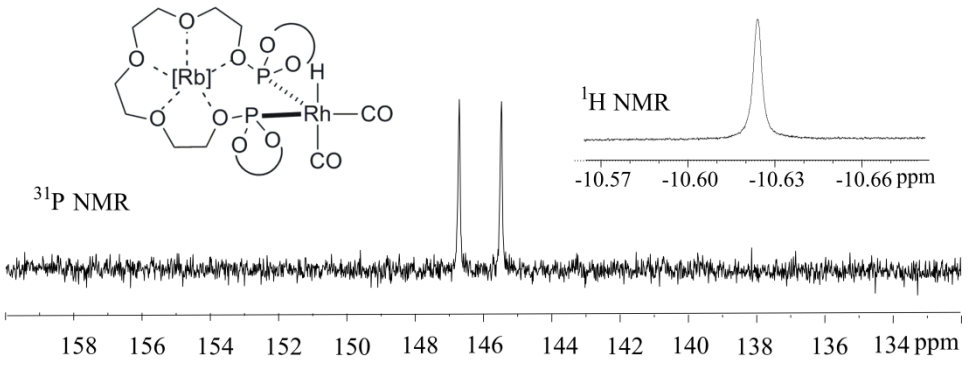

Figure 118. HP-NMR complexation studies between [Rh(κ^2O,O'-acac)(CO)$_2$], **46d**, and RbBArF under 10 bar of 1:1 CO/H$_2$ at 25 ºC in toluene-d_8/THF-d_8 (97/3 v/v)

Table 36. NMR spectral data for rhodium complexes derived from RbBArF•**46d** and CsBArF•**46a**[a]

	NMR spectroscopic data		
Complex	**δ ^{31}P (ppm)**	**J_{Rh-P} (Hz)**	**δ ^{1}H (ppm)**
[Rh(H)(CO)$_2$(CsBArF•**46a**)]	150.0	247	–10.5
[Rh(H)(CO)$_2$(RbBArF•**46d**)]	146.3	249	–10.6

[a] NMR data was acquired at 25 ºC under 10 bar of 1:1 CO/H$_2$ in a 5 mm sapphire NMR tube in toluene-d_8/THF-d_8 (97/3).

The P-H coupling could be confirmed by ^{1}H-^{31}P HMBC spectroscopy, which showed a cross-peak between the hydrido and the phosphite signals (see Figure 119). Such a small P-H and large Rh-P couplings (see Table 36) are indicative that the hydrido ligand has a strong preference for a *cis*-arrangement relative to the P-atoms, which are coordinated in an equatorial-equatorial fashion to a trigonal-bipyramidal rhodium center.

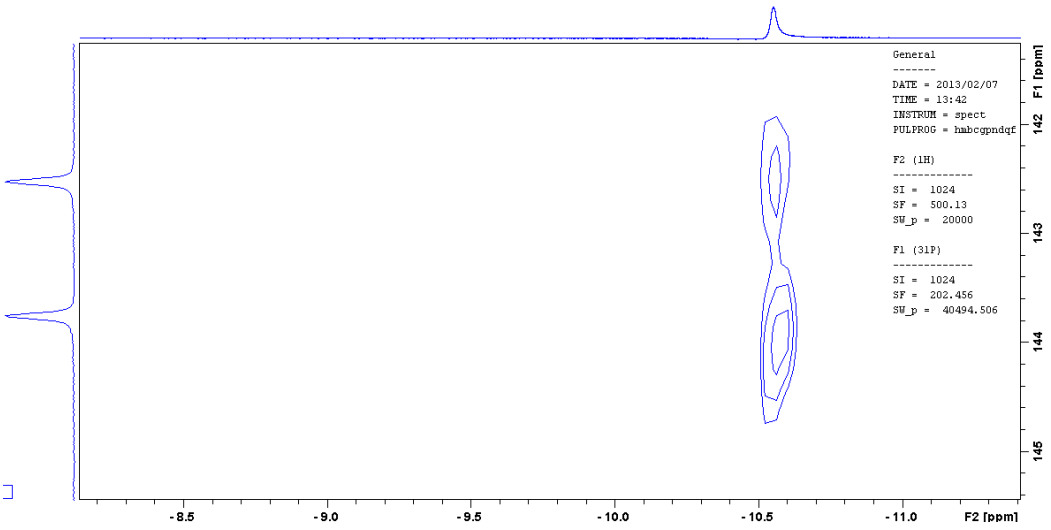

Figure 119. High Pressure ^{1}H-^{31}P HMBC spectrum of the rhodium complex derived from RbBArF•**46d** acquired at 25 ºC in toluene-d_8/THF-d_8 (97/3 v/v)

The formation of this rhodium chelate could also be proved by mass spectrometry, since the molecular ion for [Rh(**46a**)]$^{+}$ (*m/z* calculated for $C_{76}H_{88}O_{12}P_2RhSi_4$: 1469.39; found: 1469.5; see Figure 120) was detected in MALDI analysis of complexation reaction mixtures. MALDI-MS analysis also ruled out the formation of other rhodium complexes, as no other cationic species were

detected up to *m/z* = 4000. Our results are in agreement with other studies carried out with chelating bidentate-phosphorus ligands by the groups of Claver,[183] van Leeuwen[184] and others;[185] where generally only the [Rh(H)$(CO)_2$(P-P)] complexes have been observed.

[183] a) Axet, M. R.; Benet-Buchholz, J.; Claver, C.; Castillón, S. *Adv. Synth. Catal.* **2007**, *349*, 1983. b) Dieguez, M.; Pamies, O.; Ruiz, A.; Claver, C. *N. J. Chem.* **2002**, *26*, 827. c) Diéguez, M.; Pàmies, O.; Ruiz, A.; Castillón, S.; Claver, C. *Chem. Eur. J.* **2001**, *7*, 3086. d) del Río, I.; Pàmies, O.; van Leeuwen, P. W. N. M.; Claver, C. *J. Organomet. Chem.* **2000**, *608*, 115.
[184] a) Deerenberg, S.; Kamer, P. C. J.; van Leeuwen, P. W. N. M. *Organometallics* **2000**, *19*, 2065. b) Nettekoven, U.; Kamer, P. C. J.; Widhalm, M.; van Leeuwen, P. W. N. M. *Organometallics* **2000**, *19*, 4596. c) Buisman, G. J. H.; van der Veen, L. A.; Kamer, P. C. J.; van Leeuwen, P. W. N. M. *Organometallics* **1997**, *16*, 5681.
[185] a) Chikkali, S. H.; Bellini, R.; de Bruin, B.; van der Vlugt, J. I.; Reek, J. N. H. *J. Am. Chem. Soc.* **2012**, *134*, 6607. b) Damoense, L.; Datt, M.; Green, M.; Steenkamp, C. *Coord. Chem. Rev.* **2004**, *248*, 2393. c) Nozaki, K.; Sakai, N.; Nanno, T.; Higashijima, T.; Mano, S.; Horiuchi, T.; Takaya, H. *J. Am. Chem. Soc.* **1997**, *119*, 4413.

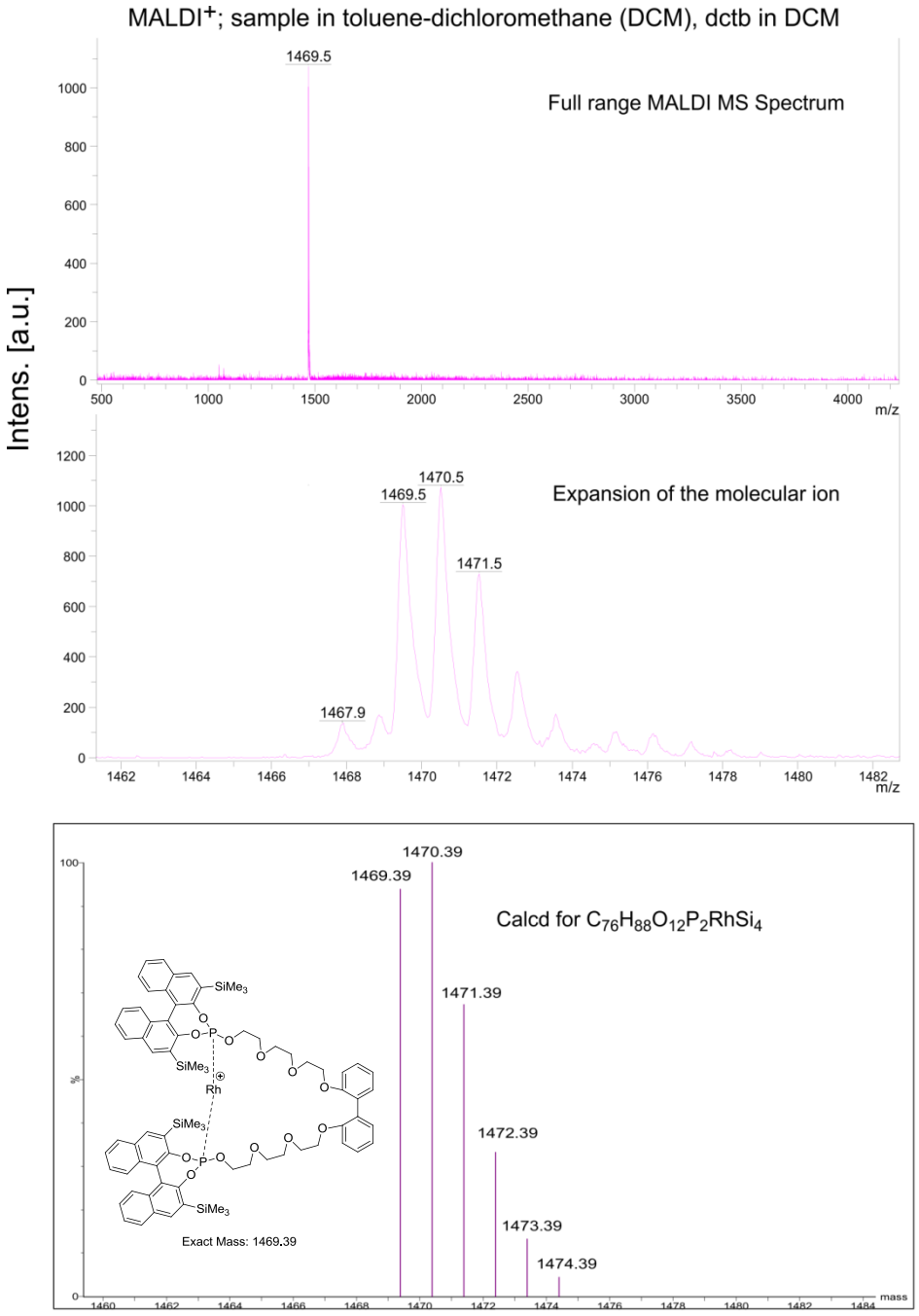

Figure 120. MALDI mass spectrum of Rh(I) catalyst derived from CsBArF•**46a** using (*E*)-2-(3-(4-(*t*butyl)phenyl)-2-methylallylidene)malononitrile (dctb) as matrix

In line with our HP-NMR studies, only one set of carbonyl signals at 2076 and 2029 cm^{-1} (C=O stretching vibration modes) were observed in the High Pressure Infrarred (HP-IR) experiments carried out with [Rh(H)$(CO)_2$(CsBArF•**46a**)]. For this *in situ* experiment, a solution of **46a** (1 equiv., 1 mM), CsBArF (1.3 equiv.), and [Rh(κ^2O,O'-acac$(CO)_2$] (1 equiv.) in toluene/THF (97/3 v/v) was transferred into an IR autoclave reactor equipped with

a mechanical stirrer, temperature controller, and a pressure device. The reactor was pressurized with 10 bar of 1:1 CO/H_2, heated at 40 ºC, left stirring for 2 hours, and the IR spectra were subsequently recorded in a FT-IR spectrometer (see Figure 121 and Figure 122). Our results are in agreement with the previous NMR experiments that indicate an equatorial-equatorial coordination mode of the ligand to the rhodium center, since typical carbonyl absorptions for the equatorial-equatorial coordination mode are observed at around 2015 and 2075 cm^{-1}, whereas the absorptions for equatorial-apical coordination modes are found at lower frequencies (*i.e. ca.* 1990 and 2030 cm^{-1}).

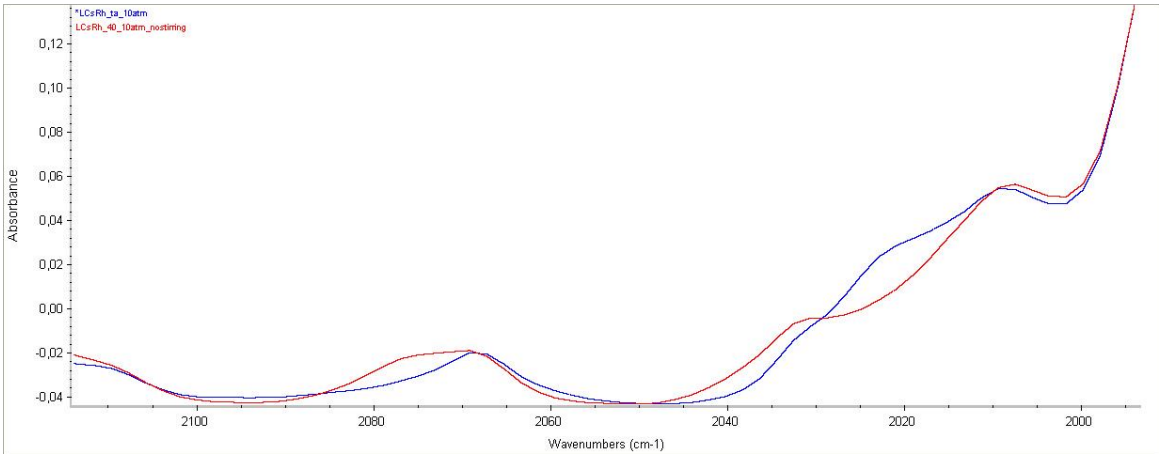

Figure 121. HP-IR spectra before (blue) and after (red) formation of $[Rh(H)(CO)_2(CsBArF$•**46a**$)]$ in toluene/THF (97/3 v/v) under 10 bar of 1:1 CO/H_2 at 40 ºC

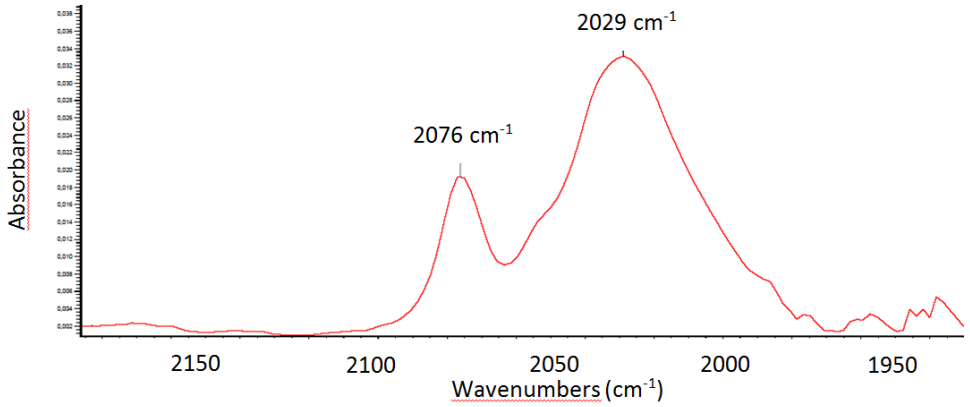

Figure 122. HP-IR spectrum of $[Rh(H)(CO)_2(CsBArF$•**46a**$)]$ in toluene/THF (97/3 v/v) under 10 bar of 1:1 CO/H_2 at 40 ºC (difference between red and blue lines in Figure 121).

*2.2.3.3 Computational studies on the geometry of the [Rh(H)(CO)$_2$(BArF salts•**46d**)] complexes*

As the process of growing crystals suitable for X-Ray analysis from the inclusion compounds derived from bisphosphite ligands **46** and the different regulation agents (alkali metal BArF salts) proved to be difficult, we decided to gain insight into the structural and/or geometrical changes induced by the regulation agents on the geometry of the resulting complexes by computational studies. These *in silico* studies were performed by Frontera *et al.*[186] at the DFT level of theory on the hydrido-dicarbonyl Rh(I) complexes derived from ligand **46d** and the different regulation agents: [Rh(H)(CO)$_2$(BArF salts•**46d**)]. These complexes have proved to be the catalyst resting states in hydroformylation reactions,[182] and studying the effects of the regulation agents on their geometry appeared to us to be the best way to start gaining an understanding of the regulation mechanism in our supramolecular catalytic systems. The optimized structures of the trigonal bipyramidal hydrido-dicarbonyl rhodium complexes derived from bisphosphite **46d** were calculated at the DFT[186] level of theory without any coordinated cation and with Na^+, K^+, Rb^+ and Cs^+ bound cations on the polyether binding motif of the ligand.

From all the structural information obtained from these computational studies, we just turned our attention in this initial analysis to those geometrical parameters that could potentially have a greater impact on the performance of the catalyst:

[186] Prof. A. Frontera is the leader of a computational group from the *Universitat de les Illes Balears* (UiB, Spain) that possesses a sound expertise in studying supramolecular interactions at the computational level. The geometry of all the complexes included in this study was optimized at the BP86-D3/def2-TZVPD level of theory within the program TURBOMOLE version 6.4 (Ahlrichs, R.; Bär, M.; Hacer, M.; Horn, H.; Kömel, C. *Chem. Phys. Lett.* **1989**, *162*, 165). The def2-TZVPD basis set was used for all atoms. It employs effective core potentials for Rh (ECP-28, as indicated in Andrae, D.; Haeussermann, U.; Dolg, M.; Stoll, H.; Preuss, H. *Theor. Chim. Acta* **1990**, *77*, 123). For the calculations we have used the BP86 functional with Grimme's latest available correction for dispersion (D3, as reported by Grimme, S.; Antony, J.; Ehrlich, S.; Krieg, H. *J. Chem. Phys.* **2010**, *132*, 154104).

- Bite angle or P-Rh-P bond angle (β): Angle formed between the Rh center and the two P atoms.
- Dihedral angle (θ) in the binaphthyl group: Mean value of the two dihedral angles in the two binaphthyl units (OC_{Ar}-C_{Ar}-C_{Ar}-$C_{Ar}O$ dihedral angle).
- Phosphorus-rhodium distance ($d_{P\text{-}Rh}$): Mean value of the two phosphorus-rhodium bond distances.

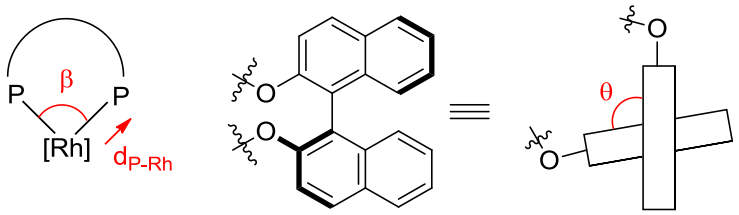

Figure 123. Geometrical parameters considered as potentially important in our hydroformylation catalytic studies

Calculated parameters have been summarized in Table 37 and in Figure 125. This figure also shows the experimental enantiomeric excesses obtained from the asymmetric hydroformylation (AHF) of vinyl acetate using the Rh(I) catalysts derived from ligand **46d** and the different alkali metal BArF salts.

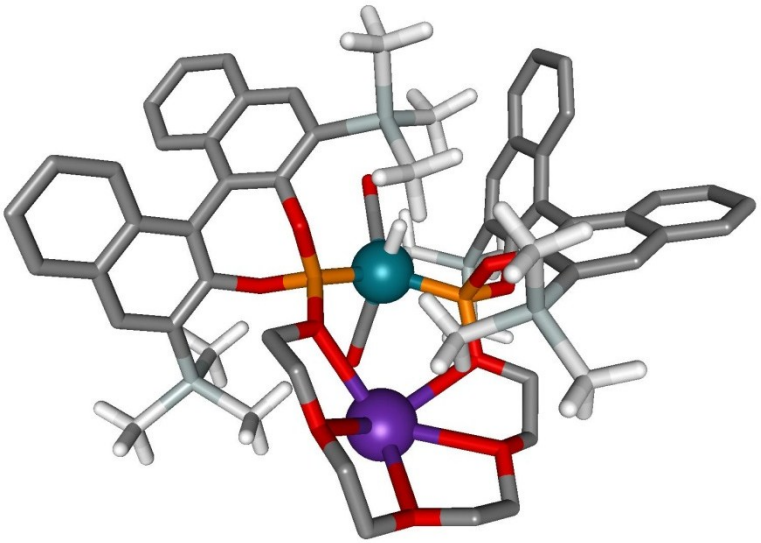

Figure 124. Calculated structure for the rhodium complex derived from ligand **46d** with the Rb^+ ion bound to the polyether binding motif

Table 37. Calculated geometrical parameters for the rhodium complexes derived from ligand **46d** with none, Na^+, K^+, Rb^+ and Cs^+ ions bound to the polyether binding motif[a]

Entry	Cation	Ionic radius (Å)	Bite-angle β (degree)	Dihedral-angle θ (mean value, degree)	$d_{P\text{-}Rh}$ (mean value, Å)
1	-	0	113.2	–57.9	2.27
2	Na^+	1.9	115.8	–58.7	2.25
3	K^+	2.3	122.1	–58.3	2.26
4	Rb^+	2.5	121.5	–58.5	2.27
5	Cs^+	2.7	121.5	–58.3	2.27

[a] See footnote 186 for the details on the computational method employed.

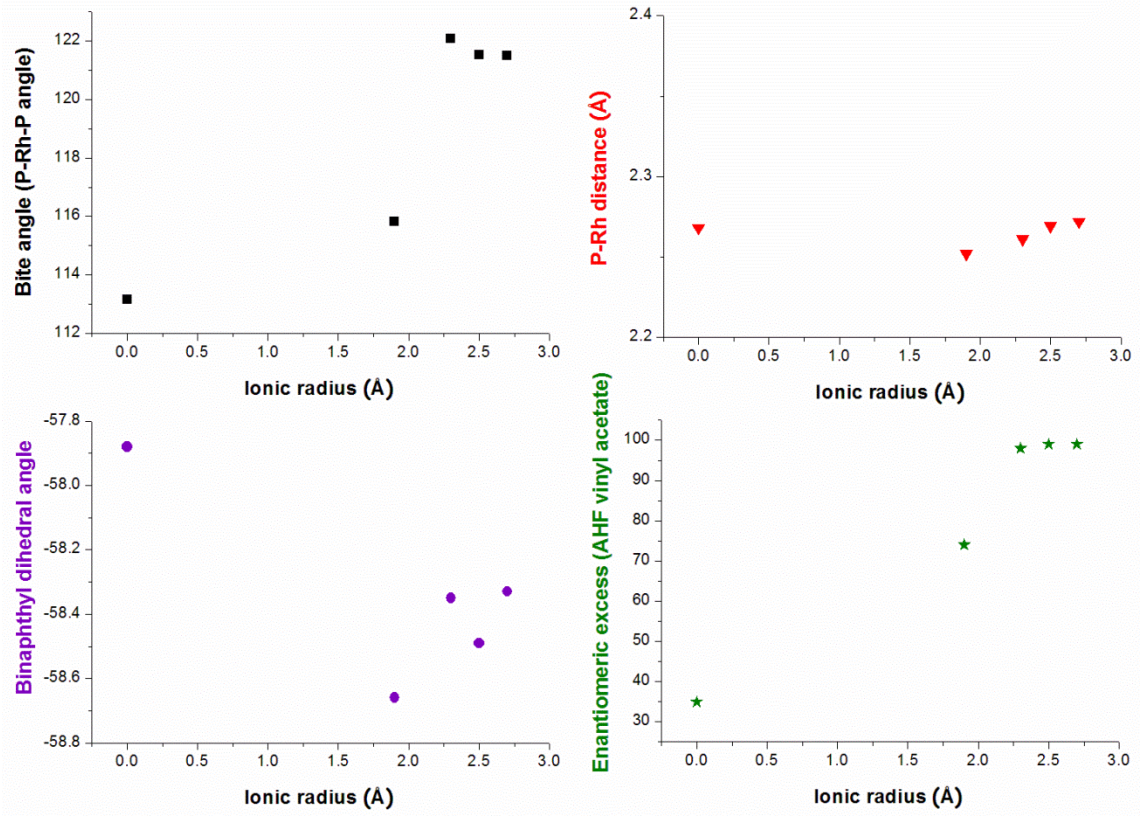

Figure 125. Calculated geometrical parameters and experimental enantiomeric excess for the AHF of vinyl acetate versus the ionic radius of the cation employed

With regard to the effects of the regulation agent in the bite angle, the general trend observed indicates that the coordination of cations of increasing ionic radius makes the bite angle (β) increase from 113º to *ca.* 121º. Calculated values for the P-Rh distance ($d_{P\text{-}Rh}$) were found to be the same when no

regulation agent was used or for the largest regulation agents of the series (Rb^+ or Cs^+) and this parameter slightly dropped for Na^+ and K^+ (largest $\Delta d_{P\text{-}Rh}$ = –0.02 Å for Na^+). The calculated values for the binaphthyl dihedral angle (θ) indicate that the regulation agent forces the binaphthyl units to adopt a conformation with a lower dihedral angle θ (from –57.9º when no regulation agent was used to *ca.* –58.4º as the average value), with small differences in this geometrical parameter for the studied regulation agents.

Most interestingly, the plot of the enantiomeric excesses obtained in the AHF of vinyl acetate using the rhodium complexes derived from ligand **46d** and different BArF salts as catalysts versus the ionic radius of the cation from the regulation agent shows a similar trend with those obtained by plotting the P-Rh distance, P-Rh-P bond angle or the binaphthyl dihedral angle as a function of the ionic radius of the cation. The best example is the close similarity observed between the plots of the calculated P-Rh-P bond angles (β) and the enantioselectivity of the AHF of vinyl acetate as a function of the ionic radius. Therefore, one of the possible explanations for the increase in the enantiomeric excess when using regulation agents might be the adaptation of the P-Rh-P bond angle of the catalyst from a non-ideal value to the required value for high enantioselectivity.

In conclusion, computational studies at the DFT level of theory on the geometry of the [Rh(H)$(CO)_2$(BArF salt•**46d**)] complexes have indicated possible changes on the catalyst geometry induced by the coordination of the regulation agent. Some trends on key geometrical parameters for catalysis (*i.e.* P-Rh distance, P-Rh-P bond angle and binaphthyl dihedral angle) have been observed when plotted versus the ionic radius of the bound cations. It has been demonstrated that the coordination of cationic species on the distal regulation site of the resting state of the catalyst influences the geometry of relevant rhodium complexes in the catalytic cycle, not only in the proximity of the polyether chain but also in areas close to the catalytic active center. Thus, the results on enantioselective catalysis that have been mentioned in the previous sections together with these preliminary computational studies validate our ligand design and proposed regulation mechanism.

2.2.3.4 Rationalization of the stereochemical outcome of the hydroformylation reactions

As has been indicated in the previous sections, asymmetric hydroformylation of styrene **6a**, vinyl esters **6b**,**e**,**f** and TMS-protected allyl alcohol **6d** with Rh(I) complexes derived from ligands **46** have preferentially provided the (*S*)-configured branched products **7a**,**b**,**d**–**f**. We have also shown in complexation studies of ligands **46** to the standard rhodium(I) precursor in hydroformylation reactions ([Rh(κ^2O,O'-acac)(CO)$_2$]) under 10 bar of 1:1 CO/H$_2$ in the presence of an excess of the regulation agent (1.3 equiv. with respect to ligand **46**), that hydrido-dicarbonyl rhodium complexes with the two phosphite groups bound to the equatorial positions of the rhodium center are obtained (*i.e.* [Rh(H)(CO)$_2$(BArF salt•**46**)] complexes).

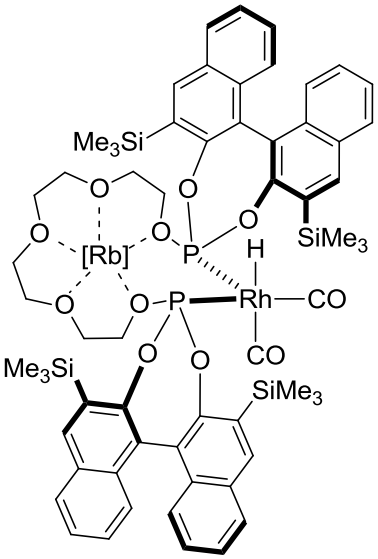

[Rh(H)(CO)$_2$(RbBArF•**46d**)]

Figure 126. Equatorial-equatorial coordination mode of ligand **46d** in the resting state complex [Rh(H)(CO)$_2$(RbBArF•**46d**)]

Quadrant diagrams provide a simplified view of the hydroformylation reaction.[187] Assuming that bisphosphite ligands **46** remain coordinated in a equatorial-equatorial fashion to the Rh(I) center in the pseudo-five coordinate

[187] Quadrant analysis in hydroformylation reactions was introduced by Landis *et al.* (see: Clark, T. P.; Landis, C. R.; Freed, S. L.; Klosin, J.; Abboud, K. A. *J. Am. Chem. Soc.* **2005**, *127*, 5040.)

transition state (after the decoordination of a CO group),[188] the quadrant diagram indicated in Figure 127 schematically represents this transition state. The quadrant diagram is constructed such that the rhodium center is placed in the center of the diagram. A rough analysis of the geometries of the [Rh(H)(CO)$_2$(BArF salts•**46d**)] complexes (see Section 2.2.3.3) indicate that three quadrants are sterically blocked (in grey color) by the binaphthyl groups in the ligand. In this simplified view of the transition state, the Rh-H bond lies parallel to the plane of alkene C=C group. Alkene coordination with the substituent placed on any of the two bottom quadrants would lead to the branched hydroformylation products ((*R*)- or (*S*)-configured aldehydes depending on the alkene coordination face, Figure 127). It should also be mentioned that coordination of the alkene with the substituent placed on any of the two upper quadrants would lead to linear products. These hydroformylation products are generally obtained in a lower ratio than the branched ones, which indicates that our hydroformylation catalytic system electronically disfavors placement of the substituent in any of the two upper quadrants (disfavorable electronic effects are indicated with red lines in Figure 127).

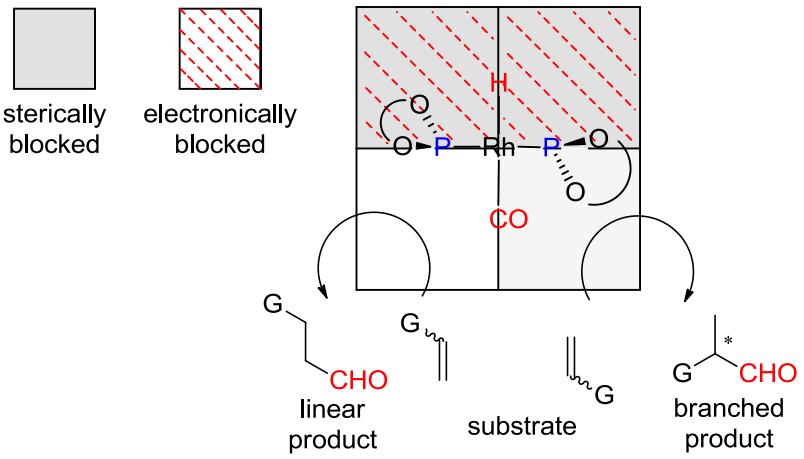

Figure 127. Regioselectivity rationalization for the hydroformylation of different terminal alkenes with our designed quadrant diagram

Indeed, electronic effects have a deep impact on regioselectivity in hydroformylation; some authors have hypothesized that the large prevalence of

[188] It is normally assumed that the chelation coordination mode of the phosphorus bidentate ligand (*i.e.* equatorial-equatorial or apical-equatorial) is maintained through the hydroformylation catalytic cycle (see for example: ref. Carbo, J. J.; Lledos, A.; Vogt, D.; Bo, C. *Chem. Eur. J.* **2006**, *12*, 1457.).

the branched product in hydroformylation of different substrates (*e.g.* styrene) is probably due to the polarization required for the formation of a rhodium-carbon bond with a partial negative charge on the adjacent carbon and a partial positive charge on the rhodium atom. Thus, only the intermediate that leads to the branched isomer can stabilize the partial negative charge by delocalization (Figure 128).[189]

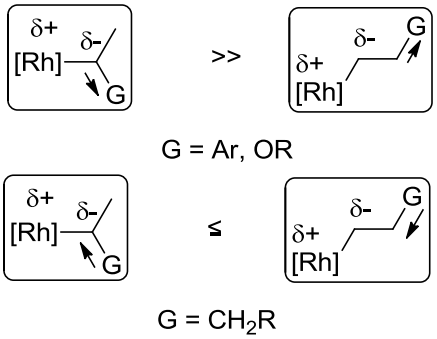

Figure 128. Stabilization of alkylrhodium intermediates from the hydroformylation of different alkenes

These mentioned electronic effects can also tentatively explain the regioselectivities obtained for the different substrates studied with our catalytic systems. As a reminder, AHF using Rh(I) catalysts derived from ligand **46d** led to regioselectivities higher than 95:5 branched-to-linear ratio in the case of substrates **6a**,**b**,**e**,**f** whereas **6d** was hydroformylated in only *ca.* 60:40 branched-to-linear ratio. A plausible explanation for such a big difference in regioselectivity can be extracted from the hypotheses that the alkylrhodium intermediates that lead to the branched hydroformylated products of styrene **6a** and vinyl esters **6b**,**e**,**f** are stabilized by the above mentioned delocalization effect, whereas the same stabilization mechanism is not possible in alkylrhodium intermediates derived from substrate **6d** (Figure 129).

[189] a) Lazzaroni, R.; Settambolo, R.; Alagona, G.; Ghio, C. *Coord. Chem. Rev.* **2011**, *255*, 3031.
b) Lazzaroni, R.; Settambolo, R.; Alagona, G.; Ghio, C. *Coord. Chem. Rev.* **2010**, *254*, 696.
c) Lazzaroni, R.; Raffaelli, A.; Settambolo, R.; Bertozzi, S.; Vitulli, G. *J. Mol. Catal.* **1989**, *50*, 1.

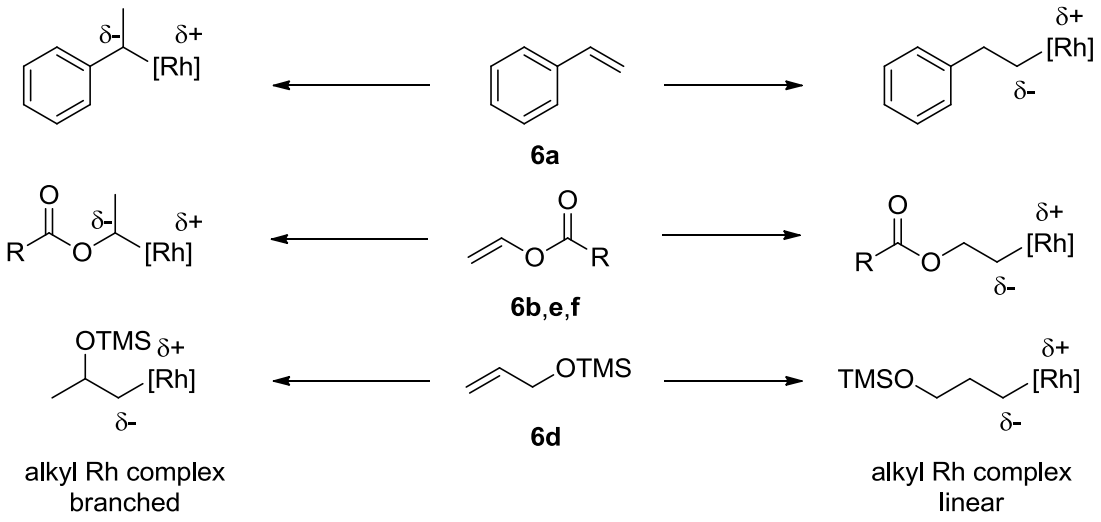

Figure 129. Stabilization of alkylrhodium intermediates derived from substrates **6** leading to the linear or the branched products

The quadram diagram depicted in Figure 130, based on the assumption of a trigonal bipyramidal coordination environment with diequatorial phosphorus atoms, helps in rationalizing the stereochemical outcome of the reaction. Approach of styrene **6a** and (allyloxy)trimethylsilane **6d** to the rhodium center by their *Si*-face leads to the predominantly formed (*S*)-configured hydroformylation products. We would like to emphasize that this model is purely mnemonic, as characterization of intermediates along the hydroformylation catalytic cycle by spectroscopic and computational models has not been performed.

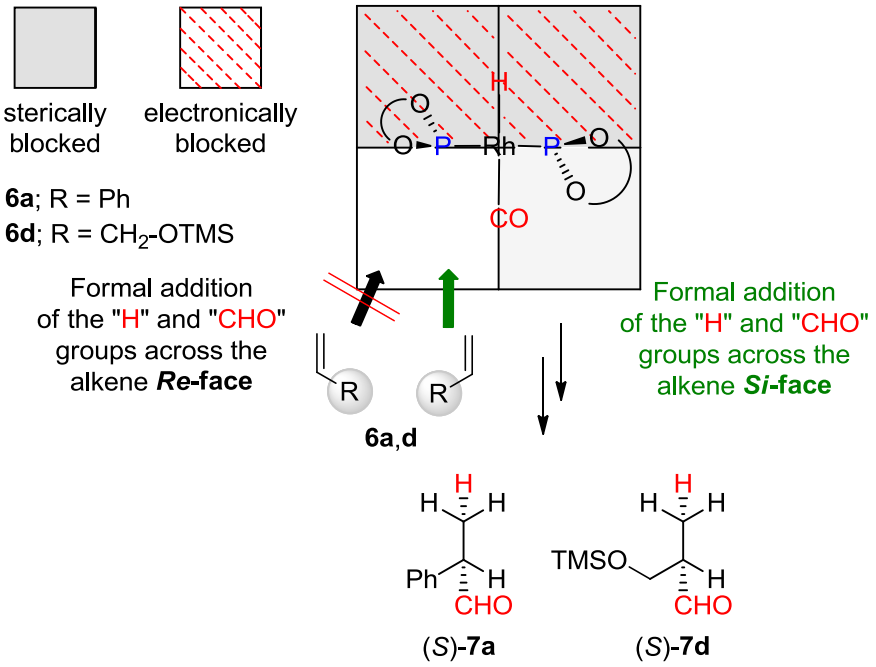

Figure 130. Quadrant diagram indicating the stereochemical outcome of the hydroformylation for substrates **6a**,**d**

It is noteworthy, that this stereochemical model is not valid for vinyl acetate **6b** and its analogues **6e**,**f**. In these cases, alkenes approach the rhodium center by their *Re*-face (see Figure 131), which indicates that the formal addition of the "H" and "CHO" groups across the C=C bond occurs in vinyl esters at the opposite enantioface than that for styrene **6a** and allyl alcohol derivative **6d**.[190]

[190] The fact that all hydroformylation products have the (*S*)-configuration may be misleading and may lead to the reader to think that "H" and "CHO" groups add across the C=C bond at the same enantioface for all products. It should be noted at this point, that there is a change in the CIP priority rules for the branched hydroformylation products derived from vinyl esters and those for styrene **6a** and allyl alcohol derivative **6d**. For this reason, all hydroformylation products have the (*S*)-configuration, although "H" and "CHO" groups add across the C=C bond at different alkene enantiofaces for the two classes of substrates.

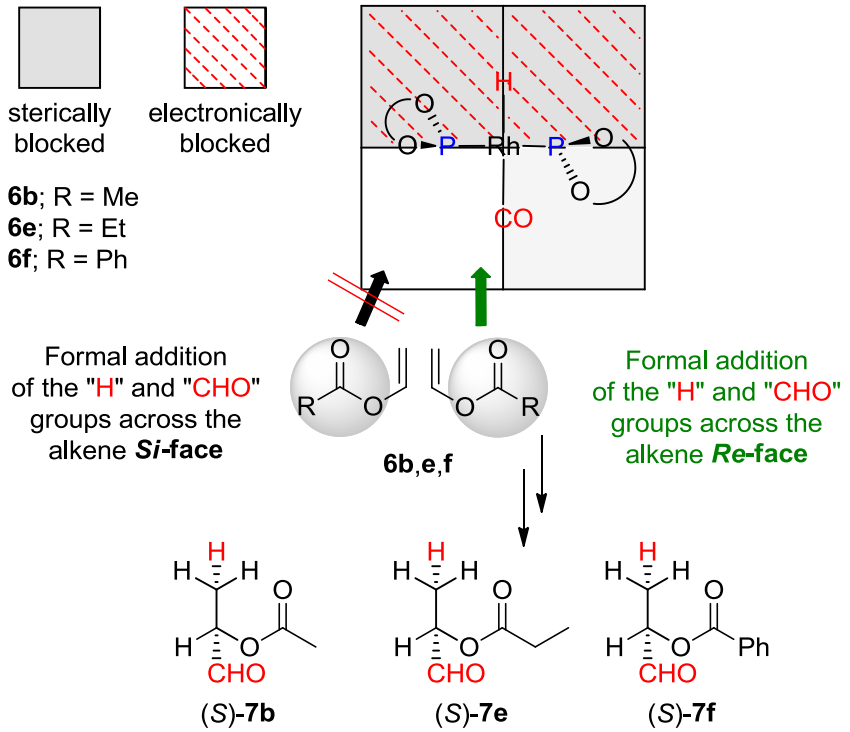

Figure 131. Quadrant diagram indicating the stereochemical outcome of the hydroformylation for substrates **6b**,**e**,**f**

Some other researches have noted that hydroformylation of vinyl acetate has some discrete features that lead to a different stereochemical outcome of the reaction.[191] Although it has not been definitely proved, some authors claim that the double bond polarization due to the inductive effect of the ester carbonyl group and the chelating effect of the vinyl ester carbonyl group to the rhodium center (Figure 132) could account for the differences on the reactivity, regioselectivity and/or enantiodiscrimination of the reaction, when compared to other terminal alkenes such as styrene or protected allyl alcohols.[192]

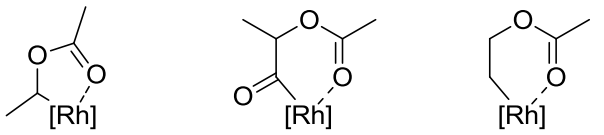

Figure 132. Proposed 5- and 6-membered chelate intermediates involved in the hydroformylation of vinyl acetate

[191] Klosin, J.; Landis, C. R. *Acc. Chem. Res.* **2007**, *40*, 1251.
[192] Dabbawala, A. A.; Bajaj, H. C.; Rao, G. V. S.; Abdi, S. H. R. *Appl. Catal., A* **2012**, *419-420*, 185.

2.2.4 Rh-mediated asymmetric hydrogenation of diverse alkenes

Encouraged by our results on asymmetric hydroformylation, we then turned our attention to developing ligands with a distal regulation site for asymmetric hydrogenations.

Asymmetric hydrogenation has been used for decades as a simple and economical way to introduce chirality into molecules of interest and production processes. Actually, homogeneous hydrogenation is one of the most deeply studied transformations in homogeneous catalysis.[193] The ability of different metal complexes to accomplish this transformation has attracted the interest of an increasing number of chemists and has led to the development of efficient methodologies for the asymmetric reduction of C=C, C=O and C=N bonds. Enantiomerically pure metallorganic compounds derived from iridium, ruthenium and rhodium are the most commonly used catalyst precursors in the asymmetric hydrogenation of diverse substrate classes (alkenes, ketones, imines or heteroaromatic compounds). It should be mentioned that we focused on the asymmetric reduction of alkenes for its undeniable importance in asymmetric synthesis. Actually, chemists have devoted a substantial research effort to the development of efficient enantioselective hydrogenation catayst for alkenes from the onset of asymmetric catalysis. The asymmetric reduction of an alkene to an alkane is considered a particularly important synthetic reaction, since construction of a C=C bond is often achieved by straightforward and reliable synthetic transformations and C=C bonds can then be subsequently converted into the corresponding C-C bonds, with one or two new stereogenic carbons being generated. Iridium-based hydrogenation catalysts do not require the presence of coordinating groups on the substrates and have permitted the reduction of polyalkyl-substituted alkenes.[194] On the other hand, enantiomerically pure rhodium and ruthenium-based complexes are the most commonly used catalysts, the former being extensively utilized in the asymmetric hydrogenation of dehydroamino acid derivatives and other functionalized alkenes to afford biologically relevant enantiomerically enriched (or pure) compounds (see Scheme

[193] a) Ager, D. J.; de Vries, A. H. M.; de Vries, J. G. *Chem. Soc. Rev.* **2012**, *41*, 3340. b) Xie, J.-H.; Zhu, S.-F.; Zhou, Q.-L. *Chem. Rev.* **2011**, *111*, 1713. c) Palmer, A. M.; Zanotti-Gerosa, A. *Curr. Opin. Drug Discovery Dev.* **2010**, *13*, 698.
[194] Cadu, A.; Andersson, P. G. *Dalton Trans.* **2013**, *42*, 14345.

45).[195] Rh-based catalysts mediate the asymmetric hydrogenation of alkenes with high efficiency (*i.e.* TON and TOF values)[196] and enantioselectivity in mild conditions. Besides, they have been applied to a broad substrate scope with demonstrated robustness in different solvents and selectivity towards diverse functional groups. Most of these rhodium complexes derive from enantiopure phosphorus ligands, mainly comprising bidentate chelating phosphorus compounds[197]or monodentate phosphorus derivatives.[198] It should be mentioned that metal-free organocatalysts that mediate asymmetric transfer hydrogenations are also under study.[199]

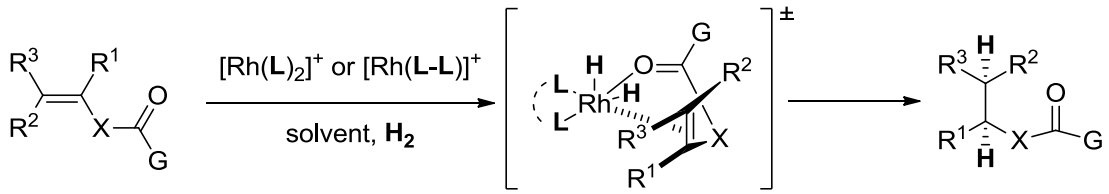

Scheme 45. Rh-catalyzed asymmetric hydrogenation of functionalized alkenes

Thus, we combined the same ligand cores and polyether units with the privileged phosphite fragments that we used for hydroformylation reactions (described in previous chapter of this Thesis) in supramolecular ligands suitable for asymmetric hydrogenation (ligands **46b** and **46e**, which incorporate the phosphite fragment derived from 3,3'-unsubstituted [1,1'-binaphthalene]-2,2'-diol).

[195] Etayo, P.; Vidal-Ferran, A. *Chem. Soc. Rev.* **2013**, *42*, 728.
[196] Arai, N.; Ohkuma, T. *Chem. Rec.* **2012**, *12*, 284.
[197] a) Czauderna, C. F.; Cordes, D. B.; Slawin, A. M. Z.; Mueller, C.; van der Vlugt, J. I.; Vogt, D.; Kamer, P. C. J. *Eur. J. Inorg. Chem.* **2013**, DOI: 10.1002/ejic.201301255 b) Fernández-Pérez, H.; Etayo, P.; Panossian, A.; Vidal-Ferran, A. *Chem. Rev.* **2011**, *111*, 2119. c) Goudriaan, P. E.; van Leeuwen, P. W. N. M.; Birkholz, M.-N.; Reek, J. N. H. *Eur. J. Inorg. Chem.* **2008**, 2939.
[198] See, for example, the following reference and those cited therein: Frank, D. J.; Franzke, A.; Pfaltz, A. *Chem. Eur. J.* **2013**, *19*, 2405.
[199] a) de Vries, J. G.; Mrsic, N. *Catal. Sci. Tech.* **2011**, *1*, 727. b) Wang, C.; Wu, X.; Xiao, J. *Chem. - Asian J.* **2008**, *3*, 1750.

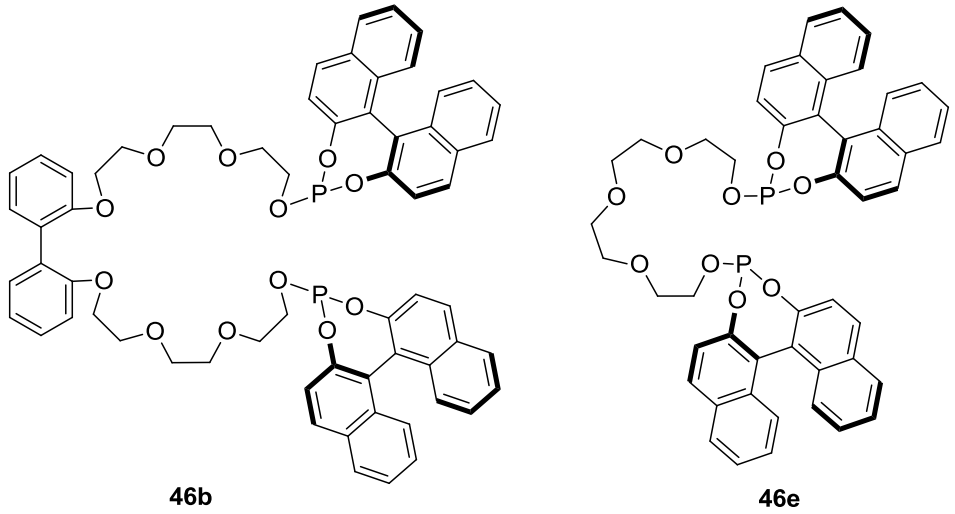

Figure 133. Bisphosphite ligands **46b** and **46e** for Rh-mediated asymmetric hydrogenation studies

*2.2.4.1 In situ NMR studies on the binding of Na•**46b** with Rh(I) precatalysts*

Analogous complexation and binding studies to the ones previously discussed between a suitable rhodium precursor for asymmetric hydrogenation ([Rh(cod)$_2$]BArF), ligand **46b** and a plausible polyether binder (NaBArF) were carried out.

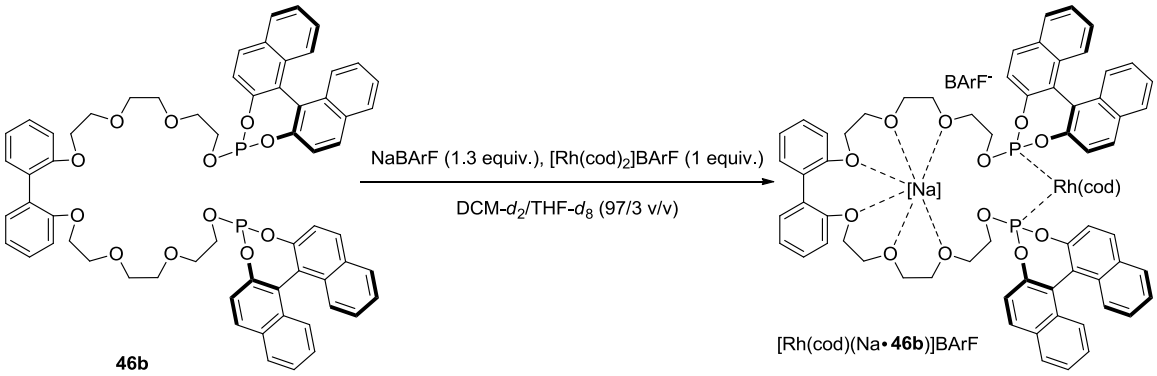

Scheme 46. Coordination studies between ligand **46b**, NaBArF and [Rh(cod)$_2$]BArF

We first studied the behavior between ligand **46b** and a suitable cationic rhodium(I) precursor for asymmetric hydrogenations ([Rh(cod)$_2$]BArF). When ligand **46b** was added to a solution of this cationic rhodium complex in DCM-d_2/THF-d_8 (97/3 v/v), we observed in ^{31}P NMR only a broad doublet ($^1J_{Rh-P}$ = 258.5 Hz, signal width at half height = 38 Hz) centered at 124.02 ppm (see, spectrum B in Figure 134). Such chemical shift in ^{31}P NMR clearly indicates that

the bisphosphite ligand is coordinated to the rhodium center. Furthermore, the observed spectral data (^{31}P and ^{1}H NMR) is in agreement with a dynamic chelate structure (*i.e.* [Rh(cod)(**46b**)]BArF), given the high flexibility of the proposed structure.

When an analogous complexation experiment was carried out with a preformed complex between NaBArF and bisphosphite **46b**, an analogous chelate was obtained ([Rh(cod)(Na•**46b**)]BArF) according to the spectral data obtained with the different spectroscopic techniques. However, the presence of NaBArF during the complexation experiments translated into a more rigid rhodium complex, as ^{31}P NMR analysis revealed: a sharp doublet ($^{1}J_{Rh-P}$ = 258.7 Hz, signal width at half height = 7 Hz) centered at 126.79 ppm (Spectrum C in Figure 134).

Overall, these binding studies between **46b** and Na•**46b** led to the conclusion that suitable rhodium-chelates for asymmetric hydrogenation are efficiently and selectively formed: [Rh(cod)(**46b**)]BArF or [Rh(cod)(Na•**46b**)]BArF (see Figure 134).

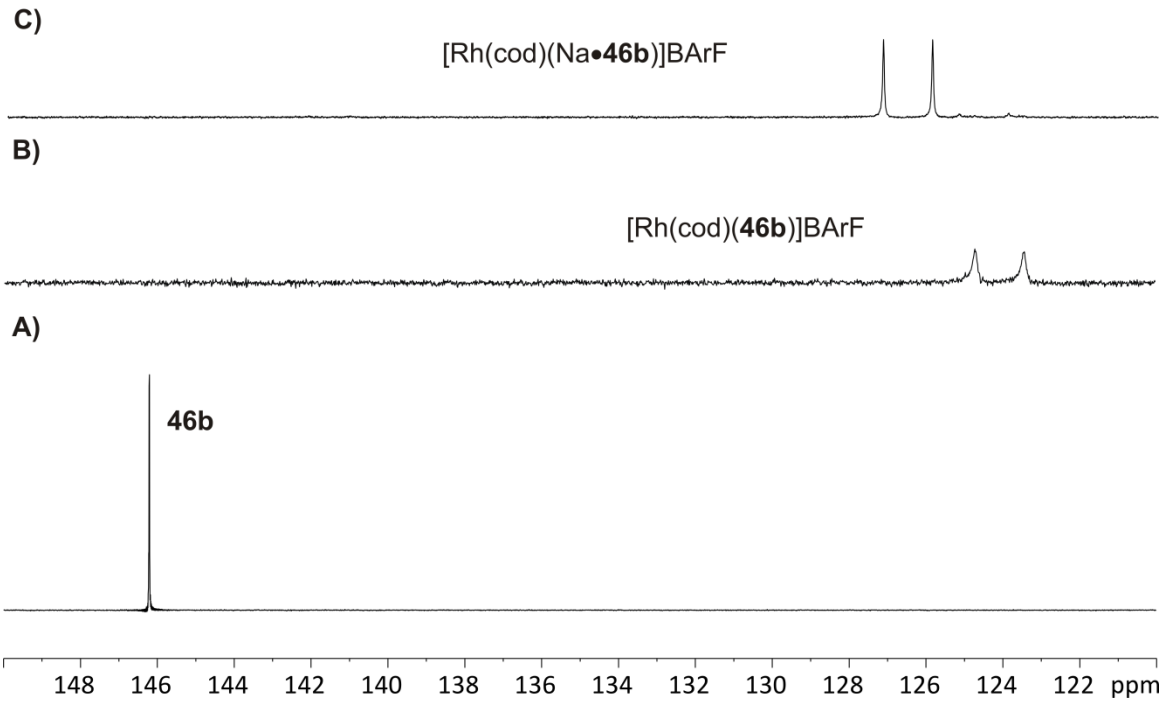

Figure 134. ^{31}P NMR spectra of: (A) free ligand **46b**, (B) rhodium complex [Rh(cod)(**46b**)]BArF and (C) rhodium complex [Rh(cod)(Na•**46b**)]BArF in DCM-d_2/THF-d_8 (97/3 v/v) at 298K

*2.2.4.2 Catalytic results on the asymmetric hydrogenation of an array of structurally diverse alkenes with bisphosphite ligands **46***

After studying the binding behavior of our supramolecular bisphosphite ligands towards rhodium precursors suitable for asymmetric hydrogenation and the effect of the regulation agents on the bisphosphites binding properties, we then turned our attention to assess the efficiency of our ligands and the effectiveness of our regulation mechanism on the aforementioned transformation.

Seven different substrates were assessed (**39a**,**b**,**d**–**h**; Scheme 47), comprising one itaconic acid derivative (**39a**), two dehydro-α-amino acid derivatives (**39b**,**d**), three α-arylenamides (**39e**,**f**,**h**) and one dehydro-β-amino acid derivative (**39g**). Standard hydrogenation screening conditions were used (1.0 mol % of precatalyst formed *in situ* from $[Rh(cod)_2]BArF$ and ligand **46b** or **46e**, addition of 1.3 equiv. of polyether binder relative to ligand, 20 bar of H_2, dichloromethane as solvent, room temperature, and overnight reactions), unless otherwise stated. Bisphosphite ligands **46b** and **46e** were used throughout the entire study, as they provided higher enantioselectivity than did the *ortho*-substituted analogues: **46a** and **46d**, respectively.[200] A summary of results without any distal regulator can be found in Table 38.

[200] The presence of substituents at the 3,3' positions of a [1,1'-biaryl]-2,2'-diol-derived phosphite can be detrimental to catalytic activity in hydrogenation reactions. For example, see: Korostylev, A.; Monsees, A.; Fischer, C.; Börner, A. *Tetrahedron: Asymmetry* **2004**, *15*, 1001.

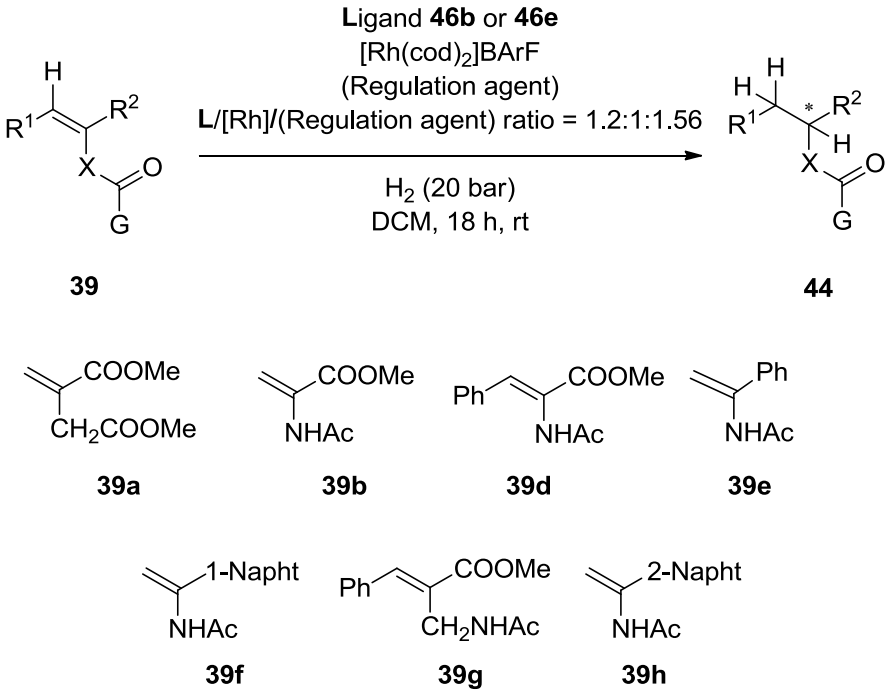

Scheme 47. Asymmetric hydrogenation mediated by Rh(I) catalysts derived from ligands **46b** or **46e**

Table 38. Catalytic studies on the hydrogenation[a] of **39a**,**b**,**d–h** using rhodium complexes derived from ligands **46** without distal regulation agents

Entry	L	Hydrogenation Results						
		Conv.[b] ee (%)[c] (config)	Conv.[b] ee (%)[c] (config)	Conv.[b] ee (%)[c] (config)	Conv.[b] ee (%)[c] (config)	Conv.[b] ee (%)[c] (config)	Conv.[b] ee (%)[c] (config)	Conv.[b] ee (%)[c] (config)
		39a	**39b**	**39d**	**39e**	**39f**	**39g**	**39h**
1	**46b**	> 99, 98, (*R*)	> 99, 94, (*S*)	> 99, 92, (*S*)	> 99, 95, (*S*)	> 99, 93, (*S*)	59, 94, (*S*)	> 99, 94, (*S*)
2	**46e**	> 99, 97, (*R*)	> 99, 94, (*S*)	> 99, 92, (*S*)	> 99, 90, (*S*)	> 99, 73, (*R*)	48, 93, (*S*)	n.d.[e]
3	**46a**	n.d.[e]	> 99, 74, (*S*)	n.d.[e]	n.d.[e]	n.d.[e]	n.d.[e]	n.d.[e]
4	**46d**	n.d.[e]	> 99, 86, (*S*)	n.d.[e]	n.d.[e]	n.d.[e]	n.d.[e]	n.d.[e]

[a] Unless otherwise stated: S/C = 100:1; [S] = 0.2 M; room temperature. The values shown are the average values of at least two independent runs. [b] Conversion, as determined by ^{1}H NMR analysis. [c] Enantioselectivity, as determined by GC or HPLC using chiral stationary phases. Absolute configuration was assigned by comparison of the elution order (GC or HPLC analysis) or specific rotation with reported data. [e] Not done.

In all cases conversion was complete, except for substrate **39g**, and enantioselectivity was generally very high (from 92% to 98% ee). These results are in agreement with recently published work, which describes that rhodium complexes derived from phosphorus bidentate ligands with long alkyl or polyether chains between the two phosphorus binding groups mediate asymmetric hydrogenations with high enantioselectivity.[201] Remarkably, ligands **46b** and **46e** gave very similar results except for substrate **39f**, but in this case the ligand chain structure demonstrated to be a key parameter. The hydrogenation product (*R*)-**44f** was obtained in a 73% of enantiomeric excess when using ligand **46e**, whereas with ligand **46b** reversed and improved enantioinduction was observed affording product (*S*)-**44f** in a 93% of enantiomeric excess (compare entries 1 and 2 in Table 38).

[201] a) Farkas, G.; Balogh, S.; Madarasz, J.; Szollosy, A.; Darvas, F.; Urge, L.; Gouygou, M.; Bakos, J. *Dalton Trans.* **2012**, *41*, 9493. b) Reetz, M. T.; Mehler, G.; Bondarev, O. *Chem. Commun.* **2006**, 2292.

We then studied the effect of alkali metal-derived regulation agents (NaBArF, KBArF, CsBArF) and ammonium BArF salts (**95**, (*R,R*)-**94** or (*S,S*)-**94**) in the asymmetric hydrogenation reaction (Table 39 and Table 40, respectively).

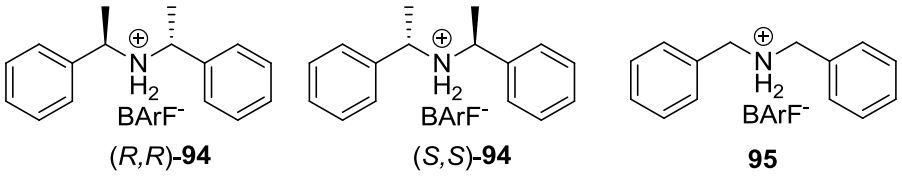

Figure 135. Ammonium BArF salts utilized in the asymmetric hydrogenation studies

Table 39. Catalytic studies on the hydrogenation[a] of **39a**,**b**,**d**–**h** using rhodium complexes derived from ligands **46** with diverse alkali metal BArF salts as distal regulation agents

		Hydrogenation Results						
Entry	Salt•**L**	Conv.[b] ee (%)[c] (config) **39a**	Conv.[b] ee (%)[c] (config) **39b**	Conv.[b] ee (%)[c] (config) **39d**	Conv.[b] ee (%)[c] (config) **39e**	Conv.[b] ee (%)[c] (config) **39f**	Conv.[b] ee (%)[c] (config) **39g**	Conv.[b] ee (%)[c] (config) **39h**
1	Na•**46b**	> 99, 97, (*R*)	> 99, 94, (*S*)	> 99, 91, (*S*)	> 99, 95, (*S*)	> 99, 94, (*S*)	58, 93, (*S*)	> 99, 94, (*S*)
2	K•**46b**	> 99, 91, (*R*)	> 99, 93, (*S*)	> 99, 92, (*S*)	> 99, 94, (*S*)	> 99, 89, (*S*)	49, 85, (*S*)	> 99, 94, (*S*)
3	Cs•**46b**	> 99, 99, (*R*)	> 99, 97,[d] (*S*)	> 99, 92, (*S*)	> 99, 95, (*S*)	> 99, 93, (*S*)	52, 91, (*S*)	> 99, 94, (*S*)
4	Na•**46e**	> 99, 97, (*R*)	> 99, 94, (*S*)	> 99, 91, (*S*)	> 99, 90, (*S*)	> 99, 73, (*R*)	66, 88, (*S*)	n.d.[e]
5	Cs•**46e**	> 99, 97, (*R*)	> 99, 95, (*S*)	> 99, 90, (*S*)	> 99, 89, (*S*)	> 99, 78, (*R*)	41, 87, (*S*)	n.d.[e]

For experimental details (footnotes a, b and c) see Table 38 [d] 2.0 equivalents (relative to ligand **46b**) of CsBArF was added. Product **44b** was obtained in 95% ee towards the (*S*)-configured product when 1.3 equiv. of CsBArF were added. [e] Not done.

Table 40. Catalytic studies on the hydrogenation[a] of **39a,b,d–h** using rhodium complexes derived from ligands **46** with diverse ammonium BArF salts as distal regulation agents

Entry	Salt•L	Hydrogenation Results						
		Conv.[b] ee (%)[c] (config)	Conv.[b] ee (%)[c] (config)	Conv.[b] ee (%)[c] (config)	Conv.[b] ee (%)[c] (config)	Conv.[b] ee (%)[c] (config)	Conv.[b] ee (%)[c] (config)	Conv.[b] ee (%)[c] (config)
		39a	**39b**	**39d**	**39e**	**39f**	**39g**	**39h**
1	**95•46b**	> 99, 97, (*R*)	> 99, 94, (*S*)	> 99, 91, (*S*)	> 99, 94, (*S*)	> 99, 92, (*S*)	39, 91, (*S*)	> 99, 94, (*S*)
2	(*R*,*R*)-**94•46b**	> 99, 98, (*R*)	> 99, 95, (*S*)	> 99, 92, (*S*)	> 99, 95, (*S*)	> 99, 93, (*S*)	21, 94, (*S*)	n.d.[d]
3	(*S*,*S*)-**94•46e**	> 99, 96, (*R*)	> 99, 94, (*S*)	> 99, 90, (*S*)	> 99, 90, (*S*)	> 99, 74, (*R*)	32, 92, (*S*)	n.d.[d]
4	(*R*,*R*)-**94•46e**	> 99, 97, (*R*)	> 99, 96, (*S*)	> 99, 90, (*S*)	> 99, 93, (*S*)	> 99, 78, (*R*)	50, 95, (*S*)	n.d.[d]

For experimental details (footnotes a, b, c and d) see Table 38

In general terms, the regulation agents studied affected the enantioselectivities, whilst conversions remained complete except for substrate **39g**, whose conversion ranged from 21 to 66%. Interestingly, addition of an excess of CsBArF to ligand **46b** (2.0 equiv. relative to ligand) led to a measurable increase in the enantioselectivity of the hydrogenation product **44b** (3% increase in the ee, see Table 39, entry 3). When the usual amount of polyether binder (1.3 equiv. of CsBArF) was used for the hydrogenation of substrate **39b**, a minor, but measurable, 1% increase in the ee was observed (Table 39, footnote d). CsBArF had the same effect on the hydrogenation of itaconic acid derivative **39a** and NaBArF on the hydrogenation of 1-(naphthyl)vinyl acetamide **39f** with Rh(I) catalysts derived from ligand **46b** (up to 1% increase in the ee; compare entry 1 in Table 38 with entries 1 and 3 in Table 39). This small, but positive, regulation effects on enantioselectivity observed for **39a** and **39f** could not be further improved by increasing the amount of regulator agent (up to 2.0 equiv. relative to ligand **46b**). Although asymmetric hydrogenation of substrates **39d**,**e**,**g**,**h**

mediated by ligand **46b** afforded products **44d**,**e**,**g**,**h** with high enantioselectivity (ranging from 92% to 95%), the distal regulation agents studied did not produce a clear improvement in the enantioselectivity of the process.

Asymmetric hydrogenation of substrate **39b** mediated by ligand **46e** was achieved in 94% ee. The enantioselectivity of the process was appreciably improved by addition of CsBArF or chiral ammonium salt (*R,R*)-**94** (95% or 96% ee, respectively; see entry 5 on Table 39 and entry 4 in Table 40). Similarly, CsBArF and/or (*R,R*)-**94** improved the results obtained for substrates **39e**, **39f** and **39g**; up to 5% increases in the ee were detected for the asymmetric hydrogenation of substrate **39f** when CsBArF or (*R,R*)-**94** were added (compare entries 2, 5 and 4 in Table 38, Table 39 and Table 40, respectively). Substrates **39e** and **39g** were hydrogenated in 90 and 93% ee, respectively, with Rh(I) catalysts derived from ligand **46e**. Gratifyingly, the enantiomeric excesses were improved in the presence of (*R*,*R*)-**94** up to 93 and 95% for substrates **39e** and **39g**, respectively. Unfortunately, the high levels of enantioselectivity achieved with the Rh(I) complexes derived from "naked ligand" **46e** for substrates **39a** and **39d** could not be further improved by addition of different regulation agents.

Thus, appropriate combinations of $[Rh(cod)_2]BArF$ and bisphosphite ligands **46b** or **46e**, plus a regulation agent (NaBArF, CsBArF or **94**), afford in some cases an adaptive catalytic system specific to the substrate geometry: the enantioselectivity of the hydrogenation product can be enhanced without any further synthetic effort, simply by choosing the adequate distal regulation agent for each substrate or by not using one at all. In fact, our catalytic results with this supramolecular strategy are close, in terms of enantioselectivity, to the results reported for the highest performing catalytic systems that have been reported up to date. Results of some of the best Rh(I) catalysts derived from high performing ligands from the literature for asymmetric hydrogenation of substrates **39a**,**b**,**d**–**h** are compared to our best results in Table 41.

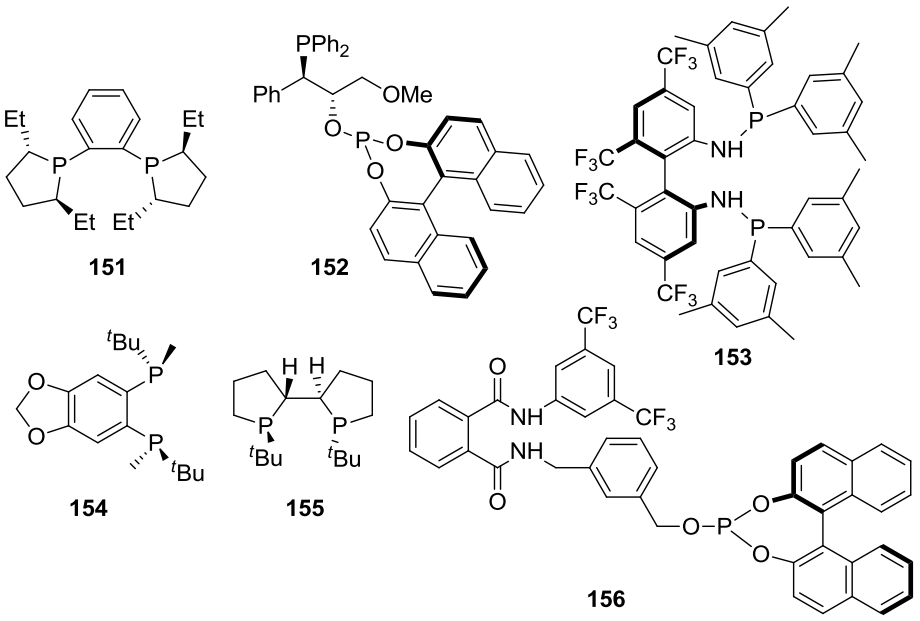

Figure 136. High performing ligands for Rh(I) asymmetric hydrogenation of **39a**,**b**,**d–h**

Table 41. Comparison between ligands from the literature and ligand **46b** for the asymmetric hydrogenation of substrates **39a**,**b**,**d–h**

Entry	Alkene	Hydrogenation Results	
		Salt•**Ligand**, ee (%)	**Ligand**, ee (%)
1	**39a**	Cs•**46b**, 99	**152**, 99
2	**39b**	Cs•**46b**, 97	**151**, 99
3	**39d**	**46b**, 92	**152**, 99
4	**39e**	**46b**, 95	**153**, 99
5	**39f**	Na•**46b**, 94	**154**, 97
6	**39g**	**46b**, 94	**156**, 99
7	**39h**	**46b**, 94	**155**, 99

Many catalytic systems derived from diverse ligands have mediated the hydrogenation of alkenes **39a**, **39b** and **39d** with perfect enantioselectivity. As a representative example, we have included in the table the milestone bisphosphine ligand Et-DUPHOS **151** and phosphine-phosphite ligand **152**.[202] Rh-mediated asymmetric hydrogenation results for α-arylenamides **39e**,**f**,**h** have been recently reviewed in two extensive articles.[203] Here, we have selected atropisomerically enantiopure bis(aminophosphine) ligand **153**[204], bisphosphines with stereogenic P atoms **154** (DioxyBenzP*)[205] and **155** (TangPhos)[206] as examples of outstanding ligands for the Rh-mediated asymmetric hydrogenation of substrates **39e**, **39f** and **39h**, respectively. Challenging dehydro-β-amino acid derivative **39g** was also hydrogenated with excellent results by Pignataro *et al.* with Rh(I) catalysts derived from monophosphite **156**.[207]

As a final conclusion, our supramolecular strategy has enabled the possibility to hydrogenate an array of structurally diverse prochiral alkenes in high levels of enantioselectivity with Rh(I) catalysts derived from simple bisphosphite ligands, that can be straightforwardly prepared. Moreover, addition of distal regulation agents has permitted the possibility to enhance the results achieved.

2.2.4.3 Rationalization of the stereochemical outcome of the hydrogenation reactions

As has been indicated in the previous section, cationic rhodium(I) complexes incorporating ligand **46b** catalyzed asymmetric hydrogenations of functionalized alkenes lead to (*S*)-configured products from dehydro-α-amino acid derivatives (**39b**,**d**) and two different α-arylenamides (**39e**,**f**,**h**). Ligand **46e** showed an opposite sense of enantiodiscrimination for substrate **39f**. The hydrogenation product derived from dimethyl itaconate (**39a**) is always obtained with the (*R*)-configuration with ligands **46b**,**e**. It is worth mentioning at this point

[202] Fernández-Pérez, H.; Donald, S. M. A.; Munslow, I. J.; Benet-Buchholz, J.; Maseras, F.; Vidal-Ferran, A. *Chem. Eur. J.* **2010**, *16*, 6495.
[203] a) Xie, J.-H.; Zhu, S.-F.; Zhou, Q.-L. *Chem. Rev.* **2011**, *111*, 1713. b) Gopalaiah, K.; Kagan, H. B. *Chem. Rev.* **2011**, *111*, 4599.
[204] Wang, C.-J.; Gao, F.; Liang, G. *Org. Lett.* **2008**, *10*, 4711.
[205] Imamoto, T.; Tamura, K.; Zhang, Z.; Horiuchi, Y.; Sugiya, M.; Yoshida, K.; Yanagisawa, A.; Gridnev, I. D. *J. Am. Chem. Soc.* **2012**, *134*, 1754.
[206] Tang, W.; Zhang, X. *Angew. Chem., Int. Ed.* **2002**, *41*, 1612.
[207] Pignataro, L.; Boghi, M.; Civera, M.; Carboni, S.; Piarulli, U.; Gennari, C. *Chem. Eur. J.* **2012**, *18*, 1383.

that the change to the (*R*)-configuration in the case of the hydrogenation product of dimethyl itaconate (**39a**) is due to an inversion in the CIP priority rules.

The successful application of enantiomerically pure rhodium complexes in asymmetric hydrogenation relies on the ability of the substrate to form a rhodium chelate involving the C=C double bond and a donor atom, which is normally placed in the γ-position of a substitutent attached to the C=C double bond (see Scheme 48, in which chelating assistance by a X-C=O group is shown). In general, theoretical studies on hydrogenation indicate competition between oxidative addition and migratory insertion as possible rate- and stereo-determining steps.[208] For ligands not being electron-rich alkyl-phosphines mediating hydrogenations in non-polar solvents, the "*dihydride mechanism*" with migratory insertion as the stereodetermining step seems quite unlikely to be operating.[209] Thus, we suggest that asymmetric hydrogenation mediated by rhodium complexes of bisphosphite ligands **46** follows the quite common "*unsaturated mechanism*".[210] In this case, dihydrogen will be added across the coordinated olefin, thus forming new carbon-hydrogen bonds from the side of the metal during the stereospecific catalytic process (See Scheme 48).

A schematic view of the hydrogenation reaction mediated by rhodium complexes derived from ligand **46b** is presented in Scheme 48, which helps in predicting the direction of stereoinduction by showing the lowest energy direction of approach of the hydrido groups to the C=C group. In this way, (*S*)-configured hydrogenation products are obtained from α-acylamino(acrylates) and α-arylenamides, whilst the hydrogenation of the itaconic acid derivative leads to the (*R*)-configured product ((*R*)-**44a**) indicated in Scheme 48.

[208] Donoghue, P. J.; Helquist, P.; Norrby, P.-O.; Wiest, O. *J. Am. Chem. Soc.* **2009**, *131*, 410.
[209] Fernández-Pérez, H.; Donald, S. M. A.; Munslow, I. J.; Benet-Buchholz, J.; Maseras, F.; Vidal-Ferran, A. *Chem. Eur. J.* **2010**, *16*, 6495.
[210] See the seminal work from Halpern and Brown *et al.* (Halpern, J.; Riley, D. P.; Chan, A. S. C.; Pluth, J. J. *J. Am. Chem. Soc.* **1977**, *99*, 8055 and Brown, J. M. *Chem. Soc. Rev.* **1993**, *22*, 25), and more recent contributions from Landis *et al.* and the references cited therein: a) Feldgus, S.; Landis, C. R. *Organometallics* **2001**, *20*, 2374. b) Feldgus, S.; Landis, C. R. *J. Am. Chem. Soc.* **2000**, *122*, 12714. c) Landis, C. R.; Feldgus, S. *Angew. Chem., Int. Ed.* **2000**, *39*, 2863.

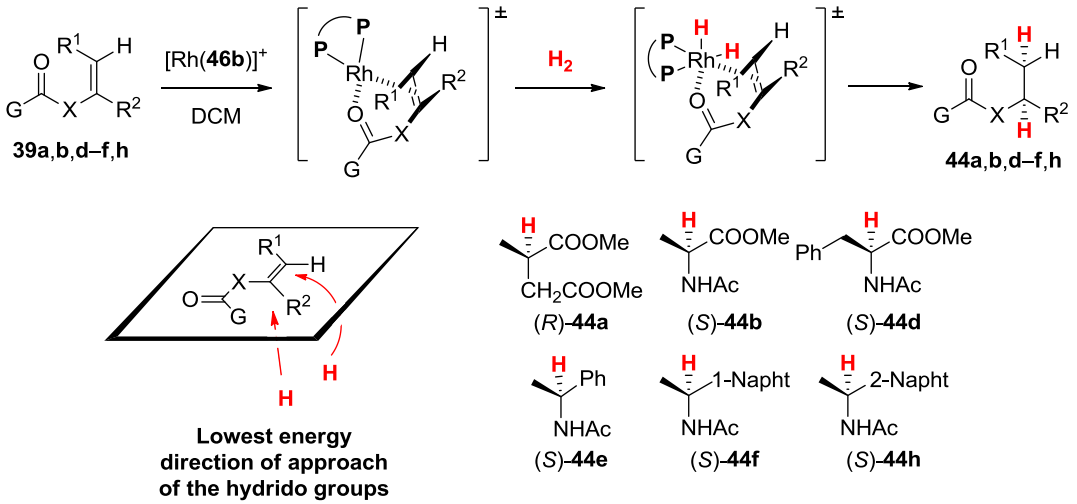

Scheme 48. Schematic view of the favored hydrogenation route of functionalized alkenes **39a**,**b**,**d–f**,**h** catalyzed by rhodium complexes derived from **46b**

On the other hand, asymmetric hydrogenation of substrate **39g** afforded product (*S*)-**44g** with both ligands **46b** and **46e**. It should be noted at this stage that this substrate forms a six-membered chelate with the rhodium center by coordination of the *N*-acetyl and C=C groups instead of the five-membered one, which is formed for the previously mentioned substrates. This change in the coordination mode for substrate **39g** translates to a formal delivery of the hydrido groups at the opposite alkene face with respect to that involved for the other substrates (compare Scheme 48 and Scheme 49). However, the final configuration of the hydrogenation product of **39g** is the same for α-acylamino(acrylates) and α-arylenamides, as both the attacked alkene face in **39g** and CIP priority rules of the substituents in the hydrogenation product **44g** change with respect to those observed for the other products.

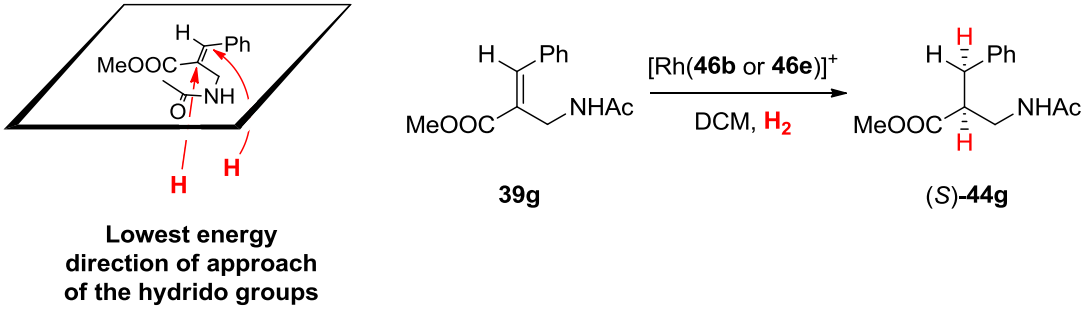

Scheme 49. Schematic view of the favored hydrogenation route of functionalized alkene **39g** catalyzed by rhodium complex derived from **46b** and **46e**

As already mentioned in Section 2.2.3.4 during the discussion of the stereochemical outcome of hydroformylation reactions, quadrant analysis provides a simplified view of the hydrogenation process. Assuming an octahedral coordination environment for the rhodium center and placement of the C=C bond in the apparently less crowded lower left quadrant and with the substrate orientations indicated in Figure 137, the observed configurations for the hydrogenation products can be predicted. We would like to emphasize that this model is purely mnemonic, as it only helps in predicting the absolute configuration of the hydrogenation products obtained. The elucidation of the most favorable reaction manifold(s) and discrimination of the less favorable one(s) could only arise from detailed computational studies for all the reaction manifolds derived from all possible binding modes of the substrate by its two enantiotopic faces. Unfortunately, the required computational studies on the origin of stereoselectivity have not been performed yet.

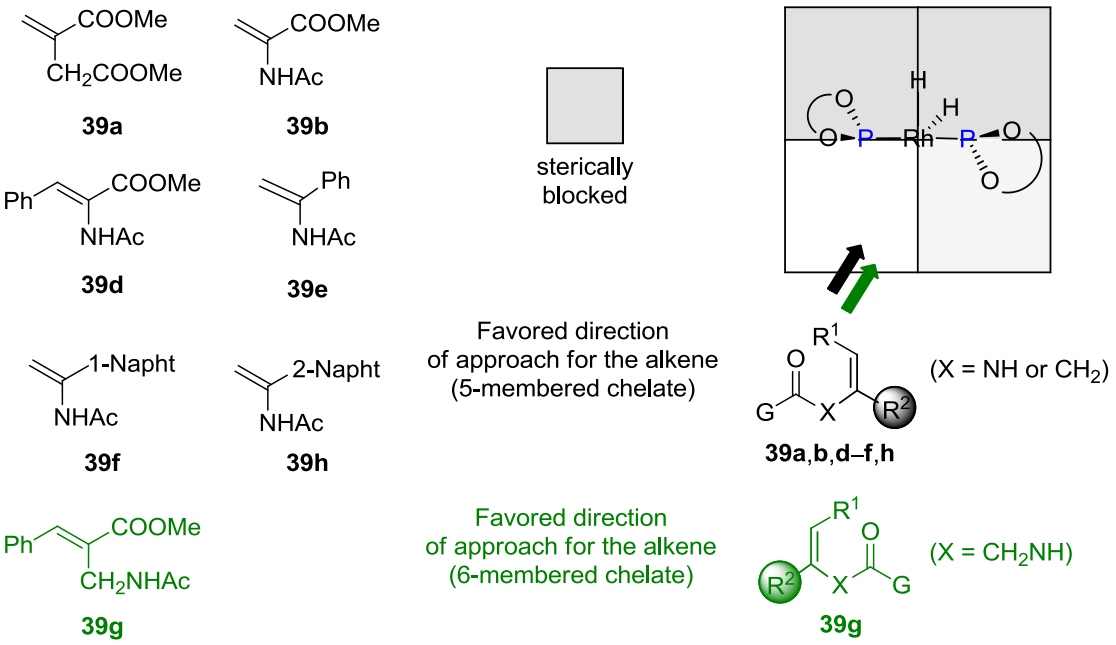

Figure 137. Quadrant diagram showing the preferential coordination face for substrates **39a**,**b**,**d–h**, which are coordinated to the rhodium center forming a five- or six-membered chelate ring, when ligand **46b** is used

EXPERIMENTAL PART

2.3 EXPERIMENTAL PART

2.3.1 General remarks

All syntheses were carried out using chemicals as purchased from commercial sources unless otherwise cited. All manipulations and reactions were performed under inert atmosphere. Glassware was dried *in vacuo* before use with a hot air gun. All solvents were dried and deoxygenated by using a Solvent Purification System (SPS). Silica gel 60 (230–400 mesh) or spherical Silica-C18 (200–400 mesh) was used for column chromatography. NMR spectra were recorded in $CDCl_3$ unless otherwise cited using a Bruker Avance 400 and 500 MHz Ultrashield spectrometers. ^{1}H NMR and ^{13}C NMR chemical shifts were quoted in ppm relative to residual solvent peaks, whereas $^{31}P\{^{1}H\}$ NMR chemical shifts were quoted in ppm relative to 85% phosphoric acid in water. IR spectra were recorded using Attenuated Total Reflection (ATR) technique unless otherwise cited. High-resolution mass spectra (HRMS) were recorded by using an electrospray ionization (ESI) method in positive mode on a Waters LCT Premier mass spectrometer. Melting points were determined in open capillaries and are uncorrected. UV spectra were recorded on a UV-Vis spectrometer using 10 mm quartz cells. Emission spectra were recorded on an Aminco·Bowman Series 2 spectrofluorimeter using 10 mm quartz cells. Optical rotations were measured on a Jasco P-1030 polarimeter. ITC data were obtained on a VP-ITC Microcalorimeter, MicroCal, LLC (Northampton, MA). Enantiomeric excesses were determined by GC or HPLC on using chiral stationary phases. GC analyses were performed on an Agilent 6890N chromatograph equipped with a FID detector. HPLC analyses were performed on an Agilent 1200 Series chromatograph equipped with a diode array UV detector. Elemental analyses were performed on a LECO CHNS-932 elemental analyzer.

2.3.2 Synthetic procedure of bisphosphite ligands 46

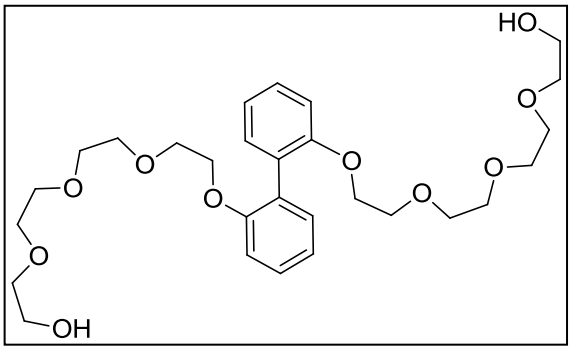

Compound 113: A mixture of 2,2'-biphenol (**87**) (1.15 g, 6.16 mmol), monotosylated diol (**129**)[211] (4.21 g, 12.10 mmol) and K_2CO_3 (8.64 g, 26.5 mmol) in dry DMF (150 mL) was refluxed for 60 h. The reaction mixture was filtered and then concentrated under reduced pressure. The crude product was purified by column chromatography over silica gel (EtOAc/MeOH 95:5 as the eluent) to afford the desired product **113** (1.5 g, 45% yield) as colorless oil; IR (neat, cm^{-1}) υ 3431, 2868, 1593, 1503, 1105; ^1H NMR (400 MHz, $CDCl_3$) δ 7.34–7.26 (m, 2H), 7.05–6.96 (m, 2H), 4.14–4.08 (t, *J* = 5.1 Hz, 2H), 3.75–3.69 (m, 4H), 3.67–3.57 (m, 6H), 3.56–3.51 (m, 4H); $^{13}C\{^1H\}$ NMR (125 MHz, $CDCl_3$) δ 156.2, 131.4, 128.2, 128.1, 120.3, 112.3, 72.4, 70.5, 70.4, 70.3, 70.1, 69.4, 68.3, 61.3; HRMS (ESI^+): m/z $[M+Na]^+$ calcd for $C_{28}H_{42}O_{10}Na$ 561.2687, found 561.2676.

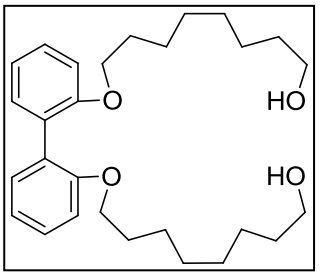

Compound 116: A mixture of 2,2'-biphenol (**87**) (0.52 g, 2.82 mmol), monotosylated diol (**127**)[212] (1.70 g, 5.64 mmol) and K_2CO_3 (1.68 g, 12.1 mmol) in dry acetonitrile (24 mL) was refluxed for 72 h. The reaction mixture was filtered and then concentrated under reduced pressure. The crude product was purified by column chromatography over silica gel (EtOAc/MeOH 95:5 as the eluent) to afford the desired product **116** (0.70 g, 56% yield) as a white solid. Mp: 31–33 ºC; IR (neat, cm^{-1}) υ 3323, 2923, 2851, 1582, 1228; ^1H NMR (400 MHz, $CDCl_3$) δ 7.34–7.24 (m, 2H), 7.03–6.92 (m, 2H), 3.95–3.88 (t, *J* = 6.6 Hz, 2H), 3.69–3.61 (t, *J* = 6.6 Hz, 2H), 1.69–1.51 (m, 4H), 1.37–1.22 (m, 8H); $^{13}C\{^1H\}$ NMR (125 MHz, $CDCl_3$) δ 156.7, 131.7, 128.5, 128.4, 120.1, 112.3, 68.5, 63.2, 32.9, 29.5, 29.4, 29.3, 26.0, 25.7; HRMS (ESI^+): m/z $[M+Na]^+$ calcd for $C_{28}H_{42}O_4Na$ 465.2975, found 465.2979.

---

[211] Rubinshtein, M.; James, C. R.; Young, J. L.; Ma, Y. J.; Kobayashi, Y.; Gianneschi, N. C.; Yang, J. *Org. Lett.* **2010**, *12*, 3560.
[212] Junk, M. J. N.; Li, W.; Schlueter, A. D.; Wegner, G.; Spiess, H. W.; Zhang, A.; Hinderberger, D. *Angew. Chem., Int. Ed.* **2010**, *49*, 5683.

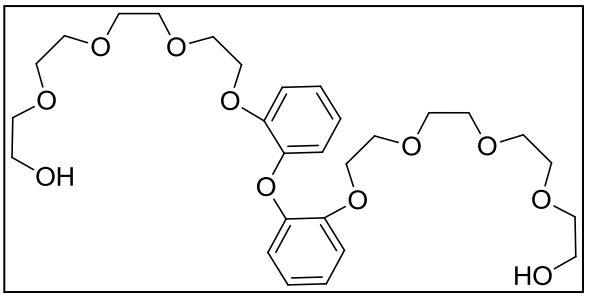

Compound 115: A mixture of 2,2'-oxydiphenol (**131**) (0.49 g, 2.40 mmol), monotosylated diol (**129**)[211] (1.67 g, 4.80 mmol) and K_2CO_3 (1.43 g, 10.3 mmol) in dry acetonitrile (24 mL) was refluxed for 60 h. The reaction mixture was filtered and then concentrated under reduced pressure. The crude product was purified by column chromatography over silica gel (EtOAc/MeOH 95:5 as the eluent) to afford the desired product **115** (0.50 g, 46% yield) as pale yellow oil. IR (neat, cm^{-1}) υ 3440, 2869, 1598, 1496, 1452; ^1H NMR (400 MHz, $CDCl_3$) δ 7.11–7.04 (m, 2H), 6.95–6.89 (m, 1H), 6.88–6.83 (m, 1H), 4.22–4.15 (m, 2H), 3.81–3.74 (m, 2H), 3.71–3.67 (m, 2H), 3.66–3.53 (m, 10H); $^{13}C\{^1H\}$ NMR (125 MHz, $CDCl_3$) δ 150.0, 146.8, 124.1, 121,8; 119.4; 115.1; 72.9; 71.0; 70.8; 70.8; 70.6; 69.9; 69.2; 61.9; HRMS (ESI^+): m/z $[M+Na]^+$ calcd for $C_{28}H_{42}O_{11}Na$ 577.2625, found 577.2599.

General synthetic procedures for bisphosphite ligands **46**:

Under argon atmosphere diol (**120**,[213] **124**[214] or **126**) (0.88 mmol) was azeotropically dried with toluene (3 x 1 mL). The remaining solid was dissolved in anhydrous toluene (14 mL) and slowly added to a stirred solution of PCl_3 (1.11 mmol) and NEt_3 (2.52 mmol) in dry toluene (14 mL) at 0 ºC. The solution was allowed to reach room temperature and was stirred overnight. The turbid reaction mixture was filtered and the solvent evaporated under reduced pressure. The resulting residue was dissolved in 14 mL of dry toluene and NEt_3 (0.35 mL, 2.52 mmol). A solution of the corresponding diol (**88**,[215] **113**, **114**, **116**, **115**) (0.41 mmol, in 14 mL of toluene) was slowly added to the previous solution and allowed to react overnight at room temperature. The reaction mixture was filtered and the solvent evaporated under reduced pressure. The resulting crude mixture was purified by column chromatography on silica gel C18 using acetonitrile/ethyl acetate 1:1 as elution solvent to provide the expected bisphosphite (*ca.* 85% yield) as a white solid.

[213] Kauch, M.; Snieckus, V.; Hoppe, D. *J. Org. Chem.* **2005**, *70*, 7149.
[214] Erre, G.; Junge, K.; Enthaler, S.; Addis, D.; Michalik, D.; Spannenberg, A.; Beller, M. *Chem. - Asian J.* **2008**, *3*, 887.
[215] For the synthetic procedure of **88** see Experimental part in chapter 1.

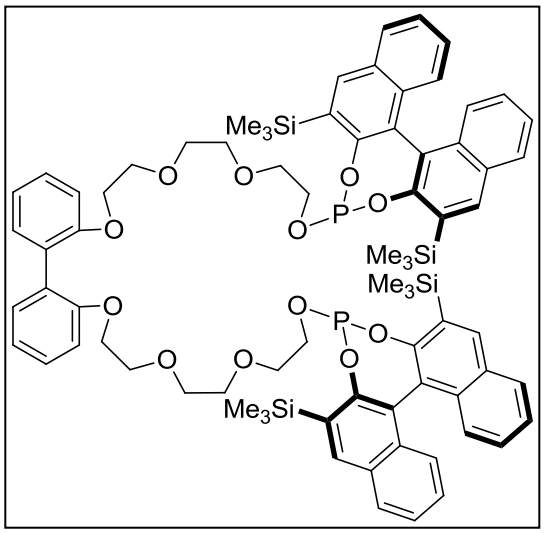

Compound 46a: Compound **46a** was synthesized following the general strategy from (R_a)-3,3'-bis(trimethylsilyl)-[1,1'-binaphtalene]-2,2'-diol (**120**) (666 mg, 1.55 mmol), PCl_3 (170 μL, 1.95 mmol), NEt_3 (615 μL, 4.42 mmol) and the slow addition of **88** (320 mg, 0.71 mmol) with NEt_3 (615 μL, 4.42 mmol) as base. Purification by C18 column chromatography using acetonitrile/ethyl acetate 1:1 afforded the expected bisphosphite ligand **46a** as a white solid (840 mg, 86% yield). Mp: 145–163 ºC; $[\alpha]_D^{25}$ = –563.8 (*c* 0.12, toluene); IR (neat, cm^{-1}) υ 1617, 1576, 1221; ^1H NMR (400 MHz, CD_2Cl_2) δ 8.14–8.07 (m, 4H), 7.96–7.88 (m, 4H), 7.43–7.36 (m, 4H), 7.25–7.11 (m, 10H), 7.09–7.03 (m, 2H), 6.94–6.84 (m, 4H), 4.01–3.97 (m, 4H), 3.96–3.88 (m, 2H), 3.61–3.53 (m, 4H), 3.43–3.33 (m, 14H), 0.46 (s, 18H), 0.45 (s, 18H); $^{13}C\{^1H,^{31}P\}$ NMR (125 MHz, CD_2Cl_2) δ 156.7, 153.0, 152.2, 137.6, 137.5, 134.3, 134.2, 133.0, 132.3, 132.0, 131.4, 131.0, 128.8, 128.8, 128.8, 128.5, 127.0, 126.9, 126.8, 125.2, 125.2, 123.0, 122.2, 120.8, 112.7, 71.0, 70.9, 70.8, 70.0, 68.7, 64.2, 0.1, 0.0; $^{31}P\{^1H\}$ NMR (202 MHz, CD_2Cl_2) δ 138.7; HRMS (ESI^+): m/z $[M+Na]^+$ calcd for $C_{76}H_{88}O_{12}P_2Si_4Na$ 1389.4726, found 1389.4757.

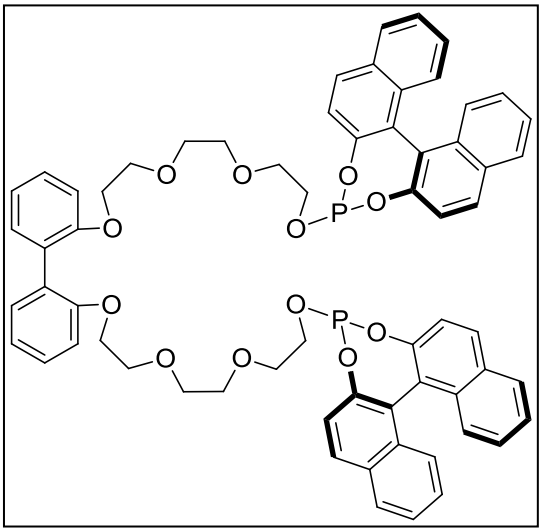

Compound 46b: Compound **46b** was synthesized following the general strategy from commercial phosphochloridite **117b** (364 mg, 1.01 mmol) with NEt_3 (280 μL, 2.01 mmol) as base and diol **88** (206 mg, 0.46 mmol). Purification by C18 column chromatography using acetonitrile afforded the expected bisphosphite ligand **46b** as a white solid (432 mg, 83% yield). Mp: 155–174 ºC; $[\alpha]_D^{25}$ = –452.5 (*c* 0.80, toluene); IR (neat, cm^{-1}) υ 1589, 1504,

1228, 1125, 1036; ^{1}H NMR (400 MHz, CD_2Cl_2) δ 7.99–7.98 (m, 2H), 7.97–7.89 (m, 6H), 7.51–7.50 (m, 2H), 7.45–7.40 (m, 6H), 7.36–7.30 (m, 4H), 7.30–7.20 (m, 8H), 6.98–6.90 (m, 4H), 4.08–3.99 (m, 6H), 3.91–3.83 (m, 2H), 3.68–3.61 (m, 4H), 3.55–3.45 (m, 12H); ^{13}C{^{1}H,^{31}P} NMR (125 MHz, CD_2Cl_2) δ 156.4, 148.6, 147.6, 132.8, 132.5, 131.6, 131.1, 130.4, 130.1, 128.4, 128.4, 128.2, 126.8, 126.7, 126.3, 126.3, 125.1, 125.0, 124.0, 122.7, 121.8, 120.4, 112.3, 70.7, 70.6, 69.7, 68.3, 64.4; ^{31}P{^{1}H} NMR (202 MHz, CD_2Cl_2) δ 146.2; HRMS (ESI^{+}): m/z $[M+Na]^{+}$ calcd for $C_{64}H_{56}O_{12}P_2Na$ 1101.3145, found 1101.3176.

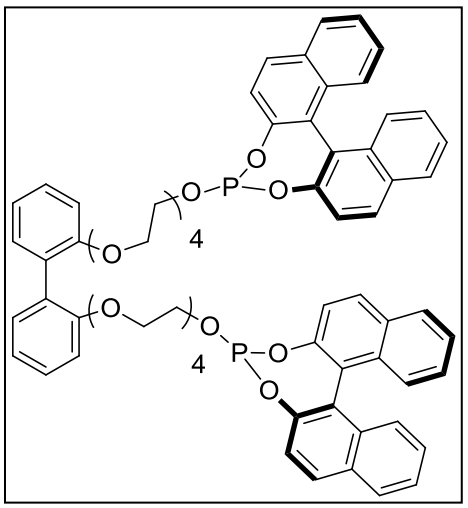

Compound 46c: Compound **46c** was synthesized following the general strategy from commercial phosphochloridite **117b** (245 mg, 0.70 mmol) with NEt_3 (194 μL, 1.40 mmol) as base and diol **113** (171 mg, 0.32 mmol). Purification by C18 column chromatography using acetonitrile afforded the expected bisphosphite ligand **46c** as a white solid (320 mg, 86% yield). Mp: 149–158 ºC; $[\alpha]_D^{25}$ = –409.8 (*c* 0.67, toluene); IR (neat, cm^{-1}) υ 2867, 1589, 1229, 937; ^{1}H NMR (400 MHz, CD_2Cl_2) δ 7.97–7.84 (m, 4H), 7.49–7.44 (m, 1H), 7.42–7.35 (m, 3H), 7.29–7.25 (m, 2H), 7.24–7.16 (m, 4H), 6.94–6.86 (m, 2H), 4.05–3.97 (m, 3H), 4.89–3.80 (m, 1H), 3.60–3.56 (m, 2H), 3.55–3.46 (m, 6H), 3.45–3.39 (m, 4H); ^{13}C{^{1}H,^{31}P} NMR (125 MHz, CD_2Cl_2) δ 156.8, 149.1, 148.0, 133.2, 132.9, 132.0, 131.5, 130.9, 130.5, 128.9, 128.8, 128.7, 128.6, 127.2, 127.1, 127.0, 126.7, 126.6, 125.5, 125.4, 124.4, 123.1, 122.2, 120.8, 112.8, 71.1, 71.0, 71.0, 70.9, 70.8, 70.0, 68.7, 64.8; ^{31}P{^{1}H} NMR (202 MHz, CD_2Cl_2) δ 146.2; HRMS (ESI^{+}): m/z $[M+Na]^{+}$ calcd for $C_{68}H_{64}O_{14}P_2Na$ 1189.3669, found 1189.3687.

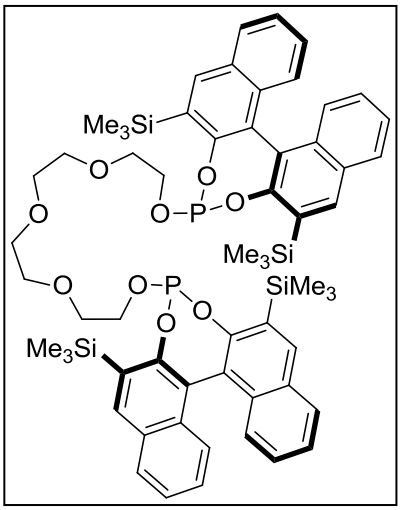

Compound 46d: Compound **46d** was synthesized following the general strategy from diol **120** (482 mg, 1.12 mmol), PCl_3 (123 μL, 1.41 mmol), NEt_3 (445 μL, 3.20 mmol) and a slow addition of tetraethylenglycol **114** (100 mg, 0.51 mmol). Purification by C18 column chromatography using acetonitrile/ethyl acetate 1:1 afforded the expected bisphosphite ligand **46d** as a white solid (481 mg, 84% yield). Mp: 64–68 ºC; $[\alpha]_D^{25}$ = –668.2 (*c* 0.26, toluene); IR (neat, cm^{-1}) υ 1276, 823, 743; ^1H NMR (400 MHz, CD_2Cl_2) δ 8.17–8.11 (m, 4H), 8.00–7.93 (m, 4H), 7.47–7.41 (m, 4H), 7.24–7.17 (m, 4H), 7.17–7.11 (m, 2H), 7.10–7.03 (m, 2H), 4.02–3.88 (m, 2H), 3.54–3.40 (m, 14H), 0.46 (s, 18H), 0.45 (s, 18H); $^{13}C\{^1H,^{31}P\}$ NMR (125 MHz, CD_2Cl_2) δ 153.0, 152.2, 137.6, 137.5, 134.3, 134.2, 133.0, 132.3, 131.4, 131.0, 128.8, 128.7, 127.0, 126.9, 126.8, 125.2, 125.1, 123.0, 122.2, 70.9, 70.9, 70.8, 64.2, 0.1, 0.0; $^{31}P\{^1H\}$ NMR (202 MHz, CD_2Cl_2) δ 135.7; HRMS (ESI^+): m/z $[M+Na]^+$ calcd for $C_{60}H_{72}O_9P_2Si_4Na$ 1133.3621, found 1133.3643.

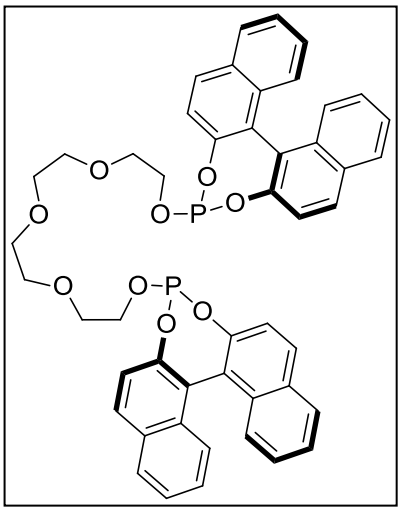

Compound 46e: Compound **46e** was synthesized following the general strategy from commercial phosphochloridite **117b** (542 mg, 1.50 mmol) and a slow addition of tetraethylenglycol **114** (134 mg, 0.69 mmol) with NEt_3 (420 μL, 3.02 mmol) as base. Purification by C18 column chromatography using acetonitrile afforded the expected bisphosphite ligand **46e** as a white solid (440 mg, 75% yield). Spectroscopic data were in agreement with the reported ones.[216]

[216] Reetz, M.T.; Meiswinkel, A.; Mehler, G. Chiral Di- and Triphosphites. WO Patent 2005047299, 2005.

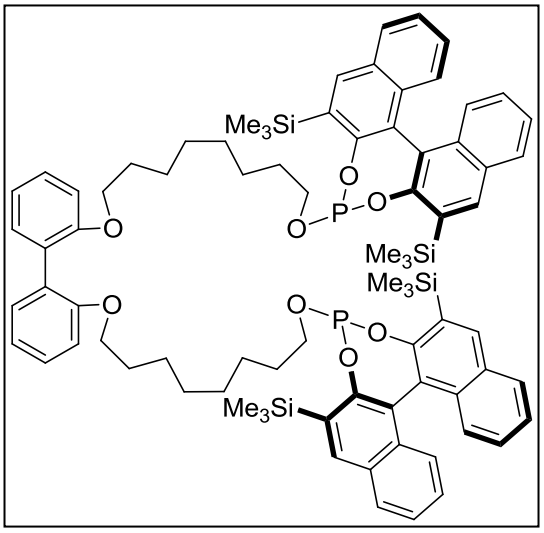

Compound 46f: Compound **46f** was synthesized following the general strategy from diol (**120**) (379 mg, 0.88 mmol), PCl_3 (97 μL, 1.11 mmol), NEt_3 (350 μL, 2.52 mmol) and the slow addition of diol **116** (179 mg, 0.41 mmol) with NEt_3 (350 μL, 2.52 mmol) as base. Purification by C18 column chromatography using acetonitrile/ethyl acetate 1:1 afforded the expected bisphosphite ligand **46f** as a white solid (509 mg, 92% yield). Mp: 68–72 ºC; $[\alpha]_D^{25}$ = –597.5 (*c* 0.18, toluene); IR (neat, cm^{-1}) υ 1276, 823, 743; ^1H NMR (400 MHz, CD_2Cl_2) δ 8.14–8.07 (m, 2H), 7.96–7.87 (m, 2H), 7.44–7.34 (m, 2H), 7.26–7.11 (m, 5H), 7.10–7.03 (m, 1H), 6.94–6.83 (m, 2H), 3.91–3.78 (m, 3H), 3.40–3.30 (m, 1H), 1.58–1.04 (m, 12H), 0.46 (s, 9H), 0.45 (s, 9H); $^{13}C\{^1H,^{31}P\}$ NMR (125 MHz, CD_2Cl_2) δ 156.9, 153.2, 152.3, 137.5, 134.3, 134.2, 133.0, 132.3, 131.9, 131.4, 131.0, 128.8, 128.7, 128.7, 128.5, 126.9, 126.8, 125.1, 125.0, 123.0, 122.1, 120.2, 112.3, 68.6, 65.5, 31.3, 29.6, 29.5, 29.4, 26.2, 25.9, 0.1, 0.0; $^{31}P\{^1H\}$ NMR (202 MHz, CD_2Cl_2) δ 136.7; HRMS (ESI^+): m/z $[M+Na]^+$ calcd for $C_{80}H_{96}O_8P_2Si_4Na$ 1381.5550, found 1381.5574.

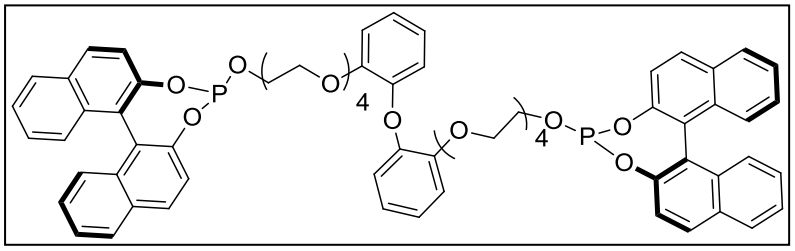

Compound 46g: Compound **46g** was synthesized following the general strategy from commercial phosphochloridite **117b** (711 mg, 1.97 mmol) with NEt_3 (547 μL, 3.93 mmol) as base and diol **113** (496 mg, 0.89 mmol). Purification by C18 column chromatography using acetonitrile afforded the expected bisphosphite ligand **46g** as a white solid (512 mg, 48% yield). Mp: 112–137 ºC; $[\alpha]_D^{25}$ = –501.8 (*c* 0.14, toluene); IR (neat, cm^{-1}) υ 2867, 1496, 1229, 1200, 936; ^1H NMR (400 MHz, CD_2Cl_2) δ 8.08–7.92 (m, 4H), 7.60–7.42 (m, 4H), 7.41–7.25 (m, 4H), 7.09–6.98 (m, 2H), 6.93–6.79 (m, 2H), 4.20–4.05 (m, 3H), 3.98–3.88 (m, 1H), 3.80–3.70 (m,

2H), 3.67–3.53 (m, 10H); $^{13}C\{^{1}H,^{31}P\}$ NMR (125 MHz, CD_2Cl_2) δ 150.0, 149.0, 148.0, 147.0, 133.2, 132.9, 132.0, 131.5, 130.8, 130.5, 128.8, 128.8, 127.1, 126.7, 126.6, 125.5, 125.3, 124.4, 124.2, 123.1, 122.2, 121.8, 119.5, 115.2, 71.1, 71.0, 70.9, 70.9, 70.0, 69.2, 64.8; $^{31}P\{^{1}H\}$ NMR (202 MHz, CD_2Cl_2) δ 146.3; HRMS (ESI^+): m/z $[M+Na]^+$ calcd for $C_{68}H_{64}O_{15}P_2Na$ 1205.3618, found 1205.3695.

Compound 46h: Compound **46h** was synthesized following the general strategy from diol **124** (297 mg, 0.65 mmol), PCl_3 (72 μL, 0.83 mmol), NEt_3 (261 μL, 1.87 mmol) and the slow addition of diol **88** (136 mg, 0.30 mmol) with NEt_3 (261 μL, 1.87 mmol) as base. Purification by C18 column chromatography using acetonitrile/ethyl acetate 1:1 afforded the expected bisphosphite ligand **46h** as a white solid (357 mg, 85% yield). Mp: 94–97 ºC; $[\alpha]_D^{25}$ = –372.1 (*c* 0.20, toluene); IR (neat, cm^{-1}) υ 2927, 2858, 1226, 756; ^{1}H NMR (400 MHz, CD_2Cl_2) δ 7.65–7.56 (m, 4H), 7.44–7.37 (m, 4H), 7.35–7.20 (m, 6H), 7.01–6.93 (m, 2H), 4.07–4.00 (m, 2H), 3.63–3.57 (m, 2H), 3.40–3.31 (m, 3H), 3.31–3.25 (m, 2H), 3.16–3.03 (m, 2H), 3.01–2.88 (m, 5H), 2.82–2.71 (m, 2H), 2.47–2.36 (m, 2H), 1.96–1.83 (m, 6H), 1.79–1.66 (m, 2H); $^{13}C\{^{1}H,^{31}P\}$ NMR (125 MHz, CD_2Cl_2) δ 156.7, 143.3, 138.7, 138.2, 138.1, 137.5, 135.2, 134.6, 132.3, 132.0, 131.8, 130.9, 130.8, 130.5, 130.1, 129.9, 129.7, 128.8, 128.5, 128.5, 127.5, 127.3, 120.8, 112.8, 70.9, 70.7, 70.6, 70.0, 68.6, 63.3, 29.6, 28.2, 28.1, 23.2, 23.1, 23.1; $^{31}P\{^{1}H\}$ NMR (202 MHz, CD_2Cl_2) δ 142.9; HRMS (ESI^+): m/z $[M+Na]^+$ calcd for $C_{88}H_{88}O_{12}P_2Na$ 1421.5649, found 1421.5670.

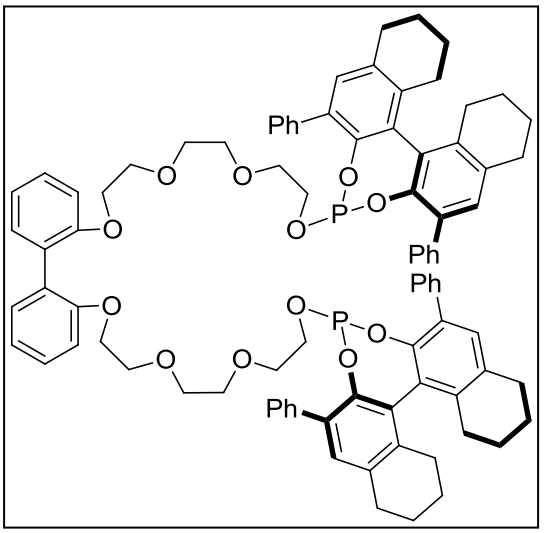

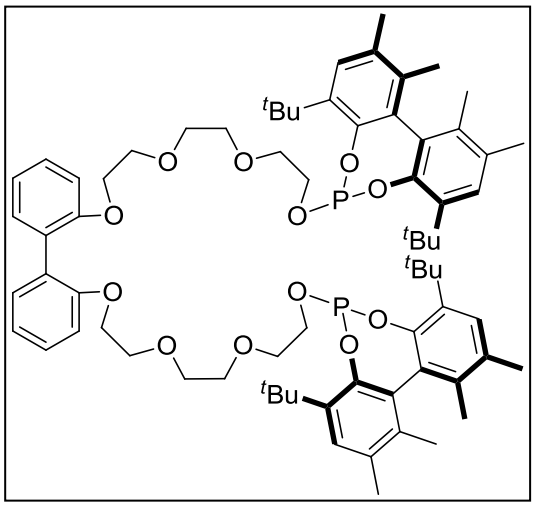

Compound 46i: Compound **46i** was synthesized following the general strategy from diol **126** (250 mg, 0.70 mmol), PCl_3 (77 μL, 0.88 mmol), NEt_3 (278 μL, 2.00 mmol) and the slow addition of diol **88** (145 mg, 0.32 mmol) with NEt_3 (278 μL, 2.00 mmol) as base. Purification by C18 column chromatography using acetonitrile/ethyl acetate 1:1 afforded the expected bisphosphite ligand **46i** as a white solid (325 mg, 83% yield). Mp: 102–122 ºC; $[\alpha]_D^{25}$ = –317.9 (*c* 0.14, toluene); IR (neat, cm^{-1}) υ 2954, 2868, 1438, 1227, 1025; ^1H NMR (400 MHz, CD_2Cl_2) δ 7.28–7.15 (m, 4H), 6.98–6.11 (m, 2H), 4.08–4.01 (m, 2H), 3.94–3.84 (m, 1H), 3.66–3.60 (m, 2H), 3.56–3.47 (m, 1H), 3.47–3.39 (m, 6H), 2.26 (s, 6H), 1.85 (s, 3H), 1.78 (s, 3H), 1.44 (s, 9H), 1.41 (s, 9H); $^{13}C\{^1H,^{31}P\}$ NMR (125 MHz, CD_2Cl_2) δ 156.7, 145.7, 145.6, 138.5, 137.4, 135.4, 134.8, 132.9, 132.2, 132.0, 132.0, 131.0, 128.8, 128.6, 128.5, 128.1, 120.8, 112.7, 71.1, 71.0, 70.9, 70.0, 68.7, 64.1, 35.0, 31.5, 31.3, 20.5, 16.8, 16.5; $^{31}P\{^1H\}$ NMR (202 MHz, CD_2Cl_2) δ 134.8; HRMS (ESI^+): m/z $[M+Na]^+$ calcd for $C_{72}H_{96}O_{12}P_2Na$ 1237.6275, found 1237.6271.

2.3.3 Measurements of binding constants by UV-vis absorption and emission spectroscopy

2.3.3.1 Measurements of binding constants by UV-vis absorption spectrophotometry

Solutions of the ligands **46** (5 x 10^{-5} – 5 x 10^{-6} M) were prepared in DCM/THF (98/2 v/v). Solutions of the corresponding BArF salts (ca. 5 x 10^{-4} M – 1 x 10^{-4} M) were also prepared in the same solvent mixture. The receptor solution was placed in a 1 cm quartz cell. The titration was carried out by adding at 298 K incremental amounts of guest (BArF salts) to the host solution (ligands **46**), which led to changes in the absorbance. The binding constants were extracted by non-linear curve fitting of the UV-vis absorption data considering a 1:1 binding model.

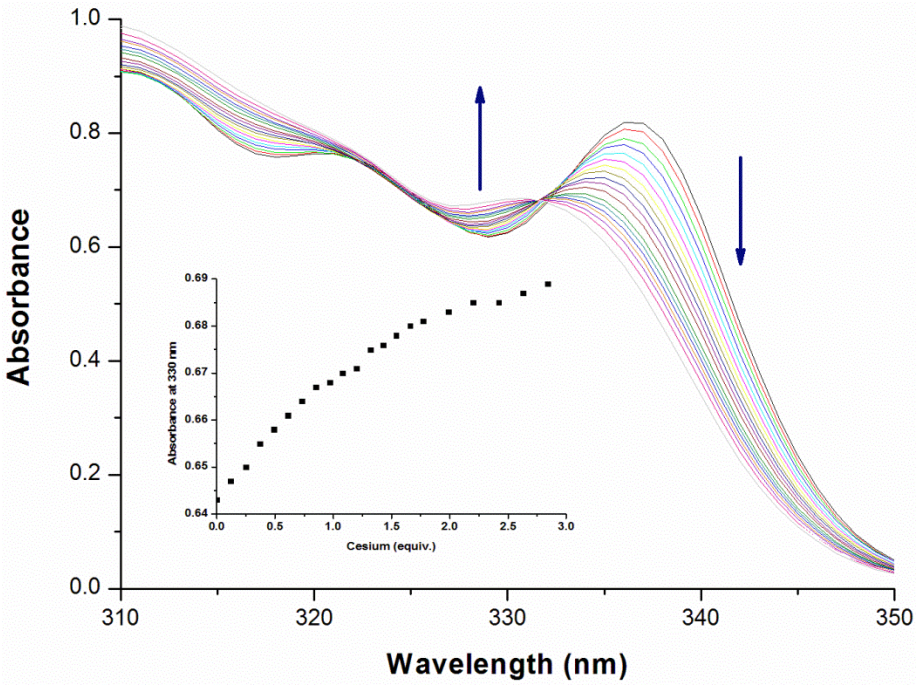

Figure 138. UV-vis titration: as a representative example see ligand **46d** (5×10^{-5} M) upon addition of Cs^+ (6.2×10^{-6} M – 1.4×10^{-4} M) in DCM/THF (98/2 v/v) at 298 K

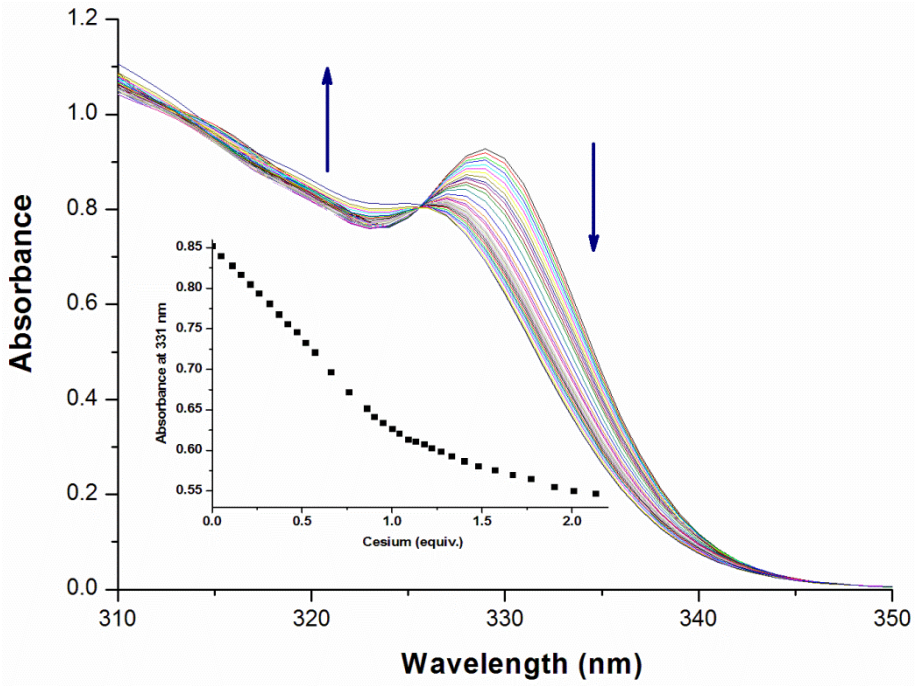

Figure 139. UV-vis titration: as a representative example see ligand **46e** (5×10^{-5} M) upon addition of Cs^+ (2.7×10^{-6} M – 1.1×10^{-4} M) in Toluene/THF (98/2 v/v) at 298 K

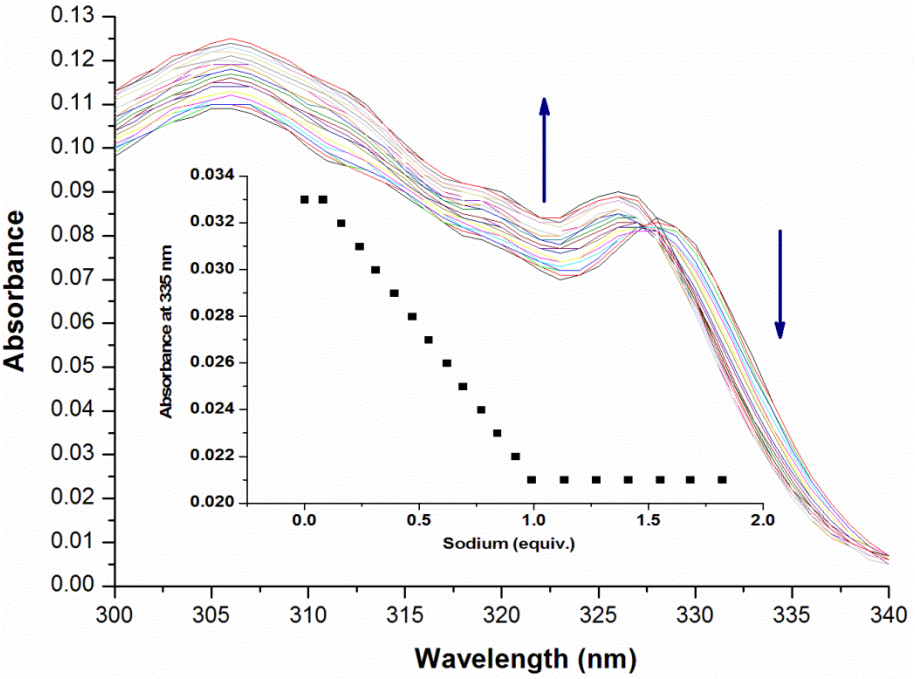

Figure 140. UV-vis titration: as a representative example see ligand **46e** (5 x 10^{-6} M) upon addition of Na^+ (4.0 x 10^{-7} M – 9.1 x 10^{-6} M) in DCM/THF (98/2 v/v) at 298 K

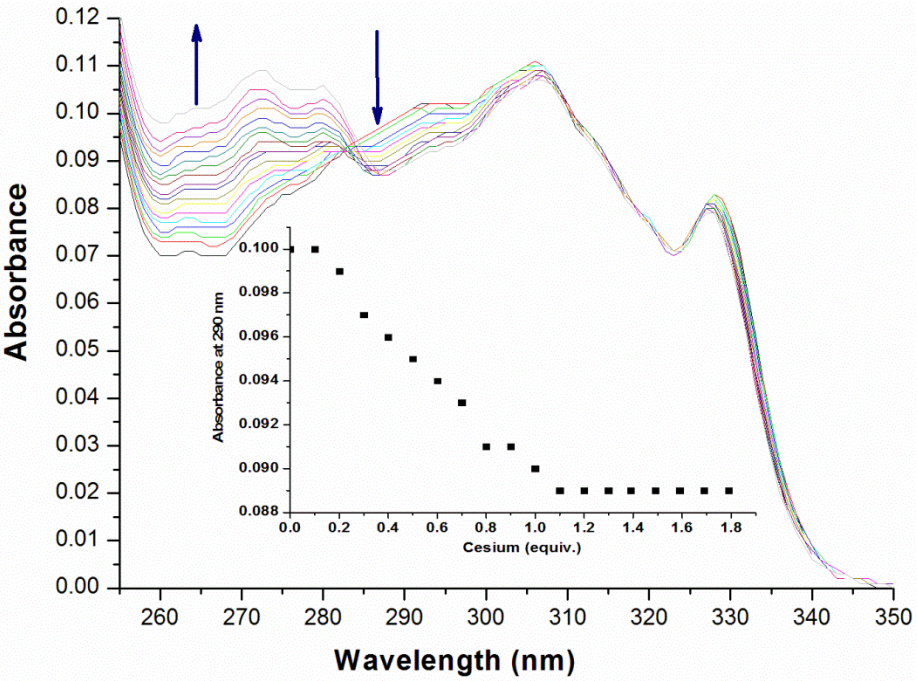

Figure 141. UV-vis titration: as a representative example see ligand **46b** (5 x 10^{-6} M) upon addition of Cs^+ (5.0 x 10^{-7} M – 8.4 x 10^{-6} M) in DCM/THF (98/2 v/v) at 298 K

2.3.3.2 Measurements of binding constants by emission spectrophotometry

Stock solutions of ligand **46** (10^{-5} M) were prepared in Toluene/THF (98/2 v/v). Solutions of CsBArF (10^{-4} M) were also prepared in the same solvent mixture. The receptor solution was placed in a 1 cm quartz cell. The titration was carried out adding at 298 K incremental amounts of CsBArF to the host solution (**46**) leading to changes in the emission spectra. Binding constants were extracted by non-linear curve fitting of the emission data considering a 1:1 binding model.

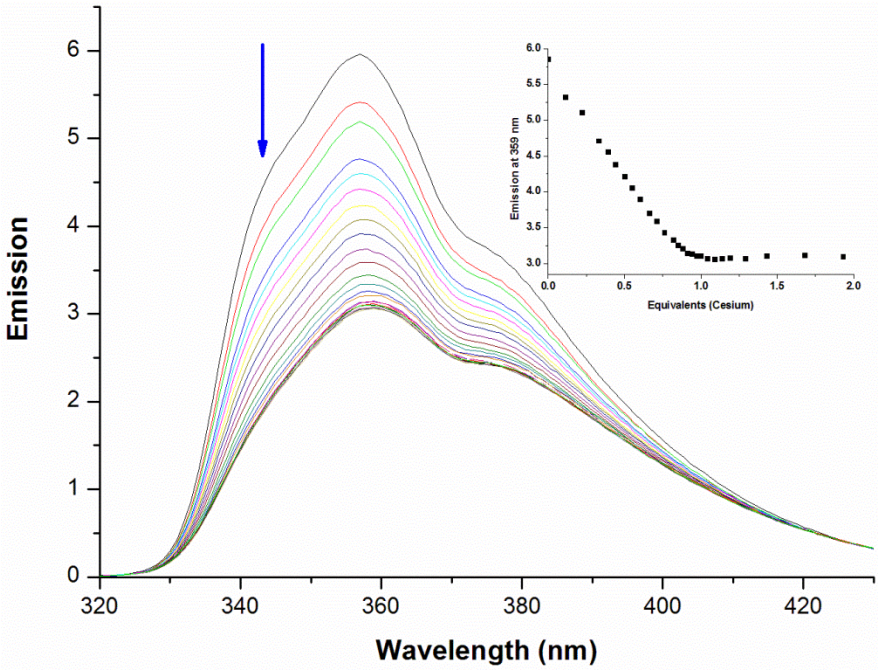

Figure 142. Fluorescence titration: as a representative example see ligand **46e** (4.7 x 10^{-5} M) upon addition of Cs^+ (5.2 x 10^{-6} M – 9.0 x 10^{-5} M) in toluene/THF (98/2 v/v) at 298 K

2.3.4 Measurements of binding constants by ITC

A solution of ligand **46** (1 x 10^{-3} M) in DCM was added in the cell of an isothermal calorimeter. Known volumes of a solution of ammonium salts **94** in DCM (7 x 10^{-3} M) were syringed into the host solution and the evolved heat measured. After the reference titration was substrated, the association constants and the thermodynamics parameters were obtained from the fit of the revised titration data to a theoretical titration curve using the one set of sites model of the MicroCal ITC Data Analysis module provided by MicroCal, LLC.

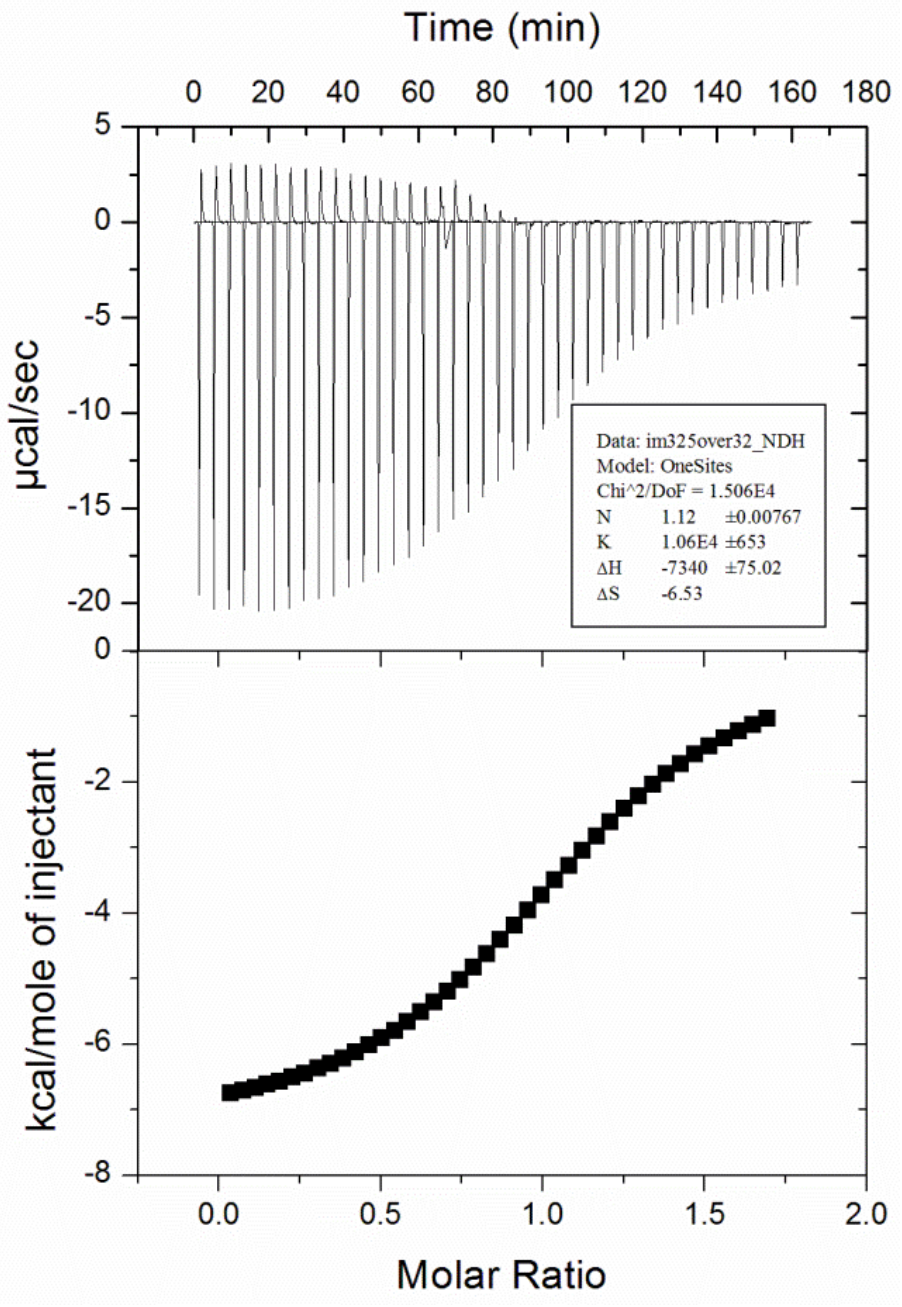

Figure 143. ITC titration data of **46e** and (*S*,*S*)-**94** in DCM at 298K

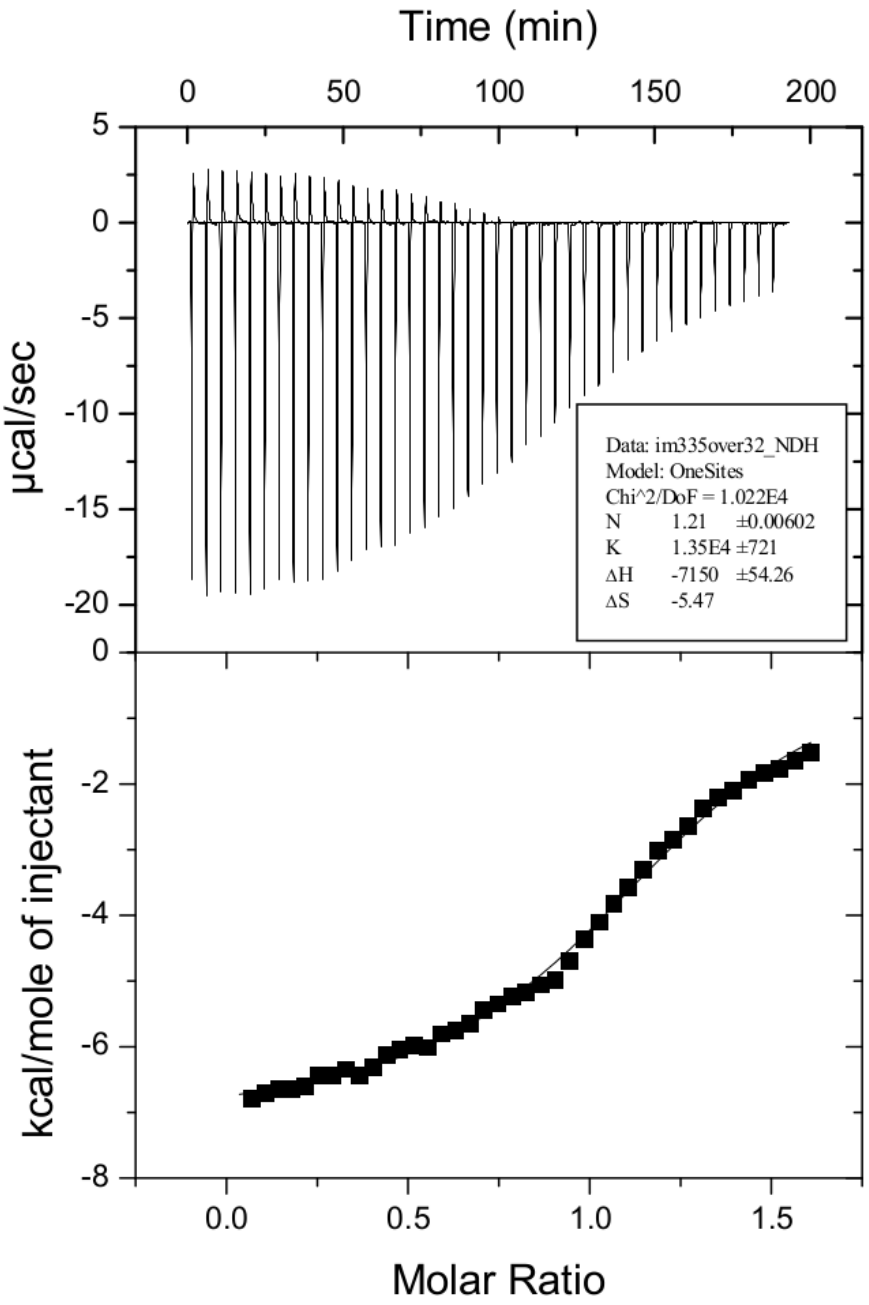

Figure 144. ITC titration data of **46e** and (*R*,*R*)-**94** in DCM at 298K

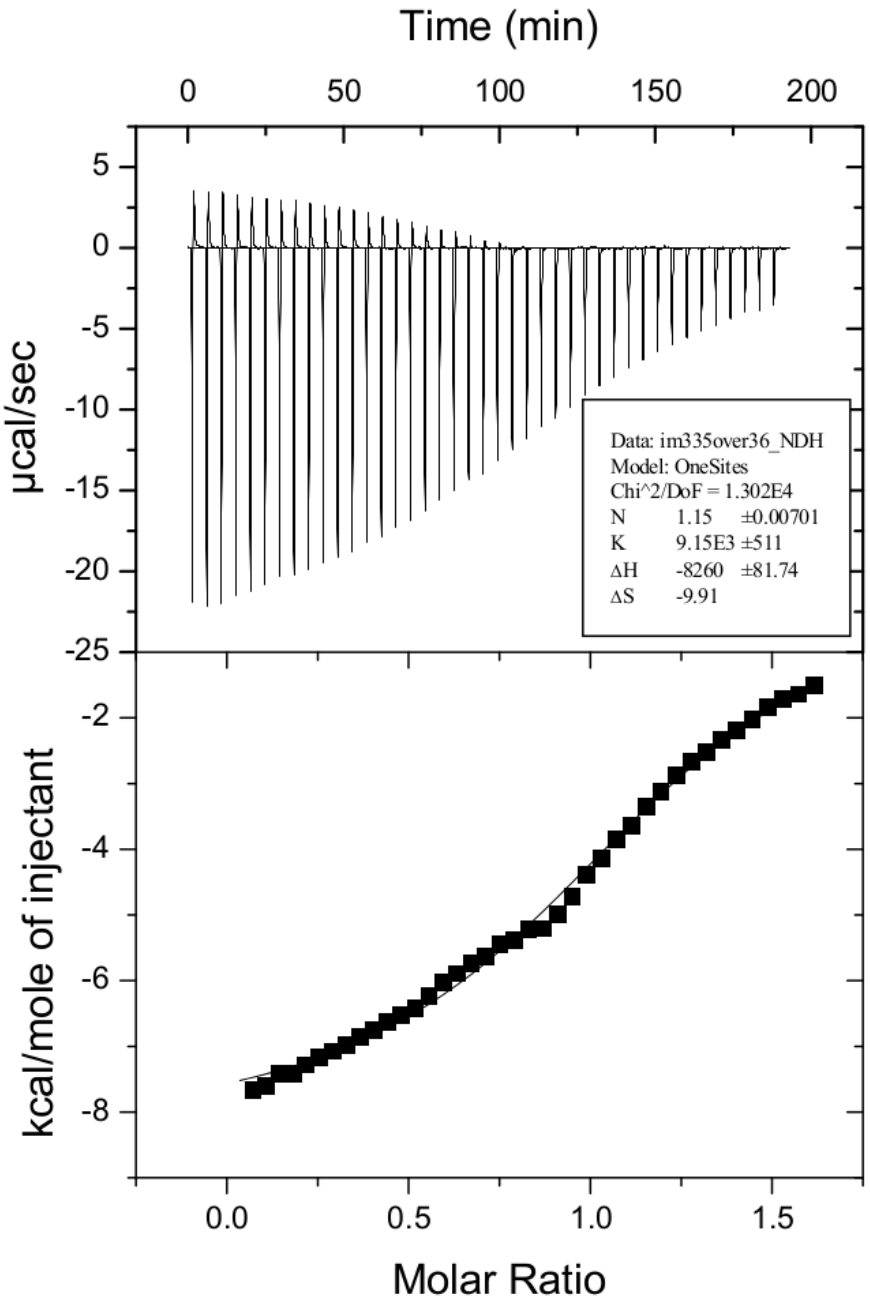

Figure 145. ITC titration data of **46d** and (*R*,*R*)-**94** in DCM at 298K

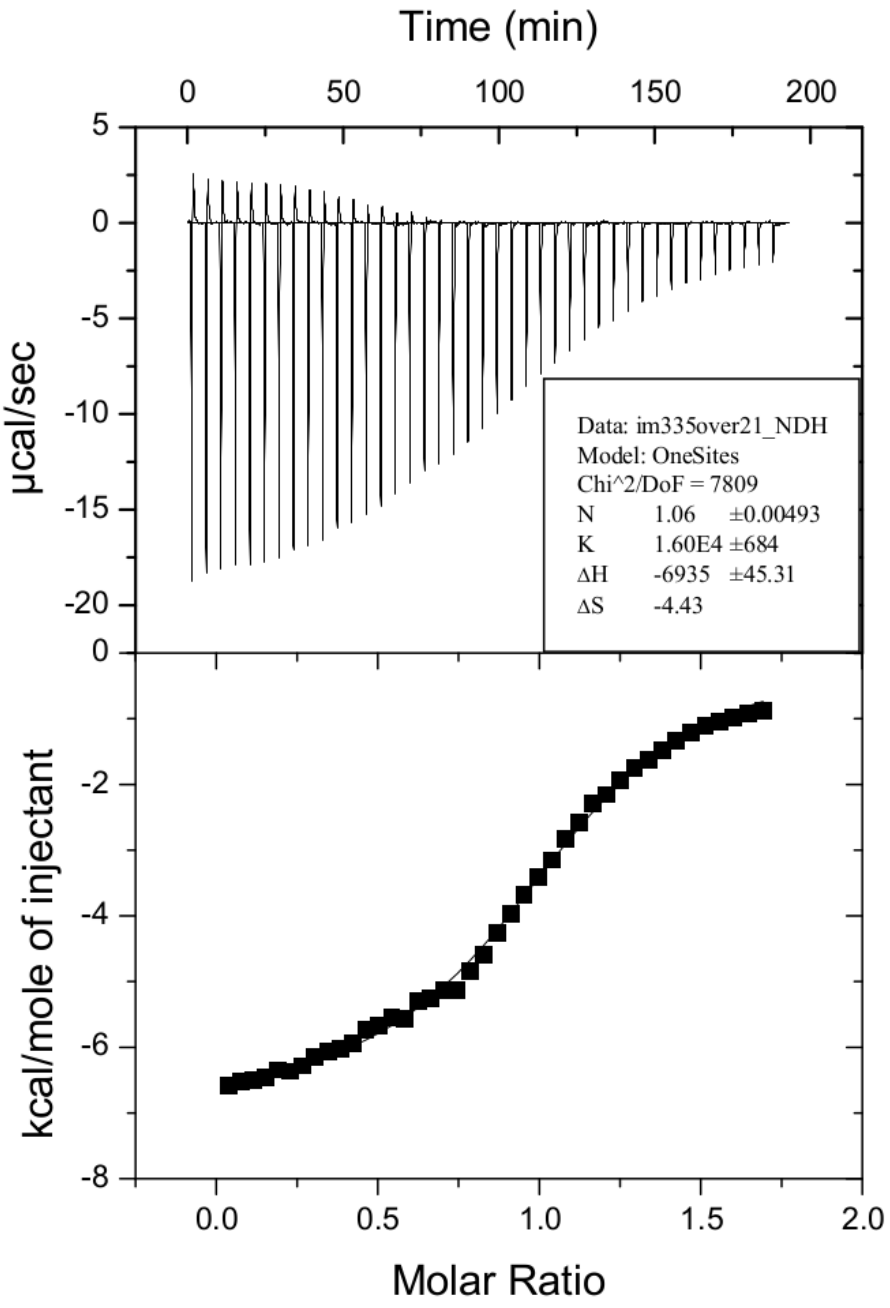

Figure 146. ITC titration data of **46b** and (*R*,*R*)-**94** in DCM at 298K

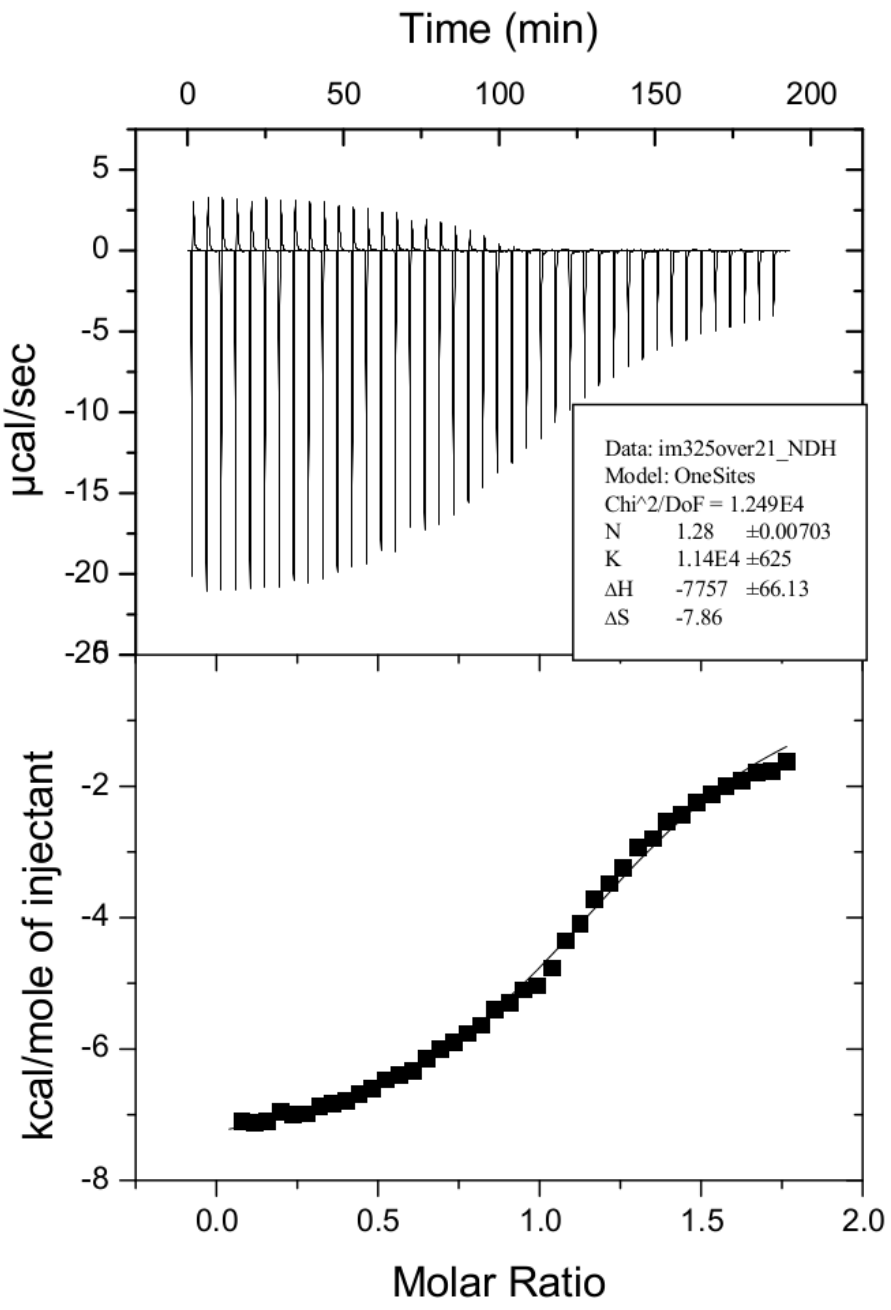

Figure 147. ITC titration data of **46b** and (*S*,*S*)-**94** in DCM at 298K

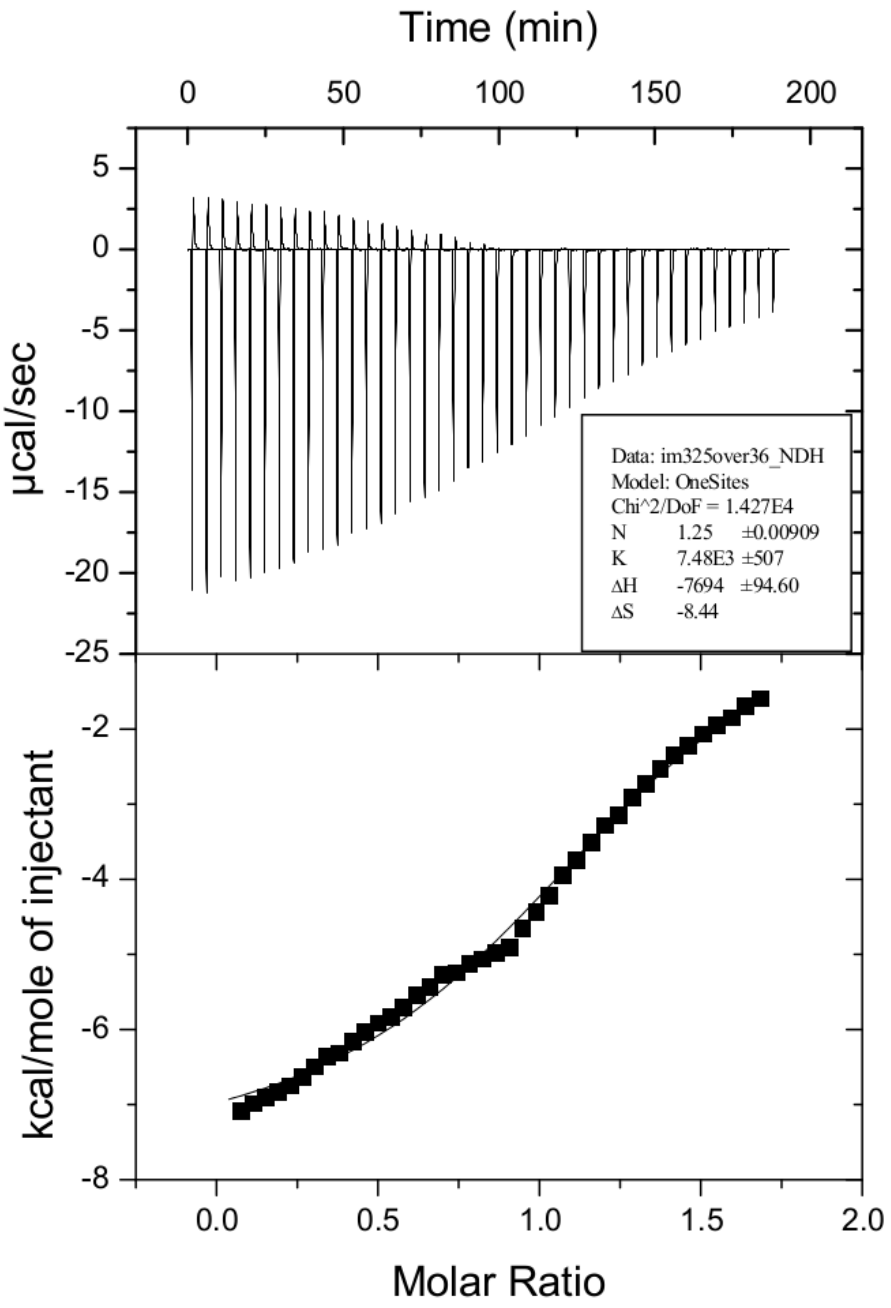

Figure 148. ITC titration data of **46d** and (*S*,*S*)-**94** in DCM at 298K

2.3.5 NMR Titrations & measurement of binding constants

Solutions of the ligands **46** (*ca.* 10^{-2} M) were prepared in toluene-d_8/THF-d_8 (95/5 v/v). Solutions of BArF salts (*ca.* 10^{-1} M) were prepared in the same solvent mixture. The host solution (0.5 mL) was placed in a NMR tube. The titration was carried out adding at 298 K incremental amounts of guest (BArF salt) to the host solution (**46**), which led to changes in the chemical shift and signal width in the NMR spectra. Binding constants were extracted by non-linear curve fitting of the

^{31}P NMR and/or ^{1}H NMR chemical shift values, considering a 1:1 binding model in the fast exchange-limit. Blue line represents the percentage of formed complex and the green line represents the percentage of remaining free ligand (host) relative to the initial ligand concentration during the titration.

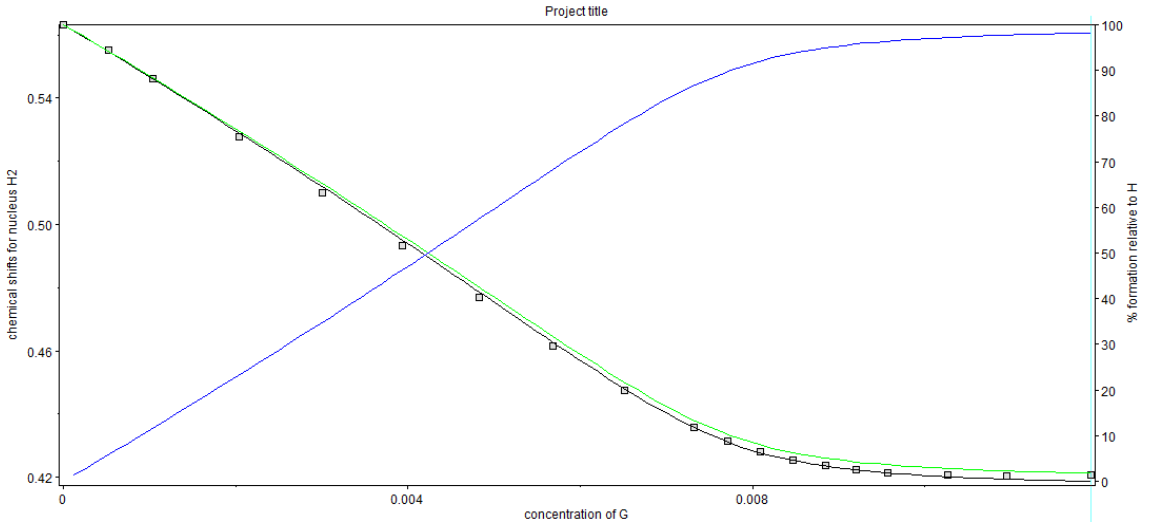

Figure 149. Changes in the ^{1}H NMR of Me_3Si- signal spectra (400 MHz, toluene-d_8/THF-d_8 (95/5 v/v)) acquired at 298 K during the titration of **46d** with Cs^+ ([**46d**] = 9 x 10^{-3} M)

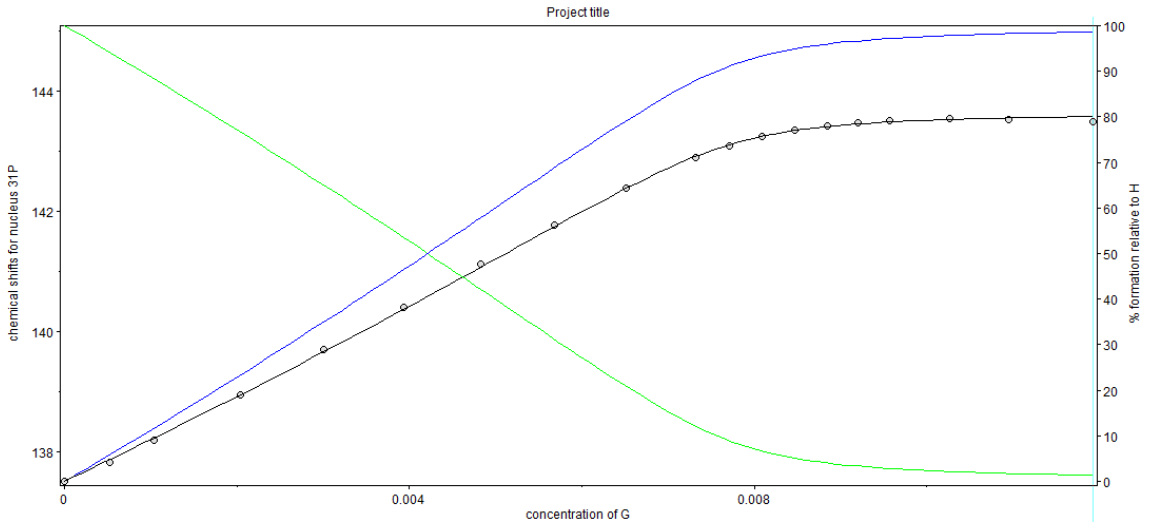

Figure 150. Changes in the ^{31}P{^{1}H} NMR (162 MHz, toluene-d_8/THF-d_8 (95/5 v/v)) spectra acquired at 298 K during the titration of **46d** with Cs^+ ([**46d**] = 9 x 10^{-3} M)

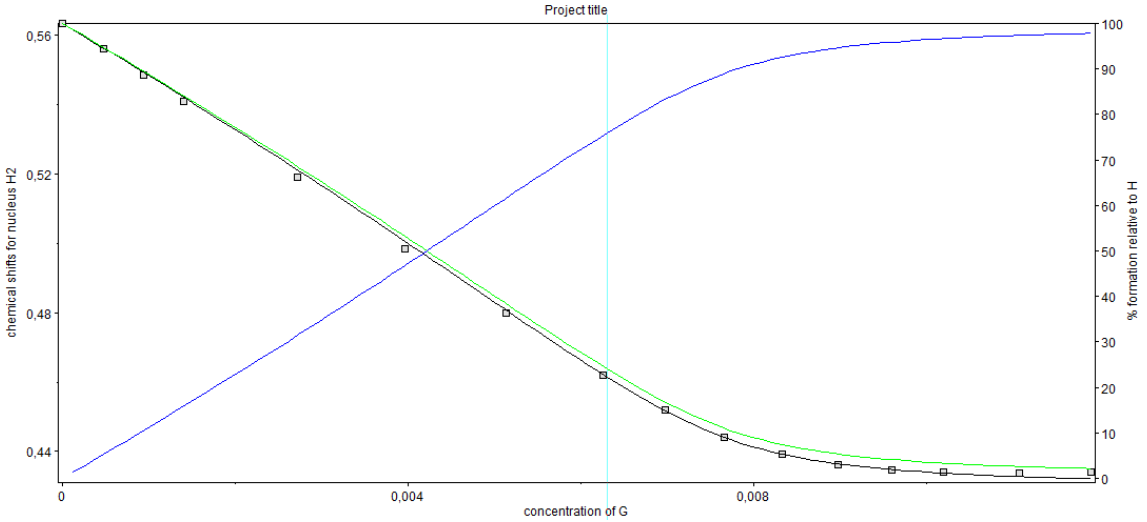

Figure 151. Changes in the ^{1}H NMR of Me_3Si- signal spectra (400 MHz, toluene-d_8/THF-d_8 (95/5 v/v)) acquired at 298 K during the titration of **46d** with Rb^+ ([**46d**] = 9 x 10^{-3} M)

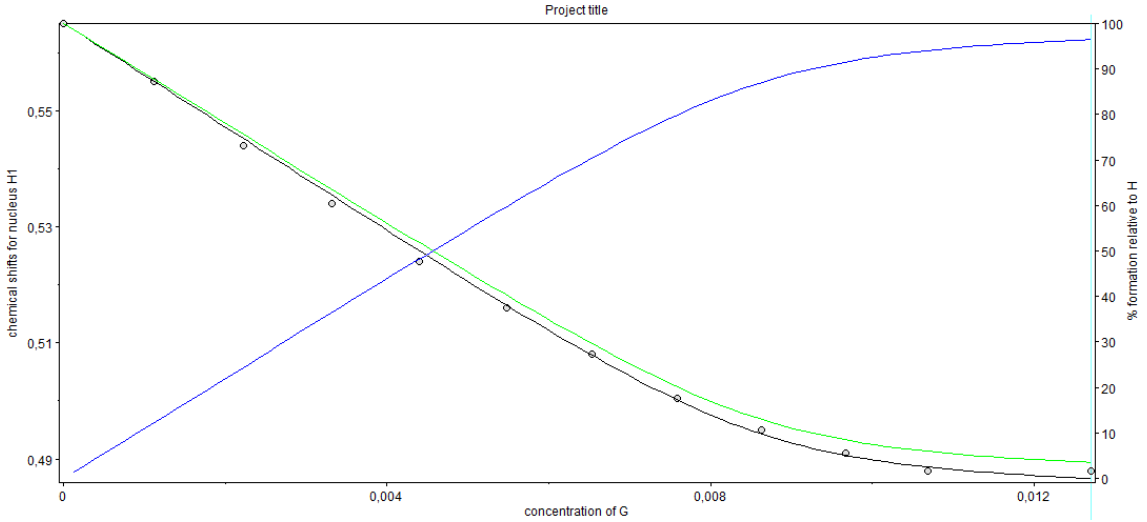

Figure 152. Changes in the ^{1}H NMR of Me_3Si- signal spectra (400 MHz, toluene-d_8/THF-d_8 (95/5 v/v)) acquired at 298 K during the titration of **46d** with Na^+ ([**46d**] = 9 x 10^{-3} M)

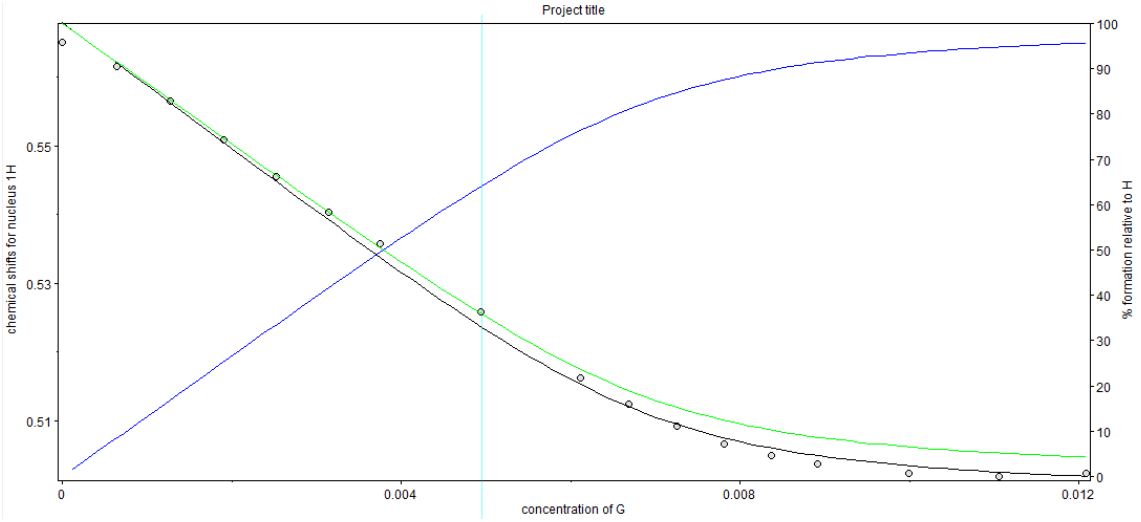

Figure 153. Changes in the ^{1}H NMR spectra of Me_3Si- signal (400 MHz, toluene-d_8/THF-d_8 (95/5 v/v)) acquired at 298 K during the titration of **46a** with Na^+ ([**46a**] = 7 x 10^{-3} M)

2.3.6 Stoichiometry determination: Job plots

Stock solutions of the same concentration of **46** and BArF salts were prepared in toluene-d_8/THF-d_8 (80:20 v/v) for NMR experiments (*ca.* 6 x 10^{-3} M) or dichloromethane/THF (80:20 v/v) for UV-vis stoichiometry determination (5 x 10^{-5} M). ^{1}H NMR or UV-vis spectra with different host-guest ratios at constant overall concentration were recorded.

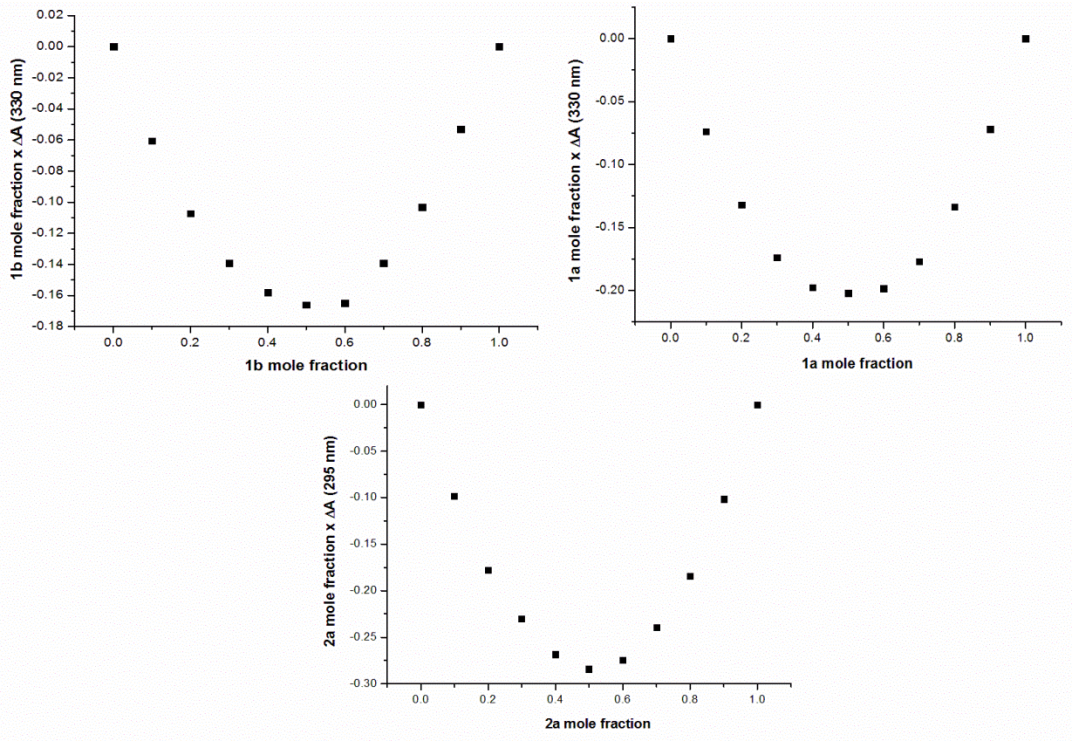

Figure 154. UV-vis Job plots for **46d** upon addition of Cs^+ (top left), **46e** upon addition of Cs^+ (top right) and **46b** upon addition of Na^+ (bottom) in DCM/THF (80/20 v/v) at 298 K

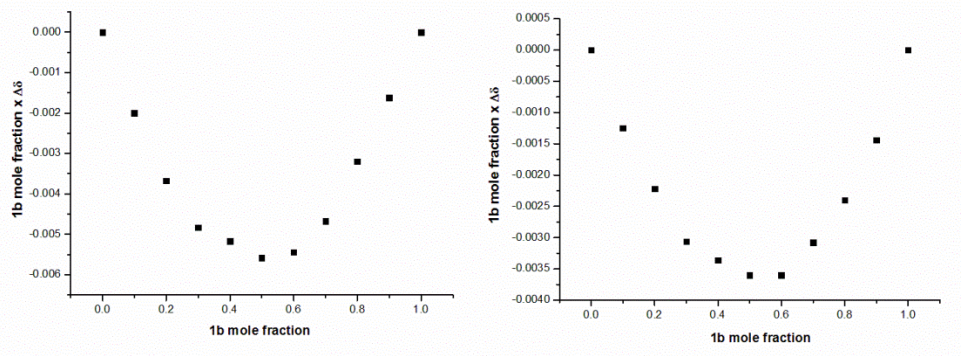

Figure 155. ^1H NMR Job plots for **46d** upon addition of: Rb^+ (left), and Na^+ (right) in toluene-d_8/THF-d_8 (80/20 v/v) at 298 K

2.3.7 Synthesis of substrates for asymmetric hydrogenation

Substrates **39e**,**f**,**h**[217] are already known compounds and were prepared by following Burk's two step methodology for α-aryl enamides synthesis.[218] **39g**[219] and **39d**[220] were prepared following a previously reported procedure. Spectroscopic data were in agreement with the reported ones.

2.3.8 General procedure for the Rh-mediated asymmetric hydrogenation

In a glovebox filled with nitrogen, to a 2 mL vial equipped with a magnetic bar and the substrate (*ca* 15 mg, 1 equiv.) was added $[Rh(cod)_2]BArF$ (0.01 equiv. in dichloromethane). To this solution, ligand **46** (0.012 equiv.) and BArF salt (0.0156 equiv.) were added from a previously stirred for 10 minutes solution. Additional dichloromethane was charged to provide the desired final concentration of substrate (0.2 M). The vial was transferred into an autoclave and taken out of the glovebox. The autoclave was purged three times with H_2 at a pressure not higher than 20 bar and, finally, the autoclave was pressurized with H_2 to the desired pressure. The reaction mixture was stirred at room temperature for 18 h. The pressure was carefully released in a well-ventilated hood. The conversion was determined by ^1H NMR and enantiomeric excesses were determined by GC or HPLC analysis using chiral stationary phases.

2.3.9 General procedure for the Rh-mediated asymmetric hydroformylation

In a glove box filled with nitrogen, to a 2 mL vial equipped with a magnetic bar was added ligand **46** (2.7 μmol in 360 μL of toluene), BArF salt (3.6 μmol in 27 μL of THF), and $[Rh(\kappa^2O,O'\text{–acac})(CO)_2]$ (2.3 μmol in 65 μL of toluene). Substrate (230 μmol), dodecane (69 μmol), and additional toluene were charged to provide the desired final solution of toluene/THF (97/3 v/v). The vial was transferred into an autoclave and taken out of the glove box. The autoclave was

[217] a) For a full characterization of **39e**, see: Gridnev, I. D.; Yasutake, M.; Higashi, N.; Imamoto, T. *J. Am. Chem. Soc.* **2001**, *123*, 5268. b) For a full characterization of **39f**, see: Liu, Z.; Xu, D.; Tang, W.; Xu, L.; Mo, J.; Xiao, J. *Tetrahedron Lett.* **2008**, *49*, 2756. c) For a full characterization of **39h**, see: Guan, Z.-H.; Zhang, Z.-Y.; Ren, Z.-H.; Wang, Y.-Y.; Zhang, X. *J. Org. Chem.* **2011**, *76*, 339.
[218] Burk, M. J.; Casy, G.; Johnson, N. B. *J. Org. Chem.* **1998**, *63*, 6084.
[219] Hoen, R.; Tiemersma-Wegman, T.; Procuranti, B.; Lefort, L.; de Vries, J. G.; Minnaard, A. J.; Feringa, B. L. *Org. Biomol. Chem.* **2007**, *5*, 267.
[220] Lee, J.; Bernard, S.; Liu, X.-C. *React. Funct. Polym.* **2009**, *69*, 650.

purged three times with syngas (1:1 H_2/CO at a pressure not higher than 10 bar) and finally, the autoclave was pressurized with syngas to the desired pressure. The reaction mixture was stirred at 40 °C (oil bath) for 5 or 18 h. The reaction was cooled and the pressure was carefully released in a well-ventilated hood. The enantiomeric excesses for the hydroformylation products of **6** were determined by GC with a Supelco Beta Dex™ 225 or 120 chiral column or HPLC analysis with a chiral column from the crude reaction mixture. Conversion and branched-to-linear product ratio for the hydroformylation products of **6** were determined by GC analysis with a Supelco Beta Dex™ 225 or 120 chiral column by using dodecane as internal standard. Conversion and branch/linear ratio for the hydroformylation product of **6d** were determined by ^{1}H NMR analysis from the crude reaction mixture.

2.3.10 Characterization of hydrogenated and hydroformylated products: 7 and 44

Hydrogenated products: **44a**[221], **44b**[222], **44e**[221], **44f**[223], **44h**[224], **44g**[225] and **44d**[222] have previously been studied. Spectroscopic data were in agreement with the reported ones.

Hydroformylated products **7**[226] are all known compounds previously described in the literature. Spectroscopic data were in agreement with the reported ones.

2.3.11 Determination of enantiomeric excess and absolute configuration of hydroformylated and hydrogenated products

The absolute configuration of the products was assigned by elution order of the enantiomers in the analysis conditions reported below.

[221] Yu, L.; Wang, Z.; Wu, J.; Tu, S.; Ding, K. *Angew. Chem., Int. Ed.* **2010**, *49*, 3627.
[222] Burk, M. J.; Feaster, J. E.; Nugent, W. A.; Harlow, R. L. *J. Am. Chem. Soc.* **1993**, *115*, 10125.
[223] Li, G.; Antilla, J. C. *Org. Lett.* **2009**, *11*, 1075.
[224] Burk, M. J.; Wang, Y. M.; Lee, J. R. *J. Am. Chem. Soc.* **1996**, *118*, 5142.
[225] Guo, Y.; Shao, G.; Li, L.; Wu, W.; Li, R.; Li, J.; Song, J.; Qiu, L.; Prashad, M.; Kwong, F. Y. *Adv. Synth. Catal.* **2010**, *352*, 1539.
[226] See the corresponding references cited in the analytical conditions for enantiomeric excess determination of each product.

GC analysis conditions for the asymmetric hydrogenation products of 39a.[227] GC analysis, Supelco Beta DEX™ 225 (30 m x 0.25 mm x 0.25 mm), isothermal 70 ºC, 15 psi He, $t_R(S)$ = 48.3 min, $t_R(R)$ = 53.2 min.

GC analysis conditions for the asymmetric hydrogenation products of 39b.[227] GC analysis, Supelco Beta DEX™ 120 (30 m x 0.25 mm x 0.25 mm), isothermal 90 ºC, 15 psi He, $t_R(S)$ = 59.5 min, $t_R(R)$ = 60.5 min.

HPLC analysis conditions for the asymmetric hydrogenation products of 39d.[227] Daicel Chiralcel® OJ-H (25 cm x 0.46 cm), 93/7 hexane/2-propanol, 1.0 mL/min, 216 nm, $t_R(R)$ = 19.4 min, $t_R(S)$ = 30.1 min.

HPLC analysis conditions for the asymmetric hydrogenation products of 39e.[227] HPLC analysis, Daicel Chiralcel® AD-H (25 cm x 0.46 cm), 95/5 hexane/2-propanol, 1.0 mL/min, 216 nm, $t_R(R)$ = 11.2 min, $t_R(S)$ = 14.2 min.

GC analysis conditions for the asymmetric hydrogenation products of 39f.[228] GC analysis, Supelco Beta DEX™ 120 (30 m x 0.25 mm x 0.25 mm), isothermal 170 ºC, 15 psi He, $t_R(S)$ = 147.8 min, $t_R(R)$ = 148.8 min.

HPLC analysis conditions for the asymmetric hydrogenation products of 39g.[229] HPLC analysis, Daicel Chiralcel® OD-H (25 cm x 0.46 cm), 93/7 hexane/2-propanol, 0.5 mL/min, 216 nm, $t_R(R)$ = 40.6 min, $t_R(S)$ = 44.6 min.

HPLC analysis conditions for the asymmetric hydrogenation products of 39h.[220] HPLC analysis, Daicel Chiralcel® AD-H (25 cm x 0.46 cm), 95/5 hexane/2-propanol, 1.0 mL/min, 216 nm, $t_R(R)$ = 15.2 min, $t_R(S)$ = 22.9 min.

GC analysis conditions for the asymmetric hydroformylation products of 6a:[230] Enantiomeric excess was determined by GC analysis with a Supelco Beta Dex™ 225 column (30 m x 0.25 mm x 0.25 μm). Flow rate: 1 mL/min. Temperature program: 100 °C for 5 min, then 4 ºC/min to 160 ºC.

[227] Etayo, P.; Núñez-Rico, J. L.; Vidal-Ferran, A. *Organometallics* **2011**, *30*, 6718.
[228] Etayo, P.; Núñez-Rico, J. L.; Fernández-Pérez, H.; Vidal-Ferran, A. *Chem. Eur. J.* **2011**, *17*, 13978.
[229] The absolute configuration was assigned by comparison of the specific optical rotation obtained for this product: $[\alpha]_D^{25}$ –12.0 (94% *ee*, c 2.0, $CHCl_3$) with the reported value: $[\alpha]_D^{20}$ (*R*) +14.7 (99% *ee*, c 2.0, $CHCl_3$).[225]

Retention times: 4.3 min for **6a**, 12.0 (*R*) and 12.2 (*S*) min for the enantiomers of **7a** (branched regioisomer), 15.7 min for **8a** (linear regioisomer).

GC analysis conditions for the asymmetric hydroformylation products of 6b:[230] Enantiomeric excess was determined by GC analysis with a Supelco Beta Dex^{TM} 225 column (30 m x 0.25 mm x 0.25 μm). Flow rate: 1 mL/min. Temperature program: 100 °C for 5 min, then 4 ºC/min to 160 ºC. Retention times: 2.2 min for **6b**, 6.5 (*R*) and 8.0 (*S*) min for the enantiomers of **7b** (branched regioisomer), 11.4 min for **8b** (linear regioisomer).

GC analysis conditions for the asymmetric hydroformylation products of 6c:[231] Branched-to-linear ratio and conversion was determined by GC analysis with a Supelco Beta Dex^{TM} 120 column (30 m x 0.25 mm x 0.25 μm). Flow rate: 1 mL/min. Temperature program: 80 °C for 5 min, then 10 ºC/min to 130 ºC. Retention times: 3.7 min for **6c**, 12.5 min for dodecane, 11.7 min for **7c** (branched regioisomer), 13.6 min for **8c** (linear regioisomer). The enantiomeric excess of the product **7c** was determined by GC analysis of its methyl ester[232] on a Supelco Beta Dex^{TM} 120 column (30 m x 0.25 mm x 0.25 μm). Flow rate: 1 mL/min. Temperature program: 80 ºC for 0 min, then 1 ºC/min to 100 ºC, 100 ºC for 8 min, then 4 ºC/min to 130 ºC. Retention times: 26.3 min for (*S*)-**7c** and 26.6 min for (*R*)-**7c**.

GC analysis conditions for the asymmetric hydroformylation products of 6d:[233] Enantiomeric excess was determined by GC analysis with a Supelco Beta Dex^{TM} 225 column (30 m x 0.25 mm x 0.25 μm). Flow rate: 1 mL/min. Temperature program: isothermal 70 °C. Retention times: 16.9 (*R*) and 17.4 (*S*) min for the enantiomers of **7d** (branched regioisomer).

GC analysis conditions for the asymmetric hydroformylation products of 6e:[234] Enantiomeric excess was determined by GC analysis with a

[230] a) Cobley, C. J.; Klosin, J.; Qin, C.; Whiteker, G. T. *Org. Lett.* **2004**, *6*, 3277. b) Cobley, C. J.; Klosin, J.; Qin, C.; Whiteker, G. T. *Org. Lett.* **2005**, *7*, 1197.
[231] Zhao, B.; Peng, X.; Wang, Z.; Xia, C.; Ding, K. *Chem. Eur. J.* **2008**, *14*, 7847.
[232] The methyl ester was obtained by oxidation with Jones reagent to give initially carboxylic acids, followed by esterification using $CH_2N_2 \cdot Et_2O$ solution.
[233] McDonald, R. I.; Wong, G. W.; Neupane, R. P.; Stahl, S. S.; Landis, C. R. *J. Am. Chem. Soc.* **2010**, *132*, 14027.
[234] Zhang, X.; Cao, B.; Yan, Y.; Yu, S.; Ji, B.; Zhang, X. *Chem. Eur. J.* **2010**, *16*, 871.

Supelco Beta Dex™ 225 column (30 m x 0.25 mm x 0.25 μm). Flow rate: 1 mL/min. Temperature program: isothermal 100 ºC. Retention times: 2.5 min for **6e**, 7.9 (*R*) and 8.8 (*S*) min for the enantiomers of **7e** (branched regioisomer), 19.6 min for **8e** (linear regioisomer).

GC analysis conditions for the asymmetric hydroformylation products of 6f:[234] Enantiomeric excess was determined by GC analysis with a Supelco Beta Dex™ 225 column (30 m x 0.25 mm x 0.25 μm). Flow rate: 1 mL/min. Temperature program: isothermal 135 ºC. Retention times: 5.7 min for **6f**, 20.7 (*S*) and 22.8 (*R*) min for the enantiomers of the **7f** (branched regioisomer), 47.7 min for **8f** (linear regioisomer).

GC analysis conditions for the asymmetric hydroformylation products of 6g:[233] Enantiomeric excess was determined by GC analysis with a Supelco Beta Dex™ 225 column (30 m x 0.25 mm x 0.25 μm). Flow rate: 1 mL/min. Temperature program: 100 °C for 5 min, then 1.5 ºC/min to 160 ºC. Retention times: 35.9 (*R*) and 39.4 (*S*) min for the enantiomers of **7g** (branched regioisomer).

HPLC analysis conditions for the asymmetric hydroformylation products of 6h:[233] Enantiomeric excess was determined by HPLC analysis with a Daicel Chiralcel® OJ-H (25 cm x 0.46 cm), 97/3 hexane/2-propanol, 0.5 mL/min, 220 nm, t_R(*R*) = 30.3 min, t_R(*S*) = 32.3 min.

GC analysis conditions for the asymmetric hydroformylation products of 6i: Enantiomeric excess was determined by GC analysis with a Supelco Beta Dex™ 225 column (30 m x 0.25 mm x 0.25 μm). Flow rate: 1 mL/min. Temperature program: 100 ºC for 5 min, then 4 ºC/min to 160 ºC, then 4 ºC/min to 132 ºC. Retention times: 27.1 (1) and 27.9 (2) min for the enantiomers of **7i** (branched regioisomer).

GC analysis conditions for the asymmetric hydroformylation products of 6j:[233] Enantiomeric excess was determined by GC analysis with a Supelco Beta Dex™ 225 column (30 m x 0.25 mm x 0.25 μm). Flow rate: 1 mL/min. Temperature program: isothermal 100 °C. Retention times: 11.3 (*R*) and 11.5 (*S*) min for the enantiomers of **7j** (branched regioisomer).

GC analysis conditions for the asymmetric hydroformylation products of 6k:[233] Enantiomeric excess was determined by GC analysis with a Supelco Beta Dex™ 225 column (30 m x 0.25 mm x 0.25 μm). Flow rate: 1 mL/min. Temperature program: isothermal 65 °C. Retention times: 60.8 (*R*) and 62.4 (*S*) min for the enantiomers of **7k** (branched regioisomer).

GC analysis conditions for the asymmetric hydroformylation products of 6l:[235] Enantiomeric excess was determined by GC analysis with a Supelco Beta Dex™ 225 column (30 m x 0.25 mm x 0.25 μm). Flow rate: 1 mL/min. Temperature program: 90 ºC, then 1 ºC/min to 108 ºC, then 4 ºC/min to 132 ºC. Retention times: 15.9 (1) and 16.4 (2) min for the enantiomers of **7l** (branched regioisomer).

HPLC analysis conditions for the asymmetric hydroformylation products of 6m:[235] Enantiomeric excess was determined by HPLC analysis of its methyl ester[232] with a Daicel Chiralcel® OD-H column (25 cm x 0.46 cm), 90/10 hexane/2-propanol, 0.5 mL/min, 254 nm, t_R(*R*) = 19.6 min, t_R(*S*) = 21.9 min.

[235] Zhang, X.; Cao, B.; Yu, S.; Zhang, X. *Angew. Chem., Int. Ed.* **2010**, *49*, 4047.

CONCLUSIONS

CONCLUSIONS

- An efficient synthesis of an array of enantiomerically pure conformationally stable bisphosphine ligands has been described. The design of these ligands included a crown ether unit of variable size and morphology for distal regulation *via* ion-dipole supramolecular interactions, and a stereogenic biaryl unit containing two phosphino binding groups for enantioselective organometallic catalysis after coordination to a transition metal center. Changes in the biaryl dihedral angle were considered to be the linking mechanism capable of communicating the regulation and catalytic sites.

- The immediate precursors of these bisphosphine ligands (*i.e.* bisphosphine dioxide derivatives) proved to have a high affinity for cationic species (*K* around 10^5 M^{-1}) according to binding studies carried out with different techniques such as fluorescence or calorimetry. The latter method also allowed the determination of the thermodynamic parameters of the binding process and the stoichiometry of the formed complexes, which was found to be 1:1 between the bisphosphine dioxide derivative and the studied cationic species (*i.e.* barium salts).

- The above-mentioned bisphosphine ligands were shown to be active in the rhodium-mediated asymmetric hydrogenation of different functionalized alkenes. However, the results, in terms of enantioselectivity, were modest. Furthermore, the addition of different cationic species did not provoke any important improvement in the enantioselectivity of the reaction. It is suggested that for future ligand design with a distal regulation site substituents at the 3 and 3’ positions of the biphenyl unit are included to raise the enantioselectivity of the process by sterically restricting the movement of the P-substituents.

- The design and synthesis of enantiomerically pure bisphosphite ligands from simple achiral diols and an array of structurally diverse enantiopure phosphochloridites *via* *O*-phosphorylation were described. These ligands combine a polyoxyethylene skeleton and two enantiomerically pure conformationally stable phosphite units. The ability of these ligands to act as podands towards cationic species was tested by performing binding studies

between them and different salts (alkali metal and ammonium salts). Different techniques were used, including UV-vis, fluorescence, NMR and ITC (isothermal calorimetry) in the case of ammonium-type species. High binding constants were obtained in all cases. For example, chiral secondary ammonium type cations bound bisphosphite ligands with *K*-values as high as *ca.* 10^4 M^{-1} according to calorimetric titrations (a 1:1 stoichiometry for the resulting complexes was revealed from these ITC studies). Association constants determined for the alkali metal salts studied (NaBArF, KBArF, RbBArF and CsBArF) ranged from 5 x 10^3 to > 5 x 10^6 M^{-1} and 1:1 complex stoichiometries were determined (Job plot analysis).

- These bisphosphite ligands were employed in two asymmetric reactions mediated by Rh(I) complexes: hydroformylation and hydrogenation. In the first reaction, hydroformylation of different vinylic or allylic substrates resulted in low enantioselectivities. However, in the presence of different cationic species as regulation agents, enantioselectivity, regioselectivity and the rate of the reaction could be improved in some cases. The best example of this improvement was found in the hydroformylation reaction of vinylic ester substrates. Enantiomeric excess could be improved up to 82% ee for the case of the hydroformylation of vinyl benzoate in the presence of Rb^+ cations as the regulation agent. With this regulation strategy, enantioselectivities and regioselectivities were raised to the same level obtained with the highest performing ligands reported in the literature for asymmetric hydroformylation of vinyl esters. On the other hand, asymmetric hydrogenation of substrates from different families such as one itaconic acid derivative, one dehydro-α-amino acid derivative, three α-arylenamides, one dehydro-β-amino acid and one dehydro-α-amino acid resulted in highly enantioselective processes (up to 92 – 98% ee with the best ligand) even in the absence of a regulation agent. Further addition of different regulation agents resulted in these cases in less notable improvements (*e.g.* 98 to 99% for **39a**, 93 to 94% for **39f** and 94 to 97% for **39b** using in each case the optimal salt as regulation agent).

- Coordination studies of the bisphosphite ligands with the different Rh(I) precatalysts employed in the catalytic experiments revealed the ability of these ligands to form chelates. High pressure studies (HP-NMR and HP-IR) under a CO/H_2 atmosphere revealed the formation of complexes of the type [Rh(H)$(CO)_2$(BArF salt•**46**)] derived from the rhodium precursor [Rh(κ^2O,O'-acac)$(CO)_2$] and the salt-bisphosphite supramolecular complexes (BArF salt•**46**). In these supramolecular structures the bisphosphite ligand is coordinated in an equatorial-equatorial fashion to the rhodium center and *cis* to the hydride ligand, which occupies an apical position in a trigonal-bipyramidal metal complex. Chelate complexes of the type [Rh(cod)(**46**)]BArF were also formed from the rhodium(I) precursor [$Rh(cod)_2$]BArF and the corresponding bisphosphite ligands. Addition of metal alkali salts as regulation agents (*i.e.* BArF salts) led in this case to a sharpening of the ^{31}P NMR signals and a downfield shift of the signals, suggesting a change in the direct environment of the P atoms and more rigidity in the supramolecular complexes. Overall, these coordination studies confirmed the formation of rhodium(I) chelates incorporating the supramolecular complexes that are formed between the bisphosphite and the salts (regulating agent).

- As an appendix to the Thesis, a family of racemic bisphosphine dioxide receptors that are the direct synthetic precursors of the above-mentioned bisphosphine ligands **45** was also presented. These receptors were found to effectively bind dicarboxylic acids such as oxalic and malonic acids according to binding studies made by UV-vis analysis (*K ca.* 5 x 10^3 M^{-1}). Besides, the affinity towards these dicarboxylic acids increased when these receptors were previously complexed to alkali cations. In the most noteworthy case, the binding constant increased by a factor of 7. Therefore one of the few allosteric receptors reported for dicarboxylic acids has been presented in this Thesis.

ACRONYMS AND ABBREVIATIONS

1,2-DME	1,2-Dimethoxyethane
a.u.	Arbitrary units
ACN	Acetonitrile
AHF	Asymmetric hydroformylation
API	Active pharmaceutical ingredient
AT	Adenine-thymine base pair
atm	Atmosphere
BArF	Tetra[3,5-bis(trifluoromethyl)phenyl]borate
ca.	*Circa* (about)
Cbz	Carboxybenzyl
CIP priority rules	Cahn-Ingold-Prelog priority rules
cod	Cyclooctadiene
DBTA	2,3-*O*,*O*-dibenzoyl tartaric acid
DCM	Dichloromethane
dctb	(*E*)-2-(3-(4-(tert-butyl)phenyl)-2-methylallylidene)malononitrile
deg	Degree
DFT	Density-functional theory
DMAP	4-(Dimethylamino)pyridine
DMF	Dimethylformamide
DNA	Deoxyribonucleic acid
DOPA	3,4-Dihydroxyphenylalanine
e.g.	*Exempli gratia* (for example)
ee	Enantiomeric excess
equiv.	Equivalent
et al.	*Et alii* (and co-workers)
EtOAc	Ethyl acetate
GC	Guanine-cytosine base pair or gas chromatography
HMBC	Heteronuclear multiple-bond correlation spectroscopy
HPLC	High-performance liquid chromatography
i.e.	*Id est* (in other words)

ITC	Isothermal titration calorimetry
LDA	Lithium diisopropylamide
MeOH	Methanol
MM	Molecular mechanics
n.d.	Not determined
nbd	Norbornadiene
NMR	Nuclear magnetic resonance
$OCN^{i}Pr$	Isopropyl isocyanate
PET	Photoinduced electron transfer
PG	Protecting group
RNA	Ribonucleic acid
rt	Room temperature
TA	Thymine-adenine base pair
TBDMS	^{t}Bu-dimethylsilyl
THF	Tetrahydrofuran
TMEDA	Tetramethylethylenediamine
$TMSN_3$	Trimethylsilyl azide
TMSOTf	Trimethylsilyl triflate
t_R	Retention time
UV-vis	Ultraviolet-visible
ZMac	(*Z*)-methyl 2-acetamido-3-phenylacrylate

APPENDIX I: BISPHOSPHINE DIOXIDE COMPOUNDS 81 AS ALLOSTERIC RECEPTORS FOR DICARBOXYLIC ACIDS

APPENDIX I: BISPHOSPHINE DIOXIDE COMPOUNDS 81 AS ALLOSTERIC RECEPTORS FOR DICARBOXYLIC ACIDS

LITERATURE REVIEW

Recognition of mono- and dicarboxylic acids by synthetic receptors is an important research area due to the biological importance and wide application of carboxylic acids in the pharmaceutical science. They are present in many biological processes and thus, they are included in many naturally occurring structures (*e.g.* amino acids, which are the protein building blocks; fatty acids and keto acids, which are present in the Krebs citric acid cycle; etc.).[236]

Over the past years, a variety of receptors containing different functional groups have been reported for selective binding of dicarboxylic acids.[237] The main interactions involved in carboxylic acid recognition are hydrogen bonding and steric complementarity. The amidopyridine motif (Figure 156) is one of the most utilized binding groups in the different reported receptors, since it provides two relatively strong complementary hydrogen bonds with carboxylic acid groups (Figure 156).

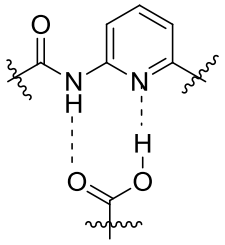

Figure 156. Binding of amidopyridines and carboxylic acid groups

This strategy was introduced by Hamilton *et al.* in their work on recognition of carboxylic acids with receptors **167** and **168a** (Figure 157).[238] The bisamidopyridine cavity **167** was found to bind ethylmalonic (K = 7.3 x 10^3 M^{-1}) and diethylmalonic dicarboxylic acids (K = 1.1 x 10^3 M^{-1}) in $CDCl_3$. The relatively

[236] Stryer, L. *Biochemistry*; Freeman: New York, 1995.
[237] Reviews: a) Bell, T. W.; Hext, N. M. *Chem. Soc. Rev.* **2004**, *33*, 589. b) Fitzmaurice, R. J.; Kyne, G. M.; Douheret, D.; Kilburn, J. D. *J. Chem. Soc., Perkin Trans. 1* **2002**, 841. c) Chen, H.; Weiner, W. S.; Hamilton, A. D. *Curr. Opin. Chem. Biol.* **1997**, *1*, 458. d) Rebek, J., Jr. *Mol. Struct. Energ.* **1988**, *10*, 219.
[238] **167** and **168a** receptors: Garcia-Tellado, F.; Goswami, S.; Chang, S. K.; Geib, S. J.; Hamilton, A. D. *J. Am. Chem. Soc.* **1990**, *112*, 7393.

low binding constants presumably reflect the unfavorable planar conformation of the diacid, which is required for complexation into the cavity. On the other hand, the more flexible acyclic host **168a** binds stronger with a range of diacids and particularly with adipic acid ($K > 1 \times 10^5$ M^{-1}). Nevertheless, other binding motifs found applicability in the dicarboxylic acid recognition field.[237] Some relevant examples of different receptors for dicarboxylic acids and, in some cases, their complexes with guests are shown in Figure 157.

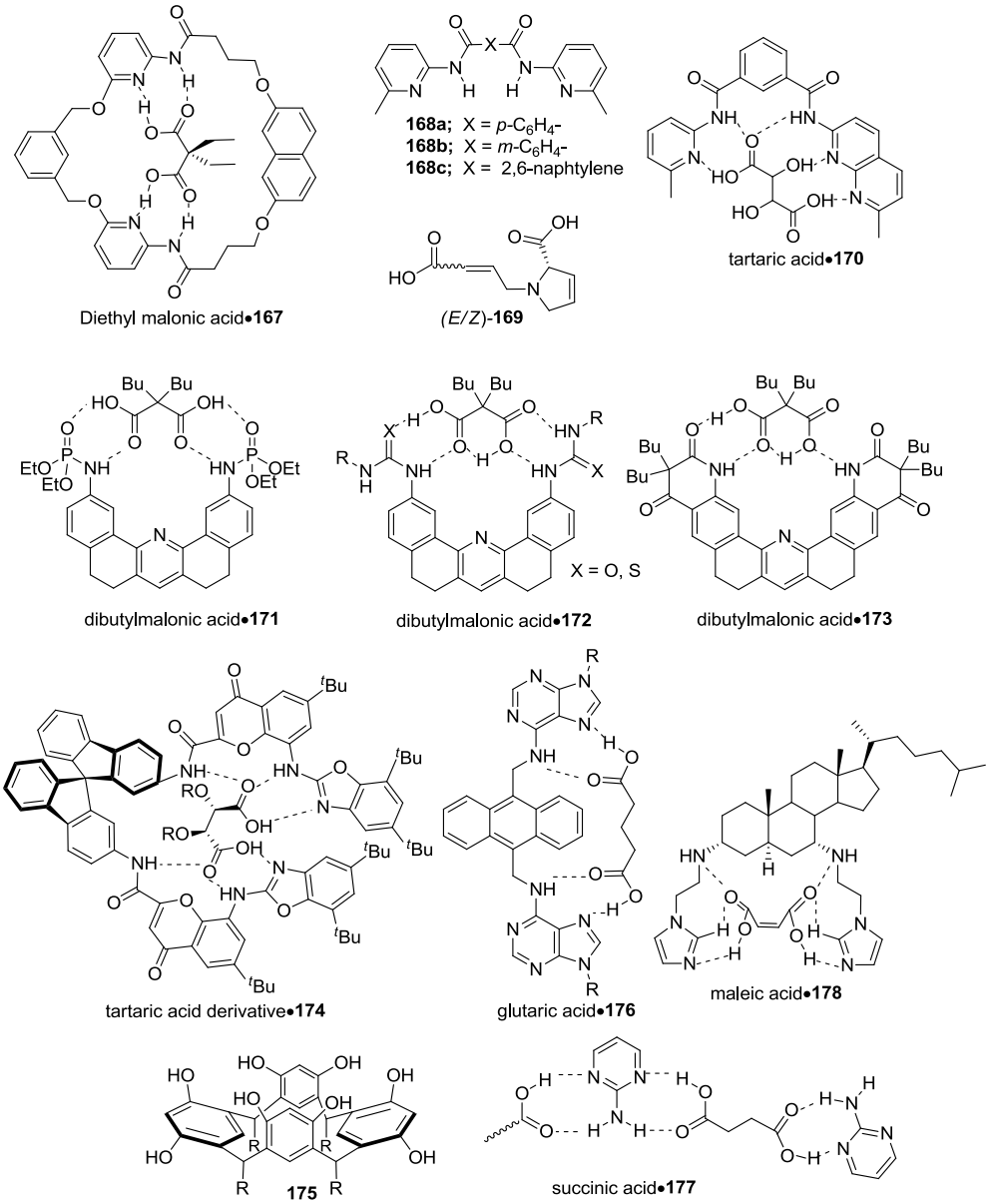

Figure 157. Dicarboxylic acid recognition. The design of dicarboxylic acid receptors utilizes a number of different approaches. Receptors **167**–**168**[238,239] utilize amidopyridine groups and **170**[240] incorporates an amidonaphthyridine binding motif.[241] Receptor **171**[242] utilizes phosphoric amide groups. Receptor **172**[242] bears urea or thiourea binding groups. Compound **173**[242] is a lactam-based host. Receptor **174**[243] utilizes benzoxazole units. Receptor **175**[244] is a polyol. Compound **176**[245] is an adenine-based receptor. Receptor **177**[246] utilizes aminopyrimidine motifs.[247] Receptor 2-Aminoethylimidazole-based **178**[248] is also reported to bind diacids

[239] Receptors **168b** and **168c**: Vicent, C.; Hirst, S. C.; Garcia-Tellado, F.; Hamilton, A. D. *J. Am. Chem. Soc.* **1991**, *113*, 5466.
[240] Goswami, S.; Ghosh, K.; Mukherjee, R. *Tetrahedron* **2001**, *57*, 4987.
[241] Other receptors based on amido(pyridine/naphthyridine) binding groups. a) Self-assembled amidopyridines through Pt(II) coordination: Shanmugaraju, S.; Bar, A. K.; Jadhav, H.; Moon, D.; Mukherjee, P. S. *Dalton Trans.* **2013**, *42*, 2998. b) Discrimination of fumaric and maleic acids:

For example, receptors **168b** and **168c** found applicability in the discrimination of (*E*)- and (*Z*)-proline diacid **169**. Receptor **170** binds tartaric acid through multiple hydrogen bonds. Tartaric acid derivatives could be enantioselectively recognized by receptor **174**. The receptor **175** has a pronounced length-dependent affinity towards dicarboxylic acids and it selectively binds glutaric acid. Another selective receptor for glutaric acid is the adenine-based ligand **176** (K = 3.5 x 10^4 M^{-1}). Early interesting co-crystallization studies reported on receptor **177** showed the binding preferences of aminopyrimidine receptors with different carboxylic acids. Receptor **178** showed a good selectivity toward maleic acid. Despite the great quantity of different strategies in the design of receptors for dicarboxylic acids, only one example of P=O-based receptors has been documented (see receptor **171** in Figure 157).

Receptors with the capability to control their binding ability towards dicarboxylic acids by allosteric modulation are scarce in the literature.[249]

Ghosh, K.; Sen, T.; Patra, A.; Mancini, J. S.; Cook, J. M.; Parish, C. A. *J. Phys. Chem. B* **2011**, *115*, 8597. c) Triphenylamine-based receptors (aminopyridine and amidopyridine as binding motifs): Ghosh, K.; Masanta, G.; Frohlich, R.; Petsalakis, I. D.; Theodorakopoulos, G. *J. Phys. Chem. B* **2009**, *113*, 7800. d) Binding studies in solution and in the solid state: Goswami, S.; Jana, S.; Fun, H.-K. *CrystEngComm* **2008**, *10*, 507. e) Citric acid sensing: Ghosh, K.; Sen, T.; Fröhlich, R. *Tetrahedron Lett.* **2007**, *48*, 2935. f) Dicarboxylic acid sensor with amidopyridine and quinoline as binding motifs: Ghosh, K.; Adhikari, S. *Tetrahedron Lett.* **2006**, *47*, 3577. g) Triphenylamine-based PET sensors: Ghosh, K.; Masanta, G. *Tetrahedron Lett.* **2006**, *47*, 2365. h) Tröger's base amidopyridine receptor selective for suberic acid: Goswami, S.; Ghosh, K. *Tetrahedron Lett.* **1997**, *38*, 4503. i) Organic receptor assembled around a transition metal template: Prevot-Halter, I.; Smith, T. J.; Weiss, J. *J. Org. Chem.* **1997**, *62*, 2186. j) 1,3-Bis[(pyrid-2-ylamino)carbonyl]adamantine as receptor for dicarboxylic acids: Karle, I. L.; Ranganathan, D.; Haridas, V. *J. Am. Chem. Soc.* **1997**, *119*, 2777. k) Heptanedioic acid binding: Koenig, B.; Moeller, O.; Bubenitschek, P.; Jones, P. G. *J. Org. Chem.* **1995**, *60*, 4291. l) Metal templated receptor for glutaric acid and related diacids: Goodman, M. S.; Hamilton, A. D.; Weiss, J. *J. Am. Chem. Soc.* **1995**, *117*, 8447. m) An helicopodand-based receptor for α,ω-dicarboxylic acids: Owens, L.; Thilgen, C.; Diederich, F.; Knobler, C. B. *Helv. Chim. Acta* **1993**, *76*, 2757. Chiral spirobifluorene-based receptor for enantioselective complexation of dicarboxylic acids: n) Cuntze, J.; Diederich, F. *Helv. Chim. Acta* **1997**, *80*, 897. o) Alcázar Montero, V.; Tomlinson, L.; Houk, K. N.; Diederich, F. *Tetrahedron Lett.* **1991**, *32*, 5309.

[242] Mussons, M.; Raposo, C.; de la Torre, M.; Morán, J. R.; Caballero, M. *Tetrahedron* **1999**, *55*, 4077.

[243] Hernández, J.; Almaraz, M.; Raposo, C.; Martín, M.; Lithgow, A.; Crego, M.; Caballero, C.; Morán, J. R. *Tetrahedron Lett.* **1998**, *39*, 7401.

[244] Tanaka, Y.; Kato, Y.; Aoyama, Y. *J. Am. Chem. Soc.* **1990**, *112*, 2807.

[245] Ghosh, K.; Sen, T.; Fröhlich, R. *Tetrahedron Lett.* **2007**, *48*, 7022.

[246] Etter, M. C.; Adsmond, D. A. *J. Chem. Soc., Chem. Commun.* **1990**, 589.

[247] Glutaric acid selective bis pyrimidine amine linked xylene spacer: Goswami, S.; Hazra, A.; Fun, H.-K. *J. Inclusion Phenom. Macrocyclic Chem.* **2010**, *68*, 461.

[248] Jadhav, J. R.; Ahmad, M. W.; Kim, H.-S. *Tetrahedron Lett.* **2010**, *51*, 5954.

[249] a) Ikeda, T.; Hirata, O.; Takeuchi, M.; Shinkai, S. *J. Am. Chem. Soc.* **2006**, *128*, 16008. b) Takeuchi, M.; Imada, T.; Shinkai, S. *Angew. Chem., Int. Ed.* **1998**, *37*, 2096. c) Lustenberger, P.; Welti, R.; Diederich, F. *Helv. Chim. Acta* **1998**, *81*, 2190.

Moreover, the reported systems are homotropically regulated (the binding of the first dicarboxylic guest provokes a change in the receptor that modifies its affinity towards the following dicarboxylic guest molecules). For example, Shinkai *et al.*[249a,b] designed allosteric cerium(IV)bisporphyrinato double decker complexes as receptors for dicarboxylic acids. In receptor **179**, both porphyrin units can rotate freely around the porphyrin-cerium-porphyrin axis until the binding of the first dicarboxylic acid at the pyridine units rigidifies the resulting complex and inhibits the rotation process. With the conformational process locked, the subsequent binding events are energetically more favorable, thereby the affinity of the receptor towards the guests is enhanced resulting in an overall positive cooperativity.[249b] In Scheme 50 the binding of four (*R*,*R*)-cyclohexanedicarboxylic acid **180** to allosteric receptor **179** by hydrogen bonds is represented.

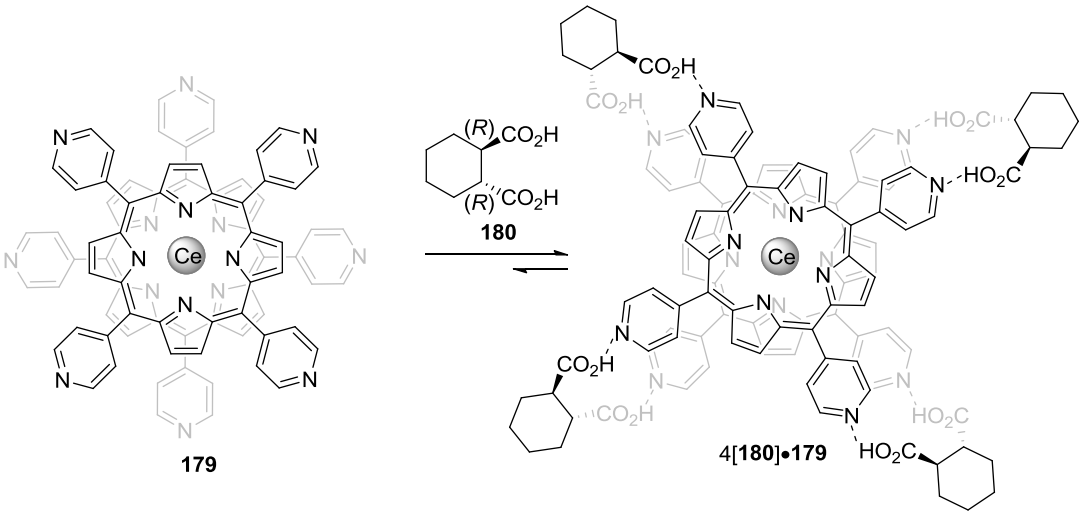

Scheme 50. Shinkai's homotropic allosteric receptor **179** for dicarboxylic acids

An example of a receptor for dicarboxylic acids with negative homotropic allosterism was reported by Diederich *et al.*[249c] in 1998. They designed an amidopyridine ditopic receptor bridged by two BINOL units **181** in which the binding of a dicarboxylic acid, such as the *N*-Cbz-glutamic acid **182**, strongly decreased the affinity of the other amidopyridine motif for the same guest **182** (Figure 158).

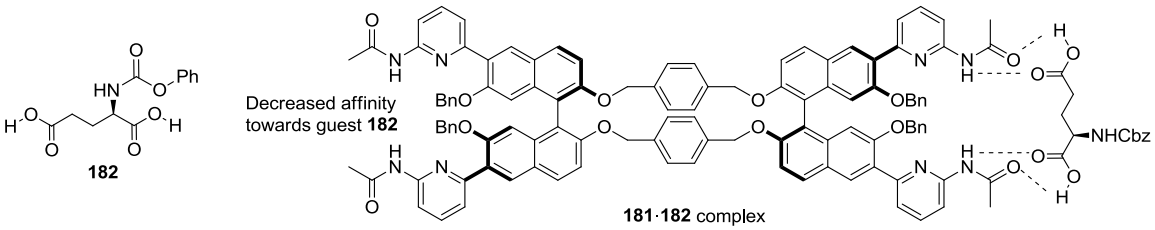

Figure 158. Ditopic receptor **181** with homotropic negative allosteric recognition of glutamic acid derivative **182**

RESULTS AND DISCUSSION

Binding studies: binding constant determination of diverse hydrogen bond donors with crown ether containing allosteric P=O receptors

As has been described in chapter 1 of this Thesis, we have developed an efficient synthesis for 2,2'-diphosphino-1,1'-biphenyl derivatives with an appended crown ether moiety. We considered that the structure of these compounds was highly interesting and suitable as allosteric receptors for a wide variety of guests. It should be noted at this point that our receptors incorporate two P=O binding groups capable of hydrogen-bonding for a wide array of guests, such as diols, ureas and dicarboxylic acids, and also a crow-ether motif, whose binding properties towards salts have already been discussed in chapter 1 of the present Thesis. Thus, we became interested in studying the properties of derivatives **81** as allosteric receptors, as well as the effectiveness of our regulation mechanism in the molecular recognition of the aforementioned guests.[250]

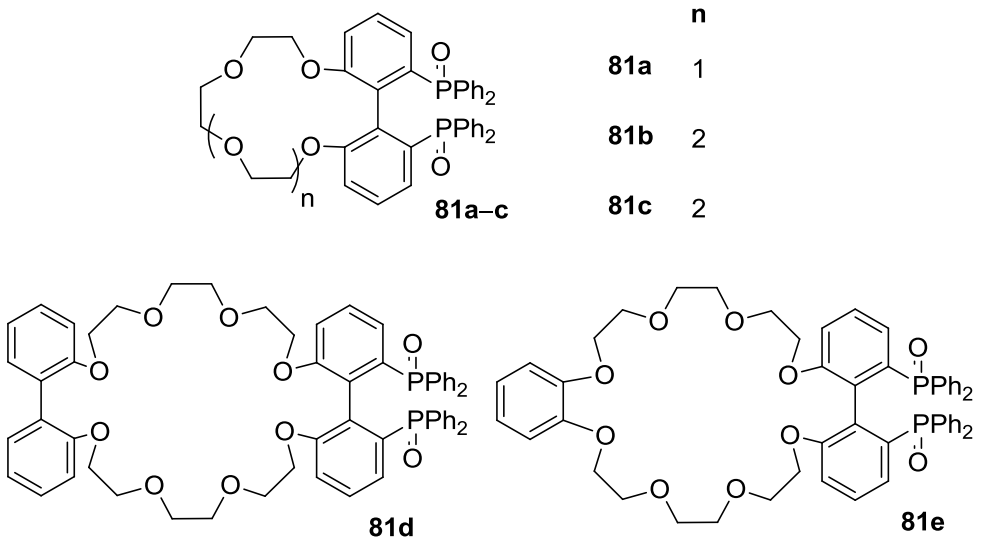

Figure 159. Allosteric receptors **81a–e**

As the first step in this study, we turned our attention to the H-bond acceptor properties of the P=O groups present in our receptors towards an array of hydrogen-bonding complementary partners to P=O groups. Preliminary

[250] These binding studies were carried out in collaboration with Dr. Amilan D. Jose.

binding studies were carried out with different guests, such as ureas **183**, diols **184** and dicarboxylic acids **185** (Figure 160).

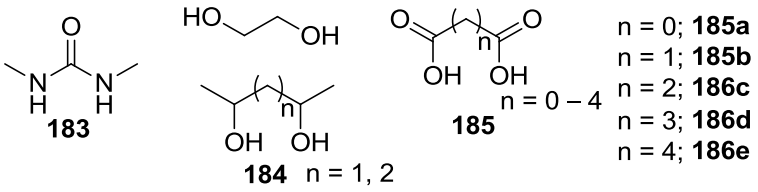

Figure 160. H-bond donor species tested as potential guests for **81**

For this purpose, fluorescence spectra of (*rac*)-**81a** in the usual solvent mixture (DCM/MeOH 99.5/0.5 v/v) was recorded before and after the addition of increasing quantities of the assayed analytes dissolved in the same solvent. Only in the case of some dicarboxylic acids, **185a** and **185b**, a change of emission intensity of receptor **81a** was observed, which indicated that a measurable association process between them and receptor (*rac*)-**81a** could be taking place (Figure 161).

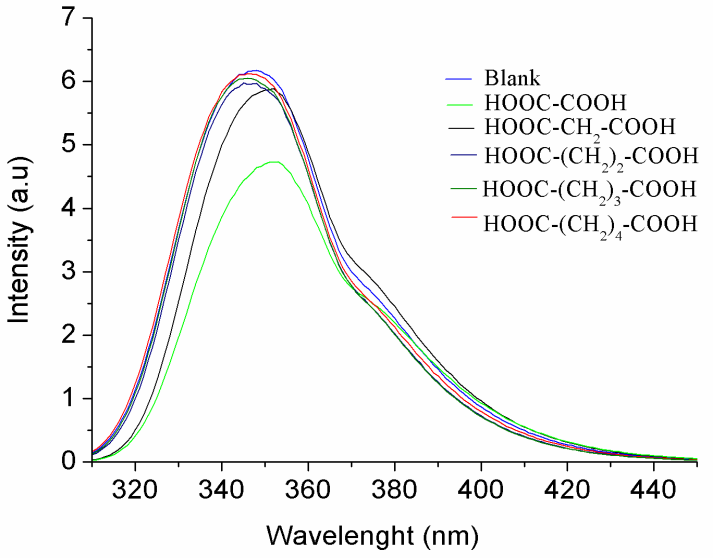

Figure 161. Change in emission spectrum of (*rac*)-**81a** (1.60×10^{-4} M) upon addition of an excess amount (10 equiv.) of different dicarboxylic acids in a DCM/MeOH mixture (99.5/0.5 v/v) at 298 K

Binding properties of P=O-based crown receptors (*rac*)-**81** with different dicarboxylic acids were further studied with several spectroscopic techniques. Indeed, changes in the UV-spectra of (*rac*)-**81** were observed after the addition of increasing amounts of oxalic **185a** and malonic **185b** solutions (*ca.* 10^{-2} M) to

solutions of (*rac*)-**81** (*ca.* 10^{-4} M) in DCM/MeOH (99.5/0.5 v/v): the absorption band at *ca.* 300 nm experienced a 5 nm bathochromic shift upon binding and association constants between (*rac*)-**81** with oxalic and malonic acids could in this way be determined (see Table 42). The UV-visible titration data was analyzed using multivariate factor analysis and considering a binding model with two colored stoichiometric states of the receptors: unbound and a 1:1 complex with the corresponding diacid. SPECFIT software (Version 3.0; Spectra Software Associates) was used for this purpose.[251]

Table 42. Association constants of receptors **81a**,**b**,**c**,**e** with dicarboxylic acids

		Binding constants (M^{-1})[a,b]	
Entry	Receptor	Oxalic acid	Malonic acid
1	(*rac*)-**81a**	6.7×10^3	4.5×10^3 [c]
2	(*rac*)-**81b**	4.9×10^3	4.4×10^3
3	(*rac*)-**81c**	6.2×10^3	4.6×10^3
4	(*rac*)-**81e**	7.4×10^3	5.0×10^3

[a] Measured in DCM/MeOH (99.5/0.5 v/v) at 25 ºC with UV-vis absorption spectroscopy. [b] Average value of at least two measurements. [c] This binding constant was also measured by ^{31}P NMR and its value found to be 2.8×10^3 M^{-1}.

Other dicarboxylic acids with a longer spacer between the carboxylic groups (*i.e.* succinic **185c**, glutaric **185d** and adipic acids **185e**) induced very small changes in the absorption spectra, which led us to conclude that weak binding could be taking place in these cases (Figure 162). Binding studies consistently revealed that binding affinity of the receptor decreased upon increasing the spacer chain length of the dicarboxylic acid, thus the selectivity order was: HOOC-COOH **185a** > HOOC-CH_2-COOH **185b** > HOOC-$(CH_2)_2$-COOH **185c** >> HOOC-$(CH_2)_{n>2}$-COOH. It is worth mentioning that the ring size and shape of the crown ether in the receptors **81a**,**b**,**c**,**e** does not seem to influence the affinity of the *P=O* binding groups towards oxalic and malonic acids.

[251] a) Gampp, H.; Maeder, M.; Meyer, C. J.; Zuberbuehler, A. D. *Talanta* **1986**, *33*, 943.
b) Gampp, H.; Maeder, M.; Meyer, C. J.; Zuberbuehler, A. D. *Talanta* **1985**, *32*, 95.

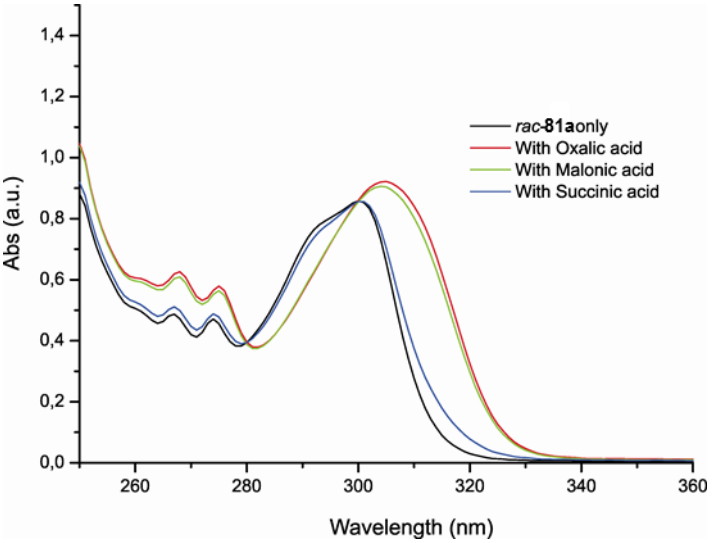

Figure 162. Change in UV-vis spectrum of (*rac*)-**81a** (1.17 x 10^{-4} M) upon addition of excess amount (10 equiv.) of different dicarboxylic acids in a DCM/MeOH mixture (99.5/0.5 v/v) at 298 K

The fact that only short-chain dicarboxylic acids showed binding with our receptors might suggest that both P=O units might be cooperating in the binding process. Long chain dicarboxylic acids may not have the suitable distance to form a chelate.

The stoichiometries of the formed complexes were studied by the continuous variations method (Job's plot)[252] for the receptor (*rac*)-**81b** with oxalic and malonic acids. Stock solutions of the same concentration of receptor (*rac*)-**81b** (*ca.* 1 x 10^{-4} M) and dicarboxylic acids **185a** and **185b** were prepared in DCM/MeOH (99.5/0.5 v/v). Then, UV-vis spectra with different host-guest ratios at constant total concentration were recorded. Job plots were made by plotting the changes in absorbance at 300 nm versus χ_{host} (Figure 163). The maximum of the curve was found at χ_{host} = *ca*. 0.5 suggesting a 1:1 binding mode.

[252] Huang, C. Y. *Methods Enzymol.* **1982**, *87*, 509.

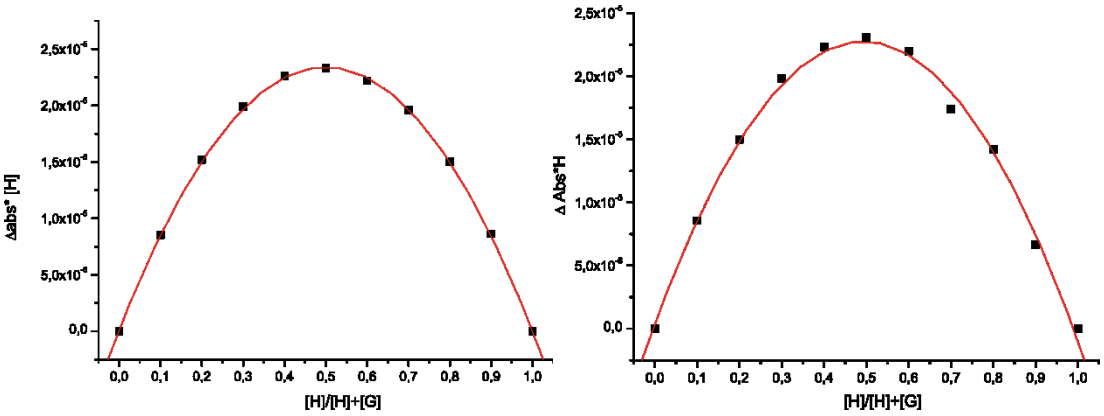

Figure 163. Job plots of (*rac*)-**81b** upon addition of oxalic (left) and malonic acid (right) in DCM/MeOH (99.5/0.5 v/v) at 298 K

For the sake of comparison, the binding constant between (*rac*)-**81a** and malonic acid was also determined by ^{31}P NMR. For this experiment, a solution of the receptor (*rac*)-**81a** (*ca.* 10^{-4} M) and malonic acid (*ca.* 10^{-2} M) were prepared in DCM-d_2/MeOH-d_4 (99.5/0.5 v/v). The host solution (0.6 mL) was placed in a NMR tube. The titration was carried out adding at 298 K incremental amounts of guest (malonic acid) to the host solution ((*rac*)-**81a**), which led to changes in the chemical shift and signal width in the NMR spectra. Binding constants were extracted by multivariate factor analysis of the ^{31}P NMR chemical shift values, considering a 1:1 binding model in the fast exchange-limit. SPECFIT software was used. The binding constant determined by NMR (2.8 x 10^3 M^{-1}) (Figure 164) was in good agreement with the one determined by UV-vis spectrophotometry (4.5 x 10^3 M^{-1}), validating the methodology employed. However, the magnitude of the binding contants (*ca.* 10^3 M^{-1}) forced us to use dilute solutions of (*rac*)-**81a** during the NMR-titration (the concentration to measure an association constant depends on the *K*-value, and the recommended concentration has been set to *ca.* 1/*K*, which implied working in our case with *ca.* 10^{-4} M solutions),[253] with the correspondingly long acquisition times and duration of experiments. The interaction between the COOH and the P=O groups between receptor (*rac*)-**81b** and oxalic and malonic acids was also confirmed by ^{31}P NMR. The ^{31}P NMR analysis of a qualitative titration of the receptor **81b** with **185a** and **185b** acid showed a broadening and a downfield shift (2.8 ppm and 2.6 ppm, respectively) of the phosphorus signal. For

[253] Hirose, K. in *Analytical Methods in Supramolecular Chemistry*; Schalley, C. A., Ed.; Wiley-VCH: Weinheim, 2007.

example, the ^{31}P NMR spectra of the qualitative titration between **81b** and **185a** are presented in Figure 165.

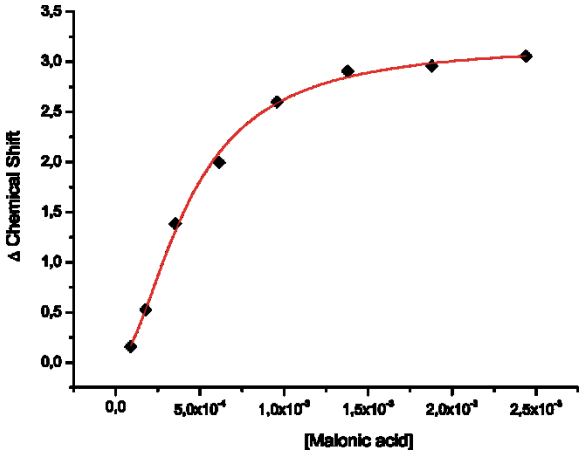

Figure 164. NMR Titration to measure the binding constant between (*rac*)-**81a** (8.91 x 10^{-4} M – 8.42 x 10^{-4} M) and malonic acid: Changes in the ^{31}P NMR (202 MHz, DCM-d_2/MeOH-d_4 [99.5/0.5 v/v]) upon addition of **185b** (8.90 x 10^{-5} – 2.44 x 10^{-3} M)

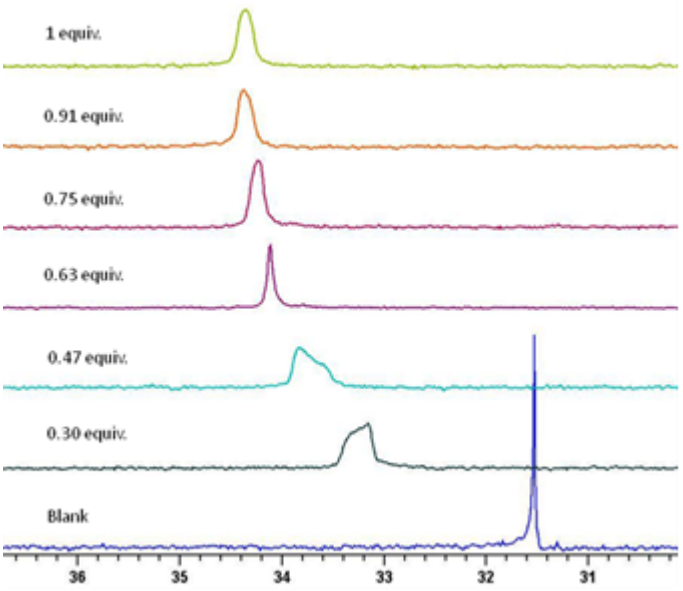

Figure 165. Changes in the ^{31}P NMR (202 MHz, DCM-d_2/MeOH-d_4 [99.5/0.5 v/v]) spectra acquired at 298 K during the titration of (*rac*)-**81b** with oxalic acid ([(*rac*)-**81b**] = 1.3 x 10^{-2} M)

Crystals of the complex between (*rac*)-**81b** and oxalic acid suitable for X-ray analysis could be grown by slow evaporation of a solution of the complex in dichloromethane. In the solid state, the substrate molecules formed hydrogen bonds between the P=O and COOH groups (see dashed lines in Figure 166;

$d_{P=O\text{-}HOOC}$ = 2.580 Å and $d_{P=O\text{-}HOOC}$ = 1.70 Å), leading to a well-defined linear complex with an overall 1:1 stoichiometry.

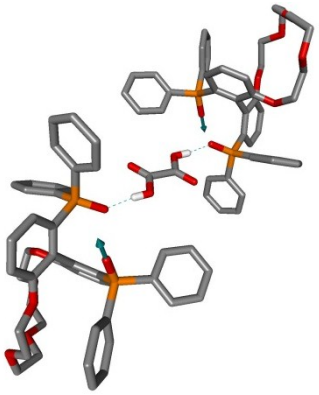

Figure 166. X-ray structure of (*rac*)-**81b** with oxalic acid (dotted lines indicate binding groups for further oxalic acid molecules)

Binding studies: binding constant determination of hydrogen bond donors with crown ether containing allosteric P=O receptors

After studying the binding affinities of several cationic species toward the different crown ether moieties, and the association constants between different dicarboxylic acids with the P=O groups of our receptors **81**, we turned our attention to the effect of Li^+ and Na^+ as potential allosteric effectors in the recognition of oxalic and malonic acids by receptors **81a**–**c**,**e**. We proceeded as follows: solutions of the receptors **81a**–**c**,**e** (*ca.* 10^{-4} M) were prepared in DCM/MeOH (99.5/0.5 v/v). Solutions of the corresponding dicarboxylic acids (*ca.* 10^{-2} M) or crown ether binders (*ca.* 10^{-2} M) were also prepared in the same solvent mixture. The receptor solution was placed in a 1 cm quartz cell. The titration was carried out by adding incremental amounts of guest **185a** or **185b** at 298 K to the host solution (Li^+• or Na^+•(*rac*)-**81a**–**c**,**e** [prepared *in situ* by adding 10 equivalents of the corresponding perchlorate to (*rac*)-**81a**–**c**,**e**]), which led to changes in the absorbance spectrum of the receptor. See, for example, the UV-vis spectra changes in the case of receptor **81a** and complex Li^+•**81a** upon addition of malonic acid **185b** (Figure 167).

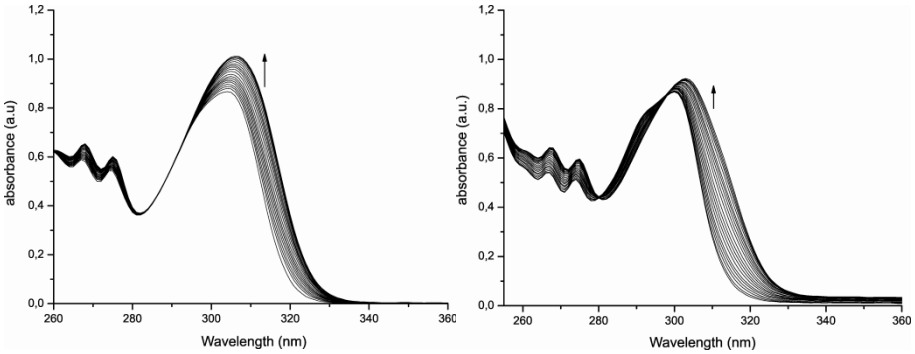

Figure 167. UV-vis titrations. Left: Li^+•(*rac*)-**81a** (1.17 x 10^{-4} M – 1.13 x 10^{-4} M in (*rac*)-**81a** and 10 equivalents of $LiClO_4$) upon addition of different amounts of **185b** (0 M – 4.87 x 10^{-4} M) and right: (*rac*)-**81a** (1.23 x 10^{-4} – 1.17 x 10^{-4} M) upon addition of different amounts of **185b** (0 M – 6.80 x 10^{-4} M) in DCM/MeOH (99.5/0.5 v/v) at 298 K

The UV-vis titration data was again analyzed using multivariate factor analysis and considering a binding model with two colored stoichiometric states of the crown ether receptors: unbound and 1:1 complex. SPECFIT software (Version 3.0; Spectra Software Associates) was used. The results are summarized in Table 43.

Table 43. Allosteric effects on binding of (*rac*)-**81a**,**b**,**c**,**e** with dicarboxylic acids

		Binding constants (M^{-1}); K_{rel}[a]	
Entry	Complex	Oxalic acid	Malonic acid
1	Li^+•**81a**	1.1 x 10^4; 1.7	3.3 x 10^4; 7.4
2	Na^+•**81a**	4.3 x 10^4; 6.5	1.3 x 10^4; 2.9
3	Li^+•**81b**	1.8 x 10^4; 3.7	1.3 x 10^4; 2.9
4	Na^+•**81b**	1.6 x 10^4; 3.3	1.4 x 10^4; 3.1
5	Li^+•**81c**	1.0 x 10^4; 1.7	1.4 x 10^4; 3.1
6	Na^+•**81c**	2.0 x 10^4; 3.3	8.5 x 10^3; 1.9
7	Li^+•**81e**	3.9 x 10^4; 5.3	8.2 x 10^3; 1.6
8	Na^+•**81e**	1.4 x 10^4; 1.9	7.7 x 10^3; 1.5

[a] Binding constant quotient with and without allosteric effector calculated from UV-vis absorption titrations.

To our delight, binding constant values were found to be higher in comparison to those determined for the same receptor with unbound cationic species. As a remarkable example, the highest allosteric effect was found with

receptor **81a** that binds to malonic acid about 7 times more tightly when a lithium salt is present than to "free" receptor **81a** (compare entries 1 in Table 42 and Table 43).

In the case of oxalic acid, a similar impact on the binding was found on the binding with **81b**. In this case, sodium perchlorate increased the binding constant from 6.7 x 10^3 to 4.3 x 10^4 M^{-1} (K_{rel} = 6.4, compare entries 2 in Table 42 and Table 43).

Unfortunately, despite many attempts it was not possible to grow suitable crystals for X-Ray analysis of any of the complexes indicated in Table 43 to get structural information of the supramolecular entities formed. We hypothesize that changes in the torsion angle between the central aryl rings and rigidification of the receptor structure produced by the inclusion of the cations into the crown ether strengthen binding of the dicarboxylic acid guests at the P=O motifs.

In conclusion, we have described a straightforward synthesis of new P=O-disubstituted biphenyl derivatives with appended crown ethers **81**. The properties as receptors for dicarboxylic acids have been evaluated by UV-vis titrations, and high affinities have been found (ranging from 4.9 x 10^3 to 7.4 x 10^3 M^{-1}). The affinity of the receptors for cationic species amenable to bind the crown ether moiety was also determined by fluorescence. Binding of cationic species (Na^+ or Li^+) proved to increase the affinity of the receptors for dicarboxylic acid guests. In the best case, the binding constant of receptor **81a** towards malonic acid **185b** increased up to 7.4 times its value when Li^+ was bound to the receptor.

The successful application of our modulation mechanism by ion-dipole interactions in a distal crown ether regulation site in the design of allosteric receptors encourages us to keep working on the development of new receptors for interesting guest molecules.

APPENDIX II: SELECTED NMR SPECTRA AND X-RAY DATA

APPENDIX II: SELECTED NMR SPECTRA AND X-RAY DATA

I. SELECTED NMR SPECTRA OF FINAL COMPOUNDS

^{1}H NMR spectrum of compound **45a:**

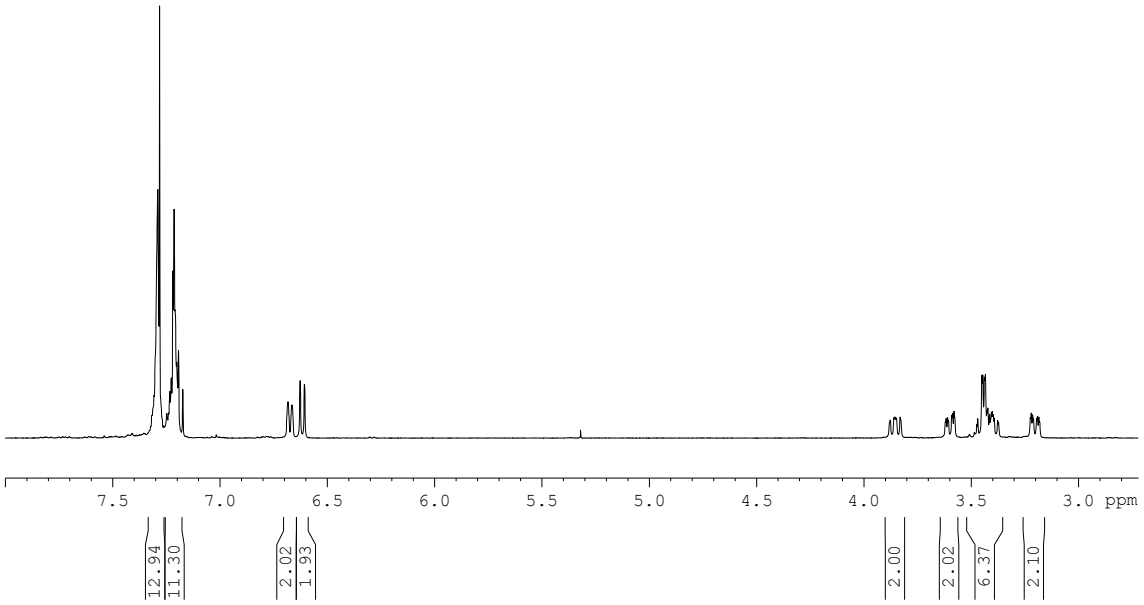

^{13}C{^{1}H,^{31}P} NMR spectrum of compound **45a:**

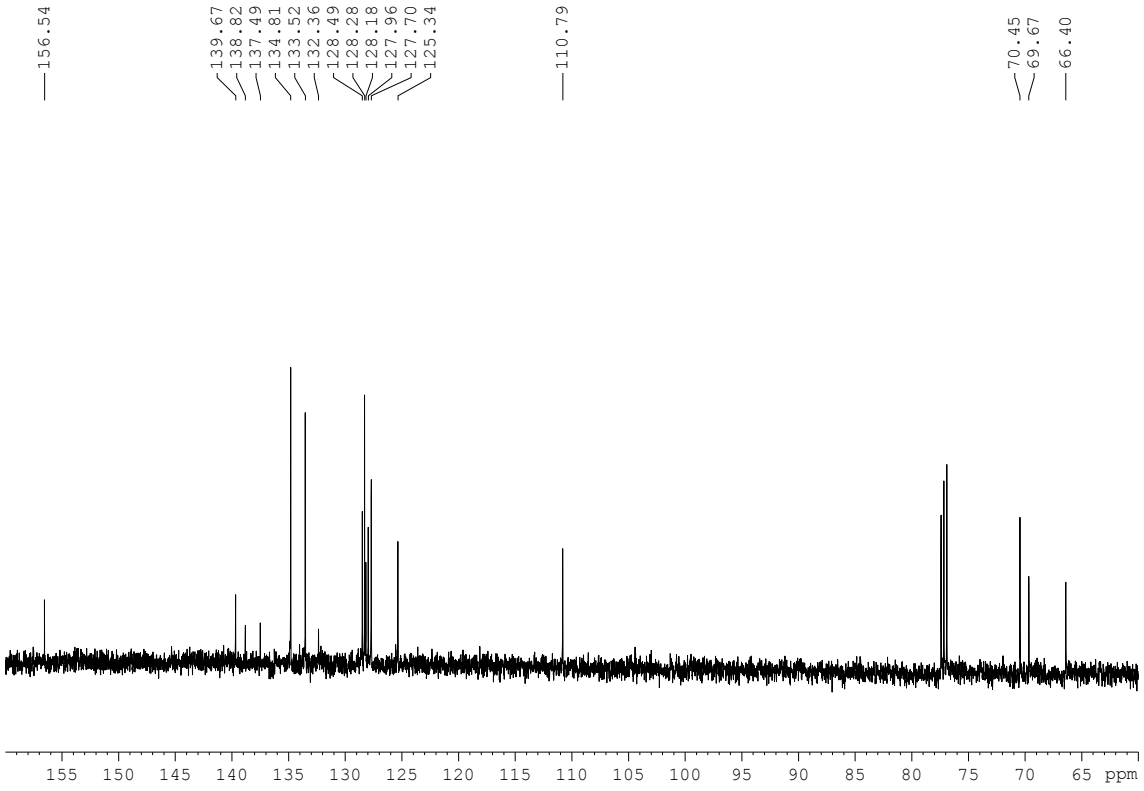

^{31}P NMR spectrum of compound **45a:**

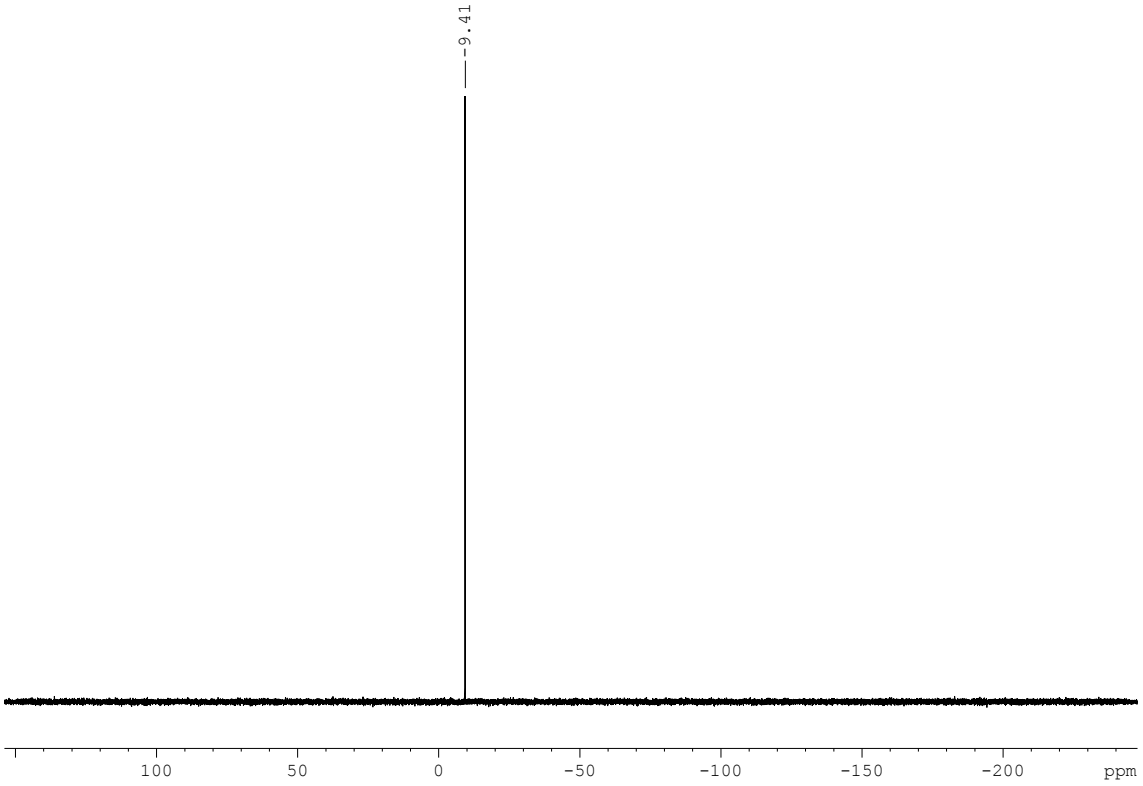

^{1}H NMR spectrum of compound **45b:**

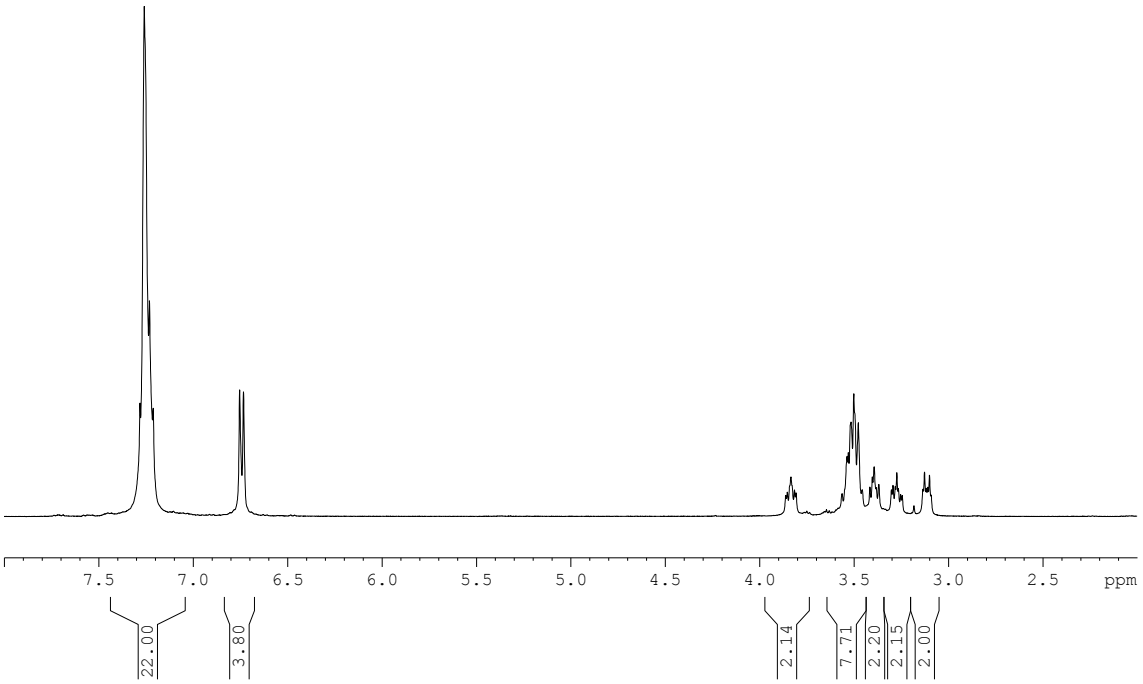

$^{13}C\{^{1}H,^{31}P\}$ NMR spectrum of compound **45b:**

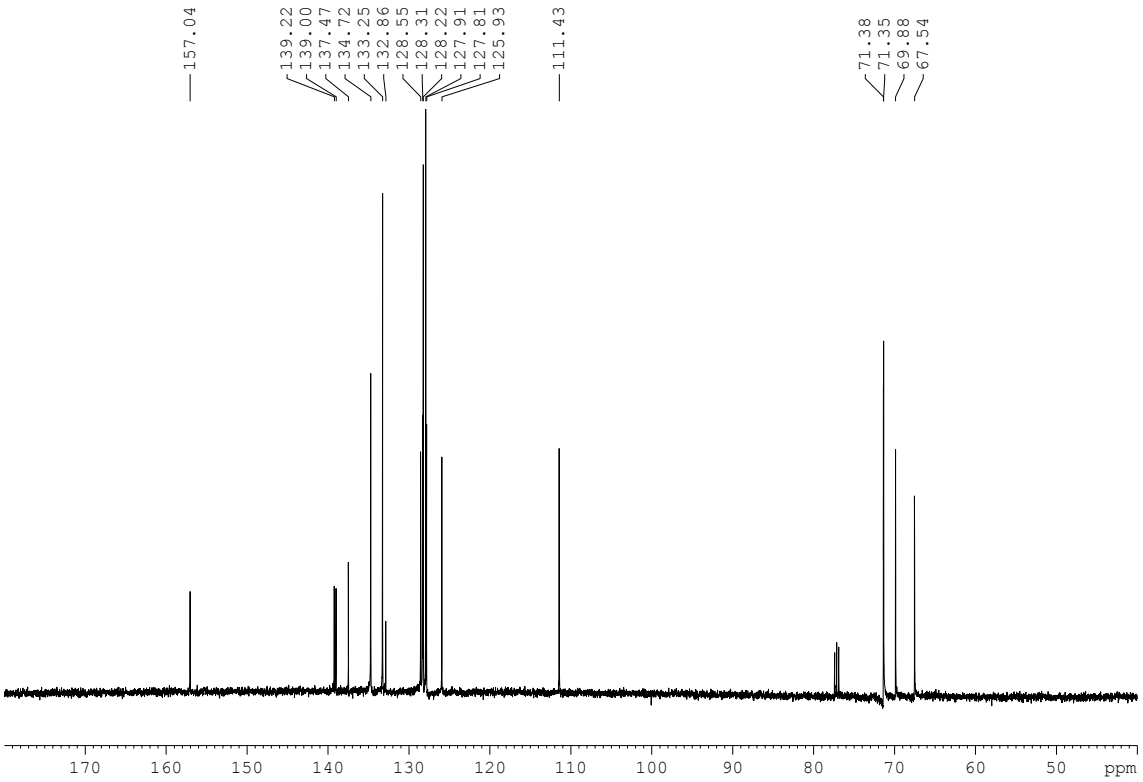

^{31}P NMR spectrum of compound **45b:**

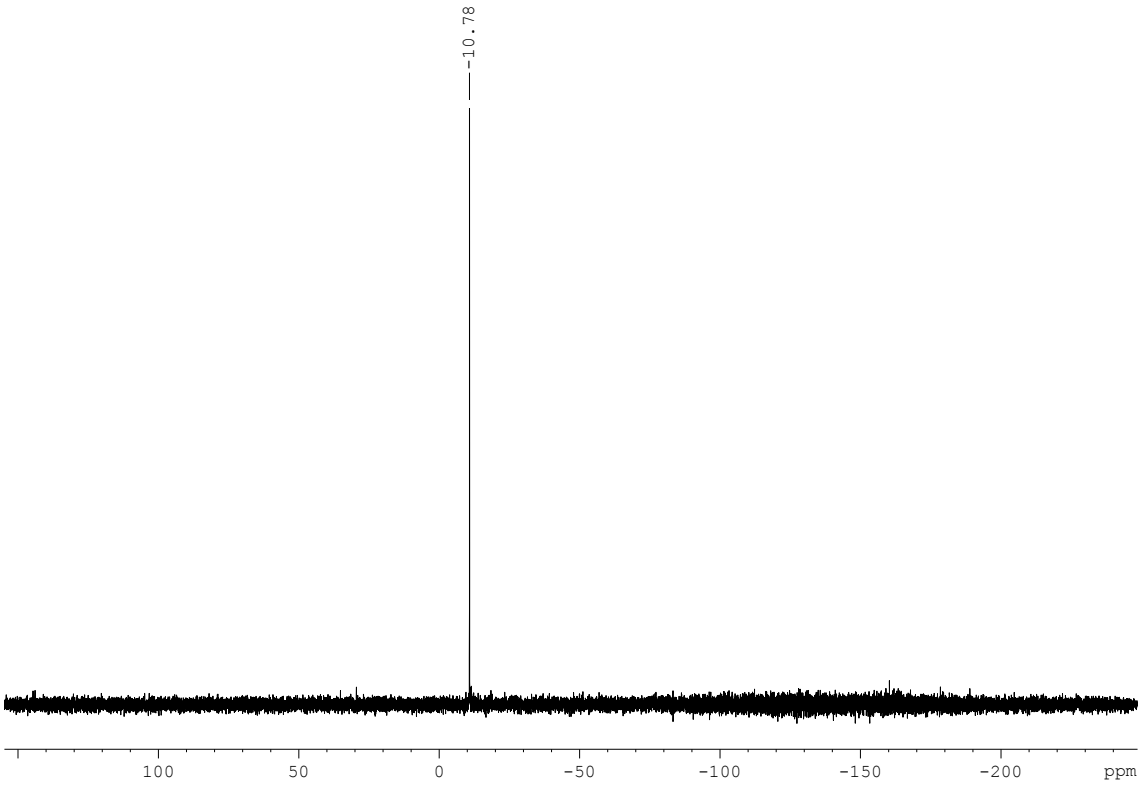

^{1}H NMR spectrum of compound **45e:**

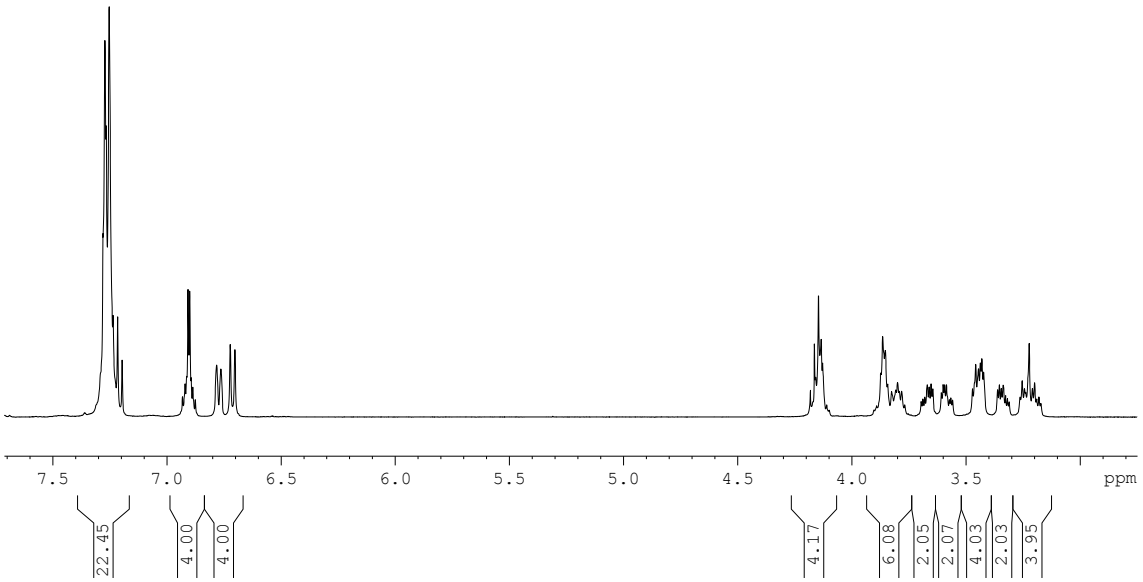

^{13}C{^{1}H,^{31}P} NMR spectrum of compound **45e:**

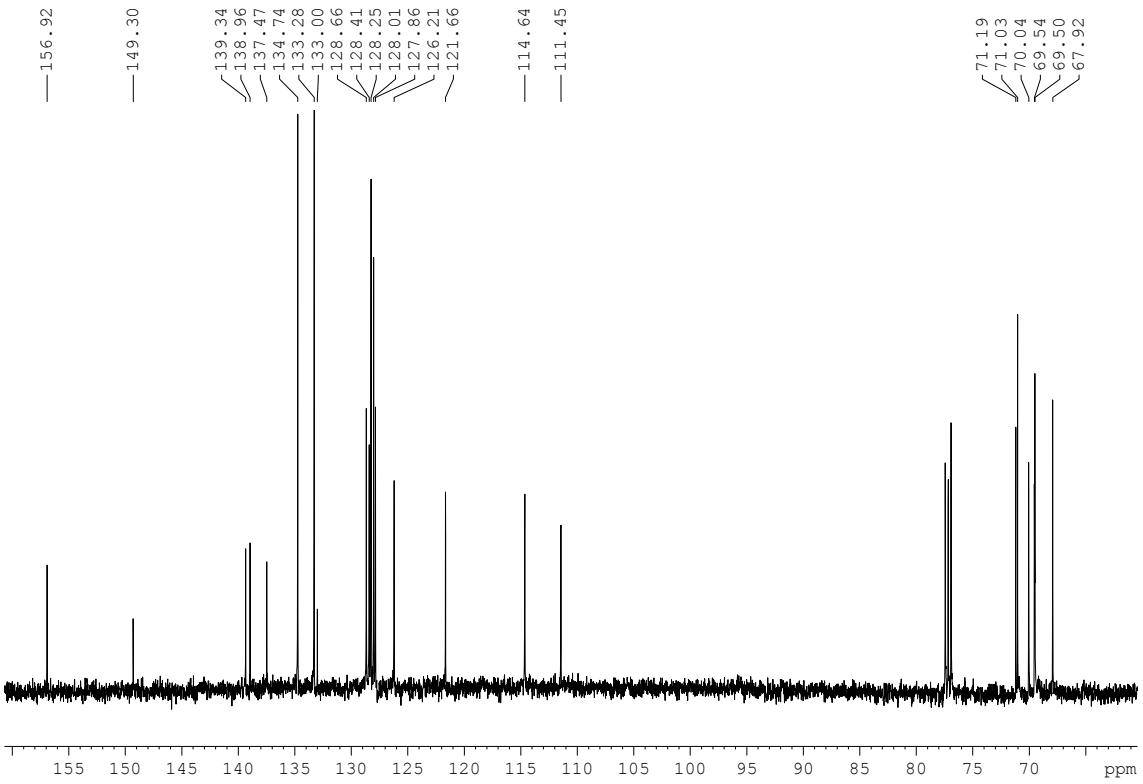

^{31}P NMR spectrum of compound **45e:**

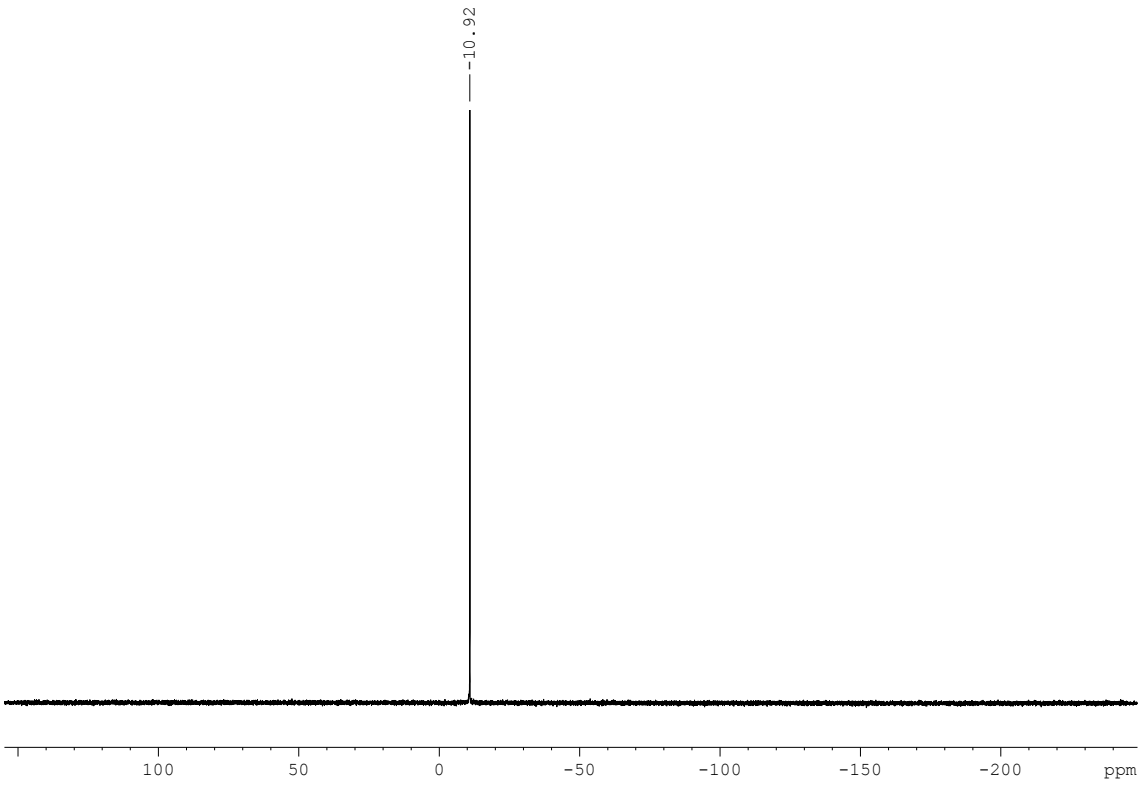

^{1}H NMR spectrum of compound **46a:**

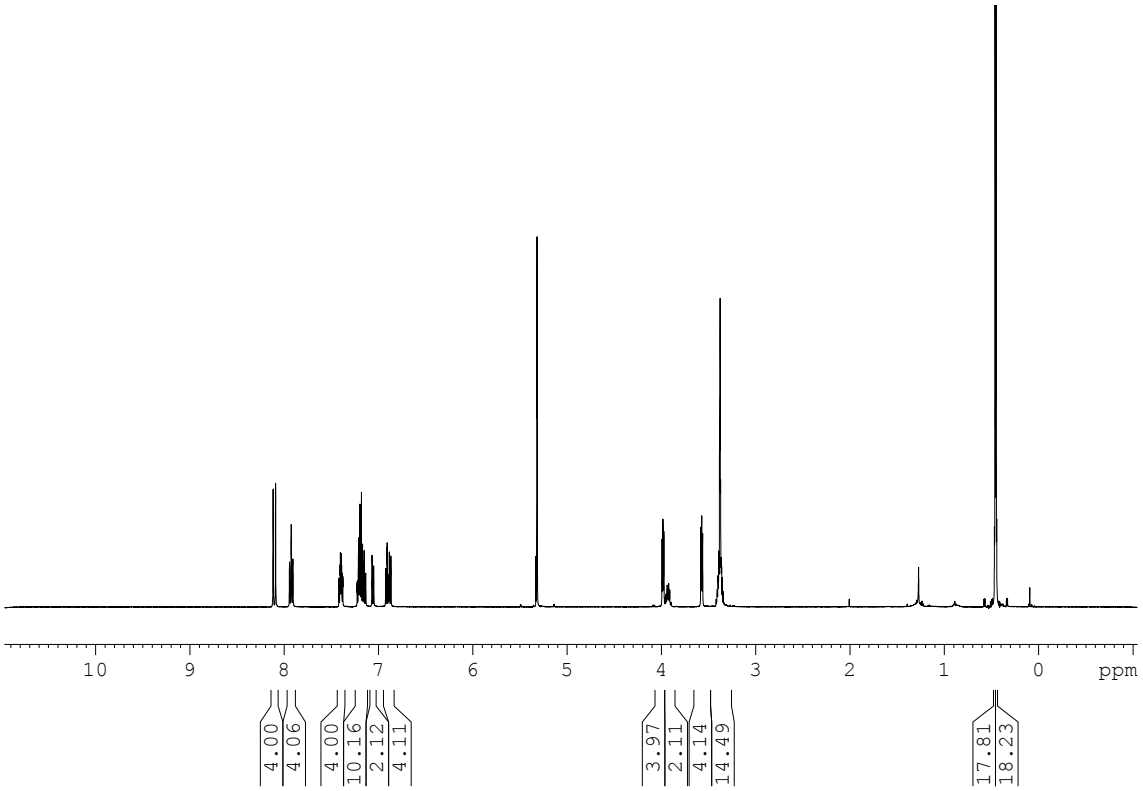

$^{13}C\{^{1}H,^{31}P\}$ NMR spectrum of compound **46a:**

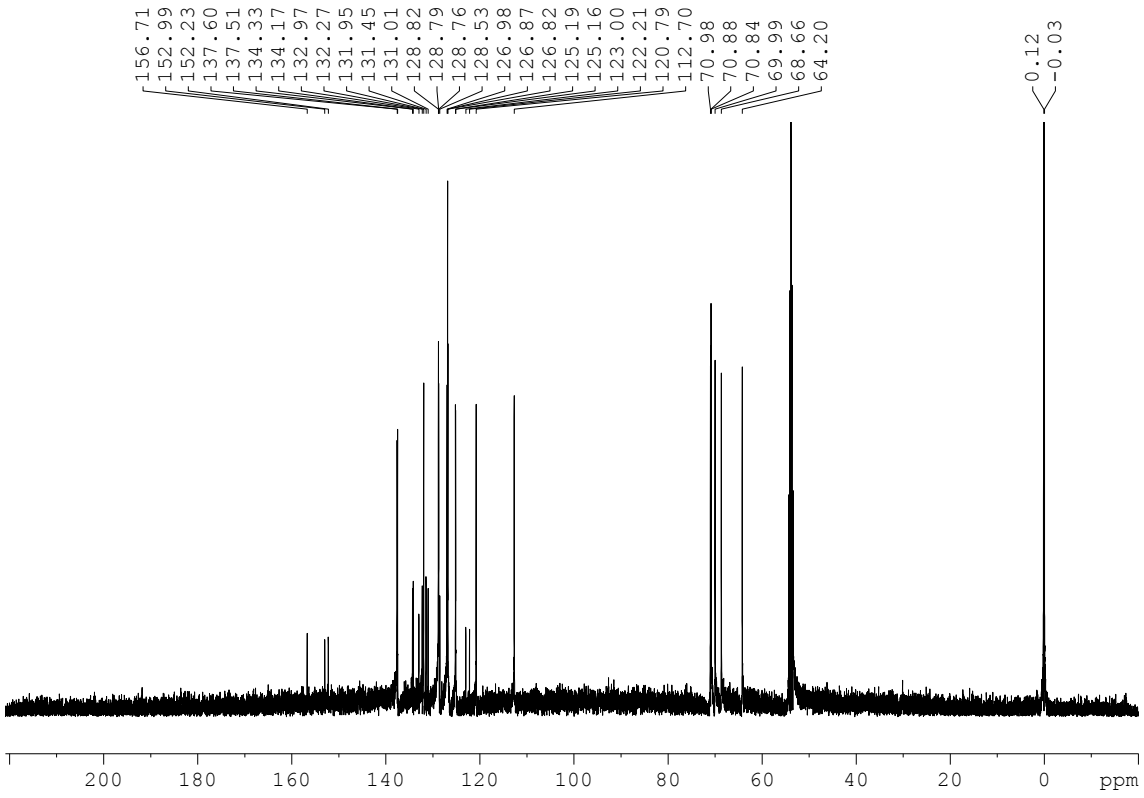

^{31}P NMR spectrum of compound **46a:**

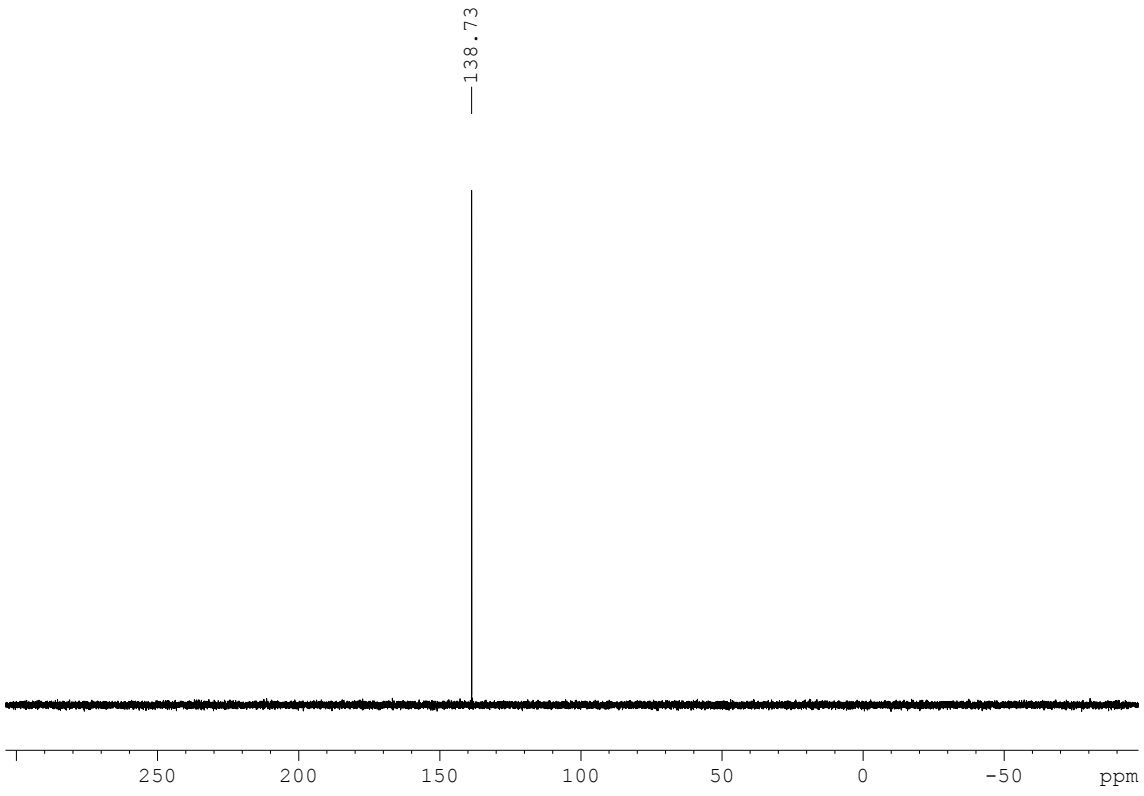

^{1}H NMR spectrum of compound **46b:**

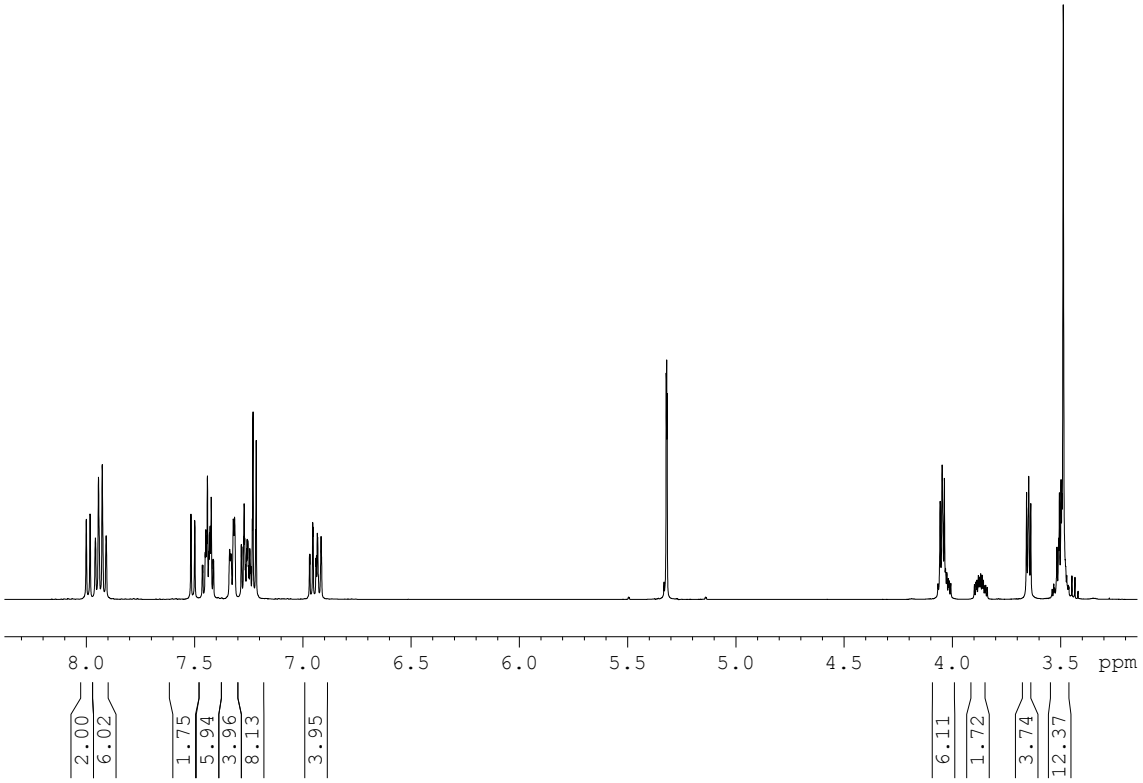

^{13}C{^{1}H,^{31}P} NMR spectrum of compound **46b:**

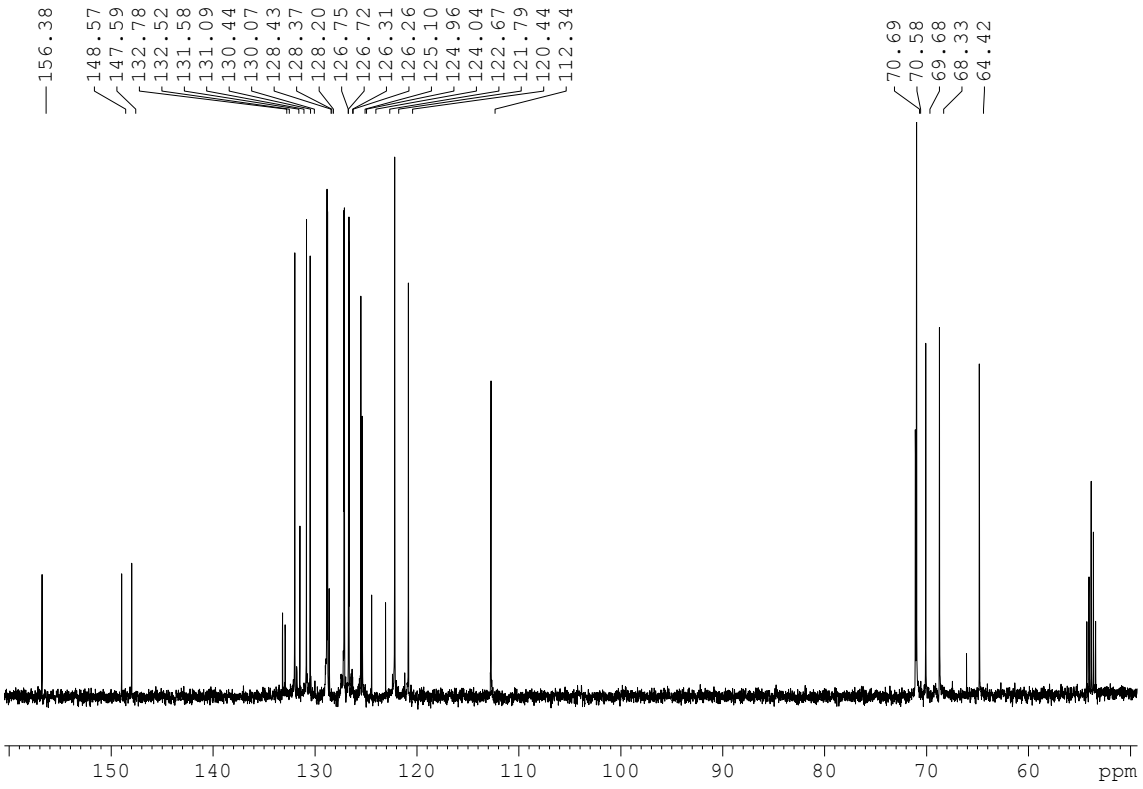

^{31}P NMR spectrum of compound **46b:**

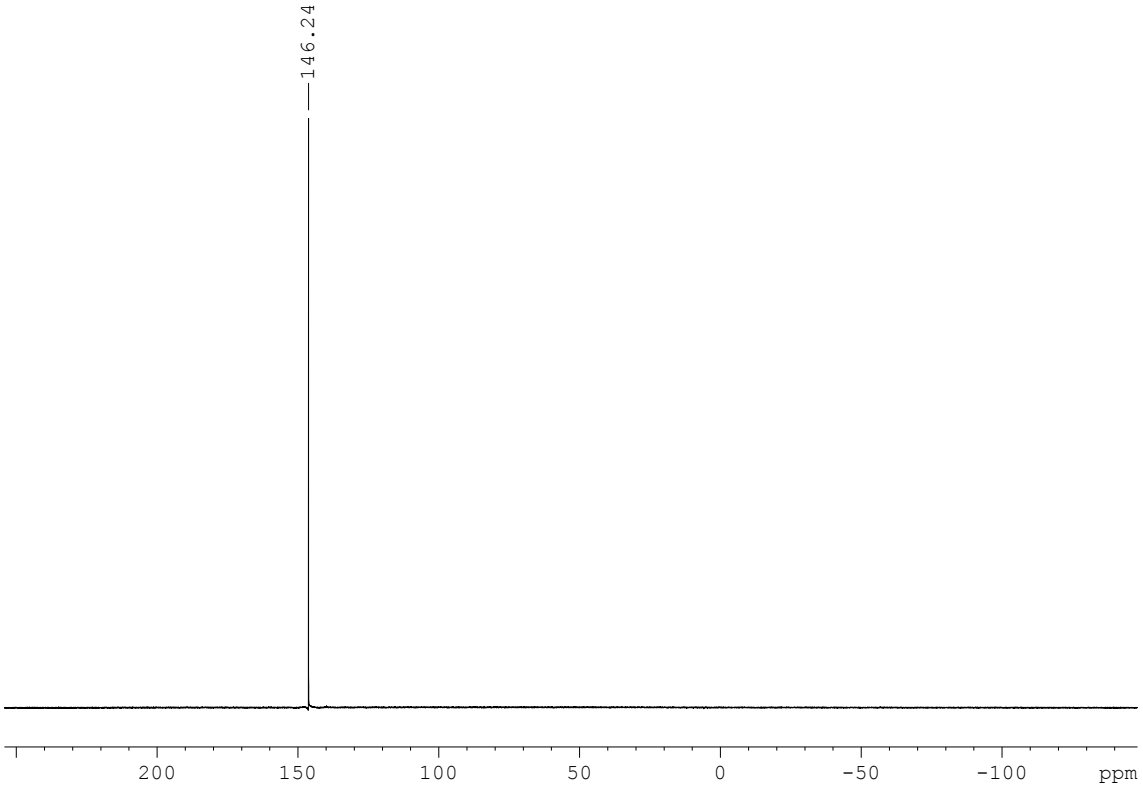

^{1}H NMR spectrum of compound **46c:**

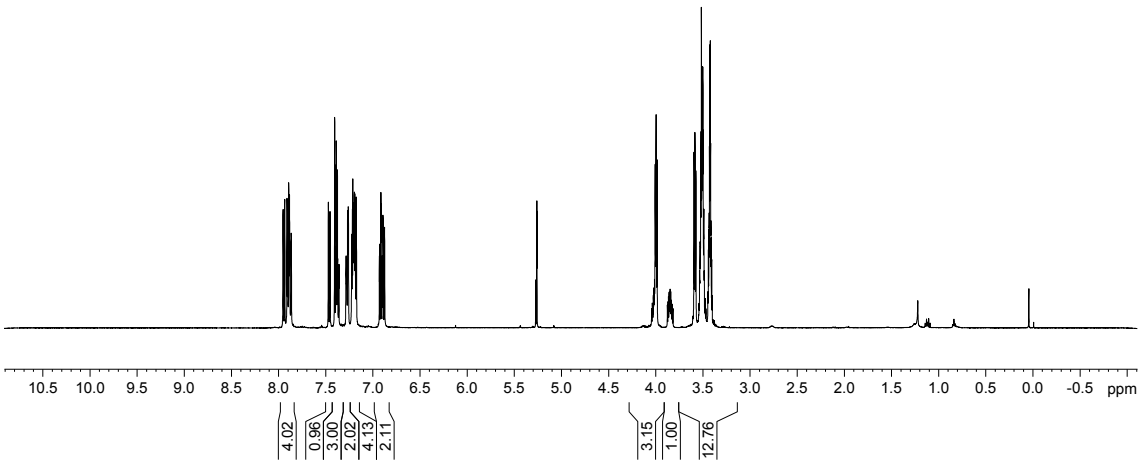

$^{13}C\{^{1}H,^{31}P\}$ NMR spectrum of compound **46c:**

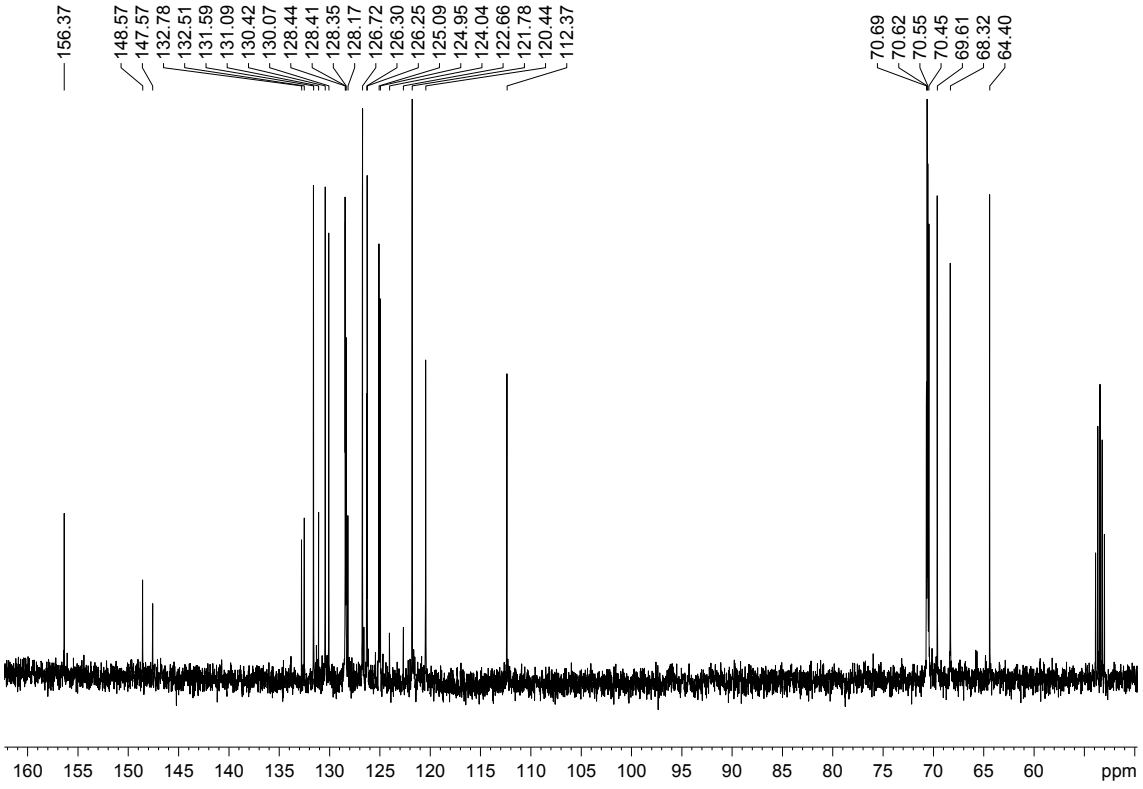

^{31}P NMR spectrum of compound **46c:**

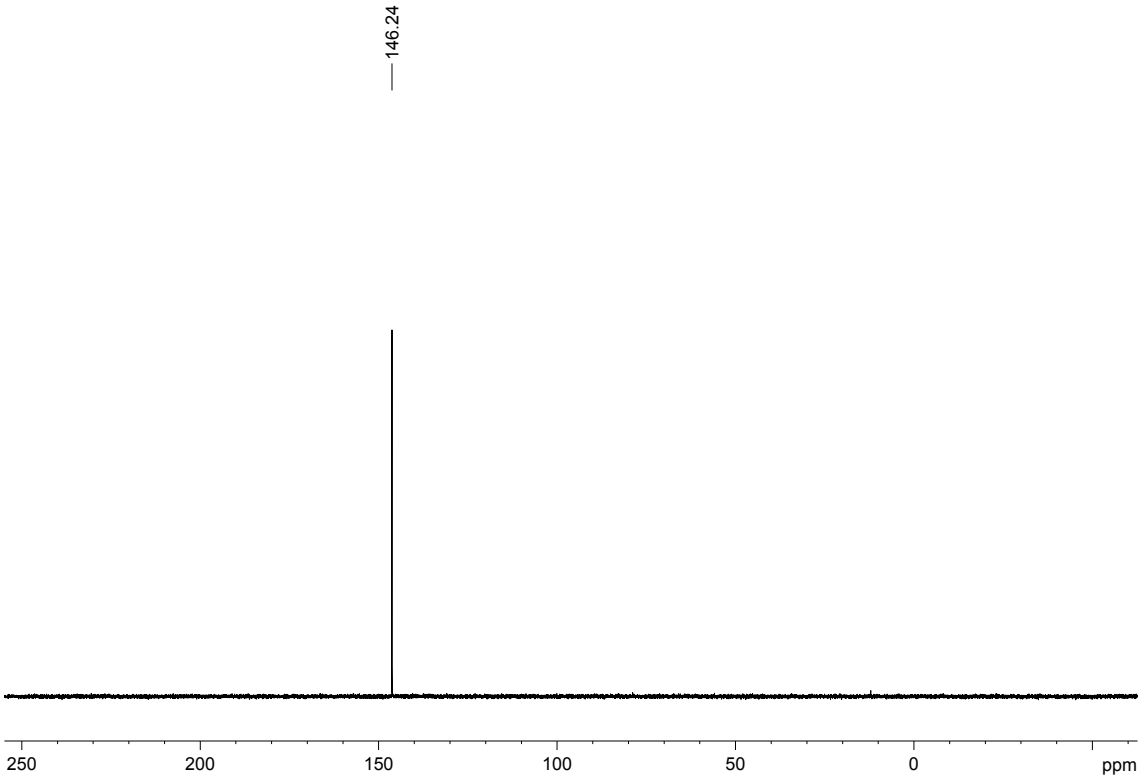

^{1}H NMR spectrum of compound **46d:**

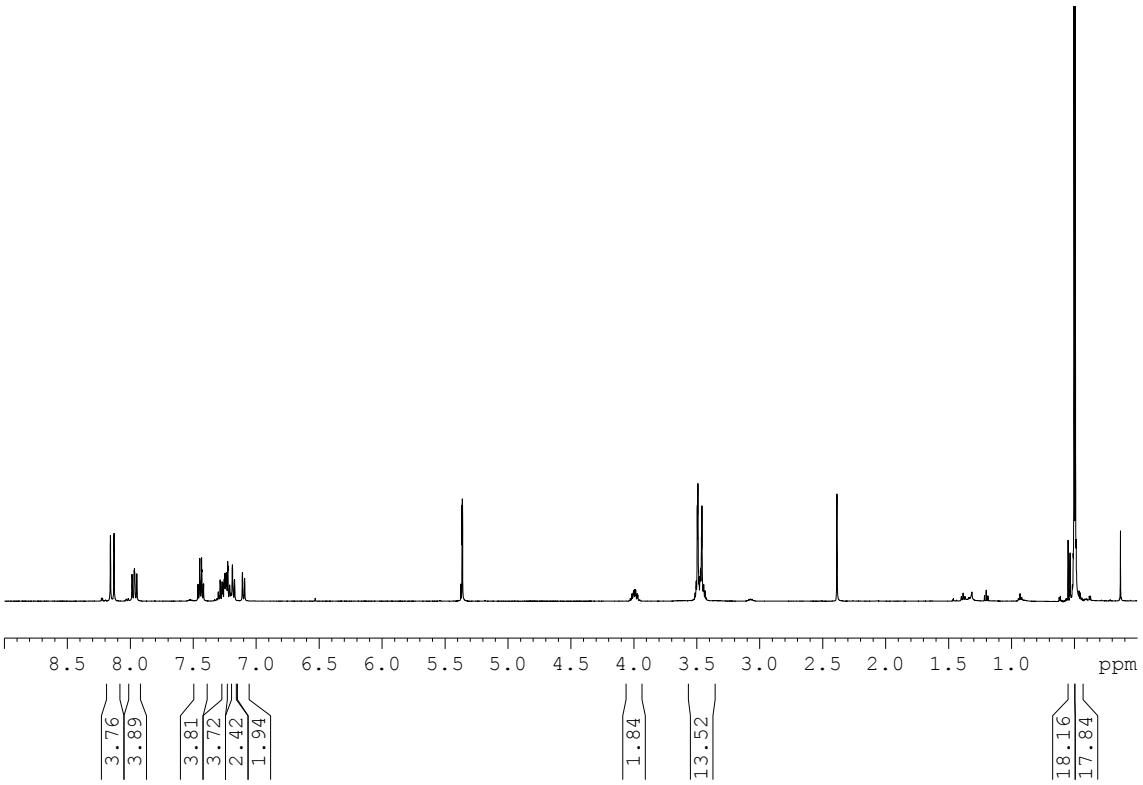

^{13}C{^{1}H,^{31}P} NMR spectrum of compound **46d:**

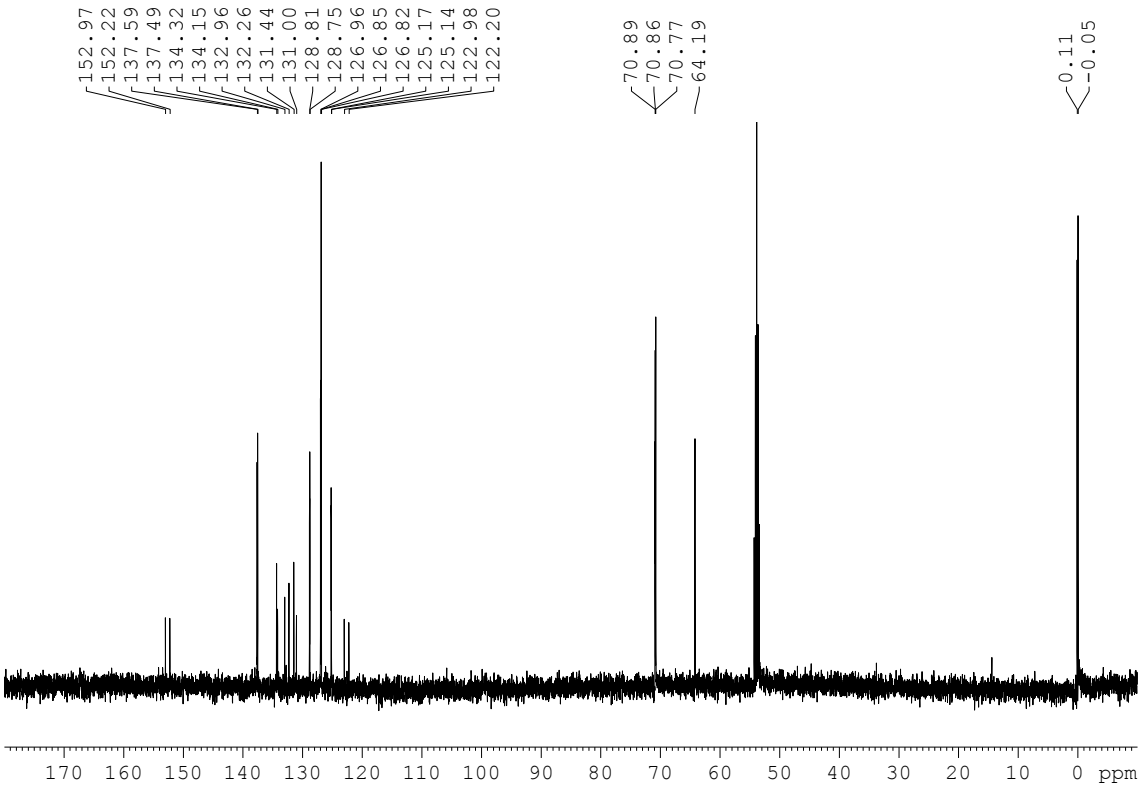

^{31}P NMR spectrum of compound **46d:**

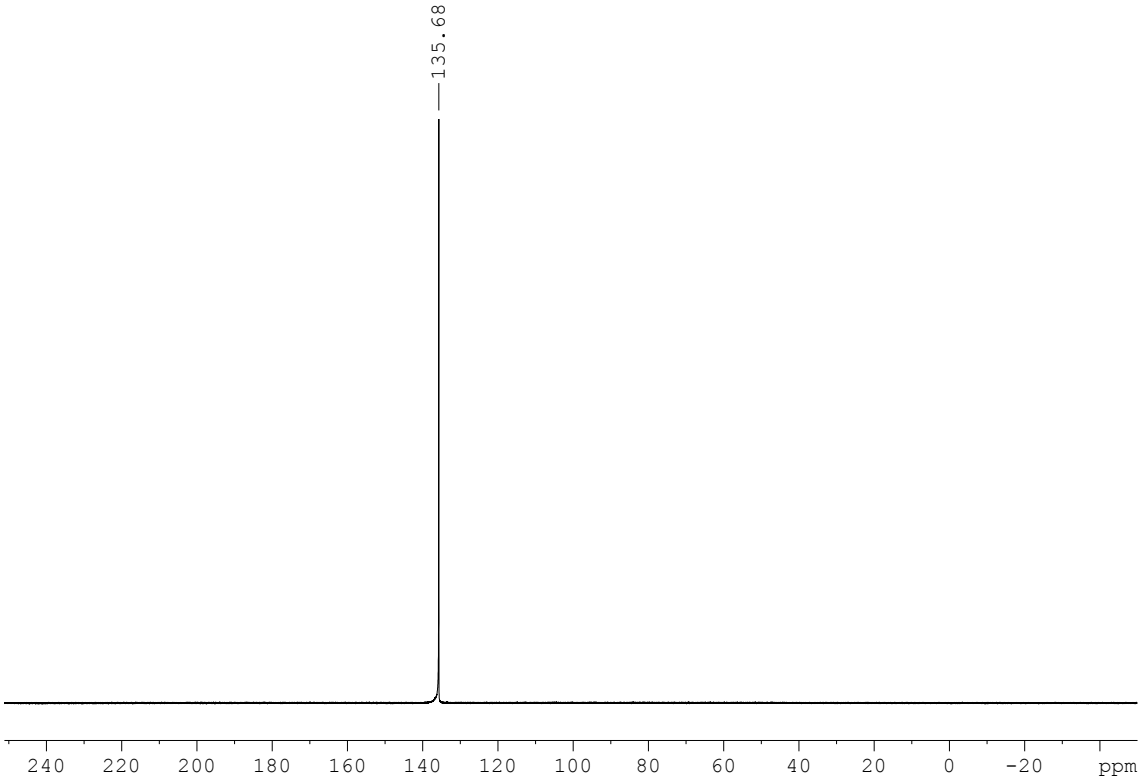

^{1}H NMR spectrum of compound **46f:**

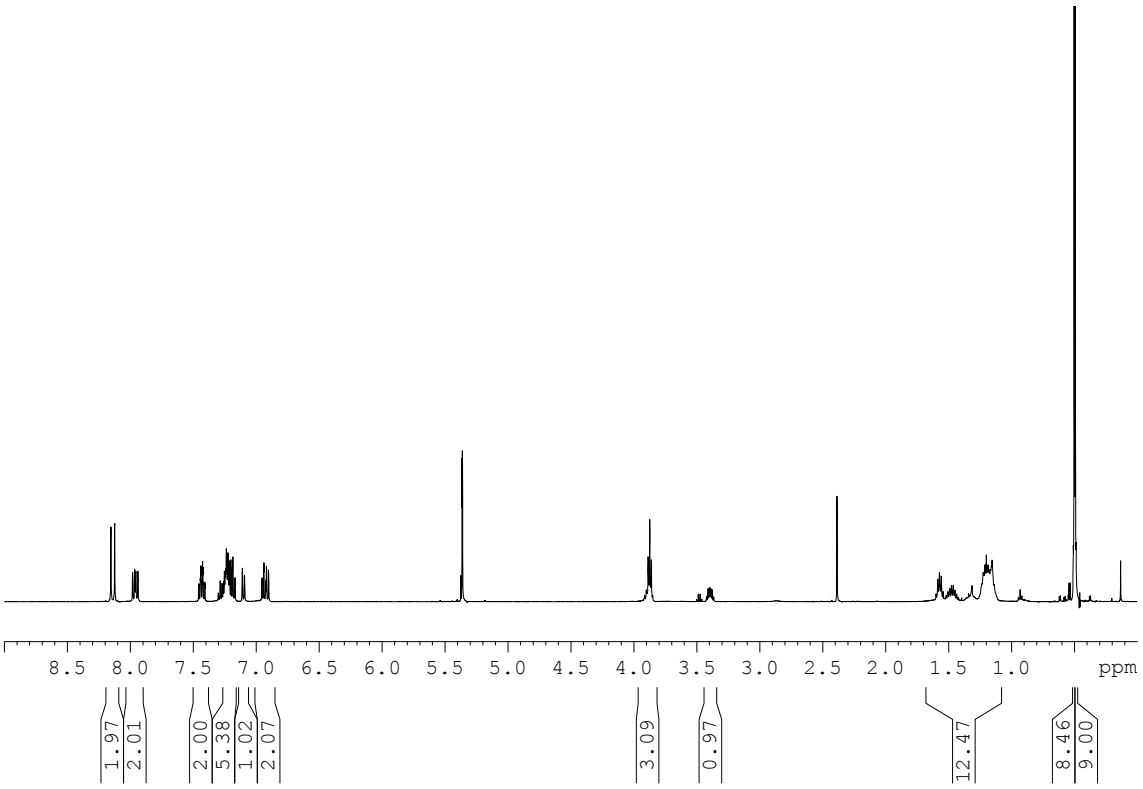

$^{13}C\{^{1}H,^{31}P\}$ NMR spectrum of compound **46f:**

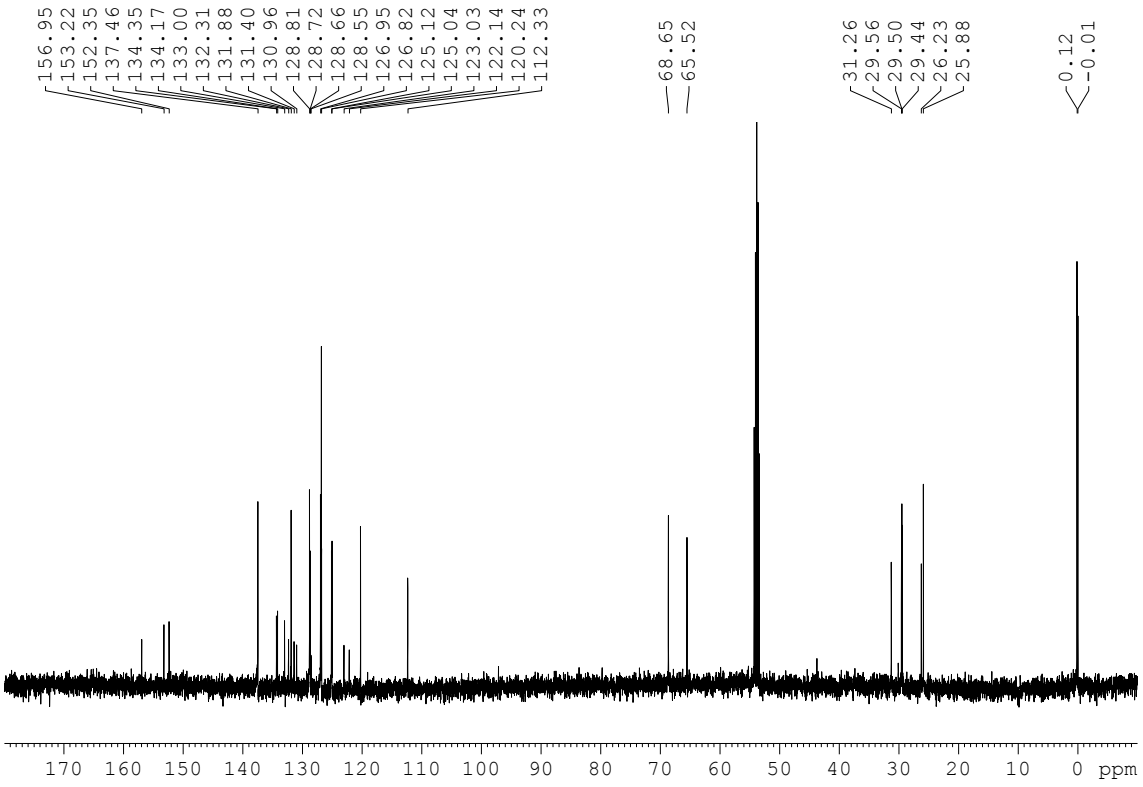

^{31}P NMR spectrum of compound **46f:**

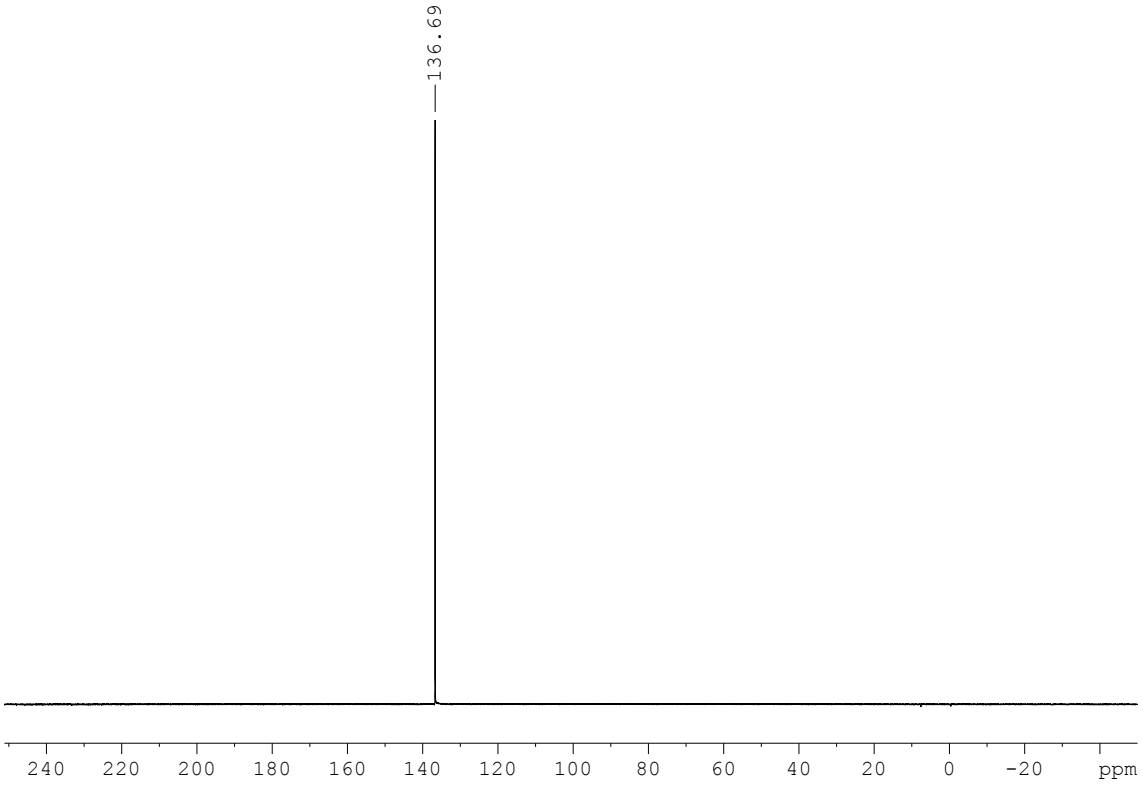

^{1}H NMR spectrum of compound **46g:**

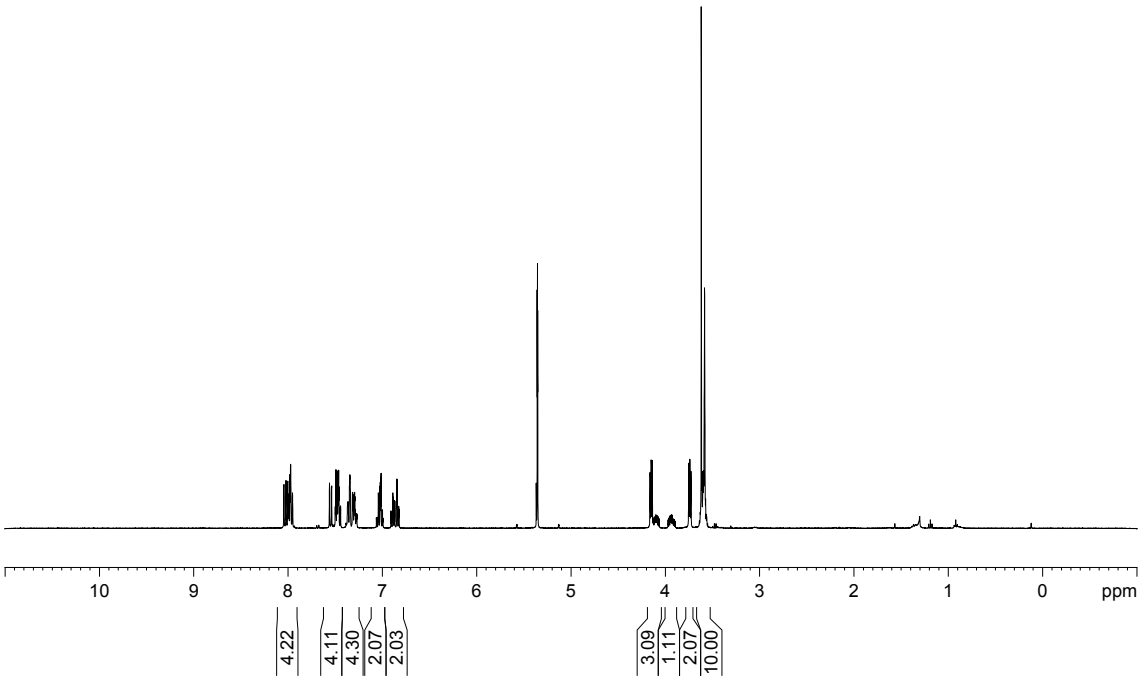

^{13}C{^{1}H,^{31}P} NMR spectrum of compound **46g:**

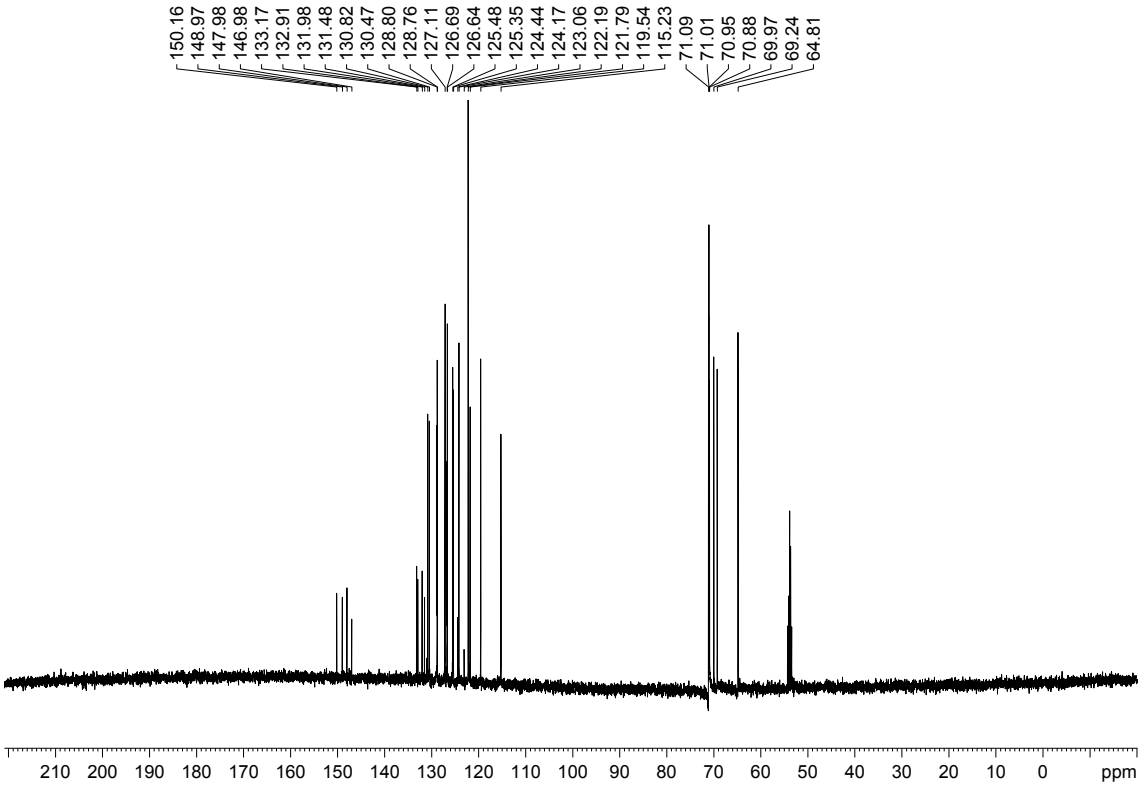

^{31}P NMR spectrum of compound **46g:**

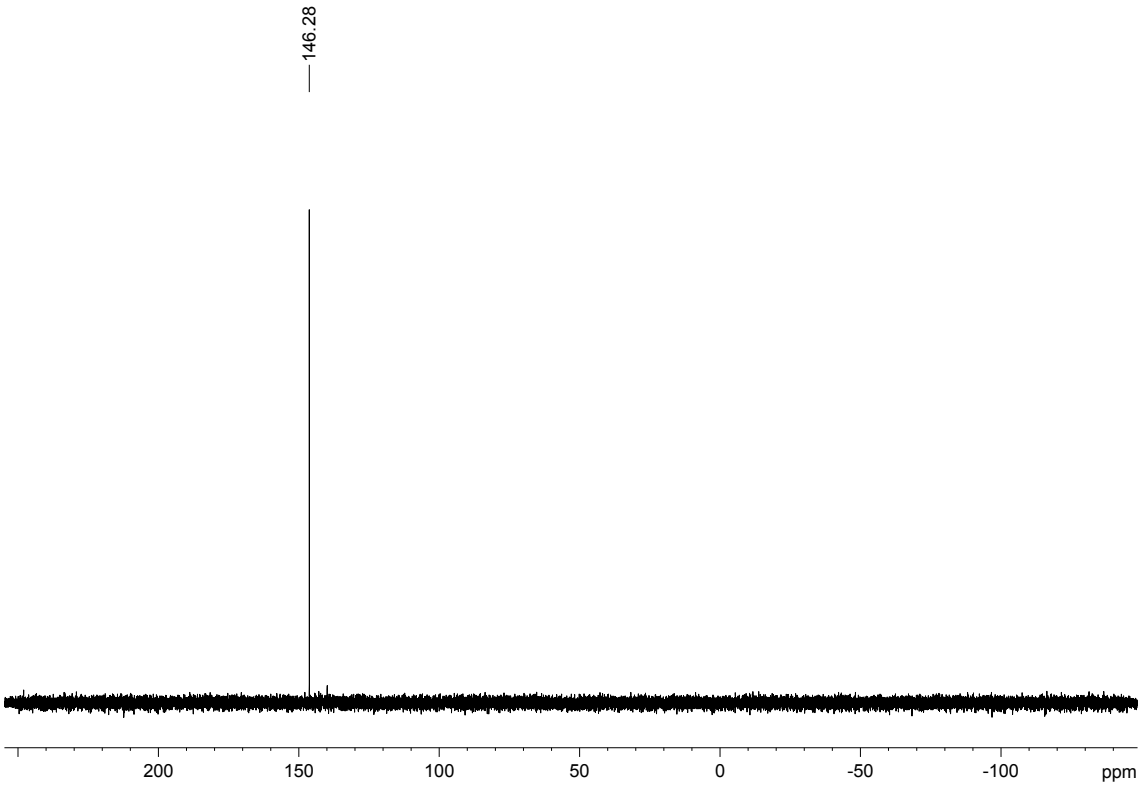

^{1}H NMR spectrum of compound **46h:**

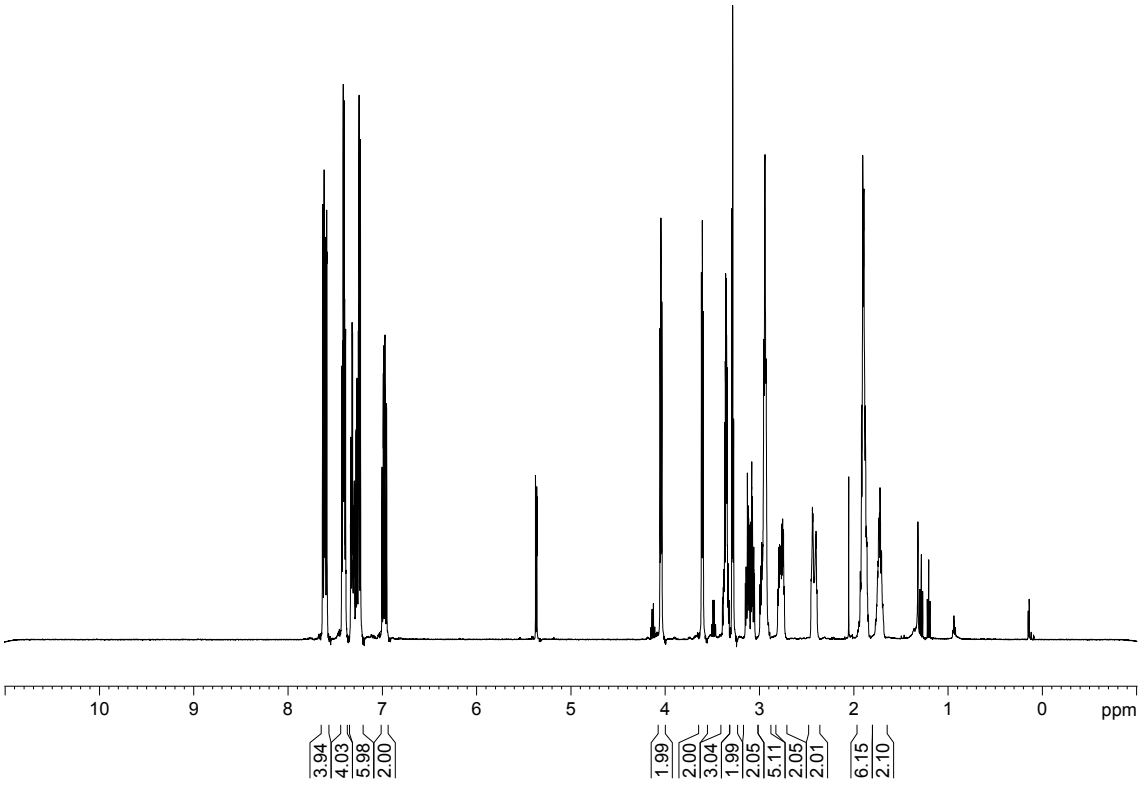

$^{13}C\{^{1}H,^{31}P\}$ NMR spectrum of compound **46h:**

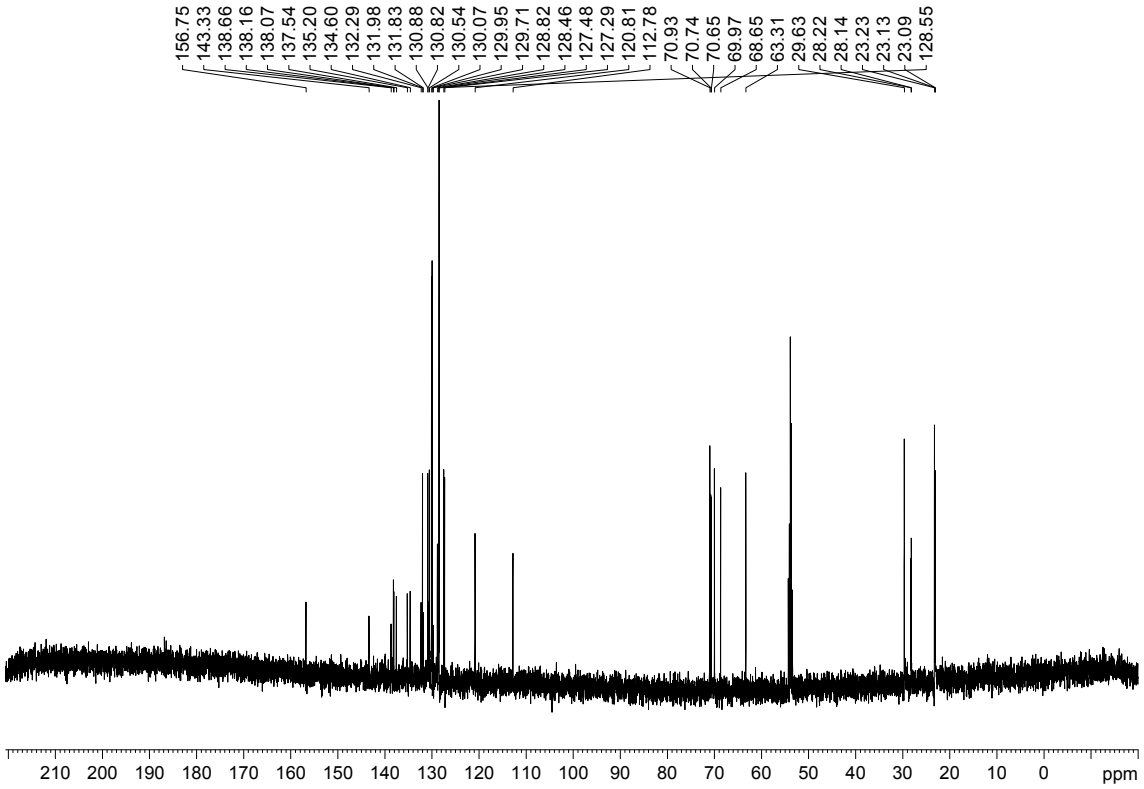

^{31}P NMR spectrum of compound **46h:**

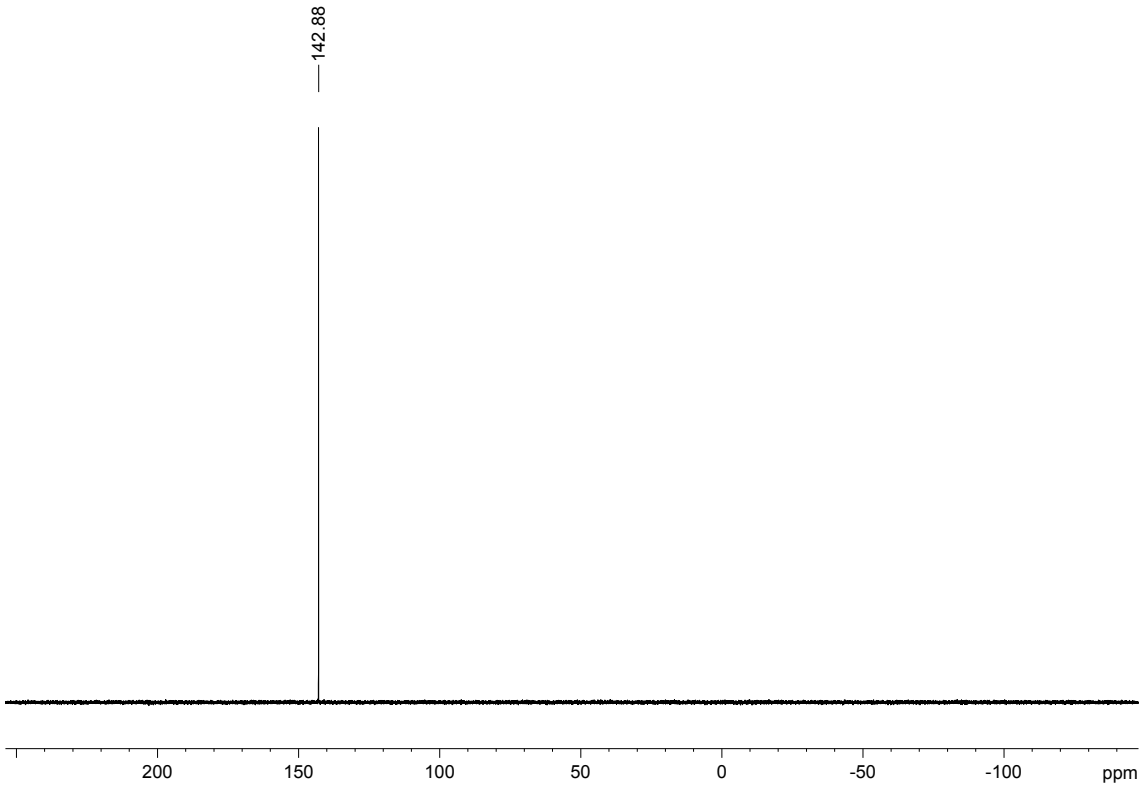

^{1}H NMR spectrum of compound **46i:**

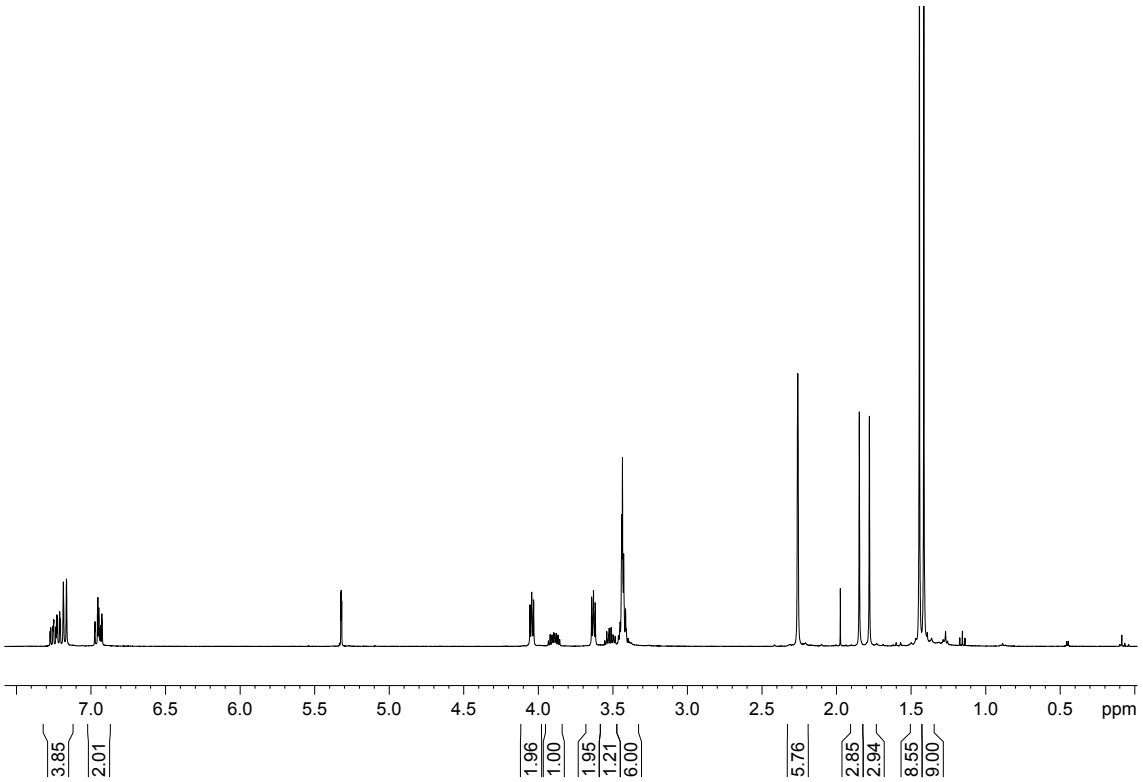

^{13}C{^{1}H,^{31}P} NMR spectrum of compound **46i:**

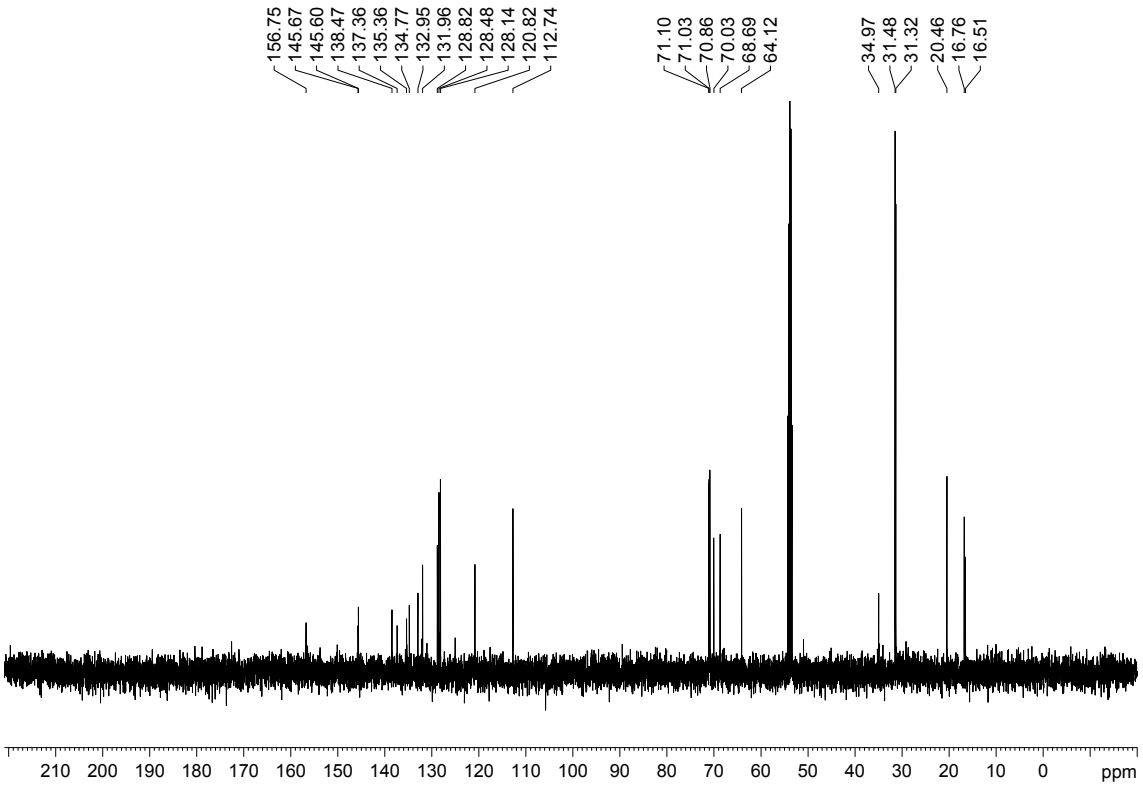

^{31}P NMR spectrum of compound **46i:**

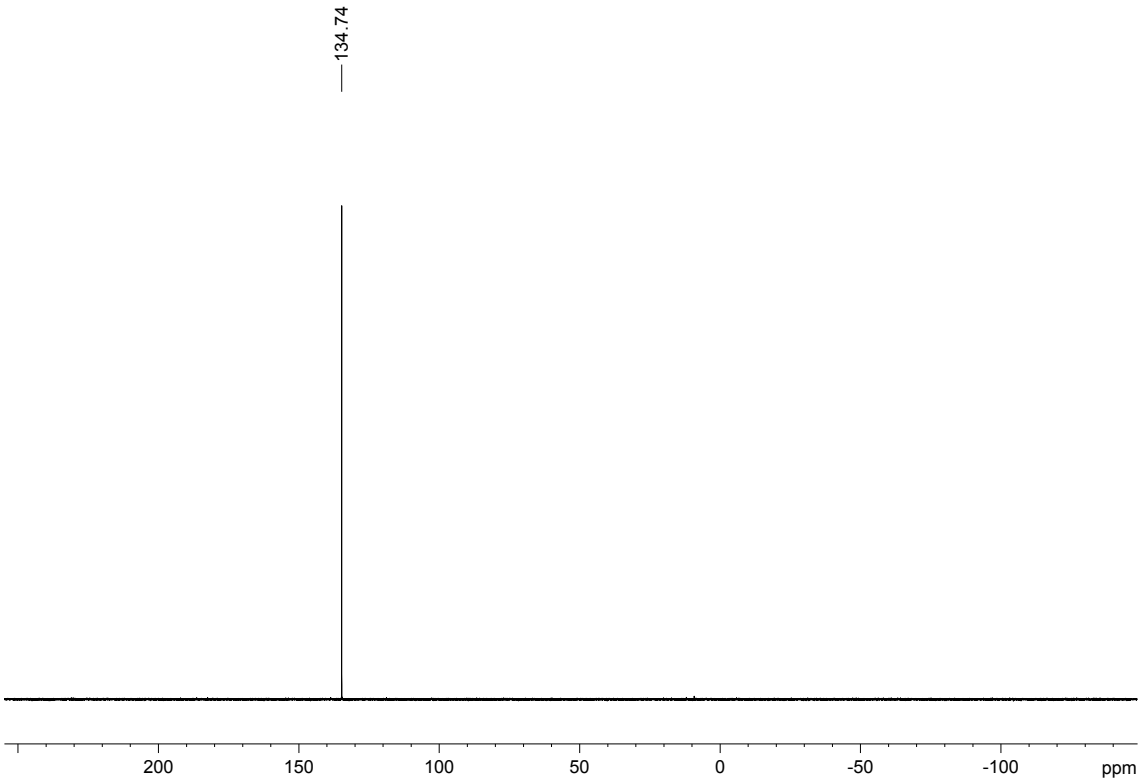

^{1}H NMR spectrum of compound (*rac*)-**81a:**

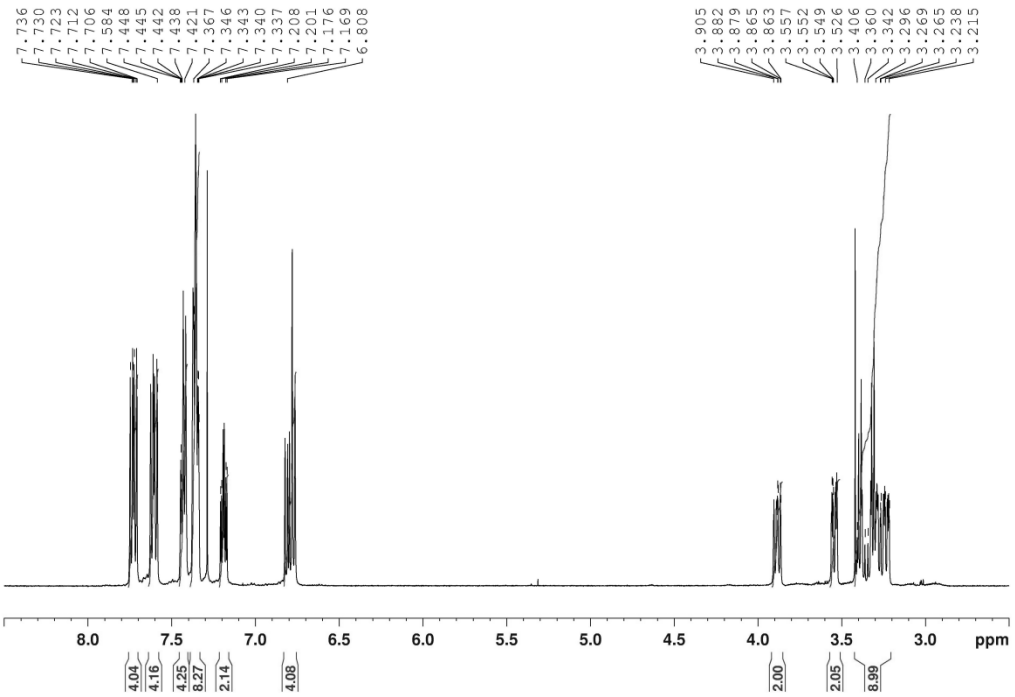

$^{13}C\{^{1}H,^{31}P\}$ NMR spectrum of compound (*rac*)-**81a:**

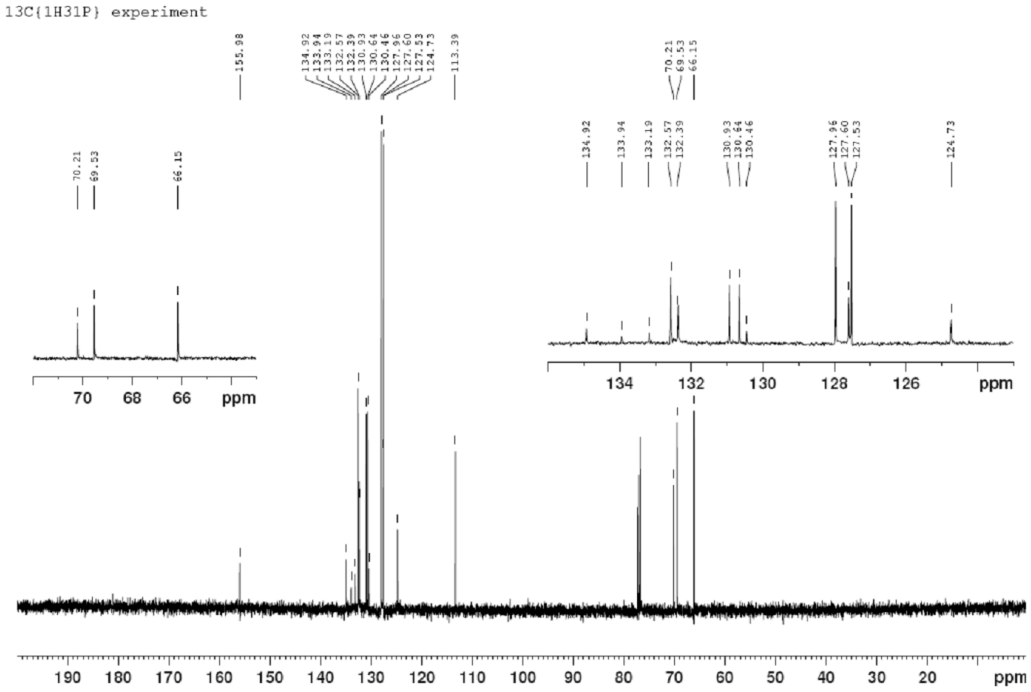

^{1}H NMR spectrum of compound (*rac*)-**81b:**

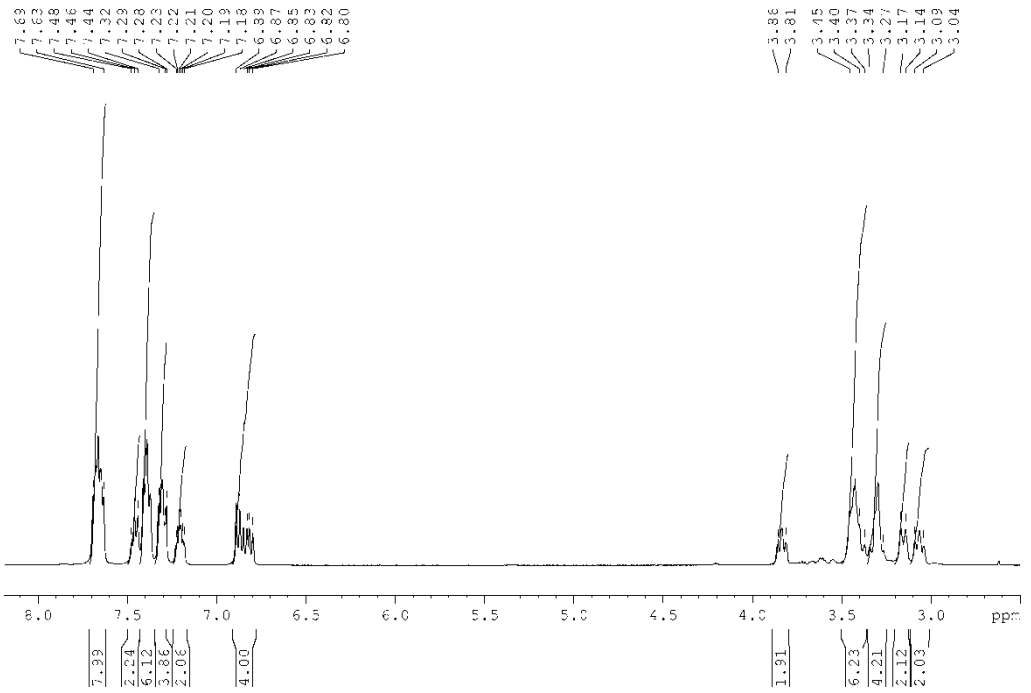

$^{13}C\{^{1}H,^{31}P\}$ NMR spectrum of compound (*rac*)-**81b:**

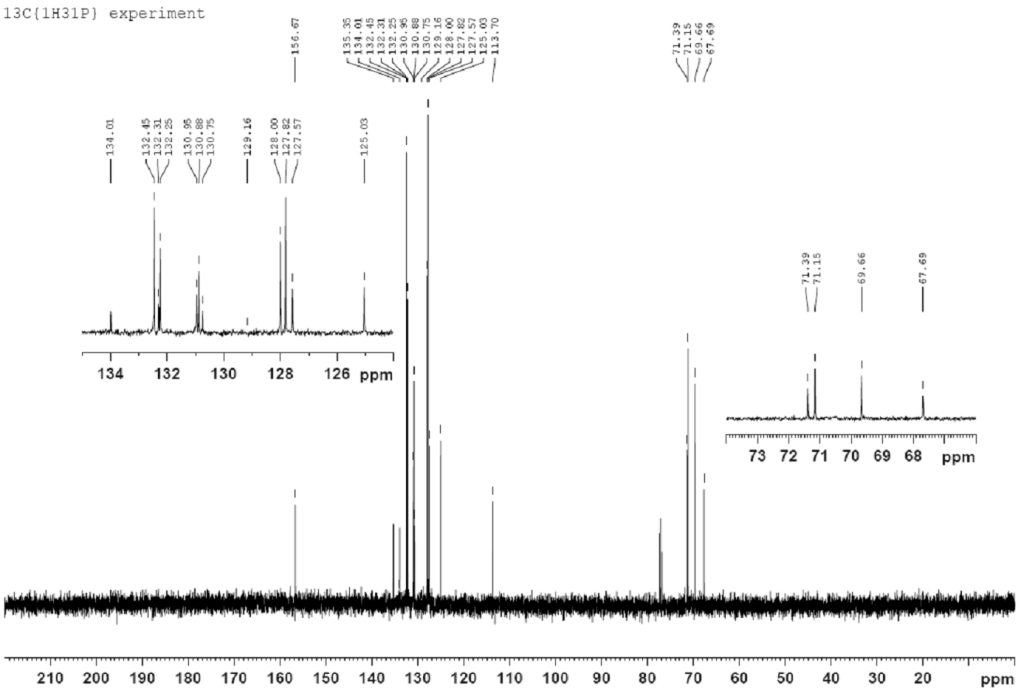

^{1}H NMR spectrum of compound (*rac*)-**81c:**

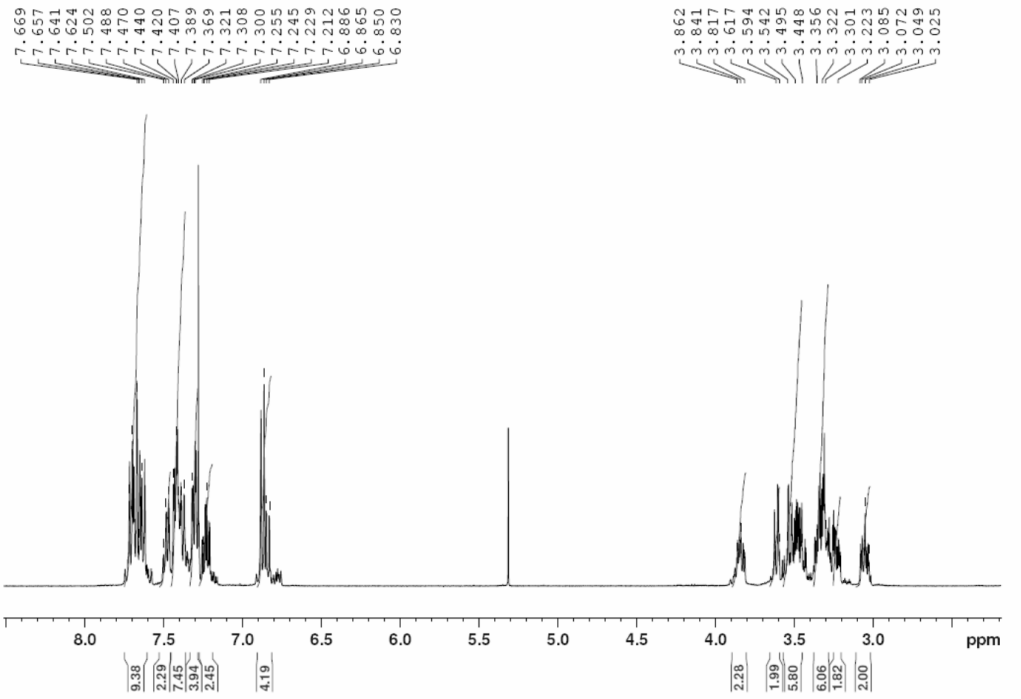

$^{13}C\{^{1}H,^{31}P\}$ NMR spectrum of compound (*rac*)-**81c:**

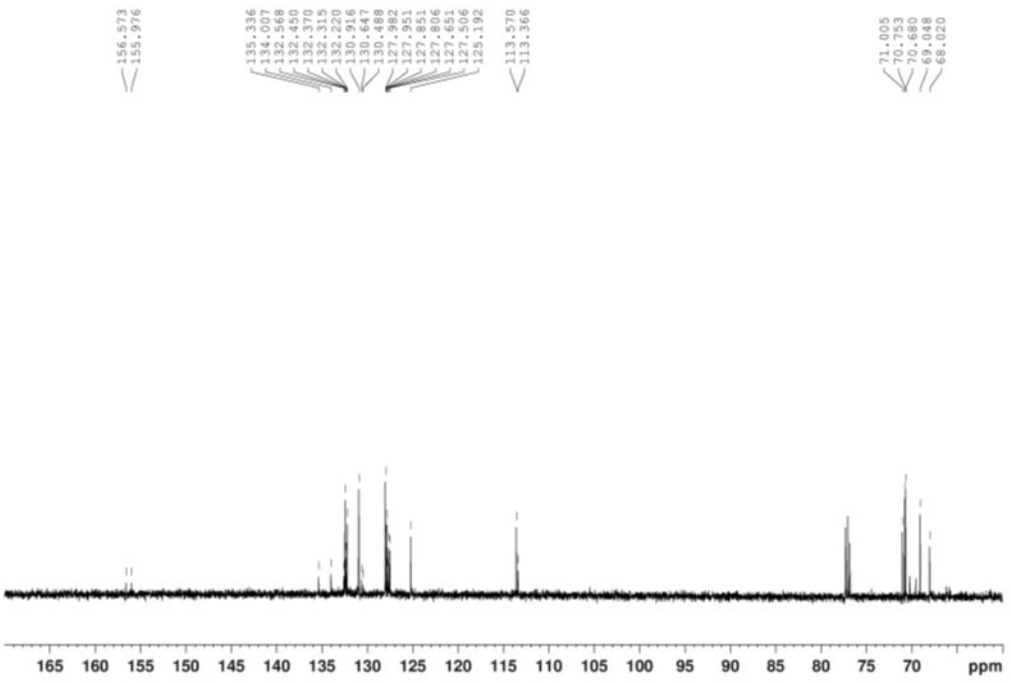

^{1}H NMR spectrum of compound (*rac*)-**81d:**

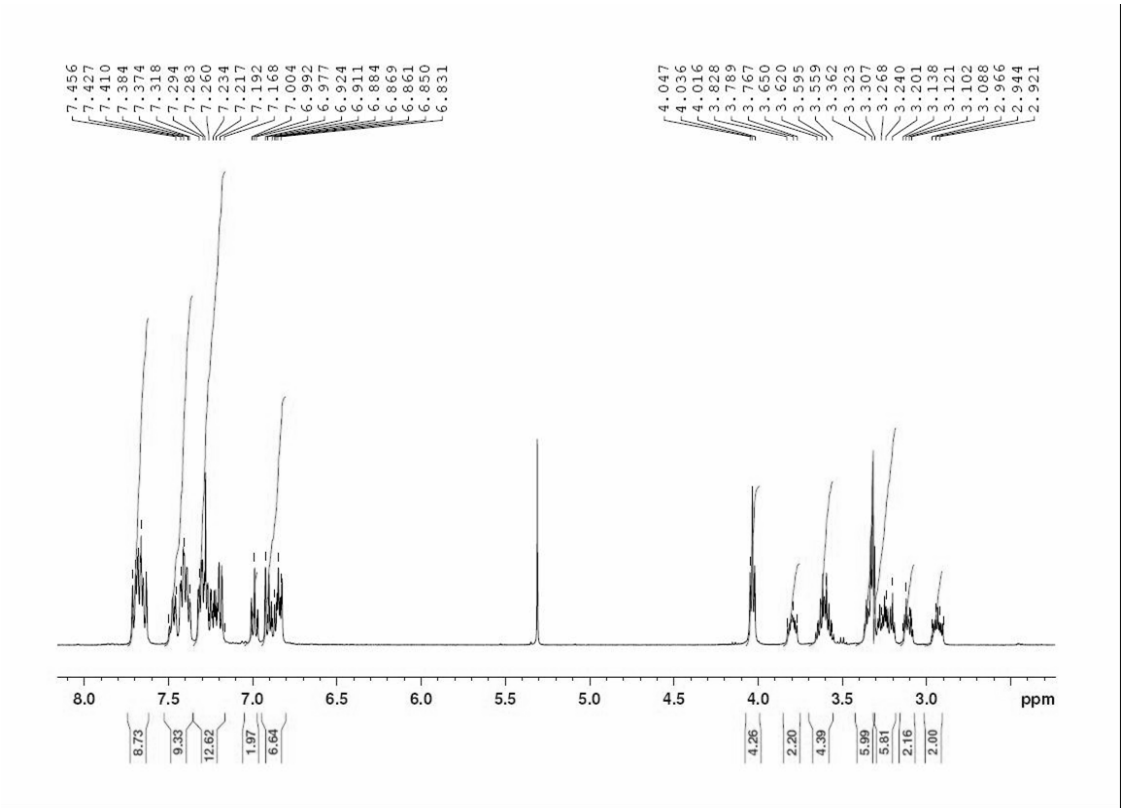

$^{13}C\{^{1}H,^{31}P\}$ NMR spectrum of compound (*rac*)-**81d:**

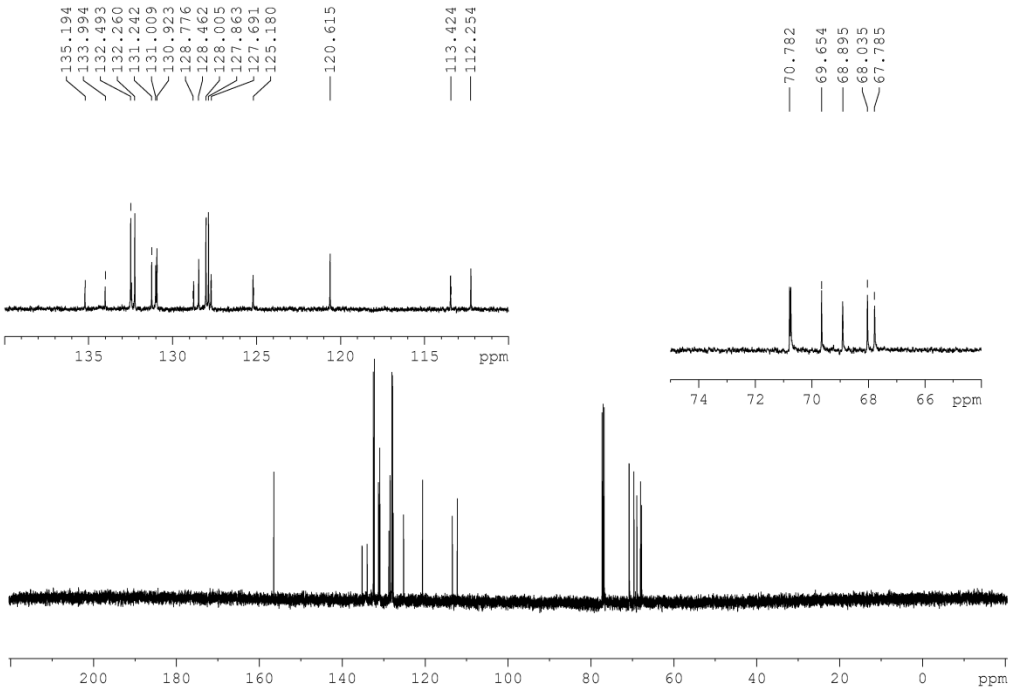

^{1}H NMR spectrum of compound (*rac*)-**81e:**

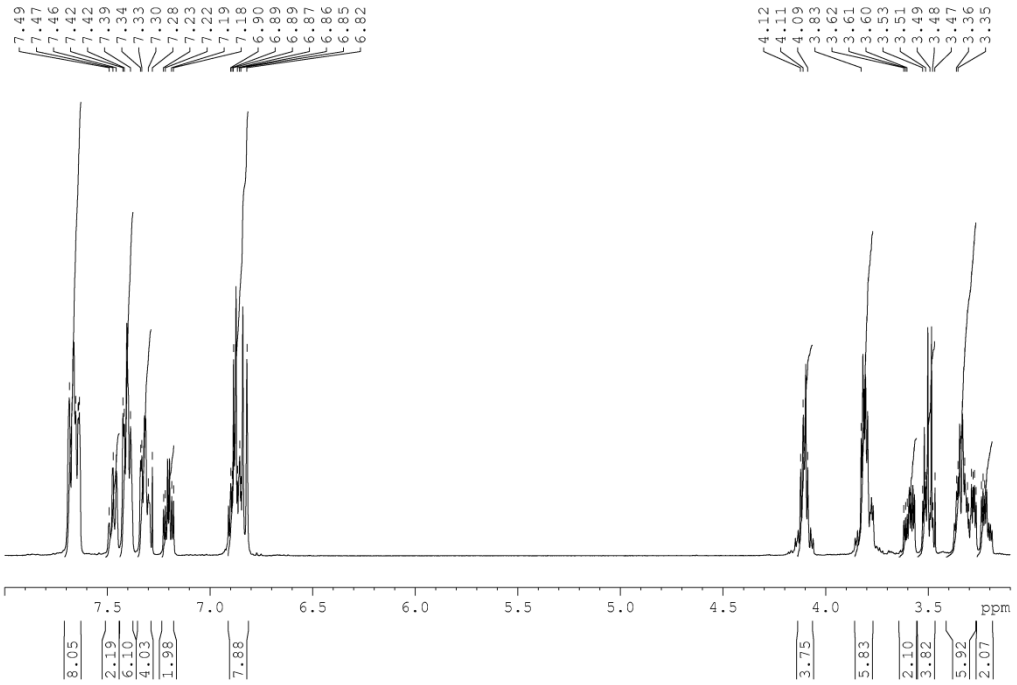

$^{13}C\{^{1}H,^{31}P\}$ NMR spectrum of compound (*rac*)-**81e:**

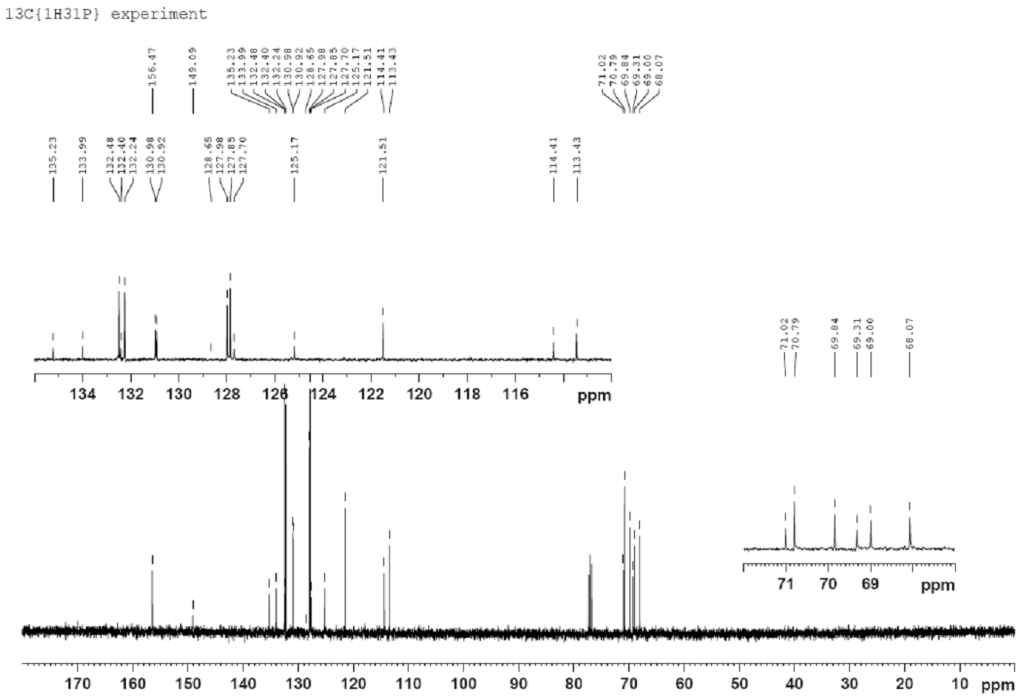

^{1}H NMR spectrum of compound (*R*)-**93:**

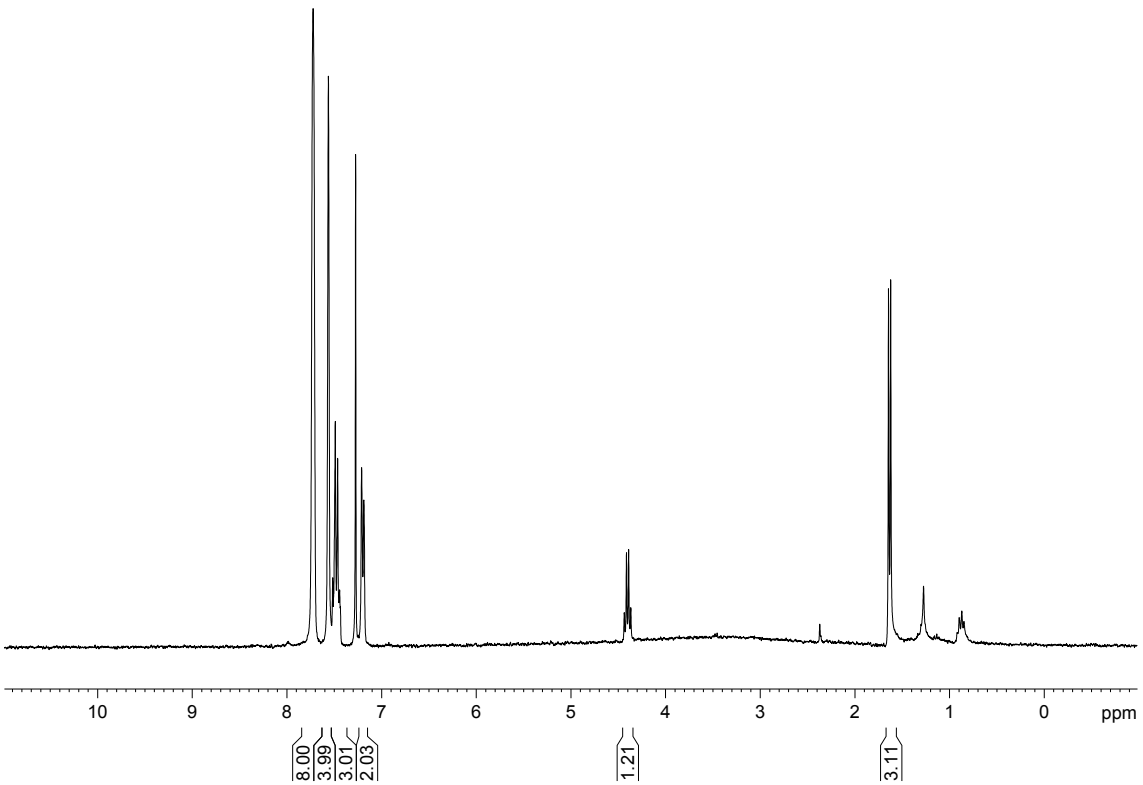

$^{13}C\{^{1}H\}$ NMR spectrum of compound (*R*)-**93:**

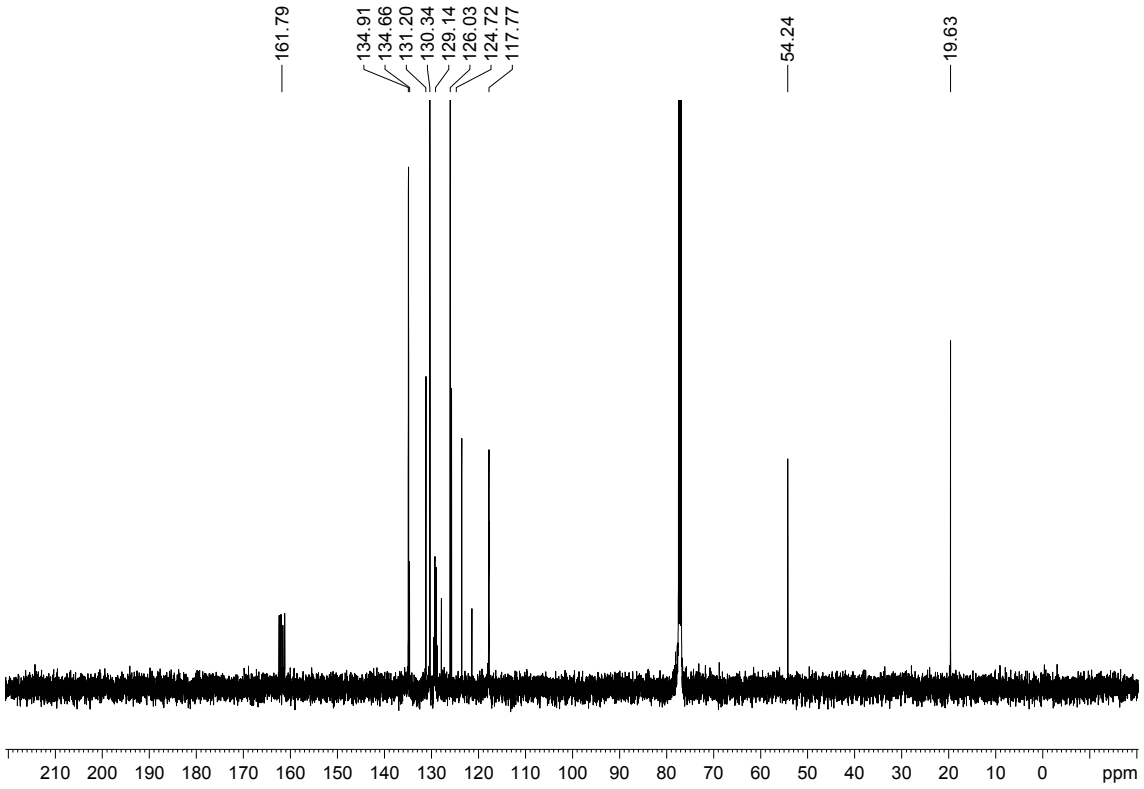

^{1}H NMR spectrum of compound (*R,R*)-**94:**

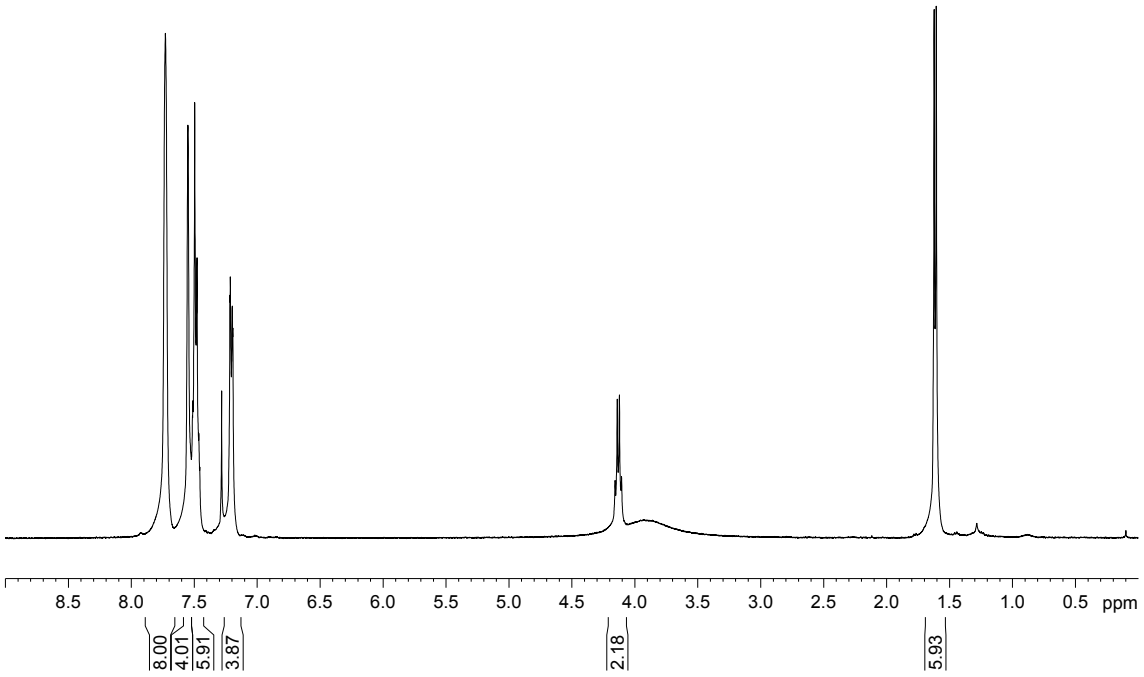

$^{13}C\{^{1}H\}$ NMR spectrum of compound (*R,R*)-**94:**

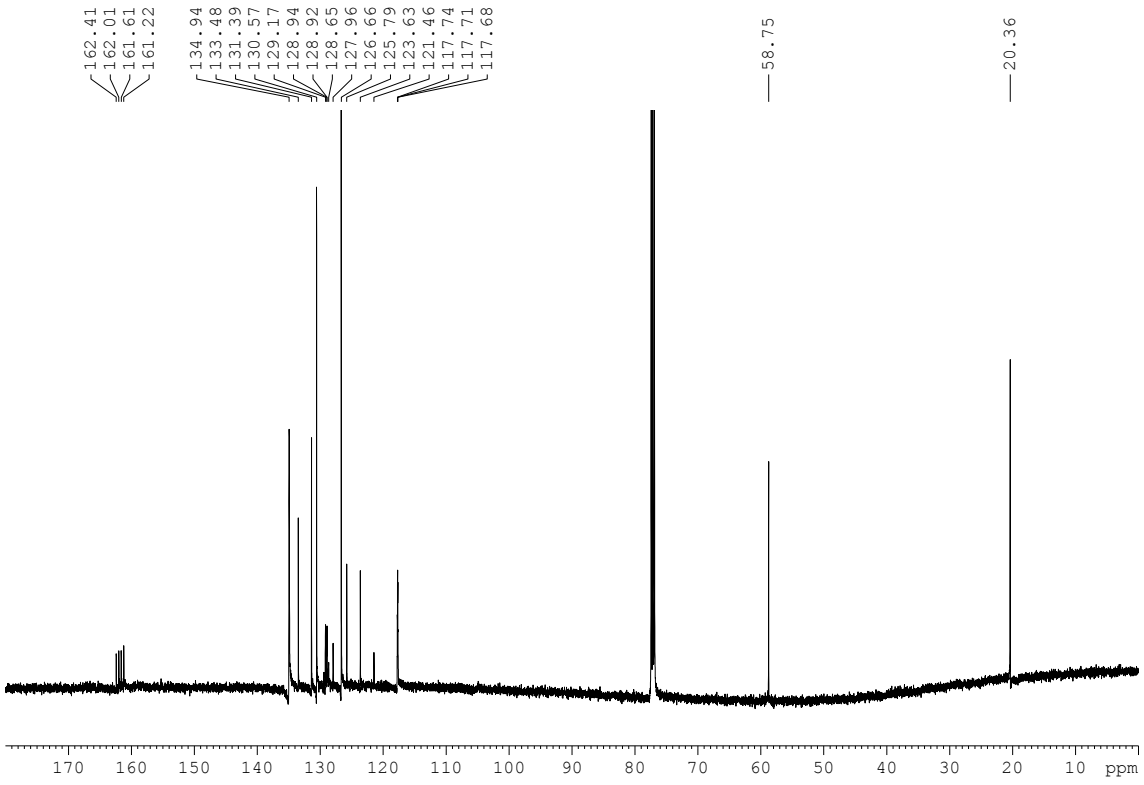

II. X-RAY STRUCTURE DATA

Compound	(*rac*)-**45a**
Formula	$C_{42}H_{38}O_4P_2$
Formula weight	668.66
Crystal size (mm^3)	0.10x0.10x0.03
Crystal color	Colorless
Crystal system	Monoclinic
Space group	P2(1)/n
a (Å)	12.508(2)
b (Å)	16.721(3)
c (Å)	16.132(4)
α (deg)	90.00 °
β (deg)	93.820(9) °
γ (deg)	90.00 °.
Volume ($Å^3$)	3366.4(12)
Z	4
ρ (g/cm^3)	1.319
μ (mm^{-1})	0.173
θ_{max} (°)	30.81
Reflec. measured	10216
Unique reflections	6584 [R_{int} = 0.0797]
Absorpt. correct.	Empirical
Trans. min/max	0.9948/0.9829
R1/wR2 [I>2σ(I)]	0.0503 / 0.1098
R1/wR2 [all data]	0.0956 / 0.1312
Goodness-of-fit (F^2)	1.008
Peak/hole ($e/Å^3$)	0.569 / -0.413

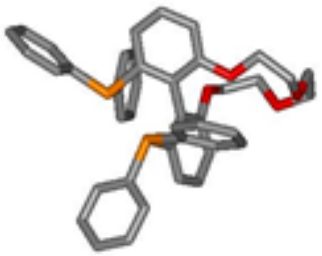

Figure 168. X-ray structure of (*rac*)-**45a**

Compound	(*rac*)-**81a**	(*rac*)-**81b**	(*rac*)-**81c**
Formula	$C_{42}H_{38}O_6P_2$	$C_{44}H_{43}O_7P_2$	$C_{46}H_{46}O_8P_2$
Formula weight	700.66	744.24	788.77
Crystal size (mm^3)	0.20 x 0.20 x 0.03	0.20 x 0.05 x 0.01	0.50 x 0.40 x 0.30
Crystal color	Colorless	Colorless	Colorless
Crystal system	monoclinic	orthorhombic	Monoclinic
Space group	P2(1)/n	Pbca	P2(1)/c
a (Å)	12.4330(10)	20.497(9)	14.5572(11)
b (Å)	17.0318(14)	16.860(4)	14.0426(9)
c (Å)	16.3075(14) Å	21.701(11)	19.6973(19)
α (deg)	90	90	90
β (deg)	95.204(2)	90	103.384(4)
γ (deg)	90	90	90
Volume ($Å^3$)	3439.0(5)	7499(5)	3917.2(5)
Z	4	15	4
ρ (g/cm^3)	1.353	1.319	1.337
μ (mm^{-1})	0.177	0.169	0.167
θ_{max} (°)	36.97	25.37	36.31
Reflec. measured	16911	6348	17679
Unique reflections	12898 [R_{int} =0.0392]	3082 [R_{int} = 0.1774]	11164 [R_{int} = 0.0445]
Absorpt. correct.	Empirical	Empirical	Empirical
Trans. min/max	0.9655/0.9947	0.9671/0.9983	0.9210/0.9515
R1/wR2 [I>2σ(I)]	0.0464 / 0.1213	0.0679 / 0.1231	0.0583 / 0.1499
R1/wR2 [all data]	0.0660/ 0.1327	0.1720 /0.1622	0.1024/ 0.1753
Goodness-of-fit (F^2)	1.053	0.952	1.046
Peak/hole ($e/Å^3$)	0.720 /-0.254	0.489 /-0.408	0.636 / -0.592

Compound	(*rac*)-**81d**	(*rac*)-**81e**	(*rac*)-**81b**•oxalic
Formula	$C_{60}H_{58}O_{10}P_2$	$C_{56}H_{59}O_{10}P_2$	$C_{46}H_{44}O_{11}P_2$
Formula weight	1000.33	961.97	834.75
Crystal size (mm^3)	0.40 x 0.40 x 0.30	1.00 x 0.60 x 0.40	0.40 x 0.20 x 0.15
Crystal color	Colorless	Colorless	Colorless
Crystal system	Triclinic	Monoclinic	Monoclinic
Space group	P-1	P2(1)/n	P2(1)/n
a (Å)	14.7422(6)	13.9857(4)	11.6798(6)
b (Å)	15.6498(6)	17.0527(5)	21.8055(11)
c (Å)	25.5926(10)	20.7173(5)	16.6189(7)
α (deg)	103.740(2)	90	90
β (deg)	93.977(2)	99.004(2)	104.011(2)
γ (deg)	108.190(2)	90	90
Volume ($Å^3$)	5382.7(4)	4880.1(2)	4106.6(3)
Z	2	4	4
ρ (g/cm^3)	1.295	1.309	1.350
μ (mm^{-1})	0.143	0.151	0.169
θ_{max} (°)	32.98	36.39	30.08
Reflec. measured	37806	23162	11841
Unique reflections	28567 [R_{int} = 0.0286]	14295 [R_{int} = 0.0395]	8226 [R_{int} = 0.0562]
Absorpt. correct.	Empirical	Empirical	Empirical
Trans. min/max	0.9450/0.9583	0.8637/0.9421	0.9355/0.9751
R1/wR2 [I>2σ(I)]	0.0583 / 0.1537	0.0658 / 0.1791	0.0630 / 0.1587
R1/wR2 [all data]	0.0809 / 0.1757	0.1114 /.2133	0.0955 / 0.1793
Goodness-of-fit (F^2)	1.042	0.987	1.036
Peak/hole ($e/Å^3$)	0.840 / -0.973	0.995 / -0.898	1.009 / -0.469

SUMMARY IN CATALAN

SUMMARY IN CATALAN

En la present tesi s'ha estudiat el disseny, la síntesi i l'aplicació en catàlisi asimètrica o reconeixement molecular de tres noves famílies de lligands i receptors amb potencial per a la regulació de la seva activitat o afinitat per interaccions supramoleculars de tipus ió-dipol amb espècies catiòniques (E^+). Concretament, s'ha preparat: a) Una família de lligands enantiopurs de tipus bisfosfit que s'ha aplicat en hidrogenació i hidroformilació asimètrica mediada per rodi **46**. b) Una família de lligands enantiopurs de tipus bisfosfina que s'ha aplicat en hidrogenació asimètrica **45** i c) una família de receptors amb regulació distal en forma racèmica de tipus òxid de bisfosfina per a reconeixement de molècules neutres mitjançant enllaços d'hidrogen **81** (Figura 1).

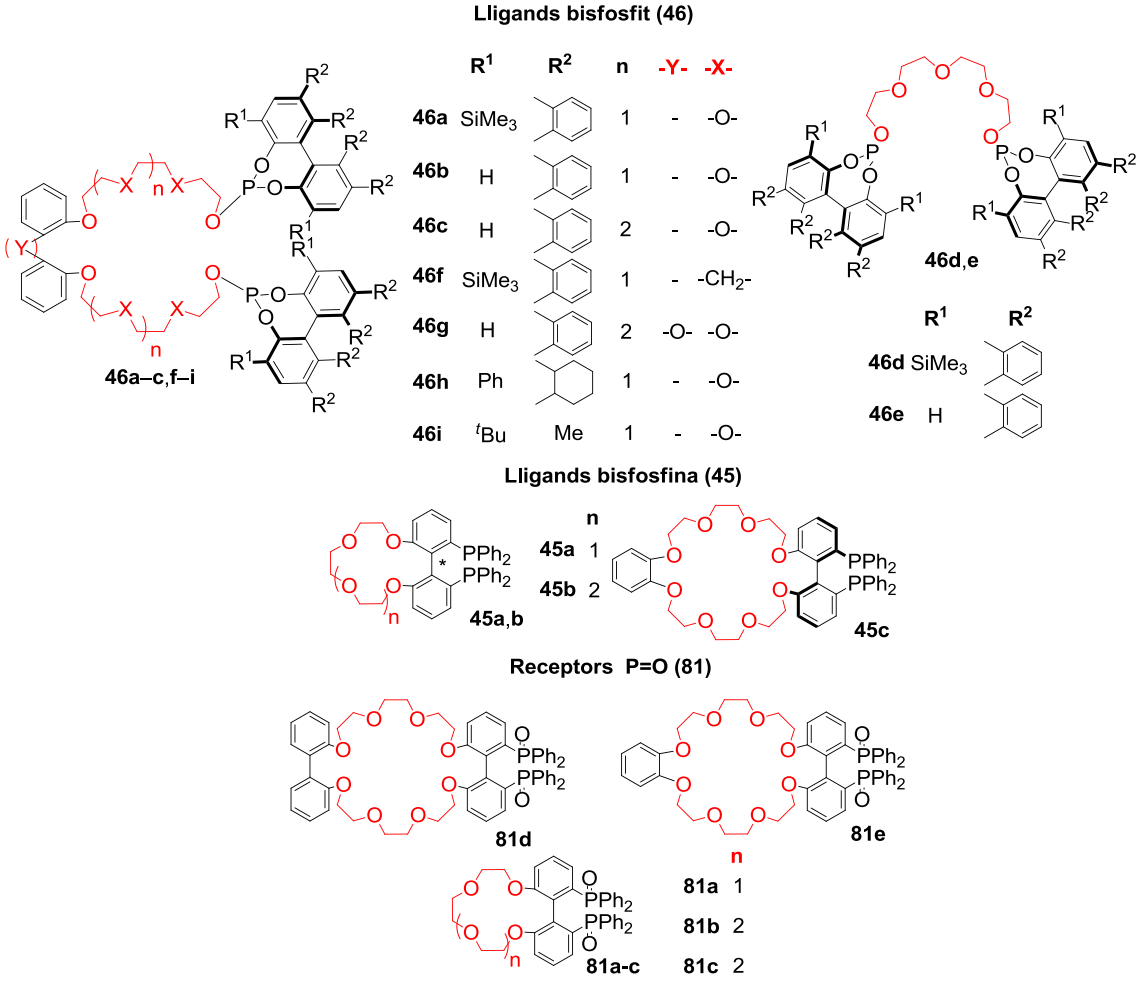

Figura 1. Lligands supramoleculars enantiopurs tipus bisfosfit **46**, bisfosfina **45** i receptors en forma racèmica **81**

Tant en el cas dels receptors **81** com en el cas dels lligands sintetitzats **45** i **46**, la part responsable de la regulació de la seva activitat a través d'interaccions supramoleculars amb cations és la cadena polioxietilènica present en les diferents estructures (en vermell). No obstant, el sistema de regulació proposat difereix segons les diferents famílies preparades. Així, pels cas dels bisfosfits **46** la introducció d'espècies catiòniques (E^+) té dos efectes: a) Efecte plantilla que orienta els grups fosfit per a la coordinació d'aquests al centre actiu de rodi i facilita la generació d'espècies

quelat per a la catàlisi asimètrica. b) Depenent de les característiques de l'espècie introduïda, com la mida del catió, el lligand pot patir canvis de flexibilitat i geometria que afecten l'estructura final del catalitzador, variant d'aquesta manera l'activitat catalítica d'aquest (Esquema 1).

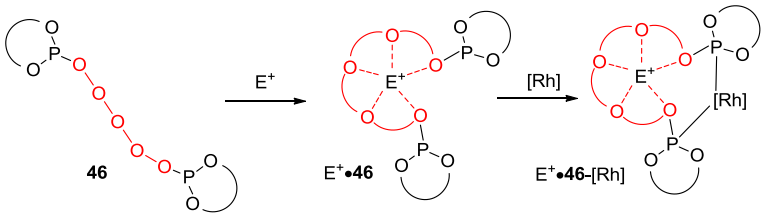

Esquema 1. Estratègia de modulació supramolecular amb els bisfosfits **46**

D'altra banda, l'estratègia per a la modulació de l'afinitat dels receptors **81** i l'activitat dels lligands **45** és diferent. Aquesta està basada en la possibilitat de variar l'angle diedre del bifenil present a l'estructura a través de la coordinació de diferents cations (E^+) en els èters corona directament units a aquest. En el cas dels lligands **45** aquest canvi geomètric tindria com a conseqüència immediata la variació del "bite angle", que ha demostrat ser un factor de màxima importància en la catàlisi asimètrica. D'una manera anàloga, els receptors **81** també veurien afectada l'afinitat a diferents substrats degut al canvi geomètric que afectaria els grups responsables del reconeixement molecular (P=O) (Esquema 2).

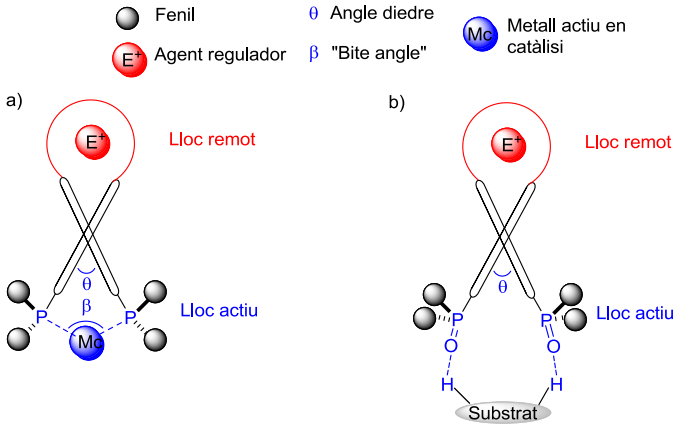

Esquema 2. Estratègia de modulació supramolecular amb a) els lligands **45** i b) els receptors **81**

Com a estudis previs, es van mesurar constants d'associació dels lligands i els receptors sintetitzats vers diferents espècies catiòniques amb diferents tècniques: espectrofotometria d'absorció (UV-vis), ressonància magnètica nuclear, espectrofotometria d'emissió (fluorescència) i/o tècniques calorimètriques. Es van trobar afinitats molt altes: *K* majors de 10^6 M^{-1} en el cas de lligands de la família **46** i sensiblement menors pels receptors **81** (*K ca.* 10^5 M^{-1}) amb cations alcalins. Aquesta afinitat dels receptors i dels lligands cap a espècies catiòniques permeten la total complexació dels receptors o lligands amb els cations (E^+) sense necessitat d'un gran excés d'aquests. D'altra banda, els grups fosfit o fosfina en el cas dels lligands **46** i **45**, respectivament, o fosforil (P=O) en el cas dels receptors **81** queden lliures per a processos coordinatius. Aquesta coordinació pot ser amb un metall de transició que

possibiliti la catàlisi en el cas dels lligands **45** i **46** o amb donadors de ponts d'hidrogen aprofitant el caràcter acceptor dels grups fosforil en els receptors **81**.

Els lligands de tipus bisfosfit **46c** i **46i** van demostrar ser molt efectius en la hidrogenació asimètrica de dobles enllaços C=C mediada per complexes de rodi derivats d'aquests lligands. Substrats de diferents famílies (**39**) com: dimetil itaconat **39a**, derivats de dehidro-α-aminoàcids **39b** i **39d**, α-arilenamides **39e,f,h** i el derivat de dehidro-β-aminoàcid **39g** van ser hidrogenats amb altes enantioselectivitats (92–99% ee). Es van obtenir millores apreciables en els excessos enantiomèrics obtinguts mitjançant l'adició de diferents cations (E^+), l'afinitat dels quals amb **46b** i **46e** s'havia demostrat en els estudis previs de complexació. Així es demostra que els catalitzadors de rodi derivats d'aquests lligands poden millorar la seva activitat catalítica mitjançant interaccions supramoleculars en un centre de regulació separat del centre catalític (Esquema 3).

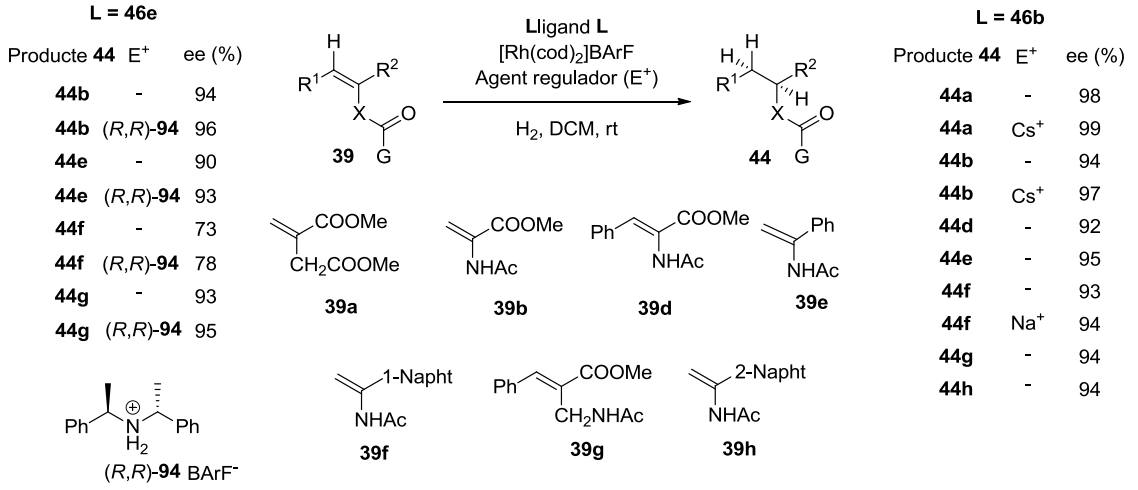

Esquema 3. Hidrogenació asimètrica de diferents substrats olefínics **39**

Aquests lligands bisfosfit (**46**) també van ser aplicats en la hidroformilació asimètrica de diferents alquens mediada per complexes de rodi derivats de **46**. En aquesta transformació, es demostra que en el cas dels substrats de tipus èster vinílic **6b**,**e**,**f**, l'adició de cations alcalins de la grandària adequada a la mida de la cavitat del lligand millora l'activitat, la regioselectivitat i l'enantioselectivitat del procés. El major increment en la enantioselectivitat va ser observat en la hidroformilació del benzoat de vinil **6f** amb el catalitzador de rodi derivat del lligand **46d**. De fet, **6f** és hidroformilat amb una enantioselectivitat molt baixa (14% ee), però si el lligand **46d** està prèviament complexat amb el catió Rb^+, l'excès enantiomèric del procés puja a un 96% (Esquema 4). S'aconsegueix, doncs, amb lligands de fàcil preparació, i mitjançant interaccions ió-dipol en un lloc allunyat del centre actiu del catalitzador, la modulació de l'activitat dels catalitzadors de rodi derivats. Obtenint, d'aquesta manera, resultats comparables o millors que els prèviament descrits a la literatura en hidroformilació asimètrica d'èsters de vinil.

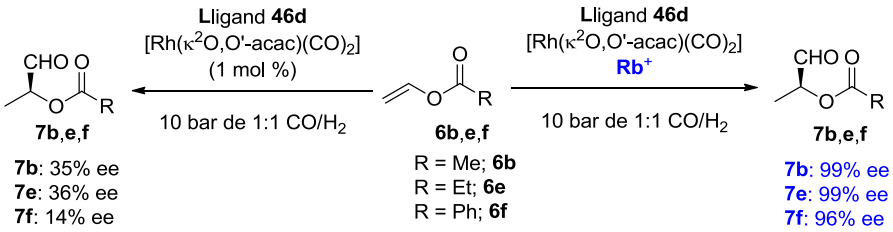

Esquema 4. Hidroformilació asimètrica d'èsters vinílics **6** amb i sense Rb^+

Els receptors **81** van demostrar tenir una alta afinitat per a àcids dicarboxílics; amb valors de *K* en DCM/MeOH (99.5/0.5 v/v) al voltant de 10^4 M^{-1} en gairebé tots els casos. Aquests àcids són reconeguts pels receptors sintetitzats a través de ponts d'hidrogen entre els protons carboxílics i els oxígens dels grups fosforil (P=O) (Figura 2). La coordinació d'agents catiònics (E^+) a la unitat èter corona va resultar en efectes reguladors positius, incrementant, en el millor dels casos fins a 7 vegades la *K* determinada sense agent regulador (E^+). Com a exemple representatiu, el gràfic de la Figura 2 mostra l'augment de les *K* del receptor **81a** vers els àcids malònic i oxàlic per l'adició de catió Li^+. En el marc d'aquest treball s'ha descrit, doncs, la preparació d'un dels pocs receptors al·lostèrics per a àcids dicarboxílics de la literatura.

a) b)

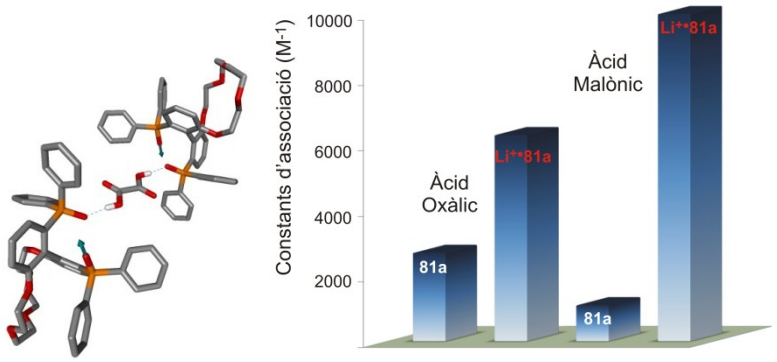

Figura 2. a) Estructura del complex de **81b** amb l'àcid malònic. b) Efecte de Li^+ en les constants d'associació determinades entre el receptor **81a** i els àcids dicarboxílics oxàlic i malònic

D'altra banda, els lligands supramoleculars **45a** i **45b** van ser provats en la hidrogenació asimètrica mediada per rodi dels substrats **39a**,**b**,**d**. No obstant, tot i que els catalitzadors derivats d'aquests lligands es van mostrar actius en catàlisi, l'enantioselectivitat assolida va ser molt baixa en els casos de **39b** i **39d** (2–15% ee) i moderada en el cas de **39a** (64% ee). L'adició de diferents cations (E^+) per a la regulació de l'activitat dels catalitzadors a través d'interaccions supramoleculars amb els lligands no va resultar en una millora substancial dels excessos enantiomèrics aconseguits. Es conclou que seria necessari, en el cas d'aquests lligands, un canvi estructural que millorés l'eficàcia en l'enantioinducció. Com a possible solució, es proposa l'increment de volum estèric en les proximitats al centre catalític per incorporació de substituents en posició 3, 3' de la unitat bifenil.